United States
Environmental Protection
Agency

Industrial Environmental Research
Laboratory
Research Triangle Park NC 27711

EPA-600/9-84-025c
November 1984

Research and Development

EPA

Fourth Symposium on the Transfer and Utilization of Particulate Control Technology:

METEOROLOGY

Volume III. Economics, Mechanical Collectors, Coal Characteristics, Inhalable Particulates, Advanced Energy and Novel Devices

EPA-600/9-84-025c
November 1984

FOURTH SYMPOSIUM ON THE TRANSFER AND UTILIZATION OF PARTICULATE CONTROL TECHNOLOGY: VOLUME III. ECONOMICS, MECHANICAL COLLECTORS, COAL CHARACTERISTICS, INHALABLE PARTICULATES, ADVANCED ENERGY AND NOVEL DEVICES

Compiled by:

F. P. Venditti, J. A. Armstrong, and Michael D. Durham

Denver Research Institute
P. O. Box 10127
Denver, Colorado 80210

Grant Number: CR 809301

Project Officer

Dale L. Harmon
Office of Environmental Engineering and Technology
Industrial Environmental Research Laboratory
Research Triangle Park, North Carolina 27711

INDUSTRIAL ENVIRONMENTAL RESEARCH LABORATORY
OFFICE OF RESEARCH AND DEVELOPMENT
U. S. ENVIRONMENTAL PROTECTION AGENCY
RESEARCH TRIANGLE PARK, NORTH CAROLINA 27711

DISCLAIMER

This document has been reviewed in accordance with U.S. Environmental Protection Agency policy and approved for publication. Mention of trade names or commercial products does not constitute endorsement or recommendation for use.

ABSTRACT

The papers in these three volumes of Proceedings were presented at the Fourth Symposium on the Transfer and Utilization of Paticulate Control Technology held in Houston, Texas during 11 October through 14 October 1982, sponsored by the Particulate Technology Branch of the Industrial Environmental Research Laboratory of the Environmental Protection Agency and coordinated by the Denver Research Institute of the University of Denver.

The purpose of the symposium was to bring together researchers, manufacturers, users, government agencies, educators and students to discuss new technology and to provide an effective means for the transfer of this technology out of the laboratories and into the hands of the users.

The three major categories of control technologies - electrostatic precipitators, scrubbers, and fabric filters - were the major concern of the symposium. These technologies were discussed from the perspectives of economics; new technical advancements in science and engineering; and applications. Several papers dealt with combinations of devices and technologies, leading to a concept of using a systems approach to particulate control rather than device control. Additional topic areas included novel control devices, high temperature/high pressure applications, fugitive emissions, measurement techniques, and economics and cost analysis.

Each volume of these proceedings contains a set of related session topics to provide easy access to a unified technology area.

Since the spirit and style of the panel discussion are not reproducible in print, the initial remarks presented by the panelists have been included in the volume to which their input to the panel pertained, in the interest of providing unified technological organization.

CONTENTS

Page

VOLUME III - CONTENTS v
VOLUME I - CONTENTS viii
VOLUME II - CONTENTS xi

Keynote Address

PARTICULATE CONTROL TECHNOLOGY AND WHERE IT IS GOING xv
K.E. Yeager

Section A - Economic Comparisons

A COMPARISON OF A BAGHOUSE VS. ESP'S WITH AND WITHOUT GAS CONDITIONING FOR LOW SULFUR COAL APPLICATIONS 1
W.H. Cole

APPLICATION OF THE BUBBLE CONCEPT TO FUEL BURNING SOURCES AT A NAVAL INDUSTRIAL COMPLEX 12
C.S Thompson

Section B - Mechanical Collectors

CYCLONE PERFORMANCE: A COMPARISON OF THEORY WITH EXPERIMENTS 26
J.A. Dirgo, D. Leith

HIGH FLOW CYCLONE DEVELOPMENT 41
W.B. Giles

CYCLONE SCALING EXPERIMENTS 53
W.B. Giles

TEST METHODS AND EVALUATION OF MIST ELIMINATOR CARRYOVER 66
V. Boscak, A. Demian

Section C - Coal Characterization

FILTRATION CHARACTERISTICS OF FLY ASHES FROM VARIOUS COAL PRODUCING REGIONS 81
J.A. Dirgo, M.A. Grant, R. Dennis, L.S. Hovis

FLY ASH FROM TEXAS LIGNITE AND WESTERN SUBBITUMINOUS COAL: A COMPARATIVE CHARACTERIZATION 97
D.R. Sears, S.A. Benson, D.P. McCollor, S.J. Miller

USE OF FUEL DATABANKS FOR THE EFFECTIVE DESIGN OF STEAM GENERATORS AND AQC EQUIPMENT 114
N.W. Frisch, T.P. Dorchak

Section D - Inhalable Particulate Matter

DEVELOPMENT OF INHALABLE PARTICULATE (IP) EMISSION FACTORS . . . 131
D.L. Harmon

INHALABLE PARTICULATE MATTER RESEARCH COMPLETED BY GCA/TECHNOLOGY DIVISION 141
S. Gronberg

RESULTS OF TESTING FOR INHALABLE PARTICULATE MATTER AT MIDWEST RESEARCH INSTITUTE 154
K. Wilcox, F. Bergman, J. Kinsey, T. Cuscino

INHALABLE PARTICULATE EMISSION FACTORS TEST PROGRAMS 166
J.W. Davison,

CHARACTERIZATION OF PARTICULATE EMISSION FACTORS FOR INDUSTRIAL PAVED AND UNPAVED ROADS 183
C. Cowherd, Jr., J.P. Reider, P.J. Englehart

CONDENSIBLE EMISSIONS MEASUREMENTS IN THE INHALABLE PARTICULATE PROGRAM 198
A.D. Williamson, J.D. McCain

Section E - Advanced Energy Applications

GAS CLEANING AND ENERGY RECOVERY FOR PRESSURIZED FLUIDIZED BED COMBUSTION 211
A. Brinkmann, P.M. Kutemeyer

DEMONSTRATION OF THE FEASIBILITY OF A MAGNETICALLY STABILIZED BED FOR THE REMOVAL OF PARTICULATE AND ALKALI 226
L.P. Golan, J.L. Goodwin, E.S. Matulevicius

TEST RESULTS OF A HIGH TEMPERATURE, HIGH PRESSURE ELECTROSTATIC PRECIPITATOR 241
D. Rugg, G. Rinard, J. Armstrong, T. Yamamoto, M. Durham

COAL-ASH DEPOSITION IN A HIGH TEMPERATURE CYCLONE 256
K.C. Tsao, A. Rehmat, D.M. Mason

DUST FILTRATION USING CERAMIC FIBER FILTER MEDIA — A STATE-OF-THE-ART SUMMARY — 271
R. Chang, J. Sawyer, W. Kuby, M. Shackleton,
O.J. Tassicker, S. Drenker

HIGH TEMPERATURE AND PRESSURE PARTICULATE FILTERS FOR FLUID BED COMBUSTION 282
D.F. Ciliberti, T.E. Lippert, O.J. Tassicker, S. Drenker

MOVING BED-CERAMIC FILTER FOR HIGH EFFICIENCY PARTICULATE AND ALKALI VAPOR REMOVAL AT HIGH TEMPERATURE AND PRESSURE . . . 300
D. Stelman, A.L. Kohl, C.A. Trilling

TESTING AND VERIFICATION OF GRANULAR BED FILTERS FOR REMOVAL OF PARTICULATES AND ALKALIS 318
T.E. Lippert, D.F. Ciliberti, R. O'Rourke

BAGHOUSE OPERATION IN GEORGETOWN UNIVERSITY COAL-FIRED, FLUIDIZED-BED BOILER PLANT, WASHINGTON, D.C. 335
V. Buck, D. Suhre

Section F - Novel Devices

PARTICLE CAPTURE MECHANISMS ON SINGLE FIBERS IN THE PRESENCE OF ELECTROSTATIC FIELDS 347
M.A. Ranade, F.L. Chen, D.S. Ensor, L.S. Hovis

PILOT DEMONSTRATION OF PARTICULATE REMOVAL USING A CHARGED FILTER BED 362
P.H. Sorenson

PILOT DEMONSTRATION OF MAGNETIC FILTRATION WITH CONTINUOUS MEDIA REGENERATION 370
C.E. Ball, D.W. Coy

Section G - Plenary Session

NOVEL PARTICULATE CONTROL TECHNOLOGY 386
S. Masuda

AUTHOR INDEX 406

VOLUME I

FABRIC FILTRATION

Section A - Fabric Filters: Fundamentals

THEORY OF THE TEMPORAL DEVELOPMENT OF PRESSURE DROP ACROSS A FABRIC FILTER DURING CAKE INITIATION 1
E.A. Samuel

PULSE JET FILTRATION THEORY - A STATE-OF-THE-ART ASSESSMENT. . . 22
R. Dennis, L.S. Hovis

LABORATORY TECHNIQUES FOR DEVELOPING PULSE JET COLLECTORS. . . . 37
R.R. Banks, J.T. Foster

OFF-LINE PULSE-JET CLEANING SYSTEM 48
T.C. Sunter

Section B - Fabric Filters: Measurement Techniques

FIELD EVALUATION OF THE DRAG OF INDIVIDUAL FILTER BAGS 62
W.T. Grubb, R.R. Banks

A DUAL-DETECTOR BETA-PARTICLE BACKSCATTER GAUGE FOR MEASURING DUST CAKE THICKNESS ON OPERATING BAG FILTER AND ESP UNITS. . . . 77
R.P. Gardner, R.P. Donovan, L.S. Hovis

MIT FLEX ENDURANCE TESTS AT ELEVATED TEMPERATURE 91
J.T. Foster, W.T. Grubb

THE ONE-POINT IN-SITU CALIBRATION METHOD FOR USING A BETA-PARTICLE BACKSCATTER GAUGE FOR CONTINUOUSLY MEASURING DUST CAKE THICKNESS ON OPERATING BAG FILTER AND ESP UNITS 107
R.P. Gardner, R.P. Donovan, L.S. Hovis

Section C - Fabric Filters: Coal Fired Boilers

PULSE-JET FABRIC FILTER EXPERIENCE USING NON-GLASS MEDIA AT AIR TO CLOTH RATIOS OF 5 TO 1 ON A PULVERIZED COAL FIRED BOILER 121
G. Pearson, D.D. Capps

START-UP AND OPERATION OF A FABRIC FILTER CONTROLLING PARTICULATE EMISSIONS FROM A 250 MW PULVERIZED COAL-FIRED BOILER 132
C.B. Barranger, N. Spence, J. Saibini

VOLUME I CONTENTS (Cont.)

PERFORMANCE OF A 10 MW FABRIC FILTER PILOT PLANT AND COMPARISON TO FULL-SCALE UNITS 148
W.B. Smith, K.M. Cushing, R.C. Carr

THE DESIGN, INSTALLATION, AND INITIAL OPERATION OF THE W.H. SAMMIS PLANT, UNIT 3 FABRIC FILTER 164
D.R. Ross, J.R. Howard, R.M. Golightley

RESULTS FROM THE FABRIC FILTER EVALUATION PROGRAM AT COYOTE UNIT #1 179
H.J. Peters, A.A. Reisinger, W.T. Grubb, M. Lewis

BAGHOUSE PERFORMANCE AND ASH CHARACTERIZATION AT THE ARAPAHOE POWER STATION 192
R.S. Dahlin, D.R. Sears, G.P. Green

AN EVALUATION OF FULL-SCALE FABRIC FILTERS ON UTILITY BOILERS. 210
J.W. Richardson, J.D. McKenna, J.C. Mycock

STATUS OF SPS INVESTIGATION OF HARRINGTON STATION UNIT 2 FABRIC FILTER SYSTEM 226
R. Chambers, D. Harmon

UPDATE OF SPS PILOT BAGHOUSE OPERATION 239
R. Chambers, S. Kunka, D. Harmon

THE USE OF SONIC AIR HORNS AS AN ASSIST TO REVERSE AIR CLEANING OF A FABRIC FILTER DUST COLLECTOR 255
A. Menard, R.M. Richards

Section D - Fabric Filters: Electrostatic Enhancement

ELECTROSTATIC STIMULATION OF REVERSE-AIR-CLEANED FABRIC FILTERS 287
D.A. Furlong, G.P. Greiner, D.W. VanOsdell, L.S. Hovis

ELECTRICAL STIMULATION OF FABRIC FILTRATION: ENHANCEMENT BY PARTICLE PRECHARGING 303
G.E.R. Lamb, R. Jones, W. Lee

ESFF AS A FIELD EFFECT 316
L.S. Hovis, G.H. Ramsey, R.P. Donovan

ELECTRICAL ENHANCEMENT OF FABRIC FILTRATION: PRECHARGING VS. BAG ELECTRODES 327
R.P. Donovan, L.S. Hovis, G.H. Ramsey

PERMEABILITY OF DUST CAKES COLLECTED UNDER THE INFLUENCE OF AN ELECTRIC FIELD 342
D.W. VanOsdell, R.P. Donovan, D.A. Furlong, L.S. Hovis

Section E - Fabric Filters: Practical Considerations

HIGH VELOCITY FABRIC FILTRATION FOR INDUSTRIAL COAL-FIRED BOILERS 357
G.P. Greiner, S. Delaney, L.S. Hovis

OPTIMIZING THE LOCATION OF ANTI-COLLAPSE RINGS IN FABRIC BAGS 382
J. Musgrove

PULSE JET ON-LINE CLEANING FILTER FOR FLY ASH 420
W.G. Wellan

TOP INLET VERSUS BOTTOM INLET BAGHOUSE DESIGN 431
R.M. Jensen

UPGRADE OF FLY ASH COLLECTION CAPABILITY AT THE CROMBY STATION 446
T.J. Ingram, R.J. Biese, R.O. Jacob

HIGH SULFUR FUEL, FABRIC FILTER STARTUP EXPERIENCE 460
P. Hanson, L. Adair, R.N. Roop, R.B. Moyer

FUNDAMENTAL STRATEGIES FOR CLEANING REVERSE AIR BAGHOUSES. . . . 482
M. Ketchuck, M.A. Walsh, O.F. Fortune,
M.L. Miller, M. Whittlesey,

Section F - Dry Scrubbers

DESIGN CONSIDERATIONS FOR BAGHOUSE - DRY SO_2 SCRUBBER SYSTEMS 494
O.F. Fortune, R.L. Miller

RESULTS OF BAGHOUSE AND FABRIC TESTING AT RIVERSIDE 506
H.W. Spencer III, Y.J. Chen, M.T. Quach

REACTIVITY OF FLY ASHES IN A SPRAY DRYER/FABRIC FILTER FGD PILOT PLANT 521
W.T. Davis, R.E. Pudelek, G.D. Reed

Section G - Plenary Session

FABRIC FILTRATION - AS IT WAS, HAS BEEN, IS NOW AND SHALL BE 536
E.R. Frederick

AUTHOR INDEX 551

VOLUME II

ELECTROSTATIC PRECIPITATION

Section A - Industrial Applications

MODELING OF WET BOTTOM AGITATOR SYSTEMS FOR ELECTROSTATIC PRECIPITATORS ON RECOVERY BOILERS 1
M.A. Sandell, R.R. Crynack

DESIGN AND PERFORMANCE OF ELECTROSTATIC PRECIPITATORS UTILIZING A NEW RIGID DISCHARGE ELECTRODE DESIGN 17
G.R. Gawreluk, R.L. Bump

DEVELOPMENT AND EVALUATION OF NEW PRECIPITATOR EMITTER ELECTRODE 35
R.L. Adams, P. Gelfand,

INDUSTRIAL APPLICATIONS OF TWO STAGE TUBULAR ELECTROSTATIC PRECIPITATORS 51
H. Surati, M.R. Beltran

Section B - Advanced Technology

PILOT DEMONSTRATION TWO-STAGE ESP TEST RESULTS 65
P. Vann Bush, D.H. Pontius

EVALUATION OF PRECHARGERS FOR TWO-STAGE ELECTROSTATIC PRECIPITATORS 84
G. Rinard, D. Rugg, M. Durham

INITIAL EXPERIMENTS WITH AN ELECTRON BEAM PRECIPITATOR TEST SYSTEM 96
W.C. Finney, R.H. Davis, J.S. Clements, E.C. Trexler, J.S. Halow, O. Tokunaga

EXPERIMENTS WITH WIDE DUCTS IN ELECTROSTATIC PRECIPITATORS . . . 111
E. Weber

A RECONCILIATION: WIDE VERSUS NARROW SPACED COLLECTING PLATES FOR PRECIPITATORS 126
D.G. Puttick

PULSE CORONA AS ION SOURCE AND ITS BEHAVIORS IN MONOPOLAR CURRENT EMISSION 139
S. Masuda, Y. Shishikui

Section C - Fundamentals

A NEW CORRECTION METHOD OF MIGRATION VELOCITY IN DEUTSCH EFFICIENCY EQUATION FOR CONVERSION OF ELECTROSTATIC PRECIPITATOR SIZING FROM A PILOT-SCALE TO FULL-SCALE 154
F. Isahaya

DISTORTION OF PULSE VOLTAGE WAVE FORM ON CORONA WIRES DUE TO CORONA DISCHARGE 169
S. Masuda, H. Nakatani

ELECTROSTATIC PRECIPITATOR ANALYSIS AND SYNTHESIS 184
T. Chiang, T.W. Lugar

COMPUTER MODEL USE FOR PRECIPITATOR SIZING 194
G.W. Driggers, A.A. Arstikaitis, L.A. Hawkins

IMPROVEMENTS IN THE EPA/SRI ESP PERFORMANCE MODEL 204
M.G. Faulkner, R.B.Mosley, J.R. McDonald, L.E. Sparks

NUMERICAL SIMULATION OF THE EFFECTS OF VELOCITY FLUCTUATIONS ON THE ELECTROSTATIC PRECIPITATOR PERFORMANCE 218
E.A. Samuel

CORONA - INDUCED TURBULENCE 230
M. Mitchner, G.L. Leonard, S.A. Self

VELOCITY AND TURBULENCE FIELDS IN NEGATIVE CORONA WIRE-PLATE PRECIPITATOR 243
H.P. Thomsen, P.S. Larsen, E.M. Christensen, J.V. Christiansen

THE EFFECT OF TURBULENCE ON ELECTROSTATIC PRECIPITATOR PERFORMANCE 261
D.E. Stock

FACTORS LEADING TO ELECTRICAL BREAKDOWN OF RESISTIVE DUST LAYERS AND SUSTAINED BACK CORONA 271
P.A. Lawless, L.E. Sparks

ELECTRICAL BREAKDOWN OF PARTICULATE LAYERS 288
G.B. Moslehi, S.A. Self

ELECTROMECHANICS OF PARTICULATE LAYERS 306
G.B. Moslehi, S.A. Self

LATERAL PROPAGATION OF BACK CORONA IN TWIN-ELECTRODE TYPE PRECIPITATORS 322
S. Masuda, T. Itagaki

FIRST MEASUREMENTS OF AEROSOL PARTICLE CHARGING BY FREE ELECTRONS 337
J.L. DuBard, M.G. Faulkner, L.E. Sparks

VOLUME II CONTENTS (Cont.)

Section D - Operation & Maintenance

GAS FLOW DISTRIBUTION MODEL TESTING 349
D.R. Cook, J.M. Ebrey, D. Novogoratz

AIR FLOW MODEL STUDIES 369
L.H. Bradley

COLLECTING ELECTRODE RAPPING DESIGNED FOR HIGH EFFICIENCY ELECTRIC UTILITY BOILER ELECTROSTATIC PRECIPITATORS 384
A. Russell-Jones, A.P. Baylis

ELECTROSTATIC PRECIPITATOR AND FABRIC FILTER OPERATING AND MAINTENANCE EXPERIENCE 401
P.R. Goldbrunner, W. Piulle

Section E - Conditioning

ECONOMICAL FLY ASH COLLECTION BY FLUE GAS CONDITIONING 416
E.L. Coe, Jr.

EXPERIENCES AT DETROIT EDISON COMPANY WITH DECLINING PERFORMANCE OF SULFUR TRIOXIDE FLUE GAS CONDITIONING EQUIPMENT 430
L.A. Kasik, W.A. Rugenstein, J.L. Gibbs

ESP CONDITIONING WITH AMMONIA AT THE MONROE POWER PLANT OF DETROIT EDISON COMPANY 444
E.B. Dismukes, J.P. Gooch, G.H. Marchant, Jr.

FLY ASH CHEMISTRY INDICES FOR RESISTIVITY AND EFFECTS ON ELECTROSTATIC PRECIPITATOR DESIGN AND PERFORMANCE 459
H.J. Hall

Section F - Control Systems

A NEW ENERGIZATION METHOD FOR ELECTROSTATIC PRECIPITATORS MITSUBISHI INTERMITTENT ENERGIZATION SYSTEM 474
T. Ando, N. Tachibana, Y. Matsumoto

SOME MEASURED CHARACTERISTICS OF AN ELECTROSTATIC PRECIPITATOR OBTAINED USING A MICROCOMPUTER CONTROLLER 489
M.J. Duffy, T.S. Ng, Z. Herceg, K.L. McLean

ELECTROSTATIC PRECIPITATOR ENERGIZATION AND CONTROL SYSTEMS . . 499
K.M. Bradburn, K. Darby

VOLUME II CONTENTS (Cont.)

APPLYING MODULAR MICROCOMPUTER CONTROL ELEMENTS IN A PRECIPITATOR CONTROL SYSTEM 521
I.M. Wexler

Section G - Plenary Session

THE CURRENT STATUS, FUTURE DIRECTIONS, AND ECONOMIC CONDITIONS IN THE APPLICATION OF ESP'S 534
S. Oglesby

AUTHOR INDEX 539

PARTICULATE CONTROL TECHNOLOGY AND WHERE IT IS GOING

by: K. E. Yeager
Electric Power Research Institute
Palo Alto, California 94303

ABSTRACT

This keynote address underscores the key role of particulate control technology in any practical strategy for reducing the emissions associated with coal utilization. Its importance results from the long-standing and successful cooperative efforts among user, supplier, and government to achieve control methods which are as reliable, simple and low cost as possible. Opportunities are discussed for capitalizing on this established and accepted base to solve the current and emerging set of air pollution issues facing the utility industry.

INTRODUCTION

Thank you Mr. Chairman, ladies and gentlemen. I particularly welcome this opportunity to speak to you because I believe particulate control must be the foundation for a rational emission control strategy. Before we examine where particulate control technology is going, let us look at where it has been.

Nearly 100 years ago particulate control began in earnest to resolve the obvious smoke emissions of heavy industry. A cooperative effort over the ensuing years among user, supplier, and government has brought particulate control to be an accepted, integral part of our industrial and combustion processes.

This development has been successful because it never forgot that it was the function of particulate control not just to clean the stack but to do so in as reliable, simple and least costly manner as possible. In other words, good industrial engineering practice guided the emission control effort as it would all other aspects of commercial process development.

During the 1970s, the politicization of the environment, in my judgement, led us away from building on this successful foundation. Instead, alternatives sacrificing good commercial practice were imposed in return for promise of maximum theoretical emission control efficiency. Legislative and administrative decisions were made which ignored the technical principles necessary

for successful control technology application. An adversial relationship rapidly developed between user, supplier and government in which lawyers, not scientists and engineers, were responsible for defining the state of control technology. I submit that this results in the very antithesis of progress by installing a psychology of contradiction not cooperation.

REQUIREMENTS

The basic issue in control requirements as they have evolved over the last 25 or 30 years has been the dramatic increase in removal efficiency demanded of particulate control. In the 1950s and even 1960s, control requirements were in the 90 percent range. Today we're two orders of magnitude higher in requirement. As a result, we are as close to zero particulate discharge as is measurable. This has forced a revolutionary change in our control considerations. Where we were once well within the state of the art in particulate control, we have now exceeded the state of the art in precipitators. We are also evaluating fabric filtration because of its potential cost and performance advantages. In summary, we are going from a technology which is widely available and well known, but marginal in performance, to a technology that promises a performance margin. However, its current design base and reliability in the utility industry are not well established.

As we go into the future, we are faced with toxic substances control standards demanding not just a relative level of control, but absolute control. This emerging requirement has also been connected to fine particulate. We are also challenged by a major secondary particulate issue, which has changed the arena of argument for the application of flue gas desulfurization and NO_x control.

From an engineering standpoint, we also have to be aware of some of the control issues that may not be reflected in removal efficiency, but will have a major impact on the way we design and operate equipment. First, preconstruction review requires agreement on the level of control capability for all pollutants prior to commencing construction. This may mean agreement not just between the regulatory agency and the utility, but with interveners as well.

Second, and perhaps more important, operation and maintenance standards will require the technology to meet a predetermined level of reliability in order for the power plant to be permitted to operate at all.

What are some of the issues facing the utility industry which must guide our actions? These include, in addition to environmental requirements:

- uncertain petroleum availability
- skyrocketing fuel prices
- declining demand growth rates
- restricted capital investment capability
- loss of public confidence in the nuclear initiative
- withdrawal of government R&D support
- rapidly increasing electrical rates.

Several factors in the utility response to these issues seem clear:

1. Electric generation will depend increasingly on coal

2. Priority will be placed on improving the reliability and longevity of existing generating capacity. This includes reducing sensitivity to fuel quality.

3. The utility user will assume greater leadership for the selection, development and commercialization of technology.

4. U.S. supplier priority is likely to focus more and more on competing in the international market to maintain market size.

What does all this mean for the particulate control technology developer?

ELECTROSTATIC PRECIPITATION--This has long been the backbone of environmental control in the utility industry. If we look at the impact of changing control requirements from a precipitator standpoint, we would find that the demand for increase in control capability has led to about a fivefold increase in electrostatic precipitator size and at least a threefold increase in cost in constant 1981 dollar terms. We've gone from a low-cost technology, operating well, to a high-cost technology, often operating not very well.

More and more the public perception of environmental acceptability is based on a clear stack, irrespective of regulatory requirements. This is also becoming an industry measure and one I might add which has the positive attention of the utility industry. It means that retrofit measures must be advanced to reduce the sensitivity of the high efficiency precipitator to changing fuel quality and resulting ash characteristics. Chemical conditioning therefore has become one important solution to this issue and one which has advanced from a black art to real engineering credibility. Second, as reduced economic strength and slowed electricity demand growth reduces capacity expansion, we must look even more to increasing the long-term reliability of our equipment to last not just 30-40 years but 50 years and more. Third, a revitalized effort to advance the technology of ESP is needed to maintain its competitiveness in the face of ever more stringent emission control requirements.

FABRIC FILTERS--In the face of very stringent standards and the desire to maintain a clear stack under all conditions, fabric filters are rapidly becoming a competitive, if not preferred, alternative for new plant applications. This is creating a healthy technical competition between fabric filters and precipitators.

Although in use for many years, we have, however, found major opportunities for improving the reliability, operability and cost of this technology as it applies to the utility industry. These opportunities encompass among others; improved aerodynamic design, bag materials, cleaning frequency and method, optimized dust loading on bags, and electrostatic enhancement.

INTEGRATED EMISSION CONTROL--If we look at the growth in environmental control requirements on power plants since 1965 we find revolutionary technical and economic changes. In 1965 a precipitator was the primary control device. Its cost was about 10% of a new plant. Today, typically 40% of the cost of a new plant is for environmental control. By 1985 these requirements provide the opportunity for the emission control technology tail to wag the power plant, not only in dimensions, but also in investment.

This forces us to take a hard look at our conventional way of viewing emission control. We can't afford to deal with each control requirement as an individial black box. Rather, we have to integrate them in a systematic way that provides simplification and improved reliability. Integrated Emission Control (IEC) is, therefore, more than anything, a state of mind. As the cost of meeting environmental regulations on a new coal fired power plant increases to 40% or more of a billion dollar investment, I think we are all faced with the realization that business as usual, i.e., adding piece meal more and more auxiliary control devices is a bankrupt approach. Fundamentally, IEC means elevating the engineering priority of environmental control to a level equivalent to its economic importance.

Nowhere, in my judgement, are the opportunities for particulate control technology greater. Issues which are accelerating the need for this approach are closely associated with the total atmospheric loading of pollutants. These include, for example, visibility/long-range transport and acid precipitation.

Acid precipitation is the latest and most politically potent in a series of issues that may require expanded retrofit emission control. It is therefore imperative from a cost and practicality standpoint that we base any resulting retrofit strategy on the existing particulate control capability. Coal cleaning is important but can only reduce SO_2 emissions by about 2 million tons per year. Coal switching is likely to be politically, if not economically, limited. Therefore, many companies in the industrial midwestern states may be required to create a technology to achieve 40-60% SO_2 removal utilizing dry removal in conjunction with existing particulate control capabilities. Failure to do so may add billions of dollars per year to the local cost of control.

As an example of the IEC approach, our tests indicate a strong correlation between reduced NO_x formation and reduced fine particulate formation. This leads EPRI to urge combustion control opportunities which may cost-effectively combine these two effects. Such an approach begins to integrate particulate control with the combustion process itself.

NEW TECHNOLOGY

The present utility conditions present an opportunity to carry IEC one step further as the utility industry actively develops and commercializes new coal utilization technology for its next generation of plants. Foremost among these technologies, in my judgement, is fluid bed combustion which provides an evolutionary improvement in our use of coal. Specific advantages include:

- Increased fuel flexibility
- Less cost sensitivity to size
- Integral environmental control - except particulate.

A 100-200 MWe utility demonstration of this new steam generating technology is planned by EPRI and the utility industry for operation this decade. This will be based on the 20 MWe TVA/EPRI engineering prototype now successfully operating at Paducah, Kentucky.

In the pressurized form, fluid bed combustion has growth potential to provide several additional advantages including:

- Shop fabricated, barge transportable, standardized power modules for rapidly and cost effectively adding generating capacity.

- Lowest busbar energy cost of any coal option

The key to its success, however, is reliable high pressure, high temperature filtration to insure gas turbine reliability and emission compliance. This is an area demanding concentrated effort by the development community.

EPRI'S ROLE

It has been EPRI's role to help fill the void surrounding determination of the cost, reliability and operability issues affecting required or proposed control technology. Through the vehicle of large-scale tests, particularly at our Arapahoe Test Facility and the new Shawnee AFBC Facility, we endeavor to manage and limit the level of risk associated with commercial innovation. We include efforts to:

- Determine under actual utility operating conditions the factors which may limit practical application of controls.

- Where appropriate, help resolve these issues.

- Determine objectively the status of new technology.

- Avoid large and expensive commercial failures which may cost large sums and kill otherwise promising technologies.

- Train utility technicians and operators.

- Provide a credible and realistic data base for establishing technical policy on environmental control.

CONCLUSIONS

I applaud EPA for working to reconstruct the former spirit of cooperation necessary for the advancement of environmental control technology. Having just returned from Europe, I am even more convinced that throughout the Western World and Japan, environmental progress must be made within the fundamental economic and productivity strength of our societies.

Within this context are three principles which I believe are crucial to successful advancement of environmental control.

1. The affected industry must be given greater freedom in selecting the means of control. Over the past decade industry has too often found itself reacting to legislative determinations of technology status without constructive opportunity to participate in this determination. The regulator and regulated must work together in the technical arena without counterproductive administrative and legal constraints.

2. Conversely, government must accept at least joint responsibility for resolving with industry the practical issues of reliability, cost and operability which limit productive use of new control technology. These issues will not be effectively reduced by simply dumping them in the lap of industry.

3. Particulate control technology remains the key to practical control of the full set of emissions affecting coal utilization. The challenge to all of you is tc capitalize on this established and accepted base and aggressively provide the technical leadership and ingenuity necessary to achieve practical solutions. EPRI and the utilities look forward to working with you in this endeavor.

Thank you for your kind attention and my very best to you all.

A COMPARISON OF A BAGHOUSE VS. ESP'S WITH AND WITHOUT GAS CONDITIONING FOR LOW SULFUR COAL APPLICATIONS

by: William H. Cole
Gibbs & Hill, Inc.
New York, N.Y. 10001

ABSTRACT

The new source emission standard of 0.03 lbs/10^6 Btu for electric utilities suggests that the selection of particulate removal equipment will increasingly favor the baghouse as compared to conventional ESP's for low sulfur coal applications. This paper investigates a third alternative of a relatively small ESP used in conjunction with SO_3 gas conditioning for new generating units, which typically require efficiency levels of 99.70 percent or higher. The three alternatives are compared for a 500 MW unit burning low sulfur western coal. Emphasis is placed on the comparable economics of investment, and present worth of annual costs including fixed charges, incremental energy, bag replacement, sulfur feed stock, and maintenance. Cost sensitivity is illustrated for assumed escalation rates from zero to 10 percent. A preliminary review indicates that ESP's in conjunction with gas conditioning, offer an attractive alternative to a conventionally sized ESP or baghouse, and may restore the dominance of ESP's in equipment selection.

INTRODUCTION

During the past few years, there has been a significant decline in the use of electrostatic precipitators (ESP's) as compared to an increasing use of the baghouse by the electric utility industry. This has resulted from a number of factors as follows:

(1) Typical efficiency levels in the 99.7 to 99.8 percent range are generally required to satisfy the current maximum emission regulation of 0.03 lbs/10^6 Btu for new generating units.

(2) The increased use of low sulfur coal, particularly of the western variety, requires relatively large ESP's.

(3) A broad range of critical coal and ash characteristics is often used in the precipitator equipment specification for performance guarantees. This clearly tends to result in an overly conservative design based on the "worst" coal.

The combined effect of the above factors has made the baghouse cost competitive with the precipitator for low sulfur coal applications, with the added benefit of performance that is essentially independent of normal variation in the coal characteristics. The trend to the use of baghouse is substantiated by statistics from one vendor which indicate that the baghouse obtained 14 and 17 percent of the electric utility megawatt orders in 1979 and 1980, respectively. Even more indicative are Industrial Gas Cleaning Institute statistics which show that the baghouse market share for all flyash collectors increased from 24 to 45 percent of total dollar bookings during the same period (1).

There is now another option deserving of full consideration in the process of equipment selection for new generating units. This is the use of a relatively small ESP equipped with a sulfur burner type gas conditioning system which introduces small quantities of sulfur trioxide into the flue gas as the conditioning agent. Although the effectiveness of sulfur conditioning has been known for many years, there was insufficient demand to justify commercialization of the equipment design prior to the Clean Air Act of 1970. When intially developed in the early 1970's, the system appeared to have limited application to the upgrading of substandard performance of existing precipitators designed for relatively low efficiency, and subsequently being used to collect a marginal or high resistivity fly ash. However, in recent years there have been major improvements in both the conditioning process and equipment design. The experience with more than 100 installations to date indicates that the equipment meets all of the criteria of automation, reliability, and availability required by the electric utility application. On this basis, it is logical to evaluate the use of a relatively small ESP designed for use with gas conditioning for a new generating unit. Although systems have been designed with this objective, this paper summarizes the results of a technical and economic comparison of this alternative with a full size precipitator and baghouse for a hypothetical 500 MW unit burning a low sulfur western coal.

EQUIPMENT DESCRIPTION

The only equipment requiring description is the gas conditioning system, and space limitations require that this be brief. Suffice it to say that numerous publications are available with details of the process and equipment, whereas the objective of this paper is a comparison of the technical and economic aspects of the system when used with an ESP as compared to other alternatives.

The gas conditioning equipment required for a new 500 MW generating unit comprises a liquid sulfur storage tank of nominal 100 ton capacity, a metering pump skid including the unloading pump, and a single burner/converter skid to serve both precipitators. As noted previously, of salient importance is the control system and level of automation. Assuming the sulfur is in the liquid state at startup, a push button activates the electric ambient air heaters to raise the temperature of

the vanadium pentoxide catalyst to the required process temperature of 800 F. This requires approximately 4 hours from a cold start at which point a second push button activates the sulfur feed to the burner/converter skid for controlled feed of sulfur trioxide to the ESP inlet probes. The feed rate is optimized following installation of the system, and is automatically regulated by a boiler signal to maintain the optimum injection rate over the total range of boiler load. If desired, the feed will automatically shut off at a predetermined boiler load at which point gas conditioning is no longer required because of reduced gas flow rate to the ESP, and the system has a turn down ratio of at least 20 to 1 in the event of an upset condition.

The equipment causes minimal problems with general arrangement, particularly with a new generating unit. The sulfur storage tank and pump skid can be remotely located, and only the converter skid should be located as closely as possible to the ESP inlet ducts to minimize the stainless steel piping to the inlet probes. The system also causes no constraints on ductwork layout since only one second of treatment time is required to condition the ash upstream of the precipitator inlet flange.

SYSTEM DESIGN PARAMETERS

The system design and performance requirements are summarized as follows:

Unit Size	500 MW
Gas Flow Rate	1,800,000 ACFM
Gas Temperature	300 F
Heat Input	5000 MMBtu/hr
Coal Firing Rate	625,000 lbs/hr
Maximum Emission	0.03 lbs/MMBtu
Inlet Grain Loading	3.28 GR/ACF
Guarantee Efficiency	99.70 percent
Maximum Outlet Loading	0.010 GR/ACF

The above requirements were based on the coal and ash analyses in Table 1 which represent a composite of several Wyoming coals from the Powder River Basin.

TABLE 1. DESIGN COAL AND ASH ANALYSES

Coal	Percent	Fly Ash	Percent
Moisture	28.0	Silica	35.0
Carbon	46.0	Aluminum Oxide	19.0
Ash*	9.0	Iron Oxide	5.5
Hydrogen	3.4	Calcium Oxide	22.0
Nitrogen	0.8	Magnesium Oxide	4.4
Oxygen	12.3	Potassium Oxide	0.4
Sulfur	0.5	Sodium Oxide	1.0
Heating Value	8000 Btu/lb	Titanium Oxide	1.0
		Sulfur Trioxide	11.3

*Assume 90 percent ash to flyash.

EQUIPMENT DESIGN

In an effort to achieve objectivity, the sizing and design of all equipment was obtained from experienced vendors. Since there is often more disparity in baghouse design among suppliers, this information was obtained from two vendors, and it lends credence to the technical comparison to note that both designs were virtually identical.

PRECIPITATOR DESIGNS

A rigid frame precipitator with hammer rapping was selected for the full sized unit not equipped with gas conditioning. This design appears appropriate for a high resistivity ash application based on adequate rapping intensity, and reliability of the semi-rigid discharge electrodes of the scalloped ribbon or twisted square type.

A mast type electrode design that can be used with overhead hammer or magnetic impulse rapping was selected for the unit to be equipped with gas conditioning. This is also appropriate due to the relatively small precipitator size which can create problems with electrical sectionalization with a rigid frame design.

A comparison of the basic design parameters is shown in Table 2.

TABLE 2. ESP DESIGN PARAMETERS

(One ESP of 2 Required)	Rigid Electrode (with Conditioning)	Rigid Frame (without Conditioning)
Gas Flow @ 300 F (acfm)	900,000	900,000
Efficiency (%)	99.70	99.70
No. of Gas Passages (12 in.)	108	80
Plate Height (ft)	36	45
Effective Duct Length (ft)	45	87.6
Collecting Area (sq ft)	349,920	629,856
Gas Velocity (ft/sec)	3.86	4.17
Bus Sections (Series/Parallel)	5/4	6/4
Connected Ma/1000 sq ft	51	38
Connected Watts/sq ft	2.83	2.10
SCA (sq ft/1000 acfm)	389	700
Migration Velocity Wk (ft/sec)	1.447	0.804
Migration Velocity W (ft/sec)	0.249	0.138

The most significant difference between the two designs is obviously the SCA's (or design migration velocities) which indicate that the precipitator equipped with gas conditioning has only 56 percent as much collecting plate area as compared to the full size ESP. It may be coincidental, but it is of interest to note that both SCA's agreed with

that of the writer within less than 1.5 percent. The question may arise as to a procedure for sizing precipitators designed specifically for use with gas conditioning. A good guideline is to consider the application as though it were a 2 percent sulfur coal. Although the latter can be adjusted by the sulfur trioxide injection rate, a 2 percent sulfur is generally about optimum for stability of electrical operation without undue concern about re-entrainment.

BAGHOUSE DESIGN

The baghouse design provided by two equipment suppliers was virtually identical, and is summarized in Table 3. Of the design features shown, the only one specified for this paper was the use of reverse air cleaning.

TABLE 3. BAGHOUSE DESIGN PARAMETERS

(One Baghouse of Two Required)	
Gas Flow/Baghouse @ 300 F (acfm)	900,000
Efficiency (%)	99.80
No. of Compartments/Baghouse	12
No. Bags/Comp't. (3 Bag Reach)	393
Cloth Area/Baghouse (sq ft)	488,106
Bag Material (12 in. x 35 ft Bags)	Glass
Bag Cleaning	Reverse Air
Reverse Air/Cloth Ratio	1.75:1
Gross Air/Cloth Ratio (12 Comp'ts.)	1.84:1
Net Air/Cloth Ratio (10 Comp'ts.)	2.38:1

GAS CONDITIONING SYSTEM DESIGN

The sulfur burner gas conditioning system comprises a 100 ton liquid sulfur storage tank, a metering pump skid, a single sulfur burner/converter skid serving both precipitators, and two sets of sulfur trioxide injection probes. The sulfur burner is rated at 300 lbs/hr with an expected maximum use rate of 190 lbs/hr to provide a sulfur trioxide injection rate of 25 ppm by volume. Maximum electrical requirement is 200 kw.

ECONOMIC FACTORS

The assumed economic parameters are critical to the cost comparison, and were obtained from a number of sources. The factors include those typically provided to Gibbs & Hill by the electric utilities for economic studies, such as plant life, fixed charges, capacity charge, and interest rates. Other factors such as incremental

energy cost, bag life, and cost of liquid sulfur were obtained specifically for the requirements of this study. The economic factors used as a basis for the cost comparison are summarized in Table 4.

TABLE 4. ECONOMIC FACTORS

Plant Life	30 yrs.
Capacity Charge	$1,000/kw
Fixed Charge Rate	17 percent
R.O.I. For Present Worth	10 percent
Incremental Energy Cost	$0.025/kwhr
Avg. ESP Pressure Loss	1.0 in wg
Avg. Baghouse Pressure Loss	4.5 in wg
Steam Cost (Sat. @ 45 psig)	$0.003/lb
Liquid Superbrite Sulfur	$160.00/ton
Bag Life	3 yrs.
Annual Maintenance Costs:	
ESP's (% of Material Cost)	5.0 percent
Baghouse (% of Material Cost)	2.5 percent
Interest Rate	10 percent
Escalation Rate*	0, 5, & 10 percent
Operating Hours/Yr	8200/yr
Avg. Load Factor	75 percent

*Escalation is applied to cost of energy, sulfur, steam, replacement filter bags, and maintenance.

Several of the above parameters which are critical to this study are based on the following:

(1) Incremental energy charge is based on a G&H estimate for the use of low sulfur western coal in the midwest region.

(2) A fabric filter bag life of 3 years was suggested by equipment suppliers based on the economics of replacement of an entire compartment at one time.

(3) The cost of liquid "superbrite" sulfur is based on two recent price quotations including delivery to a Gulf Port. It also includes a nominal $20 per ton inland freight charge to the plant destination.

(4) Maintenance costs were the single most difficult cost to assess. Utility records will sometimes include routine shift inspection, or only special maintenance requirements. There is insufficient experience to estimate routine maintenance costs on a baghouse. However, it was assumed to be one half that for a precipitator as a percentage of material cost. The assumption of 5 percent of material cost for the gas conditioning system was within $14,000 per year when compared to detailed records on one specific installation.

COST COMPARISON

The overall cost comparison of the various alternatives is made on the basis of investment cost, and present worth of annual cost assuming 0, 5, and 10 percent escalation. In my opinion, the initial investment cost and present worth of annual costs with zero escalation is particularly pertinent. However, the extension of these costs to include assumed rates of escalation provides a sensitivity analysis which is of value in interpreting the effect of escalation on critical annual costs.

INVESTMENT COSTS

The investment costs for the three alternatives were obtained from the vendors based on a semi-turnkey installation. The costs include all flange to flange material and auxiliaries including erection, with the exception of ductwork and the ash handling system. However, differentials in these items were examined and included in the investment cost.

Costs for the ESP's were in accordance with the past experience of Gibbs & Hill. However, there was a discrepancy of approximately 10 percent in the baghouse flange to flange erected cost provided by the two vendors. This differential was minimized based on the overall semi-turnkey price, and the two costs were averaged. It is also noted that the average cost used for this comparison is still significantly less than comparable costs obtained for a baghouse installation a year ago.

The investment costs for a turnkey installation of the three alternatives are summarized in Table 5.

TABLE 5. COMPARISON OF INVESTMENT COST (000's OF $)

Investment Costs	ESP w/Cond.	ESP w/o Cond.	Baghouse
ESP/Baghouse (Material)	$ 3,658	$ 6,280	$ 5,772
ESP/Baghouse (Erection)	2,940	5,310	3,975
Auxiliaries (Installed)*	4,969	7,172	4,981
Gas Cond. Syst. (Installed)	1,980	-	-
Installed System Cost	$13,547	$18,762	$14,728
Capacity Charge			
ESP/Baghouse	$ 2,334	$ 2,502	$ 3,683
Gas Cond. System	261	-	-
Total Investment Cost	$16,142	$21,264	$18,411
Investment Cost Diff.	Base	$ 5,122	$ 2,269

*Includes ESP nozzles and duct manifolds, all support steel and insulation, accessways, low voltage wiring, hopper heaters & level alarms, and ash handling connections. Baghouse also includes interior insulation (top & bottom), and bypass duct.

As noted below the table, the scope of supply approaches the cost of a turnkey installation. The initial intent in the cost comparison was to eliminate considerations of ductwork and ash handling as being base to both the precipitator and baghouse systems. However, it became apparent that both of these factors are inherently favorable to the baghouse, and cost adjustments were made as follows:

(1) A terminal point was assumed for ductwork at the entrance and exit of the precipitators and baghouse. No cost was accessed for any ductwork from these terminal points to the inlet and outlet flanges of the baghouse. In the case of the ESP's, an inlet manifold connecting four inlet nozzles, and a similar outlet manifold was assumed without nozzles. The cost of the manifolds, nozzles, support steel and insulation required for the precipitators exceeded $1,000,000, and is included in the investment cost for precipitators in Table 5.

(2) It was further recognized that ash handling is generally more costly for a precipitator because of the increased number of hopper connections. A recent cost quotation of $8000 per hopper was assessed as an investment cost for all alternatives. This resulted in a $128,000 cost differential adder for the ESP equipped with gas conditioning as compared to the baghouse. This cost is also included in the investment costs in Table 5.

A review of the total investment costs in Table 5 indicates the precipitators equipped with a gas conditioning system to be the least costly. The cost differential in favor of this system is $2,269,000 and $5,122,000 as compared to the baghouse and full sized precipitator, respectively. This substantial differential will be reflected in the present worth of annual cost for variable escalation rates to follow.

COMPARISON OF ANNUAL COST-NO ESCALATION

This comparison of annual costs is very significant since it provides first year costs which are not affected by assumed escalation rates. The latter can greatly distort the care taken in establishing valid investment and annual operating cost estimates. This comparison without escalation is shown in Table 6(a).

TABLE 6(a). COMPARISON OF ANNUAL COST-NO ESCALATION (000's of $)

	ESP w/Cond.	ESP w/o Cond.	Baghouse
Total Investment	$16,142	$21,264	$18,411
Annual Costs			
Fixed Charges	$ 2,744	$ 3,615	$ 3,130
Incremental Energy	490	474	526
Sulfur	94	-	-
Steam	6	-	-
Bag Replacement	-	-	212
Maintenance	253	314	144
Total Annual Cost	$ 3,587	$ 4,403	$ 4,012
Annual Cost Differential	Base	$ 816	$ 425
P.W. of Annual Cost	$33,814	$41,507	$37,821
P.W. Differential	Base	$ 7,693	$ 4,007

The summary in Table 6(a) indicates that the annual cost of the precipitators equipped with gas conditioning is the least costly, with a differential of $425,000 per year as compared to the baghouse. The present worth of annual cost over 30 years is $4,007,000 in favor of the gas conditioned ESP's.

COMPARISON OF P.W. OF ANNUAL COST ASSUMING 5% ESCALATION

The cost comparison shown in Table 6(b) will indicate the effect of any annual costs that are sufficiently sensitive to escalation such that they have a significant effect on the comparison shown in Table 6(a). It will be noted that by assuming escalation, it is necessary to capitalize (i.e., use the present worth) of each cost factor.

TABLE 6(b). COMPARISON OF P.W. OF ANNUAL COST - 5% ESCAL. (000's of $)

	ESP w/Cond.	ESP w/o Cond.	Baghouse
Total Investment Cost	$16,142	$21,264	$18,411
P.W. Of Annual Costs (30 yrs)			
Fixed Charges	$25,867	$34,078	$29,506
Incremental Energy	7,741	7,489	8,310
Sulfur	1,485	-	-
Steam	95	-	-
Bag Replacement	-	-	3,349
Maintenance	3,997	4,961	2,275
Total P.W. Of Annual Costs	$39,185	$46,528	$43,440
P.W. Differential	Base	7,343	$ 4,255

The results summarized in Table 6(b) indicate the present worth of annual cost of the ESP with gas conditioning to be $4,255,000 less costly than the baghouse. This is a larger cost advantage than that which resulted from the assumption of no escalation in Table 6(a). This indicates that annual costs subject to escalation for the baghouse system exceed those for the ESP equipped with a gas conditioning system.

COMPARISON OF P.W. OF ANNUAL COST ASSUMING 10% ESCALATION

The comparison shown in Table 6(c) is somewhat academic except to show that by assuming an increasing escalation rate will result in a more favorable cost position for the ESP with gas conditioning. It should also be evident that assuming a rate greater than the return on investment will cause a rapid acceleration in the cost advantage.

TABLE 6(c). COMPARISON OF P.W. OF ANNUAL COST - 10% ESCAL. (000's of $)

	ESP w/Cond.	ESP w/o Cond.	Baghouse
Total Investment Cost	$16,142	$21,264	$18,411
P.W. of Annual Costs (30 yrs)			
Fixed Charges	$25,867	$34,078	$29,506
Incremental Energy	14,700	14,220	15,780
Sulfur	2,820	-	-
Steam	180	-	-
Bag Replacement	-	-	6,360
Maintenance	7,590	9,420	4,320
Total P.W. Of Annual Costs	$51,157	$57,718	$55,966
P.W. Differential	Base	6,561	$ 4,809

As expected, the present worth differential in favor of the precipitator with conditioning has increased to $4,809,000 as compared to $4,007,000 and $4,255,000 for the case of zero and 5 percent escalation, respectively.

SUMMARY AND CONCLUSIONS

The results of the study indicate the following summary and conclusions:

(1) The use of relatively small precipitators equipped with a sulfur burner type gas conditioning system provides an attractive alternative which should be considered in the selection of equipment for new generating units burning a low sulfur western coal.

(2) The cost advantage without distortion by assumed escalation rates indicates an annual cost savings of $425,000 per year, and a savings in present worth of annual costs over 30 years of $4,007,000 as compared to a baghouse. The major factor which results in these differentials is a lower initial investment of $2,269,000 for the total installed system including auxiliaries.

(3) The cost differentials for the comparison in (2) above further increase in favor of the gas conditioned ESP's with any assumed escalation rate applied to operating costs.

(4) A comparison with the full size precipitator indicates this to be the most costly alternative with a present worth cost differential of $7,693,000 vs. $4,007,000 for the baghouse, using the gas conditioned ESP's as base.

(5) Aside from the economic comparison, a primary objective of the study was a technical evaluation of the alternative systems. I believe that up to this point, a general consensus of opinion would favor the baghouse from the standpoint of reliability and maintenance. Although judgmental, it is my opinion that gas conditioning used in conjunction with ESP's greatly enhances the electrical operating stability and reliability of the precipitator collecting high resistivity ash. The automation which permits selection of an optimum sulfur trioxide injection rate that remains constant in parts per million with variable boiler load, should eliminate arcing and minimize maintenance with discharge electrodes, transformer rectifier sets, and controls due to reduced transients.

(6) Discussions with several utility engineers about a year ago, indicated no unusual maintenance with the sulfur burner system, and availability was estimated at better than 98 percent. On this basis, it is not unreasonable to equate the technical operating characteristics of gas conditioned ESP's with the baghouse. This combined with the economic advantages, may restore the precipitator to a dominant position in equipment selection for the electric utilities for low sulfur western coal applications.

The work described in this paper was not funded by the U.S. Environmental Protection Agency, and therefore the contents do not necessarily reflect the views of the Agency, and no official endorsement should be inferred.

REFERENCES

(1) Walker, A.B. and Gawreluck, G. Performance capability and utilization of electrostatic precipitators past and future. International Conference on Electrostatic Precipitation, October, 1981.

APPLICATION OF THE BUBBLE CONCEPT TO FUEL BURNING SOURCES AT A NAVAL INDUSTRIAL COMPLEX

by: CHARLES THOMPSON
ATLANTIC DIVISION
NAVAL FACILITIES ENGINEERING COMMAND
UTILITIES, ENERGY AND ENVIRONMENTAL DIVISION
NORFOLK, VIRGINIA 23511

ABSTRACT

The Norfolk Naval Shipyard, Portsmouth, Virginia, consists of a large Industrial Ship Repair Complex. There are over 50 gas and oil-fired industrial size boilers located in the Shipyard. These boilers serve such diversified functions as generating power, space heating, hot water, and process steam and ship system testing. Eight of these boilers exceed Virginia's particulate emission limits by as much as 90 percent. Engineering studies outlined methods to achieve compliance with Air Pollution Control Equipment at a total cost of $9 million. A change in the Virginia regulations for particulate emissions from Fuel Burning Equipment in 1979 allowed a Bubble policy to be applied. This change allowed a combination of Bubble concept and control equipment techniques to be used. The cost savings in applying this technique was approximately $6 million. Discussed are the problems and procedures in formulating an acceptable Bubble concept policy and control program to allow compliance for the boiler plants.

INTRODUCTION

The Norfolk Naval Shipyard, Portsmouth, Virginia is a naval ship repair activity. The Shipyard is located in the Hampton Roads intrastate Air Quality Control Region of Virginia. This region is currently in compliance with the total suspended particulate matter air standard.

The industrial activity that is accomplished at the Shipyard include construction overall, repair, alterations, drydocking and outfitting of ships and other water crafts. The industrial processes used that generate air pollution are painting, sand and grit blasting, plating, degreasing, metal forgering and boilers. The boilers provide steam for process equipment, equipment testing, generating electricity and space heating. The electric power generated is distributed to ships and production loads at the pier facilities and to offices, barracks and ships located throughout the Shipyard. The steam is distributed to ship's pier facilities, offices, barracks and industrial processes. To provide this power and steam requirements, it takes 56 boilers located at numerous locations around the Shipyard. The boilers heat input ranges from one million BTU per hour up to one hundred and fifty million BTU per hour. The types of fuel burned includes natural gas, distillate and residual oil and refuse. Table 1 is a list of the Shipyard's boilers and their heat input.

The Shipyard is comprised of many land areas that are separated from each other by waterways, railroads, public roadways, and private property. Figure 1 shows the relationship of the Shipyard land areas to each other. Each separate area has a different and specific function.

The New Gosport and Stanley Court areas are housing tracts for Navy personnel. These areas are located up to three miles from the main Shipyard Industrial Area. The South and St. Helena's Annexes are used to mothball ships for extended layup. St. Julien's Creek Annex is now being used for extended shipyard services such as electronic engineering, warehouse storage and property disposal.

The Shipyard's industrial boilers are spread throughout these areas. The housing areas and the South Annex contain numerous small oil fired boilers that run separate steam heating systems from the main industrial area. The two areas known as St. Julien's Creek and St. Helena's Annex are permitted separately with the State Air Board and are therefore not included under the Shipyard Bubble.

BUBBLE CONCEPT

The Environmental Protection Agency over the years has formulated and approved the Bubble Concept. Today the concept is one of innovative

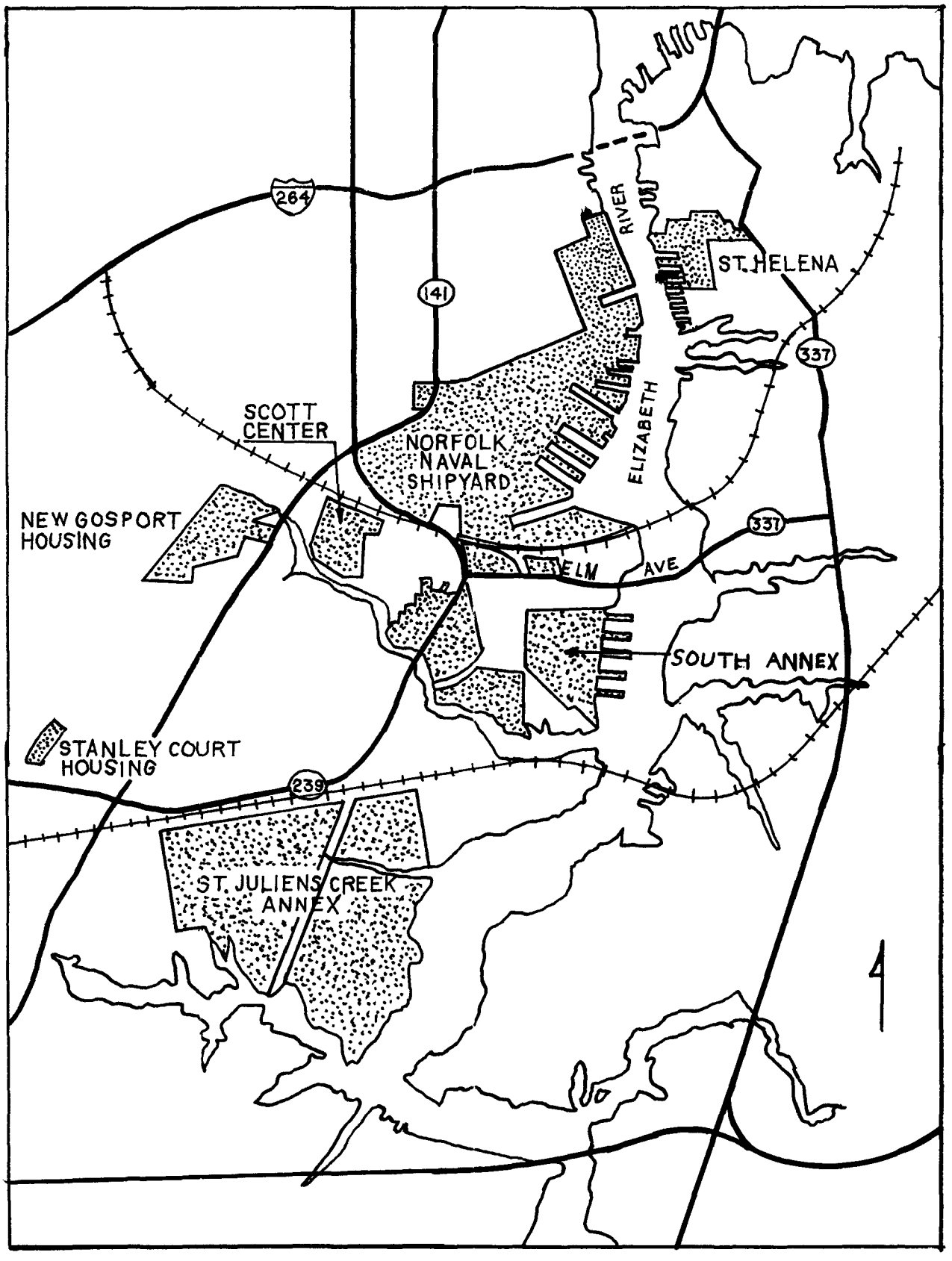

Figure 1. Shipyard Vicinity Map

emission trading for existing emission sources. The Bubble gives plant engineers and managers the ability to develop less costly ways of meeting air quality requirements. The Bubble Concept allows a plant with multiple emission sources through compensating emission trades among the sources to comply with regulatory air standards.

The State of Virginia endorsed a version of the Bubble Policy in 1976. The Air Board approved a modification to rule EX-3, "Particulant Emission from Fuel Burning Equipment," of the Virginia's Air Pollution Control Regulation. Under Section 4.31(e) the rule states, "The emission contribution allocation for each of the fuel burning units of the affective facilities shall be its designated portion of the maximum allowable particulant emissions from the affective facility when operating at total capacity."(1)

APPLICATION OF THE BUBBLE

BACKGROUND

In the time period between 1979 and early 1980, the Shipyard was attempting to bring two boiler plants into compliance with Virginia Air Pollution Control Regulation for fuel burning sources.

The sources were the Main Steam and Power Plant, Building 174 and Salvage Fuel Fired Boiler Plant, Building 1460. These plants had both failed stack emission tests. Table 2 shows measured versus regulation allowed emissions for each plant. The Main Steam and Power Plant exceeded air standards by approximately 60 percent. The Salvage Fuel Fired Boiler also exceeded its emission limits by up to 90 percent.

The Main Steam and Power Plant consists of six boilers. The boilers were constructed between 1939 and 1944. They were originally designed to burn pulverzied coal and later converted to residual oil in the mid 60's. The particulant emissions from the Main Steam and Power Plant were controlled by large diameter cyclones. The operating efficiency of these cyclones was unknown.

The Salvage Fired Fuel Boiler plant consists of two water wall boilers. The boilers were completed in 1977 and burned refuse, as received, on recipicating grates. At the Salvage Fuel Fired Boiler, the particulate emissions were controlled by a single field electrostatic precipitator. The measured precipitator efficiency was approximately 90 percent.

RELEVANT ENGINEERING STUDIES

During 1979 engineering studies were funded to review each situation and present possible corrective solutions. For the Main Steam Plant, this became a complicated and almost insurmountable task. The plant was approximately 40 years old and had become incapable of fully supplying the Shipyard's steam and power demands. It also was known that the efficiency of the boilers had deteriorated over the years to an estimated 70 percent. A review of stack emission tests showed that unburned carbon made up approximately 60 percent of the particulate being emitted from the stack. The plant has a long horizontal breaching leading to a 200 foot stack. The breaching would readily fill up with fly ash. Theoretically it was felt that improving boiler efficiency could bring the plant back into compliance with Virginia Air Pollution standards. However due to the plants age and nebulous factors regarding equipment performance variables and preliminary stack emission results of 29.5 lb. per hour, final compliance could not be guaranteed.

The Salvage Fuel Fired Boiler electrostatic precipitator was reviewed and found to be deficient in many areas. The deficiencies noted were power levels, size of the unit, spark rate control and transformers/ rectifying controls. (2) The electrostatic precipitator consultant recommended a new electrostatic precipitator upstream of the existing one. The electrostatic precipitator would act as a precleaner and together with repairs to the existing precipitator would bring the facilities into compliance.

The cost of these corrective items were estimated to be approximately $6 million for the Main Steam Plant and $2.6 million for the Salvage Fuel Fired Boiler Plant. Table 3 is a summary and break down of each items cost. For the Main Steam Plant, the estimate shows that approximately $2.6 million of the cost was just to repair and improve boiler efficiency. The Shipyard has attempted since 1974 to bring the Main Steam Plant into compliance. Past work on the boilers and the future work scheduled, Table 3, was intended by the Shipyard to bring the Main Steam and Power Plant into compliance. However, the Virginia Air Pollution Control Board insisted that the Main Steam and Power Plant be brought into compliance as rapidly as possible and that no more delays would be tolerated. Therefore, a $3.7 million appropriation for an electrostatic precipitator was included. The use of the precipitator would guarantee compliance of the boilers with Virginia Air Standards.

While the above studies was being completed, two events took place that impacted upon the Shipyard's decision. First, a preliminary plan and location for a regional Trash Burning Plant was being finalized. A decision has been made to locate this facility at the Norfolk Naval Shipyard if a contract could be agreed to. The new facility would then replace the existing Main Steam and Power Plant and Salvage Fuel Fired Boiler Plant. The time schedule, even though not finalized, was

estimated to be approximately five years for construction completion. The Shipyard's ultimate decision was that spending $8.9 million on the existing plants that would be shut down in five years was not the best alternative. However, the Virginia Air Pollution Control Board would not grant a long term, five years, variances to operate at higher particulate emission levels for these two plants. The second event was notification in January 1980, by the Virginia Air Pollution Control Board of their Bubble Policy and suggested allocation of allowed particulate emissions. The suggested allocation by the State had totaled the heat input for all 54 boilers located at the Shipyard and calculating total pounds per hour of particulate emissions allowed. The total emissions were then divided between boilers by the ratio of each boiler heat input divided by total heat input of all boilers.

It was felt that this contingency placed an unequitable burden upon the small (10 x 10/6 BTU/HR) residual oil fired boilers. Further, this policy had reduced the overall allowed emissions at the Shipyard by approximately 160 pounds per hour. Since the proposed Bubble terms by Virginia Air Pollution Control Board would have to be modified, it was considered feasible to also used the new Virginia Bubble Concept to assist in bringing the Main Steam and Power Plant and Salvage Fuel Fired Boiler Plant into compliance.

BUBBLE CONCEPT

There are 54 boilers located on the Shipyard in three different distinct land areas, separated by public or private property. The boilers consist of large industrial size boilers burning residual fuel down to very small process steam type boiler burning natural gas. The boilers also fall into two distinct categories, stationary-permanent, and stationary-portable.

The portable boilers consist of both barge and skid mounted package boilers. These boiler range in size from 1.5 to 17 million BTU per hour heat input. The portable boilers are used to supply steam for testing ship's steam systems. Therefore, the boilers are moved frequently within the Shipyard from pier location to pier location. These boilers can also moved into other sections of the Shipyard as well, such as the South Annex and St. Helena's Annex.

The applicable Virginia Air Pollution Standard that the boilers had to comply with involved a sliding scale of allowed emissions; for example, when the heat input rises the amount of emissions allowed decreases. As discussed previously, the Shipyard was concerned that as the number of boilers increase, the total allowed emissions would decrease, putting an unfair burden upon small Residual Oil Fired Boilers. Finally many of the boilers were located not on the main Shipyard property, but in separate distinguishable sites and these boilers emissions also would be penalized.

To take all these considerations into account, four Bubbles were formed around the Shipyard. A Bubble was formed over the main Shipyard land area for the stationary-permanent boilers; a Bubble was formed for the portable boilers at the Shipyard; a Bubble was formed for the South Annex boilers, and finally a Bubble was formed for the remote housing site boilers. It was felt that by setting up four Bubbles a fair and equitable solution was made between allowable emission and actual operation of the Shipyard. Table 1 demonstrates each Bubble location, boilers involved, the boiler heat input and the allowed emissions, both before and after application of the Bubble.

ALLOWED EMISSIONS

The allowed emissions were calculated using the following procedure. For the main Shipyard Bubble the boiler reference numbers 15 through 19, 24 through 25, and 2,001 through 2,008 were calculated using EPA air emission factors from publication AP 42, and current fuel usage. These allowed emissions were totaled and substracted from the total allowed under the Bubble. The quantity of emissions left were then split between the Main Steam and Power Plant, reference numbers 9 through 14, and the Salvage Fuel Fired Boiler Plant, reference numbers SS-101 and SS-102. For the other Shipyard areas the total emissions allowed for each Bubble were divided between boilers base on the ratio of boiler heat input to total heat input.

CONCLUSION

The accomplishment of the four Bubbles has allowed the Norfolk Naval Shipyard to comply with all emission limits, at a reasonable cost and time frame. The Bubble policy has allowed the Main Steam Plant to come into compliance and at the same time not have to include an electrostatic precipitator. The estimated control efficiency of the multi-cyclone installed and the improvement in the boiler combustion will give a final outlet emission within the 31 pounds per hour limit. Preliminary stack testing of the Main Steam Plant has shown emissions to be 29.5 pounds an hour. The saving due to the Bubble has been approximately $3.7 million.

The Salvage Fuel Fired Boiler compliance is to be accomplished by upgrading the existing electrostatic precipitator and installing a precleaning multi-cylcone. The use of the multi-cyclone is to remove large particles that were degrading electrostatic precipitation operation. The precipitator should now operate at its fullest potential. The cost of this project is approximately $400,000. This represents a saving of approximately $2.2 million over installing a new electrostatic precipitator and reconstructing and moving the existing precipitator.

Current ongoing performance testing of the Main Steam and Power Plant and Salvage Fuel Fired Boiler are showing new problems. It is now expected that the Bubble will not be required for the Main Steam and Power Plant compliance. Preliminary stack testing has shown emissions to range between 15 and 19 pounds per hour. The current performance of the new multi-cylcones and upgraded precipitators at the Salvage Fuel Fired Boiler, however, has been very disappointing. Emission testing has not yet taken place but visible emissions are at times exceeding 20 percent opacity. It is now expected that the Bubble Concept will have to be used to shift allowed emissions to the Salvage Fuel Fired Boiler for final compliance.

The total allowed emissions from the Norfolk Naval Shipyard under its State Registration No. 62040 has been decreased by application of the Bubble Concept. The decrease has taken place even while two facilities Main Steam Plant and Salvage Fuel Fired Boilers are allowed to increase emission levels. The accomplishment of these two goals at the same time have saved the U.S. taxpayers approximately $5.9 million in capital cost and approximately $55,000 in annual operating costs under the Virginia Bubble Concept.

The work described in this paper was not funded by the U.S. Environmental Protection Agency and therefore, the contents do not necessarily reflect the views of the agency and no official endorsement should be inferred.

REFERENCES

1. Stone, D., Editor, VirginiAir, Publication of Virginia Air Pollution Control Board. Vol. 12, No. 2, June 1982.

2. Hall, H. J., Summary Analysis and Recommendations for Precipitator System Improvement to meet State Regulations on Incinerator Gases at Naval Shipyard, Portsmouth, Virginia, Technical Report HAR79-222, June 1979.

TABLE 1 - PARTICULATE EMISSION CONTRIBUTION

REFERENCE NUMBER	EQUIPMENT MANUFACTURER AND MODEL NUMBER	RATED HEAT CAPACITY (10/6 BTU/HR)	TOTAL PARTICULATES ALLOWED BEFORE BUBBLE (LBS/HR)	TOTAL PARTICULATES ALLOWED UNDER BUBBLE (LBS/HR)
1. Main Shipyard Area				
9 10 12	Combustion Engineering (Bldg. 174) Contract 139	150 ea.	28.0 ea.	31.0 ea.
11 13 14	Riley Stoker Corp (Bldg. 174) Contract 1534	150 ea.	28.0 ea.	31.0 ea.
15 16	Singer Co.; Model H-52-E4748-YIHK (Bldg. 171)	6.75 ea.	3.4 ea.	0.07 ea.
17	Singer Co.; Model G10-E5973-UNK 40 Superheater (Bldg. 171)	4	3.4 ea.	0.04
24 25	Orr and Sem Bower, Inc.; Model A-7 (Bldg. 171)	1.15 ea.	.7 ea.	0.2 ea.
S-101	E. Keeler Co; Model 15687-2 (Bldg. 1460)	29	11.0	8.45
S-102	E. Keeler; Model 15687-2 (Bldg. 1460)	29	11.0	8.45
2001	NID-035627-RS Products Furnace; no model number (Bldg. 163)	9.8	4.5	0.1

TABLE 1 - PARTICULATE EMISSION CONTRIBUTION (CONTINUED)

REFERENCE NUMBER	EQUIPMENT MANUFACTURER AND MODEL NUMBER	RATED HEAT CAPACITY (10/6 BTU/HR)	TOTAL PARTICULATES ALLOWED BEFORE BUBBLE (LBS/HR)	TOTAL PARTICULATES ALLOWED UNDER BUBBLE (LBS/HR)
2002	NID-016040-Eclipse Engineering Co. Furnace; no model number (Bldg. 163)	1.3	.6	0.01
2003	NID-015566 Mires Furnace NID-015567 Mires Furnace (Bldg. 163)	1.5 1.5	.7 .7	0.015 0.015
2004	NID-015564 Mires Furnace NID-015565 Mires Furnace (Bldg. 163)	1.5 1.5	.7 .7	0.015 0.015
2005	NID-015728 Rust Furnace; no model number (Bldg. 163)	2.8	1.3	0.02
2006	4 - Small heating furnaces Manufacturer/model number unknown (Bldg. 163)	.7 ea.	.3 ea.	0.01 ea.
2007	8 - Small forging furnaces; Manufacturer/model number unknown (Bldg. 163)	.6 ea.	.3 ea.	0.01 ea.
2008	NOD-D16019-NNSY furnace; no model number (Bldg. 163)	1.2	.5	0.01
18	Electromotive Division of General Motors; Model 20-645E4/2 cycle diesel driven electrical generators - 4 units	26 ea.	7.5 ea.	0.2

TABLE 1 - PARTICULATE EMISSION CONTRIBUTION (CONTINUED)

REFERENCE NUMBER	EQUIPMENT MANUFACTURER AND MODEL NUMBER	RATED HEAT CAPACITY (10/6 BTU/HR)	TOTAL PARTICULATES ALLOWED BEFORE BUBBLE (LBS/HR)	TOTAL PARTICULATES ALLOWED UNDER BUBBLE (LBS/HR)
19	Detroit Diesel Allison Div of General Motors Model 501-K14C Gas Turbine driven electrical generators - 2 units	33 ea.	9.5 ea.	0.25
		1177.2	357.0	205.1
2. Portables				
S-29	Continental Boiler; model APA-170A-5 (Portable)	5.695	3.4	2.1
F-1	Lookout Mfg. Co. (Barge YD-145)	3.77	2.3	1.4
S-128	Ames Iron Works Boiler Model C-150 (Barge YSR-30)	4.75	2.9	1.8
S-129	Ames Iron Works Boiler; Model C-150 (Barge YSR-30)	4.75	2.9	1.8
S-126	Ames Iron Works Boiler; Model C-150 (Barge YSR-33)	4.75	2.8	1.8
S-127	Ames Iron Works Boiler Model C-150 (Barge YSR-33)	4.75	2.8	1.8
S-130	Ames Iron Works Boiler; Model C-150 (Barge YSR-37)	4.75	2.8	1.8

TABLE 1 - PARTICULATE EMISSION CONTRIBUTION (CONTINUED)

REFERENCE NUMBER	EQUIPMENT MANUFACTURER AND MODEL NUMBER	RATED HEAT CAPACITY (10/6 BTU/HR)	TOTAL PARTICULATES ALLOWED BEFORE BUBBLE (LBS/HR)	TOTAL PARTICULATES ALLOWED UNDER BUBBLE (LBS/HR)
S-131	Ames Iron Works Boiler; Model C-150 (Barge YSR-37)	4.75	2.9	1.8
S-22	Wicks Boiler Co.; Type A-3 (Portable)	17	8.9	6.4
S-18	Cyclotherm Div., U.S. Radiator Corp; Model C-80 (Portable)	3.672	2,2	1.4
S-23	Clever-Brooks; Model PSM-50 (Portable)	1.638	1.0	0.6
	TOTAL	60.3	34.9	22.7
3. Southgate Annex				
1	Boiler Engineering & Supply	7 ea.	3.5 ea.	3.5 ea.
2	Continental Model			
3	Model (Bldg. 481)			
	TOTAL	21 ea.	10.4	10.4
4. Stanley Court				
4	Boiler Engineering & Supply	7 ea.	3.5 ea.	3.5 ea.
5	Continental Model (Stanley Court)			
6	Boiler Engineering & Supply Superior Model (Stanley Model)	7 ea.	3.5 ea.	3.5 ea.
	TOTAL	21 ea.	10.4 ea.	10.4 ea.
	GRAND TOTAL OF EMISSIONS ALLOWED		412.7 ea.	248.6 ea.

TABLE 2 - EMISSIONS

	MEASURED EMISSIONS	STANDARD
Main steam and power plant boilers	45 lb/hr	28 lb/hr
Salvage fuel fired boiler plant boiler 1	12.4 lb/hr	11 lb/hr
boiler 2	19.8 lb/hr	11 lb/hr

TABLE 3 - COSTS

Main steam and power plant

1.	Repair combustion controls	154,000
2.	Replace dust collectors	441,000
3.	Repair breeching	673,000
4.	Rehabilitate boiler No. 10	421,000
5.	Replace oxygen meters	15,000
6.	Rehabilitate boiler No. 11	722,000
7.	Repair smoke stack	206,000
8.	Additional pollution control device	3,700,000
		$6,332,000

Salvage fuel fired boiler plant

1.	Repairs to electrostatic precipatator	110,000
2.	Construct new multi-cyclones	300,000
3.	Install opacity meters	15,000
4.	Additional electrostatic precipitators	2,200,000
		$2,625,000

CYCLONE PERFORMANCE: A COMPARISON OF THEORY WITH EXPERIMENTS

by: John A. Dirgo
David Leith

Harvard School of Public Health
Department of Environmental Health Sciences
665 Huntington Avenue
Boston, MA 02115

ABSTRACT

This paper describes the results of tests conducted on a Stairmand high-efficiency cyclone. The cyclone was pilot plant scale with a design air flow of 0.14 m^3/s (300 cfm). Collection efficiency and pressure drop were measured over a range of air flows at ambient temperature and pressure. An oil mist was used as a test aerosol because it consists of spherical drops of uniform density, which are unlikely to bounce or re-entrain after striking the cyclone wall. At each air flow, a fractional efficiency curve (collection efficiency vs. particle diameter) was determined. Each experimental curve was compared with fractional efficiency curves generated by several cyclone efficiency models. A comparison of this type is more valid than one based on cyclone cut diameter (the particle size collected with 50 percent efficiency). This work represents the initial phase of a study of optimized cyclone design.

INTRODUCTION

Cyclones have been used since the late 1800's for the removal of dust from industrial gas streams. Because they rely on inertial forces to collect particles, cyclones are inefficient collectors of particles smaller than about 5 μm in diameter. In spite of this disadvantage, there has been a renewed interest in cyclones, particularly as precollectors in atmospheric and pressurized fluidized bed combustion systems.

Many different types of cyclones have been built, but the reverse-flow cyclone with a tangential inlet is most often used for industrial gas cleaning. Figure 1 shows a typical reverse-flow cyclone. This collector can be characterized completely by eight dimensions, which are often expressed in terms of their ratio to the cyclone body diameter, D. Figure 1 also shows the dimension ratios and the actual dimensions for the cyclone used in this study--the Stairmand high-efficiency design cyclone (1). This design is one example of standard cyclone designs that have been developed. Many of these designs arose through a trial and error approach as "the result of 'hunches' or

Dimension ratio	Dimension (m)
D = 1.0	0.305
a = 0.5	0.153
b = 0.2	0.061
D_e = 0.5	0.153
S = 0.5	0.153
h = 1.5	0.458
H = 4.0	1.220
B = 0.375	0.114

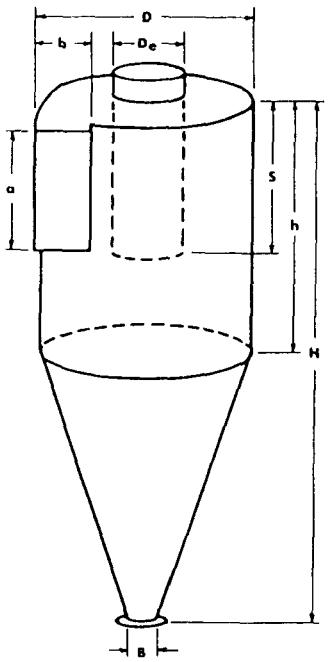

Figure 1. Reverse-flow cyclone with dimension ratios and dimensions for a Stairmand high-efficiency design.

efforts to overcome operating difficulties (2)." According to Swift (3), "...cyclones have been developed almost wholly by experiment, and it would be difficult to prove mathematically that [they] are of the best design..."

There is no reason to assume that standard cyclone designs represent the optimum possible performance. In fact, cyclone theories predict that substantial improvements (increased collection efficiency at constant pressure drop or reduced pressure drop at constant efficiency) can be obtained by altering cyclone dimensions. This paper presents the results of the initial phase of a study of improved cyclone design, in which fractional efficiency curves for a Stairmand high-efficiency cyclone were determined over a range of gas flow rates. The results will be used to evaluate the predictive capabilities of cyclone efficiency theories and to establish a "baseline" performance level for this cyclone. Later changes in performance due to changes in cyclone dimensions can be measured against this baseline.

THEORY

Cyclone collection efficiency theories differ greatly in complexity. Some are almost entirely empirical while others are completely theoretical. There is a general agreement that operating parameters of the system should be used to predict performance, and most theories have some sort of impaction parameter grouping that accounts for the influence of particle diameter and density, gas velocity and viscosity, and cyclone diameter. There is less agreement on the effects of cyclone dimensions and geometry. Some theories consider all eight cyclone dimensions while others include as few as two.

All theories set up a balance between the outward centrifugal force on a particle caused by the spinning gas stream and the inward drag force resisting the radially

outward motion. By assuming various flow conditions within the cyclone, different authors have dismissed different terms in this force balance as insignificant. Because the relative importance of these terms will change with cyclone design and operating conditions, it is unlikely that any one theory will accurately predict performance for all applications (4). At least three general classes of cyclone efficiency theories have been published (4). These are described below with examples given for each type.

CRITICAL DIAMETER: STATIC PARTICLE APPROACH

The static particle approach determines the particle diameter for which the outward centrifugal force is exactly balanced by the drag force caused by gas flowing radially inward to the cyclone core. Theoretically, these "static" particles should remain suspended indefinitely at the boundary between the vortex and the cyclone core; smaller particles flow to the core and out of the cyclone while larger particles move to the cyclone wall for collection. Theories of this type predict an abrupt change in collection efficiency from zero to 100 percent as particle diameter increases beyond the critical size. In practice, this sharp cut is not realized because of variations in radial and tangential gas velocities along the cyclone axis, and the efficiency for the critically sized particle is often taken as 50 percent.

An example of the static particle approach is the theory of Barth (5). Barth calculates the diameter of the particle for which the centrifugal and drag forces are equal. The resulting expression for diameter is used to determine the terminal settling velocity, v_{ts}^*, for the critically sized particle:

$$v_{ts}^* = \frac{Q\,g}{2\pi(H-S)v_t^2} \tag{1}$$

[Terms in Eq. (1) and subsequent equations are defined in the NOMENCLATURE section at the end of the paper.] Here, v_{ts}^* is used mainly as a measure of aerodynamic resistance. Tangential gas velocity in the vortex, v_t, is evaluated at radial position $D_e/2$.

The terminal settling velocity of any particle size, v_{ts}, can be related to v_{ts}^* by:

$$\frac{v_{ts}}{v_{ts}^*} = \frac{\pi(H-S)v_t^2\rho_p\,d_p^2}{9\,Q\,\mu} \tag{2}$$

Barth gives a generalized plot of cyclone collection efficiency as a function of this ratio.

CRITICAL DIAMETER: TIMED FLIGHT APPROACH

The timed flight approach assumes an initial radial position for particles entering the cyclone. The critically sized particle is one that can cross the distance from this initial radial position to the cyclone wall during its time in the cyclone. One of the most commonly used theories of this type is the Lapple "cut diameter" theory (6). Lapple assumes that the particle size that enters the cyclone at the inlet half-width ($D/2 - b/2$) and travels the distance to the wall during its residence time is collected with 50 percent efficiency. Lapple's expression for this particle size, called the cut diameter, is:

$$d_{50} = \sqrt{\frac{9\mu b}{2\pi\rho_p\,v_t\,N_e}} \tag{3}$$

The collection efficiency for any other particle size can be found from its ratio to the cut diameter. A plot of fractional efficiency versus this ratio, reported by Lapple, has

been fit to the equation (7)

$$\eta_c = \frac{1}{1 + (d_{50}/d_p)^2} \tag{4}$$

This relationship was developed experimentally for a Lapple general purpose cyclone design (6); similar relationships for other cyclone designs have not been reported.

FRACTIONAL EFFICIENCY APPROACH

While both critical diameter methods rely on generalized plots to determine the collection efficiency for particles other than the critical size, the fractional efficiency approach allows a direct calculation of the efficiency for any particle size. Examples of this type of theory are the Leith-Licht model (8) and a more recent model by Dietz (9).

Leith and Licht assume that the tangential gas velocity in the cyclone is related to the distance from the cyclone axis by

$$v_t r^n = CONSTANT \tag{5}$$

where n is the vortex exponent. Experimental studies of cyclone flow patterns have reported values of 0.5 to 0.9 for n, with most values falling in the lower end of this range. According to Alexander (10), the vortex exponent can be calculated from

$$n = 1 - [(T/283)^{0.3}(1 - 0.67\, D_m{}^{0.14})] \tag{6}$$

where T is the gas temperature in °K and D_m is the cyclone diameter in meters.

Leith and Licht also assume that radial gas velocity is zero and that the drag force on particles travelling radially outward toward the cyclone wall is described by Stokes' law. This model accounts for turbulence within the cyclone by assuming that in any plane perpendicular to the cyclone axis, uncollected particles are uniformly mixed. Cyclone dimensions are considered in the determination of an average residence time for the gas in the cyclone. The resultant expression for collection efficiency is

$$\eta_c = 1 - \exp[-2\,(C\Psi)^{\frac{1}{(2n+2)}}] \tag{7}$$

The influence of particle and gas properties are combined into Ψ, a modified inertia parameter

$$\Psi = \frac{\rho_p\, d_p{}^2\, v_i\, (n + 1)}{18\, \mu\, D} \tag{8}$$

The term C is a dimensionless cyclone geometry parameter that depends only on the eight cyclone dimension ratios and is independent of the size of the cyclone (8).

The Dietz (9) model represents a refinement of the Leith-Licht method and divides the cyclone into three regions. These regions are the entrance region (the annular space around the outlet duct at the top of the cyclone), the downflow region (corresponding to the vortex below the level of the outlet duct), and the core region (formed by the extension of the outlet duct to the bottom of the cyclone). Turbulence within each region is assumed to produce a uniform radial concentration profile for uncollected particles. To approximate a distribution of particle residence times in the cyclone, the theory allows for the exchange of particles between the downflow and core regions. The Dietz model determines cyclone collection efficiency as

$$\eta_c = 1 - (K_0 - \sqrt{K_1^2 + K_2}) \exp\left[\frac{-\pi(2S - a)\rho_p d_p^2 v_i}{18\mu a b}\right] \quad (9)$$

where the subscripted K terms are functions of particle and gas properties as well as cyclone dimensions.

EXPERIMENTS

All experiments were carried out on the cyclone test system shown in Figure 2. In this system, room air was pulled through an absolute filter to remove ambient particles. Air flow rate was measured by the pressure drop across a calibrated Stairmand disc. A Stairmand high-efficiency cyclone, with D = 0.305 m, was used.

Arcoprime 200 (a mineral oil with ρ_p = 860 kg/m^3) was nebulized using a Laskin nozzle aerosol generator (11) with a compressed air gauge pressure of 27.6 kPa (4 psig) and was injected through a cylindrical probe that introduced the aerosol at the center of the duct. This aerosol generation system was chosen for several reasons. First, because the liquid droplets produced are spherical, their aerodynamic behavior is easily described. All of the theories described above assume spherical particles. Second, collected liquid droplets should not bounce or re-entrain after striking the cyclone wall. Again, cyclone collection efficiency theories assume this to be the case. Finally, this generation system produced sufficient particles over a range of sizes ($1\mu m < d_p < 5\mu m$) where cyclone fractional efficiency should increase from ≈0 to ≈1.

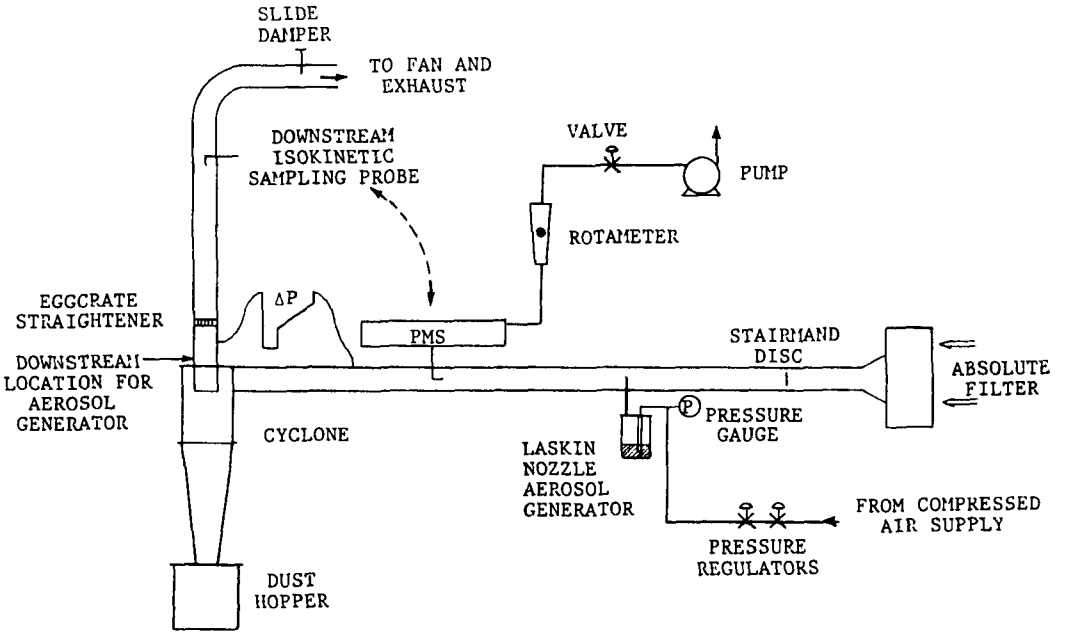

Figure 2. Schematic drawing of cyclone test system.

Aerosol samples were taken isokinetically through sampling probes at the duct centerline upstream and downstream of the cyclone. Particles were sized and counted with a Particle Measuring Systems (PMS), Inc. (Boulder, CO 80301) aerosol scattering spectrometer. The maximum number concentration counted was $< 10^4/cm^3$ without dilution, well below the concentration for which coincidence is significant for this instrument. To minimize sampling line losses, the PMS was moved between the upstream and downstream sampling locations; in each case, the sampling line consisted of a 23 cm long horizontal run from the duct centerline to the PMS inlet.

Accurate sampling of the aerosol downstream from the cyclone is difficult because the gas flowing from the cyclone is swirling. Techniques for sampling from a swirling gas flow are available, but because of transient velocity patterns, these techniques are difficult to use at best, and unreliable at worst. To eliminate this problem, an "egg crate" flow straightener was installed three duct diameters downstream from the entrance to the cyclone outlet duct. According to Browne and Strauss (12), this device will not affect flow patterns and collection within the cyclone if it is more than two duct diameters from the outlet duct entrance. As reported by Ferguson, et al. (13), we found that a straightener with each cell $D/6$ in height, width, and depth (where D is the duct diameter) produced a flat axial velocity profile with negligible tangential velocity downstream of the cyclone.

An efficiency determined from a measurement of aerosol concentration downstream of the flow straightener will reflect collection by both the cyclone and the straightener. Accordingly, measurements of efficiency that include collection by the straightener must be corrected. We accomplished this by injecting aerosol downstream of the cyclone but upstream of the flow straightener as shown in Figure 2. The concentration and size distribution of aerosol injected at this point were assumed identical to the concentration and size distribution of aerosol injected upstream of the cyclone as measured at the upstream sampling location. Because the operating parameters of the aerosol generator are not affected by its location, this assumption is reasonable. The distance between the aerosol injection and sampling locations was the same, both upstream and downstream of the cyclone.

Three sets of measurements, each set consisting of eight replicate samples, were made for each test. For the first set of measurements, aerosol was injected and sampled upstream of the cyclone. The second set sampled the aerosol downstream of the cyclone after it had been injected upstream. For the third set, the aerosol was injected between the cyclone and straightener and sampled downstream of the straightener. For particles of any size, the combined efficiency of the cyclone and straightener can be measured directly by

$$\eta_{c+s} = 1 - \frac{N_{up,down}}{N_{up,up}} \tag{10}$$

where N is the count rate for particles of that size, the first subscript refers to the aerosol injection site relative to the cyclone (up for upstream and $down$ for downstream), and the second subscript refers to the sampling location relative to the cyclone. The efficiency of the straightener can also be measured directly from

$$\eta_s = 1 - \frac{N_{down,down}}{N_{up,up}} \tag{11}$$

The combined efficiency of the cyclone and straightener in series is related to the individual efficiencies of each by

$$\eta_{c+s} = 1 - (1-\eta_c)(1-\eta_s) \tag{12}$$

By substituting Eqs. 10 and 11 into Eq. 12 and solving for η_c, cyclone efficiency can be expressed as

$$\eta_c = 1 - \frac{N_{up,down}}{N_{down,down}} \tag{13}$$

Prior to making the measurements described above, it was necessary to relate a single sample, taken at the duct centerline, to the average particle count rate across the duct. Samples were taken at six radial positions across the duct both upstream of the cyclone and downstream of the straightener. By combining these six counts, it was possible to estimate an average count rate for the duct. Downstream of the straightener, the concentration profile was uniform and a single centerline sample was representative of the duct average. Upstream profiles were less uniform (higher counts near the center of the duct), but for each cyclone inlet velocity, a single average correction factor was sufficient to relate the centerline sample to the average count for the duct.

Tests were conducted at cyclone inlet velocities of 5, 10, 15, 20, and 25 m/s. The design inlet velocity for a Stairmand high-efficiency cyclone with D = 0.305 m is 15 m/s, corresponding to a flow rate of 0.14 m^3/s (300 cfm). Three separate tests were conducted at each inlet velocity, for a total of fifteen experiments. For each experiment, all particles ≥ 1 μm in diameter were counted and sized into intervals of width 0.75 μm by the PMS. Cyclone collection efficiency for the midpoint of each size interval was calculated from Eq. 13, where $N_{up,down}$ and $N_{down,down}$ were the average counts for the eight replicate samples. The total number of particles counted per test ranged from 7×10^4 to 5×10^5.

For each inlet velocity, pressure drop across the cyclone was measured. The downstream pressure taps were located between the cyclone and the flow straightener so that any additional pressure loss due to the straightener was not included in the measurement.

RESULTS AND DISCUSSION

Cyclone pressure drop values for each of the five inlet velocities are shown in Table 1. Pressure loss also can be expressed as a number of inlet velocity heads, ΔH, which should be constant for all inlet velocities. The average value for ΔH was 5.7, higher than the value of 5.3 reported by Stairmand (1) for this cyclone design.

TABLE 1. EXPERIMENTAL CYCLONE PRESSURE DROP

Inlet velocity (m/s)	Pressure Drop (Pa)
5	87
10	336
15	785
20	1407
25	2205

Figure 3 shows the experimental fractional efficiency curves for all five cyclone inlet velocities. Each data point represents the mean cyclone efficiency for the three tests involving that particular particle diameter and inlet velocity combination The effects of both of these parameters on cyclone efficiency are in general agreement with theoretical predictions. For any particle diameter, Figure 3 shows that an increase in inlet velocity, holding all other parameters constant, results in increased fractional efficiency. For a given cyclone inlet velocity, efficiency increases with particle diameter.

Figures 4-8 compare experimental results with predictions of the four cyclone efficiency theories discussed previously. The theoretical predictions are presented as smooth curves. Experimental data points from Figure 3 have been replotted, without the connecting lines, in Figures 4-8. To indicate the reproducibility of the experimental results, a 95 percent confidence interval is indicated by the *'s above and below each data point. For the three determinations of efficiency represented by each data point, the 95 percent confidence interval is given by $\bar{\eta}_c \pm (\frac{4.30\sqrt{s_\eta^2}}{\sqrt{3}})$ where s_η^2 is the variance of the three efficiency measurements and 4.30 is the appropriate value for Student's t with two degrees of freedom. Where confidence intervals do not appear symmetrical, it is because they have not been extended beyond the range of fractional efficiency from 0 to 1.

For ideally collected liquid droplets, the experimental fractional efficiency curves indicate a much sharper separation by the cyclone than predicted by most of the theories. With no particle bounce or re-entrainment, large increases in collection efficiency occur for relatively small increases in particle diameter. For example, at cyclone inlet velocities of 10 and 15 m/s (Figures 5 and 6), increases of ≈ 2 μm in particle diameter cause fractional efficiency to increase from <0.2 to >0.8. The theories of Lapple, Leith and Licht, and Dietz all predict much flatter fractional efficiency curves. Only the Barth theory matches the experimental curves in steepness.

The Lapple theory underestimates collection efficiency for most of the data. Only for cyclone inlet velocities ≤ 10 m/s and fractional efficiency ≤ 0.2 do the Lapple predictions and the experimental results agree. One major drawback to the Lapple theory is the use of the term N_e in the expression for cyclone cut diameter, Eq. 3. This empirical term describes the effective number of turns made by the gas stream in the cyclone and is necessary to calculate residence time. Lapple (6) recommended that N_e be determined experimentally for different cyclone designs, but the value of 5 that he reported is often used.

Although $N_e = 5$ was used to calculate the Lapple curves in Figures 4-8, the experimental data suggest that N_e is substantially higher. Using experimentally determined cut diameters from the curves in Figure 3, experimental values of N_e can be calculated from Eq. 3. Calculated values of N_e are not constant for the cyclone design as suggested by Lapple (6), but increase from ≈ 12 at $v_i = 5$ m/s to ≈ 30 at $v_i = 25$ m/s. These "calibrated" values of N_e can be used to calculate new fractional efficiency curves for the Lapple theory. However, the new curves would fit the experimental data only at the cut diameter, underestimating efficiency for larger particles and overestimating for smaller particles.

The predictions of the Dietz theory fall in the same range as the Lapple curves in Figures 4-8. Experimental cyclone efficiency is generally much higher than predicted by the Dietz theory, except for the lower ends of the fractional efficiency curves at

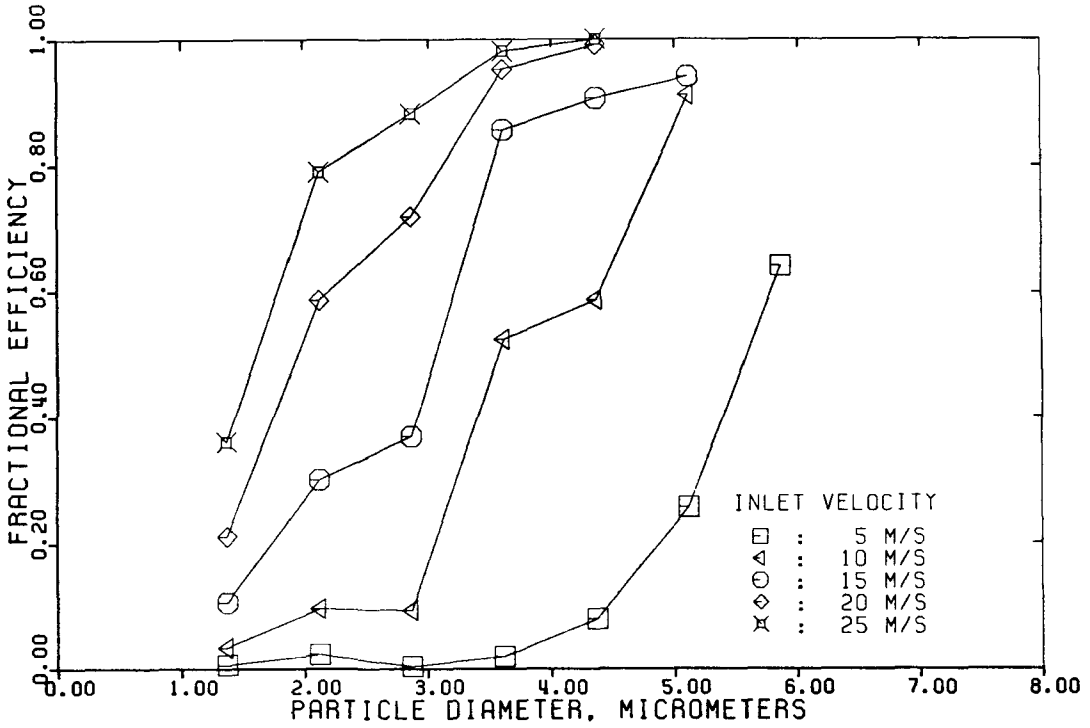

Figure 3. Experimental fractional efficiency curves for Stairmand high-efficiency cyclone for inlet velocities from 5 m/s to 25 m/s.

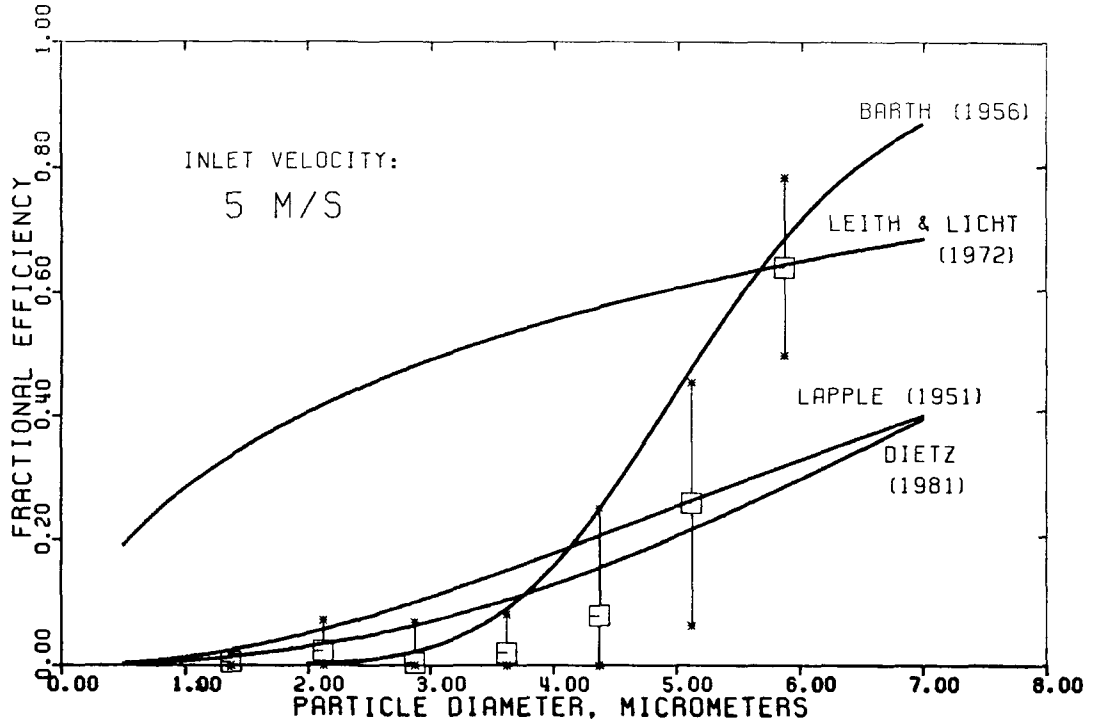

Figure 4. Experimental and theoretical cyclone efficiency for cyclone inlet velocity = 5 m/s. (For Figures 4-8, open squares indicate experimentally determined efficiency; asterisks indicate 95% confidence intervals; solid lines indicate theoretical predictions.)

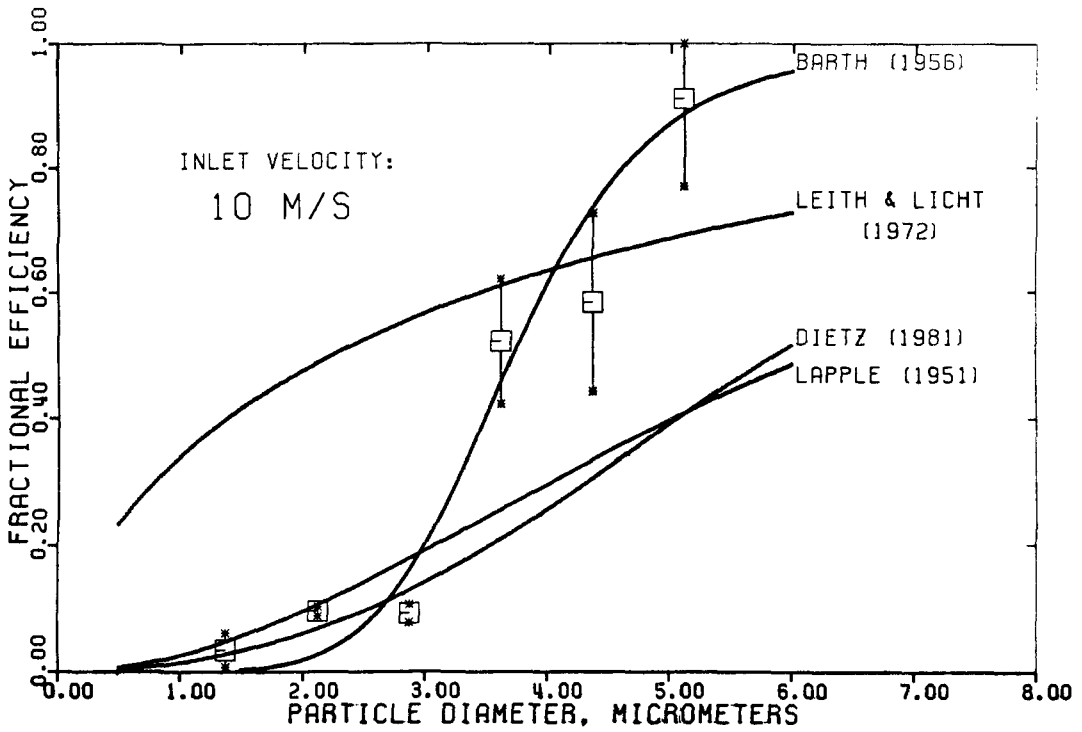

Figure 5. Experimental and theoretical cyclone efficiency for cyclone inlet velocity = 10 m/s.

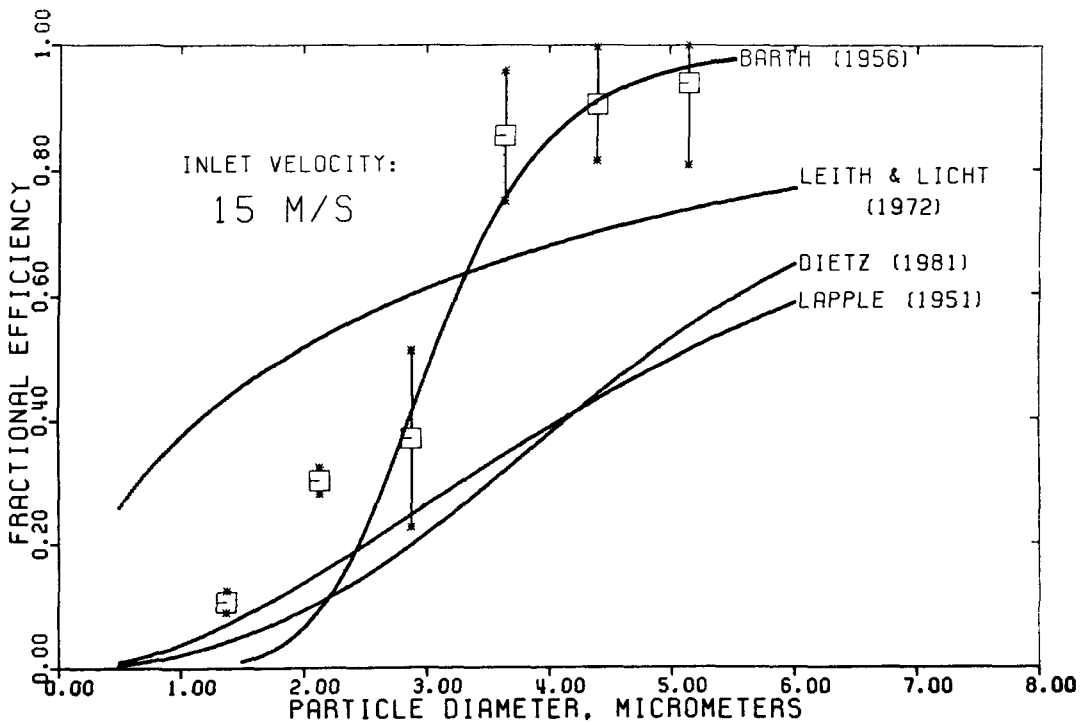

Figure 6. Experimental and theoretical cyclone efficiency for cyclone inlet velocity = 15 m/s.

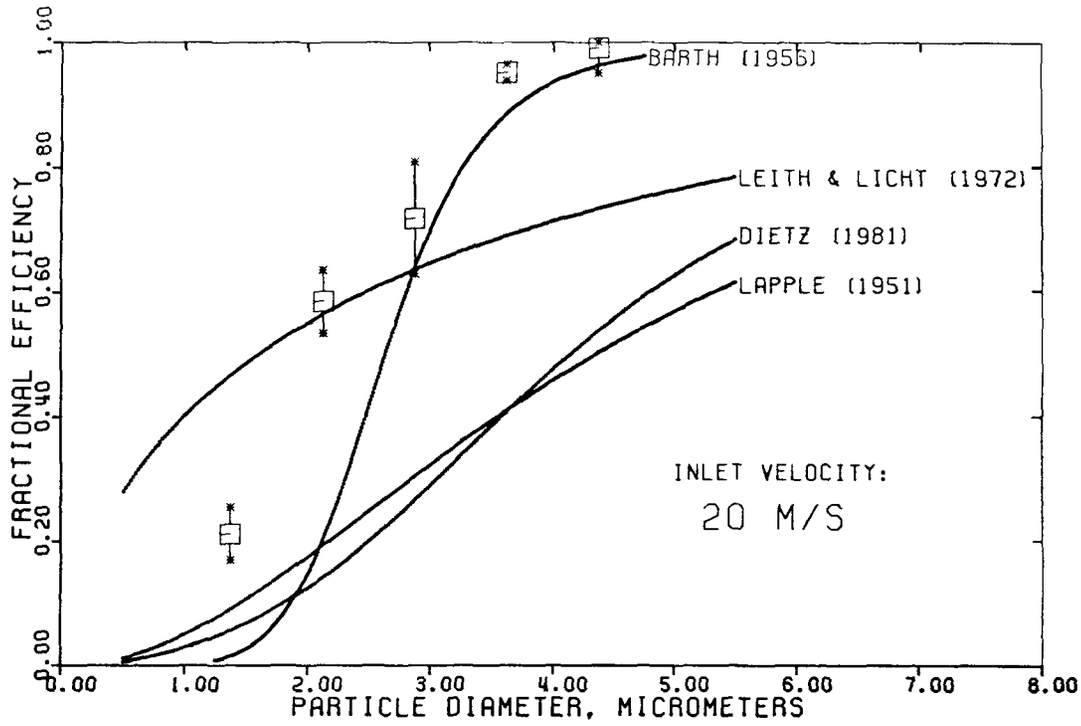

Figure 7. Experimental and theoretical cyclone efficiency for cyclone inlet velocity = 20 m/s.

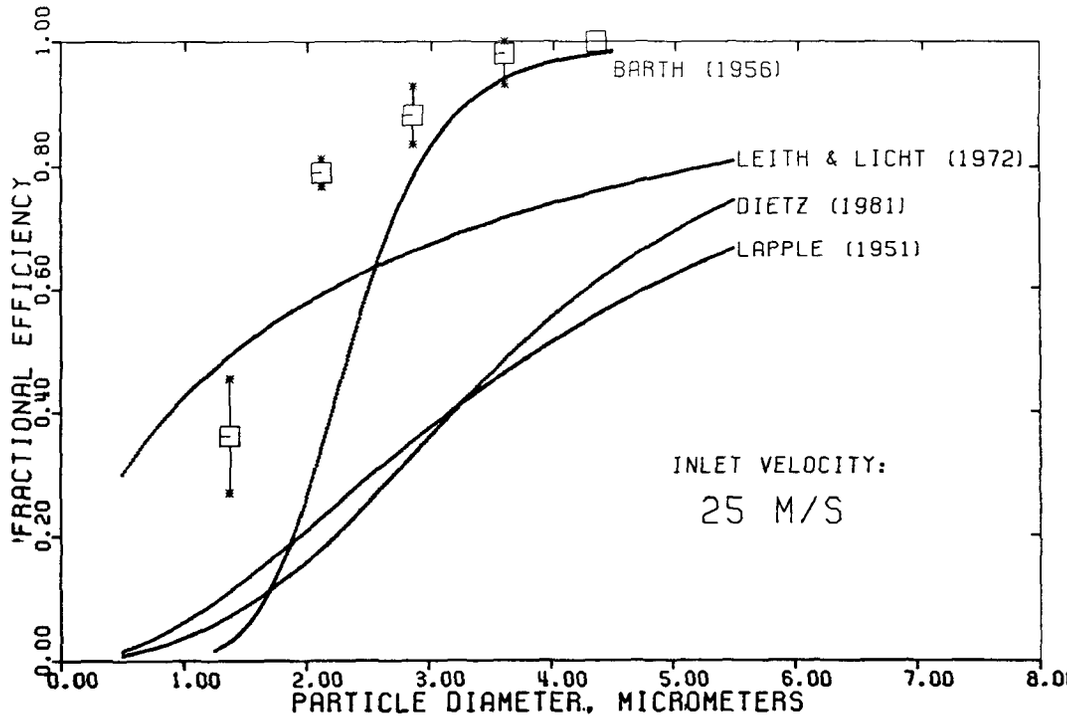

Figure 8. Experimental and theoretical cyclone efficiency for cyclone inlet velocity = 25 m/s.

inlet velocities of 5 and 10 m/s. The Dietz curves were calculated using a vortex exponent of 0.56, obtained from Eq. 6, although Dietz (9) recommends a higher value of 0.7. Higher values for n imply higher tangential velocity in the vortex and greater centrifugal forces acting on the particles in the gas stream. While the use of $n = 0.7$ would increase the efficiencies predicted by the Dietz theory, the Dietz curves in Figures 4-8 would be shifted only slightly upward from their present positions.

The theoretical curves based on the Leith-Licht cyclone model predict higher collection efficiency than either the Lapple or Dietz models. For all of the inlet velocities tested, the Leith-Licht model agrees with the experimental results in the middle of the fractional efficiency range, $\eta_c \approx 0.4$ to 0.6. Since the Leith-Licht curves are flatter than the experimental fractional efficiency curves, this model underestimates efficiency for most particle diameters larger than the experimental d_{50}. For smaller particles, the model greatly overestimates cyclone efficiency.

Both the Leith-Licht and Dietz theories assume that turbulence within the cyclone is sufficient to cause complete radial back-mixing of uncollected particles in any plane perpendicular to the cyclone axis. This, in part, accounts for the relatively flat theoretical fractional efficiency curves calculated from the two models. The steep slope of the experimental curves suggests that turbulence is less important than predicted. Recent work by Mothes and Loffler (14) and a previous study by Hejma (15) indicate that there is a concentration gradient for particles in the vortex of the cyclone. Mothes and Loffler found that larger particle ($\approx$3.5 μm) concentrations were much higher near the cyclone wall and decreased by nearly two orders of magnitude from the wall to the cyclone core. Smaller particle ($\approx$0.5 μm) concentrations were much more uniform as radial position changed. Hejma found similar results in the cone of the cyclone, although in the cylinder above the cone, he found that dust concentration was nearly independent of radial position. These studies indicate that the assumptions of complete radial back-mixing made by the Leith-Licht and Dietz theories are not justified, at least for larger particles. Smaller particles, with less centrifugal force, might be more strongly influenced by turbulence. The distinction between large and small particles probably depends on cyclone geometry and operating conditions.

Of the four cyclone theories presented here, the Barth theory fits the experimental data best. At inlet velocities up to 15 m/s (Figures 4-6), the Barth curves fall within the 95 percent confidence intervals for most experimental data points. At velocities of 20 m/s and above (Figures 7-8), the theoretical curves are steeper than the experimental data and there is agreement only at high collection efficiency.

One problem with the Barth approach is its reliance on a plot of collection efficiency as a function of a ratio of terminal settling velocities (particle diameter over critical particle) to determine the fractional efficiency for particles other than the critical size. This curve was developed from the results of experiments with a variety of cyclones. Other investigators using the static particle approach have found that there is a pronounced dependence of curves of this type on the design of the cyclone (16). While the predictions based on Barth's curve match some of the data for the Stairmand high-efficiency cyclone used here, the applicability of the Barth theory to other cyclone designs is uncertain.

SUMMARY

Collection efficiency for a Stairmand high-efficiency cyclone was measured experimentally under carefully controlled conditions over a range of inlet velocities. An

aerosol consisting of liquid droplets was used to minimize the possibility of particle re-entrainment after collection in the cyclone and to provide the spherical particles assumed by cyclone efficiency theories. Four theories, representing three different approaches for calculating collection by a cyclone, were compared with the data. Only one of these theories, the method of Barth, gave predictions that were in substantial agreement with the experimental results. The steep slope of the experimental fractional efficiency curves indicates that although gas stream turbulence influences the separation processes in the cyclone, the effects of turbulence are overestimated by the Leith-Licht and Dietz theories.

Currently available cyclone theories can provide general guidelines on how changes in operating conditions or cyclone dimensions will affect performance. We are now varying some dimensions of the Stairmand high-efficiency cyclone to improve performance above the baseline levels measured in this study. These results should be useful in improving cyclone theories through calibration -- finding parameters that can be adjusted so that the theories better predict experimental data. Efficient optimization of cyclone design, however, requires a theory capable of more precise predictions over a wide range of operating conditions and designs.

ACKNOWLEDGEMENTS

This work was supported by Grant No. CPE-8012968 from the National Science Foundation. Arcoprime 200 mineral oil was supplied by Donald Hasselstrom of ARCO Petroleum Products Company, Philadelphia, PA.

The work described in this paper was not funded by the U.S. Environmental Protection Agency and therefore the contents do not necessarily reflect the views of the Agency and no official endorsement should be inferred.

NOMENCLATURE

a	cyclone inlet height, m
B	cyclone dust outlet diameter, m
b	cyclone inlet width, m
C	cyclone geometry parameter (see Eq. 7), dimensionless
D	cyclone body diameter, m
D_e	cyclone outlet diameter, m
d_p	particle diameter, m
d_{50}	particle diameter collected with 50 percent efficiency, m
g	gravitational acceleration, m s^{-2}
H	overall cyclone height, m
h	cyclone cylinder height, m
K_0, K_1, K_2	intermediate terms for computing cyclone efficiency by Eq. 9, dimensionless
N_e	number of turns made by gas stream in cyclone (see Eq. 3), dimensionless
$N_{down,down}$	particle count rate downstream with downstream aerosol injection, min^{-1}
$N_{up,down}$	particle count rate downstream with upstream aerosol injection, min^{-1}
$N_{up,up}$	particle count rate upstream with upstream aerosol injection, min^{-1}
n	cyclone vortex exponent, dimensionless

Q	volume flow rate, $m^3\ s^{-1}$
r	radial distance from cyclone axis, m
S	cyclone outlet duct length, m
T	gas temperature, °K
v_i	cyclone inlet velocity, $m\ s^{-1}$
v_t	tangential gas velocity in cyclone vortex, $m\ s^{-1}$
v_{ts}	particle terminal settling velocity, $m\ s^{-1}$
v_{ts}^*	terminal settling velocity of critical particle, $m\ s^{-1}$
ΔH	cyclone pressure drop in inlet velocity heads, dimensionless
η_c	cyclone fractional collection efficiency, dimensionless
η_s	straightener fractional collection efficiency, dimensionless
η_{c+s}	combined fractional collection efficiency of cyclone and straightener, dimensionless
μ	gas viscosity, Pa s
ρ_p	particle density, $kg\ m^{-3}$
Ψ	cyclone inertia parameter, dimensionless

REFERENCES

1. Stairmand, C.J. The design and performance of cyclone separators. *Trans. Instn. Chem. Engrs.* 29:356, 1951.

2. Jackson, R. *Mechanical Equipment for Removing Grit and Dust from Gases.* Cheney and Sons, Banbury, England, 1963. 281 pp.

3. Swift, P. Dust control in industry--2. *Steam Heat. Engr.* 38:453, 1969.

4. Leith, D. Cyclones. *In:* N.C. Pereira and L.K. Wang (eds.), Handbook of Environmental Engineering. The Humana Press, Clifton, NJ, 1979. p. 61.

5. Barth, W. Design and layout of the cyclone separator on the basis on new investigations. *Brenn. Warme Kraft.* 8:1, 1956.

6. Lapple, C.E. Processes use many collector types. *Chem. Eng.* 58:144, 1951.

7. Theodore, L. and DePaola, V. Predicting cyclone efficiency. *J. Air Pollut. Control Assoc.* 30:1132, 1980.

8. Leith, D. and Licht, W. The collection efficiency of cyclone type particle collectors, a new theoretical approach. *A.I.Ch.E. Symposium Series.* 68:196, 1972.

9. Dietz, P.W. Collection efficiency of cyclone separators. *A.I.Ch.E. Journal.* 27:888, 1981.

10 Alexander, R. McK. Fundamentals of cyclone design and operation. *Proc. Australas Inst. Min. Met. (New Series).* 152-153:203, 1949.

11. Laskin, S. Submerged aerosol unit. AEC Project Quarterly Report, UR-38, University of Rochester, 1948.

12. Browne, J.M. and Strauss, W. Pressure drop reduction in cyclones. *Atmos. Environ.* 12:1213, 1978.

13. Ferguson, B.B., Mitchell, W.J., Reece, J.W., and Sterrett, J.D. Modeling and straightening cyclonic flows. Paper No. 81-7.6 presented at the 74th Air Pollution Control Association Annual Meeting, Philadelphia, PA. June 21-26, 1981.

14. Mothes, H. and Loffler, F. Investigation of cyclone grade efficiency using a light scattering particle size measuring technique (abstract). *J. Aerosol Sci.* 13:184, 1982.

15. Hejma, J. Influence of turbulence on the separation process in a cyclone. *Staub-Reinhalt. Luft.* 31(7):22, 1971.

16. Loffler, F. The calculation of centrifugal separators. *Staub-Reinhalt. Luft.* 30(12):1, 1970.

ADDENDUM

Since this paper was presented, it has come to our attention that the fractional efficiency curves calculated according to the Barth theory (Figures 4-8) are incorrect. An equation to determine v_t in Eqs. 1 and 2 appears in a number of references in addition to Barth's original article. In *Industrial Gas Cleaning (2nd Edition)* by W. Strauss (Pergamon Press, Elmsford, NY, 1975), the equation for the ratio of v_t to the cyclone outlet velocity gives values too high by a factor of two. Use of this secondary reference resulted in calculated v_t's that were twice those predicted by Barth's theory. Substitution of the correct values for v_t shifts the Barth fractional efficiency curves in Figures 4-8 substantially to the right. In addition, the slopes of the curves are reduced, although the Barth theory still predicts a sharper cut than any of the other theories presented.

Clearly, the curves based on the incorrect values for v_t provide a much better fit to the experimental data, suggesting that the maximum tangential velocities calculated by Barth's theory are too low. Although this result was discovered accidentially, it provides a good example of the type of calibration--adjusting parameters so that the theoretical predictions better match the data--that was discussed above.

John A. Dirgo
David Leith
February 1, 1983

HIGH FLOW CYCLONE DEVELOPMENT

by

W. B. Giles
Mechanical Systems and Technology Laboratory
Corporate Research and Development
General Electric Company
Schenectady, New York 12301

ABSTRACT

Investigative studies of an atypical cyclone configuration, designed for high flow capacity, were performed, focusing particularly on the design aspects of inlet flow and dust disengagement. The results indicate that a performance equal to or superior to conventional design can be achieved with a net savings in cyclone size and cost.

The design is characterized as a reverse flow cyclone with both a large inlet and a large outlet, plus increased engagement length between the cyclone body and the exhaust duct. Both of these features are seen as means to suppress large scale inlet turbulence. In addition, reduced penetration is found by locating a vortex shield in the base of the cyclone. The net result indicates an approximate two-to-one diameter reduction, relative to current art, for equal flow capability and a slight pressure loss penalty.

INTRODUCTION

Cyclones have long been a standard means of gas cleaning and owe their popularity to their mechanical simplicity, small size, and low capital cost. On the debit side, application is inhibited by relatively high operation cost, due to pressure loss, and a relatively modest collection efficiency compared to alternate means of gas cleaning.

Recent interest in coal utilization has reawakened the desire to optimize the performance of cyclones. This is especially germane for high temperature-high pressure applications of coal combustion, gasification, and catalytic reactive processes. In these applications, the pressure loss penalty is not as critical as with atmospheric systems and the capital cost of alternate gas cleaning concepts can adversely impact overall system economics.

Unfortunately, the mechanical simplicity of the cyclone is not matched with a corresponding understanding and control of the physical processes. Experience has indicated that triboelectric charging of the dust can occur internal to the cyclone under certain test conditions; thus, scaling to operational conditions can lead to overestimation of collection efficiency. Analytic effort is inhibited by the complexity of the flow field and the influence of turbulence on dust migration. Specifically, the well-known Leith-Licht [1] model incorporating turbulent back mixing shows reasonable agreement with data for conventional designs. Their paper, however, incorporates an oversimplification, corrected by Giles [2], that leads to overprediction of fines collection. Incorporating the back mixing mechanism into a multi-zone computer model, Dietz [3] has demonstrated excellent predictive capability with conventional designs but poor agreement with atypical designs. A promising effort is offered by Boysan, et al. [4], but as yet is judged to omit significant cyclone mechanics. As a consequence, design improvements must continue through empirical effort guided in large part by intuition.

BACKGROUND

The exploratory work and rationale for a high flow capacity cyclone design is described in an earlier report [5]. In brief, conventional cyclone design derives largely from the work of van Tongeren [6],[1] ter Linden [7], and Stairmand [8]. Typically, this work leads to the use of small inlets and small outlets for high performance cyclones with low flow capacity or large inlets and large outlets for low performance cyclones of high flow capacity. Stairmand, for example, offers two designs, one for each general design objective [8].

Earlier General Electric exploratory work [5], however, found that the Stairmand performance data significantly underpredicts performance for the "high flow" design. The result is that the "high flow" design receives serious consideration only as a rough-cut cyclone, e.g., for reducing the dust loading of coarse particulates. By improving design conditions at the cyclone inlet and at the dust hopper, it is found that equal or superior performance may be attained with a high flow capacity design for a net savings in cyclone size and cost. The present report summarizes the final investigations with this high flow capacity design development.

1. Designs marketed in the U.S. by General Electric Environmental Systems (formerly Buell), Lebanon, Pennsylvania.

CYCLONE DESIGN

The basic cyclone design is shown in Figure 1 as consisting of a specially-designed head end mounted onto a conventional cyclone body. The various inserts used during experimentation are also indicated.

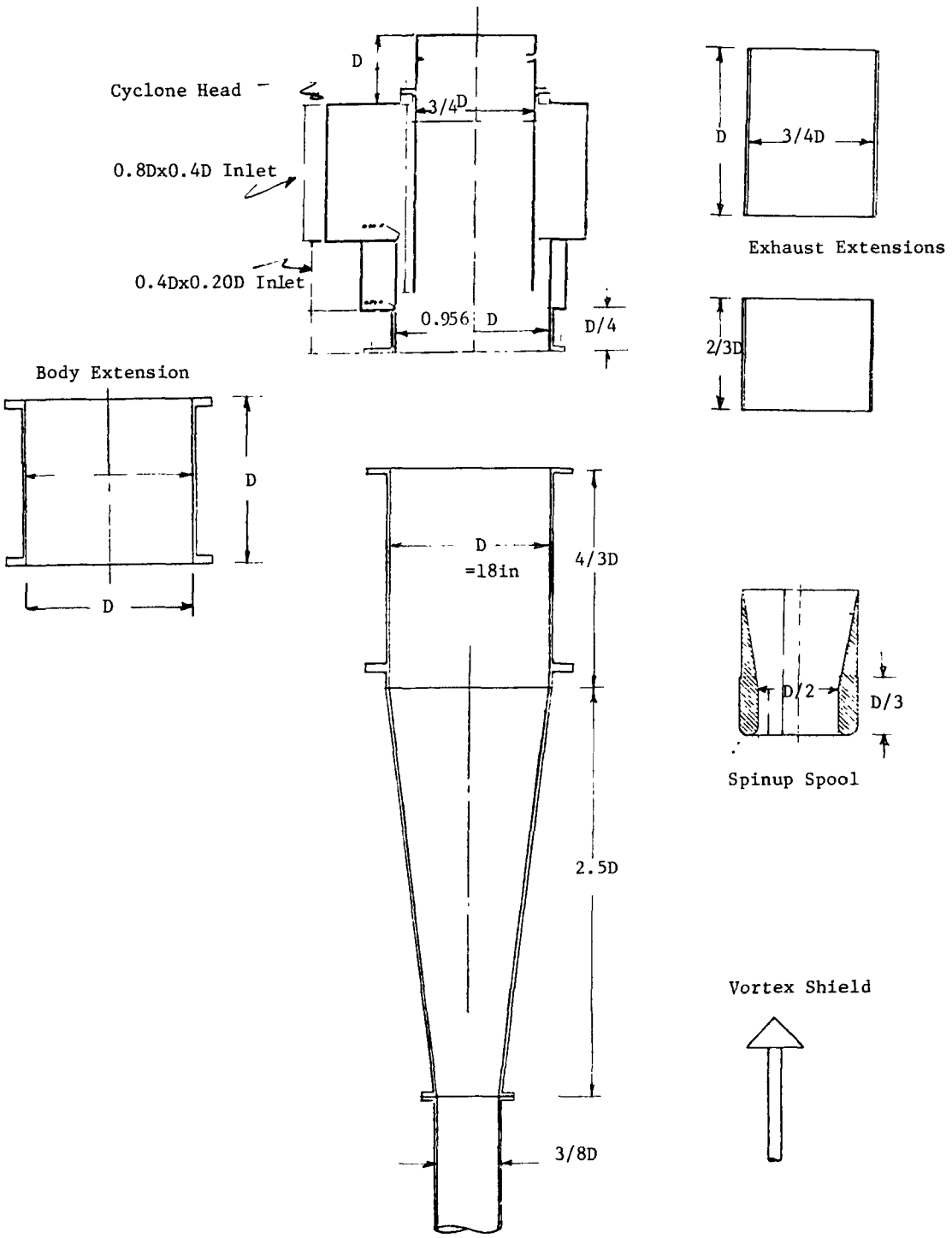

Figure 1. Schematic of high flow cyclone elements

The nominal inlet consisted of a four-point scroll supplied by an inlet of 0.9 $D \times 0.45\ D$, where $D = 18$ in. is the diameter of the cyclone body and the nominal outlet is 3/4 D. Thus the total flow capacity is

$$Q = 0.405\ D^2\ V_i$$

where V_i is the average inlet velocity. The cyclone body had a cylindrical section of 1.33 D and a conical section of length 2.5 D terminating at a pipe section of 3/8 D. The actual test unit inlet, however, included an air shield feature. This allowed assessment of the use of clean air injection between the dirty air at the wall and the central exhaust. Since this unit was designed for 80% clean air, the dirty air had an inlet of 0.4 $D \times 0.2\ D$ and the clean air had an inlet of 0.8 $D \times 0.4\ D$. The interior baffle between these two streams had a diameter of 0.956 D.

TEST PROCEDURE

The cyclone was tested as shown in Figure 2. Prefiltered air was supplied via a blower with both streams metered for flow, using flow nozzles and inclined manometers, and one stream contaminated with test dust from a blown fluidized bed. This bed provided dilute concentrations of either CURL second stage flyash ($\rho_p = 2.7$ g/cc) or nickel powder ($\rho_p = 8.5$ g/cc). Typical mass mean particle sizes were in the range of $\approx$ 2.5 to 3.2 μm.

Fractional efficiency was determined by optical measurement of input-output dust concentrations and size distributions. The overall collection efficiency was determined from two PILLS V mass concentration monitors mounted with optic windows (shop air to purged ducts). For the case of operation in the air shield mode, these sensors were mounted on the small 6-inch diameter inlet line and the 13.5-inch diameter exhaust line downstream of a perforated plate, honeycomb deswirl/mixing element. The dust injector was positioned several diameters upstream of the inlet sensor to assure turbulent mixing prior to sensing.

For particle size analysis, two Climet systems were used with isokinetic sampling[1] through 0.051-inch and 0.075-inch diameter probes for the inlet and outlet, respectively. Typical dilution ratios of approximately ten of these sampled flows were found adequate to avoid coincidence error in size counters. The resulting eight channels of size distribution information are used to compute mass distribution which, together with the overall efficiency measurement, provided means for calculating fractional efficiency.

The experiments consisted of various geometric options available within the context of this equipment. In particular, the effectiveness of the air shielding feature was assessed by measuring fractional efficiency with dirty air supplied to either the small or large inlet and with clean filtered air supplied to the other inlet. The influence of clean air dilution was accommodated in data reduction in both cases so that the data reported only reflects actual collection.

The effect of engagement length was assessed by adding exhaust pipe sections of 1 D, 2/3 D, or both to the interior. The effect of spin-up was assessed by inserting a wooden spool piece into the exhaust inlet. This allows variation of the spin-up or exhaust-to-cyclone diameter from $De/D = 3/4$ to 1/2 and extended downward a length of $D/3$ from the lip of the cylindrical exhaust. Thus, for example, a cylindrical extension of 2/3 D plus the addition

1. However, isokinetic sampling is not critical for size analysis.

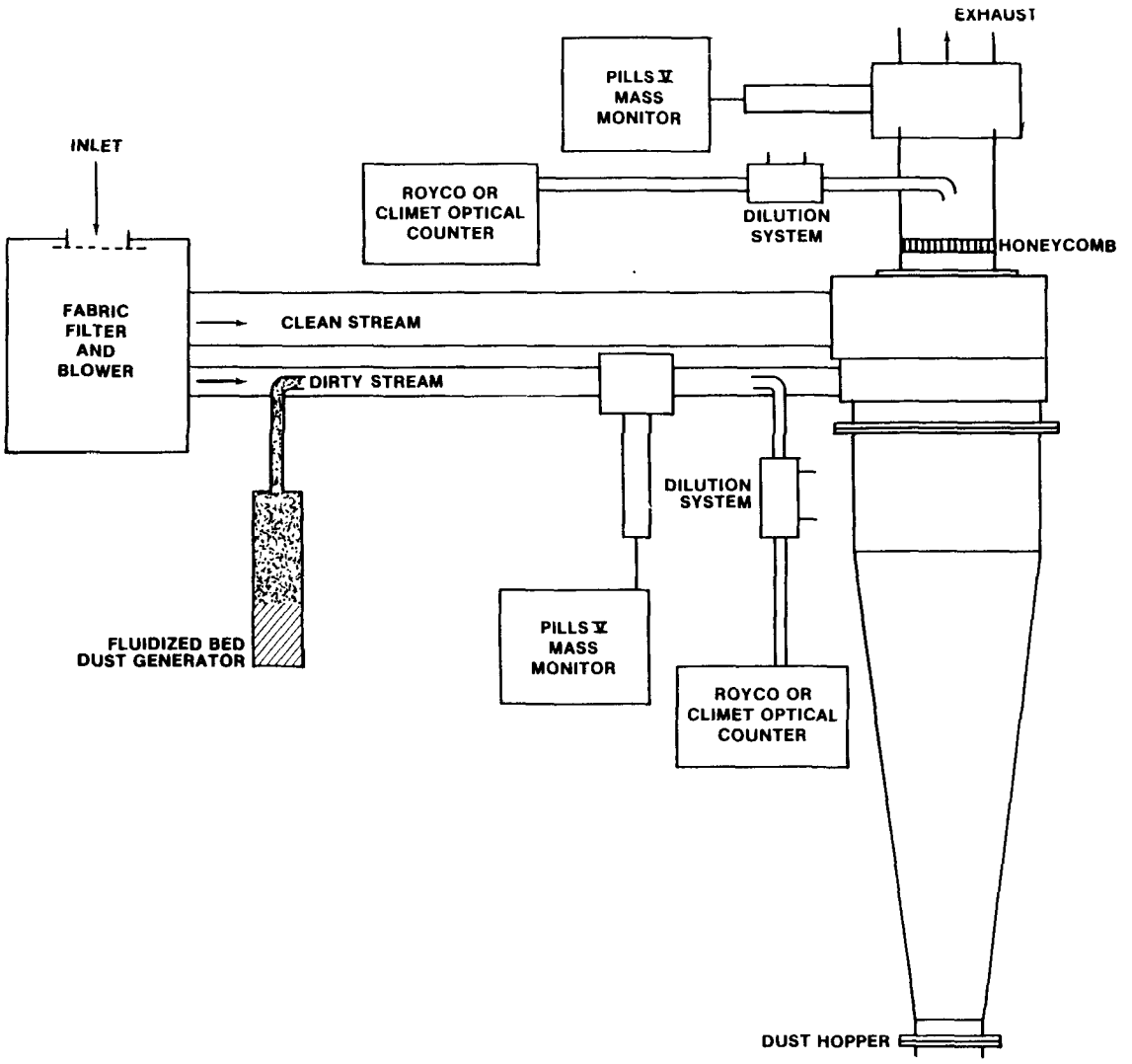

Figure 2. Cyclone test arrangement

of the wooden spool piece provides the same engagement length as a cylindrical exhaust extension of 1 D for a direct comparison of the influence of increased swirl spin-up.

In addition, tests were also conducted with the insertion of a vortex shield mounted in the conical base of the cyclone body with the apex of a 45° cone pointing upward, and finally, a cylindrical length of 1 D was added to the existing cyclone body.

TEST RESULTS AND DISCUSSION

The experiments were conducted over a range of inlet velocity and the data reduced to the form of fractional efficiency, η_f, versus nondimensional inertial separative parameter, or Stokes number,

$$\psi = \frac{\rho_p \, d_p^2 \, V_i}{18\mu \, D}$$

Also presented is the overall efficiency, η_o, versus the mass average, ψ. Here ρ_p and d_p are density and size of particle, V_i is the average inlet velocity, μ is the absolute gas viscosity, and D is the cyclone diameter.

The degree of correlation obtained over this range in velocity is used as a test to verify the dominance of inertial forces as the principal mechanism of collection.

Statistically it is anticipated that the best accuracy occurs in the vicinity of the mass mean particle size. Thus it is found that the calculated fractional efficiencies tend to be low for very large and very small particles in the population. Similarly, tests at low velocity or poor cyclone configurations afford poor discrimination in the calculation of fractional efficiency and tests at very high performance can lead to significant experimental scatter. Accordingly, the data is presented with a line drawn to reflect the "best engineering" judgment.

The following summarizes results of the various experiments.

Influence of Air Shielding

Figure 3 shows the performance of a high flow capacity cyclone with and without a clean air shield using flyash. Here the air shield data is presented as fractional efficiency, whereas the non-air shield data is based on overall efficiency. The relatively poor performance in the latter case prevented an accurate determination in fractional efficiency due to a lack of discrimination between input-output size distributions. The obvious conclusion is that there is a pronounced collection advantage in using the air shield feature.

Pressure loss measurements from inlet to ambient showed a loss of 13.5 inlet kinetic heads, as indicated.

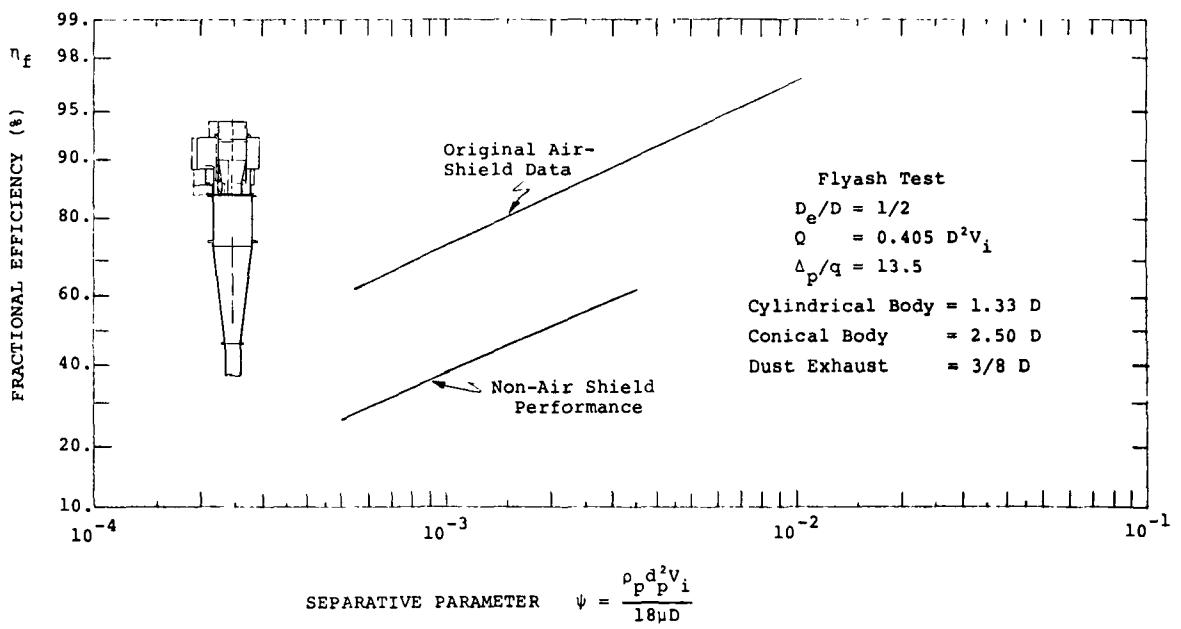

Figure 3. High flow cyclone: air shield influence

Influence of Engagement Length

In an effort to improve performance in the non-air shield configuration, the axial engagement length (e.g., the axial distance between inlet and exhaust) was increased by inserting an 18-inch extension to the exhaust duct and then an additional 12-inch extension. In these tests, the wooden spool piece was removed so that $De/D = 3/4$ and the cyclone body configuration remained constant. The results, shown in Figure 4, showed a marked improvement in performance and an expected reduction in pressure loss. The full extension of 30 inches (engagement length = 2.0 D) showed a slight performance reduction relative to the 18-inch extension, suggesting dust reentrainment due to increased proximity of the exhaust to the dip leg. The data also showed less pressure loss, due to improved recovery in the longer exhaust duct.

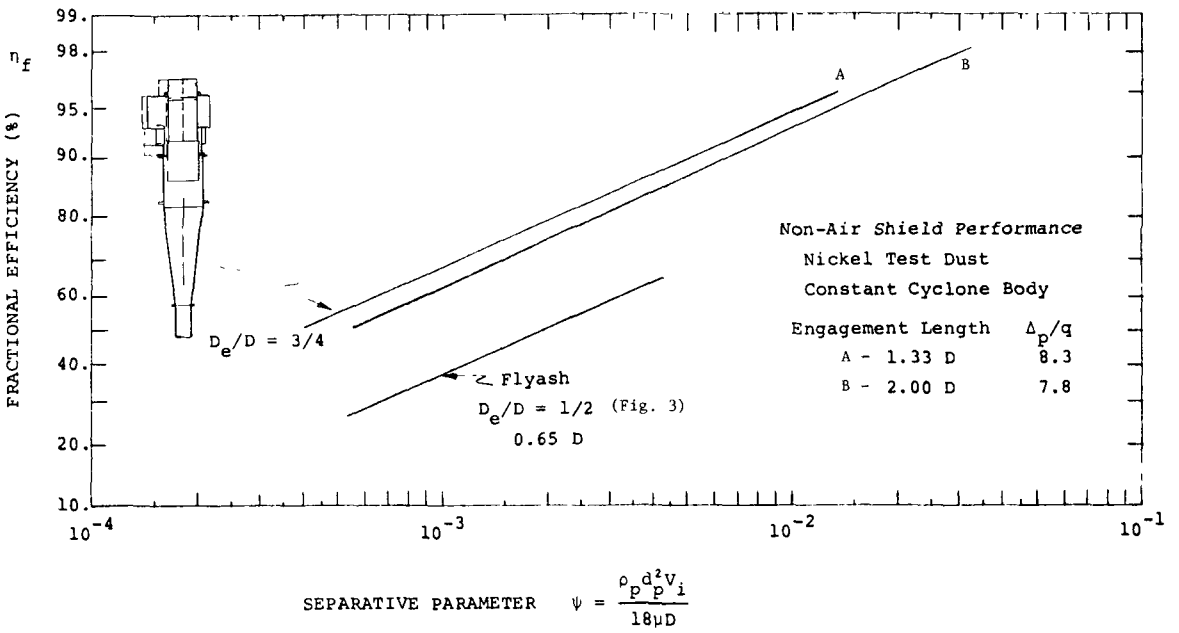

Figure 4. High flow cyclone: engagement length influence

Influence of Spin-Up

Since conventional wisdom teaches that higher vortex spin-up (generated by a smaller exhaust diameter) improves performance, the cyclone was tested in the non-air shield configuration with the same engagement length at $De/D = 1/2$ and $3/4$. The result is shown in Figure 5 and indicates a measurable performance penalty and high pressure loss associated with the constricted outlet. Further increase of the engagement length in combination with higher spin-up reduced collection efficiency and was indicative of dust reentrainment problems.

Influence of Vortex Shield

The indication of dust reentrainment led to the insertion of a vortex shield (conical point upward) above the dust exhaust, as illustrated in Figure 1. Comparative results shown in Figure 6 indicate a significant performance improvement.

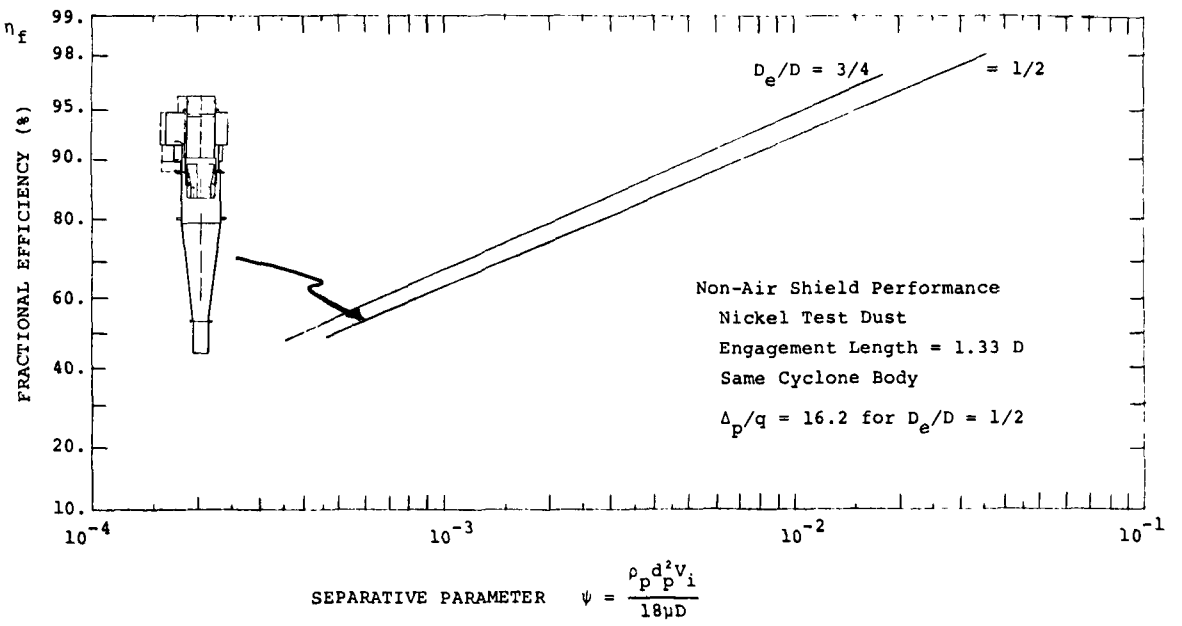

Figure 5. High flow cyclone: spin-up influence

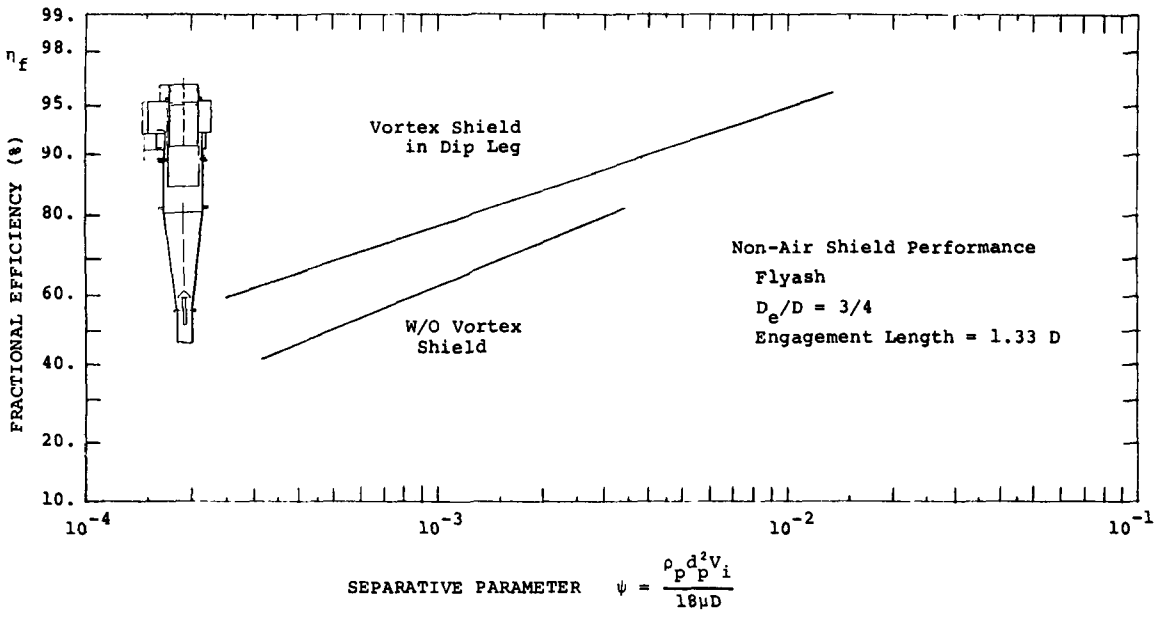

Figure 6. High flow cyclone: vortex shield influence

Test Dust Correlation

Figure 7 shows the degree of experimental accuracy obtained by using the two different test dusts. This discrepancy of ± 10% on penetration may be due to differences in particle reflectivity, which might affect the PILLS measurements, or ± 10% on particle size analysis of the Climet measurements. In general, excellent correlation is indicated.

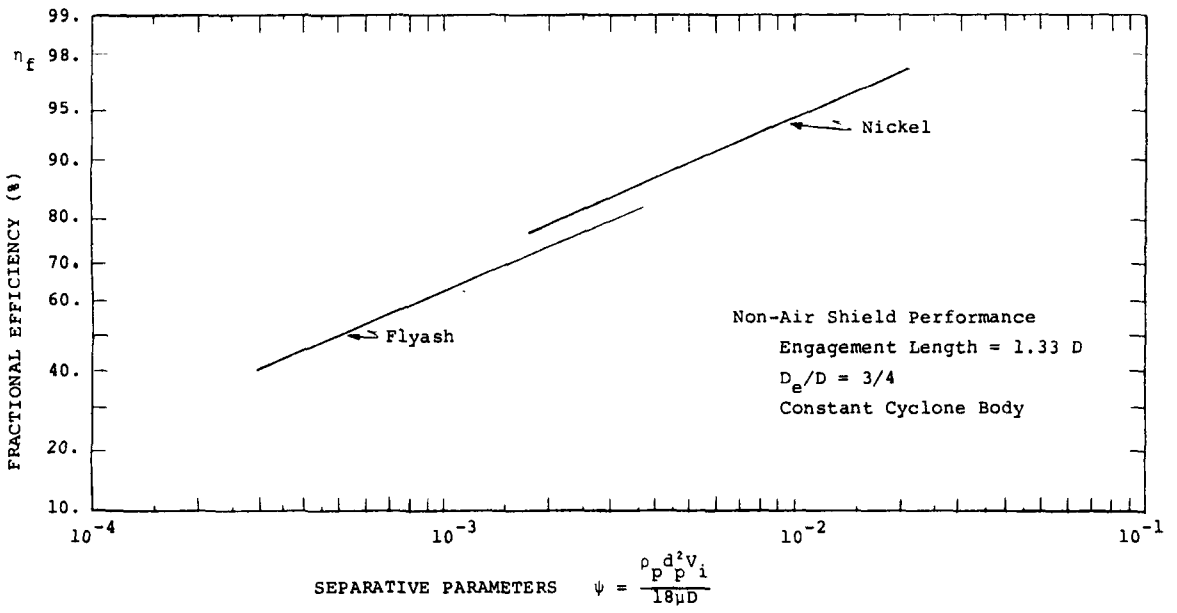

Figure 7. High flow cyclone: test dust correlation

Influence of Cylindrical Length

To assess the importance of cyclone body length, an 18-inch long cylindrical section was introduced to extend the body. Performance with and without the extension was compared (both using the vortex shield), and the results are shown in Figure 8. Accounting for the differences in test dusts, one can conclude that the longer cyclone body is not beneficial if the vortex shield is used to inhibit dust reentrainment.

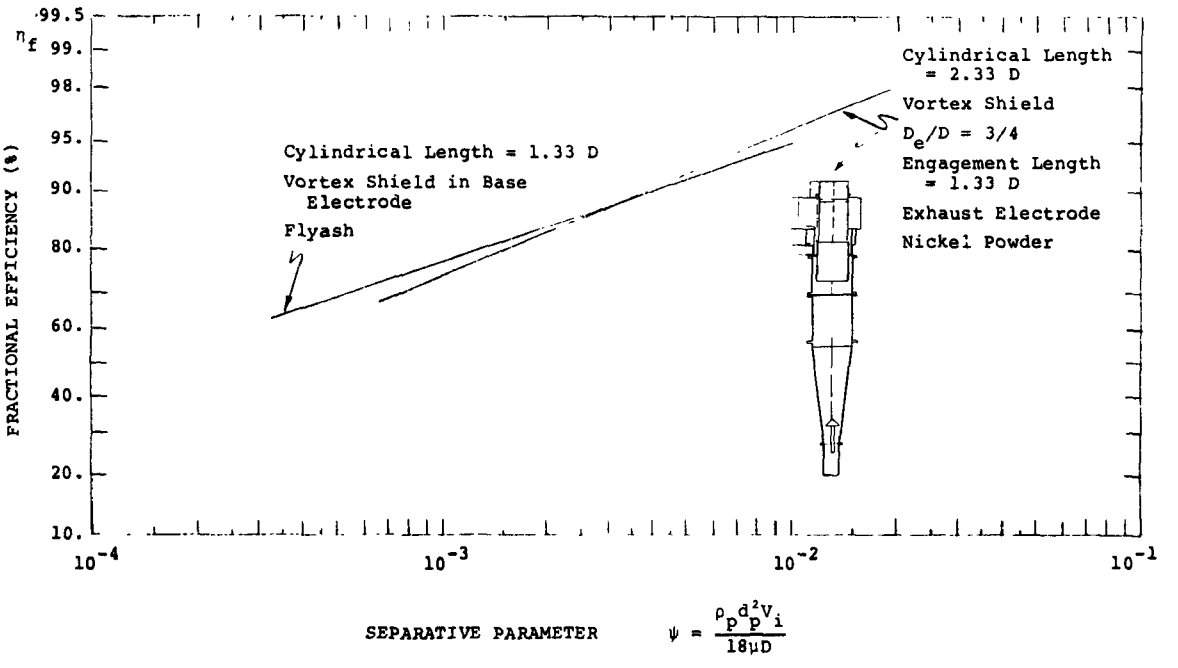

Figure 8. High flow cyclone: body length influence

High Flow Versus Low Flow Cyclone Design

In a parallel activity, testing of a Stairmand low flow or "high efficiency" design with a scroll inlet was performed using the same experimental techniques and instrumentation. These results are compared in Figure 9 with the data of the present high flow design, using increased engagement length and the base-mounted vortex shield. For the same inlet velocity, the high flow design is found to provide comparable performance at four times higher flow capacity with only a 38% higher pressure loss. Alternately, the high flow design would handle the same flow at one-half the diameter of the Stairmand design, thus shifting the ψ values by a factor of two as shown in Figure 9. With this shift, it is found that the high flow design provides substantially superior performance with a major size/cost savings. The impact of cyclone size on capital cost is anticipated to be particularly important for high pressure cleanup systems due to the required pressure vessels.

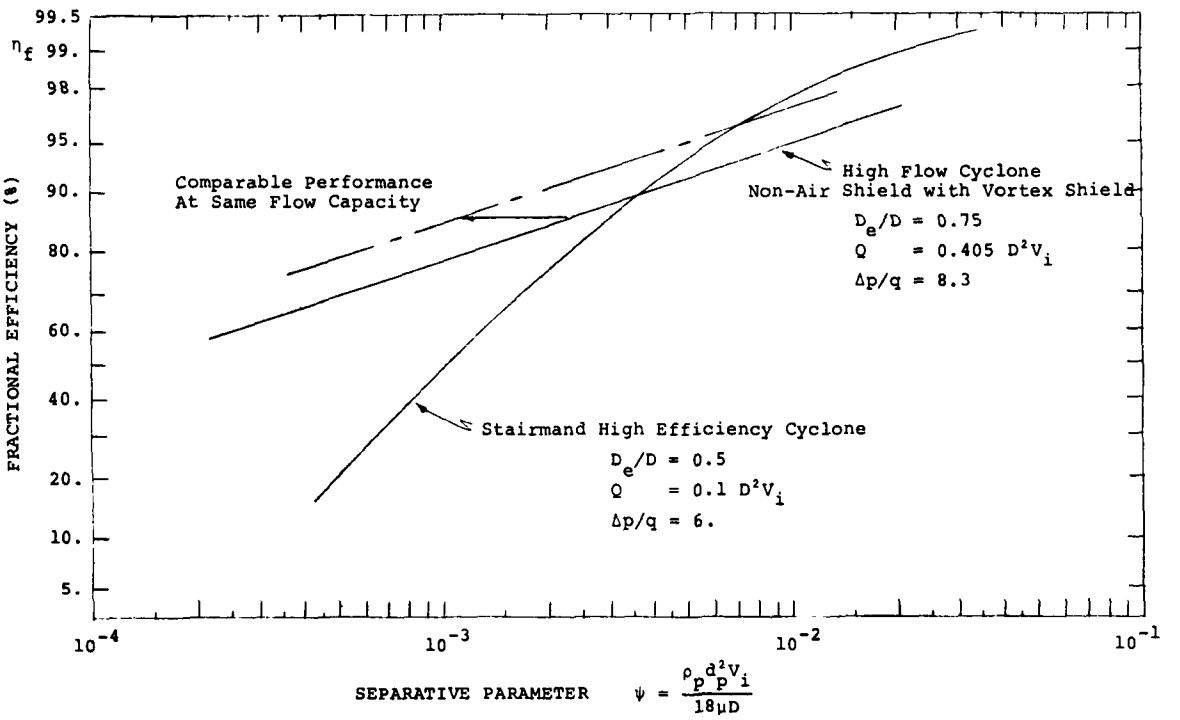

Figure 9. Low flow versus high flow cyclone performance

CONCLUSIONS

This investigation implies that typical high performance cyclone designs are inhibited in two significant areas. With small inlets and small outlets, it appears that large scale turbulence inhibits collection. The use of a large inlet contracting the flow into a relatively narrow annular region minimizes the production of large scale turbulence. Similarly, increased engagement length improves the length-to-annulus width and suppresses the turbulence that is formed. It is postulated that inlet vanes or baffling might play a similar role.

The use of air shielding is found to be an alternate means of performance improvement and is of special interest in systems that can use clean dilution gas, e.g., cyclone combustors.

The performance improvement found with the vortex shield implies that long cyclone bodies are not necessary to avoid dust reentrainment if this device is employed. This suggests that the cyclone body could be purely cylindrical with an inverted base and peripheral dust exhaust. This would result in minimizing the swirl velocity and the radial pressure gradients in the vicinity of the dust exhaust.

Contrary to conventional wisdom, it was found that increased vortex spin-up did not improve collection with the high flow design. It is theorized that this result is conditioned by the lack of the vortex shield during those tests, e.g., increased spin-up intensifies the propensity of the vortex to induce swirl and recirculation in the dust exhaust, which increases dust reentrainment.

Regarding analytical implications, it is noted that the importance of the inlet flow and dust reentrainment found in this investigation is not treated by present analytical models. At the present time, adequate means for analytically treating these two critical areas are not available, and continued cyclone development must be guided by experimental methods.

One area not addressed in the present work is the suppression of pressure loss. It is anticipated that significant pressure recovery could be achieved with an exhaust swirl diffuser.

SUMMARY

Empirical investigations show very substantial improvements in cyclone design by focusing on minimizing inlet turbulence scale and dust reentrainment at the dust discharge. These results indicate that a new high flow design can provide equal or superior collection with a cyclone of half the diameter of current high efficiency cyclones with some increase in pressure drop.

ACKNOWLEDGEMENT

The author wishes to acknowledge the support provided by K.E. Markel, Jr., Project Manager, Coal Projects Management Division, U.S. Department of Energy, Morgantown, West Virginia, in modifying and expanding the work scope of DOE Contract DE-AC21-80 ET 17091 whereby the above investigation was pursued.

The work described in this paper was not funded by the U.S. Environmental Protection Agency and therefore the contents do not necessarily reflect the view of the Agency and no official endorsement should be inferred.

REFERENCES

1. Leith, D. and Licht, W., "The Collection Efficiency of Cyclone Type Particle Collectors — A New Theoretical Approach," *AIChE Symposium Ser., Vol. 68, No. 126,* p. 126, 1972.
2. Giles, W.B., General Electric TIS Report No. 76CRD023.
3. Dietz, P.W., "Collection Efficiencies of Cyclone Separators," General Electric TIS Report No. 79CRD244, December 1979.
4. Boysan, F., Ayers, W.H., and Swithenbank, J., "Cyclone Design Fundamentals," University of Sheffield paper (unpublished).

5. Giles, W.B., "High Flow Cyclones for PFBC Hot Gas Cleanup," General Electric TIS Report No. 81CRD197, 1981.

6. van Tongeren, H., *Mech. Eng'r., 57,* p. 753, 1935.

7. ter Linden, A.J., "Investigations Into Cyclone Dust Collectors," *Inst. of Mech. Eng'rs., J., Proc. Vol. 160,* p. 233, June-December, 1949.

8. Stairmand, C.J., "The Design and Performance of Cyclone Separators," *Trans. Inst. Chem., Eng'rs., Vol. 29,* p. 356, 1951.

CYCLONE SCALING EXPERIMENTS

by

W. B. Giles
Mechanical Systems and Technology Laboratory
Corporate Research and Development
General Electric Company
Schenectady, New York 12301

ABSTRACT

A series of geometrically similar cyclones of conventional, high-efficiency design was tested to assess the normally accepted perception that cyclones act as an inertial collection device and therefore can be scaled from model to prototype size by an inertial separative parameter. These tests were conducted for three different cyclone sizes of 4, 12, and 36 in. diameter over a range of inlet velocity and at atmospheric pressure.

In using test dusts which had been shown to have a *low* propensity for triboelectric charging, good correlation was observed.

Tests were also conducted using a test dust which has been found to have a *high* propensity for triboelectric charging. The data does *not* correlate, has very high efficiency, and is characterized by relatively constant overall efficiency versus cyclone flow. The latter behavior is noted in several literature sources.

The critical user is, therefore, cautioned in the acceptance of data unless, as a minimum, the fractional efficiency can be shown to correlate with the inertial separative parameter over a range in velocity.

INTRODUCTION

Cyclone art and theory has evolved around the perception of an inertial-fluid mechanic mechanism of collection. The swirling gas flow induces a centrifugal force on the convected dust particles, which drives the particles to the wall, where axial convection transports the particles to the dust discharge. Thus it is expected that the ratio of centrifugal force to particle drag force, together with the geometric design, will describe the mechanics of collection. However, earlier experience (1) has shown that natural electrostatic forces can play a highly significant role in the collection efficiency of cyclones. This effect is to enhance performance, particularly at low operating velocities. As a consequence, model test data can lead to highly erroneous, and optimistic, expectations if natural electrostatics are present in the experiment.

Unfortunately much of the literature data is reported only at one test velocity, and from this it is not possible to assess whether or not electrostatic forces are operative. A review of the literature also discloses behavior which can now be interpreted as natural electrostatic enhancement. For example, Petroll and Langhammer (2) show approximately flat cyclone efficiency versus flow rate. Also Ludewig (3) notes the same effect in contradiction to expectation. He also cites the literature of ter Linden (4), Barth and Trunz (5), and Rammler and Breitling (6). Similar behavior was disclosed in discussion with Kraftwerk Union. Therefore, a significant risk can exist in data extrapolation.

The purpose of the present investigation was to investigate a geometrically similar design in three different sizes to assess the degree to which correlation of the data could be obtained.

In prior experiments, it was found that the phenomenon of natural electrostatic enhancement was due to triboelectric charging of the dust particles brought about by particle-wall impact. Specifically, a Faraday cage was used to measure the induced test dust charge level, as shown schematically in Figure 1. In this arrangement, gas borne dust is admitted, enshrouded by clean air. The Faraday cage then detects the image charge present in the plume, and optic equipment (not shown) is used to measure dust concentration. In this manner, the charge level per particle can be determined. It was noted that if dust was admitted directly from the fluid bed dust generator, the charge density was low. However, by using a long

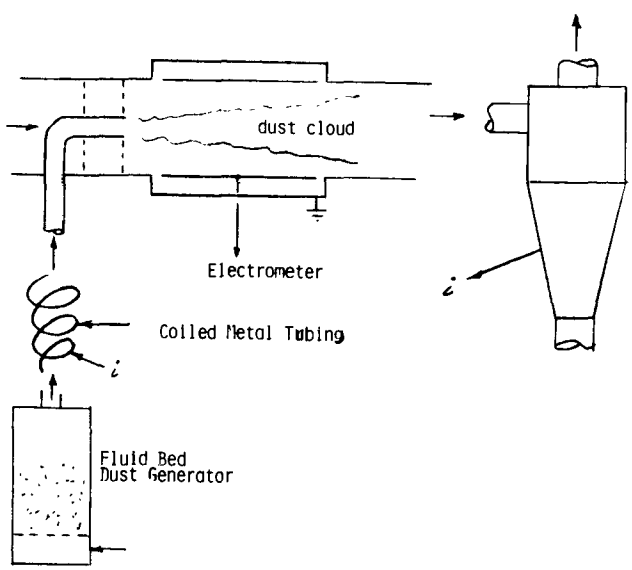

Figure 1. Faraday cage experiment

length of coiled metal tubing to ensure particle-wall impact, it was found that the charge level of PFB test dust from Exxon's Miniplant facility in Linden, New Jersey, was two orders of magnitude higher than PFB test dust from the National Coal Board Coal Utilization Research Laboratory (CURL) at Leatherhead, England. Furthermore, it was noted that the current flux into the dust was comparable to the current flux from a collecting cyclone. Therefore, it is expected that particle charging can occur internal to the cyclone given the right combination of materials, and that this accounts for the extreme difficulty in eliminating the effect, if present.

The mechanism of efficiency enhancement is theorized to be due to the mutual repulsion forces of the resulting space charge.

It was also found that electrostatics can play a major role in sampling error. If the sampling probe for particle analysis is electrically insulated from the transport dust, the probe becomes charged with very high gradients at the probe intake. This drastically reduces sample counts and shifts the size distribution (7).

With these facts in mind, CURL flyash was selected as the principal test dust and the sampling probes were grounded to avoid the anomalies of electrostatics.

TEST MODEL

The design selected for study consisted of a Stairmand (8) high-efficiency cyclone modified by use of a four-point scroll inlet. The inlet flow capacity is characterized by

$$Q = 0.1\ D^2\ V_i$$

with a pressure loss of 5.29 inlet kinetic heads. This design selection was based on its prominence in the literature and its similarity to the work of ter Linden, van Tongeren, and others so as to be representative of the state of the art. Three sizes were manufactured and tested at 4, 12, and 36 in. diameter, as shown in Figure 2.

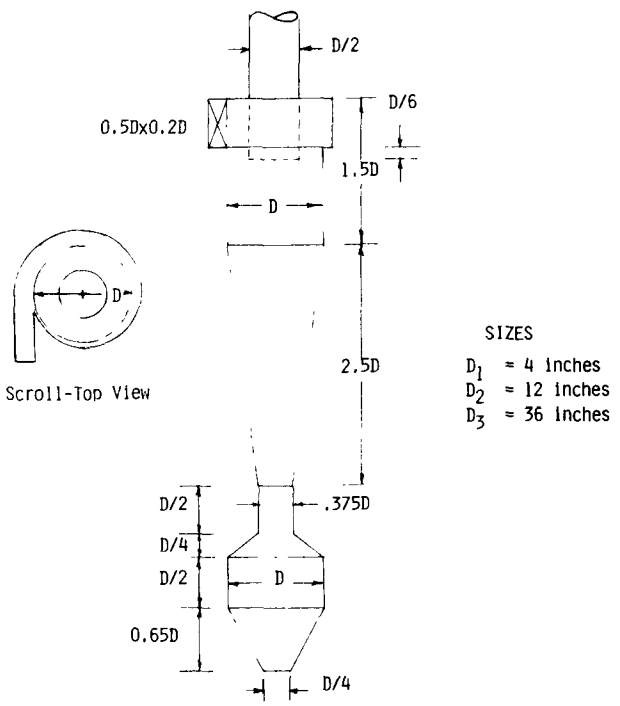

Figure 2. Test model design: Stairmand high-efficiency with four-point inlet scroll

SCALING PARAMETER

These experiments sought to assess the validity of the inertial separative parameter, Ψ, given as the ratio of centrifugal force to the Stokes drag force, or

$$\Psi = \frac{\rho_p \, d_p^2 \, V_i}{18\mu \, D}$$

where ρ_p is the particle density, d_p is the particle diameter, V_i is the average inlet velocity, μ is the absolute viscosity, and D is the diameter of the cyclone. The collection efficiency measurements are, therefore, correlated as overall efficiency, η_o, or fractional efficiency, η_f, versus Ψ. All of the parameters were varied except that of gas viscosity.

TEST PROCEDURE

These experiments consisted of blowing prefiltered room air at atmospheric conditions through the cyclone. A fluid bed dust generator was used to contaminate the supply air at relatively dilute dust loadings, several pipe diameters upstream of the test cyclone. Typical dust distributions are shown in Figure 3.

The performance of the units was determined through optical measurements of inlet-outlet dust loadings and inlet-outlet size distribution. PILLS V Mass Concentration Monitors[1] were mounted with optic windows (purged ducts at right angles to the flow) and used to determine inlet-outlet dust loadings. Particle size analysis was performed using two Climet Particle Systems.[2] The flow was sampled isokinetically and vacuum pumped through the instruments. To avoid coincidence errors with this equipment, dilution of the sample flow stream was required. A specially developed General Electric sampling system was employed to provide the functions of isokinetic sampling, flow measurement, dilution, and matching to the Climet systems. Finally, calculations converted this primary data into the form of fractional efficiency.

Measurements of cyclone pressure loss, from inlet to ambient, were also taken and normalized by inlet kinetic head, $1/2 \, \rho \, V_i^2$, based on average inlet velocity.

TEST RESULTS AND DISCUSSION

The test results of the 12 in. diameter model for different inlet velocities are shown in Figure 4 for the CURL flyash and Figure 5 for nickel powder. The data for the 36 in. diameter model is shown in Figure 6 for CURL flyash. The data set for the 4 in. diameter model is shown in Figure 7 for CURL flyash and Figure 8 for nickel powder.

A composite of all of the fractional efficiency data is shown in Figure 9, exclusive of the nickel data in the 4 in. diameter cyclone. Figure 10 shows a composite of the overall efficiency data of all of the above tests.

In general, it is noted that there is good correlation of the fractional efficiency data within the context of the experimental scatter. This indicates that inertial collection is clearly the dominant mechanism.

Inspection of the nickel data of the 4 in. cyclone, Figure 8, shows a marked lack of correlation. Efficiencies of the higher velocity test conditions, > 20 ft/sec, are markedly lower than similar data with flyash, Figure 7. It is theorized that this indicates a problem with particle bounce that is not scalable via the separation parameter.

[1] Manufactured by Environmental Systems, Inc., 200 Tech Center Drive, Knoxville, Tennessee 37917.

[2] Manufactured by Climet Instruments Company, 1320 W. Colton Avenue, Redlands, California 92373.

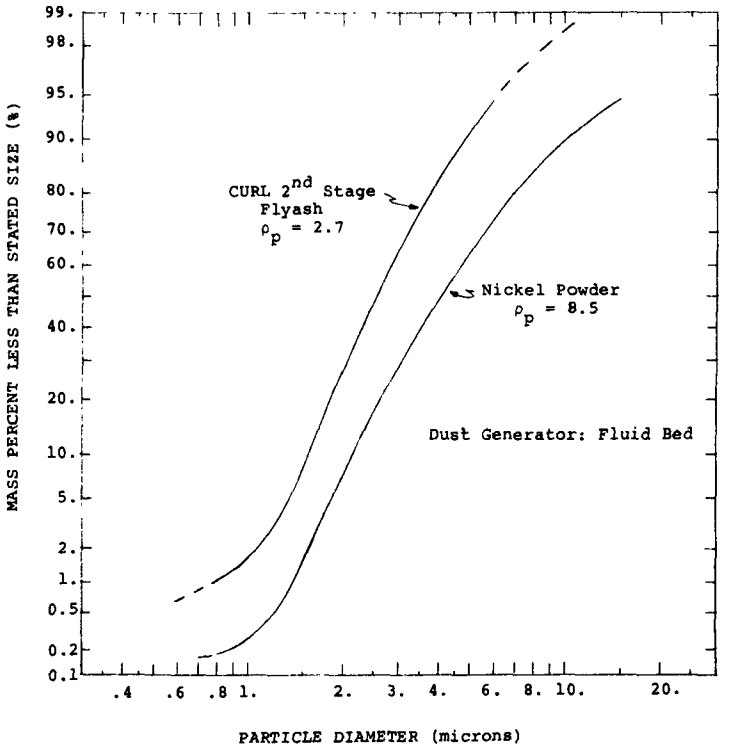

Figure 3. Typical test dust distributions at cyclone inlet

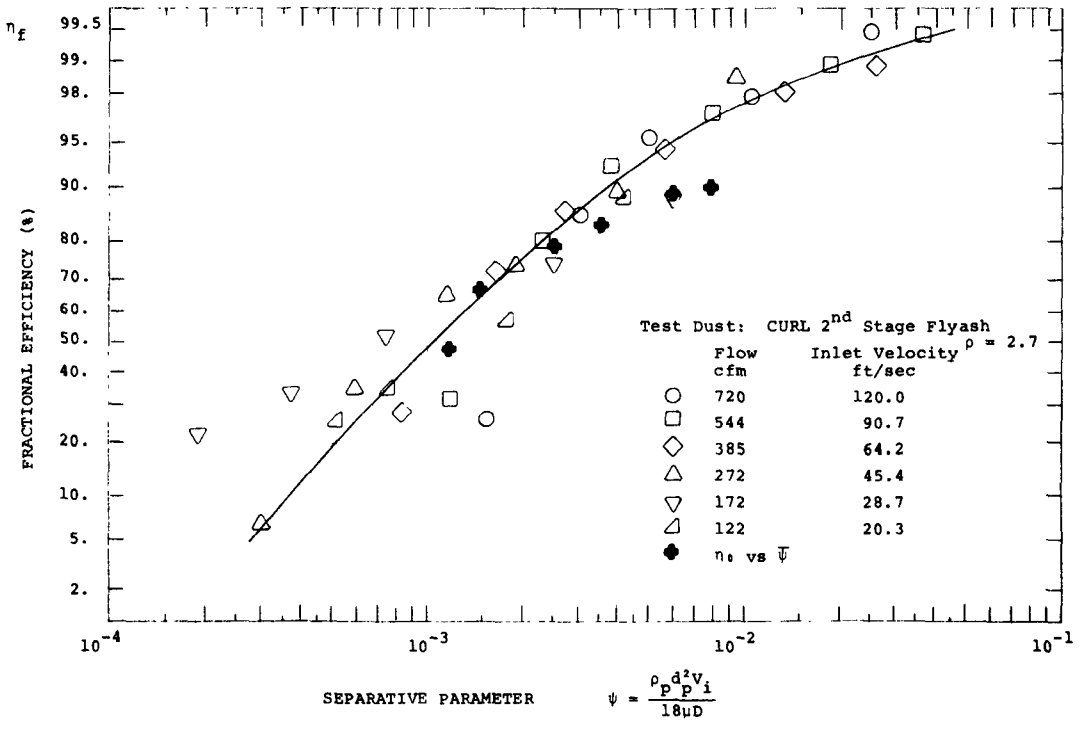

Figure 4. Fractional efficiency versus separative parameter for 12 in. diameter high-efficiency cyclone

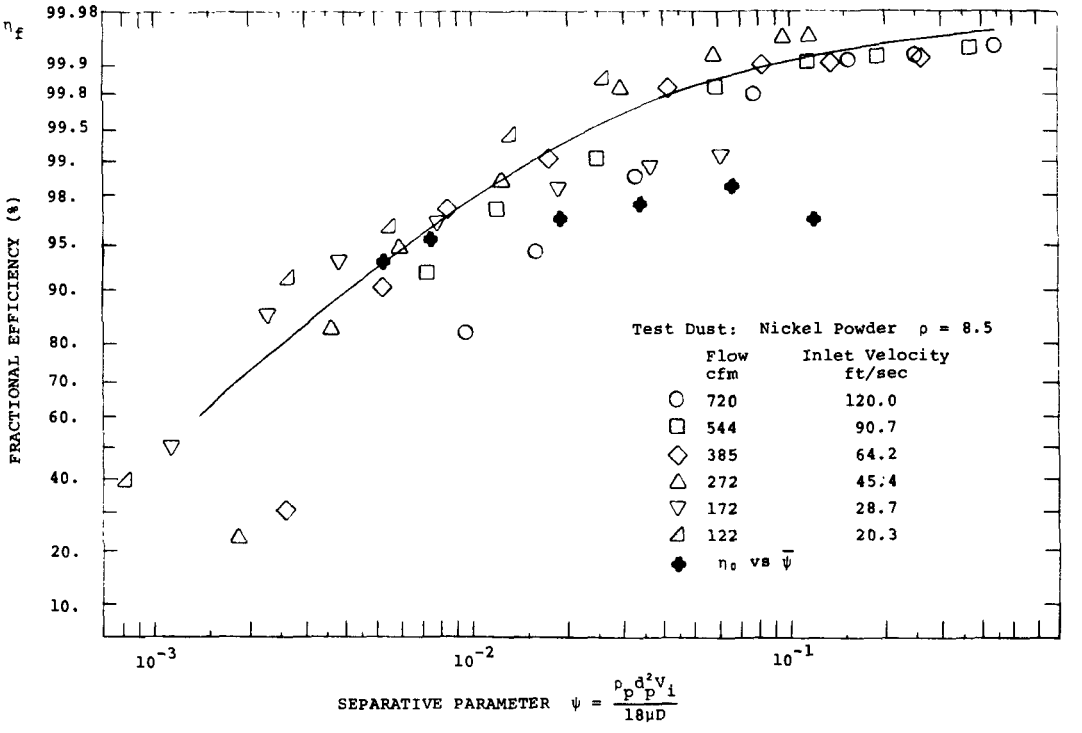

Figure 5. Fractional efficiency versus separative parameter for 12 in. diameter high-efficiency cyclone

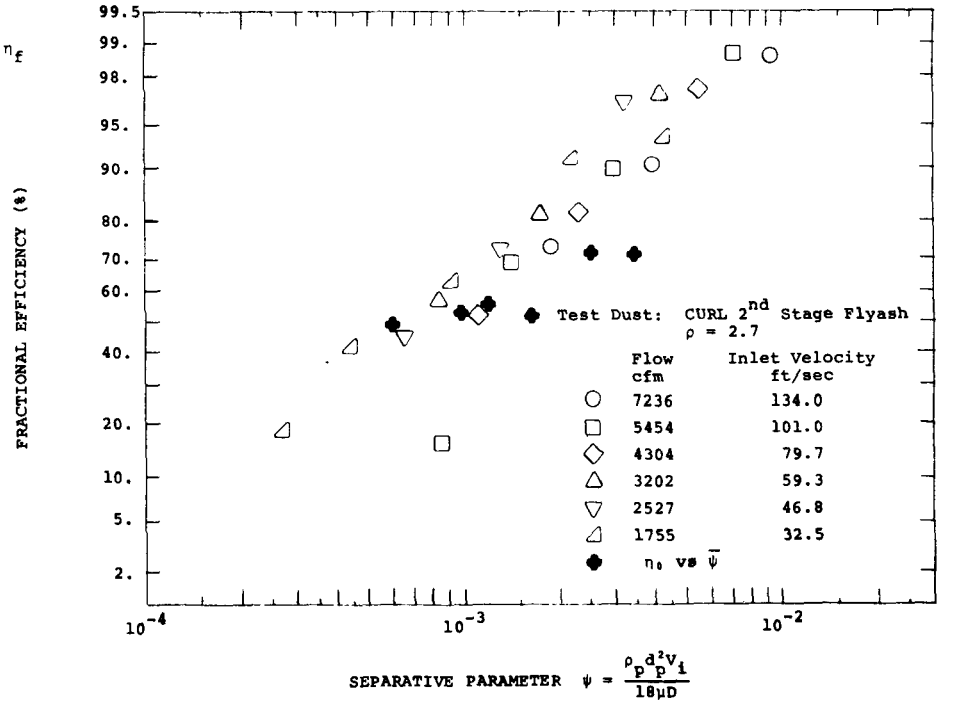

Figure 6. Fractional efficiency versus separative parameter for 36 in. diameter high-efficiency cyclone

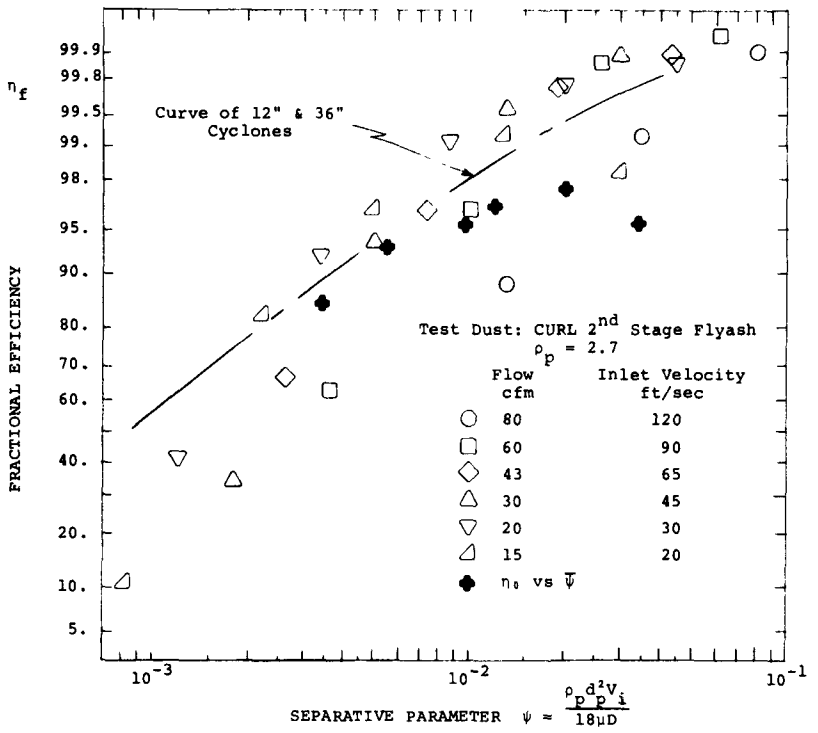

Figure 7. Fractional efficiency versus separative parameter for 4 in. diameter high-efficiency cyclone

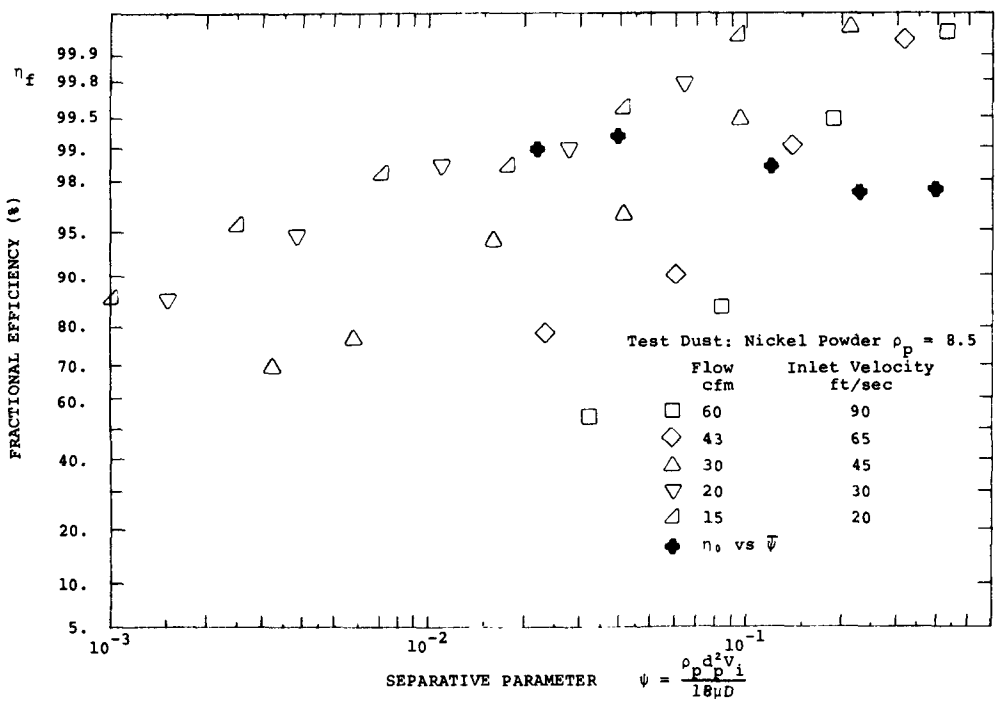

Figure 8. Fractional efficiency versus separative parameter for 4 in. diameter high-efficiency cyclone

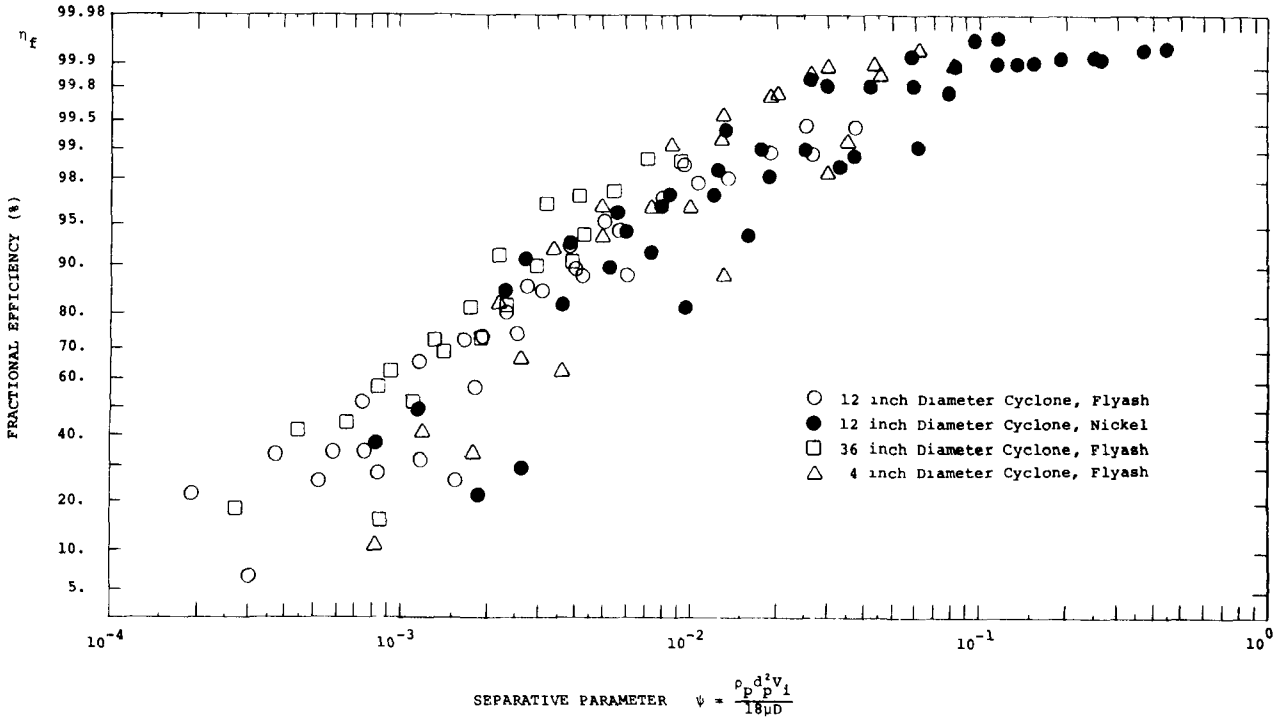

Figure 9. Fractional efficiency versus separative parameter for high-efficiency cyclone

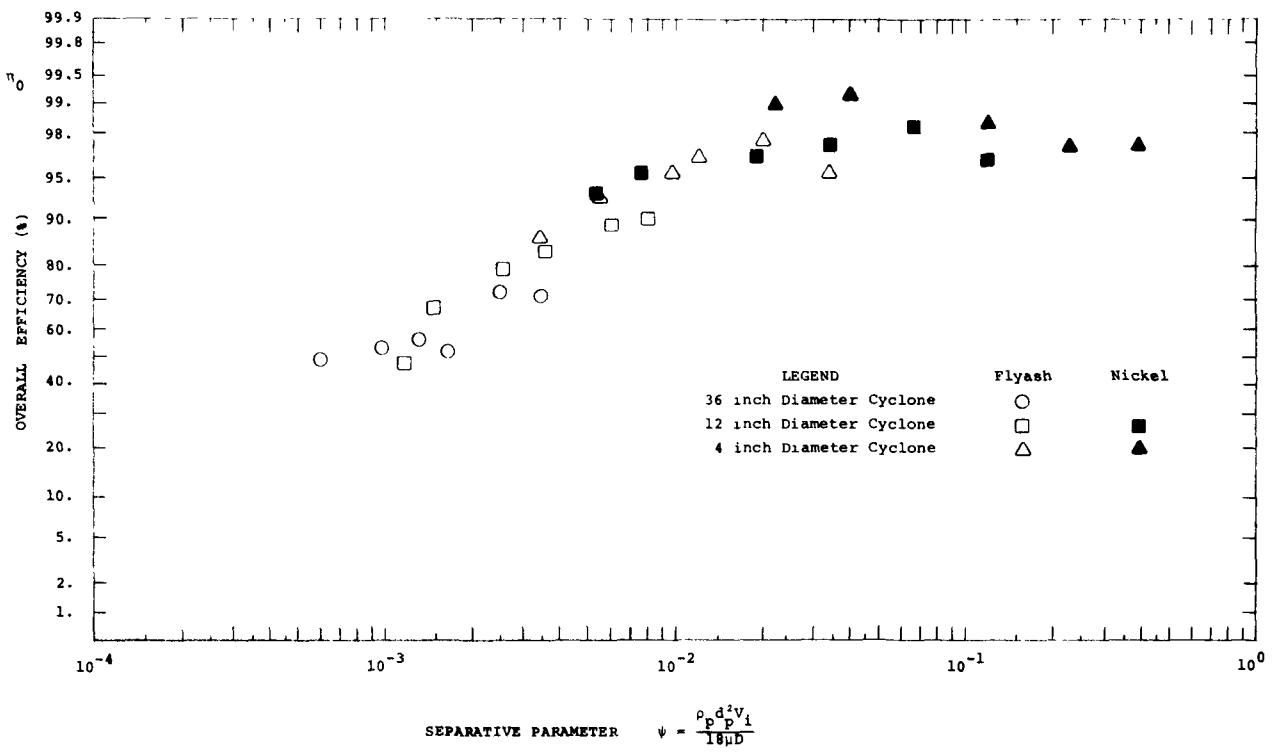

Figure 10. Composite of overall efficiency measurement of high-efficiency scaling cyclones

As noted previously, the direct measurements consist of overall efficiency plus input-output size analysis. From these measurements, the fractional efficiencies are computed. It follows that the variance that is evident between fractional and overall efficiencies (see Figures 4-8), particularly at the higher test velocities, is a direct consequence of the relatively steep slope of the fractional efficiency characteristic and the polydispersed nature of the test dust.

The final criterion of performance is, of course, the fractional efficiency. For example, the data of overall efficiency versus separative parameter, Figure 10, suggests that the particle bounce mechanism is scalable. Here the data suggests a continuous, universal curve. This suggestion, however, is belied by the fractional efficiency data of Figure 8 with nickel. This discrepancy shows that the data does not correlate with the separative parameter and indeed indicates that some other nondimensional group is required to correlate this phenomenon.

Testing with Exxon flyash, Figure 11, shows an extreme lack of correlation over the whole velocity range. The test dust has a known propensity toward charge generation, and the efficiencies at low velocity are significantly higher than the corresponding data for CURL flyash, Figure 7, except for the highest test velocity. It is concluded that triboelectric particle charging is playing a major role in collection and that this data is not scalable.

Therefore, in order to validate model test data, experiments must be conducted over a range in test velocity to demonstrate correlation. If reasonable agreement is found, inertial scaling can be employed to provide a conservative estimate of prototype performance. Unfortunately, if correlation is not found, methods must be found to eliminate, control, and/or quantify the relevant phenomena.

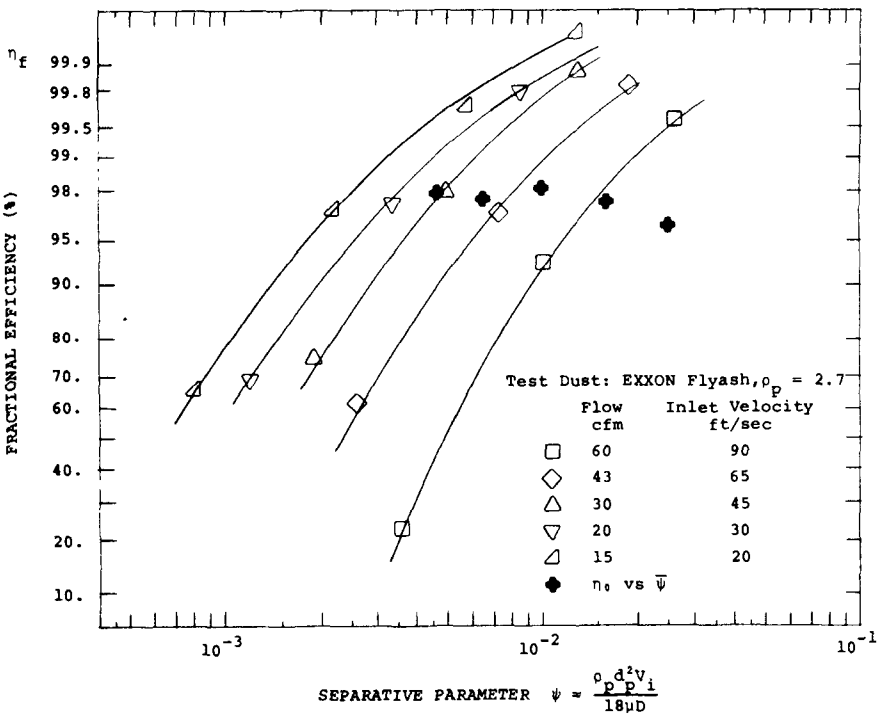

Figure 11. Fractional efficiency versus separative parameter with 4 in. diameter high-efficiency cyclone

Pressure loss measurements of the three units were normalized with inlet kinetic head, q = 1/2 ρV_i^2, and are shown in Table 1 in comparison with the reported value by Stairmand (8). The results are found to be self-consistent and 11% higher than reported by Stairmand. This is not considered a significant effect. Difference in pressure tap location could account for the discrepancy.

TABLE 1

Pressure Loss Coefficients (Inlet to Ambient)

Stairmand	$\Delta p/q = 5.3$
Scaling Cyclones	
4 inch model	$\Delta p/q = 5.7$
12 inch model	$\Delta p/q = 6.0$
36 inch model	$\Delta p/q = 5.8$

CYCLONE DATA COMPARISON

Figure 12 compares the present data against other sources of evaluation on high-performance designs. All have similar flow capacities, long cyclone bodies, and relatively small exhaust-to-barrel diameter ratios, D_e/D. The Buell[1] unit is basically similar to a van Tongeren design. It is noted that the present data is significantly higher than the data reported by Stairmand (8), whereas the recent data by CURL on a van Tongeren cyclone (9) is significantly lower than its generic data base.

Conventional theory argues that smaller exhaust-to-barrel ratio would, by the conservation of angular momentum, result in higher flow spin-up and hence provide higher particle centrifugal forces and superior collection. The relative agreement evident between the present GE data and the CURL data suggests that there is little, if any, advantage in the higher spin-up of the van Tongeren design ($D_e/D = 0.30$). The van Tongeren or Buell design does have a higher pressure loss coefficient of $\approx$ 7.7 inlet kinetic heads, versus $\approx$ 5.9 for the Stairmand design. Parallel studies of an improved high flow design (10) also found that increased spin-up did not enhance performance as would normally be expected. A possible explanation is that the advantages of higher flow spin-up are offset by the increased vortex strength inducing high reentrainment at the dust discharge. An alternate hypothesis, in the present case, is that large-scale turbulence at the inlet inhibits performance.

TRIBOELECTRIC CHARGING

To further explore the influence of natural electrostatic enhancement, as noted in the 4 in. diameter model, testing of the 12 in. diameter was conducted with Exxon flyash. These results are shown in Figure 13. Again, the data with Exxon flyash show significantly higher collection efficiency and lack of correlation, relative to the CURL flyash data. The latter is shown transposed for comparison. For example, at $\Psi = 10^{-2}$, the collection efficiency is increased from $\approx$ 97% to $\approx$ 99.5%, a four-fold reduction in penetration due to electrostatic effects. It is also noted that the high velocity performance loss is not evident with this model as was seen with the 4 in. model. Apparently the bouncing mechanism is strongly dependent on cyclone size.

[1] Now GE Environmental Systems, Inc., Lebanon, Pennsylvania.

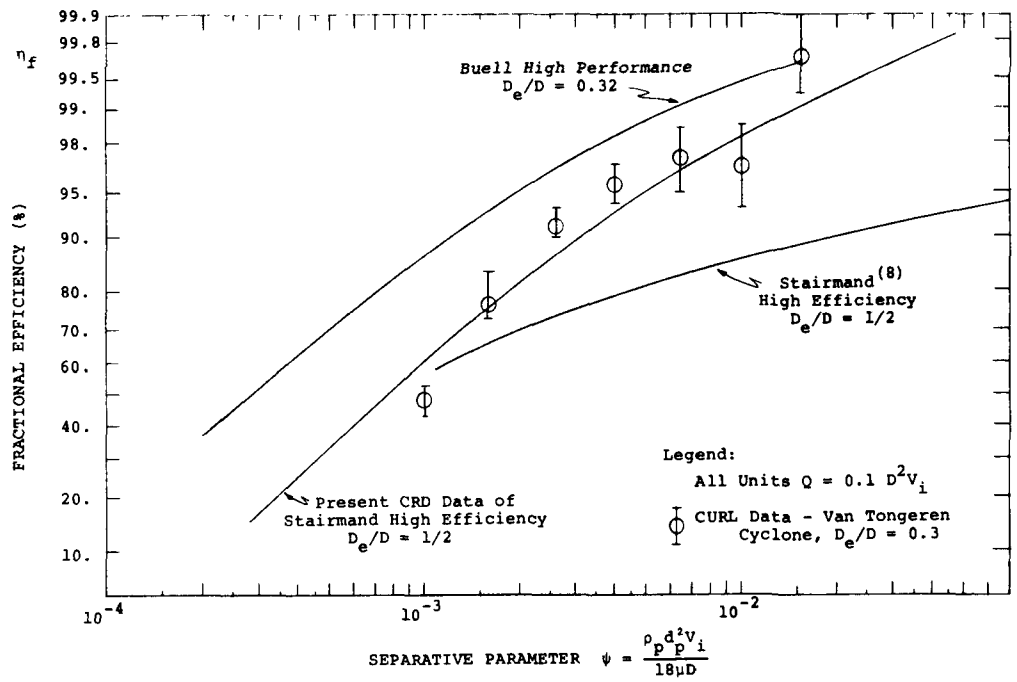

Figure 12. Comparison of high-performance cyclone data

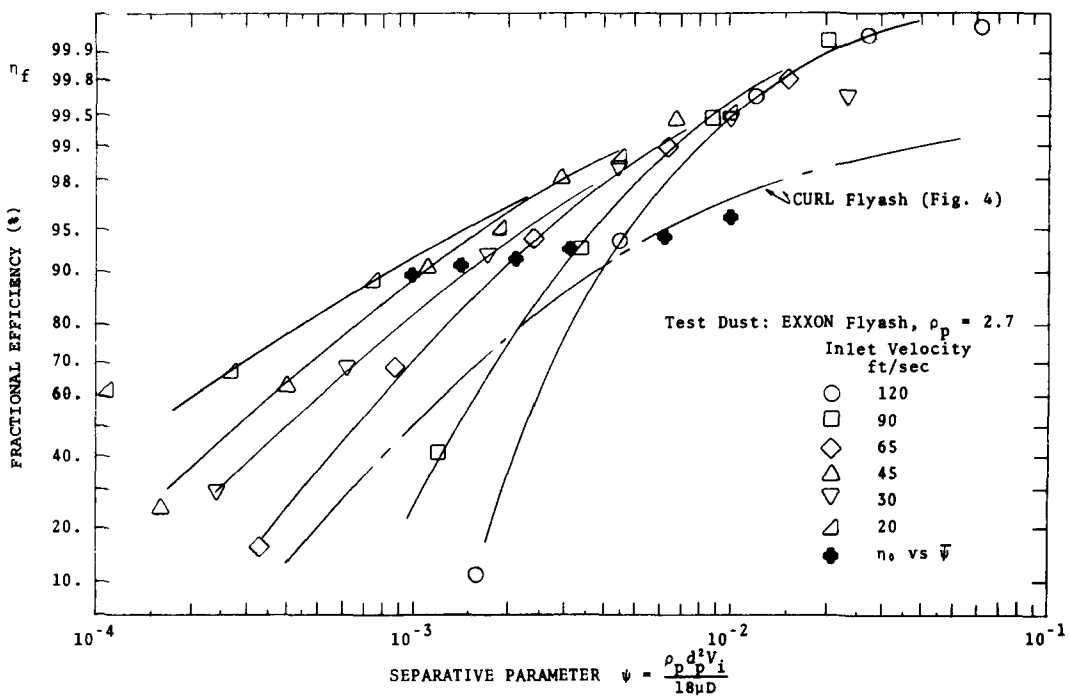

Figure 13. Fractional efficiency versus separative parameter for 12 in. diameter model

SUMMARY

It was found that the cyclone performance may or may not correlate with a simple inertial separation parameter. On one hand, parametric variations of 9 to 1 in cyclone diameter, 3 to 1 in particle density, 5 to 1 in velocity, and 6 to 1 in particle size can show good correlation, and hence data from model tests can be used to project prototype performance. On the other hand, extreme variations can exist if other phenomena are operative. The most convenient, and necessary, means of validation is to conduct experiments over a range of velocities.

Phenomena can exist that prohibit scaling from model test conditions to prototype operation. Triboelectric charging tends to enhance performance and particle bouncing tends to degrade performance. Both can produce large effects and both are poorly defined, thus *a priori* determination of the probability of these phenomena is not available. Present indications are that the condition of particle bounce may be restricted to the use of very small cyclones and high velocities. The effects of triboelectric charging are perhaps much more insidious. A literature review suggests that anomalous behavior in many experiments can now be rationalized, and, unfortunately, much of the literature must be treated with considerable skepticism.

ACKNOWLEDGMENT

This work was supported by NYS ERDA, under Contract No. 344-ET-FUC-81, through the sponsorship of General Electric's Energy Systems Programs Department. General Electric's Corporate Research and Development provided the test models.

The work described in this paper was not funded by the U.S. Environmental Protection Agency and therefore the contents do not necessarily reflect the view of the Agency and no official endorsement should be inferred.

REFERENCES

1. Giles, W. B. Electrostatic separation in cyclones. *In* Symposium on the Transfer and Utilization of Particulate Control Technology, EPA-600/7-79-044C, Vol. 3, February 1979, p. 291.

2. Petroll, J. and Langhammer, K. Comparative tests on cyclone precipitators. *In* Freiberger Forschungsheft, Vol. A220, 1962, pp. 175-196.

3. Ludewig, H. Cyclone model experiments regarding the effect of the dip pipe depth on separating efficiency and pressure drop. *In* Maschinenbantechnik, Vol. 7, No. 8, 1958, pp. 416-421.

4. ter Linden, A. J. Investigations in cyclone separators *In* VDI Seminar, Vol. 3, 1954, VDI Verlag.

5. Barth, W. and Trunz, K. Model test with water stream cyclone separator for predetermining removal efficiency. Z. F. Angew, Math and Mech., Vol. 30, No. 8/9, 1950.

6. Rammler, E. and Breitling, K. Comparative tests with centrifugal separators. *In* Freiberger Forschungsheft, Vol. A56, 1957.

7. Giles, W. B. and Dietz, P. W. Electrostatic effects on sampling through ungrounded probes. Second Symposium on the Transfer and Utilization of Particulate Control Technology, EPA-600/9-80-039D, Vol. 4, September 1980, p. 387.

8. Stairmand, C. V. The design and performance of cyclone separators. Trans. Inst. Chem. Engrs., Vol. 29, 1951, p. 356.

9. Advanced cleanup device performance design report (Task 4.3) - Volume A - Cyclone theory and data correlation of PFB CFCC Development Program. U.S. DOE DE-AC21-76ET10377, Dist. Category VC-90e, FE-2357-70, pp. 3-34.

10. Giles, W. B. High flow cyclone development. GE Report, to be published.

TEST METHODS AND EVALUATION OF MIST ELIMINATOR CARRYOVER

by: Vladimir Boscak, Atef Demian
General Electric Environmental Services, Inc.
200 North Seventh Street
Lebanon, Pennsylvania 17042

ABSTRACT

A test program was carried out at GEESI's R&D pilot plant to determine mist eliminator efficiency, carryover load and droplet size distribution from a vertical flow mist eliminator. The modified EPA Method 5 was used to determine efficiency and carryover load. The carryover load when the scrubber was operated under standard operating conditions but without mist eliminator washing was 28 to 60 mg/Nm^{3}D (0.012 to 0.024 gr/SCFD). When the bottom of the mist eliminator was washed, the carryover load above the washed section was 70 to 160 mg/Nm^{3}D (0.029 to 0.066 gr/SCFD). Mist eliminator efficiency was greater than 99%. A droplet photography technique was used to determine carryover aerosol size distribution. The average aerosol size measured above the mist eliminator was about 100 to 200 microns. Mist eliminator inlet size distribution averages about 140 microns. The carryover is probably caused by re-entrainment from the mist eliminator blades.

INTRODUCTION

Wet scrubbing flue gas desulfurization systems utilize mist eliminators to separate and remove scrubbing-liquid droplets (aerosols) contained in the flue gas. Baffles or chevron elements remove aerosols by inertial forces (1). Aerosol removal is needed to prevent carryover of suspended solids, dissolved salts and liquid to the stack as well as to avoid incrustation and corrosion of downstream system components.

There are two principal mist-eliminator configurations: horizontal gas flow and vertical gas flow types. The vertical flow arrangement has been regularly used in this country while the horizontal flow type is more common in Japan and Germany. Vertical flow eliminators generally use the chevron type design which incorporates continuous zigzag baffling comprising 2 to 6 passes. This design is favored for strength, low gas pressure drop and cost considerations. Typical design of the mist eliminator has vane spacing of 1.5 to 3.0 inches, plastic construction is most common, and wash systems typically operate intermittently to conserve plant water (2). EPRI's review of commercial FGD operating experience lists plugging/scaling, erosion, corrosion and inefficient performance of mist eliminators as detracting from high operability (3).

OPERATING EXPERIENCE WITH MIST ELIMINATORS

When aerosols entrained in flue gas are not removed in the mist eliminators, a number of problems may arise:

High particulate emission exiting stack
Deposition in ductwork and stack
Corrosion of ductwork and stack
"Rain" around stack
Corrosion - erosion of gas-gas heat exchanger
(when used for reheat)

One of the major reasons for mist eliminator operating problems in early FGD installations was insufficient understanding of FGD process chemistry. Poor performance of mist eliminators was a direct result of fouling of baffles causing upset of design for flow conditions. The fouling was a consequence of deposition of soft solids as well as formation of hard scale from precipitation of solids from a $CaSO_4$ - supersaturated liquid.

Four-pass chevron type mist eliminators are used in General Electric Environmental Services, Inc. (GEESI) FGD installations. The advantages of this mist eliminator includes a high efficiency, low pressure drop and ease of cleaning. This type of mist eliminator has been successfully used in most of GEESI's full-scale installations.

One of the problems in cleaning of mist eliminators is limited amount of available water. Occasional plugging, excessive aerosol carryover and deposition has been reported at FGD installations. The causes of the problems

were, however, traced down to operating changes like above design boiler load, overwashing of the mist eliminators, faulty valves and use of poor quality washing liquor frequently with high sulfate content.

The performance of GEESI's mist eliminators has been evaluated both on pilot and full-scale units. Figure 1 shows a full-scale mist eliminator and wash spray banks for sequential washing (4).

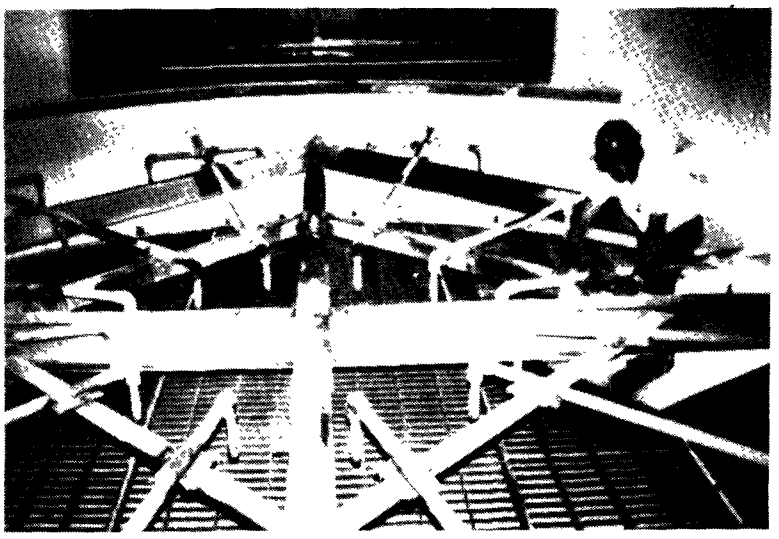

Figure 1. Mist Eliminator and Wash Spray Bank

The evaluation of a domestic full-scale unit by an independent testing laboratory indicated that mist eliminator efficiency was high even in removing submicron dust. The carryover load was reported to be in the range of 0.014 to 0.033 gr/SCFD (34-80 mg/Nm^3D). Another overseas installation reported higher carryover loads but results are somewhat doubtful because of non-isokinetic sampling technique and use of Ca tracer. In second overseas evaluation a pilot mist eliminator carryover particle size distribution was determined using a combination of cascade impactor, MgO-impactor and proprietary paper impactor, but results were inconclusive.

Since there are some reservations about the best method for measuring carryover testing GEESI decided to perform tests on a pilot unit. The same mist eliminator that is employed in a full-scale installation is installed in the pilot unit.

OBJECTIVES

The general purpose of the mist eliminator test program was fourfold:

(1) Determine the best method for mist eliminator efficiency under standard operating conditions.

(2) Measure aerosol carryover (load) during and without washing.

(3) Determine carryover droplet size distribution.

(4) Evaluate applicability of modified EPA method 5 and droplet photography technique for a full-scale mist eliminator test.

FLUE GAS DESULFURIZATION PILOT PLANT

The GEESI wet FGD pilot plant is located in Lebanon, PA. It consists of a spray absorber (3 feet diameter), recycle tank, thickener, drum filter, pumps and fan. The bottom of the spray tower (8 feet diameter) serves as a delay tank from which scrubbing media is recycled to the spray absorber. Figure 2 shows FGD pilot plant's spray absorber. Five hollow cone spray nozzles are used for atomization of scrubbing media in a spray absorber. The nozzles spray angle at pressure of 20 PSIG is 54° at 3 feet vertical distance from nozzle orifice and the arithmetic mean droplet size of a slurry is about 2000 microns.

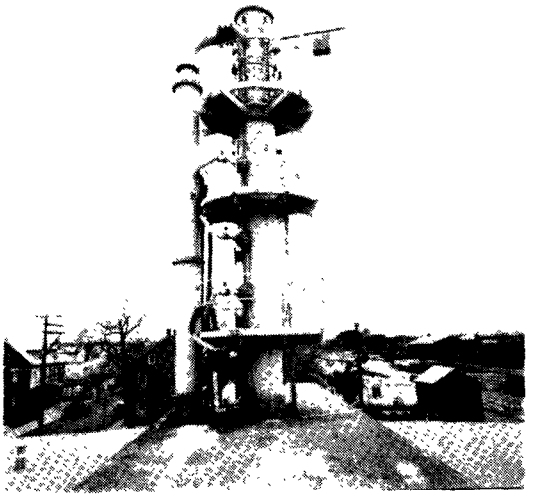

Figure 2. FGD Pilot Plant Spray Absorber

An open chevron type mist eliminator is located at top of absorber to remove entrained slurry droplets from the gas stream. It consists of four polypropylene single vane blades arranged to form an open design, four pass unit. Mist eliminator wash system consist of six spray nozzles positioned in the center of six equal areas on the bottom and another six identical nozzles on the top of mist eliminator. These wash spray nozzles when operated under standard conditions generate droplets in the range of 525 to 770 microns.

Hot flue gas from an oil fired furnace is mixed with atmospheric air and passed through absorber where it is scrubbed with liquid media. Gas then proceeds through the mist eliminator where entrained aerosol is removed prior to discharge to the atmosphere. Desired levels of SO_2 is achieved through addition of SO_2 from storage cylinder.

The pH of the recirculating slurry is maintained at preset value either by pH controller which controls the addition of lime (or limestone) to the system or by feeding lime/limestone continuously at certain rate. To maintain the material balance, a small portion of slurry is bled from the recycle system and disposed of after dewatering in a hydroclone/vacuum filter combination. The filtrate from the dewatering system is recycled.

CARRYOVER TEST METHODS

After a thorough review of test methods suitable for carryover evaluation it was decided to use a modified EPA method 5 for carryover load measurement and droplet photography for aerosol particle size distribution determination.

MODIFIED EPA METHOD 5

A modified EPA Method 5 sampling train was used to extract gas from the stack for carry-over load measurements. In this train, a stainless steel sampling nozzle of an appropriate diameter is connected to a stainless steel probe by Swagelok fittings. An S-type pitot tube and thermocouple are incorporated into the probe to measure gas velocity, pressure, temperature and temperature of the probe. The probe is heated to prevent condensation. The major distinction of modified from standard EPA Method 5 is that filter is not used in the sampling train. A glass cyclone is contained in heated sample box and the probe is connected to the cyclone inlet by leak-free glass fitting and the cyclone outlet is connected to the impingers by L-type glass connector. Greenburg-Smith type impingers are used in the impinger assembly. Four impingers are connected in series with leak-free glass fittings. The second impinger has a standard Greenburg-Smith tip, the other tips are modified by replacing the standard tip with 1/2 inch inner diameter glass tubing extending to within 1/2 inch of the flask bottom. The first and second impingers each contained 100 ml of de-ionized water, the third is empty and the fourth contain known weight of silicon gel. These four impingers was kept in an ice bath. A thermometer is placed at the outlet of the fourth impinger for monitoring purposes.

From the fourth impinger the extracted gas stream flowed through a sample line, vacuum gauge, a vacuum pump and a dry gas meter. A calibrated orifice completed the train and was used to measure instantaneous flow rates. The dual manometer across the calibrated orifice is used to measure pressure drop. During the test all the parameters such as sampling time, temperature, dry gas meter reading, pressure, etc., at each traverse point are recorded.

Velocity pressure is measured continuously and adjusted to maintain isokinetic rate. Initial and final leak tests are performed on the sampling train prior to sampling and upon completion of each test. At the end of the test the nozzle, sampling probe and connecting tubes to the impinger are washed and then wash liquor is added later to the impingers liquid. The volume of water in each impinger is measured and recorded on the data sheet. The combined liquid is kept for chemical analysis.

CHEMICAL ANALYSIS PROCEDURE

Combined wash water and impingers liquid is adjusted to 500 ml through addition of deionized water.

Initial and final recycle slurry samples (before sampling and upon completion of each test) are filtered and diluted with deionized water to desired volume.

All samples are analyzed for chloride using volumetric analysis (Mohr method).

Sodium and lithium are analyzed by flame atomic absorption (AA) technique. Sodium is analysed at 589.0 nm wave length, while lithium is analysed at 670.8 nm. In case of lithium the samples are concentrated by evaporation prior to analysis since concentration is below method's sensitivity.

In analysis of chloride, sodium and lithium it is assumed that all species are present in the liquid in ionic form and the concentrations in carryover are the same as in the slurry or wash liquid. When mist eliminator wash liquid is labeled with sodium or lithium, the concentration of this component in recycle slurry inadvertantly increase during the test. Consequently a correction is made in concentration calculation to distinguish between contributions from slurry and wash liquid. Another correction is made to adjust for presence of these species in the deionized water.

DROPLET PHOTOGRAPHY METHOD

This method employs an automated 35 mm camera tied into a drive unit, optical source and ultrahigh speed strobe unit to determine droplet particle size distribution. The optic source and the strobe unit are located opposite to the camera. Photographs are taken when the droplets passed through the slit between the camera and the optic source.

The negatives are developed and the droplet size is determined using proprietary analytical technique.

Figure 3. Two Aerosols in a Typical Photograph for Droplet Photograph

Droplet photography method has been used before for mist eliminator evaluation and is considered an adequate method for determination of droplet size distribution (5).

EXPERIMENTAL PROCEDURES

During mist eliminator carry-over study the pilot unit was operated under standard operating conditions with gas velocity of about 10 ft/s and L/G about 50. In the preliminary tests the unit was operated with gas recycle and results were widely scattered. This was attributed to distorted gas flow pattern above mist eliminator. A distorted flow pattern of flue gas is unique to pilot plant where gas recycle is used and would not be encountered in a commercial unit. Once the top of the tower was opened and unit was operated on a once through basis the gasflow distribution improved but was still somewhat skewed because of mist eliminator blades' angle. Measurement of gas flow distribution below the mist eliminator indicated rather uniform flow pattern. Two tests without mist eliminator wash were performed using three 120° traverses dictated by the absorber sampling ports.

The tests with mist eliminator wash were performed at a single sampling point (above wash nozzle in operation) with close to average gas velocity. The reason for this sampling procedure was the irregular coverage of mist eliminator with wash liquid which would prevent representative sampling if a traverse was used. Consequently, carry-over loads in these tests apply only to the mist eliminator areas covered by washing liquid. In two tests with wash the spray liquid was labeled with chloride while wash water was labeled with sodium.

Final two tests were carried out with washing but both spray and wash liquid were labeled with same conc. of chloride so that only total carry-over could be established. The total sampling time in all above tests was about one hour. No carry-over tests with top wash nozzles in operation was carried out, because the sampling was not possible.

Droplet photography tests consisted of four runs. The first traverse was carried out above mist eliminator perpendicular to the blades without wash. The second run was under the mist eliminator. The third run covered an off center traverse with and without the wash. The final test was at the selected points (velocity of about 10 fps) with and without the wash.

RESULTS AND DISCUSSION

PRELIMINARY TESTS

In preliminary tests, correlations between mist eliminator operating parameters and its pressure drop as well as percent coverage with liquid at the top were established. Table 1 shows influence of gas velocity, spray absorber L/G ratio and mist eliminator wash rate on pressure drop. Only one bottom wash nozzle was operated in these tests. The wash rate was increased from 0 to 2.5 gpm during runs at constant gas velocity and L/G ratio. The major finding of these tests was that mist eliminator pressure drop is primarily a function of gas velocity, L/G and wash rate have negligible effect. As the gas velocity is increased from 7 to 10 fps the pressure drop doubles.

Visual observation of liquid coverage on the top of mist eliminator indicate that under standard operating conditions without wash the top remains dry. Only occasional droplet emerges from mist eliminator. If droplet is large it falls back while if it is small it remains airborne and leaves the absorber. When wash takes place the top of the mist eliminator becomes wet and more droplets emerge as the wash rate is increased. About 25% of mist eliminator is washed under standard operating conditions. The maximum wash rate without significant liquid reentrainment appears to be about 1.5 gpm per square foot.

CARRY OVER LOAD TESTS

Table 2 summarizes the results of mist eliminator carryover load tests.

In the first two tests, mist eliminator carryover load was determined without washing the bottom side. In these tests the scrubbing liquid was labeled with 70,000 to 74,000 ppm of chloride. An eight sampling points traverse was used in these tests. The carryover load without wash was in the range of 28-32 mg/Nm^{3}D (0.012-0.013 gr/SCFD).

In tests 3 and 4, the mist eliminator was washed from underneath and wash liquid was labeled with sodium while spray liquid had chloride so that carryover contribution of two liquid sources can be distinguished. The total carryover from these tests was in the range of 71-110 mg/Nm^{3}D (0.023-0.046 gr/SCFD). One should note that carryover from washing relates to the area that was washed and is not representative of the total carryover.

The last two tests represent carryover load above washed area when both wash and spray liquids were labeled with chloride. The carryover load was in the range of 139-153 mg/Nm^{3}D (0.058-0.062 gr/SCFD). One can conclude that washing increases carryover mass load to double to triple of the carryover from the spray.

Since only 25% of the mist eliminator is washed at any one time under standard operating conditions, the total carryover load averages about 63 mg/Nm^{3}D (0.026 gr/SCFD).

MIST ELIMINATOR EFFICIENCY

The aerosol load in front of the mist eliminator was measured to determine its removal efficiency. An average of 5 tests using chloride tracer was about 9000 mg/Nm^{3}D (3.73 gr/SCFD). If one averages mist eliminator carryover load the removal efficiency is above 99.5%. Calvert developed an equation for the prediction of primary collection efficiency in baffle type separators based on inertial mechanisms (6):

$$E = 1 - \exp - \left(\frac{u_t}{u_G} \; \frac{n\,W\,\theta}{b \tan \theta} \right)$$

where

E = fractional collection efficiency
b = distance between baffles normal to gas flow, cm
u_t = drop terminal velocity, cm/s
u_G = superficial gas velocity, cm/s
n = number of rows of baffles
W = width of the baffle, cm
θ = angle of baffle from flow direction, radian

Substituting values for GEESI's tests:

$$E = 1 - \exp - \left(\frac{21.3^*}{304.8} \quad \left(\frac{4 \times 7.62 \times 0.52}{7.62 \times \tan 0.52} \right) \right. = 99.9\%$$

* based on 140 micron droplet size and terminal velocity for water/air system (7).

The predicted theoretical efficiency is only slightly higher then experimental.

DROPLET PHOTOGRAPHY

Table 3 summarizes the data for four sets of tests. In the first set aerosol particle size was measured on a six point traverse above the mist eliminator perpendicular to the blades when no washing took place. The average arithmetic mean diameter was 264 microns while the Sauter mean was 845 microns indicating wide particle size distribution. The probable reason for the wide particle size distribution was uneven gas flow distribution due to flue gas recycle. Gas flow measurements above mist eliminator indicated an area with downward flow. This downward flow is most likely to trap large aerosols that were reentrained from the blades and large droplets formed from the film on the lid of the absorber. If one excludes the aerosols measured in the downward flow average aerosol arithmetic mean shifts to 83 microns.

The second set of droplet photography test was carried out on a five point traverse underneath the mist eliminator where gas flow was rather uniform. Only 200 aerosols for each test representative for the whole population of aerosols were selected for measurement. The aerosol average arithmethic mean in all 5 tests was unexpectedly close with values between 139 and 143 microns.

In the third set of tests the measurement took place above mist eliminator above bottom wash nozzle with and without wash. Test without wash had average size of 78 microns while with wash average size was about 89 microns.

In the fourth set the measurement took place at the points with superficial velocity of 10 ft/s with and without wash. The cummulative of tests without wash shows 7 aerosols with arithmetic mean of 98 microns while 13 aerosols with mean of 117 microns were measured with wash. Although the number of aerosols in sets 3 and 4 is relatively small and insufficient for valid statistical analysis one interesting observation can be made. If one adds all the aerosols in these two sets without the wash the total number is 17 while with the wash total number is 36. Based on aerosol count one can conclude that aerosol carryover with wash is about double that without wash.

CONCLUSIONS

a. The pressure drop across the mist eliminator is primarily a function of gas velocity. L/G and mist eliminator wash rate have negligible effect.

b. Mist eliminator carry-over under normal operating conditions but without wash is in the range of about 28 to 60 mg/Nm^3D (0.012 to 0.025 gr/SCFD).

c. When the mist eliminator is washed from the bottom carry-over above the washed area is in the range from 70 to 160 mg/Nm^3D (0.029 to 0.066 gr/SCFD).

d. Since only 25% of mist eliminator is washed at any one time, the average carryover is about 63 mg/Nm^3D (0.026 gr/SCFD).

e. Mist concentration at the inlet of mist eliminator averages about 9,000 mg/DNm^3 (3.37 gr/SCFD), indicating mist eliminator efficiency above 99% with or without washing. Average aerosol size at the inlet is about 140 microns.

f. Carrover aerosol droplet size is about 200 microns. If one eliminates data on droplets measured in downward flow, the average carryover size is about 83 microns.

g. Modified EPA method 5 and droplet photography techniques are applicable for mist eliminator evaluation on the full scale installations.

The work described in this paper was not funded by the U.S. Environmental Protection Agency and therefore the contents do not necessarily reflect the views of the Agency and no official endorsement should be inferred.

REFERENCES

1. Ellison, W. Scrubber Demister Technology for Control of Solids Emissions from SO_2 Absorbers. Paper presented at the EPA Symposium on the Transfer and Utilization of Particulate Control Technology, Denver, Colorado. July 24-18, 1978.

2. Laseke, B.A. and Devitt, T.W. Status of FGD Systems in the United States. Paper presented at the 29th Annual Conference of the Association of Rural Electric Generating Cooperatives.

3. Balzhiser, R.E. R&D Status Report. Fossil Fuel and Advanced Systems Division, EPRI. EPRI Journal 3: 3-45-47, April 1978.

4. Saleem, A. Spray Tower: The Workhorse of Flue-Gas Desulfurization. Power, October, 1980.

5. Gavin, J.H., Hoffman, F.W. Droplet Removal Efficiency and Specific Carryover for Liquid Entrainment Separators. Paper presented at the EPA Second Symposium on the Transfer and Utilization of Particulate Control Technology. July 23-27, 1979.

6. Calvert, S., et al. Entrainment Separators for Scrubbers. Journal of the Air Pollution Control Association, Vol. 24, No. 10. October 1974.

7. Fuchs, N.A. The Mechanics of Aerosols. Pergamon Press Book. New York, 1964.

TABLE 1

PRESSURE DROP THROUGH MIST ELIMINATOR
VS
OPERATING PARAMETERS

Test Number	Gas Velocity FPS	L/G Gal/1000 ACFM	Wash Rate GPM	Relative * Pressure Drop
1	10	50	0-2.5	0.21
2	8	70	0-2.5	0.16
3	7	100	0-2.5	0.10
4	8	50	0-2.5	0.16
5	7	70	0-2.5	0.10
6	7	50	0-2.5	0.11

* Ratio of mist eliminator pressure drop to total pressure drop through spray absorber, dimensionless.

TABLE 2

CARRYOVER RESULTS SUMMARY

Test No.	Wash Rate Gpm	Calculated Carry-Over: Scrubbing Slurry mg/Nm^{3}D	Scrubbing Slurry gr/SCFD	Wash Liquid mg/Nm^{3}D	Wash Liquid gr/SCFD	Total mg/Nm^{3}D	*Total gr/SCFD
1	-	27.7*	0.012	-	-	27.7	0.012
2	-	32.2*	0.013	-	-	32.3	0.013
3	2.6	41.2*	0.017	30.1**	0.013	71.3	0.030
4	2.6	60.4*	0.025	49.4**	0.021	109.8	0.046
5	2.6					153.1*	0.063
6	2.6					138.9*	0.058

* Basis of entrainment calculation was measurement of chloride concentration

** Basis of entrainment calculation was measurement of sodium concentration

TABLE 3

DROPLET PHOTOGRAPHY RESULTS SUMMARY

Testing Position	Wash	Number of Points	Arithmetic Mean Microns	Sauter Mean Microns	Number of Drops
Above Mist Eliminator Straight Traverse	No	6	264	845	133
Under Mist Eliminator	No	5	141	161	200*
Above Mist Eliminator Off Center	No	3	78	83	10
	Yes	3	89	104	17
Above Mist Eliminator Selected Points	No	3	98	145	7
	Yes	3	117	163	19

* The number of droplets was higher but only 200 representative for size of the total population of droplets were measured

FILTRATION CHARACTERISTICS OF FLY ASHES FROM VARIOUS COAL PRODUCING REGIONS

by: John A. Dirgo
Marc A. Grant
Richard Dennis

GCA/Technology Division
213 Burlington Road
Bedford, MA 01730

Louis S. Hovis

Industrial Environmental Research Laboratory
U.S. Environmental Protection Agency
Research Triangle Park, NC 27711

ABSTRACT

The filterability of fly ashes emitted by coal burning power stations is described, including that of several ashes generated by low sulfur western coal combustion that are best controlled by fabric filtration. Chemical and mineralogical analyses of the coals were examined to determine possible relationships between coal and ash properties and filtration behavior. Both fly ash size and coal ash content correlated strongly with the fly ash specific resistance coefficient, K_2. Weaker, but discernible, correlations were shown for electrical charge behavior and method of coal firing. Coal sulfur content and ash fusion properties and chemical structures originally expected to influence particle size showed no clear-cut effects on filtration characteristics.

This paper has been reviewed in accordance with the U.S. Environmental Protection Agency's peer and administrative review policies and approved for presentation and publication.

BACKGROUND

Reliable prediction of fabric filter performance depends upon accurate estimation of two major variables: K_2, the specific resistance coefficient of the dust; and a_c, the cleaning parameter (1,2). Although the filtration process is influenced by many factors, K_2, the parameter that describes the gas permeability properties of a deposited dust layer, is especially important in determining the pressure loss for fabric filter systems cleaned by reverse air and/or mechanical shaking. Although theoretical relationships exist for predicting K_2, it would be unwise to assume better than ± 50 percent accuracy. This is due largely to the difficulty in accurately measuring key input parameters such as particle size properties, discrete particle density, and dust cake porosity.

Our first step was to survey the chemical, mineralogical, and selected physical properties of coals in conjunction with their associated seam and rock structures to provide useful insights as to how the resultant fly ashes might behave in fabric filter systems. At the inception of the study, the development of quantitative relationships between parent coal properties and the associated K_2 values for the fly ashes was considered a viable approach. Consequently, representative coal fly ash samples were sought from many cooperating electrical utility, commercial, and industrial fabric filter users. Coal and ash properties, including source data, were obtained from the field sample supplier or from the literature. Specific resistance coefficients and particle size properties for each fly ash were determined in the laboratory, thus allowing comparison of K_2 values with coal and ash properties.

SELECTION OF REPRESENTATIVE COAL FLY ASH SAMPLES

Because the study was constrained to the investigation of 12 to 15 fly ash samples, the development of a rationale for sample selection was very important. The selection process, which has been discussed extensively in a previous paper (3), is summarized next.

It was concluded that the number of fly ash samples to be investigated for any coal type should reflect the best projections for current and future use of that coal where fabric filters afford effective emission control. Figure 1 shows the geographical distribution of major United States coal fields, coal types, and the locations of coal-burning industries and utilities now using fabric filtration for particulate collection (4). Table 1 indicates the estimated 1980 tonnages of lignite, subbituminous, and bituminous coals from the six major coal producing regions. (Anthracite coal accounts for less than 1 percent of national production.) Observe that nearly 75 percent of the coals are mined in the Eastern and Midwestern States. While Western coal represented 25 percent of the 1980 total, a comparison with 1976 statistics (6) that show Western coals accounting for less than 20 percent of production, suggests that the use of these coals is increasing much faster than that for other regions. Additionally, the low sulfur content of many Western coals makes fabric filtration a more attractive control option than electrostatic precipitation. For the above reasons, Western coals were weighted more heavily in the selection process; i.e., they were represented by 8 of the 14 fly ash samples tested. Despite a broad range in coal analyses, Eastern coals from regions I, II, and III were found to be sufficiently similar to justify treatment as a single group (3). Five of the samples tested came from these regions, while the remaining sample depicted a region V coal.

The distribution of fly ash samples was representative with respect to the principal coal firing methods. Pulverized coal combustion, far more common on the basis of tonnage consumed than stoker firing, accounted for 10 of the samples tested while only 4 were generated by stoker-fired boilers.

TABLE 1. ESTIMATED 1980 COAL PRODUCTION BY COAL PRODUCING REGION (5)

Region	States	Production 10^6 tons/yr
I Northern Appalachian	PA,WV(n)[a],OH,MD,MI	189 (22.7)[b]
II Southern Appalachian	WV(s),VA,KY(e),TN(n)	192 (23.1)
III Alabama	AL, GA, TN(s)	32 (3.8)
IV Eastern Midwest	KY(w),IN,IL	171 (20.6)
V Western Midwest	AR,IA,OK,KS,MO,TX	39 (4.7)
VI Western	CO,WY,MT,SD,ND,UT, NM,AZ,ID,WA,AK	209 (25.1)

[a]Letters in parentheses refer to north, south, east, and west.

[b]Numbers in parentheses refer to percent of total.

Because high sulfur content can accentuate fly ash hygroscopicity while low sulfur contents are associated with electrical charge phenomena, coal sulfur contents ranging from 0.35 to 3.5 percent were surveyed. Total ash contents varying from 3.3 to 23 percent were investigated because it was believed that higher ash contents, in conjunction with a fixed heating rate, would reduce heat transfer to individual particles, such that large and irregularly shaped mineral particles would be less likely to melt. Among the many characterizing ratios for the mineral constituents of fly ash used to predict ash slagging and fouling properties, the base-to-acid (B/A) ratio appeared to have some predictive value through its impact on melting temperatures. Thus, several B/A levels were also included in the samplings.

Table 2 provides a general classification of the 14 fly ash samples in terms of the five selecting criteria discussed above: coal producing region, boiler firing method, coal sulfur content, coal ash content, and base-to-acid ratio. The 14 samples represented 12 different suppliers as well as a combination of electric utility, industrial, and commercial fabric filter installations. Table 3 lists the fly ash supplier and coal source region for each of the samples. In addition to furnishing fly ash samples, suppliers provided information on coal source(s), characterizing properties such as proximate and ultimate analyses, and fly ash chemical constituents.

TABLE 2. CLASSIFICATION OF FLY ASH SAMPLES BY SELECTION CRITERIA

Characteristic:						
• Coal producing region:[a]	I	II	III	IV	V	VI
# of samples	3	1	1	0	1	8
• Boiler firing method:	Pulverized coal				Stoker-fired	
# of samples	10				4	
• Sulfur content:[b]	Low (<1%)		Medium (1-3%)		High (>3%)	
# of samples	9		4		1	
• Ash content:	Low (<5%)		Medium (5-15%)		High (>15%)	
# of samples	3		9		2	
• Base/acid ratio:	Low (<0.17)		Medium (0.17-0.33)		High (>0.33)	
# of samples	4		6		4	

[a]Roman numerals refer to regions designated in Figure 1.

[b]When a range of values is used to characterize a specific coal or ash property, the midpoint of that range is used to categorize the sample.

TABLE 3. FLY ASH SUPPLIER AND COAL SOURCES

Fly ash supplier	Sample I.D.	Coal source state and coal region
Southwestern Public Service Co. Harrington Station Amarillo, Texas	SPS	Wyoming, VI
Texas Utilities Generating Co. Monticello Station Mt. Pleasant, Texas	TU	Texas, V
Nebraska Public Power District Kramer Station Bellevue, Nebraska	NPPD	Wyoming, VI
Crisp County Power Commission Cordele, Georgia	CC	Alabama, III
The Amalgamated Sugar Co.		
Union Riley Boiler	Am A	Wyoming, VI
Babcock & Wilcox Boiler	Am B	Wyoming, VI
Nampa, Idaho		
Pennsylvania Power & Light Co. Holtwood Station Holtwood, Pennsylvania	PPL	Pennsylvania and Delaware, I
Westinghouse Hanford Co. Hanford Eng. Development Lab Richland, Washington	WH	Utah, VI
The Medical Center Company Cleveland, Ohio	MCC	Ohio, I
Republic Steel Corp. Warren, Ohio	RS	Ohio, I
Colorado-Ute Electric Assoc. Nucla Station		
Hopper Sample	N(H)	Colorado, VI
Shake-down Sample	N(S)	Colorado, VI
Nucla, Colorado		
E.I. DuPont de Nemours & Co. Waynesboro Plant, No. 2 Silo Waynesboro, Virginia	D	Kentucky and West Virginia, II
United States Steel Corp. Western Steel Division Geneva Works Provo, Utah	USS	Utah and Colorado, VI

ANALYSES OF COAL AND FLY ASH PROPERTIES

The test program involved two separate efforts, the first centering on the collection of information on coal and associated fly ash properties, and the second on the laboratory determination of the specific resistance coefficient, K_2, and the particle size parameters for each fly ash sample.

DETERMINATION OF COAL PROPERTIES AND CHEMICAL CONSTITUENTS OF FLY ASH

Fly ash suppliers provided most of the information on coal properties and fly ash chemical composition. In general, data concerning the proximate analysis and sulfur content of a coal were more complete than those relating to the chemical composition of the resultant fly ash. When sample information was missing, data specified by the fly ash suppliers on the source of their coals (including state of origin, region, seam, and, where possible, mine) were used as a supplemental source. The Keystone Coal Industry Manual (7) and related publications (5,8) were instrumental in identifying coal properties for coal beds and seams not described in suppliers' responses. These sources were also used to identify the various companies mining certain seams where an ash analysis was not available for the mine in question or when the seam itself was not identified. Additional ash analyses were obtained from U.S. Bureau of Mines publications (9,10). Whenever a range of values was cited for a specific ash constituent, corresponding ranges in base/acid ratios were computed. To supplement the above sources, fly ash suppliers were later contacted to fill in critical data gaps.

LABORATORY MEASUREMENT OF K_2 AND FLY ASH SIZE PROPERTIES

All experimental measurements were performed on the bench scale apparatus shown in Figure 2. Fly ash samples were redispersed by an NBS dust generator into a test loop from which the desired aerosol quantity was extracted isokinetically for filtration tests or particle size analysis. To better simulate field conditions, the manifold upstream from the fabric filter was constructed with a bottom inlet that allowed coarser particles to settle out much as they would in many commercial systems. The filter consisted of a 15 cm x 23 cm test panel of Teflon-coated woven glass of a type commonly used for coal fly ash filtration. All tests were conducted at an air-to-cloth ratio of 0.61 m/min (2 ft/min), a flow rate typifying many reverse-air-cleaned systems. The specific resistance coefficient of the fly ash, K_2, was determined by recording pressure loss across the filter and weighing the filter and dust cake at various intervals (11). Final dust loadings on the filter ranged from approximately 300 to 700 g/m^2.

Particle size parameters were determined by Andersen Mark III cascade impactor wherein samples were extracted via a short probe from the central section of the inlet manifold. Collection at this location provided a good approximation of the size characteristics of the fly ash actually reaching the filter surface. Cumulative size distributions of the data were plotted on log-probability paper for the two impactor sizings performed for each fly ash. The aerodynamic mass median diameter (aMMD) and the geometric standard deviation (σ_g) were estimated for each pair of curves, which showed excellent agreement in most cases.

RESULTS

Relevant coal and fly ash properties for each sample are listed in Table 4 along with boiler type. Laboratory derived K_2 values, particle size properties, and a qualitative description of the electrostatic behavior of the fly ash in the test system are also presented. In Table 5, correlation coefficients are listed for selected K_2 relationships with coal and fly ash properties and the particle specific surface parameter, S_o^2, discussed in the following section.

K_2 AND PARTICLE SIZE

An adaptation of the classical Kozeny-Carman relationship investigated by Rudnick and First (12) and later modified for GCA applications (13) has been used to predict K_2 on the basis of theoretical considerations:

$$K_2 = \frac{\mu S_o^2 R}{6 \rho_p C_c} \tag{1}$$

where is the gas stream viscosity, S_o the specific surface parameter, R a complex function of dust cake porosity, $_p$ the discrete particle density, and C_c the Cunningham-Millikan slip correction. S_o characterizes the surface to volume ratio for the polydisperse particle system constituting the dust cake. S_o is readily computed from the size parameters derived from cascade impactor measurements, provided that the cumulative size curve may be approximated by a logarithmic-normal distribution; i.e.,

$$S_o = \frac{6}{MMD} \cdot 10^{1.151 \log^2 \sigma_g} \tag{2}$$

where MMD refers to the true mass median diameter and σ_g is the geometric standard deviation. As emphasized in earlier studies (13), Equation (1) is of limited use as a predictor of K_2, since small (10 percent) changes in porosity can lead to gross (~50 percent) errors in K_2 predictions. If all terms in Equation (1) remain constant except for S_o, an arithmetic plot of K_2 versus S_o^2 should appear as a straight line with its origin at zero. One infers from this relationship that K_2 must increase as the dust becomes progressively finer and the dust cake less permeable to gas flow. In fact, the actual K_2 versus S_o^2 graph (Figure 3) shows a strong positive correlation as forecast by theory. The linear regression line developed by a least squares data analysis is defined by:

$$K_2 = 0.93 + 0.42(S_o^2) \tag{3}$$

where K_2 is expressed in N-min/g-m and S_o^2 in μm^{-2}. The r^2 value for this equation, 0.54, (the fraction of the variation in K_2 that is "explained" by the equation) is statistically significant at the $p = 0.003$ level.

TABLE 4. COAL PROPERTIES AND FLY ASH FILTRATION PARAMETERS

Sample I.D.	Boiler type,[b] rate, MW_e	Coal properties: % sulfur	% ash	% moisture	% volatile	Fly ash base/acid ratio	Fly ash charge effect	Measured values[a]: K_2 N-min/g-m	aMMD μm	MMD μm	σ_g	$S_o^2 \times 10^{-8}$ cm^{-2}
SPS	(2) Pulverized, total 700	0.3-0.4	5-7	25-28	32-36	0.48	No	2.82	7.3	5.2	2.8	3.90
TU	(2) Pulverized, total 1150	0.8-1.3	16-28	31	30	0.28	Yes	0.89	9.7	6.9	2.3	1.53
NPPD	(4) Pulverized, total 113	0.5	3.3	19	36	0.22	No	3.79	5.9	4.2	2.3	4.14
CC	Pulverized, 10	0.9	9.5	6.2	38	0-17-0.33	Yes	1.61	7.5	5.3	2.5	2.96
Am A[c]	Pulverized, 29	0.5	4.0	14	40	0.22	Yes	1.49	7.7	5.4	2.5	2.81
Am B[c]	Pulverized, 28	0.5	4.0	14	40	0.22	No	4.63	6.7	4.7	2.8	4.63
PPL	Pulverized, 79	1.9	23	14	7.6	0-07-0.5	No	0.98	9.6	6.8	2.2	1.45
WH	Stoker, 7	0.5	9.2	8.3	38	0.35	Yes	4.55	8.2	5.8	3.7	5.93
MCC	Stoker	1.8-2.7	7-9	6	38	0.25-0.50	Yes	4.52	6.5	4.6	3.8	10.1
RS	Pulverized, 35	3.5	14	3.2	37	0.5-1.0	No	2.12	9.6	6.8	2.3	1.56
N(H)[d]	(3) Stoker, total 39	0.7	12	6.0	31	0.08	Yes	3.40	7.4	5.2	3.2	5.08
N(S)[e]	(3) Stoker, total 39	0.7	12	6.0	31	0.08	Yes	1.93	8.2	5.8	3.0	3.58
D	Pulverized, 76	1.1	13	6.7	29	0.28	Yes	1.86	4.7	3.3	2.2	6.07
USS	(3) Pulverized, total 90	0.7	6.4	5.6	39	0.13	No	1.73	8.6	6.1	2.3	1.95

[a]MMD and S_o^2 are derived values obtained by the following relationships:

$MMD = aMMD/\sqrt{\rho_p}$ where ρ_p is assumed to be 2 g/cm^3 for coal fly ash

$S_o = 6/MMD\ (10^{1.151 \log {}^2\sigma_g})$

[b]Number in parentheses is number of boilers.

[c]The same coal is processed by two different pulverizing/firing systems.

[d]Fly ash sample representing hopper dust.

[e]Fly ash sample depicting dust shaken from bags.

Despite the favorable statistics, the scatter of the data from which Equation (1) was calculated restricts its use as a predictive tool. The point scatter is attributed to a combination of experimental errors and real differences in particle shape, charge, and density that can also cause significant variations in cake porosity. Based on the observed point scatter, the estimated 95 percent confidence envelope about the regression line has been developed, as shown in Figure 3. If, for a certain fly ash, S_o^2 were measured as 5.0×10^{-8} cm^{-2}, Equation (3) would predict a K_2 of 3.0 N-min/g-m as a "best estimate." However, were the K_2 value for this fly ash to be determined by actual measurement, there is a 95 percent chance that its true value would fall within the range 0.85 to 5.2 N-min/g-m. Consequently, Equation (3) cannot be used for design purposes, despite the statistically significant K_2-S_o^2 correlation.

TABLE 5. CORRELATION COEFFICIENTS FOR K_2 WITH VARIOUS COAL AND FLY ASH PROPERTIES

Variable	Correlation Coefficient (r)
Specific surface parameter, S_o^2	0.733[a]
% Sulfur in coal	-0.146
% Ash in coal	-0.575[a]
% Moisture in coal	-0.148
% Volatile matter in coal	0.450
Base/acid ratio	-0.050

[a]Indicates that correlation coefficient is statistically significantly different from zero (p 0.05).

EFFECT OF BOILER TYPE AND FIRING METHOD

The method of coal firing usually influences fly ash size properties, with a stoker-fired boiler producing a coarser fly ash than that generated by a pulverized-fired or a cyclone boiler. Accordingly, one expects to see a higher K_2 value for a pulverized coal fly ash compared to that for a stoker fired effluent. Unfortunately, only semi-quantitative relationships could be inferred from the present observations, first because of limited data, and second, because additional factors not defined in this study can also affect the size properties; e.g., air/fuel ratio, load level, system geometry, gas residence time, and settlement losses.

The mass median diameters presented in Table 4, which were determined for resuspended fly ashes, do not show any striking differences when grouped according to firing method, although all four stoker-fired ashes were slightly more polydisperse. The latter effect is assumed to be the main reason for the greater S_o^2 values and hence K_2 for the stoker-fired ashes (3.6 N-min/g-m versus an average of 2.2 N-min/g-m for pulverized coal ashes). After adjustment to a common value of S_o^2, however, this K_2 difference was shown to have no statistical significance. It is emphasized, however, that for the above comparisons to be valid in the field, the expected differences in size properties between the original and resuspended states of the fly ash must be the same for both firing methods.

ELECTRICAL CHARGE PROPERTIES

The presence of ionizable salts in fly ash may produce secondary filtration effects due to electrical charging. Since the resultant charges induced by thermal dissociation or contact electrification in the combustion zone are essentially unipolar, particle repulsion effects within the close confines of the dust layer may afford the advantage of lower K_2 (and decreased pressure loss) due to increased porosity. It can also be argued that the extent to which charges induced on a fabric are able to leak off, may also affect dust dislodgement characteristics with a charge accumulation causing increased adhesion.

Electrostatic charging is often a problem in the resuspension of bulk dusts by high velocity aspiration. Although all metal components of the test system in Figure 2 were electrically grounded, there was still evidence of electrostatic charging and deposition for some of the fly ashes tested. Although no attempt was made to quantify the degree of apparent charging, samples were categorized as to the presence or absence of visible electrostatic deposition in the test system. According to Figure 3, it appears that these eight samples (circled symbols) tend to lie below the six samples (open symbols) displaying no obvious electrostatic effects. That is, for a fixed value of S_o^2, fly ashes exhibiting electrostatic effects also possessed significantly (statistically) lower K_2 properties. However, except for the fact that four of the eight samples also represented stoker-fired combustion, electrostatic behavior of the fly ashes could not be related to any other coal or ash properties. It has not been determined whether there is some intrinsic fly ash property that predisposes it to the accumulation of electrostatic charge or whether this behavior is an artifact of the experimental measurement system. Thus, although the electrostatic properties of fly ash as observed here are useful in explaining observed differences in K_2, they provide no guidance in predicting them.

COAL SULFUR CONTENT

The manner in which the sulfur content of coal affects fly ash filtration properties is not clearly understood, although it has been established that sulfur in various forms can affect ash fluid properties. The presence of suspected sulfate salts, as shown by the SO_3 assays for the coal ashes, may decrease ash softening and fluid temperatures, or at least broaden the temperature range over which an ash converts from the solid to the fluid state.

If the viscosity of the molten ash is lowered sufficiently, it is reasonable to expect that gas stream turbulence and shearing action might lead to droplet breakup. On the other hand, those particles that have been converted to the liquid phase but still remain highly viscous (and sticky) may serve as irreversible collision sites for small particles undergoing Brownian diffusion. Under these conditions, it appears that the presence of sulfates could either increase or decrease particle size parameters depending upon which mechanism prevailed.

If the coal sulfur content is due mainly to iron pyrite in the raw coal, significant separation of FeS_2 during coal upgrading will reduce the "basic" phase of the ash and hence diminish the base-to-acid ratio. Under these circumstances, one might expect an increase rather than a decrease in the softening temperature. With less chance for particle adhesion and less reduction in particle size due to droplet breakup, slightly coarser particles and hence, lower K_2 values, might be predicted. Although analyses of the 14 samples suggest an inverse effect, the low value for the correlation coeffecient (-0.05) precludes assigning any statistical significance to it. It is possible that examination of more coal samples, in which a wider range of sulfur contents is exhibited, may afford better resolution of the K_2-sulfur correlation. Since sulfur content is usually a readily attainable parameter, its use in a workable K_2 versus sulfur relationship is attractive.

COAL ASH CONTENT

The effect of ash content upon ash fusion properties was examined to determine if an increase in coal ash content might conceivably result in less heat transfer to individual mineral particles for a fixed energy input, thus slowing particle transition to the viscous and fluid states. Reduced melting might be expected to result in generally coarser and more irregularly shaped fly ash particles. Regardless of any possible impact upon particle size parameters or softening temperatures, filtration demands (cloth and fan capacity) will automatically relate to the volume of fly ash produced which, in turn, should relate directly to the amount of mineral present in the parent coal.

Data pairs representing 14 samples appear to support the proposed high ash effect; i.e., a coarser dust. Other than specific surface properties, coal ash content was the only other variable that correlated significantly with measured K_2 values. Although the data exhibit considerable scatter, Figure 4, K_2 values are seen to decrease with total ash content, as predicted. The K_2 versus ash content correlation is too broad to be of any real value. When combined with the specific surface parameter, S_o, in a multiple regression analysis, the resulting equation is:

$$K_2 = 2.04 + 0.345\ (S_o^2) - 0.079\ (\%\ \text{Ash}) \qquad (4)$$

The r^2 for Equation (4) is slightly higher than that for Equation 3, 0.65 versus 0.54, and the ratios for predicted to measured K_2 values for this equation fall within a slightly narrower range than those for Equation (3). It should be noted, however, that the coefficient for (% ash) just misses statistical significance at the $p=0.05$ level.

BASE-TO-ACID RATIO

Although a number of characterizing ratios derived from the chemical constituents of fly ash were investigated initially, only the base-to-acid (B/A) ratio appeared to offer any predictive capabilities. The basic components of the ash are Fe_2O_3, CaO, MgO, Na_2O, and K_2O while the acidic components are SiO_2, Al_2O_3, and TiO_2. Minimal ash melting points and fluid temperatures accompanied by a more rapid transition from the solid to the liquid phase are observed with a 1:1 mix of basic and acidic components. As the B/A ratio becomes larger or smaller than 1/1, melting points and fluid temperatures rise. This trend is roughly symmetrical on either side of the unity ratio, depending only on the relative difference between basic and acidic components. Thus, the effect of a B/A ratio of 1/2 is approximately the same as for a ratio of 2/1. B/A ratios were calculated for 93 ash samples (representing all 6 coal producting regions) (9). When these ratios were compared to their corresponding ash softening temperatures, the correlation coefficient was very high ($r = 0.81$, $p<0.001$).

Although the base-to-acid ratio is clearly a reliable indicator of ash melting and fusion properties, the expected link between melting and fusion properties and effluent particle size and K_2 could not be discerned, as discussed earlier in this paper. Correlation coefficients for B/A with both K_2 and S_o^2 were approximately -0.2, well below the level of significance for a sample of this size.

SUMMARY AND CONCLUSIONS

The purpose of the research described in this paper was to investigate possible relationships between coal and ash properties and fly ash filtration characteristics. It was postulated that certain chemical and physical properties of coals might have some predictive value in determining the specific resistance coefficients, K_2, of their resultant fly ashes. Since this parameter is an important index of fabric filter performance, a reliable estimation method would prove valuable in the design and analysis of reverse-air and/or mechanical-shake cleaned fabric filter systems. Six potential correlations between K_2 and selected coal and/or fly ash characteristics are reviewed in this paper. Coal sulfur content and the base-to-acid ratio appeared to be of little value in predicting K_2.

Limited data suggest that those fly ashes bearing an appreciable net electrostatic charge (based upon qualitative indications only) form a more porous dust layer on the fabric surface. The latter effect would explain the observed reduction in K_2 when S_o, the specific surface parameter, does not change.

The method of coal-firing, through its impact on the size properties of the fuel entering the combustion zone, also produces a discernible change in K_2. The much coarser size of the coal charged to the grates of a stoker-fired boiler, as compared to the 70 percent less than 200 mesh feedstock typifying a pulverized coal boiler, was expected to generate a coarser fly ash

and a lower K_2. However, for the redispersed fly ash samples tested, those from stoker-fired boilers were much more polydisperse and had higher values for S_o^2, resulting in higher K_2 values for the stoker ashes. After adjustment to a common value of S_o^2, pulverized coal and stoker ashes showed no statistically significant K_2 differences.

An empirical correlation between ash content and K_2 was displayed, although not at the statistical level where it could be used to establish filter system design or operating parameters. Lower K_2 values for high ash coals appeared to confirm the hypothesis that high ash contents would allow less heat for particle size reduction or alteration of surface properties.

A strong correlation was observed between fly ash size properties (i.e., particle specific surface) and K_2, as predicted by theory. It should be noted, however, that with concurrent variations in fuel preparation methods, size reduction processes, and air to fuel ratios, fly ash size parameters may show no relationship to parent coal properties. The fact that the equation representing the least squares regression line permits only $\pm$ 50 percent estimates for K_2 suggests that many coal fly ashes must share similar values for dust cake porosity and average discrete particle density.

There are a number of factors that mitigate against accurate prediction of fly ash filterability from coal properties alone. First, there may be several unidentified coal properties that exert secondary effects on fly ash filterability. The second order effects may be masked by strong first order parameters, such as the particle size. Because of the data scatter, a large number of samples might be required before the identity and magnitude of such secondary effects could be established with any certainty.

Another factor working against precise quantification of the effects of coal properties on K_2 is the tremendous variability that exists in coals. Coal seam overburdens, partings, and floors, the associated rock structures surrounding and separating seams, contribute to this variability. However, since coal is formed from diverse plant materials (such that heterogeneity in structure is quite common), extensive compositional variations can occur spatially and in depth for any given seam (14). This can pose serious problems for coal users with strict specification requirements and also for researchers. While the coal properties obtained from fly ash suppliers represent the best available "average" values, there is no guarantee that the particular fly ash sample received and tested was derived from coal with these same "average" properties.

REFERENCES

1. Dennis, R. and Dirgo. J.A. Comparison of Laboratory and Field Derived K_2 Values for Dust Collected on Fabric Filters. Filtration and Separation. 18: 394-396,417, 1981.

2. Dennis, R. and Klemm, H.A. A Model for Coal Fly Ash Filtration. J. Air Pollut. Control Assoc. 29: 230-234, 1979.

3. Dennis, R., Dirgo, J.A., and Hovis, L.S. Coal Properties and Fly Ash Filterability. Third Symposium on the Transfer and Utilization of Particulate Control Technology: Volume I. Control of Emissions from Coal Fired Boilers. pp. 1-10. EPA-600/9-82-005a (NTIS PB 83-149583), July 1982.

4. Gibbs and Hill, Inc. Coal Preparation for Combustion and Conversion. Prepared for Electric Power Research Institute. EPRI AF-791, Project 466-1, Final Report, May 1978.

5. Nielson, G.F. (Editor-in-Chief). 1981 Coal Mine Directory: United States and Canada. McGraw-Hill, Inc. New York, New York, 1981.

6. Energy Data Report. Coal-Bituminous and Lignite in 1976. DOE/EIA-0118/1 (1976). Prepared in the Office of Energy Data and Interpretation, U.S. Department of Energy. December 18, 1978.

7. Nielson, G.F. (Editor-in-Chief). 1979 Keystone Coal Industry Manual. McGraw-Hill, Inc., New York, New York, 1979.

8. Nielson, G.F. (Editor-in-Chief). U.S. Coal Mine Production by Seam - 1976. McGraw-Hill, Inc., New York, New York. 1977.

9. Abernethy, R.F., Gibson, F.H., and Peterson, M.J. Major Ash Constituents in U.S. Coals. U.S. Department of the Interior, Bureau of Mines, 1969.

10. Gibson, F.H. and Selvig, W.A. Analysis of Ash from United States Coals. U.S. Bureau of Mines Bulletin No. 567. U.S. Department of the Interior, Bureau of Mines, 1956.

11. Bubenick, D.V., Hall, R.R., and Dirgo, J.A. Control of Particulate Emissions from Atmospheric Fluidized-Bed Combustion with Fabric Filters and Electrostatic Precipitators. EPA-600/7-81-105 (NTIS PB 82-115528), June 1981.

12. Rudnick, S.N. and First, M.W. Specific Resistance (K_2) of Filter Dust Cakes: Comparison of Theory and Experiments. Third Symposium on Fabric Filters for Particulate Collection. p. 251-288. EPA-600/7-78-087 (NTIS PB 284969), June 1978.

13. Dennis, R. and Klemm, H.A. Fabric Filter Model Format Change. Volume I, Detailed Technical Report; Volume II, User's Guide. Industrial Environmental Research Laboratory, U.S. Environmental Protection Agency, Research Triangle Park, N.C. Report No. EPA-600/7-79-043a and -043b (NTIS PB 293551 and 294042), February 1979.

14. Haggin, J. Interest in Coal Chemistry Intensifies. Chemical and Engineering News. pp. 17-26, August 9, 1982.

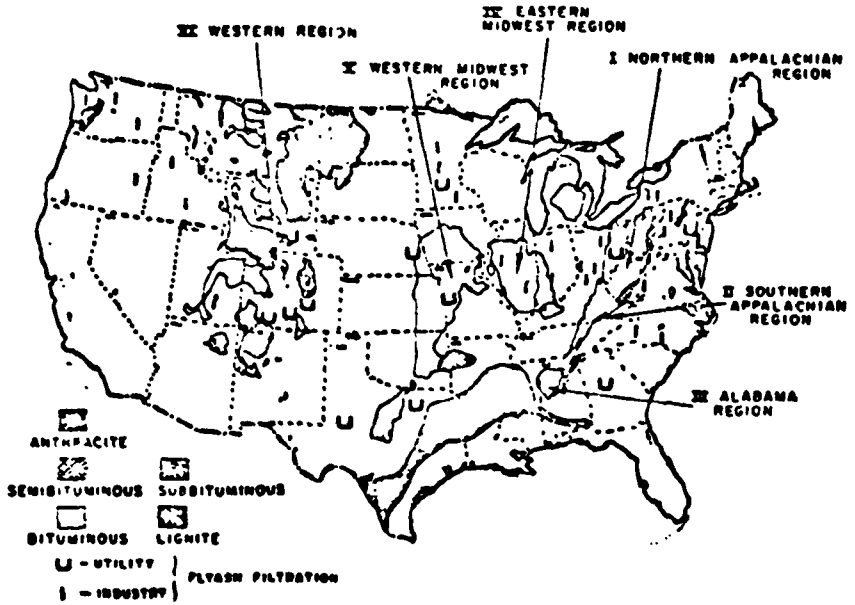

Figure 1. Coal fields of the United States and sites selected to obtain fly ash.[4]

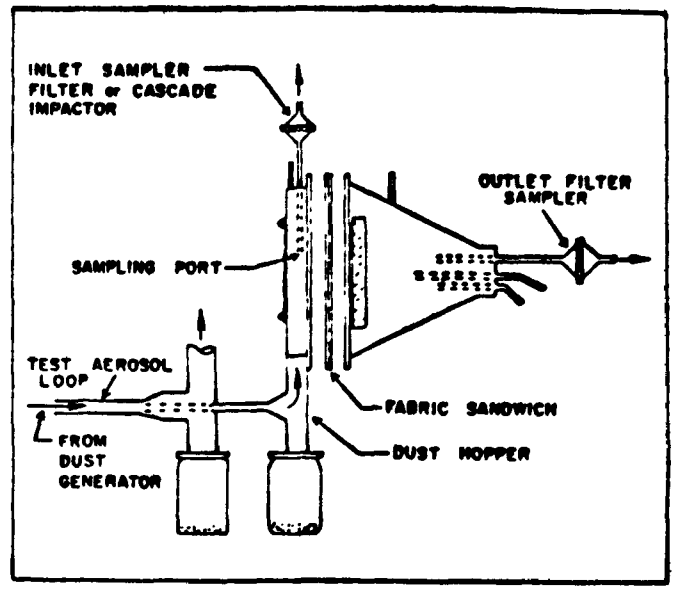

Figure 2. GCA bench scale fabric filter test assembly.

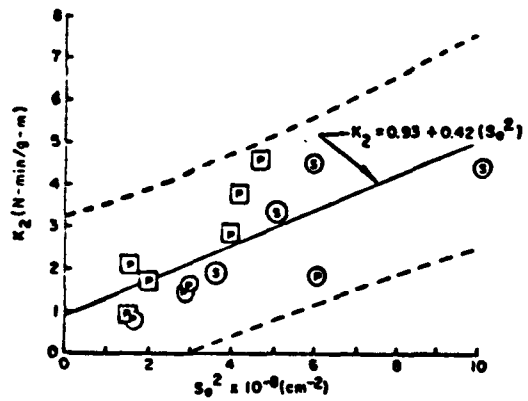

Figure 3. Specific resistance coefficient (K_2) vs. specific surface parameter (S_o^2). P (pulverized), S (stoker-fired), circles (charge effects).

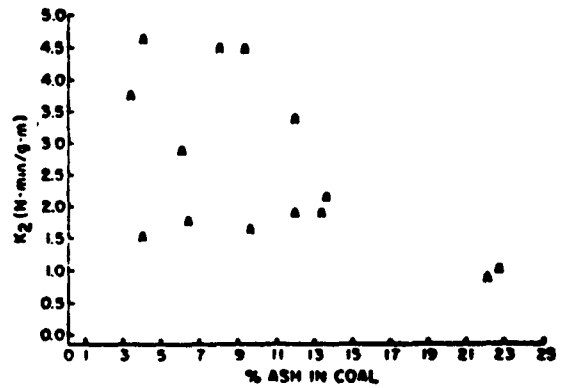

Figure 4. Dust cake specific resistance coefficient (K_2) versus percent ash in coal.

FLY ASH FROM TEXAS LIGNITE AND WESTERN SUBBITUMINOUS COAL: A COMPARATIVE CHARACTERIZATION

D. Richard Sears, Steven A. Benson,
Donald P. McCollor, and Stanley J. Miller
U.S. Department of Energy
Grand Forks Energy Technology Center
Grand Forks, North Dakota 58202

ABSTRACT

As examples, we use two Jackson group lignites from Atascosa and Fayette Counties, Texas, and a Green River Region subbituminous coal from Routt County, Colorado.

The composition of individual fly ash particles was determined using scanning electron microscopy and electron microprobe, with support from x-ray diffraction of bulk ash. Using particle sample populations large enough to permit statistical treatment, we describe the relationship of composition to particle size and the correlation between elemental concentrations, as well as particle size and composition distributions. Correlations are displayed as data maps which show the complete range of observed variation among these parameters, emphasizing the importance of coal variability.

We next use this data to produce a population distribution of ash particle resistivities calculated with Bickelhaupt's model. The relationship between calculated resistivity and particle size is also displayed, and the results are compared with measured values.

By acceptance of this article, the publisher and/or recipient acknowledges the U.S. Government's right to retain a nonexclusive royalty-free license in and to any copyright covering this paper.

INTRODUCTION

The ability to employ elemental analysis and mineral speciation of coal, in advance of mining, to reliably select, design, and size a particulate control device would reap numerous benefits. Most accomplishments in this area, particularly those of Bickelhaupt (1), Selle (2), and Frisch (3), relate to electrostatic precipitator (ESP) performance, based on bulk coal or ash composition. Frisch, loc. cit., describes an algorithm for including within-seam coal variability in the inter-relationship of ash-to-BTU ratio, resistivity, specific collection area (SCA) and efficiency.

By contrast, we have chosen to focus on populations of individual ash particles. A goal of the GFETC program is to quantify the generic and specific properties and property distribution of low rank western coal ashes as they relate to collectability, emission levels, and environmental insult. In this paper we describe work which has led us from individual particle composition to individual particle resistivities and their frequency distributions.

MATERIALS AND TECHNIQUES

We have selected three specific coals for this report: two Texas lignites notable for their high ash, low BTU, and high sulfur content and a low sulfur Colorado subbituminous coal on the borderline between subbituminous A and high volatile C bituminous. These coals are described in Table I.

Fly ash is generated using the GFETC Particulate Test Combustor (PTC). This unit is an axially upward, pulverized coal fired furnace with a nominal coal consumption of 75 lbs/hour. Equipped with an electric air preheater, provision for the usual primary, secondary, and tertiary air, and induced draft exhaust through the selected particulate control device, the unit is designed to generate ash characteristic of that produced in a utility boiler. Axial firing maximizes fly ash/(bottom ash + slag) ratios. Although the PTC is not equipped with boiler tubes, the flues are supplied with a system of heat exchangers permitting delivery of flue gas at temperatures from ~200 to ~750°F. PTC instrumentation includes redundant real-time measurement of flue gas temperature and gas concentrations.

Combustor operating parameters and the flue gas environment from which fly ash was sampled are summarized in Table 2.

Ash was sampled isokinetically and simultaneously size fractionated using a Southern Research Institute (SoRI) 5-stage multicyclone (4) which we have modified for extractive, rather than in-stack, sampling. The unit is enclosed in an oven regulated to stack temperature.

Bulk hopper ash is analyzed for major and minor elements using x-ray fluorescence (XRF). Multicyclone ash fractions are analyzed both by XRF and also by neutron activation analysis.

TABLE 1. DESCRIPTION OF COALS INVESTIGATED

Name	Arapahoe	Ledbetter	San Miguel
Mine	Energy Mine	None*	San Miguel
Location	Routt Co.,CO	Fayette Co.,TX	Atascosa Co.,TX
Power plant	Arapahoe Unit 3 Public Service Co. of Colorado Denver, CO	None*	San Miguel Station San Miguel Electric Corporative Jourdanton, TX
Type	Green River Region Subbituminous	Jackson Group lignite	Jackson Group lignite
Analysis (as burned)			
C, % dry basis	62.74	38.17	46.42
H, % " "	4.71	5.53	3.79
N, % " "	1.63	0.55	0.72
S, % " "	0.43	2.11	2.49
O, % " "	19.79	32.64	27.38
Ash, % " "	10.7	21.0	19.2
H_2O, %	7.9	25.3	13.0
Heating value Btu/lb as burned	11,058	6,578	7,719
X-ray coal ash analysis			
SiO_2	55.0	58.7	45.0
Al_2O_3	25.1	19.5	15.2
Fe_2O_3	3.7	4.0	5.8
TiO_2	1.1	0.8	0.7
P_2O_5	0.9	0.2	0.4
CaO	5.7	6.1	9.3
MgO	2.4	2.5	1.2
Na_2O	0.0	0.6	4.6
K_2O	1.5	0.9	2.1
SO_3	4.6	6.6	15.2

*Ledbetter lignite was a composite of core drillings collected at the location of a future generating station and mine to be opened by the Lower Colorado River Authority in Fayette Co., TX.

TABLE 2. COMBUSTION CONDITIONS

Coal Run No.	Arapahoe AR-183	Ledbetter LD-193	San Miguel TL-153
Coal feed, lb/hr.	45.2	83.6	69.5
Air feed, scfm	118	112.	149.
Flue gas composition			
O_2, vol %	4.9	5.9	6.6
CO_2, vol %	13.2	12.2	13.0
N_2, vol %	81.9	81.9	80.4
SO_2, ppm	353.5	2957.	3800
NO_x, ppm	~1000	697.	783
H_2O, vol %	7.9	12.6	8.8
Inlet dust loading gr/scf	2.43	7.28	13.1
Inlet temperature °F	296	325	272

For mineral speciation of coal and ash, an important tool is x-ray diffraction applied to both fly-ash and to oxygen-plasma low temperature (150°C) ashed coal (LTA). The LTA technique avoids the pyrolysis and minimizes the dehydration of mineral species which occurs in conventional ashing.

We also employ chemical fractionation (5), of coal, a technique in which sequential extractions of the coal are performed using 1M ammonium acetate and 1M HCl. The first solution removes ion-exchangeable cations and soluble salts; the second solution dissolves carbonates and acid soluble oxides. Unaffected pyrite and silicates remain in the solid residue.

Ash resistivity is measured at temperature in simulated flue gas in a laboratory unit (6). Although the PTC is equipped with an in-stack point-to-plane resistivity instrument, the laboratory unit permits investigations over the entire range from 200-825°F with control of SO_2 and H_2O concentrations over a wide range.

The major tool employed in our work has been the scanning electron microscope/energy dispersive electron microprobe (SEM)[1]. SEM is applied to

[1]GFETC employs a JEOL JSM 35 scanning electron microscope. X-rays are detected with a Kevex lithium-drifted silicon detector. Elemental analysis is performed by means of a Tracor Northern NS-880 X-ray analyzer. (Reference to specific brand names and models is done to facilitate understanding and neither consitutes nor implies endorsement by the Department of Energy).

sufficient individual particles to permit statistical analysis. To eliminate human bias in selection of particles to be measured and analyzed, photographs of SEM fields are overlaid with a grid. Random-number-generated grid coordinates are used to select particles for analysis. SEM determination of particle size and shape and SEM-electron microprobe analysis of major element composition were done on particles from each of the five multicyclone stages. The data obtained from all five stages were combined to form a population of particles and the data were analyzed using the SEM's online computational system.

RESULTS

Mineral species identified above XRD detection limits in the three coals were: Arapahoe: quartz, kaolinite, and calcite; Ledbetter: quartz, kaolinite, calcite, pyrite, and plagioclase; San Miguel: quartz, clinoptilolite (a zeolite), $CaSO_4$-$5H_2O$, plagioclase, pyrite, kaolinite, and possibly calcite. For our purposes, the most notable differences are the higher inorganic mineral content of the Texas lignites, and the absence of detectable pyrite in the Arapahoe coal. Chemical fractionation results were complex and too voluminous to report in detail here. Notable results were that Ledbetter appears to have ~87% of its calcium associated with the organic structure whereas San Miguel and Arapahoe had 44-53%, with most of the remainder as carbonate. Almost 100% of the sodium in the Texas lignites was associated with the organic structure, whereas ~75% of Arapahoe's sodium appears to be in aluminosilicates.

XRD of the bulk fly ash reveals: Arapahoe: quartz and mullite (Al_6-Si_2O_{13}); Ledbetter: quartz, mullite, anhydrite ($CaSO_4$), and cristobalite; San Miguel: quartz, anhydrite, mullite, magnetite (Fe_3O_4), hematite (Fe_2O_3) and an unusually large quantity of amorphous material or quench growth.

The presence of mullite and cristobolite is consistent with the thermal decomposition of kaolinite which proceeds through various stages including the formation of mullite and cristobalite above 1095°F (7, 8, 9).

Particle size distributions of the three fly ashes were determined by isokinetic extraction of material from the PTC flues through impactors and the SoRI multicyclone. Multicyclone data appear in Figure 1. Salient observations are: all three ashes have large amounts of material in the, 2.5-4 μm range; San Miguel has significantly more fines in the submicron range; based on an assumed maximum particle size of ~70 μm, mass median diameters (mmd) for Arapahoe, Ledbetter, and San Miguel ashes are ~15, ~15, and ~28 μm, respectively. Actual field tests at Arapahoe and San Miguel stations suggested mmd's of 20 and 16 (10, 11). Cumulative percentages at 1μm agree reasonably well with field experience; Arapahoe: 0.18% in PTC, 0.08% in the field; San Miguel: 0.65% in the PTC, 0.53% in the field.

SEM ash analyses produce quantitative results for twelve major and minor elements for each particle examined, plus size and aspect ratio. From this data, frequency distributions are calculated and displayed in Figure 2. Sulfur showed a maximum at zero concentration for all three coals, and it is omitted from the selection.

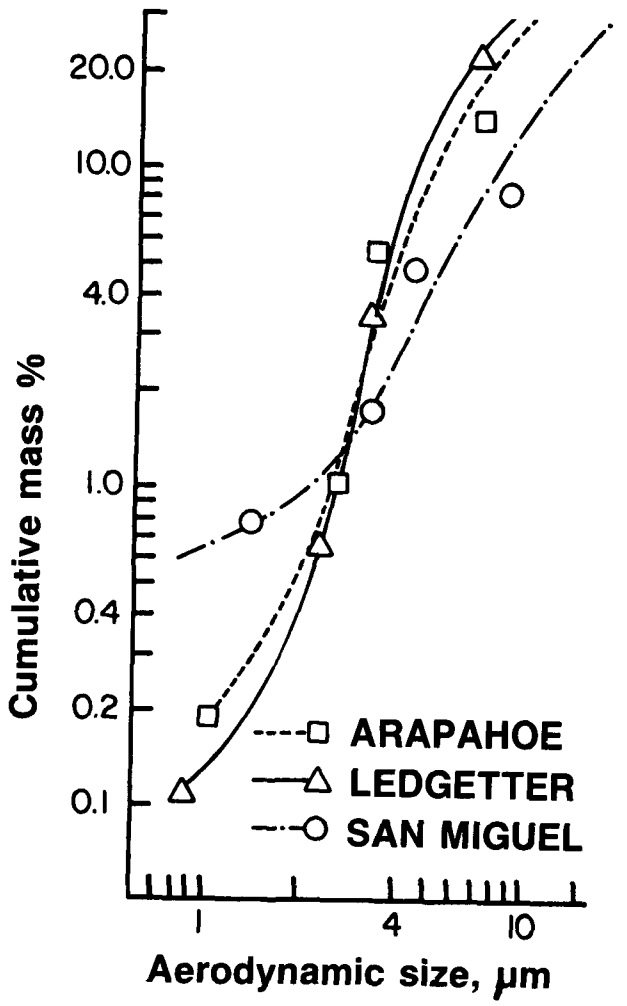

FIGURE 1. Cumulative particle size distributions.

In order to calculate particle resistivity according to the Bickelhaupt Model (1), composition of individual particles is required. This information is also needed in order to begin to understand the origin of fly ash particles in terms of coal mineral composition and the combustion process. Because each particle is a serial numbered entity in the SEM statistical system, this information is recoverable for each particle. In Figure 3, we present a few examples of binary correlations selected because they illustrate some of the diverse functional relationships encountered. These data maps represent 500, 300, and 200 particles of Arapahoe, Ledbetter, and San Miguel ashes, respectively. The same display can be produced for concentration versus size, if desired. When this is done, it is often observed that Na_2O and SO_3 are enhanced in the fine particle region. Cf. Ref. 10., for example.

Although these data may be used in conjunction with x-ray diffraction to describe some of the ash "mineralogy", in this paper we present it primarily to illustrate and emphasize the extremely non-uniform composition of real fly ash. Analyses of bulk ash fail to provide any suggestion of this diversity. Consequently, there is a temptation to assume that concentration-dependent physical properties such as resistivity are uniform for all particles. This is a very bad assumption, as we see in Figure 4, in which we display ash particle resistivities calculated by the Bickelhaupt model (1).

A point on these data maps should be interpreted as representing a bulk resistivity one would calculate for a perfectly uniform ash in which all particles have the same composition as the single particle corresponding to the plotted point. One must not assume that any one point corresponds to the resistivity one would measure in that single isolated particle. Bulk resistivity is a complicated phenomena and the semi-empirical Bickelhaupt model does not purport to apply to individual isolated particles.

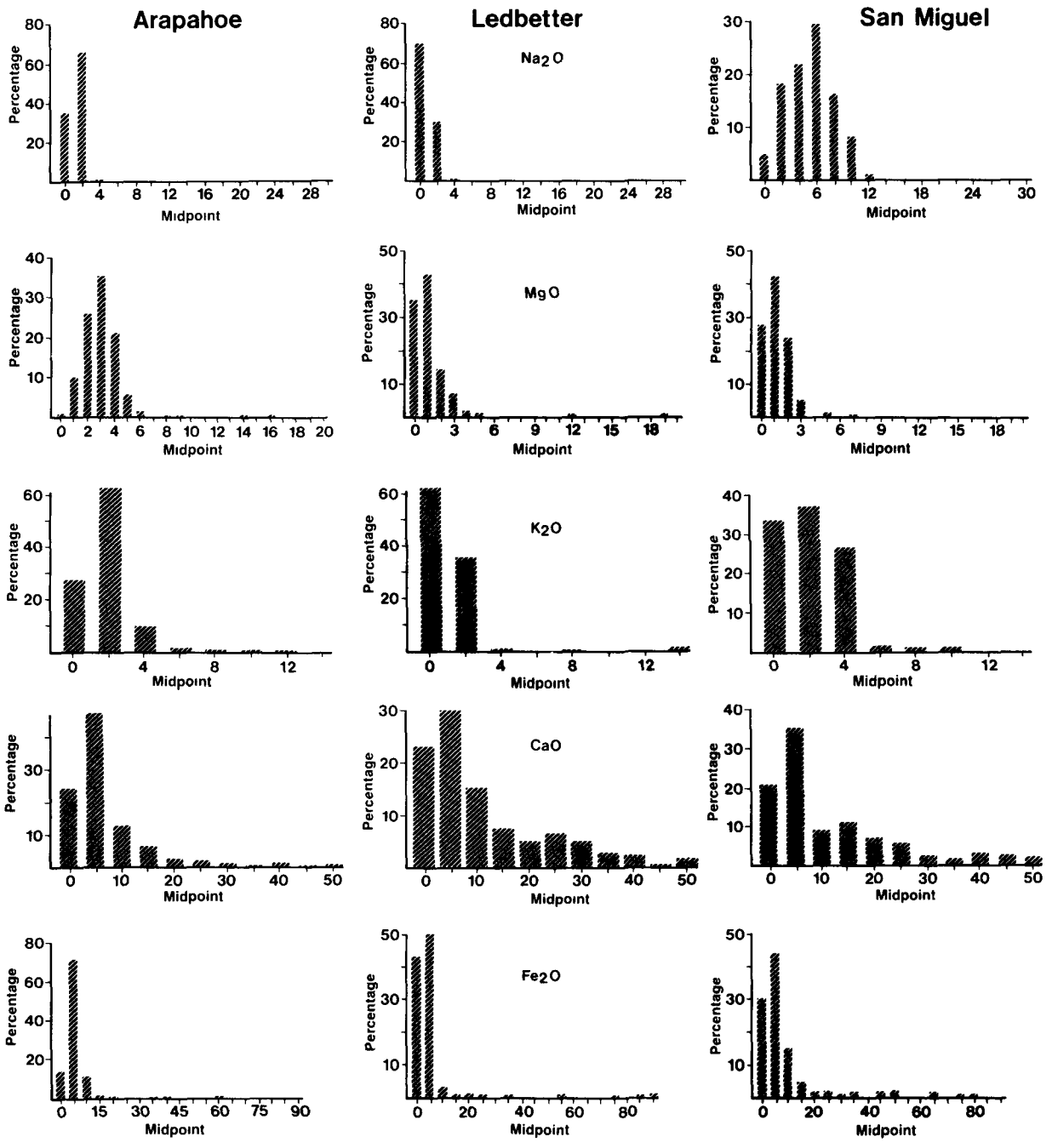

FIGURE 2. Elemental composition distributions, reported as oxide, for the three ashes.

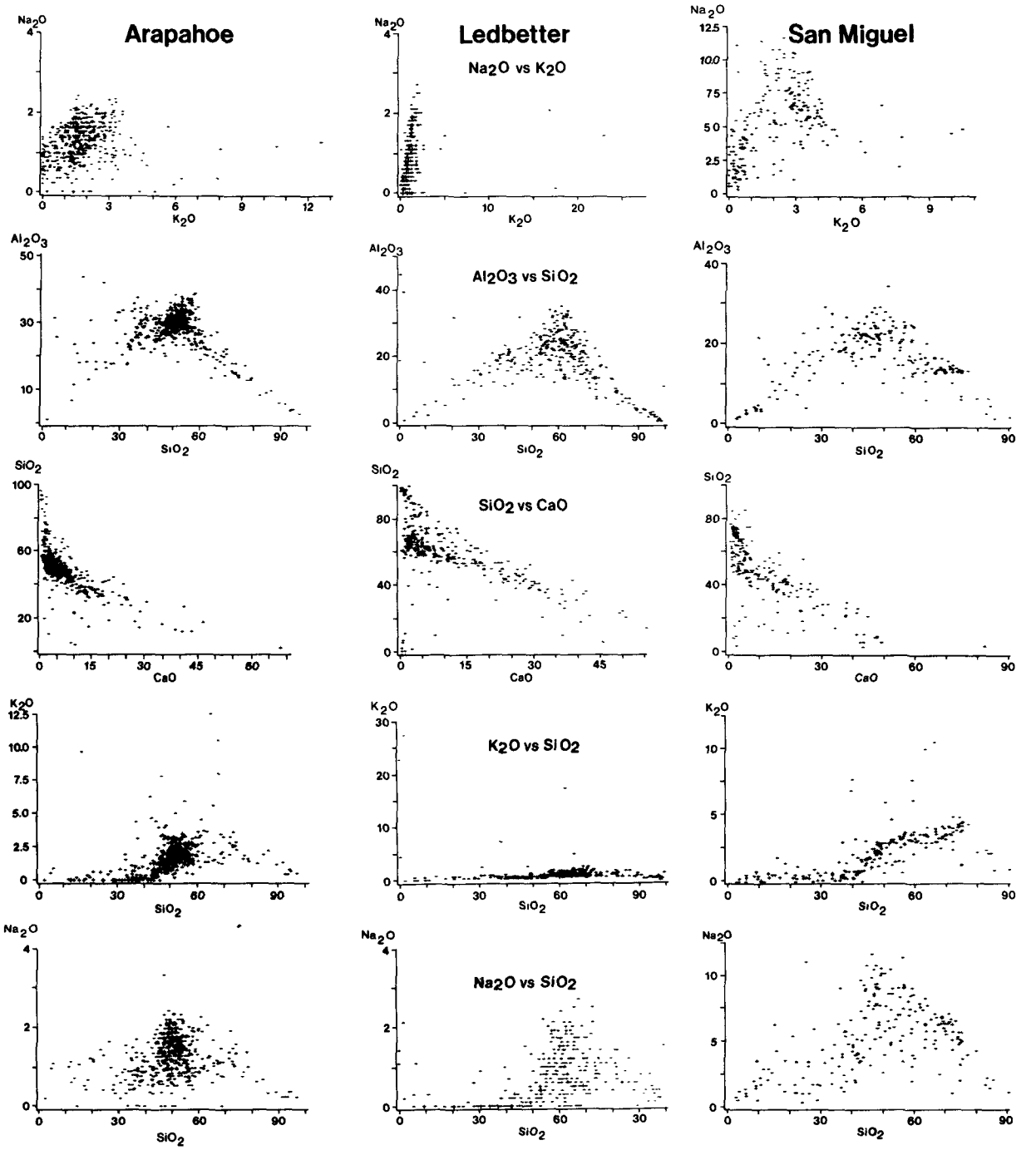

FIGURE 3. Examples of correlations between elemental concentrations. Each datum represents a specific, individual particle.

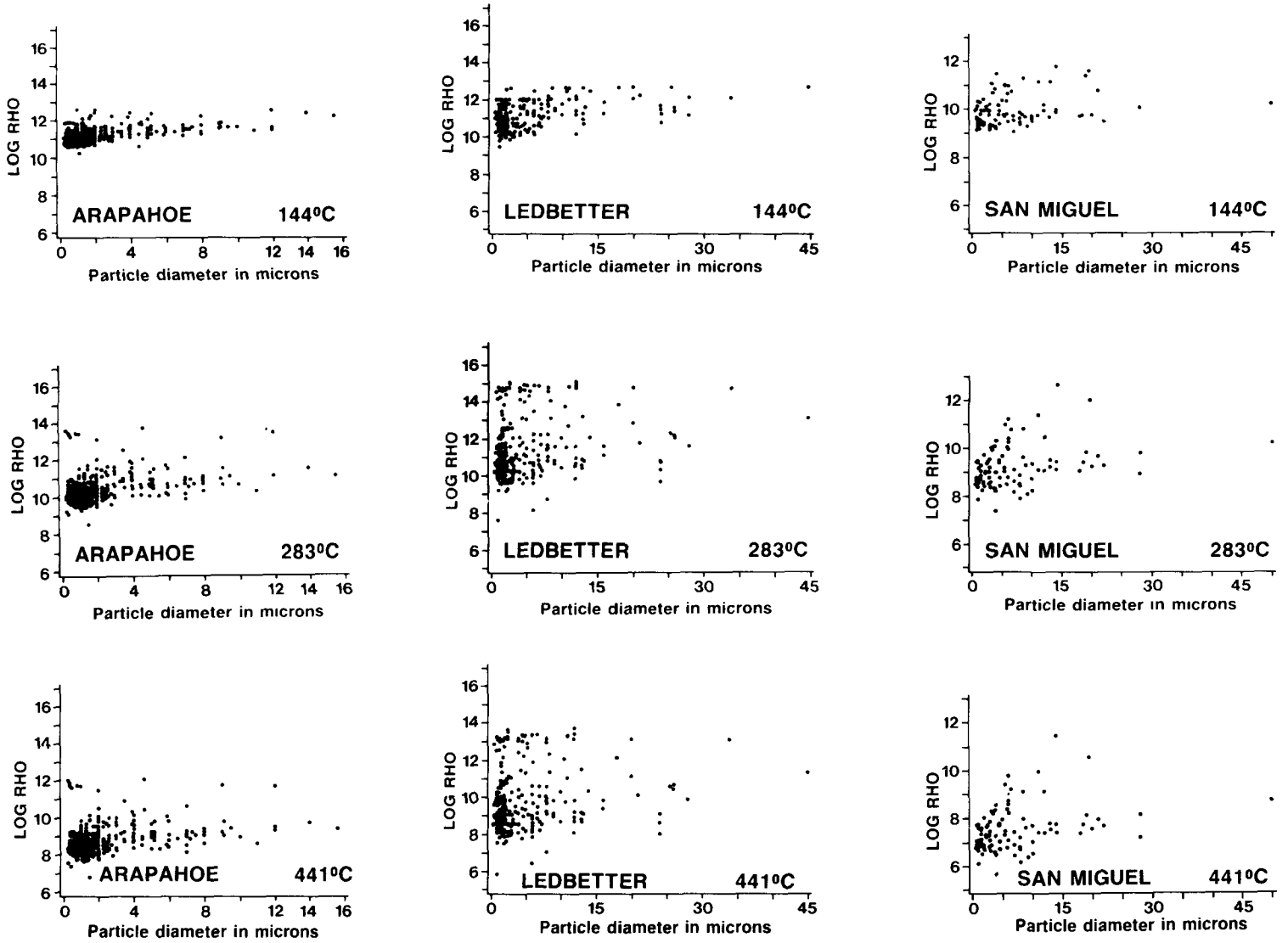

FIGURE 4. Log resistivity vs. particle size for the three coals at 144°C (291°F), 283°C (541°F), and 441°C (826°F). Resistivities calculated by the Bickelhaupt Model. See Table 3 for flue gas concentrations.

Flue gas concentrations employed in these calculation are given in Table 3. SO_3 was set at 0.29 and 0.0 ppm for Araphahoe and San Miguel because these concentrations were observed in field measurements (10, 11). Ledbetter SO_3 field data are not available; therefore its SO_3 was taken to be similar to San Miguel's. The SO_2 and H_2O concentrations are typical values observed in actual test burns in the PTC pilot unit, but are not necessarily identical to the values at the exact time of sample collection. Lithium was set at a small value, for it is not detectable by XRF.

TABLE 3. CONDITIONS EMPLOYED IN RESISTIVITY CALCULATIONS

Coal	Arapahoe	Ledbetter	San Miguel
Concentration			
H_2O wt %	8.7	17.4	8.8
SO_2 ppm	353	2957	4400
SO_3 ppm	0.29	0.0	0.0
Field, Kv/cm	1.5	1.5	1.5
Lithium concn. in ash, wt %	0.01	0.01	0.01

In Figure 5 the resistivity data are displayed in another format which may be more useful in estimating impact on precipitator performance. The high and low temperatures span much of the range of cold side and hot side precipitators. A notable feature of Figures 4 and 5 is the increasing breadth of the resistivity distribution which accompanies a shift to lower valves, as temperature is increased. Another unexpected feature is the markedly asymmetric shape of the distribution at some temperatures (e.g. Arapahoe at 441°C and San Miguel at 144°C).

Average or consolidated resistivities, i.e., pseudo-bulk resistivities, may be calculated from the voluminous individual particle values. In Figure 6, we display such averages as functions of temperature.

COMPARISON OF CALCULATED AND MEASURED RESISTIVITIES

A few comparisons with measured values are possible. For two of the coals, laboratory resistivities over a range of temperatures were obtained in the GFETC resistivity apparatus (6). The value of the maximum resistivity rho(max), which occurs at temperature t(max), is reported in Table 4, together with field measurements at specified temperatures. Also included is the value calculated for bulk field-collected ash using the Bickelhaupt Model (10).

For the two Texas lignites, average particle resistivities calculated by the methods of this paper agree well with measured values. The temperatures of maximum resistivity, however, disagree substantially. For Arapahoe subbi-

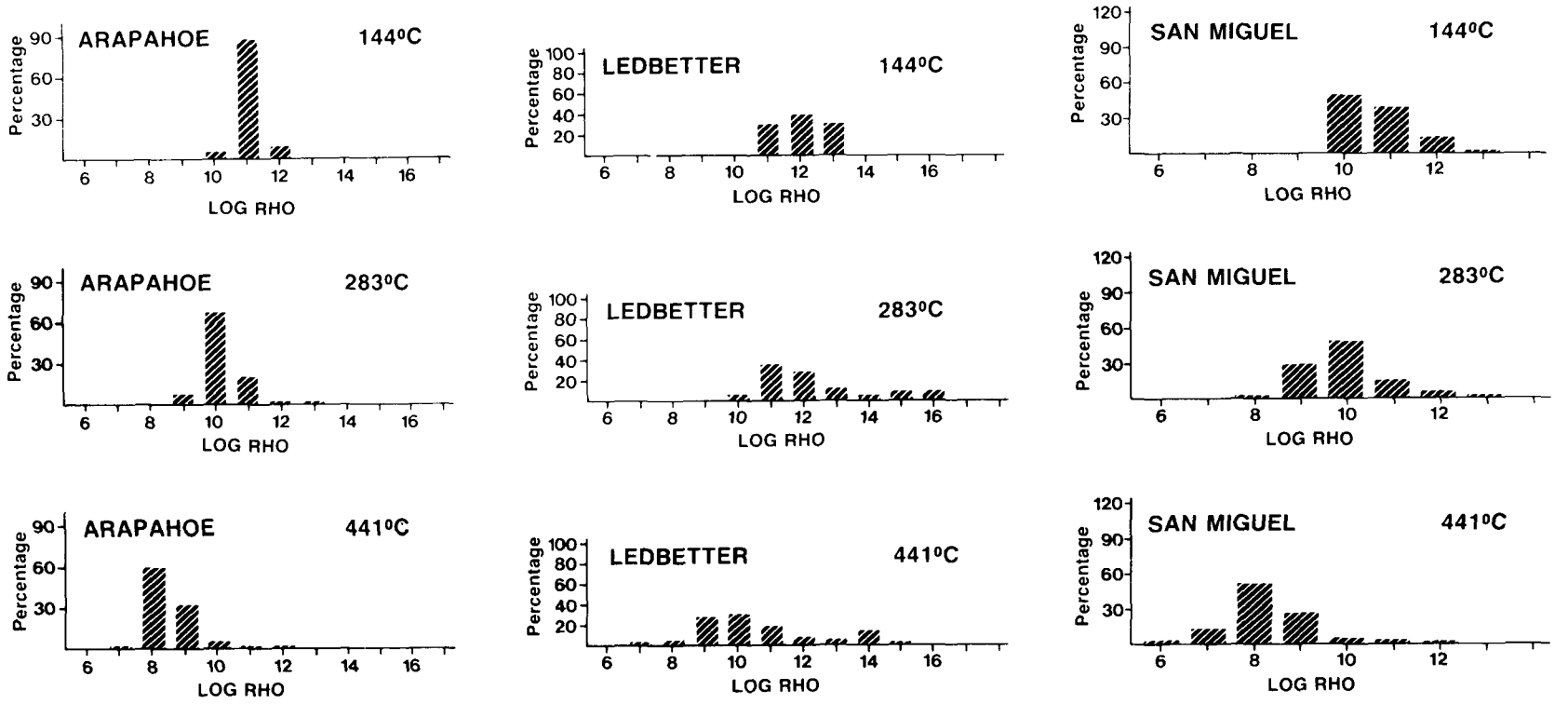

FIGURE 5. Frequency distributions of particle resistivities calculated with Bickelhaupt Model. See Table 3 for flue gas concentrations.

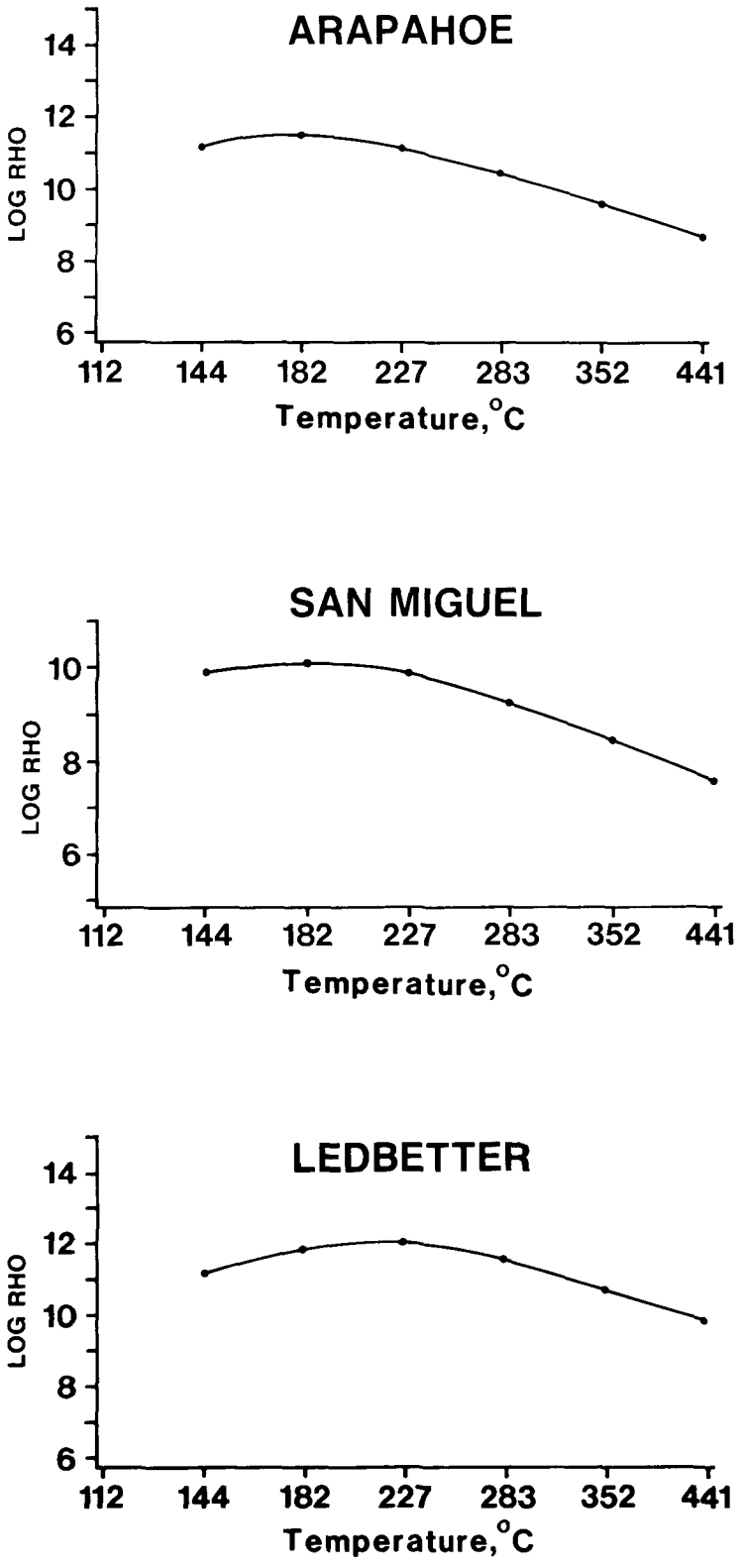

FIGURE 6. Average resistivity versus temperature.

tuminous coal, field in-situ resistivity and bulk ash calculated resistivity are both almost an order of magnitute higher than calculated here from particle chemistry.

TABLE 4. COMPARISON OF CALCULATED AND EXPERIMENTAL RESISTIVITIES

Coal	Arapahoe	Ledbetter	San Miguel
rho(max), ohm-cm			
measured†	N/A	9.5×10^{11}	1.3×10^{10}
calc.(this paper)	4×10^{11}	1×10^{12}	1×10^{10}
t(max), °F (°C)			
measured†	N/A	272 (133)	289 (143)
calc.(this paper)	360 (182)	419 (215)	370 (188)
t(field),°F(°C)	266 (130)	N/A	330 (166)
rho(field) ohm-cm			
in-situ*	6×10^{11}	N/A	1.6×10^{10}
calc.(this paper)	7×10^{10}	N/A	1×10^{10}
bulk ash (calc)≠	5×10^{11}	N/A	0.5×10^{10}

†Using A.S.M.E. laboratory unit (6).
*Measured at spark-over (10, 11).
≠Using standard Bickelhaupt method (1).

The average particle method described here is wholly dependent upon the assumption that the particle data correspond to a representative selection of particles. However, there are problems in both sample preparation and in particle selection which will tend to favor larger particles over fines.

Second, the Bickelhaupt Model is an empirical relationship which may not be applicable to these ashes or these flue gas conditions. Figure 7 displays several resistivity calculations for San Miguel with an experimental curve (ρLAB) which is the average of thirteen laboratory measurements.

In Figure 7 ρVS is the combined volume and surface resistivity and ρVSA is ρVS combined with an acid contribution (1). These resistivities are combined as follows:

$$\rho_{vs} = \frac{\rho_v \rho_s}{\rho_v + \rho_s}$$

and

$$\rho_{vsa} = \frac{\rho_a \rho_{vs}}{\rho_a + \rho_{vs}}$$

and are defined by relations of the form:

$$\log \rho_v = C_1 - C_2 \log (Li+Na) - C_3 \log (Fe) + C_4 \log (Mg + Ca)$$

$$\log \rho_s = \log \rho_{so} - K (H_2O)_{vapor}$$

where C_1 through C_4 are constants and ρ_{SO} and K contain no concentration-dependent terms. We see that ρ_v is dependent on elemental composition, including elements which may be particle size dependent. Our data for San Miguel (which do not extend into the submicron range) suggest enhancement of SO_3 and Fe_2O_3 in the fines and are inconclusive for Na_2O. Any sample preparation or particle selection problem which biases the size distribution away from fines will diminish the apparent average SO_3 and Fe_2O_3 concentrations, thereby increasing the calculated resistivity.

We do not have Arapahoe data with which to make a comparison similar to Figure 7. Our data do show sodium to be enhanced in the fines in Arapahoe ash (10). Damle et al have noted that the literature has conflicting results for sodium in various coals (12).

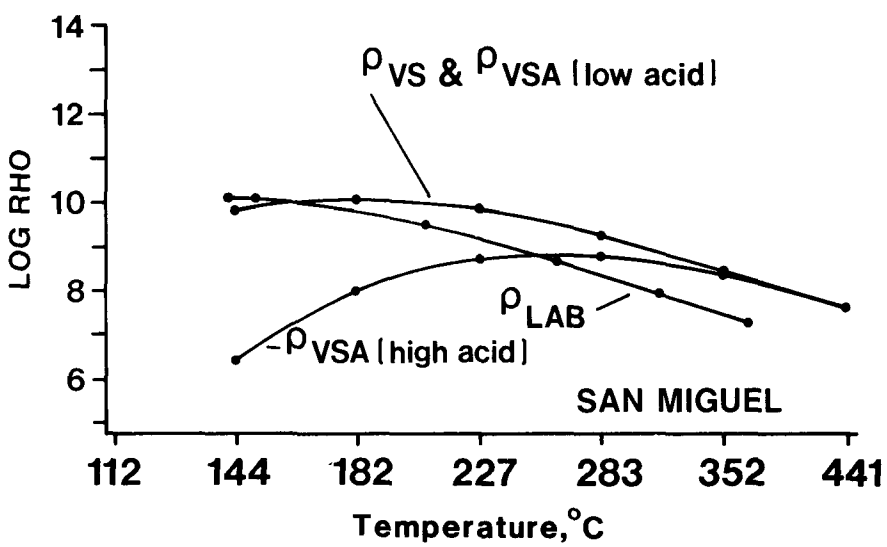

FIGURE 7. Comparison of VS and VSA resistivities with laboratory resistivity for San Miguel lignite. See Text for conditions and definitions.

Surface-sorbed SO_3 in equilibrium with the flue gas leads to the acid resistivity ρ_A. This is defined by an algorithm which differs for "eastern" ashes, for which Ca + Mg $\leq$ 3.5% or K $\geq$ 1.0%, and "western" ashes, taken as those for which Ca + Mg > 3.5% and K < 1.0%. Sorting one file of 103 San Miguel particle compositions, we found that it consisted of 75 "eastern" particles and 28 "western" particles. At low temperatures and high SO_3 concentrations, calculated ρ_{VSA}'s therefore fall into two narrow horizontal bands in a data map such as Figure 4.

In the absence of specific flue gas SO_3 concentration data, it is common to assume $(SO_3) \sim 0.004\ (SO_2)$. In our case, that would be 17.6 ppm SO_3, corresponding to the ρ_{vsa} (high acid) in Figure 7. We have used ρ_{vsa} (low acid) throughout this paper, corresponding to $(SO_3)= 0$, which approximates field measurements.

CONCLUSIONS

Reviewing Figure 7, it is apparent that the average particle resistivity calculation most closely approximates the zero-acid or volume-surface resistivity ρ_{vs}. The temperatures of resistivity maxima are poorly predicted, however. Improved sample preparation and particle selection procedures which scrupulously avoid biasing the particle size distribution may minimize the problem.

The real value of the method lies in its ability to describe the breadth of the resistivity distribution. Furthermore, resistivity vs. particle size data maps allow one to estimate the variation of this breadth over the entire range of particle sizes investigated. Although we have employed the Bickelhaupt model, alternative models may be used if they express resistivity quantitatively as a function of those elemental concentrations measurable by SEM/electron microprobe.

We feel that it is extremely important for persons sizing precipitators to be fully aware of the degree and the importance of ash particle resistivity variability. Although this application of SEM to emission control planning is extremely time-consuming, it may be justified as a routine method by those contemplating use of suspected "problem" coals.

ACKNOWLEDGMENTS

We wish to acknowledge the contributions of: Diane K. Rindt and A. L. Severson in x-ray diffraction and fluorescence analyses; Francis J. Schanilec and Clyde L. Ziegelman for particulate sampling and sizing; and Loretta A. Weckerly and Annette Ahart for pilot plant operation and engineering support.

The work described in this paper was not funded by the U.S. Environmental Protection Agency and therefore the contents do not necessarily reflect the views of the Agency and no official endorsement should be inferred.

REFERENCES

1. Bickehaupt, R.E. A technique for predicting fly ash resistivity. EPA-600/7-79-204, U.S. Environmental Protection Agency, Research Triangle Park, NC, 1979. 105 pp.

2. Selle, S.J., Hess, L.L., and Sondreal, E.A. Western fly ash composition as an indicator of resistivity and pilot ESP removal efficiency. Paper No. 75-02.5. Presented at 1975 Meeting, Air Pollution Control Association, Boston, MA. June 15-20, 1975.

3. Frisch, N.W. A technique for sizing electrostatic precipitators for highly variable fuels. J. Air Pollution Control Association. 30:574, 1980.

4. Smith, W.B., Wilson, R.R. Jr., and Harris, D.B. A five-stage cyclone system for in-situ sampling. Environmental Science and Technology. 13: 1389, 1979.

5. Miller, R.N. and Given, P.H. Variations in inorganic constituents of some low rank coals. Ash Deposits and Corrosion Due to Impurities in Combustion Gases. Hemisphere Publishing Co., Washington, D.C. 1977. pp 39-50.

6. Selle, S.J., Tuffe, P.H., and Gronhovd, G.H. A study of the electrical resistivity of fly ashes from low-sulfur western coals using various methods. Paper No. 72-107. Presented at the 1972 Meeting of the Air Pollution Control Association, Miami Beach, FL. June 18-22, 1972.

7. Deer, W.A., Howie, R.A., and Zussman, J. Rock Forming Minerals. Vol. 3. Sheet Silicates. Longman, London, 1976. pp. 202 ff.

8. Hulett, L.D. and Weinberger, A.H. Some etching studies of the microstructure and composition of large aluminosilicate particles in fly ash from coal-burning power plants. Environmental Science and Technology. 14:965 ff, 1980.

9. Stinespring, C.D. and Stewart, G.W. The surface chemistry of aluminosilicate particles--application to combustion stream chemistry. METC/RI-79/7. U.S. Department of Energy, Morgantown, WV. August 1979.

10. Dahlin, R.S., Sears, D.R., and Green, G.P. Baghouse performance and ash characterization at the Arapahoe Power Station. This Symposium, Session A-5.

11. Dahlin, R.S. San Miguel station electrostatic precipitator technical summary report, field test No. 2. DOE/GFETC/10225-2. U.S. Department of Energy, Grand Forks, ND, 1982. 29pp.

12. Damle, A.S., Ensor, D.S., and Ranade, M.B. Coal combustion aerosol formation mechanisms: A review. Aerosol Science and Technology. 1:119 ff, 1982.

USE OF FUEL DATABANKS FOR THE EFFECTIVE DESIGN OF STEAM GENERATORS AND AQC EQUIPMENT

by: N. W. Frisch* and T. P. Dorchak
AFFILIATED ENERGY & ENVIRONMENTAL TECHNOLOGIES, INC.
North Branch, New Jersey

ABSTRACT

Information concerning coal properties and their variability is critical to the proper design of steam generators and associated gas cleaning equipment (precipitators, FGD and to a lesser degree, fabric filters). For situations in which a fuel source is well defined, a databank of hundreds of coal and ash analyses may be used to assess the variability of the fuel and to develop critical sizing and design parameters.

This paper discusses a comprehensive computer approach which examines fuel databank information and generates design parameters for a set of operating conditions. Fuel parameters related to boiler design and operation, including fusion temperatures, T_{250}, fouling and slagging indices, etc., may be entered or generated for statistical analysis and presentation. Uncontrolled and corrected emission levels of particulate and SO_2, as well as acid dew point temperatures are developed.

In the case of ESP's, the program can indicate collection area requirements for any type of emission rate (mass, concentration or opacity-basis). Gas conditioning and pulse energization options are included. Both statistical and a wide range of graphical outputs provide the user with desired guidance; a typical plot would be a mine map with fuel or ESP parameters overlaid.

---

* N. W. Frisch is with N. W. FRISCH ASSOCIATES, INC., in Kingston, New Jersey.

INTRODUCTION

Information concerning coal properties and their variability is critical to the proper design of large steam generators and associated gas cleaning equipment for particulate and sulfur oxide emission control. It is well recognized that the performance of electrostatic precipitators (ESP's) and to a lesser degree fabric filters (F/F) commonly used for particulate collection, are sensitive to the properties of the coal. The design of flue gas desulfurization equipment critically depends on fuel characteristics such as sulfur and chloride content, as well as the base content of the coal ash. The boiler designer must also match the boiler design and ancillaries to the properties and rank of the coal. There is no universal boiler/furnace that can operate properly on all ranks of coal.

The nature of the coal is thus the singlemost important variable to be considered in the specification of modern-day coal-fired steam generators. Even with existing units scheduled to burn a different coal, detailed information regarding the coal must also be considered of paramount importance.

In the case of coal from a new large mine, prior to mining, exploration of the mining area may produce analyses and characteristics of hundreds of cores. A number of these cores, as shown in one scheme presented in Figure 1(1), will be completely analyzed and characterized. For each of these cores, which can be over one hundred in number in our experience, up to fifty data points may be generated per core, excluding trace element analysis. It is obvious that even for simple storage such a large data base is best placed into computer files. More and more large coal companies in the United States are today using computer storage. Typically, these files can produce limited statistics on key parameters for use by the purchaser or his architectural engineer (A/E) to specify the fuel conditions for boiler and gas cleaning equipment. These parameters may include ash, sulfur and Btu content of the coal, as well as ash oxides.

As will be demonstrated shortly, such computer files are clearly inadequate for our objective of developing and presenting the critical parameters necessary for the design of

- the boiler and furnace, as well as coal handling, storage and preparation equipment
- the particulate emission control equipment, whether ESP or F/F (in the case of the ESP, the actual size is developed)
- The flue gas desulfurization equipment

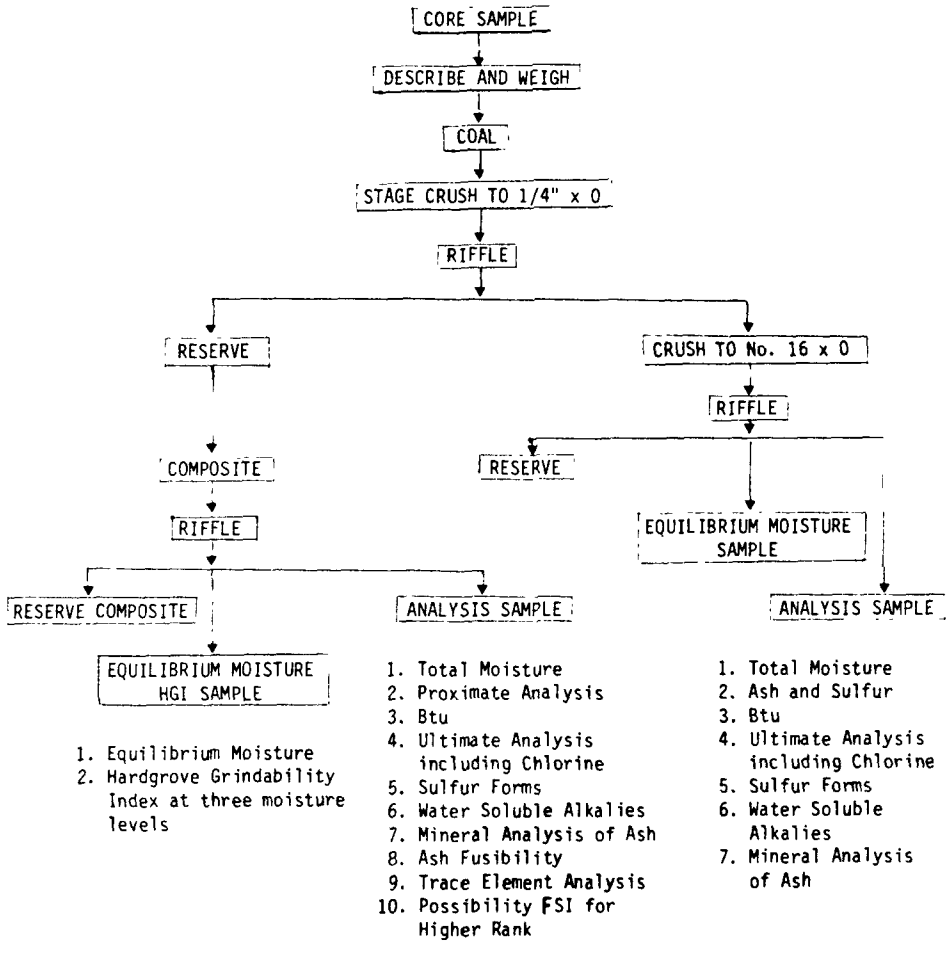

Figure 1. Preparation and Complete Analysis of a Subbituminous Coal Core.

TYPICAL COAL DATABANK FILE DEFICIENCIES

The usual databank typically stores only measured parameters; often all cores are not completely characterized for every fuel parameter. Thus, it is desirable to be able to estimate the values of the missing parameters. Then there are design parameters which are rarely measured directly, such as T_{250}, slagging index, etc. A design program must be capable of calculating these values for a wide range of fuels.

Further, one is often interested in the value of a tentative parameter, i.e., one which is not well-defined and whose form is subject to modification as time passes and better information becomes available. Capability to develop such parameters in an on-line mode is most desirable.

Additionally, one is often interested in relating various fuel parameters one to another; for example, is Hardgrove Grindability Index (HGI) related to other fuel parameters such as ash content or ash composition or coal heating value? Clearly, a wide range of plotting capability is required, encompassing at a minimum X-Y, X-Y-Z, including log coordinates, and also probability type plots.

And finally, if the program is to possess utility for sizing of AQC equipment, specialized modules must be included. In the example in this paper we use a fuel data base which contains information about core location, seam thickness, coal ultimate, proximate and ash chemical analyses, as well as HGI values. We then concern ourself with precipitator sizing for a specific (opacity) target, taking into account the variability of the fuels, including the seam thicknesses. (We, of course, develop the critical boiler design parameters as well.)

BOILER DESIGN - CRITICAL COAL PARAMETERS

For each complete analysis of the core or coal sample, critical fuel parameters are developed, as well as certain operating parameters, including gas flow for a given generator size. The most problematical of these parameters, particularly in the case of Western low sulfur coals and lignites, proves to be the ash slagging and fouling indices. Many different indices have been proposed as recently summarized by Bryers (2). Slagging indices based on measured viscosity temperature profiles are recognized as the most reliable. Unfortunately, due to the expense of the determination, the viscosity data is generally not available. AE2's COALMASTER program will calculate a slagging index based on ash composition when such ash viscosity is lacking.

For Western coals, AE2 experience and research indicates that the best expression for the slagging factor (R_{VS}) takes the following form adapted from the work of Watt and Fereday (3), (4).

$$R_{VS} = \frac{58.34\ M^{0.5}}{F_S}\left[\frac{1}{(2.4 - C)^{0.5}} - \frac{1}{(4 - C)^{0.5}}\right]$$

Table 1 below relates the level of the slagging index to the severity of slagging.

TABLE 1. VALUES OF SLAGGING INDEX

Slagging Classification	Slagging Index R_{VS}
Medium	0.5 - 0.99
High	1.0 - 1.99
Severe	Greater than 2.00

The reader is referred to the referenced work for definition of the terms above. The relationship is based on the spread between T_{250} and $T_{10,000}$ or plastic range of the ash. The COALMASTER program also independently computes the T_{250} values based on the work of Sage and Duzy, as reported by Winegartner (5). Subsequent examples show the above equation correctly predicts the high slagging properties shown by some Western subbituminous coals.

For Eastern coals, the slagging factor (R_S) may be calculated by the well-established relationship:

$$R_S = B/A \times \% S$$

where B/A is the base-to-acid ratio of constituents in the coal ash
% S is percent sulfur in the coal, dry basis

Since the acidic components react under fire zone conditions with the basic components, their balance at a ratio of approximately 1.0 produces typically the lowest melting slag. (Other components such as the silica to alumina content may modify the ash fusion temperatures.) The B/A ratio, therefore, is an indicator of the slagging potential of the coal ash. The sulfur content is included since low melting sulfates are found in the slag from Eastern high sulfur coals.

In addition to the slagging behavior expected, the designer must also contend with the fouling characteristics of the coal. The selection, design and placement of convection surfaces depends directly on the fouling index. The number of blowers in these areas will also be affected. Here one must apply different indices according to the type of ash. For Eastern coals, the fouling factor R_f longest in use and calculable from the typical data base is determined by the product of the base-to-acid ratio and the sodium oxide percentage in the coal ash.

$$R_f = B/A \times \% Na_2O$$

A refined index R_f' is based rather on the soluble sodium content of LTA ash, a parameter which is typically unavailable. If the latter value is available, the program can readily calculate this R_f'.

For Western coals, no factor has found general application. A general consensus of workers in the field is that fouling is related to the sodium oxide content of the ash, the base-to-acid ratio and the ash content. AE2 has performed regression analysis on a limited number but a wide range of fuel to develop a function encompassing these three parameters in a form which accounts for soluble sodium.

$$R_f = \frac{K\ (\% Na_2O)^a\ \ (\% Ash)^b}{1 + D/(B/A)^c}$$

where a, b, c, D and K are constants

In the example that follows, the expression does successfully predict the low-to-medium fouling characteristic of Western subbituminous coal.

An additional critical fuel parameter that impacts on the mill capacity is the Hardgrove Index. To account for the impact of the variation of this parameter in the coal on nominal mill capacity, AE2 uses the following ex-

pression:

$$\% \text{ of Rated Mill Capacity} = A \text{ Log } (HGI) + B$$

where A and B are constants for a given mill type

In our Figure 2, additional fuel parameters and related boiler design features are summarized. Our program clearly presents all the critical coal parameters for use by the boiler manufacturers for the design of a reliable low-maintenance boiler of proper size and configuration.

COAL PROPERTIES RELATED TO BOILER DESIGN	IMPACT ON P-C FIRING UNITS
Rank	Furnace Size
Moisture	Heat Release Rates - Btu/ft^2/hr
Ash	Heat Liberation Rates - Btu/ft^3/hr
Sulfur	Burners & Blowers - No., Size, Spacings
Btu/lb and Ultimate Analysis	Hoppers - Openings, Angle
Ash Composition	Pendant Heating Surface & Placement Blowers
Reactivity	Convection Surfaces & Placement
Grindability	Flue Gas Flow Rates
Abrasiveness	Coal Preparation & Storage

Figure 2. Major Boiler Design Parameters Related to Coal Properties.

Flue Gas Desulfurization Design - Critical Coal Parameters

Although there are many types of systems in use today, both wet and dry, using various basic reagents to control sulfur oxide emissions, their design and operation are critically dependent on the sulfur content of the coal. However, in the ash of many Western coals in particular, sufficient basic components such as calcium and magnesium oxides are present to naturally combine with the sulfur oxides to reduce their emission rates. This retention of sulfur by fly ash has been related to the ash chemistry by Gronhovd (6) and by Davis and Fiedler (7). The program uses a relationship of the Davis-Fiedler type as a basis to calculate the uncontrolled emission rate. The level of control, the stoichiometry and the reagent usage are directly related to these emission rates. Chlorine content in the fuel is also critical to wet processes affecting material selection and makeup composition. These key parameters are presented by the COALMASTER program in both tabular statistical form and graphical presentation for ready use in the selection and design of FGD equipment. Presentation on the mine coordinates also allows the mine engineer to avoid or blend off pockets of excessively higher sulfur content coal.

PRECIPITATOR SIZING - COAL PARAMETERS

It is generally recognized that precipitator performance is sensitive to fuel characteristics. In the case of highly variable fuels, one is faced with

the problem of developing an ESP size that is adequate to treat a very large portion of the fuel without offering an economically unattractive SCA (ft^2 collecting area/1000 acfm).

Sizing precipitators for a specific fuel has progressed from the use of a migration velocity parameter which is solely dependent upon coal sulfur content (ca 1950). A number of approaches are in use today; they include use of performance test data (analogy) (8), proprietary indices (9), migration velocity-resistivity relationships (10), (11), comprehensive regression equations (relating W_K to both fuel and operating parameters) (12), computer modeling (13), pilot precipitator tests (14), combustor burns (15), and a number of combination approaches (16). Unfortunately, the experimental effort appears to be diminishing and more and more reliance is placed on paper approaches.

It is not an objective of this paper to discuss in detail sizing approaches. Rather, we are most concerned with the presentation of variable fuel data in the ESP specification and how this data is properly treated by the ESP designer.

Commonly, the A/E will examine the individual histograms of the coal elements and ash oxides and develop minimum and maximum values for each of the components. (Subjective truncation is usually practiced at this point.) This data and the mean value are presented in tabular form in the specification. A specification of this type was prepared using published data (Table 2).

TABLE 2. EXAMPLE OF FUEL SPECIFICATION

	Ultimate Analysis (% by weight, as received)				Ash Chemical Analysis (% by weight)		
	Mean	Min	Max		Mean	Min	Max
Carbon	37.21	21.26	39.87	SiO_2	26.49	4.66	74.55
Hydrogen	2.78	1.52	3.42	Al_2O_3	12.43	2.22	19.90
Nitrogen	0.67	0.52	1.03	TiO_2	0.49	0.04	1.09
Sulfur	0.63	0.18	1.41	Fe_2O_3	8.30	2.65	20.30
Oxygen	11.74	10.71	12.45	CaO	24.61	8.80	42.80
Ash	7.14	3.89	15.95	MgO	6.83	2.70	12.00
Moisture	39.83	27.78	52.53	K_2O	0.73	0.11	2.36
Total	100.00			Na_2O	1.25	0.12	7.25
				Li_2O	--	--	--
Higher Heating Value, Btu/lb	6258	3068	7660	SO_3	17.93	3.77	32.62
				P_2O_5	0.16	.01	0.94
				Undetermined	0.78	.01	1.09
					100.00		
Equilibrium Moisture,%	35.51	24.80	4930	Ash Fusion Temperature, °F Reducing			
				IT	2183	1900	2820
				ST	2211	1940	2820
Hardgrove Grindability Index	35.90	22.00	136.00	HT	2237	1960	2820
				FT	2263	1990	2820

The use of such a fuel specification presents several problems. First, it is difficult to assign a probability of occurrence to any of the critical fuel or ash component levels. Equally important is the fact that one cannot reliably develop individual fuel and ash sample compositions from this type of specification in the general situation (17). And it is these individual fuel samples which dictate specific levels of ash loadings, ash resistivity and particle size upon the precipitator system.

Let us examine a relatively simple situation in which only three fuel parameters, A, B and C, influence ESP performance. High levels of A improve performance while high levels of B or C depress performance or require higher efficiency levels for the same design outlet level. (We may think of A as Na_2O, B as CaO and C as ash/Btu ratio.)

When the designer selects the limiting values of A, B and C, using a specification of the type shown in Table 2, the highest levels of B and C, and the lowest level of A become the basis for the design. This, in theory, determines the worst case situation. This selection is shown on Figure 3.a., points 1 and 1'.

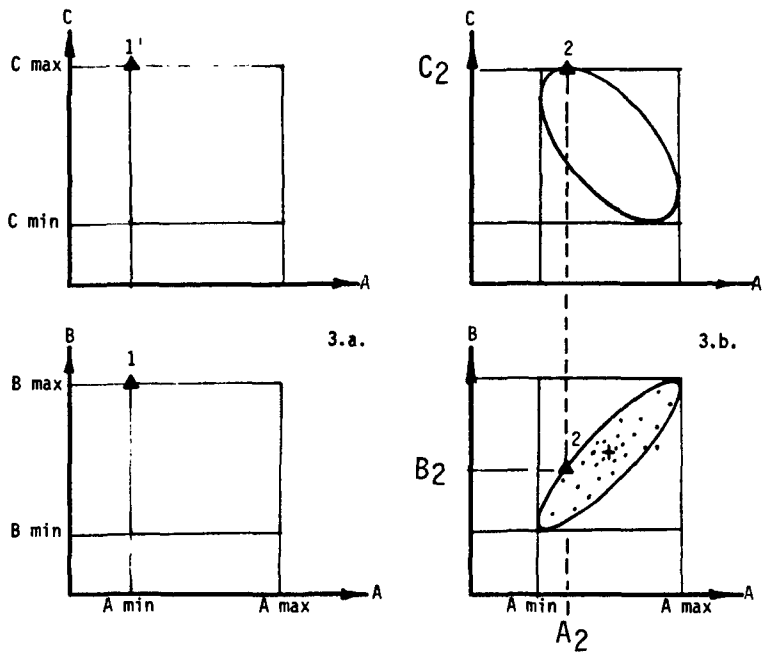

Figure 3. Locating the Limiting Values of the Design Parameters. (simple ESP situation)

But we are not even certain that this extreme combination occurs in the fuel bank and if it does, whether it describes 0.1, 1 or 5% of the fuel. Alternatively, a less conservative designer might choose another fuel basis for design, possibly even the mean composition. Coy and Frisch (18) have discussed some of the implications of these alternate choices.

If all the individual analyses are represented on Figure 3.a., we typically arrive at a plot similar to Figure 3.b. Here, many of the data points cluster about the mean and the plot exhibits a decreasing density of data points as one moves away from the mean. An elliptical boundary (contour ellipse) can be drawn to encompass a large selected proportion of the fuel. Knowing these boundaries, one is able to define a composition, namely point 2, which has a known small probability of occurrence. Compositions A_2, B_2 and C_2 occur together in a sample; A_2 and B_2 describe a relatively high resistivity ash and C_2 fixes a high efficiency requirement. Typically, a significant lower SCA requirement results for condition 2 compared to condition 1'.

Techniques for locating point 2 are readily applied in some simple cases (19). More complex situations require both definition of a significant number of statistical parameters and also computer solution. In these real-life situations, we prefer an alternate approach.

AE2's approach involves sizing of ESP's for each core analysis, taking into account coal seam thickness, and all variables which affect fuel flow rate, gas flow rate, ash loading, ash resistivity, ash particle size, gas phase composition and density. Ash loading, ash resistivity and ash particle size are especially important parameters. Loading and resistivity may exhibit wide ranges within a single fuel bank. Ash loading is best characterized by use of the ratio of ash to Btu; resistivity is estimated by the Bickelhaupt approach (20) or alternatively for a given rank fuel the use of proprietary regression equations can be applied in the computer program. The Bickelhaupt approach combines the role of various ash species (Na, Li, Ca, Mg, Fe) and gas phase components (SO_3 and H_2O) in influencing fly ash resistivity.

Clearly, a computer approach is required to handle the large data base involved and to develop the statistics of the pertinent parameters and via graphics, to present visually the relationships between various fuel and precipitator parameters. Especially useful are cumulative plots of required C.E. area or similar plots of outlet loading or opacity for a given SCA ESP. Other useful plots depict the mine area with important ESP or fuel parameters overlaid; this permits one to locate especially difficult fuel areas which may then be selectively mined, blended or eliminated from the mining plan.

A comprehensive example follows.

APPLICATION OF COALMASTER PROGRAM

A brief description of the use of the program follows.

First, the coal file is read; coal and ash parameters, as well as available boiler parameters are input. The program has been written in a most accommodating manner to handle the various means of reporting data in use today.

Parameters not in the file are calculated by the program when feasible. Thus, in the absence of ash fusion temperatures, the standard ones are estimated (IT, ST, HT and FT - both reducing and oxidizing).

Operating parameters for the precipitator are requested. Options for conditioning or pulse energization are allowed. The program performs combustion calculations, resistivity and ash loading estimates, etc., and sizes for each core. The operator then may provide a design collecting area, under the guidance of the program. The pertinent (outlet) parameters for the specified precipitator are then calculated.

Next the operator is provided with five options, including graphics and statistics. The graphical display is most useful and can provide excellent insight into various interactions between variables.

Another distinctive feature of AE2's program is the ability to define from the keyboard any new parameter in a most general form. Then one may perform statistics or graphics in a manner analogous to the manner used with the standard (built-in) parameters.

Selected output of the program is discussed in the next section.

BOILER DESIGN PARAMETERS

As shown previously, the capacity of a particular mill depends on the Hardgrove Grindability of the coal. Of equal significance, the throughput in terms of Btu per hour depends also on the heat content (Btu/lb) in the coal. When the product of the mill capacity and heat content is at a minimum level, the throughput necessarily falls to a minimum. Determining this minimum by simply multiplying minimum levels of HGI and Btu found in the coal statistics obviously results in an unrealistically low design throughput. Rather, the minimum throughput is best determined by calculating the throughput for <u>each</u> mill capacity. In the case of an existing unit, the adequacy of the existing mill system can be evaluated beforehand to avoid costly mill problems. Figure 4 presents the results of our calculations.

We note that all but two of the more than one hundred calculated values fall below the contour ellipse. Eliminating these extreme points which represent less than two percent of the coal, our design point is determined by point A, which corresponds to a heating value of 8200 Btu/lb and a 65% capacity. The contour ellipse encompassing the specified proportion of the fuel population passes through point A and exhibits a minimum throughput of $4.97(10)^5$, which becomes the basis of design. Alternatively selecting point B as the design point, corresponding values of 8500 Btu/lb and 39% are obtained, resulting in nearly a 50% jump in design mill capacity. Our next consideration might be the furnace size itself.

The size and even the type of furnace depend on several factors, but prominent among these is the slagging character of the coal. To evaluate this property, the COALMASTER program calculates the slagging index R_{VS} for each of the cores. These can then be inspected by plotting the indices as a percentage of the coal tonnage as in Figure 5. In this example, the index varies from about 0.75 to 1.8, indicating for a Western type ash, medium to moderately high slagging characteristics. (Refer to (2) for the guidelines used here.)

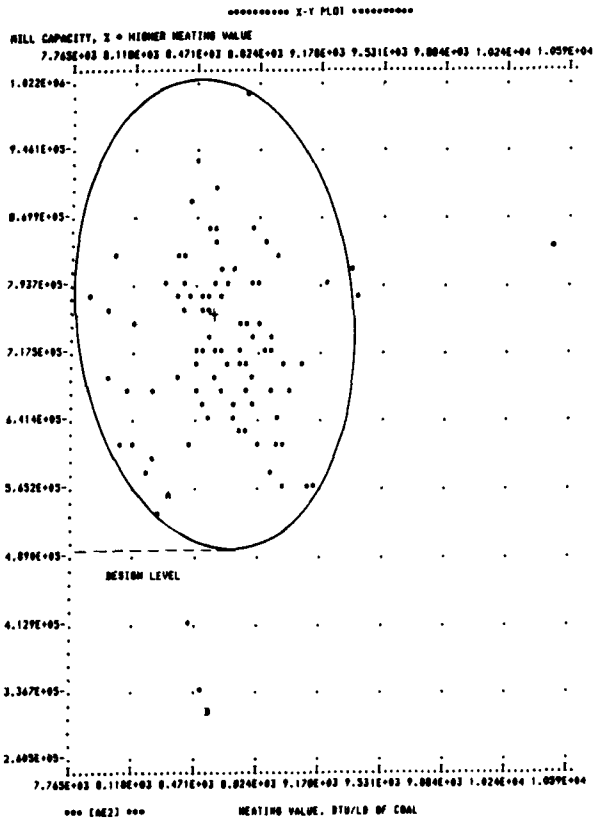

Figure 4. Relative Mill Throughput and Heating Values for Individual Cores.

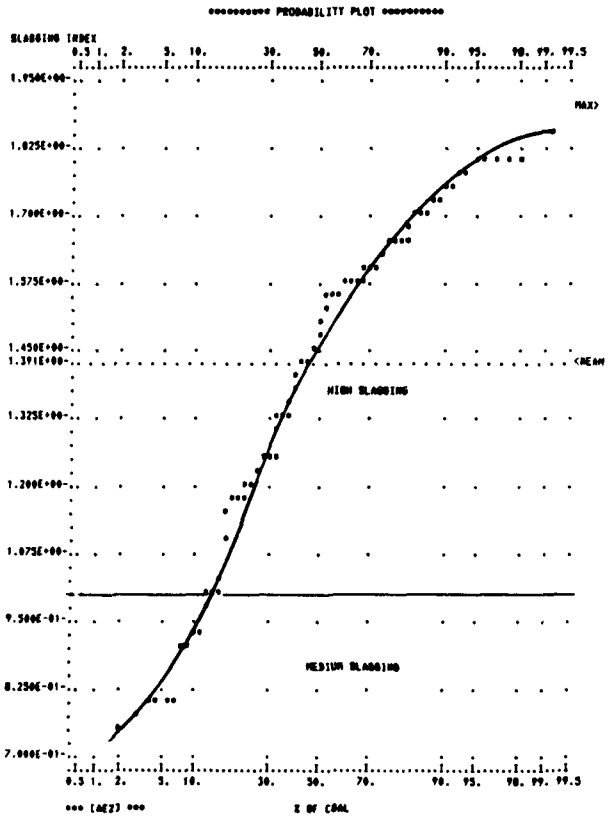

Figure 5. Probability Plot of Slagging Index.

The boiler designer would therefore select an intermediate-sized furnace corresponding to an intermediate heat-release rate (Btu/ft^2/hr). Beyond the furnace zone, other areas of the boiler are also affected by the properties of the ash.

In the back pass of the boiler, the positioning and spacing of the platens and tubing in the superheater-reheater and economizer sections are critically dependent on the fouling properties of the ash. Wider spacing is required to prevent bridging and plugging as the fouling index increases. The type of airheater can also be affected. We at AE2, however, believe the fouling index should also be evaluated along with the slagging characteristics. A situation involving an evaluated medium fouling type ash with a severe slagging characteristic represents a more difficult situation than one with a medium slagging characteristic. The severe slagging ash raises furnace temperatures, thereby raising back pass temperatures, accelerating tube fouling. The simultaneous occurrence of high slagging and medium fouling is readily determined by plotting the slagging index versus the fouling index as shown in Figure 6. The points falling in the upper-right-hand quadrant represent cores with high slagging and medium fouling properties. They represent about 18% of the cores, a significant portion of the fuel. The designer is therefore cautioned to give added weight to the indicated medium fouling character-

istics. Looking even further down the line, the control of particulate and sulfur oxide emissions must be considered.

Flue Gas Desulfurization Parameters

As previously discussed, the retention of sulfur in the ash, particularly a basic Western ash, can significantly impact on the efficiency demands on the FGD system. This is clearly demonstrated in our next example presented in Figure 7. The sulfur emission levels anticipated are shown in a cumulative plot of the coal tonnage. Levels do not exceed the old standard of 1.2 lbs per million Btu. In contrast, sulfur levels in the coal do actually range above this standard to about 1.35 lbs

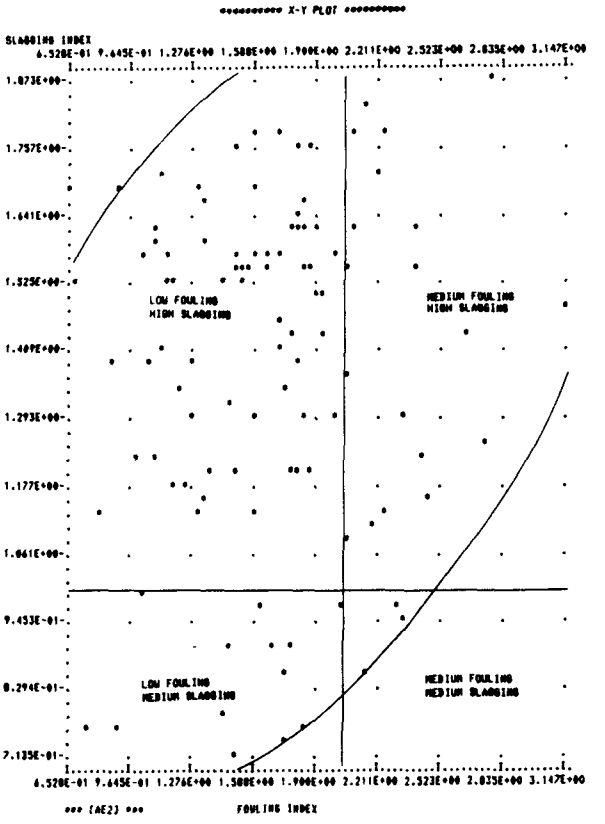

Figure 6. Slagging and Fouling Indices of Individual Ash Samples.

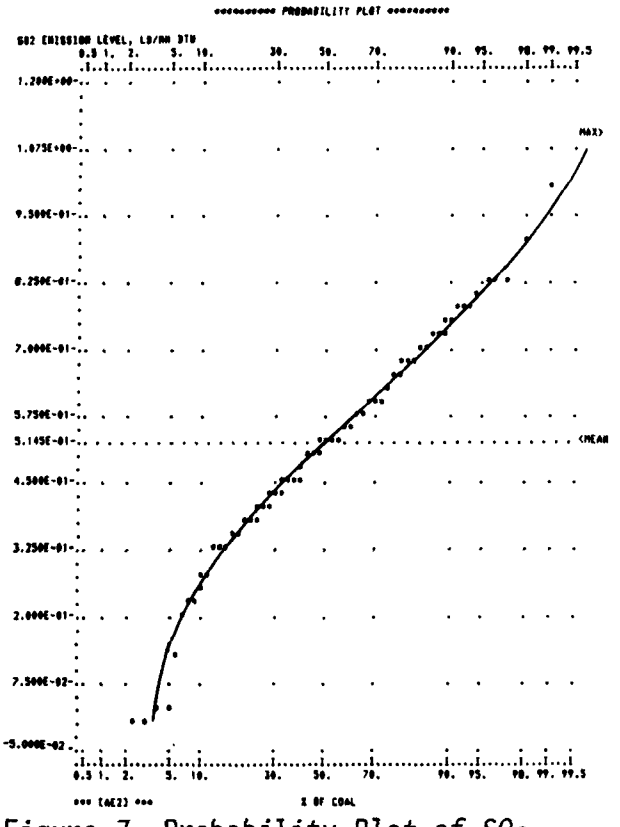

Figure 7. Probability Plot of SO_2 Emissions Level.

per million Btu. If the old standard is applicable, the calculation here demonstrates that no scrubbers would be required.

Applying the current emission standards, the minimum 70% reduction must be achieved. No more than 30% of the potential 1.35 lbs of SO_2 per million Btu associated with the coal can be emitted, i.e., 0.40 lbs/million Btu. Without the analysis here, scrubbers would therefore be designed for 70% removal efficiency. Taking advantage of ash retention shows that the scrubber actually requires an efficiency of about 53% to reduce the emissions from 0.825 lbs to 0.405 lbs per million Btu. With a 600 MW boiler, savings in capital and operating

costs amount to over 30 million dollars over the life of the plant.

PRECIPITATOR PARAMETERS

In this situation, a design opacity of 20% was specified. Figure 8 is a probability plot of outlet opacity for the design collecting area specified by the designer. This area was correctly specified and will adequately treat about 97% of the coal. Three isolated cores would require extraordinary levels of CE area; it is not appropriate to design for these cores.

Examination of the relationship between outlet opacity and various coal and ash parameters indicates that ash resistivity was the dominant factor. Figure 9 shows the dependence of outlet opacity on ash resistivity. A similar plot demonstrated that ash loading was not as critical.

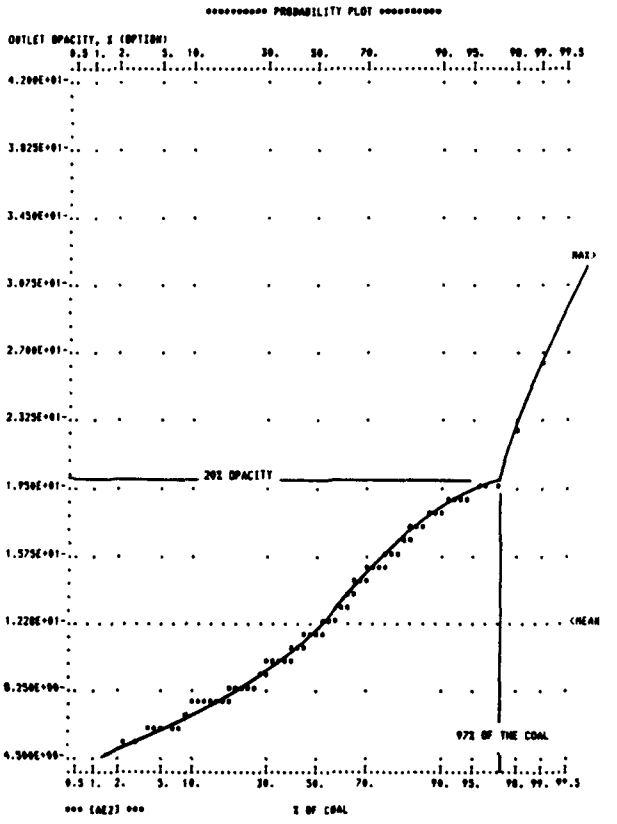

Figure 8. Probability Plot of Outlet Opacity.

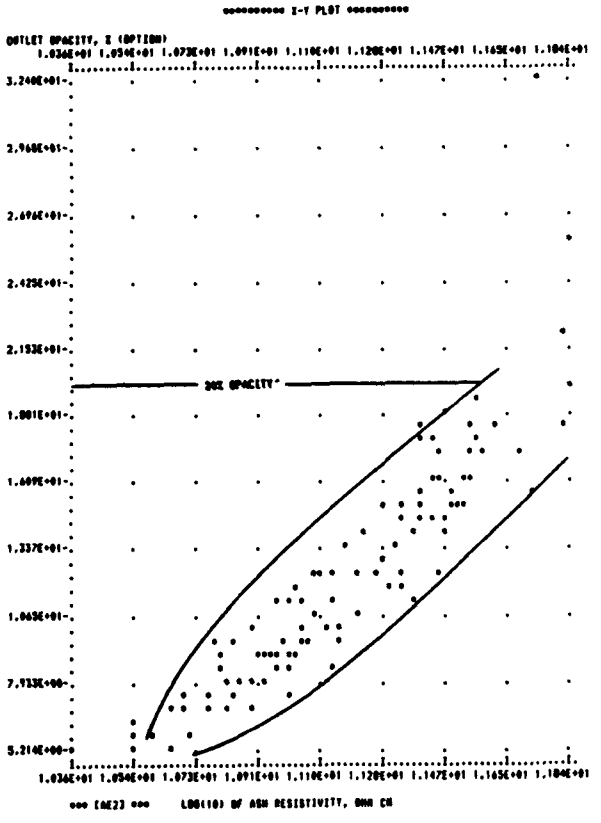

Figure 9. Dependence of Outlet Opacity on Ash Resistivity.

Figure 10 is a mine map overlaid with ash resistivity indicators. (The Z indicators, scaled from 0 to 9 in order of increasing resistivity, refer to each bore hole; the key is not shown in our paper.) We have delineated on the map two relatively low resistivity areas and one critical resistivity zone (>5(10)" ohm cm). Use of the X-Y-Z plot permits one to modify the mining plan if economically feasible or to take appropriate action to avoid unattractive coal (high resistivity, high slagging ash, etc.).

And finally, Figure 11 shows the perversity of nature. Fuels which require relatively low ESP collecting areas are those which exhibit the higher levels of fouling index. This is a consequence of the opposing dependence of ash resistivity and fouling tendency upon soluble sodium content of the ash.

CONCLUSION

The large amount of data generated during the evaluation of large coal mining properties must be handled by computers. The computer programs typically used, however, lack flexibility, particularly in the generation of new parameters and indices, as well

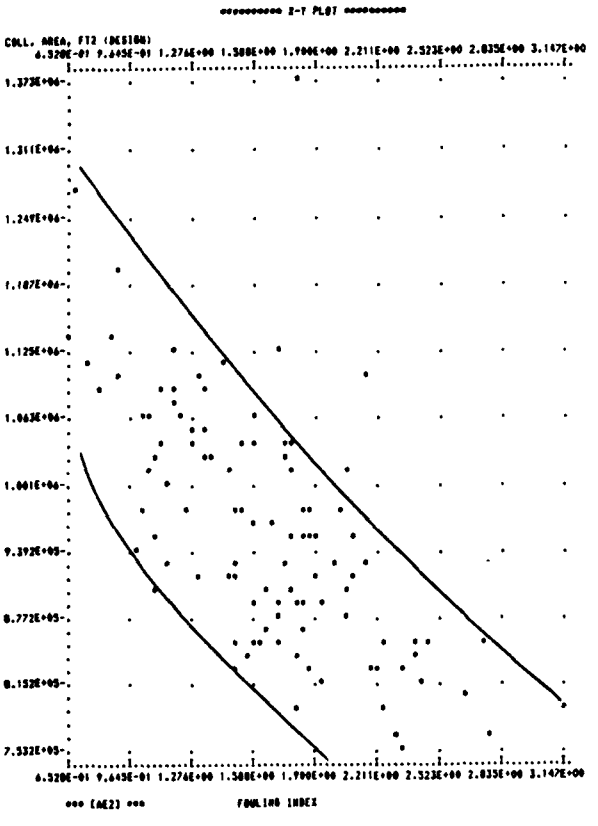

Figure 11. Relationship of Required ESP Collecting Area and Fouling Index.

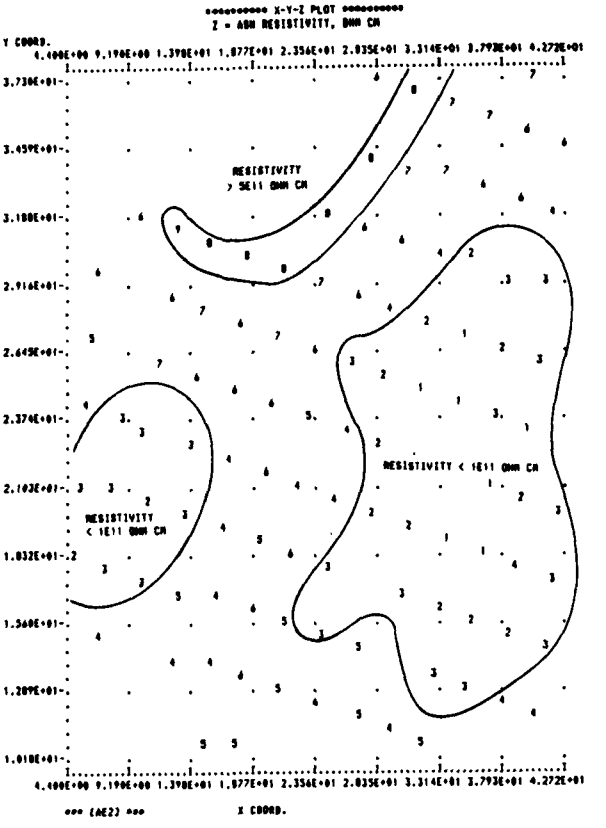

Figure 10. Mine Map Showing Location of High and Low Ash Resistivity Zones.

as in the types of plots that can be generated. The COALMASTER program was developed to overcome these shortcomings and extend the data base where necessary to produce basic design parameters for large boiler installations and associated air quality control equipment. An additional objective is to size the electrostatic precipitator required to meet any given emission target whether efficiency, mass or opacity.

The COALMASTER program, therefore, extends the basis for the technical and economic evaluation of new or even

currently mined coal deposits. Key parameters are presented in both tabular statistical form and graphical plots for the designer of equipment involved in the utilization of the resource. In light of today's high capital costs and ever-increasing maintenance costs, it is imperative that the design match the coal. The responsibility here is shared among the producer of the coal, the boiler owner and his architectural engineer, as well as the vendor of the equipment. AE2 welcomes inquiries from these parties and others regarding the use of the program.

The work described in this paper was not funded by the U.S. Environmental Protection Agency and therefore the contents do not necessarily reflect the views of the Agency and no official endorsement should be inferred.

REFERENCES

1. Duzy, A.F., et al. Western Coal Deposits, Pertinent Qualitative Evaluations Prior to Mining and Utilization. Paper presented at the 1977 Ninth Annual Lignite Symposium, May 18, 1977, Grand Forks, N. Dakota.

2. Bryers, R.W. On-Line Measurements of Fouling and Slagging and Correlation with Predictive Indices. Paper presented at the June 1981 Lignite Symposium sponsored by D.O.E. at San Antonio, Texas.

3. Watt, J.D. and Fereday, F. The Flow Properties of Slags Formed from the Ashes of British Coals: Part 1. Viscosity of Homogeneous Liquid Slags in Relation to Slag Composition. J. Inst. of Fuel XLII, No. 338, 99-103, (Mar.1969) Part 2. The Crystallizing Behaviour of the Slags, J. Inst. of Fuel XLII No. 339, 131-134 (Apr. 1969).

4. Barrick, S.M. and Moore, G.F. Empirical Correlation of Coal Ash Viscosity with Ash Chemical Composition. Paper presented at ASME Annual Meeting, Dec. 5, 1976, New York, NY.

5. Winegartner, E.C. and Rhodes, B.T. An Empirical Study of the Relation of Chemical Properties to Ash Fusion Temperatures. J. Engineering for Power 97, 395-406 (1975).

6. Gronhovd, G.H., Tufte, P.H. and Selle, S.J. Some Studies on Stack Emissions from Lignite-Fired Power Plants. Paper presented at the 1973 Lignite Symposium, May 9-10, 1973, Grand Forks, N. Dakota.

7. Davis, W.T. and Fiedler, M.A. The Retention of Sulfur in Fly Ash from Coal-Fired Boilers. J. Air Pollution Control Association 32 395-397 (April 1982).

8. Frisch, N.W. Engineering Manual for Fly Ash Precipitators (1981).

9. Matts, S. Coal-Ash Composition and Its Effects on Precipitator Performance. Flakt Engineering 1 No. 3 (Oct. 1977).

10. White, H.J. Industrial Electrostatic Precipitation, Addison-Wesley Publishing Company, Inc., Reading, MA, 1963.

11. Sproull, W.T. Collecting High Resistivity Dust and Fumes. Laboratory Performance of a Special Two-Stage Precipitator. Ind. Eng. Chem. 47 940-944 (No. 5, 1955).

12. Frisch, N.W. and Coy, D.W. Sizing Electrostatic Precipitators for High Temperature. Paper presented at Symposium on the Changing Technology of Electrostatic Precipitators, Adelaide, S. Australia, Nov. 8, 1974.

13. McDonald, J.R. A Mathematical Model of Electrostatic Precipitation, Vol. I, Modeling and Programming; Vol. II, User Manual, EPA-600/7-78-111 a,b - June 1978.

14. Saponja, W. A Systematic Approach to the Application of Electrostatic Precipitators on Lower Sulfur Coals. Paper presented at Canadian Electrical Association, Edmonton, Alberta, Oct. 1974.

15. Wagoner, C.L., Barrick, S.M., Vecci, S.J. and Piulle, W. Fuel and Ash Evaluation to Predict Electrostatic Precipitator Performance-A Progress Report. Paper presented at the IEEE-ASME Joint Power Generation Conference, Long Beach, CA, Sept. 18-21, 1977.

16. Tassicker, O.J. and Sproull, W.T. Improved Precipitator Technology by Pilot Plant Testing and Evaluation of Coal Bore-Cores. Paper presented at Particulate Control in Energy Processes Symposium held at San Francisco, California on May 11-13, 1976.

17. Engelbrecht, Heinz. Hot or Cold Precipitators for Fly Ash from Coal-Fired Boilers. Paper presented at Symposium on Coal Utilization and Air Pollution Control, Western PA section, Air Pollution Control Association, Apr. 21-22, 1976, Pittsburgh, PA.

18. Coy, D.W. and Frisch, N.W. Specifying Precipitators for High Reliability. Paper presented at Symposium on Control of Fine Particles, September 30 - October 2, 1974, Pensacola Beach, Florida.

19. Frisch, N.W. A Technique for Sizing Electrostatic Precipitators for Highly Variable Fuels. J. Air Pollution Control Association 30 574-575 (1980).

20. Bickelhaupt, R.E. A Technique for Predicting Fly Ash Resistivity. EPA-600/7-79-204, August 1979.

DEVELOPMENT OF INHALABLE PARTICULATE (IP) EMISSION FACTORS

by: Dale L. Harmon
Industrial Environmental Research Laboratory
U. S. Environmental Protection Agency
Research Triangle Park, N. C. 27711

ABSTRACT

At the request of EPA's Office of Air Quality Planning and Standards (OAQPS), ORD is conducting a study characterizing inhalable particle (IP) emissions from various sources for the development of emission factors.

Three contracts were awarded in September 1979 to conduct source characterizations for IP from major sources. The testing phase for these contracts is near completion, and individual reports on the major sources which will include the IP emission factors are being prepared. The IP emission factors are based on existing particle size data and the IP source characterization tests. This paper gives an overview of the EPA program to develop IP emission factors.

This paper has been reviewed in accordance with the U. S. Environmental Protection Agency's peer and administrative review policies and approved for presentation and publication.

INTRODUCTION

Early in 1978, a task force on inhalable particulate (IP) emission characterization was formed to develop a program for determining emission factors based on cutoff size for IPs from both controlled and uncontrolled sources. In 1978 EPA's Office of Research and Development (ORD) completed a plan for a program to obtain the IP data as specified by a priority listing developed by EPA's Office of Air Quality Planning and Standards (OAQPS). This plan is the basis for the ongoing IP emission factor development program.

DISCUSSION

The IP Emissions Factor Task Force Executive Committee which was formed in 1978 has been meeting about once a month since February 1979 to direct the work for development of IP emission factors. The committee has members from the following EPA organizations:

Office of Air Quality Planning and Standards (OAQPS),
Industrial Environmental Research Laboratory-RTP (IERL-RTP),
Industrial Environmental Research Laboratory-CIN (IERL-CIN),
Environmental Sciences Research Laboratory (ESRL), and
Division of Stationary Source Enforcement (DSSE).

An early task for the committee was to establish a list of priority sources to be tested for IP emissions. Since the range of sources emitting IP was large and the time and funds available were limited, it was necessary to make use of existing data to the maximum extent practical and test sources which would provide the highest practical level of return. The priority sources identified early in the program are listed in Table 1. Changes made in the priority list since it was developed have been to add iron foundries and industrial roads and to eliminate primary zinc smelters and incineration from the list. At the time the original priority list was developed and funding levels were established, funds were included for lower priority sources to be added when identified; however, budget reductions, delays in testing, and increased testing costs have eliminated any testing beyond that now planned.

When the IP emission factor program was first begun the Agency was examining the effects of several particulate size fractions including IP matter, then defined as ≤ 15 μm aerodynamic equivalent diameter, fine particulate, ≤ 2.5 μm aerodynamic equivalent diameter, and fractions between these size cut points. (2) The IP fraction is based on particulate matter which can deposit in the conducting airways and gas exchange areas of the human respiratory system while breathing through the mouth. A fine fraction ≤ 2.5 μm is based on chemical composition and the bimodal size distribution of airborne particles and the predominant penetration of particles ≤ 2.5 μm into the gas exchange region of the respiratory tract. (3)

A large data bank (> 300 test series) of particle size data on various industrial sources was in existence prior to initiation of the IP emission factor program. The most useful data was taken with impactors which have an upper stage cut-off of 10 μm or less. For this data to be used to develop

IP emission factors it was necessary to extrapolate from existing data to 15 μm. An extrapolation procedure was developed and data from the Fine Particle Emissions Information System (FPEIS)(4), a data bank developed for EPA containing much of the existing particle size data, has geen extrapolated to 15 μm. This data is adequate to provide IP emission factors for some industrial sources without additional testing.

During the time the IP emission factor program was being developed, it became apparent that the measurements problem for obtaining IP source data was much more difficult than originally believed. It was determined that a sizeable effort would have to be devoted to this area before any field measurements were actually undertaken. To this end a meeting was sponsored by EPA's Industrial Environmental Research Laboratory and Environmental Sciences Research Laboratory, both of Research Triangle Park (IERL-RTP and ESRL), bringing together many of the nation's measurement experts to develop a program to provide the necessary measurement and sampling techniques and expertise. These measurement experts decided that a 2-stage cyclone set would be the best device to use for point source sampling. Such a system was developed for EPA by Southern Research Institute to provide 15 and 2.5 μm size cuts. Before fabrication of these cyclone sets was complete, however, questions began to arise as to selection of a 15 μm upper limit for IPs. In the spring of 1980 it was determined that the definition of IP might be revised to some cut point less than 15 μm so that the cyclones could no longer be used. At this time, the approved point source sampling method became an impactor with a 15 μm cyclone precutter. Data is reported as a continuous plot of emission factor vs particle size from 15 μm down. When the IP cut point is finalized the appropriate emission factor can be read from the graph. An example curve is shown in Figure 1.

It is necessary to obtain IP fugitive emission data on industrial sources as well as point source data. Four test methods have been used for sampling IP fugitive emissions depending on the characteristics of the site to be sampled:

Quasi-Stack Sampling,
Roof Monitor Sampling,
Upwind/Downwind Sampling, and
Exposure Profiling.

Where cooling and dilution of ducted gas streams result in the formation of condensed particles, it is necessary to measure these condensibles as part of the IP emissions. One of the early tasks in the IP program was to develop a condensibles sampler. A prototype device was designed, fabricated, and field- and laboratory-tested by Southern Research Institute. It was intended that each of the contractors doing IP emission testing for EPA would fabricate one or more of the condensible samplers developed by Southern Research; however, by the time the sampler was developed it was not cost effective to do this with the limited funds remaining for testing, so all condensible testing for the IP emission factor program is being done with the prototype unit.

Draft copies of protocols for these test methods have been developed for those doing the IP testing. (5)(6)(7)(8)

In September 1979, as the result of a competitive procurement action, contracts were awarded to three IP characterization contractors to conduct plant surveys and source assessments for IPs and to support OAQPS in the development and implementation of an IP standard. Contracts were awarded to GCA Corporation, Midwest Research Institute, and Acurex Corporation. The scope of work for these contracts requires the contractor to conduct on-site plant inspections or surveys for the purpose of defining and evaluating the particulate pollution problems and for determining the fugitive emission sources. Following approval of a test plan developed by the contractor for the sites selected by EPA, the contractor conducted tests for ducted particulate matter, fugitive emissions, and condensible particulate matter as required.

When the IP characterization contracts were initiated, it was planned to use EPA personnel from IERL-RTP and IERL-CIN who were familiar with the industries to be tested to make test site selections. This did not work out in most cases because many of the EPA personnel did not have adequate time to devote to test site selection. It was necessary to direct the IP characterization contractors to develop priority lists for some industries and recommend specific sites for testing. Early in the program, it was decided to try to work on a cooperative basis with industrial organizations to gain access to test sites rather than use Clean Air Act Section 114 letters to gain access. Most of the industrial organizations contacted were willing to work on this project on a cooperative basis, but working out such agreements was time consuming.

It was originally planned that much of the testing would be done early in the contract period, but this was not possible. In addition to the delays in test site selection and gaining access to test sites, significant delays have resulted from the need to develop IP sampling equipment (including the condensibles sampler and size selective inlets and elutriators) for use in the fugitive measurements program.

It would have been desirable to conduct tests on several different sites for each source type, but the number of sites tested was limited by the funds available. Where possible, tests for IP emissions were combined with other EPA field tests to stretch the limited funds. Also, existing data is being used where possible to supplement IP testing. Table 2 lists the IP tests which have been completed to date. The only testing remaining to be completed with the available funds are tests of a steel mill BOF stack and an electric arc furnace and condensibles testing of a coal-fired industrial boiler, batch type asphalt plant, and (possibly) a coal-fired utility boiler.

All testing planned for paved urban roads has been completed. Testing of unpaved roads and industrial paved roads is near completion.

Tests at seven different steel plants have been completed, and tests at two additional steel plants are planned. Processes tested in steel plants include the cast house, sinter plant, quench tower, basic oxygen furnace, hot metal desulfurization, Q/BOP, paved and unpaved roads, and coal piles. Tests at one lime plant were completed. Processes tested were a kiln controlled by an ESP, a kiln controlled by a fabric filter, material transfer, and product loading fugitives. IP emissions from kilns on a dry process cement plant and a wet process cement plant have been completed.

Tests on three ferroalloy electric arc furnaces have been completed. The furnaces tested were producing silicon metal, ferromanganese, and ferrosilicon. Tests at an iron foundry were completed for pouring and cooling operations. Tests at a secondary lead smelter were completed. Processes tested were blast furnace metal and slag tapping and charging, agglomeration flue, refining kettle, and pigging machine. Slag and matte tapping operations were tested at a primary copper smelter.

Emissions from a drum mix asphalt plant have been measured, and plans are to measure the condensible emissions from a batch mix asphalt plant. Tests were completed at two pulp and paper plants. Processes tested were a nondirect contact evaporator type recovery furnace, a direct contact evaporator type recovery furnace, a lime kiln, and a smelt dissolving tank.

There is a large body of existing data available on combustion source emissions so that the only testing planned is for condensibles. Condensibles tests have been completed on a coal-fired utility plant, an oil-fired utility plant, and an oil-fired industrial boiler.

Test reports are being prepared for each field test, but it is not intended to publish these reports. As the testing is completed for a given source category, such as the ferroalloy industry, then one of the three IP characterization contractors is given the task of preparing a source category report on that category. This contractor will combine test results from all contractors, extrapolate valid pre-existing data, develop source category IP emission factors, and prepare a report which will be used for the AP-42 type input. The source category reports, which will contain summaries from the IP test reports, will be published as EPA reports.

Source category reports will be prepared for the following 10 source categories:

1. Paved Roads
2. Industrial and Unpaved Roads
3. Iron and Steel
4. Ferroalloy
5. Cement and Lime
6. Primary and Secondary Nonferrous
7. Iron Foundries
8. Asphaltic Concrete
9. Kraft Pulp Mills
10. Combustion

Preparation of source category reports has started on all source categories except industrial roads and combustion. First drafts of the paved road and the ferroalloy source category reports have been completed and reviewed by EPA. Final corrections are being made on these two reports, after which they will be submitted for peer review and publication. All of the source category reports should be completed by early spring of 1983.

REFERENCES

1. Compilation of Air Pollutant Emission Factors, Third Edition and Supplements, AP-42, U. S. Environmental Protection Agency, Research Triangle Park, N. C., August 1977 (and later).

2. Staff Paper Outline for Particulate Matter, Office of Air Quality Planning and Standards, U. S. Environmental Protection Agency, Research Triangle Park, N.C., July 31, 1980.

3. F. J. Miller, et al., "Size Considerations for Establishing a Standard for Inhalable Particles," Journal of the Air Pollution Control Association, 29(6): 610-615, 1979.

4. Reider, J. P., R. F. Hegarty, "Fine Particle Emissions Information System: Annual Report (1979)," EPA-600/7-80-092 (NTIS PB80-195753), U. S. Environmental Protection Agency, Research Triangle Park, N.C., May 1980.

5. Harris, D. B., "Procedures for Cascade Impactor Calibration and Operation in Process Streams," Revised 1979, 2nd Draft, U. S. Environmental Protection Agency, Research Triangle Park, N. C., 1979.

6. Protocol for the Measurement of Inhalable Particulate Fugitive Emissions from Stationary Industrial Sources, Draft, U. S. Environmental Protection Agency, Research Triangle Park, N. C., March 1980.

7. Wilson, R. R., W. B. Smith, Procedures Manual for Inhalable Particulate Sampler Operation, Draft, U. S. Environmental Protection Agency, Research Triangle Park, N. C., November 1979.

8. Williamson, A. D., Procedures Manual for Operation of the Dilution Stack Sampling System, Draft, U. S. Environmental Protection Agency, Research Triangle Park, N. C., October 1980.

TABLE 1. IP EMISSION FACTOR PRIORITY SOURCES

1. Paved and Unpaved Roads
2. Iron and Steel Manufacturing
3. Secondary Lead Smelters
4. Portland Cement Manufacturing
5. Lime Manufacturing
6. Asphaltic Concrete Manufacturing
7. Ferroalloy Manufacturing
8. Primary Nonferrous Smelters
   a. Copper
   b. Lead
   c. Zinc
   d. Aluminum
9. Kraft Pulp Mills
10. Combustion (Coal/Oil)
    a. Utility
    b. Industrial
    c. Commercial/Residential
11. Incineration

TABLE 2. COMPLETED IP EMISSION TESTS

Source Category	Sources Tested
Paved and Unpaved Roads	Urban Paved Roads
Iron and Steel	BOF Hot Metal Desulfurization Paved Roads Coal Storage Pile Cast House Q/BOP Sinter Plant Quench Tower
Cement and Lime	Lime Plant Kiln-ESP Kiln-fabric filter Material Transfer Product Loading Cement Plant Kiln-wet process Kiln-dry process
Ferroalloy	Electric Arc Furnace Silicon Metal Ferromanganese Ferrosilicon
Iron Foundry	Pouring and Cooling
Primary and Secondary Nonferrous	Secondary Lead-various ducted and fugitive sources Primary Copper-matte tap, slag tap, and idle ladle
Asphaltic Concrete	Drum Mix Plant
Pulp and Paper	Recovery Furnace-nondirect contact evaporator Recovery Furnace-direct contact evaporator Lime Kiln Smelt Dissolving Tank
Combustion	Coal-Fired Utility Boiler-condensibles Oil-Fired Utility Boiler-condensibles Oil-Fired Industrial Boiler-condensibles

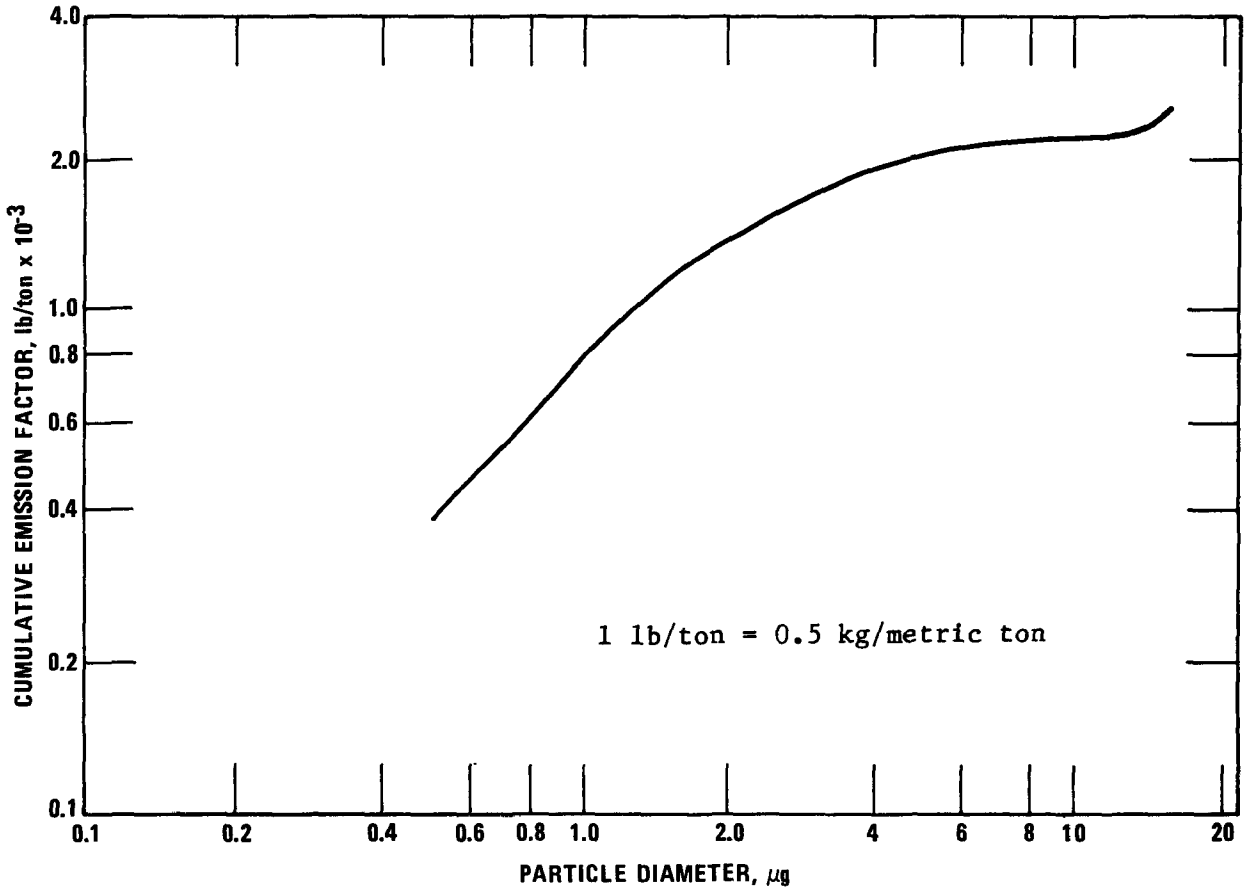

Figure 1. Emission factor for controlled emissions from hot metal desulfurization plant based on one test.

INHALABLE PARTICULATE MATTER RESEARCH COMPLETED BY GCA/TECHNOLOGY DIVISION

by: Stephen Gronberg
Senior Environmental Scientist
GCA/Technology Division
213 Burlington Road
Bedford, MA 01730

ABSTRACT

GCA/Technology Division has completed literature surveys and stack tests in order to develop reliable size-specific particulate emission factors. The majority of work concerned the iron and steel, ferroalloy and iron foundry industries. Particulate emission rates and particle size distribution were measured at eight facilities. Typically, tests were conducted before and after a control device and only in-stack techniques were used. The results of these tests and information from other test programs have been reviewed, ranked, and included in a Source Category Report for each industry. The Source Category Reports provide an updated section of AP-42 "A Compilation of Emission Factors" and present background information on industry trends, engineering specifics and control devices.

This paper has been reviewed in accordance with the U.S. Environmental Protection Agency's peer and administrative review policies and approved for presentation and publication.

INTRODUCTION

The EPA Office of Research and Development contracted GCA/Technology Division in June of 1980 to develop size-specific particulate emission factors for the iron and steel, ferroalloy production and gray iron foundry industries. Through literature searches, telephone surveys and other methods, GCA prepared test plans which were a summary of the best available particulate emissions data for each industry. Potential emission rates, control devices and test sites were described in industry-wide Test Plans. EPA subsequently requested permission to conduct IP tests at potential test sites of interest. Eight sources have been voluntarily sampled using IP procedures and two more tests programs are scheduled. Reports describing each of the completed test programs in detail have been submitted to and reviewed by EPA.

After completing several tests, EPA issued technical directives to compile Source Category Reports for each of the three industries. The Ferroalloy industry tests were completed first and this Source Category Report was prepared and submitted to EPA. Comments on the report are presently being implemented in all three Source Category Reports. The reports present background information for revised sections of AP-42 "A Compilation of Emission Factors." These reports are an up-to-date summary of reliable emissions information and are useful to States when revising Implementation Plans and to control device manufacturers, local regulatory agencies and other industrial personnel.

Present areas of IP work at GCA include more in-depth analyses of the data and samples obtained during field tests. Samples of respirable and nonrespirable particulates are being analyzed for up to 28 elements of interest, such as cadmium, lead, iron, etc. Neutron activation and x-ray fluorescence techniques are being used and the first report of results is presently under evaluation. Through these analyses, source signatures will be developed where the elemental composition of certain size particles will be determined. Only a trial set of samples from a sinter plant test have been analyzed; however, all sources tested as part of the IP program will eventually be analyzed by one or both methods. In addition, volatile and nonvolatile carbon analyses will be performed.

Draft reports of field tests are being revised in light of recent efforts by Southern Research Institute to more accurately predict particle behavior in the cyclones and impactors used in particle size determinations. The results presented in this paper may therefore change slightly in the near future.

SAMPLING AND ANALYSIS PROCEDURES

GENERAL

Prior to conducting field tests, several directives were issued to compile information on available particulate data, industry trends, control devices and to assess the availability of sampling locations. One directive

was issued to develop emission factors based on all particulate data stored in the EPA "Fine Particle Emission Inventory System" (FPEIS). Approximately 750 size distribution measurements of 15 different source categories were compiled where 350 of the measurements were performed on coal-fired boiler emissions, 100 on electric arc furnaces, 98 on lime kilns and 65 at gray iron foundries. An example of 1 of the 17 size distribution plots compiled from FPEIS data is provided in Figure 1. This distribution is based on 235 particle size measurements.

Three directives were then issued to develop Test Plans for the iron and steel, ferroalloy and iron foundry industries. Sources of emissions were ranked according to their potential (i.e., uncontrolled) yearly emission rates. Based on the iron and steel Test Plans, GCA developed and conducted field sampling programs for the top three ranked source categories, sources which in total could emit approximtely 85,000 tons per year of particulate.

In the Ferroalloy production industries, tests were conducted on three electric arc furnaces in cooperation with a Research Triangle Institute (RTI) program to characterize organic material emissions. The open furnaces tested were producing silicon metal, ferrosilicon and ferromanganese. All three were controlled by positive pressure baghouses. The major sources of emissions in the iron foundry industry were found to be the melting operations, which were also found to be well characterized in the literature. Tests were planned and conducted on a foundry pouring and cooling operation, a source for which no reliable particle size data was available.

IP PROCEDURES

Size specific emission factors are based on a combination of simultaneous total particulate and particle size distribution measurements. Total particulate emission rates were measured using a conventional EPA Method 5 sampling train. Particle size distribution was measured using Andersen cascade impactors equiped with cyclone precollectors. In addition, a dual-cyclone train was operated in order to obtain bulk size-fractionated samples for future elemental analysis.

Prior to field sampling, a presurvey of the host site was conducted in order to gather the necessary data and to arrange for installation of sampling facilities. Six inch (ID) sampling ports were needed for the dual cyclones. A detailed Test Plan for the individual site was prepared and submitted to EPA for approval. After approval, field sampling was usually completed in 1 week. Four tests, each typically consisting of one total particulate and two impactor runs, were usually conducted simultaneously before and after a control device. Inlet impactor runs were much shorter than the outlet runs and sometimes up to four inlet runs were completed during one outlet impactor run. Several tests were conducted in cooperation with other agencies. The EPA Office of Air Quality, Planning and Standards (OAQPS) funded the dual cyclone tests. EPA Region III and V provided some funds through existing contracts at GCA for iron and steel tests and as mentioned earlier, Research Triangle Institute performed the total particulate measurements at the

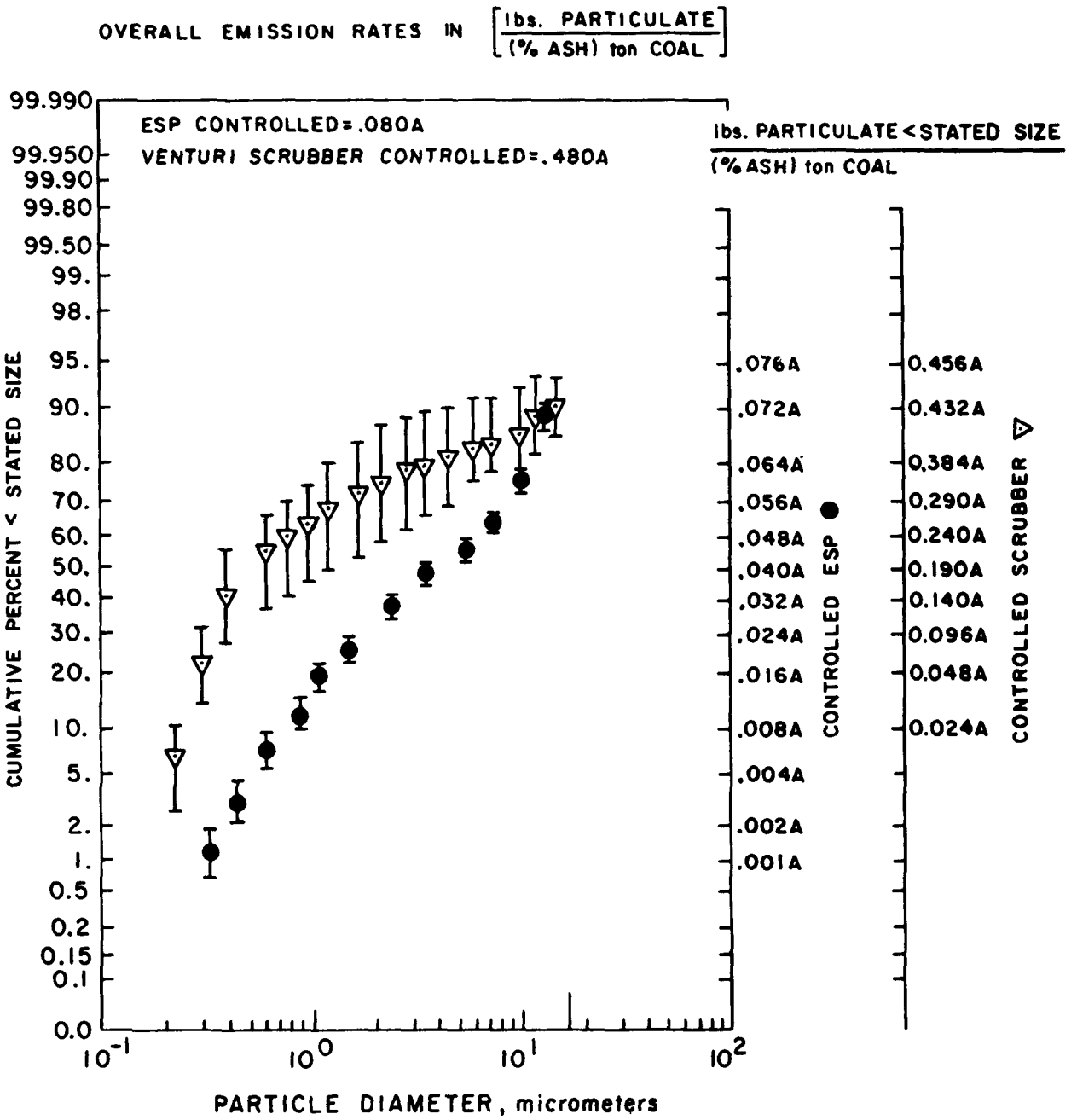

Figure 1. Example FPEIS compilation, pulverized bituminous coal combustion >100 MBtu/hr with 90 percent confidence intervals.

Ferroalloy plants. The coke quench tower tests were funded through several sources including, DOFASCO, the host source and Munters, the tower baffle system manufacturer. Typically, the added funding was used to add more depth to the programs. Additional points were sampled, more visible emissions data was obtained, and more in-depth process evaluations were conducted as a result.

Samples were obtained for ducted sources by isokinetic sampling of four or more sample points within the stack or duct. Collected particulates were weighed in order to determine concentration and size distribution. Some particulate samples will be analyzed for elemental constituents. Sampling and analytical data was reduced by computer. Verson 4.0 of the GCA Sampling Data Reduction System was used to calculate all total particulate results. Particle size distribution results were initially calculated using the Cascade Impactor Data Reduction System (CIDRS) developed by Southern Research Institute. A newer, interactive version of CIDRS was recently developed by Reseach Triangle Institute. The Particulate Data Reduction and Entry System (PADRE) is on the EPA Univac computer and is accessible to all subscribers through a telecommunications network. A program user enters data into PADRE in response to specific prompts whereas CIDRS is a batch type program where cards are punched and the program is run all at once. PADRE checks each entry and allows greater quality control of results. Cyclone precutter and dual cyclone results are calculated using equations supplied by the designers, Southern Research Institute, however, revisions to the cyclone calculations may be forthcoming since additional calibration work is underway. IP protocol called for operating the cyclone precollector/cascade impactor combination at a flow rate that would provide a 15 micron cut size in the cyclone precollector. In many cases, this flow rate was felt to be too low to obtain good impaction of particulate onto the impactor glass fiber substrates since experience dictated that a higher flow was in order. The decision was made to operate the train in favor of the impactor and to attempt to calculate the new size cut point in the cyclone precollector. Southern Research Institute is investigating the behavior of the cyclone precutters at these different flow rates.

SOURCE SIGNATURE PROCEDURES

A dual cyclone train was designed by Southern Research Institute for particle size determinations at ducted sources. The two cyclones in series have cut points of 15 and 2.5 microns when operated at the proper flow rates. The addition of a backup filter provides particulate samples of three size classifications, greater than 15, between 2.5 and 15 and smaller than 2.5 microns. The dual cyclone train was operated during most of the IP test programs with mixed results. The size fractions derived from the dual cyclone results usually agreed within a factor of 20 percent with the impactor results. However, the total particulate results were often a factor of two times different hence the size specific emission factors also varied greatly. Reasons for the variations are numerous and include single point (cyclones always operated at the center of the stack) versus multiple point sampling.

The elemental analysis results from the dual cyclone runs have yet to be finalized. Neutron Activation and X-Ray Fluorescence techniques are being employed to determine concentrations of elements such as lead, cadmium, calcium, magnesium, zinc, etc. When these results are available, the elemental composition of respirable and nonrespirable particles will be determinable. Presently, only preliminary results for tests conducted at a Sinter Plant by Midwest Research Institute are completed.

SUMMARY OF RESULTS

GENERAL

Field sampling programs have been completed by GCA at one coke quench tower, two blast furnace casthouses, one Q-BOP furnace, three ferroalloy plants, and one iron foundry pouring and cooling line. A brief summary of the results obtained follows.

COKE QUENCH TOWER

Dominion Foundries and Steel, Limited (DOFASCO) volunteered to host the IP Coke Quench Tower Test Program. Coke quenching is where hot coke, which was recently pushed out of a coke oven, is sprayed with water to stop the coking process. Coke arrives at the quench tower at 2500°F and leaves at 200°F. Some of the water used to quench the coke is recycled and 10 to 20 percent is lost to the atmosphere during quenching. IP tests were conducted in two phases, during clean and during dirty quench water usage. Clean water was defined as containing less than 1500 mg/l total dissolved solids (TDS); dirty water as containing more than 5000 mg/l TDS. Tests were conducted simultaneously above and below a set of Munters baffles installed in the tower. Nine to 12 quenches were sampled per run and 3 to 5 runs were completed during each water quality phase. The resulting IP emission factors are based on the amount of coal charged to the coke oven. The results, provided in Table 1, show the expected trends where higher emission rates resulted from dirty quench water useage. The particle size results are questionable in that water droplets may have caused a bias toward larger particles. The particle size results indicate a higher fraction of large particles (droplets) in the outlet stream than was present at the inlet to the baffles during dirty quench water usage. This study involved the efforts of Southern Research Institute in the measurement of condensable particle size distributions and water analyses were performed by several other recognized laboratories.

BLAST FURNACE CATHOUSES

Two different types of blast furnace casting emission control systems were tested using IP procedures. Dominion Foundries and Steel, Limited (DOFASCO), Hamilton, Ontario, volunteered to host tests at the No. 3 blast furnace. The roof monitor opening of this conventional, older casthouse was

TABLE 1. SIZE SPECIFIC EMISSION FACTORS, DOFASCO NO. 1 QUENCH TOWER

Test type	Total No. of quenches sampled	Cumulative	Particle aerodynamic 50% cut diameter (d_{50})					
			Total	15 μm	10 μm	5 μm	2.5 μm	1.0 μm
Clean Water								
Inlet	36	% mass $<d_{50}$	100	37.4	30.1	19.1	11.1	4.0
		lb $<d_{50}$/ton	1.1	0.4	0.3	0.2	0.1	0.0
Outlet	36	% mass $<d_{50}$	100	15.1	9.8	7.0	6.0	1.2
		lb $<d_{50}$/ton	0.3	0.1	0.0	0.0	0.0	0.0
Dirty Water								
Inlet	39	% mass $<d_{50}$	100	26.4	22.8	21.4	19.3	13.8
		lb $<d_{50}$/ton	5.2	1.4	1.2	1.1	1.0	0.7
Outlet	27	% mass $<d_{50}$	100	49.8	32.3	24.8	20.4	8.5
		lb $<d_{50}$/ton	1.4	0.7	0.5	0.3	0.3	0.1

sealed and connected via a 10 foot diameter duct to a positive pressure baghouse. Bethlehem Steel Cororation, Sparrows Point, Maryland, allowed tests of the newer L blast furnace casthouse runner evacuation system. L furnace is one of the largest in the United States and produces 10,000 tons per day. Four casting runner systems are available, each controlled by close fitting hoods connected to a positive pressure baghouse. At both test sites, the slotted roof monitor baghouse outlets prevented conducting meaningful outlet tests.

DOFASCO was tested in November 1981 and was the first IP test conducted by GCA. During the 1 week test program, 4 IP tests were completed during casting each consisting of 1 total particulate and 3 impactor runs. Two casts were sampled per total particulate run. The results are lower than the results of tests conducted in the same manner at Bethlehem Steel Corporation. The runner evacuation system emission factors are three times higher than the building evacuation system emission factors as shown in Table 2. Extensive visible emission observations were conducted during both test series. No significant differences in the apparent capture of emissions by the control systems was noted. The runner evacuation system test results also show a larger percentage of large particles. The proximity of the evacuating draft to the hot metal and slag runners is a logical reason for the higher emission factors. Note that the results presented here represent the "evacuated" emission factors and without the evacuating action of the control systems, emissions from a typical uncontrolled casthouse are probably less than the results of the tests at DOFASCO.

Q-BOP FURNACE

U.S. Steel Corporation volunteered to host IP tests at their Q-BOP shop located in Fairfield, Alabama. A Q-BOP furnace is similar to a conventional top-blown basic oxygen furnace (BOF) however oxygen is blown in from the bottom of the vessel. Furnace C, rated at 200 ton capacity, was tested at the outlet side of the quencher-scrubber control system. No sampling locations were available at the inlet to the control devices. This furnace is a closed furnace in that the hood is directly attached to the furnace shell. The combustion of off gasses is suppressed by limiting the amount of ambient air infiltration to only 10 percent of that required for complete combustion. Carbon monoxide levels of 20 percent (v/v) are typical during the oxygen blow period. A sliding doghouse enclosure is also connected to the control system whereby any emissions escaping the close fit hood are captured.

The results of the IP tests, shown in Figure 2 show effective particulate control. The quencher/scrubber combination is estimated to be 99.6 percent efficient based on an assumed inlet loading of 15 lbs particulate per ton of steel produced. The particle size results show the expected penetration of particles smaller than 10 microns. Below this size, the particulate does not have the inertia to penetrate droplets of water in the control device.

The results presented were calculated using two different assumptions regarding the validity of the backup filter weight gain. Due to the potential for particle bounce within the impactor, the backup filter weight gain is

TABLE 2. SIZE SPECIFIC EMISSION FACTORS, BLAST FURNACE CASTING EMISSIONS

Source	Units	Particle aerodynamic 50 percent cut diameter (d_{50})					
		∞ [a]	15 μm	10 μm	5 μm	2.5 μm	1.0 μm
DOFASCO No. 3 Furnace	% mass $< d_{50}$	100	67	54	35	25	15
	$\frac{lb < d_{50}}{hr}$	114.7	76.8	62	40	29	17
	$\frac{lb < d_{50}}{ton\ iron\ cast}$	0.39	0.26	0.21	0.14	0.10	0.06
Bethlehem Blast Furnace	% mass $< d_{50}$	100	26.5	23.7	20.1	15.2	9.1
	$\frac{lb < d_{50}}{hr}$	500	132	118	100	76	45
	$\frac{lb < d_{50}}{ton\ iron\ cast}$	1.30	0.34	0.31	0.26	0.20	0.12

[a]From EPA Method 5 front half data.

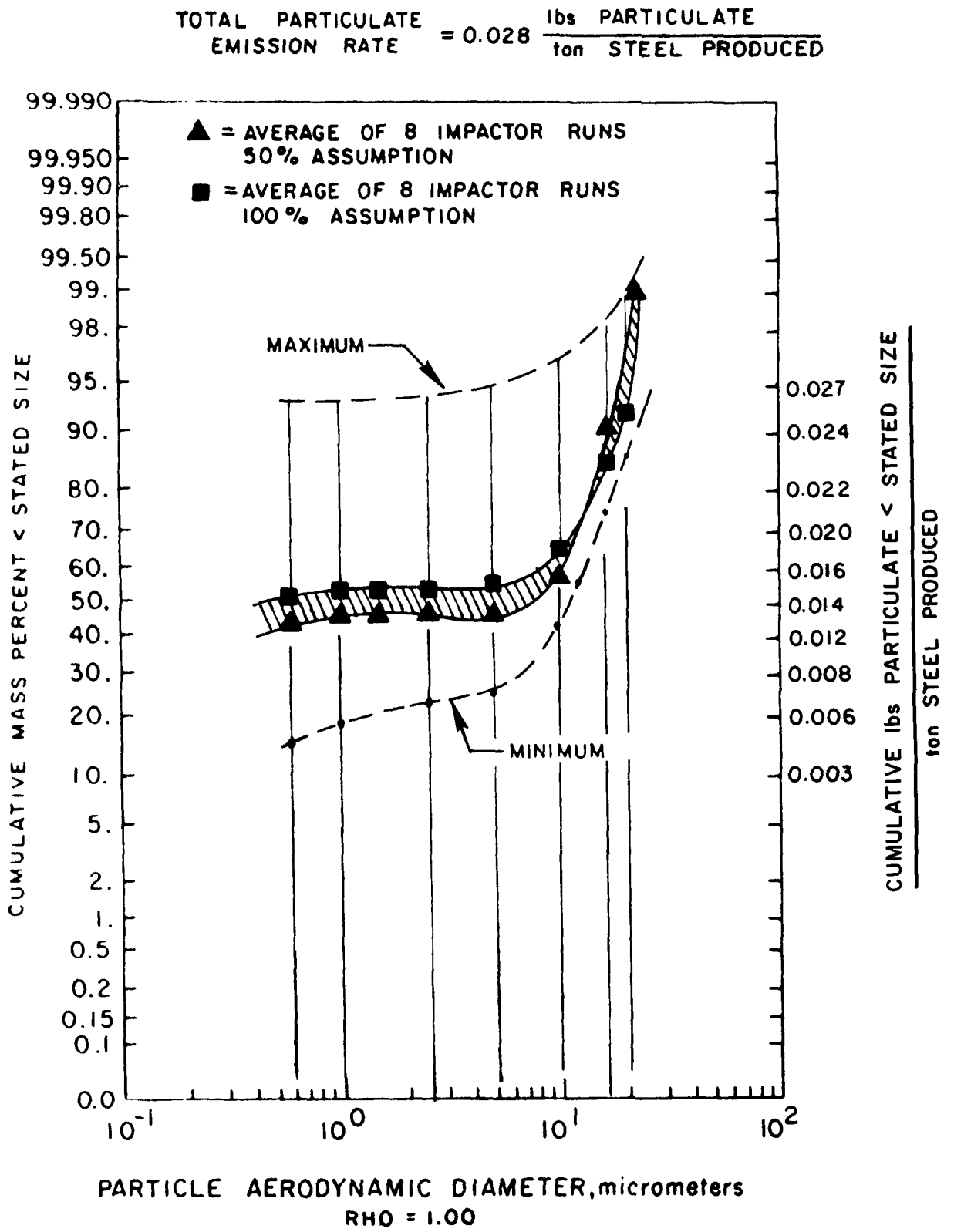

Figure 2. Average size distribution of emissions from a Q-BOP Furnace control system, U.S. Steel, Fairfield Works.

sometimes biased high resulting in erroneously high percentages of fine particles. The results were first calculated assuming that 100 percent of the weight gain was valid and then using the assumption that only half of the weight gain was actually attributable to particles smaller than the cut size of the previous impaction stage. Usually the two assumptions only affect the results in the 1 to 3 micron size ranges however the Q-BOP results were significantly affected over the 0.6 to 10 micron range. Particle bounce may have occurred since the impactors were operated at flow rates of 0.5 to 0.6 acfm and 0.7 acfm is considered the upper limit of good impactor performance.

FERROALLOY INDUSTRY

Emissons from three open electric arc furnaces producing ferroalloys were sampled using IP procedures. RTI performed the total particulate measurements through a subcontract to Entropy Environmentalists as part of a Level 2 Environmental Assessment of organic emissions. GCA/Technology Division personnel conducted particle size tests during the tests by Entropy. Isokinetic sampling was conducted simultaneously at the inlets and outlets of the baghouses controlling emissions from each furnace. The resulting size-specific emission factors are presented in Table 3 for each test series. The emission factors are based on the ferroalloy production rate during the test period.

Baghouse outlet tests were conducted at poor sampling locations. Positive pressure baghouses with roof monitor-type outlets are used at most ferroalloy facilities. These tests were all conducted in each of the individual baghouse compartments, about 6 feet above the top of the bags, at a single sample point. The flow was below detectable limits, therefore, isokinetic sampling was impossible. Since all three facilities were tested in the same manner, relative differences are notable; however, the overall accuracy is questionable. Baghouse inlet tests were all conducted isokinetically in horizontal circular ducts. Several inlet impactor runs were completed during each outlet run. The results show a wide variation in emission rates depending on the ferroalloy being produced and the results of the silicon metal tests, 800 lb/ton, were the expected results by source personnel.

IRON FOUNDRY POURING AND COOLING

The particle size distributions of emissions from foundry melting operations has been well documented in the literature. Sand handling, mulling and pouring and cooling are the next largest sources of emissions at a typical foundry. IP tests were conducted on a relatively new (1973) pouring and cooling line at Lynchburg Foundry, Lynchburg, Virginia. Ductile iron automotive parts were being cast during the test program.

Three stacks were tested simultaneously. Three stacks vent pouring emissions and three vent cooling emissions directly to the atmosphere. The total particulate results presented in Table 4 are based on one set of three simultaneous modified Method 5 runs on each operation. A third IP test, consisting of two runs on cooling stacks and one run on a pouring stack, was

TABLE 3. SIZE SPECIFIC EMISSION FACTORS, SUMMARY OF TESTS AT FERROALLOY PLANTS

Sampling location	Product	Units	Particle aerodynamic diameter (d_{50} in μm)					
			∞ [a]	15	10	5	2.5	1
Baghouse inlet	Ferrosilicon	lb/ton product	69.7	39.7	38.3	35.5	32.8	25.8
	Ferromanganese	lb/ton product	28.4	25.6	22.7	19.3	17.3	9.9
	Silicon Metal	lb/ton product	872	750	706	645	610	497
Baghouse outlet	Ferrosilicon	lb/ton product	1.84	1.38	1.29	1.03	0.83	0.53
	Ferromanganese	lb/ton product	0.48	0.42	0.38	0.29	0.22	0.11
	Silicon Metal	lb/ton product	33.0	30.4	27.7	22.4	18.5	12.54

[a]Based on EPA Methods 1 through 5 "front half" test results.

TABLE 4. SUMMARY OF EMISSION FACTORS, LYNCHBURG FOUNDRY

	Units	Pouring emissions	Cooling emissions
Production Rate	tons/hr	105	114
Total Particulate Emission Factors			
Mass Concentration[a]	gr/dscf	0.003	0.002
Mass Emission Rate[b]	lb/hr	2.21	2.52
Process Weight Rate[b,c]	lb/ton	0.021	0.022
Particle Size Distribution			
Cumulative Mass[a]	% <15 μm d_{50}	65	63
	% <2.5 μm d_{50}	22	20
Mass Emission Rate[b]	lb <15 μm d_{50}/hr	1.44	1.59
	lb <2.5 μm d_{50}/hr	0.49	0.50
Size Specific Emission Factors[c]			
lb particulate <15 μm d_{50}/ton		0.014	0.014
lb particulate <2.5 μm d_{50}/ton		0.005	0.005

[a]Average of four pouring and five cooling runs.

[b]Sum of three simultaneous runs.

[c]Based on the total weight of sand, cores and hot metal processed.

completed on the last field sampling day. The mix was chosen in the field to provide a more balanced total number of runs on both operations. When calculating emission factors, however, the total particulate emission rate from each of the three stacks venting each process is needed. The results show large differences in emission rates from each stack and the potential for variability in emission generation rates. The average of all five cooling and four pouring impactor runs were used to determine the particle size fractions. These results are multiplied by the average of three simultaneous Method 5 runs to calculate emission factors.

The total particulate results appear to correlate well with the amount of activity assocated with the area evacuated. Pouring operations were mainly performed under the hood connected to the stack where the results are six times greater than the results of the other tests on the stack which is over the area usually vacant for safety purposes among other reasons. Sometimes a second operator pours hot metal under the hoods connected to the stack for which results are in between the results of tests. The cooling room emission rates also appear to correlate with the location being vented. The highest emission rates were measured where the hot flasks first enter the room and the lowest rates were measured at the cooling room exit area. All of the results were very low and the maximum particulate catch was 67 mg after sampling 220 dscf.

CONCLUSIONS

The emission factors developed thus far are presently being reviewed in light of recent research on fine particle behavior in cyclones and impactors. Calibrations are being conducted by Southern Research Institute and modifications to the PADRE data reduction system are also underway. Most of the IP data will be reanalyzed shortly and the emission factors presented here may change slightly. Also in the near future, interesting conclusions regarding the elemental nature of the respirable particulates will be available.

RESULTS OF TESTING FOR INHALABLE PARTICULATE MATTER AT MIDWEST RESEARCH INSTITUTE

by: H. Kendall Wilcox
Fred J. Bergman
John Scott Kinsey
Tom Cuscino

Midwest Research Institute
Kansas City, Missouri 64110

ABSTRACT

Source test data collected by Midwest Research Institute for emissions of inhalable particulate matter have been presented in this paper for a variety of industrial categories. Test results for two cement plants (one wet process and one dry process), one lime plant, and one asphalt paving plant are available. Results have been presented in terms of the AP-42 format for the relative size fractions of both controlled and uncontrolled emissions from these processes. Such test results should be of interest to control device manufacturers as well as those who may need to be involved in the development of State Implementation Plans for inhalable particulate matter.

This paper has been reviewed in accordance with the U.S. Environmental Protection Agency's peer and administrative review policies and approved for presentation and publication.

RESULTS OF TESTING FOR INHALABLE PARTICULATE MATTER AT MIDWEST RESEARCH INSTITUTE

INTRODUCTION

The U.S. Environmental Protection Agency (EPA) is conducting research to characterize the emissions of the fine particles in the inhalable particulate (IP) size range for a variety of industrial sources. The purpose of this research is to develop emission factors which are to be used if revisions to the National Ambient Air Quality Standard for particulate matter are made to address fine particles. It was originally planned to determine size specific mass concentration on uncontrolled sources and to calculate emissions based on established control efficiencies. However, since most control efficiency data were based on total suspended particulate (TSP), the scope of the program was modified to simultaneously determine uncontrolled and controlled size specific mass concentrations.

Testing at Midwest Research Institute has included one lime plant, one wet process cement plant, one dry process cement plant, and one drum mix asphalt plant. This paper presents a brief overview of the testing procedures used to collect the data from ducted sources and the results of the measurements made in terms of the emission factors for each process. More detailed information regarding the plant processes, control devices and plant configurations has been reported previously. (1)(2)

GENERAL PROCEDURES

SAMPLING PROCEDURES

The basic sampling methodology used by MRI to determine the controlled and uncontrolled emissions from each plant is that specified in the protocol document developed for the EPA's IP program. (3) Certain modifications were made to the standard protocol, however, when it was deemed necessary to collect a more representative sample of the emissions.

Basically the protocol requires collecting multiple samples in each of four quadrants of the duct as shown in Figure 1. Where suitable ductwork meeting Method 5 requirements was available A and B patterns were used. If suitable ductwork was not available, pattern C was used.

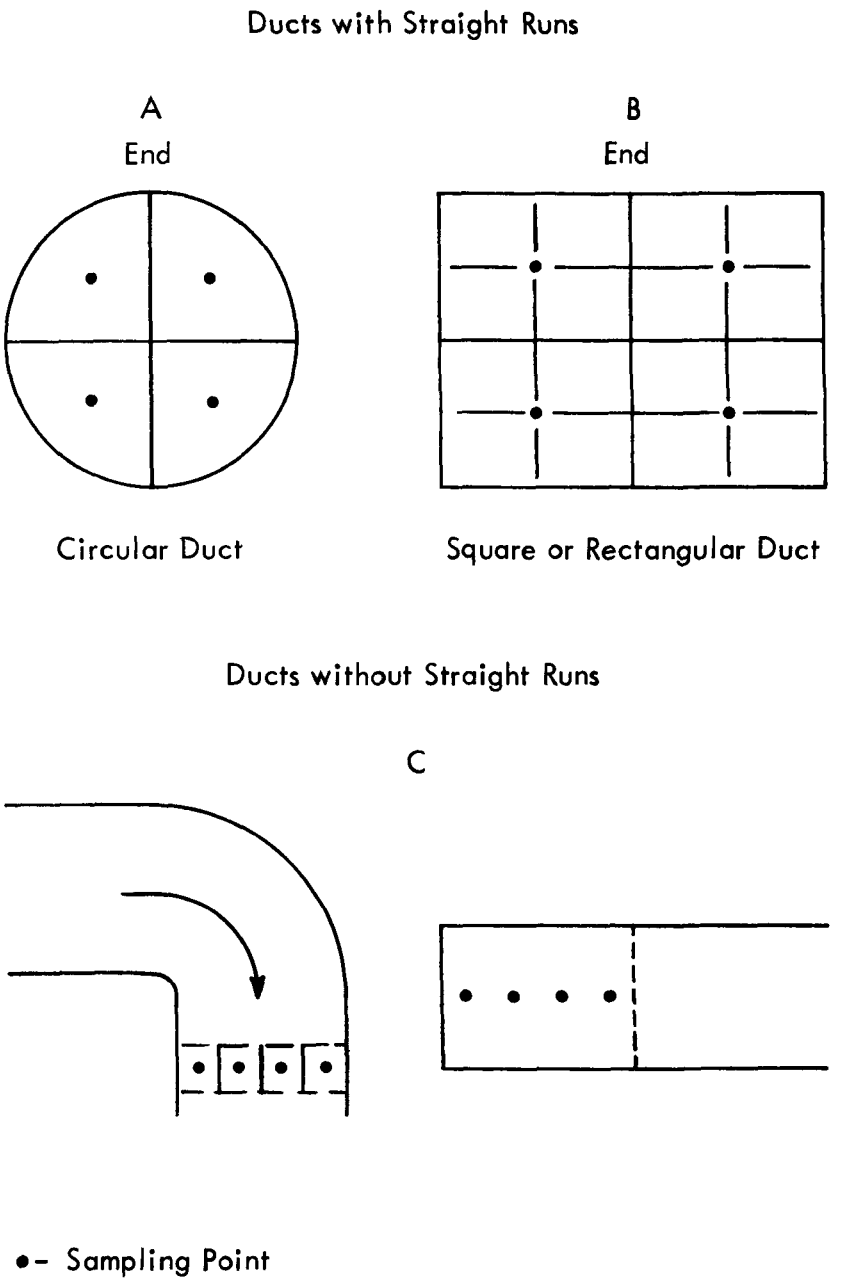

Figure 1. Sampling point locations

Two types of samples were collected at each sample point: total mass emissions; and particle size distribution. Although EPA Reference Method 2 was used to collect preliminary velocity data, the stack was not traversed during sampling. The total mass samples were collected isokinetically at each point using EPA Method 5 or Method 17 techniques. The particle size samples were collected at a constant flow rate according to manufacturer specifications using a suitable nozzle diameter to obtain as near isokinetics sampling as possible. Several types of samplers were used. For heavy loading conditions typically found at the inlet of a control device, an Andersen High Capacity Stack Sampler (HCSS) equipped with a Sierra 15 μm preseparator was used to collect the sample for all plants except the lime plant. For the lime plant a Brink 5 stage impactor was used with a 7 μm cyclone as the first stage. For the light loading conditions typically occurring for controlled emissions, an Andersen Mark III impactor equipped with the Sierra 15 μm preseparator was used. Although the sampling times varied substantially for the inlet and outlet, an effort was made to collect data from both the controlled and uncontrolled locations during the same time period.

Initially, four mass runs and four size runs were conducted from each quadrant for a total of 16 mass and 16 particle size runs for both the controlled and uncontrolled emissions. The number of samples was later reduced for the controlled emissions to two for each quadrant rather than four.

CALCULATION OF EMISSION FACTORS

The emission factors presented in this report were calculated as follows. Total emission factors were calculated from the results of the total mass runs (Modified Method 5 or Method 17) and the average production rate for the process during the test period.

Emission factors for the particle size measurement were calculated by determining the mass for each stage of the size device and calculating the cumulative percentages of the total mass for each. These percentages were then applied to the total mass emission factors from the modified Method 5 or Method 17 runs to obtain the emission factor for each stage.

A spline equation was used to fit the data and to extrapolate, where required, to the desired cutpoints. (4) Emission factors were calculated for 2.5, 10.0, and 15.0 μm. The particle diameter upper limit was assumed to be 50.0 μm for the calculations using the spline equation.

TEST RESULTS

The test results from these studies are provided in terms of the emission factors for the total particulate emissions based on the total mass determinations from the modified Method 5 and Method 17 samples. Emission factors for < 2.5 μm, < 1.00 μm, and < 15 μm were calculated based on the results particle size distribution obtained from the impactors and the total mass results.

ASPHALT PLANT

The test results from the drum-mix asphalt plant are shown in Table 1. This plant was nearly new at the time of testing and was in excellent mechanical condition. Sampling was conducted at the inlet and outlet of a baghouse collector. Test Nos. 1 through 4 were conducted with 100% virgin aggregate material. Tests A and B were conducted with approximately 34% of the aggregate comprised of recycled asphalt material. Due to process variations and the limited number of runs, it is difficult to draw any meaningful conclusions about the differences between virgin and recycled aggregate from the data. Variations included changes in production rate and in type of mix even within a one day period. However, even though the data was collected over a period of several weeks (due to unfavorable weather conditions) it is felt that the emission factors obtained are at least generally representative of most drum-mix asphalt plants.

DRY PROCESS CEMENT PLANT

The emission factors for the dry process cement plant are shown in Table 2. The kiln was operating at approximately 35 tons per hour and was equipped with a baghouse. Material exiting the kiln passes through a 3-stage suspension preheater system to remove the bulk of the larger material prior to entering the baghouse. The baghouse inlet was sampled between the preheater and the baghouse inlet. The outlet was sampled on the main exhaust stack.

LIME PLANT

The results of testing of the lime plant are shown in Table 3. Two kilns were operating in this plant. One kiln of 400 per day ton capacity was equipped with three electrostatic precipitators (ESPs) arranged in parallel, the other of 300 ton per day capacity was equipped with one 5-cell baghouse. Both controlled and uncontrolled emissions were measured for each kiln. The dust control system on the conveyor belt transfer points was also sampled.

WET PROCESS CEMENT PLANT

The emission factors for the wet process cement plant are shown in Table 4. This plant has two rotary kilns of 35 ton/hr which are each equipped with ESP units which exhaust through a common stack. The inlet to one of the two ESP units was sampled as well as the outlet prior to entry into the common stack.

During the latter part of the test the plant switched from Type II to Type I cement. Differences in ESP performance for the two types of cement are difficult to determine based on thelimited data available for Type I.

TABLE 1. SUMMARY OF INHALABLE PARTICULATE EMISSION FACTORS FOR THE ASPHALT PLANT

		Test No.	Emission factor (lb/ton)[a] Total	< 2.5 μm[b]	< 10 μm[b]	< 15 μm[b]
Baghouse Controlled side	ns	A[c]	25.2	-	-	-
		B[c]	16.3	-	-	-
		1	37.9	1.6	7.6	8.6
		2	37.6	1.5	7.6	8.9
		3	30.2	1.4	6.4	7.3
		4	27.9	2.1	7.0	7.9
		Average	30.9[d]	1.7	7.2	8.2
Baghouse Uncontrolled side		1	0.06	0.01	0.02	0.02
		2	0.07	0.01	0.02	0.03
		Average	0.07	0.01	0.02	0.03

[a] Pounds of particulate matter per short ton of asphalt paving produced.
[b] Aerodynamic diameter.
[c] Total mass runs only--no particle size information available. Tests conducted with plant using recycled asphalt paving as a raw material.
[d] Average emission factor is the arithmetic mean of the results from the eight total mass test runs and not an average of the data shown.

TABLE 2. SUMMARY OF EMISSION FACTORS FROM A DRY PROCESS CEMENT PLANT

Sampling location	Test No.	Emission factors Total (lb/ton)[a]	< 2.5 μm[b] (lb/ton)	< 10.0 μm[b] (lb/ton)	< 15.0 μm[b] (lb/ton)
Baghouse uncontrolled side	1	220	42	87	93
	2	220	31	83	90
	3	210	42	90	96
	4	210	39	94	99
	Average	220	38	88	94
Baghouse controlled side	1	0.62	0.20	0.44	0.45
	2	0.89	0.32	0.74	0.76
	Average	0.76	0.26	0.59	0.60

[a] (lb/ton) = pounds per ton of product.
[b] Aerodynamic diameter.

TABLE 3. SUMMARY OF EMISSION FACTORS FROM A LIME PLANT

	Test No.	Emission factors (lb/ton)[a]			
		Total	< 2.5 μm[b]	< 10 μm[b]	< 15 μm[b]
Baghouse uncontrolled side	1	133.8	14.2	52.0	74.8
	2	120.3	12.5	50.5	70.8
	3	118.9	15.6	53.6	72.7
	4	108.4	8.9	45.0	64.3
	Average	120.4	12.8	50.3	70.7
Controlled side	1	0.13	0.03	0.08	0.09
	2	0.09	0.02	0.05	0.06
	3	0.10	0.03	0.07	0.08
	4	0.10	0.03	0.07	0.09
	Average	0.11	0.03	0.06	0.08
Electrostatic precipitator uncontrolled side	1	354.4	3.6	50.0	134.0
	2	378.4	4.0	69.1	212.0
	3	395.5	2.6	59.7	154.1
	4	359.5	2.8	53.9	138.0
	Average	371.9	3.3	58.2	159.5
Controlled side	1	8.1	1.1	4.3	5.7
	2	10.5	1.1	4.7	5.8
	3	9.1	1.6	4.9	6.2
	4	9.5	1.2	4.6	5.3
	Average	9.3	1.3	4.6	5.8
Dust collector	1	1.8	0.06	0.15	0.17
	2	1.7	0.07	0.16	0.16
	3	3.0	0.10	0.27	0.32
	4	2.3	0.08	0.19	0.21
	Average	2.2	0.8	0.19	0.22

[a] (lb/ton) = pounds per ton of product.
[b] Aerodynamic diameter.

TABLE 4. SUMMARY OF EMISSION FACTORS--COMBINED AND INDIVIDUAL WET PROCESS CEMENT TEST RESULTS

Kiln sampling location	Test No.	Emission factors - cumulative % Total (lb/ton)[a]	> 2.5 μm[b] (lb/ton)	> 10.0 μm[b] (lb/ton)	> 15.0 μm[b] (lb/ton)
Combined cement product test results					
Electrostatic precipitator uncontrolled side	1	1,100	25	90	150
	2	1,100	22	80	130
	3	1,400	15	86	180
	4	1,400	18	84	150
Average		1,200	20	85	150
Electrostatic precipitator controlled side	1	0.10	0.079	0.087	0.099
	2	0.17	0.082	0.11	0.12
Average		0.14	0.08	0.10	0.11
Individual cement product test results[c]					
Type I cement product					
Electrostatic precipitator uncontrolled side		1,400	24	94	160
Electrostatic precipitator controlled side		0.15	0.08	0.10	0.12
Type II cement product[c]					
Electrostatic precipitator uncontrolled side		1,100	14	70	140
Electrostatic precipitator controlled side		0.13	0.079	0.10	0.10

[a] lb/ton = pounds per ton of product.
[b] Aerodynamic diameter.
[c] Data represent the average of all the sampling runs conducted during production of the specific type of cement product.

SUMMARY OF DATA

Two summaries of the data are shown in Tables 5 and 6. Table 5 shows a comparison of the particle size distribution for the uncontrolled and controlled emissions for each of the processes tested. It is generally expected that controlled emissions will contain higher percentages of fine particulate than the uncontrolled emissions. The data does show increased percentages of fine (< 2.5 μm) particulate in the controlled emissions by a factor of two or three for baghouses and from 15 to 35 for ESP's.

Table 6 presents a summary of the control device efficiencies for each device tested. As can be seen for the lime plant the baghouse represents a considerably better control device for this process.

TABLE 5. SIZE DISTRIBUTION, UNCONTROLLED VS. CONTROLLED

Process	Total E.F. lb/ton	Size Distribution wt. % less than stated size < 2.5 μm	< 10 μm	< 15 μm
Lime Plant				
Baghouse				
Uncontrolled	120	11	42	59
Controlled	0.11	27	54	73
ESP				
Uncontrolled	372	0.9	16	43
Controlled	9.3	14	49	62
Cement, Wet Process				
ESP				
Uncontrolled	1200	1.6	7.1	13
Controlled	0.14	57	71	79
Cement, Dry Process				
Baghouse				
Uncontrolled	220	17	40	43
Controlled	0.76	34	78	79
Asphalt, Drum Mix				
Baghouse				
Uncontrolled	30.9	5.5	23	27
Controlled	0.07	14	29	43

TABLE 6. CONTROL DEVICE EFFICIENCY

	Emission Factor, lb/ton		
	Uncontrolled	Controlled	% Eff.
Lime Plant			
Baghouse			
Total	120	0.11	99.91
< 15 μm	70.7	0.08	99.89
< 10 μm	50.3	0.06	99.88
< 2.5 μm	12.8	0.03	99.77
ESP			
Total	372	9.3	97.50
< 15 μm	159	5.8	96.35
< 10 μm	58.2	4.6	92.10
< 2.5 μm	3.3	1.3	60.61
Wet Process Cement Plant			
ESP			
Total	1200	0.14	99.988 +
< 15 μm	150	0.11	99.93
< 10 μm	85	0.10	99.88
< 2.5 μm	25	0.08	99.68
Dry Process Cement Plant			
Baghouse			
Total	220	0.62	99.7
< 15 μm	94	0.45	99.5
< 10 μm	88	0.44	99.5
< 2.5 μm	38	0.20	99.5
Asphalt Drum Mix Plant			
Baghouse			
Total	30.9	0.07	99.77
< 15 μm	8.2	0.03	99.63
< 10 μm	7.2	0.02	99.72
< 2.5 μm	1.7	0.01	99.41

REFERENCES

1. Bergman, Fred J. and Wilcox, H. Kendall. Inhalable Particulate Testing at Cement and Lime Plants. Paper presented at the 75th Annual Meeting of the Air Pollution Control Association, New Orleans, LA. June 20-25, 1982.

2. Kinsey, John Scott, Walker, T. and Wilcox, H. K. A Determination of Fine Particulate Emissions from a Drum-Mix Asphalt Plant. Paper presented at the 75th Annual Meeting of the Air Pollution Control Association, New Orleans, LA. June 20-25, 1982.

3. Wilson, R. R. and Smith, W. B. Procedures Manual for Inhalable Particulate Sampler Operation, Report No. SoRI-EAS-79-761, Southern Research Institute, Birmingham, AL. November 30, 1979.

4. Johnson, J. W., Clinard, G. I., Felix, L. G. and McCain, J. D. A Computer-Based Cascade Impactor Data Reduction System, EPA-600/7-78-042, U.S. Environmental Protection Agency, Washington, D.C. March 1978.

INHALABLE PARTICULATE EMISSION FACTORS TEST PROGRAMS

by: Jim Davison
Acurex Corporation
485 Clyde Avenue
Mountain View, California 94042

ABSTRACT

The Energy & Environmental Division of Acurex Corporation was contracted by the Industrial Environmental Research Laboratory (IERL) of the U.S. Environmental Protection Agency (EPA) to obtain uncontrolled/controlled emissions data from various stationary sources of air pollution. The emission factors derived from this data will assist in the determination of the need to set a national ambient air quality standard for inhalable particulate matter.

An extensive series of particulate mass and particle size distribution tests were conducted at several major sources, including Kaiser Steel (hot metal desulfurization and BOF), and Kennecott Minerals (matte and slab tapping).

This paper presents a review of each process, test equipment and procedures, and test results expressed as emission factors relative to process operations, and as a percent of the particulate emissions less than a selected micron size.

This paper has been reviewed in accordance with the U.S. Environmental Protection Agency's peer and administrative review policies and approved for presentation and publication.

TEST EQUIPMENT

Uncontrolled and controlled particulate mass emissions data was obtained using the Acurex High Volume Stack Sampler (HVSS). Particle size measurements were made using the SoRI two-cyclone train, the SoRI dilution stack sampling system, and the Andersen Mark III cascade impactor.

First, a brief review of the sampling trains and test equipment used during these programs.

All particulate mass measurements were made with the HVSS, which is an EPA Method 5 sampler consisting of the following components:

- A 316 stainless-steel sampling nozzle (buttonhook) properly sized for isokinetic sampling
- A 316 stainless-steel-lined sampling probe, 5-ft long, equipped with a thermocouple to measure probe temperature, a thermocouple to measure stack gas temperature, and an S-type pitot tube to measure velocity pressure
- A 316 stainless-steel 3-μm cyclone for large particulate collection (inlet test location only)
- A Teflon-coated stainless-steel filter holder containing a 142-mm glass fiber filter
- A temperature-controlled oven to maintain the cyclone and filter holder at 250°F
- A Teflon-lined, braided stainless-steel hose, 5-ft long to connect the outlet of the filter holder to the inlet of the impinger train
- An impinger train containing four glass bottles to collect moisture and condensible inorganic and organic material escaping the filter and cyclone (bottles 1, 2 -- 250 ml distilled water, bottle 3 -- dry, bottle 4 -- silica gel)
- A 10-cfm carbon vane pump modified for very low leakage around the shaft
- A control module, containing a dry gas meter and an orifice meter, to monitor temperature, pressure, and flowrate throughout the sampling train

Figure 1 illustrates the Acurex HVSS train.

The Andersen Mark III cascade impactor was equipped with a 15-μm precutter. The sampler contains nine jet plates, each having a pattern of precision drilled orifices. The resulting increased gas stream velocity through the plates distribute the sample into eight fractions or particle size

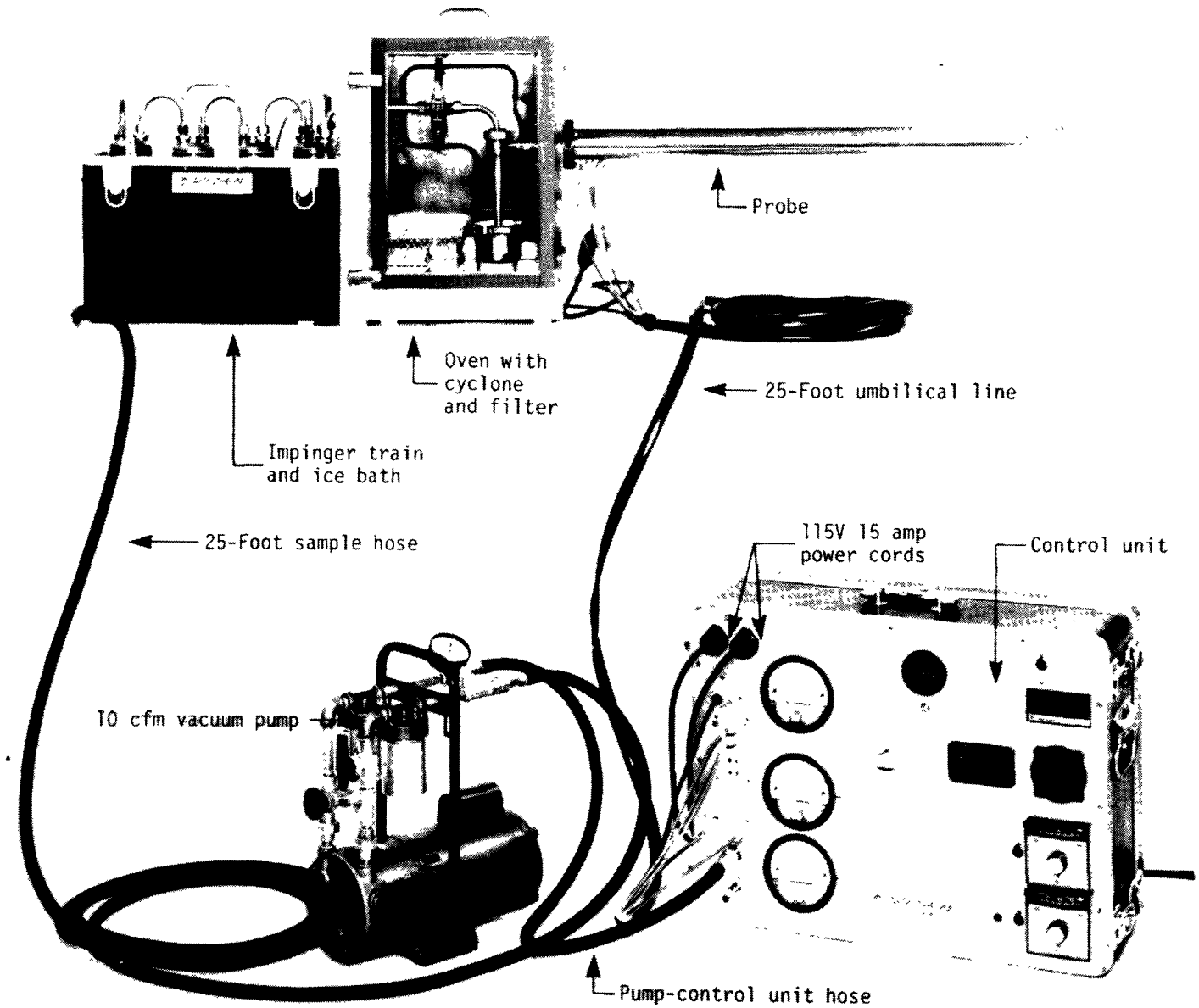

Figure 1. Acurex High Volume Stack Sampler.

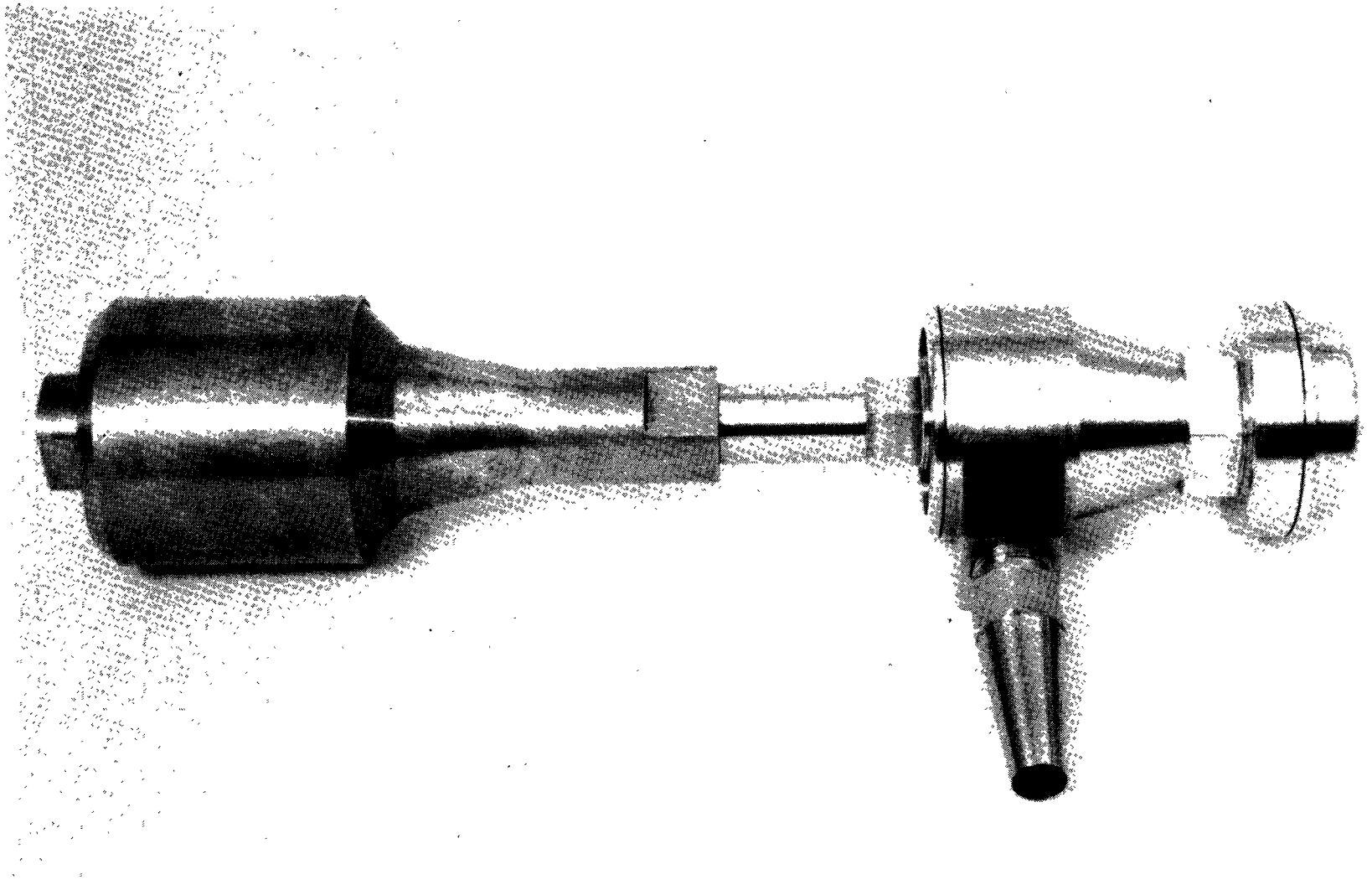

Figure 2. Andersen Mark III impactor with 15-μm precutter.

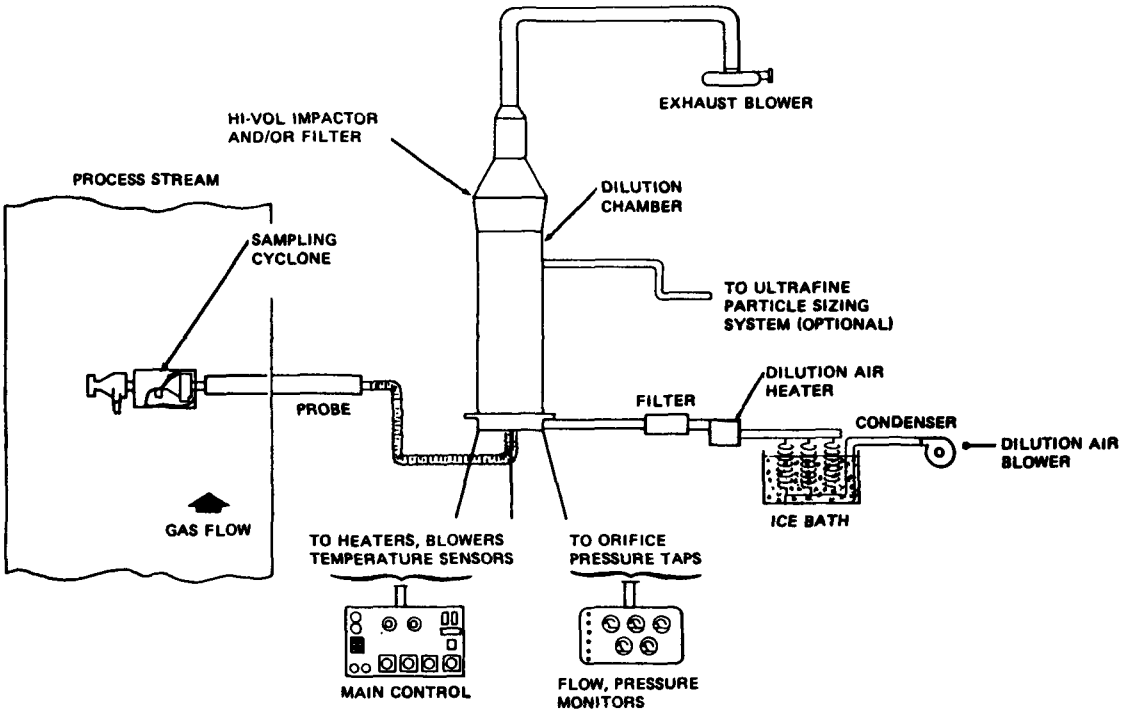

Figure 3. Diagram of stack dilution sampling system.

ranges. The device was mounted directly on the end of a 6-ft stainless-steel probe connected by a stainless-steel hose to an impinger train followed by the pump and control module (see Figure 2).

A diagram of the major components of the SoRI dilution stack sampling system is shown in Figure 3. In normal operation, gases from the process stream are drawn through the IP dual-cyclone sampler, in which particles with aerodynamic diameter greater than 15 μm and those in the range 2.5 to 15 μm are removed in two stages. The stack gas containing the fine particle fraction (<2.5 μm) and condensible vapors pass through the heat-traced probe and flexible sample line and are introduced into the bottom of the cylindrical dilution chamber. At this point the stack gas is mixed with dilution air to form a simulated plume which flows upward through the dilution chamber, through a standard high-volume filter which collects the fine particulate and any new particulate formed by condensation. The diluted stream is exhausted by a 1-hp blower or optionally by a standard high-volume blower. Stack gas flowrate is measured by an orifice at the base of the dilution chamber. Dilution and exhaust flow are measured by orifices in the inlet and outlet lines, respectively.

KAISER STEEL PROGRAM

The first phase of the Kaiser Steel program included a series of particulate mass and particle size distribution tests conducted on the emissions from the Hot Metal Desulfurization (HMDS) Plant of Kaiser Steel in Fontana, California. Measurements were made to quantify uncontrolled emissions (inlet to baghouse) and controlled emissions (outlet of baghouse), and to develop emission factors for the process.

Hot metal from the blast furnace arrives at the HMDS plant in torpedo cars which are positioned into a partially open shed attached to the HMDS building. Lances are inserted into as many as three torpedo cars at one time, and a predetermined amount of calcium carbide and calcium carbonate is blown into the hot metal using nitrogen. The hot metal is normally desulfurized by this process to less than 0.03 percent sulfur. A stopper on the lance fits the opening of the torpedo car to minimize emissions during the desulfurization process. Emissions that escape are captured by a local hood and ducted to a six-compartment, positive pressure Wheelabrator-Frye baghouse.

Samples of the uncontrolled emissions from the HMDS process were collected at the inlet to the baghouse as indicated in Figure 4. The sampling ports installed in the rectangular duct included six ports (three on each side) for particle size trains and three ports for particulate mass sampling. Measurements were made at nine sampling points at each of these locations. (Three points per port.)

The controlled emissions were measured at the baghouse outlet. Sampling ports were located on stacks 2 and 5; a 6-in. diameter port on each stack was used for particle size determination, and two 4-in. diameter ports were used for particulate mass sampling.

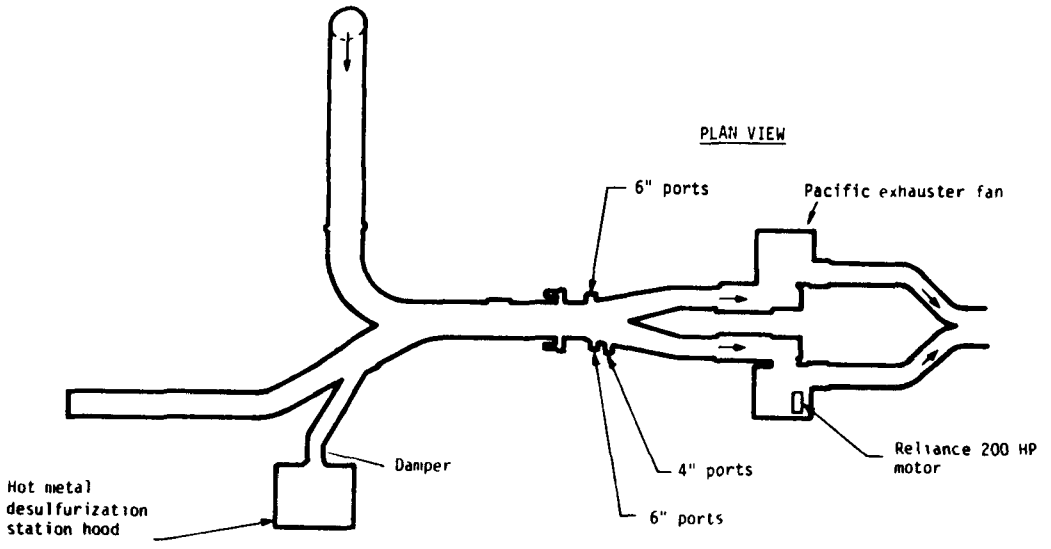

a) Uncontrolled emission sampling port locations.

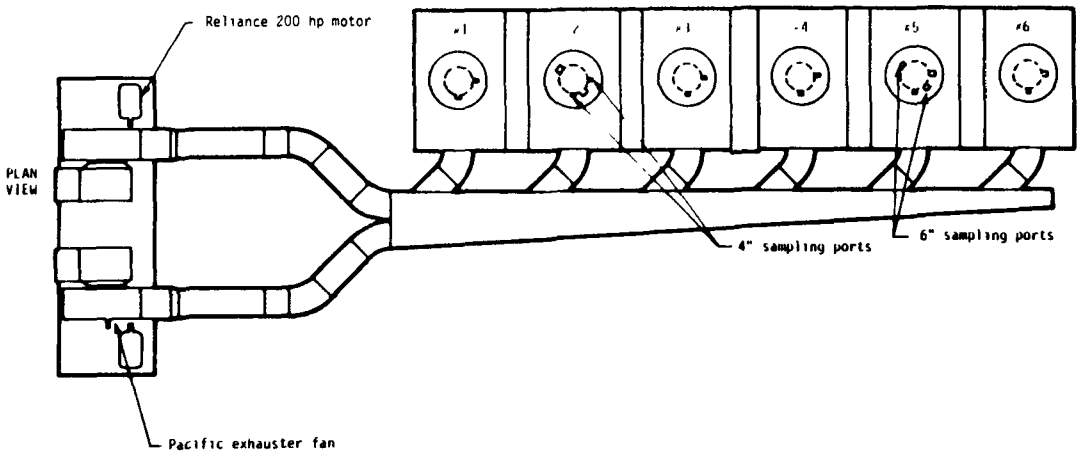

b) Controlled emission sampling port locations.

Figure 4. Hot metal desulfurization emissions control system.

Measurements obtained with the EPA Method 5 particulate mass and SoRI two-cyclone particle size trains, indicate the uncontrolled emission factor ranged from 4.62×10^{-1} to 15.33×10^{-1} lb (average 11.53×10^{-1}) of particulate emitted per ton of hot metal desulfurized. Thirty-two percent of these emissions were less than 15 μm in size.

Based on measurements made with the EPA 5 and Andersen Mark III impactor trains, the controlled emission factor ranged from 15.40×10^{-4} to 34.62×10^{-4} lb (average 27.80×10^{-4}) of particulate emitted per ton of hot metal desulfurized. Eighty-one percent of these emissions were less than 15 μm in size.

Test results are presented in Table 1. The particulate mass removal of the baghouse averaged 99.91 percent, and emission factors were higher for heats requiring more desulfurization.

Phase II of the test program at Kaiser Steel involved a series of particulate mass and particle size tests conducted on the emissions from the basic oxygen plant (BOP). Measurements were made to quantify uncontrolled (baghouse inlet) and controlled (baghouse outlet) secondary fugitive emissions, and to develop emission factors for the process. The test program included the hot metal charging and tapping portions of the BOP cycle.

Each vessel of the two-vessel plant is capable of producing 230 tons of steel per heat. Oxygen steelmaking begins with the charging of approximately 100 tons of steel scrap. Nearly 200 tons of molten iron is charged onto the scrap in the vessel. A door on the vessel enclosure is used to completely seal the enclosure for capture of the fugitive emissions generated during the charging operations. A lance is lowered into the vessel and blows oxygen into the mixture increasing the temperature to 2,900°F. After about 40 min, molten steel is tapped into a ladle. Fugitive emissions from tapping are also captured in the vessel enclosure.

Emissions from the BOP steelmaking facilities are controlled by separate primary and secondary air pollution control systems.

The primary emission control system consists of two closed-hood, suppressed combustion systems with high-energy venturi scrubbers. Dust-laden gases are captured in a hood above each vessel. The hood carries the gases to a quencher and then to the scrubber. The cleaned gases, containing carbon monoxide are burned at the top of a stack. The water used in the gas cleaning process is then piped outside the shop to large clarifying tanks. Particulates are removed from the water which is recycled back through the scrubber system.

The steelmaking facility's secondary fugitive emission control system is designed to handle all the emissions not captured by the primary system. These include fumes generated when steel scrap and molten iron are added to the open mouth of the steelmaking vessel and when steel is tapped into a ladle. Fumes are drawn off from both sides of the enclosure through ductwork which travels under the charge floor, up the outside vertical face of the shop and across a roadway to the dirty gas fans and the baghouse. The secondary

TABLE 1. KAISER STEEL HOT METAL DESULFURIZATION PLANT TEST RESULTS

Test location	Desulfurization rate (tons/min)	Particulate mass concentration (gr/dscf)	Particulate mass emission rate (lb/min)	Emission factor (lb/ton)	Percent less than 15 μm
Baghouse inlet uncontrolled emissions[a]	26.89	2.3038	27.72	11.53×10^{-1}	32.1
Baghouse outlet controlled emissions[b]	65.98	13.77×10^{-3}	0.17	27.80×10^{-4}	81.0

[a]Average of tests 18 through 28
[b]Average of tests 15 through 17

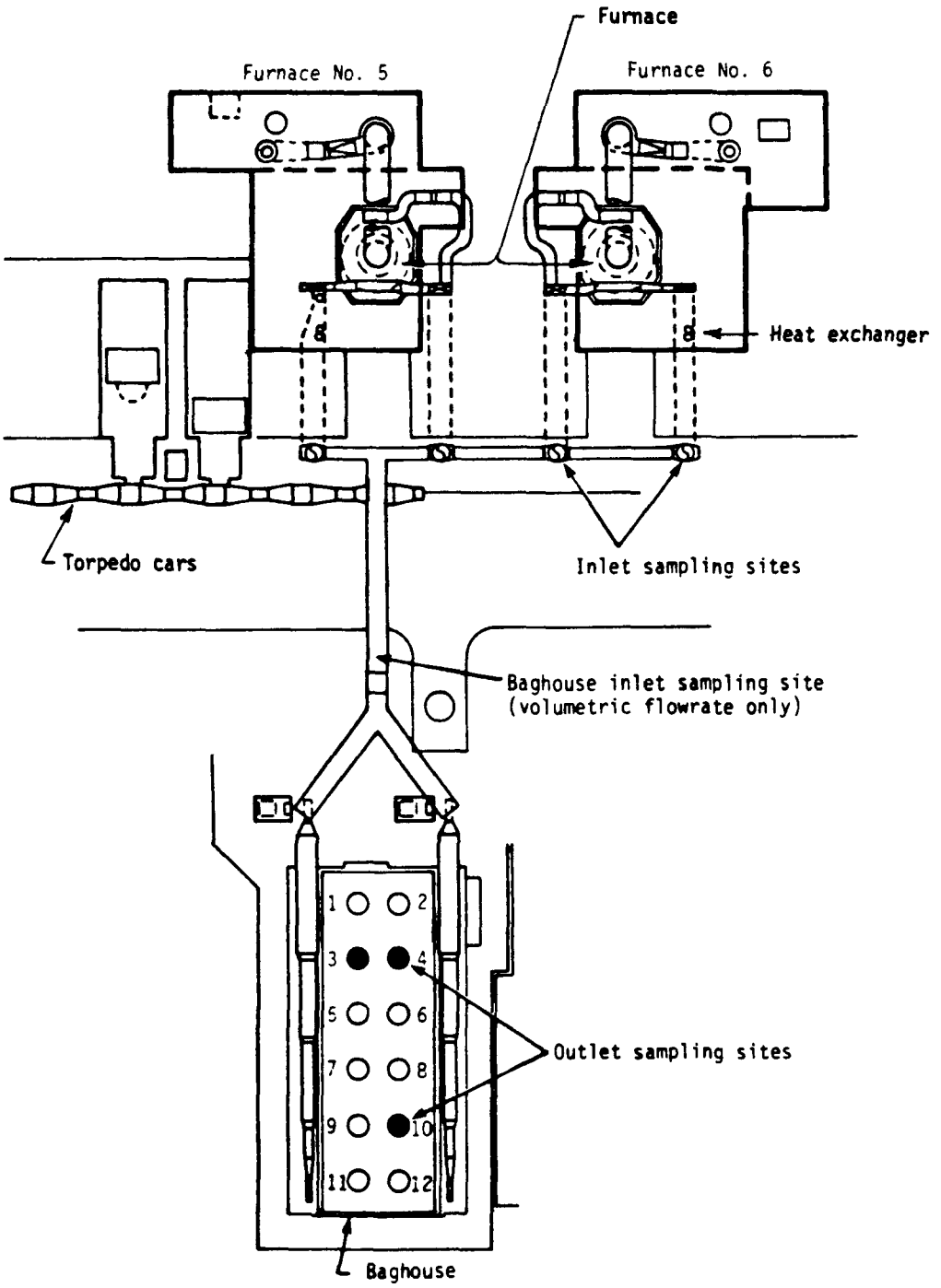

Figure 5. Top view of BOP secondary fugitive particulate emission control system ductwork and baghouse.

fugitive emission control system, designed by PECOR, handles 630,000 acfm of gases. This system has a separate hood and duct to capture tapping emissions. Fugitive emissions from the hot metal transfer station and skimming station (inside the BOP) are also captured and cleaned by this control system.

Figure 5 illustrates the location of the inlet and outlet sampling ports in the BOP secondary fugitive particulate emission control system.

Samples of the uncontrolled secondary fugitive particulate emissions from the hot metal charging and tapping portions of the BOP cycle were collected in the two ducts of the secondary emission control system for each vessel. The two ducts for each control system were designated east and west for testing purposes and are illustrated in Figure 5. All four ducts were manifolded together into a common duct leading to the baghouse inlet.

The particulate mass and particle size sampling ports were located on the vertical side of each rectangular inlet duct. Each rectangular inlet duct was 11-ft wide and 4-ft deep. The particulate mass and particle size sampling ports for each duct consisted of four equidistant 6-in. ports while velocity and temperature measurements were made in four 4-in. ports placed 30 in. above the particulate mass and particle size ports.

Samples of the controlled secondary fugitive particulate emissions from the hot metal charging and tapping portions of the BOP cycle were collected at three of the 12 outlet stacks serving the baghouse. Budget and manpower limitations prevented simultaneous testing of all 12 outlet stacks. Stacks 3 and 10 at the front and rear of the two rows of outlet stacks were selected as representative sampling locations.

The particulate mass sampling ports (two ports at 90° on each of stacks 3, 4, and 10) were located 8 ft downstream from the top of the baghouse and 5 ft upstream of the stack exit. The particle size sampling port (one port, located at 45° to the mass sampling ports) on stacks 3 and 10 were located at the same level as the mass sampling ports. Stack 4 did not have a 6-in. port and, hence, the 4-in. ports were used for the particle size tests as well.

All particulate mass measurements were obtained with the Acurex HVSS and in accordance with EPA Method 5 procedures. Sampling involved strict timing and coordination since particle size and mass determination were made simultaneously, and were dependent on the hot metal charging and tapping times (variable from heat to heat). Particle size determinations were made with the SoRI two-cyclone train for all inlet tests (high grain loading), and the Andersen Mark III impactor with a 15-μm cyclone precutter was used for the baghouse outlet tests (very low grain loading).

Table 2 illustrates the results of testing conducted during the changing and tapping cycles.

Based on measurements made with EPA Method 5 particulate mass and SoRI two-cyclone particle size trains, the uncontrolled secondary fugitive emission factor for hot metal charging ranged from 8.08×10^{-2} to 33.34×10^{-2} lb of particulate emitted per ton of hot metal charged (average 14.65×10^{-2}) and

TABLE 2. KAISER STEEL BOP TEST RESULTS

Test location	Hot metal charged (tons/heat)	Steel tapped (tons/heat)	Particulate mass emission rate (lb/min)	Particulate emission factor (lb/ton)	Percent less than 15 μm
Baghouse inlet uncontrolled emissions charging[a]	186	--	27.62	14.65×10^{-2}	56.3
Baghouse outlet controlled emissions charging[b]	249	--	0.1505	5.97×10^{-4}	63.0
Baghouse inlet uncontrolled emissions tapping[c]	--	219	4.95	14.62×10^{-2}	49.7
Baghouse outlet controlled emissions tapping[d]	--	226	0.1348	2.58×10^{-3}	40.0

[a]Average during 24 heats
[b]Average during 16 heats
[c]Average during 14 heats
[d]Average during 8 heats

from 6.94×10^{-2} to 29.21×10^{-2} lb of particulate emitted per ton of steel tapped (average 12.48×10^{-2}). The SoRI particle size showed 56.3 percent of these emissions were less than 15 μm in size.

Based on measurements made with EPA Method 5 particulate mass and Andersen Mark III impactor trains, the controlled secondary fugitive emission factor for hot metal charging ranged from 3.37×10^{-4} to 10.96×10^{-4} lb of particulates emitted per ton of hot metal charged (average 5.97×10^{-4}) and from 2.63×10^{-4} to 8.91×10^{-4} lb of particulate emitted per ton of steel tapped (average 4.80×10^{-4}). Of these amounts, 63 percent were less than 15 μm in size.

The uncontrolled secondary fugitive emission for tapping ranged from 4.94×10^{-2} to 24.05×10^{-2} lb of particulate emitted per ton of steel tapped (average 14.62×10^{-2}). Of this amount, 49.7 percent of the emissions were less than 15 μm in size.

The controlled secondary fugitive emission factor for tapping ranged from 1.11×10^{-3} to 5.06×10^{-3} lb of particulate emitted per ton of steel tapped (average 2.58×10^{-3}). Of this amount, 40 percent of the emissions were less than 15 μm in size.

The particulate mass removal efficiency of the baghouse averaged 99.58 percent for hot metal charging and 99.11 percent for tapping.

KENNECOTT MINERALS PROGRAM

A series of particulate mass, particle size, and sulfur dioxide tests were conducted on the fugitive emissions generated during matte and slag tapping operations on the reverberatory furnace of Kennecott Minerals Company in Hayden, Arizona. These measurements were made to quantify the uncontrolled fugitive emissions from these operations, and to develop emission factors for the tapping process.

Both copper matte and slag are tapped by means of a tap hole in the side of the reverberatory furnace. The molten material flows down a launder chute into a ladle which is positioned one floor below the tap hole. The slag ladle is carried by a slag hauler to the plant dump site. The approximately 18 tons of matte per ladle are used to charge the converters for concentration of the copper to about 98 percent.

At the time of the test program, there were no particulate controls on the hoods collecting the fugitive particulate emissions generated during the matte and slag tap operations. The emissions captured by the hoods are ducted through the plant roof to the atmosphere.

Figure 6 illustrates the matte sampling location. The sampling ports consisted of two 6-in. diameter flanges and two 3-in. diameter male pipe couplings. These ports were at the 47-ft level of the 34-in. diameter stack. The stack is connected directly to a fan which drew air from the movable hood over the matte tap station (the hood was lowered into place during tapping).

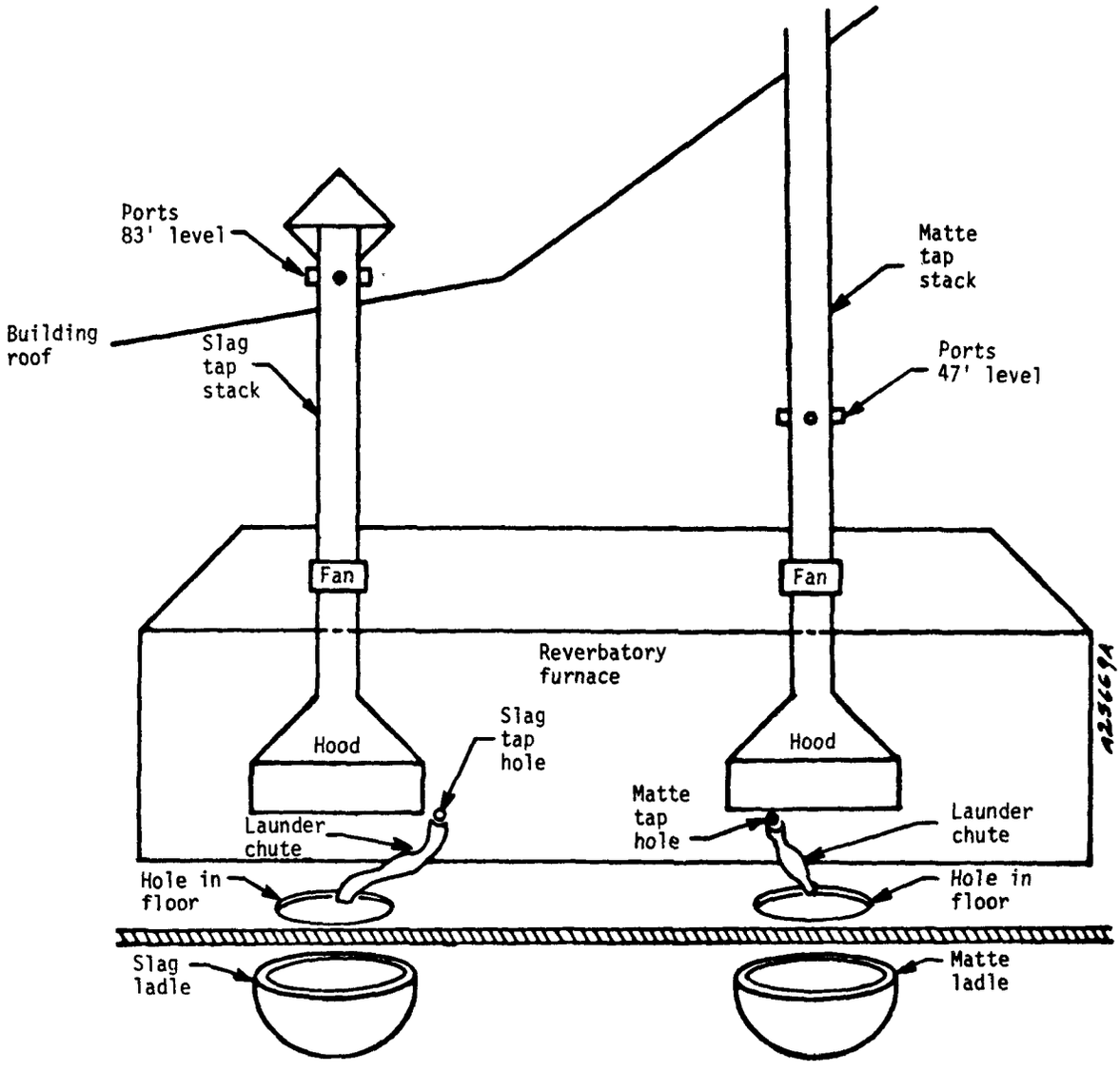

Figure 6. Sampling locations for matte and slag.

Figure 6 also illustrates the slag sampling site. This site was located very near the top of the stack on the roof of the building. Two 6-in. flanges and two 3-in. diameter male pipe coupling ports were located at the 83-ft level of the 34-in. diameter stack.

The sampling equipment used during the particulate mass testing compared with requirements of EPA Method 5/8. All particle size tests were conducted with the Andersen 2000 Mark III in-stack cascade impactor fitted with a 15-μm cyclone precutter and straight sampling nozzle.

Prior to conducting the actual tests on each stack, a series of preliminary measurements were made to determine stack gas velocities (to size sampling nozzles), approximate grain loadings (to avoid overloading impactors) and the need to condition the glass fiber filter substrates in the stack gases prior to use (to compensate for SO_x filter reaction forming artifact sulfates). The significance of the last two variables was determined by drawing 10 ft^3 of gas from each stack through the impactor which was preceded by a flat 47-mm filter (to remove particulates but allow passage of the SO_2-laden gases). The results of this preliminary measurement indicated SO_x filter reactions were not a problem at either source and, hence, in situ conditioning of the impactor substrates was not required.

For the matte tap tests, the stack was traversed in two directions at 90° using 12 sampling points per traverse (total 24 points). Each test was 24 min in length, which was sufficient to collect at least 100 mg of particulate in the front half of the train. Several matte tap operations were sampled for each test and four separate tests were conducted to characterize the particulate emissions.

For the slag tap tests, the same procedures were used (both stacks were the same diameter) except the sampling time was extended to 48 min to collect a sufficiently large sample. Multiple slag taps were sampled for each test and a total of four separate tests were performed.

Particle size measurements were made at the same time as the particulate mass tests. A total of four points (average point on each radius of each stack) were sampled for 20 min during matte tap and 40 min during slag tap to collect a weighable sample.

Measurements made with a combined EPA Method 5/8 train indicate that the uncontrolled emissions from the matte tapping operations range between 0.12 and 0.17 lb of particulate emitted for each ton of matt tapped (average 0.13 lb/ton). Measurements made with the Andersen 2000 Mark III cascade impactor precutter indicate that 76 percent of the particulates are <15 μm in size.

Similar measurements made on the slag tapping emissions resulted in uncontrolled emissions which range between 0.01 and 0.04 lb of particulate emitted for each ton of slag tapped (average 0.03 lb/ton). Approximately 33 percent of these emissions were less than 15 μm in size.

Table 3 provides a summary of the test results.

TABLE 3. KENNECOTT MINERALS REVERBERATORY FURNACE TEST RESULTS

Test location	Tapping rate (tons/min)	Particulate mass concentration (Gr/DSCF)	Particulate mass emission (lb/min)	Emission factor (lb/ton)	Percent less than 15 μm
Matte hood uncontrolled emissions[a]	2.25	0.1066	0.27	0.13	76
Slag hood uncontrolled emissions[b]	1.68	0.0353	0.04	0.03	33

[a]Average of tests M-1 through M-4
[b]Average of tests S-1 through S-4

As a result of these tests it appears that fugitive emissions generated during matte removal from the reverberatory furnace are approximately an order of magnitude higher than slag-generated fugitive emissions and are considerably smaller in particle size. The average fugitive particulate mass emission factor (based on Method 5) for matte tap was 0.13 lb/ton versus 0.03 lb/ton for slag tap operations. Approximately 76 percent of the matte emissions were less than 15 μm in size, whereas only 33 percent of the slag emissions were less than 15 μm in size.

CHARACTERIZATION OF PARTICULATE EMISSION FACTORS FOR INDUSTRIAL PAVED AND UNPAVED ROADS

by: Chatten Cowherd, Jr.
J. Patrick Reider
Phillip J. Englehart
Midwest Research Institute
Kansas City, Missouri 64110

ABSTRACT

This paper presents the results of an expanded measurement program to characterize uncontrolled particulate emissions generated by traffic entrainment of surface particulate matter from industrial paved and unpaved roads. The emission sampling procedure used in this program provided emission factors for the following particle size ranges: < 15 μm, < 10 μm, and < 2.5 μm aerodynamic diameter. Testing was performed at sites that were representative of significant paved and unpaved road emission sources within the following industrial categories: crushed stone and gravel processing, primary nonferrous smelting, and asphalt and concrete batching. Measured emissions in each particle size range were correlated with road and traffic parameters as a preliminary step to the development of predictive emission factor equations for industrial paved and unpaved roads. Previously collected field test data for integrated iron and steel plants and surface coal mines were also integrated into the industrial road emission factor data bases.

This paper has been reviewed in accordance with the U.S. Environmental Protection Agency's peer and administrative review policies and approved for presentation and publication.

INTRODUCTION

Over the past few years traffic-generated dust emissions from unpaved and paved industrial roads have become recognized as a formidable source of atmospheric particulate emissions, especially within those industries involved in the mining and processing of mineral deposits. Frequently, road dust emissions exceed emissions from other open dust sources associated with the transfer and storage of mined materials. For example, in western surface coal mines, dust emissions from uncontrolled unpaved roads usually account for more than three-fourths of the total particulate emissions, including typically controlled process sources such as crushing operations (1). Therefore, the quantification of this source is necessary to the development of effective strategies for the attainment and maintenance of the total suspended particulate (TSP)* standards, as well as the anticipated particulate standard based on particle size.

Although a considerable amount of field testing of industrial roads has been performed, those studies have focused primarily on TSP emissions. Only relatively recently has the emphasis shifted to development of size specific emission factors in the small particle range (< 15 μm aerodynamic diameter). The following particle size fractions have been of interest in these studies:

IP = Inhalable particulate matter consisting of particles smaller than 15 μm in aerodynamic diameter.

PM_{10} = Particulate matter consisting of particles smaller than 10 μm in aerodynamic diameter.

FP = Fine particulate matter consisting of particles smaller than 2.5 μm in aerodynamic diameter.

One major field study was directed to development of size-specific emission factors for western surface coal mines (1). Field testing was conducted at three mines, each representing a major western coal field. The study included testing of unpaved haul roads and unpaved access roads in the absence of dust control measures. Although the primary sampling method for road testing was exposure profiling, the conventional upwind-downwind method was used for a few tests. Particle size distributions were determined at two or more heights in the plume by use of dichotomous samplers and high-volume cascade impactors with cyclone preseparators. Road dust emission factors in the form of predictive equations were developed for the TSP, IP, and FP fractions.

In a second study directed to evaluation of open dust source controls in the iron and steel industry, uncontrolled emissions from paved and unpaved roads were tested prior to application of control measures (2). The testing was performed at two steel plants, in Ohio and Texas. Exposure profiling, the primary test method, was supplemented by the use of high-volume

(*) TSP denotes the size fraction of the total airborne particulate that is captured by a standard high volume sampler.

cascade impactors with cyclone precollectors for particle sizing at two heights in the plume. Emission factors were determined for total particulate (TP) matter as well as IP and FP fractions.

In a related nonindustrial study, IP, PM_{10}, and FP emission factors were developed for urban paved roads (3). Exposure profiling was used to measure emissions at representative sites in the Kansas City and St. Louis areas. Particle sizing at two heights in the plume was performed with high-volume samplers equipped with size-specific (IP) inlets and cascade impactors. A generalized emission factor equation was derived from the test data, containing parameters that vary with particle size fraction and road category.

This paper reports on a field study which utilized exposure profiling to provide size-specific emission factors for uncontrolled paved and unpaved roads within other industries having significant road dust sources. Testing was performed at representative sites within the following industrial categories: crushed stone and gravel processing, primary nonferrous smelting, and asphalt and concrete batching. By combining the test data from this study with the data from the two prior industrial studies referenced above, it was anticipated that the resulting data base would be adequate to develop reliable emission factors for the range of road and traffic conditions which characterize major industrial road dust sources. The sampling methodologies and emission factors derived in this study are presented below.

SAMPLING SITE SELECTION

Plant surveys were performed within each of the specified industries to locate suitable test sites which at the same time were representative of road and traffic conditions within these industries.

Three major criteria were used to determine the suitability of each candidate site for sampling of road dust emissions by the exposure profiling technique:

1. Adequate space for sampling equipment and easy accessibility to the area.

2. Sufficient traffic and/or road surface dust loading so that adequate mass would be captured on the lightest loaded collection substrate during a reasonable sampling time period.

3. A wide range of acceptable wind directions, taking into account: (a) the test road orientation relative to the predominant wind directions for the locality; and (b) possible effect of nearby structures on wind flow across the test road.

Table 1 gives the general geographical location of test sites within each industry, the distribution of tests performed, and the sampling periods for each industry. Note that this study also entailed testing of rural unpaved roads. For purposes of comparison, Table 1 also lists appropriate data for the three prior studies. It is apparent that the data base represented in this table represents a diversity of industrial settings and seasonal conditions.

TABLE 1. FIELD TEST MATRIX

Industrial category	Test site location	Road tests conducted		Sampling period
		Unpaved	Paved	
Asphalt batching	Missouri	0	4	Oct. 1981
Concrete batching	Missouri	0	3	Nov. 1981
Copper smelting	Arizona	3	3	Apr. 1982
Sand and gravel processing	Colorado	0	3	Apr. 1982
	Kansas	3	0	July 1982
Stone crushing	Kansas	5	0	Dec. 1981
Rural roads	Kansas	6	0	Aug.-Sept. 1981
	Missouri	4	0	Mar. 1982
	Colorado	2	0	Apr. 1982
Surface coal mining*	Montana	12	0	Aug., Dec. 1979
	North Dakota	10	0	Oct. 1979
	New Mexico	7	0	July-Aug. 1980
Iron and steel†	Ohio	7	7	July 1980 Oct.-Nov. 1980
	Texas	0	4	July 1981
Urban roads≠	Missouri	0	11	Feb.-Mar. 1980 May 1980
	Kansas	0	5	Feb.-Mar. 1980
	Illinois	0	3	May 1980

* Reference 1.
† Reference 2.
≠ Reference 3.

SAMPLING EQUIPMENT

A variety of sampling equipment was utilized in this study to measure particulate emissions, roadway surface particulate loadings, and traffic characteristics.

The primary tool for quantification of emissions was the MRI exposure profiler, which was developed under EPA Contract No. 68-02-0619 (4). Normally, the exposure profiler was positioned at a distance of 5 m from the downwind edge of the road. The profiler consisted of a portable mast (6 m height) supporting an array of five sampling heads spaced at 1 m intervals above the ground. Each sampling head was operated as an isokinetic TP exposure sampler directing passage of the flow stream through a settling chamber (trapping particles larger than about 50 μm in diameter) and then upward through a standard 8- by 10-in.* glass fiber filter positioned horizontally. Sampling intakes were pointed into the wind, and sampling velocity of each intake was adjusted to match the local mean wind speed, as determined prior to each test. Throughout each test, wind speed was monitored by recording anemometers at two heights, and the vertical profile of wind speed was determined by assuming a logarithmic distribution. A wind vane at the top of the mast was used to monitor wind direction.

To obtain the particle size distribution of the particulate emissions, high-volume parallel-slot cascade impactors with cyclone preseparators were positioned along side of the profiler at heights of 1 and 3 m. At the operating flow rate of 20 scfm, the cutpoints of the impactor stages were 10, 4.2, 2.1, 1.4, and 0.73 μm aerodynamic diameter, and the cyclone cutpoint was 11 μm aerodynamic diameter. In addition, a standard high-volume air sampler and a high-volume sampler equipped with a size-selective IP inlet were operated at a height of 2 m.

For measurement of background particulate concentration, a standard high-volume sampler and a high-volume sampler with an IP inlet were operated upwind of the test road, at a height of 2 m. Care was taken to locate the upwind samplers away from any localized upwind emission source.

Samples of the dust found on the road surface were collected as part of each source test. In order to collect this surface dust, it was necessary to close each traffic lane for a period of approximately 15 min. Normally, an area that was about 0.3 m by the width of the road was sampled. A portable vacuum cleaner was used to collect surface dust from the paved roads. The attached brush on the collection inlet was used to abrade surface compacted dust and to remove dust from the crevices of the road surface. Vacuuming was preceded by broom sweeping if large aggregate was present. For the unpaved roads, broom sweeping was used to collect samples of loose particulate matter from the road surface. Unpaved roads were not vacuumed.

(*) Readers more familiar with metric units may use the conversion factors at the end of this paper.

The characteristics of the vehicular traffic during the source testing were determined by both automatic and manual means. The vehicular characteristics included: (a) total traffic count; (b) mean traffic speed; and (c) vehicle mix.

Total vehicle count was determined by direct observation. Vehicles were classified into functional categories keyed to the number of axles and wheels. The average speed of the traveling vehicles was determined by direct observation with verification from plant operators. The weights of the vehicle types were estimated by consulting plant operators for industrial sites. Automobile literature was used to estimate curb weights of vehicles traveling on rural roads.

SAMPLING AND ANALYSIS PROCEDURES

The sampling and analysis procedures employed in this study were subject to the Quality Control (QC) guidelines which met or exceeded the requirements specified by EPA (5,6). As part of the QC program for this study, routine audits of sampling and analysis procedures were performed. The purpose of the audits was to demonstrate that measurements were made within acceptable control conditions for particulate source sampling and to assess the source testing data for precision and accuracy. Examples of items audited include gravimetric analysis, flow rate calibration, data processing, and emission factor calculation.

Particulate samples were collected on Type A slotted glass fiber impactor substrates and on Type AE (8- by 10-in.) glass fiber filters. To minimize the problem of particle bounce, the glass fiber cascade impactor substrates were greased. The grease solution was prepared by dissolving 140 g of stopcock grease in 1 liter of reagent grade toluene. No grease was applied to the borders and backs of the substrates. The substrates were handled, transported, and stored in specially designed frames which protected the greased surfaces.

Prior to the initial weighing, the greased substrates and filters were equilibrated for at least 24 hr at constant temperature and humidity in a special gravimetrics laboratory. During weighing, the balance was checked at frequent intervals with standard weights to ensure accuracy. The substrates and filters remained in the same controlled environment for another 24 hr, after which a second analyst reweighed them as a precision check. Substrates or filters that could not pass audit limits were discarded. Ten percent of the substrates and filters taken to the field were used as blanks.

Prior to equipment deployment, a number of decisions were made as to the potential for acceptable source testing conditions. These decisions were based on forecast information obtained from the local U.S. Weather Service office. A specific sampling location was identified based on the anticipated wind direction. Sampling would be initiated only if the wind speed

was forecast between 4 and 20 mph. Sampling was not planned if there was a high probability of measurable precipitation (normally > 20%) or if the road surface was damp.

Emission sampling usually lasted about 1 hr for unpaved roads and 4 hr for paved roads. Occasionally, sampling was interrupted due to occurrence of unacceptable meteorological conditions and then restarted when suitable conditions returned. The unacceptable meteorological conditions most frequently encountered consisted of light winds (below 4 mph) and insufficient angle (< 45 degrees) between mean (15-min average) wind direction and road direction.

To prevent particulate losses, the exposed sampling media were carefully transferred at the end of each run to protective containers within the MRI instrument van. Exposed filters and substrates were placed in individual glassine envelopes and numbered file folders and then returned to the MRI laboratory. Particulate that collected on the interior surfaces of each exposure probe and cyclone precollector was rinsed with distilled water into separate glass jars.

When exposed substrates and filters (and the associated blanks) were returned from the field, they were equilibrated under the same conditions as the initial weighing. After reweighing, 20% were audited to check precision.

The vacuum bags and the polyethylene bags containing road sweepings were weighed to determine total net mass collected. Then the dust was removed from the bags and was dry sieved. The screen sizes used for the dry sieving process were the following: 3/8-in., 4, 10, 20, 40, 100, 140, and 200 mesh. The material passing a 200 mesh screen is referred to as silt content.

The vertical distributions of the product of plume concentration and mean wind speed were numerically integrated to calculate emission factors. The cyclone/cascade impactor sampler combinations provided reliable point concentrations for IP and finer particle size fractions. Plume height was determined by extrapolation of the vertical profile of TP concentration as measured by the MRI exposure profiler.

TEST RESULTS

Tables 2 and 3 summarize by industry category the size-specific particulate emission factors determined for unpaved roads and paved roads, respectively. Geometric means and geometric standard deviations of emission factors are given because road dust emission factor data sets are found to follow log normal rather than normal distributions (1). For purposes of comparison, data from References 1 to 3 are also presented.

TABLE 2. UNPAVED ROAD EMISSION FACTORS (UNCONTROLLED)

Industrial category*	No. of tests	Emission factor (kg/VKT)†							
		TP		IP		PM_{10}		FP	
		$\bar{x}$	σ	$\bar{x}$	σ	$\bar{x}$	σ	$\bar{x}$	σ
Copper smelting	3	23.4	1.1	6.64	1.1	0.42	1.1	0.06	1.9
Sand and gravel processing	2	3.76	1.5	1.42	2.4	0.97	2.7	0.24	3.2
Stone crushing	4	4.28	2.5	2.98	3.2	0.50	2.4	0.08	2.2
Rural roads	9	9.93	3.5	2.54	3.9	0.97	4.3	0.21	4.8
Surface coal mining (haul trucks)≠	20	7.62	2.4	1.57	3.1	-	-	0.06	3.2
Surface coal mining (light/ med. duty)≠	10	1.77	1.8	0.503	3.8	-	-	0.03	3.6
Iron and steel (light duty)§	4	3.30	1.2	0.67	2.1	0.57	1.9	0.21	2.1
Iron and steel (heavy duty)§	3	36.9	1.0	8.69	1.1	6.80	1.2	2.35	1.1

* Parenthetical notation refers to vehicle type.

† $\bar{x}$ = geometric mean; σ = geometric standard deviation; VKT = vehicular km traveled.

≠ Reference 1.

§ Reference 2.

TABLE 3. PAVED ROAD EMISSION FACTORS (UNCONTROLLED)

Industrial category	No. of tests	Emission factor (kg/VKT)*							
		TP		IP		PM_{10}		FP	
		$\bar{x}$	σ	$\bar{x}$	σ	$\bar{x}$	σ	$\bar{x}$	σ
Asphalt batching	3	0.60	1.9	0.25	1.5	0.11	1.2	0.05	1.2
Concrete batching	3	1.22	1.7	0.76	1.4	0.29	1.5	0.10	1.6
Copper smelting	3	3.25	1.5	1.16	1.7	0.79	1.8	0.17	2.0
Sand and gravel processing	2	1.88	1.8	0.41	2.5	0.23	2.8	0.16	4.0
Iron and steel	10	0.72	1.6	0.22	1.5	0.17	1.5	0.06	1.6
Urban roads	10	-	-	0.001	4.3	0.001	4.2	0.001	3.6

* $\bar{x}$ = geometric mean; σ = geometric standard deviation; VKT = vehicular km traveled.
Source: Reference 3.

The average small particle fractions of the unpaved and paved road emissions for each industry are given in Table 4. It is evident that paved road emissions contain substantially larger portions of small particles than unpaved road emissions.

The road and traffic parameters measured during each test included: total loading of loose surface particulate on the traveled portion of the road; silt content of the total loading; silt loading, which is the product of total loading and silt content; average vehicle speed; average vehicle weight; and average number of vehicle wheels. These source characterization parameters are summarized for unpaved and paved roads in Tables 5 and 6, respectively. Again, data from References 1 to 3 are presented for purposes of comparison. Although the moisture content of the road surface particulate was measured, it was not included as a reliable source parameter because of the difficulty of collecting a sample without altering its moisture content.

The parameters are being evaluated as possible correction parameters for development of predictive emission factor equations by stepwise multiple linear regression. Previous studies have shown that predictive emission factor equations for unpaved and paved roads substantially reduce the uncertainty in estimating road dust emissions on a site-specific basis (1,3,7).

TABLE 4. EMISSION FACTOR RATIOS BY INDUSTRIAL CATEGORY

Industrial category	IP/TP		PM_{10}/TP		FP/TP	
	Unpaved	Paved	Unpaved	Paved	Unpaved	Paved
Asphalt batching	-	0.42	-	0.18	-	0.083
Concrete batching	-	0.62	-	0.24	-	0.082
Copper smelting	0.28	0.36	0.018	0.24	0.0026	0.052
Sand and gravel processing	0.38	0.22	0.26	0.12	0.064	0.085
Stone crushing	0.70	-	0.12	-	0.019	-
Rural roads	0.26	-	0.098	-	0.021	-
Surface coal mining (haul trucks)	0.21	-	-	-	0.0079	-
Surface coal mining (light/med. duty)	0.28	-	-	-	0.017	-
Iron and steel	-	0.31	-	0.24	-	0.083
Iron and steel (light duty)	0.20	-	0.17	-	0.064	
Iron and steel (heavy duty)	0.24	-	0.18	-	0.064	-

TABLE 5. SOURCE CHARACTERIZATION PARAMETERS - UNPAVED ROADS (UNCONTROLLED)**

Industrial category	No. of tests	Total loading (g/m^2)		Silt content (%)		Silt loading (g/m^2)		Veh. speed (kph)		Veh. weight (tonnes)		Veh. wheels	
		$\bar{x}$	σ	$\bar{x}$	σ	$\bar{x}$	σ	$\bar{x}$	σ	$\bar{x}$	σ	$\bar{x}$	σ
Copper smelting	3	2,710	1.3	16.9	1.1	460	1.2	16	1.0*	2	1.1	4.4	1.1
Sand and gravel processing	3	14,100	1.1	4.7	1.2	660	1.3	8	1.0*	28	1.0	14.4	1.2
Stone crushing	5	4,930	1.4	14.0	1.2	690	1.4	19	1.3	12	1.2	4.8	1.1
Rural roads	11	2,700	1.7	9.7	1.8	260	2.9	47	1.2	2	1.1	4.0	1.0*
Surface coal mining (haul trucks)	18	310	2.3	7.7	1.7	24	2.8	41	1.3	65	1.5	7.8	1.2
Surface coal mining (light/med. duty)	10	240	2.6	6.2	1.3	15	2.8	54	1.3	2	1.1	4.0	1.0
Iron and steel (heavy duty)	3	4,560	1.7	15	1.1	710	1.5	32	1.0*	36	1.7	8.4	1.4
Iron and steel (light duty)	4	-	-	10	-	-	-	24	1.0*	3	1.0*	4.0	1.0*

** $\bar{x}$ = geometric mean; σ = geometric standard deviation.
* Captive vehicles were used to generate traffic.

TABLE 6. SOURCE CHARACTERIZATION PARAMETERS - PAVED ROADS (UNCONTROLLED)**

Industrial category	No. of tests	Total loading (g/m^2)		Silt content (%)		Silt loading (g/m^2)		Veh. speed (kph)		Veh. weight (tonnes)		Veh. wheels	
		$\bar{x}$	σ	$\bar{x}$	σ	$\bar{x}$	σ	$\bar{x}$	σ	$\bar{x}$	σ	$\bar{x}$	σ
Asphalt batching	4	3,630	1.2	3.5	1.4	127	1.6	16	1.0†	4	1.0	6.4	1.1
Concrete batching	3	221	1.2	5.4	1.1	12	1.1	21	1.3	8	1.0†	10.0	1.0†
Copper smelting	3	1,482	1.2	18.8	1.2	278	1.5	23	1.4	5	1.5	5.8	1.3
Sand and gravel processing	3	966	1.5	7.1	1.1	68	1.4	37	1.0†	40	1.0	14.1	1.3
Iron and steel	10	43	2.5	16.3	1.6	7.5	2.8	-	-	17	1.6	6.0	1.2
Urban	10	2	4.9	10.8	2.1	0.25	3.9	54	1.4	3	1.4	5.1	1.2

** $\bar{x}$ = geometric mean; σ = geometric standard deviation.
† Captive vehicles were used to generate traffic.

As a preliminary step in the development of emission factor equations for this expanded data base derived from this study in combination with References 1 to 3, a nonparametric analysis was performed. The purpose of this analysis was to determine whether the associations between source characteristics and emissions intensity found to be important in the earlier studies were reflected in the expanded data base.

Spearman's (rank-order) correlation (r) was computed based on rankings of the geometric mean values (by industry type) of the various size-specific emission factors and corresponding source characteristics (8). Pearson's r is typically used to test for association; however, its use can be limited by the restrictive assumption of a bivariate (joint) normal distribution (8). Rank correlation methods are not limited by the form of the distribution. It should be noted that these are only first order (simple) correlations. They do not reflect the partial correlations that are represented in earlier MRI equations (e.g., as given in References 1, 3, and 7).

In general, the analysis confirms earlier work which indicated that emissions were most directly related to roadway surface loading. There are some indications that the expression of the loading parameter will change depending upon the particle size fraction, but no significant correlations emerge for FP emissions. This preliminary analysis also suggests that the relationships between source characteristics and emissions intensity are stronger for unpaved roads than for paved roads.

For unpaved roads, IP emissions correlate significantly with both silt content ($p = 0.044$) and silt loading ($p = 0.068$); and PM_{10} emissions also correlate with silt loading ($p = 0.042$), where p is the probability that the relationship is due to chance. The strongest relationship was found between the ratio PM_{10}/TP and vehicle weight, as illustrated in Figure 1. This indicates that the more intense road surface grinding by heavy vehicles produces a greater portion of small particles in the emissions.

For paved roads, the strongest correlation is found between IP emissions and silt loading ($p = 0.051$). This is consistent with the emission factor equation previously developed for urban streets (3).

CONCLUSIONS

The field testing program described herein was performed to expand the small particle emission factor data base on industrial paved and unpaved roads. The ultimate objective of this research is to provide reliable small particle emission factors for the range of road and traffic conditions which characterize major industrial road dust sources.

The past approach to this problem has been to develop emission factors in the form of predictive equations which relate particulate emissions to road and traffic parameters. Such equations have been developed for TSP emissions from industrial roads based on combined data crossing industry

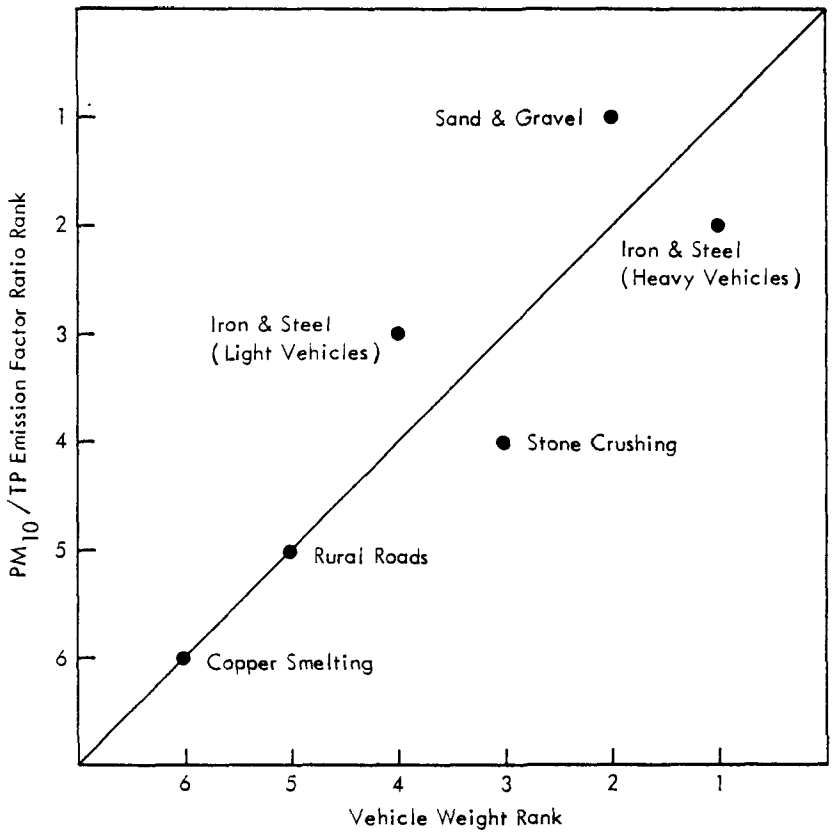

Figure 1. Rank-order correlation for unpaved roads: PM_{10}/TP emission factor ratio versus vehicle weight ($p = 0.017$).

lines. These equations have been shown to be far more accurate than single-valued averages in estimating site-specific road dust emissions.

The nonparametric analysis performed in this study indicates that the associations between emissions intensity and source characteristics found to be important in earlier studies, are reflected in the expanded data base. Thus, it appears likely that reliable emission factor equations can be developed from the data base. However, the equations for different particle size fractions will probably contain different functional dependencies on source parameters.

ACKNOWLEDGMENT

The work upon which this paper is based was performed pursuant to EPA Contract No. 68-02-3158. William B. Kuykendal served as EPA project officer for the study.

REFERENCES

1. Axetell, K., Jr., and Cowherd, C., Jr. Improved emission factors for fugitive dust from western surface coal mining sources - Vol. II: Emission factors. (Draft final.) Contract 68-03-2924, W.D. 1, U.S. EPA, Cincinnati, OH, November 1981.

2. Cuscino, T., Jr., Muleski, G. E., and Cowherd, C., Jr. Iron and steel plant open source fugitive emission control evaluation. (Draft final.) Contract 68-02-3177, W.A. 4, U.S. EPA, Research Triangle Park, NC, August 1982.

3. Bohn, R., Cowherd, C., Jr., and Englehart, P. J. Paved road particulate emissions. (Draft final.) Contract 68-02-3158, T.D. 19, U.S. EPA, Research Triangle Park, NC, February 1982.

4. Cowherd, C., Jr., Axetell, K., Jr., Guenther, C. M., and Jutze, G. Development of emission factors for fugitive dust sources. EPA-450/3-74-037 (NTIS PB238262). U.S. EPA, Research Triangle Park, NC, June 1974.

5. Quality Assurance Handbook for Air Pollution Measurement Systems. Vol. II - Ambient Air Specific Methods. EPA 600/4-77-027a. U.S. EPA, Research Triangle Park, NC, May 1977.

6. Ambient Monitoring Guidelines for Prevention of Significant Deterioration. EPA 450/2-78-019 (NTIS PB283696). U.S. EPA, Research Triangle Park, NC, May 1978.

7. Cowherd, C., Jr., Bohn, R., and Cuscino, T., Jr. Iron and steel plant open source fugitive emission evaluation. EPA-600/2-79-103 (NTIS PB299385). U.S. EPA, Research Triangle Park, NC, May 1979.

8. Bhattacharyya, G., and Johnson, R. Statistical concepts and methods. New York: John Wylie and Sons, pp 526-533, 1977.

CONVERSION FACTORS

Readers more familiar with metric units may use the following conversion factors:

Non-metric	Times	Equals metric
in.	2.54	cm
mph	1.61	km/hr (kph)
scfm	28.32	std liters/min

CONDENSIBLE EMISSIONS MEASUREMENTS IN THE INHALABLE PARTICULATE PROGRAM

by: Ashley D. Williamson and Joseph D. McCain
Southern Research Institute
Birmingham, AL 35255

ABSTRACT

In order to meet the EPA's inhalable particulate program goal of obtaining measurements of condensible matter in process streams, a Stack Dilution Sampling System was designed at Southern Research Institute under EPA contract. The principal component of the system is a cylindrical dilution chamber in which flue gas is mixed with filtered air and the resulting aerosol-laden mixture analyzed. As the sample is cooled by dilution, condensible vapors form particles under conditions similar to those which occur in actual plumes. Field measurements have been performed at a continuous drum mix asphalt plant, two kraft recovery boilers, a coke quenching tower, and an oil-fired package boiler. Data from these tests show that significant fractions of the total emissions at some sources consist of condensible vapors.

This paper has been reviewed in accordance with the U.S. Environmental Protection Agency's peer and administrative review policies and approved for presentation and publication.

INTRODUCTION

One concern in stack sampling of particulate is the realization that the ultimate particulate emissions from a stationary source may well be greater than those emissions measured instack. Many process streams contain significant amounts of condensible compounds which pass through the stack in vapor phase, but which undergo a physical change of state as the plume is diluted and cooled, and ultimately add to the particulate emission inventory of the ambient environment. The added mass is expected to accumulate almost entirely in the fine particle range below 10-15 μm.

In order to simulate this plume condensation process, a Stack Dilution Sampling System (SDSS) was designed and built at Southern Research Institute under EPA contract. This system attempts to form a replica plume from dilution of extracted stack gases with filtered ambient air so that the condensed portion of the particulate emissions can be studied. As part of its Inhalable Particulate (IP) Emission Factor Measurement Program, the EPA chose to include condensible measurements at several industry sources using the SDSS. This paper will briefly describe this instrument and report on the condensibles tests performed thus far.

DESCRIPTION OF SAMPLING SYSTEM

A diagram of the SDSS is shown in Figure 1. The design and operation of the device have been described previously (1), so will only be summarized here. Stack gases are extracted through the EPA IP Dual Cyclone sampler (1,2), in which particles with aerodynamic diameters greater than 15 μm are captured in one cyclone (Cyclone X), and particles in the 2.5-15.0 μm size range are captured in a second (Cyclone III). Particles with aerodynamic diameters less than 2.5 μm pass through the sampler and remain in the gas stream as it passes through a heat-traced probe and flexible hose, through a flow metering venturi, and into the cylindrical dilution chamber. Use of the present cyclone train as a precutter represents a design compromise. It would be patently unrealistic to filter all particulate matter from the undiluted stream and thereby remove centers on which condensation occurs in the stack plume. The cut at 2.5 μm preserves most of the condensation sites in the diluted stream while removing the larger particles which would have greater probability of loss in the probe and sample lines. The condensible material is thus combined with the respirable fraction (<2.5 μm) of the nonvolatile particulate matter. Dilution air is forced through an ice bath condenser, reheated to the desired temperature, filtered, and introduced tangentially into the inlet assembly at the bottom of the dilution chamber. The dilution air flow is directed upward in an annulus bordered on the outside by the walls of the 21.3 cm ID dilution chamber and on the inside by the 4.27 cm ID sample inlet tube. The major purpose of the condenser/heater combination is to allow dilution air with reproducible constant temperature and humidity to be used at all sampling locations. A "standard" dilution air at 21.1°C and 24 percent relative humidity is used. These values are easily achieved and within the range of typical ambient air conditions.

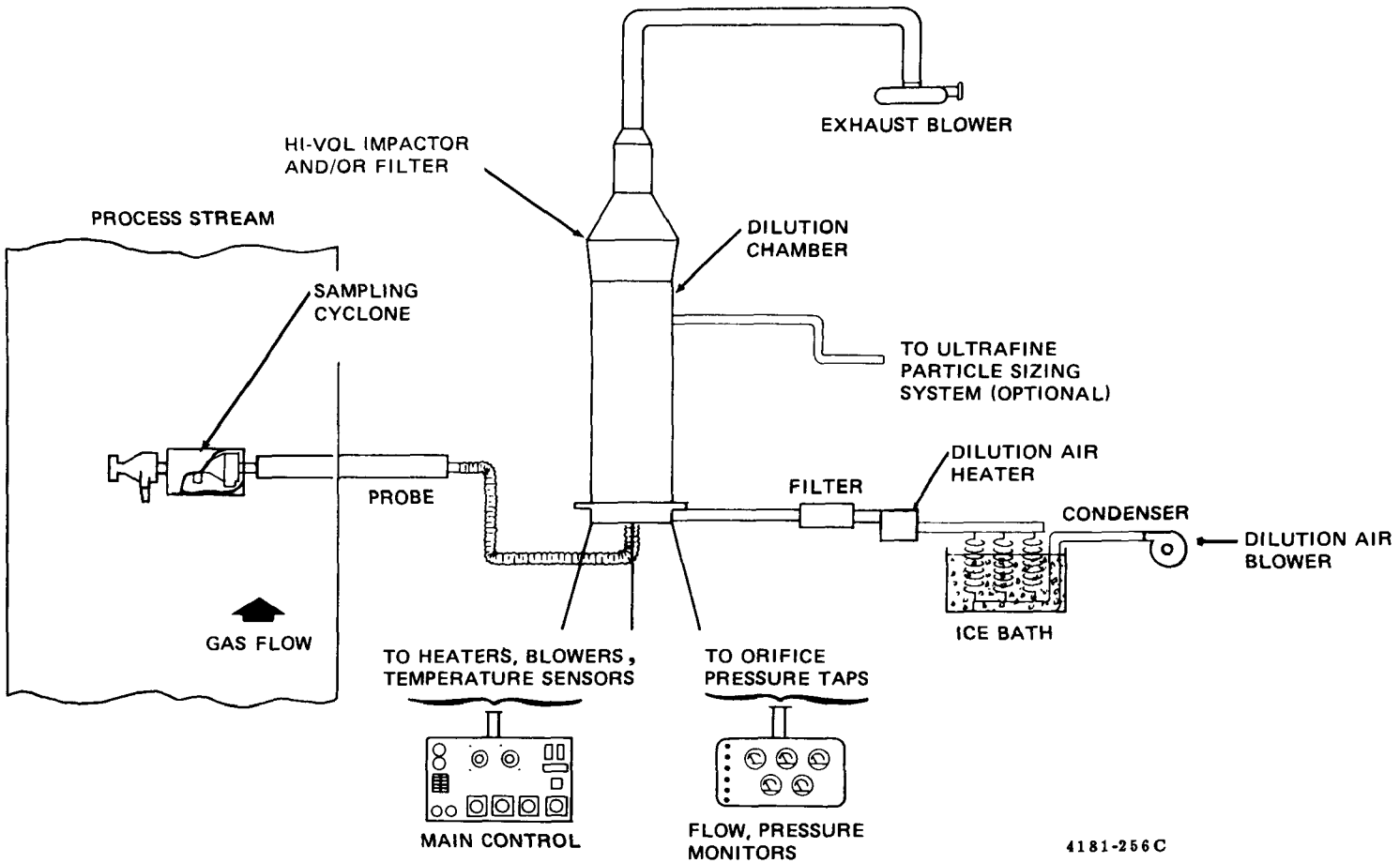

Figure 1. Diagram of Stack Dilution Sampling System.

The principal component of the system is the 1.22 m long cylindrical dilution chamber in which mixing of sample and dilution air occurs. The mixing mechanism chosen for the device is injection of a jet of extracted stack gas into the center of a confined stream of dilution air moving at a lower velocity. This choice seems to be the closest approximation to a jet exhausting from a stack exit into a nearly stagnant ambient atmosphere. The diameters of the sample inlet tube and the overall dilution chamber were chosen to give cross-sectional areas for sample gas and dilution air inlets to the dilution chamber that are proportional to the mass flows of these two gas streams at the design dilution ratio of 25:1. Thus, if the sample gas temperature were the same as the 21°C dilution air, the two streams would merge isokinetically. Heated sample gas streams will have extra velocity, as indeed occurs in a buoyant plume. The sample gas flowrate is constrained by the requirement that the first IP cyclone cut at 15 μm. The necessary flow varies with temperature and composition of the stack gas, but is approximately equivalent to a mass flow of 17 normal ℓ/min over a range of typical conditions. The total diluted flow of 425 ℓ/min is monitored by an orifice in the exhaust line. In practice, it is preferable to maintain this standard exhaust flow rather than a standard dilution ratio. Gas flowrates are adjusted using the two blowers shown in Figure 1.

IP sampling protocol for particulate measurements calls for single point samples at the centroids of each of the four quadrants of the duct cross section, and calls for four samples at each point. For SDSS sampling, this protocol was modified due to cost factors, the restricted mobility of the SDSS, and the general lack of port access when several other parallel measurements are in progress. At most sites the choice was made to make three or four total runs at two positions in the ductwork. The SDSS was run at the centroid of one quadrant of duct cross-section. At the centroid of a second quadrant a second train was run simultaneously. The second train consists of the instack inhalable-particulate precollectors used on the SDSS followed by an instack filter. For ducts without stratification of particulate matter, the instack precollectors should collect equivalent amounts of particulate matter. Any mass on the SDSS filter in excess of that accounted for by the catch of the instack filter can be attributed to condensible matter. On alternate runs, the two trains are switched in order to minimize the effects of stratification.

At one of the test sites it was not possible to use the first IP cyclone (Cyclone X) due to confined duct space. For these tests, the second cyclone was used with a buttonhook nozzle. The sample flowrate for this run was calculated in the usual manner as if Cyclone X were used.

FIELD SAMPLING STUDIES

In the course of the IP Emission Factor Measurement Program, six field sampling tests have been performed using the SDSS. Data are available from two kraft recovery boilers, a continuous drum mix asphalt plant, a coke quench tower, and an oil-fired package boiler. Results from the sixth test, at an oil-fired utility boiler, were not available in time to be included in this paper.

The first test series was performed at two kraft recovery boilers downstream of the electrostatic precipitator (ESP) particulate control devices at each source. One of the two furnaces was of the direct contact evaporator (DCE) design; the second did not use contact evaporators. The results of the tests are shown in Table 1. At the non-DCE boiler A, only two useful runs were possible due to ESP failure. The desired four runs were obtained at the DCE boiler B. The runs at those sites were somewhat unusual in that a substantial fraction of the mass collected in the SDSS was found in the sample line rinses, as shown in Table 1. The rinses at non-DCE boiler A contained over four times the mass collected by the SDSS filter. The probe deposits at the DCE boiler were not as high, but were still comparable to the filter catches. The color of the evaporated residues varied from white to yellow to red-brown.

The large sample line catches at the recovery boilers were unexpected in view of the results of other field tests in which less than 5 percent of the fine particulate fraction of the SDSS sample was collected in the sample lines and in view of laboratory tests with dye aerosol which showed line depositions on the order of 15 percent of the filter catch. A possible explanation lies in the fact that a portion of the exit end of the Method 5 probe used for the test was found to be unheated and therefore operated at a temperature below that of the stack gas. Condensation of volatile species (including water vapor) on this cooled portion of the probe was quite possible under these conditions. It is also possible that some of the probe rinse material may contain reaction products of the stainless steel sampling probe with the corrosive stack vapors. Thus, the condensible fractions noted in Table 1 should be taken as upper limits. In either case, there was definitely a condensible or reactive component present in the exhaust streams at both recovery boilers, and the non-contact evaporation boiler A emitted significantly more of this component than DCE boiler B. It should be noted in this regard that the Method 5 tests at boiler A also had large fractions in the probe rinse and had loadings significantly higher than were measured with instack impactors.

A second SDSS test series was performed at the quench tower of a steel industry coke oven. Coke quenching is a cyclic process in which individual carloads of hot coke from the oven are doused with a stream of water, giving a burst of emissions including steam, entrained particulate matter, organic material, quench water residue, and chemical reaction products. Sampling was performed only during the course of each 3 to 4 minute quench. In order to prevent accumulation of water droplets in the sampling trains, the second IP cyclone (III) of both trains and the instack filter of the IP train were heated with heating tapes. Cyclone X was left unheated and served as a large droplet scalper. All samples were taken from a single port downstream of the demister baffles. The first three runs were conducted with the usual mode of quench operation in which excess quench water is collected and recycled. The fourth run sampled emissions from single-pass "clean" quench water operation.

The results of the SDSS tests are shown in Table 2. Fairly significant instantaneous particulate loadings were observed during the quench cycles, with most of the collected mass in the fine particle size range (under 2.5 μm). As in the first test, a significant fraction of the SDSS sample was found in

TABLE 1. RESULTS OF STACK DILUTION SAMPLING SYSTEM TESTS ON TWO KRAFT RECOVERY BOILER ESP EXHAUST STREAMS

Run	Sample Volume, dnm^3	Catch Weights, mg				Mass Concentration, mg/dnm^3				
		Cyclone X	Cyclone III	Probe Wash	Filter	Cyclone X (15 μm)	Cyclone III (2.5-15 μm)	Filter+ Probe (<2.5 μm)	Total	Percent Condensible
BOILER A - NON-DCE PROCESS										
1-SDSS	2.029	53.11	2.85	128.96	5.00	26.17	1.40	66.01	93.58	-
2-SDSS	2.000	3.11	0.22	157.56	35.20	1.55	0.11	96.28	97.94	82.8
2-IP	2.194	12.23	5.38		33.19	5.77	2.45	15.13	23.15	
2-M5									172	
3-SDSS	1.793	0.69	0.05	99.79	10.2	0.38	0.03	61.35	61.75	80.8
3-IP	2.28	4.10	4.57		26.14	1.80	2.00	11.46	15.26	
3-M5									45.3	
BOILER B - DCE PROCESS										
4-SDSS	1.854	0.86	5.96	12.83	28.0	0.46	3.21	22.02	25.69	40.9
4-IP	2.180	8.68	13.48	---	25.06	3.98	6.18	11.50	21.66	
5-SDSS	1.888	3.06	12.85	24.06	20.4	1.62	6.80	23.54	31.97	33.7
5-IP	2.121	13.98	20.55	---	27.08	6.59	9.69	12.77	29.05	
6-SDSS	1.888	1.97	6.82	13.51	3.80	1.04	3.61	9.17	14.36	16.2
6-IP	2.090	4.52	5.43	---	14.30	2.16	2.60	6.84	11.60	
7-SDSS	1.882	2.35	4.93	10.08	19.9	1.25	2.62	15.93	19.80	41.8
7-IP	1.930	0.55	3.94		14.8	0.28	2.04	7.66	9.99	

TABLE 2. RESULTS FROM STACK DILUTION SAMPLING SYSTEM TESTS OF COKE QUENCH OPERATIONS

Run	Sample Duration (min)	No. of Quench Cycles Sampled	Sample Gas Vol. dnm^3	Mass Concentration, mg/dnm^3					Percent Condensibles
				Cyclone X (>15 μm)	Cyclone III (2.5-15 μm)	Probe, Hose (<2.5 μm)	Filter	Total	
1-SDSS	66	18	0.459	59.12	5.86	138.97	111.75	315.70	33.7
1-IP	44	12	0.306	65.94	17.32	--	144.42	227.68	
2-SDSS	49	16	0.481	49.25	11.51	93.21	103.82	257.79	34.0
2-IP	49	16	0.481	32.73	8.57	--	109.44	150.74	
3-SDSS	33	12	0.324	34.42	16.74	114.62	96.08	261.86	24.5
3-IP	33	12	0.324	30.80	10.53	--	146.43	187.76	
4-SDSS[a]	70	21	0.687	20.17	7.38	57.81	29.27	114.63	44.6
4-IP[a]	70	21	0.687	20.52	6.00	--	35.97	62.49	

[a]Quench water changed from recycle to single pass operation.

the probe rinse. In this case, the rinses were approximately equal in mass to the filter catch. Comparison of the two trains indicates an average of 86 mg/dnm^3 condensible material in the recycle runs, corresponding to 30.9 percent of the total particulate emissions. The "clean" water run contained 51 mg/dnm^3 condensible; but since the overall particulate emissions were lower for this mode, this concentration represents 44.6 percent of the total measured emissions. These amounts of volatile material are substantial. It should be mentioned, however, that since the instack samplers and SDSS sample lines were heated above the average duct temperature, much of the measured condensible fraction may represent volatile material that is re-evaporated in the instack portions of the sampling trains.

A third test which dramatically demonstrates the presence of condensible emissions was performed at a continuous drum mix asphalt plant. The plant in question was a modern stationary unit with 325 tons per hour capacity and a highly efficient particulate control baghouse. The burner is fired by natural gas, and the tests were run under conditions of approximately 30 percent recycle aggregate feed.

As shown in Table 3, the majority of the controlled particulate emissions as measured at stack temperatures are over 15 μm aerodynamic diameter and presumably consist of resuspended rock dust. The diluted stack gas, however, contains an equivalent loading of fine particles not seen by the instack IP train. This test gave the largest unambiguous ratio of condensible to nonvolatile fine particles of any of the SDSS tests, with an 8:1 ratio of filter catches. When the SDSS sample line washes (which average about 25 percent of the SDSS filter catches) are added, the SDSS condensible catch represents 90 percent of the fine particle fraction and 45 percent of the total particulate emissions.

The high condensible fraction of the SDSS filter catch allowed a striking confirmation of residual volatility of the particulate even at room temperature. As shown in Figure 2, the three SDSS filters lost up to 20 percent of their original particulate mass over a period of 4 days after sampling. This effect is expected to be general for condensible emissions which are not saturated in the local air and are not stabilized by oxidation, water uptake, or other chemical reaction.

The final SDSS test for which data are available took place at the EPA facilities at Research Triangle Park, North Carolina. A 2.5×10^6 BTU/hr Scotch Marine Package boiler was sampled with the SDSS and IP trains, with an EPA Method 5 train, an Andersen Mark III impactor, and extensive continuous gaseous emissions monitors. The boiler emissions were measured using three fuel oils:a No. 2 distillate oil, a No. 5 residual oil with 1 percent sulfur, and a No. 6 residual oil containing 2.8 percent sulfur. Table 4 contains the average emissions from three runs with each oil measured by the SDSS and IP trains and by Method 5. Comparison of the SDSS and IP trains indicates that significant concentrations of condensible matter can be measured for the two residual oils. The concentrations shown in Table 4 represent 10-15 percent of the total SDSS emissions, and 30-60 percent of the fine particle fraction of the diluted stream. Significantly, the Method 5 front-half loadings agree closely with the SDSS, indicating that the dew point of

TABLE 3. RESULTS OF STACK DILUTION SAMPLING SYSTEM TESTS AT A CONTINUOUS DRUM MIX ASPHALT PLANT

Run	Sample Volume, dnm^3	Mass Concentration, mg/dnm^3			Percent Condensibles
		Cyclone X (>15 μm)	Cyclone III (2.5-15 μm)	Filter + Probe (<2.5 μm)	
1-IP	1.765	5.78	1.57	1.59	
1-SDSS	1.559	19.03	2.80	--	--
2-IP	1.681	18.76	0.94	1.49	
2-SDSS	1.375	14.92	2.01	15.78	43.7
3-IP	2.104	36.74	4.36	1.66	
3-SDSS	1.704	25.61	5.52	19.79	35.6
4-IP	1.115	9.70	2.14	2.42	
4-SDSS	1.112	14.47	2.13	27.81	57.2
AVERAGE-IP		17.75	2.25	1.79	
AVERAGE-SDSS		18.51	3.11	21.13	45.3

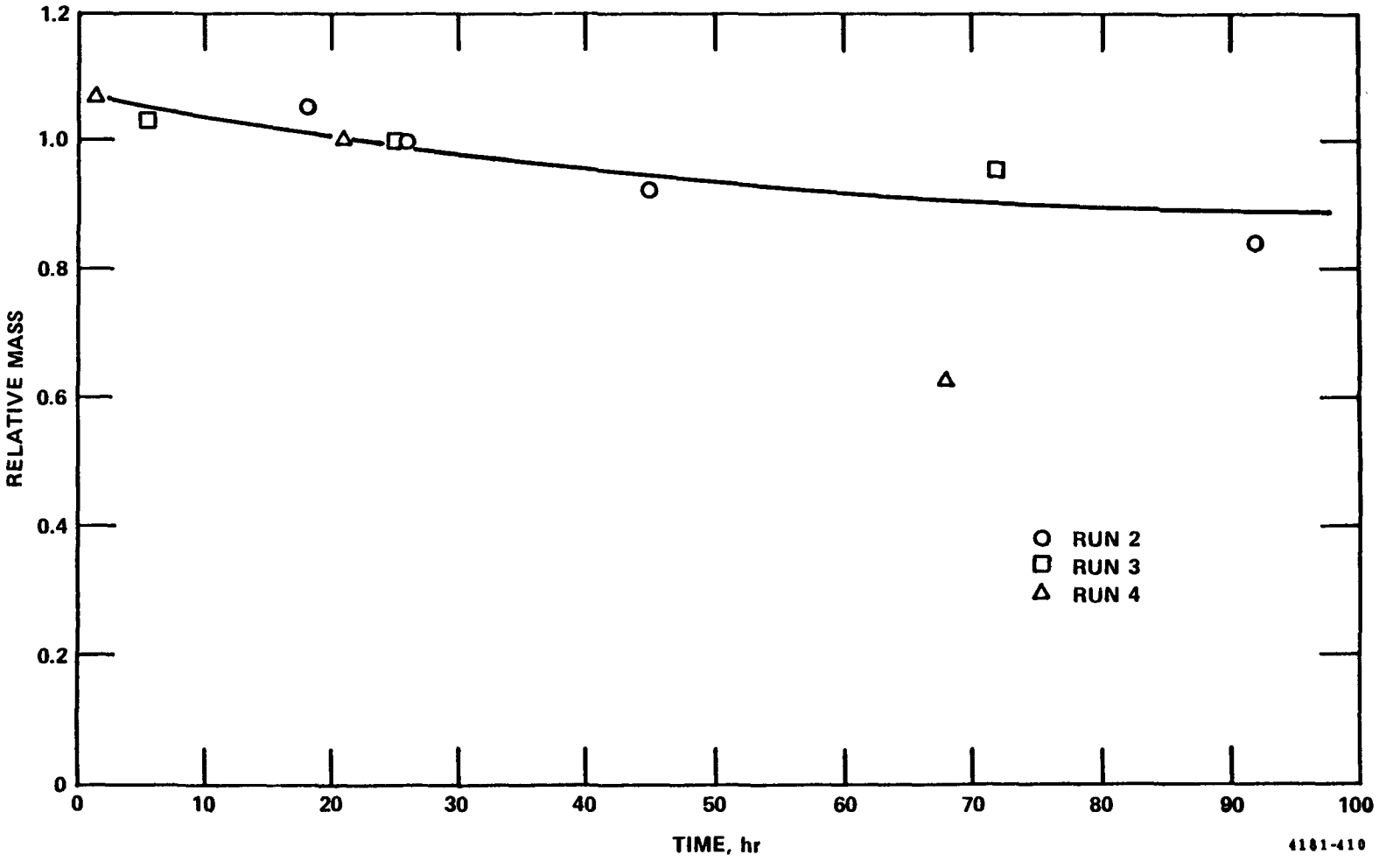

Figure 2. Relative variation of particulate mass on SDSS filter with time after sampling. All data for each run are normalized with respect to mass measured one day (21-26 hr) after sampling.

TABLE 4. RESULTS OF STACK DILUTION SAMPLING SYSTEM TESTS AT AN OIL-FIRED PACKAGE BOILER[a]

Oil	Device	Mass Concentration (mg/dnm^3) Cyclone (>2.5 μm)	Filter (<2.5 μm)	Total	Calculated Condensible
No. 2 distillate	IP	<0.1	0.7	0.8	
	SDSS	0.1	3.3	3.4	2.5
	M5			5.7	
No. 5 residual	IP	41.7	18.1	59.8	
	SDSS	41.2	28.5	69.9	10.0
	M5			71.8	
No. 6 high sulfur	IP	188.4	16.4	204.8	
	SDSS	203.6	41.3	244.6	25.0
	M5			253.0	

[a]Each value represents the average of three runs for the oil used.

the condensible material is higher than the 120°C Method 5 oven temperature. In addition, the loaded SDSS filters showed a definite tendency to gain weight when exposed to room air, indicating a hygroscopic component in the particulate catch. These factors strongly suggest sulfuric acid vapor to be the condensible component in this case. Soluble sulfate analyses of the SDSS and IP filters are in progress to check this hypothesis.

In conclusion, the Stack Dilution Sampling System has been used for testing at five sites in four source categories where condensible emissions were anticipated during formulation of the Inhalable Particulate sampling program. Some indication of condensible emission was found in each test. For at least one source, particulate matter formed by condensible vapors accounts for almost half the source contribution to the ambient total suspended particulate. The condensible contribution is even greater to particulate matter in the size range of respiratory interest. These results indicate that from many emissions sources, the contribution of condensible material connot be ignored.

ACKNOWLEDGEMENTS

This research was supported by the U.S. Environmental Protection Agency under Contract No. 68-02-3118, D.B. Harris, Project Officer. Field tests at the kraft recovery boilers and at the oil-fired package boiler were performed via subcontract from Acurex Corporation under EPA primary Contract 68-02-3159. Field tests at the asphalt plant were performed via subcontract from Midwest Research Institute under their primary Contract 68-02-3158. Tests at the coke quench tower were performed via subcontract to GCA Technology Corporation under EPA primary Contract No. 68-02-3157. EPA program manager for all field is D.L. Harmon.

REFERENCES

1. Williamson, A.D., and Smith, W.B. Development of a sampling train for stack measurement of inhalable particulate. In: Third Symposium on the Transfer and Utilization of Particulate Control Technology, Volume IV. Atypical Applications. EPA-600/9-82-005d (NTIS PB83-149617. U.S. Environmental Protection Agency, Research Triangle Park, North Carolina, 1982. p.297.

2. Smith, W.B., Cushing, K.M., Wilson, R.R., Jr., and Harris, D. B. Cyclone samplers for measuring the concentration of inhalabla particles in process streams. J. Aer. Sci. 13:259, 1982.

GAS CLEANING AND ENERGY RECOVERY

for

PRESSURIZED FLUIDIZED BED COMBUSTION

By: Dr. Albert Brinkmann
Gottfried Bischoff GmbH & Co.
Essen, West Germany

Mr. Peter Kutemeyer
Bischoff Environmental Systems
Pittsburgh, PA

ABSTRACT

THE DEVELOPMENT OF FLUIDIZED BED COMBUSTION

In an effort to reduce the consumption of oil and natural gas the search for a new technology, capable of utilizing low grade fuels, as well as more fully extracting available energy from high grade coal, led to the development of fluidized bed combustion (FBC).

The advantages of FBC are:

A. Lower and more uniform combustion temperatures, resulting in lower generation of NO_x.

B. Acceptably low SO_2 emissions by addition of limestone, thus eliminating expensive desulfurization equipment.

C. Smaller heat exchangers, and thus smaller boilers, due to higher heat transfer coefficients.

D. Use of low grade fuels.

The first operational FBC systems used in Germany operated at atmospheric pressure. These classic FBC plants required a relatively low capital investment and presented no development problems during installation or operation. Figure 1 shows the flow diagram of a 35 MW thermal output plant.

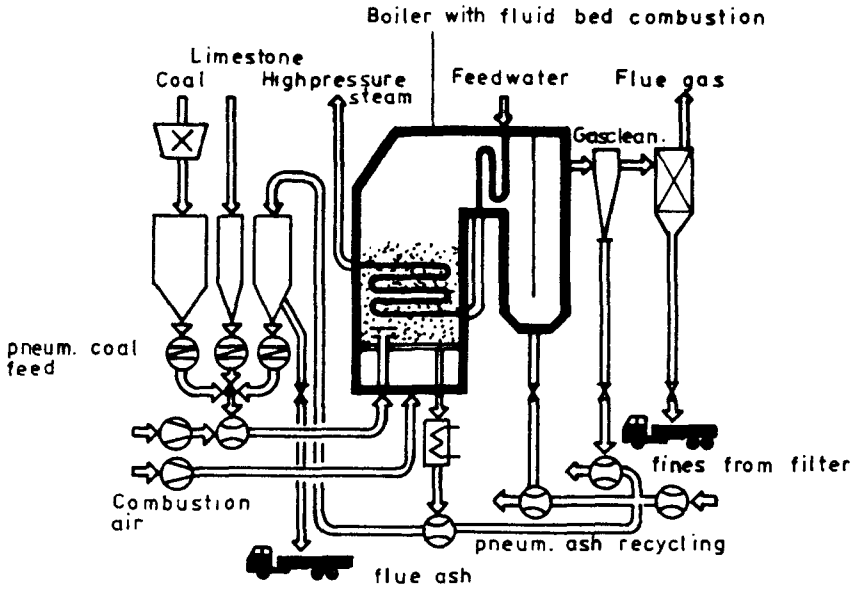

Figure 1: Flow scheme of a fluidized bed combustion plant (35 MW) operating at atmospheric pressure.

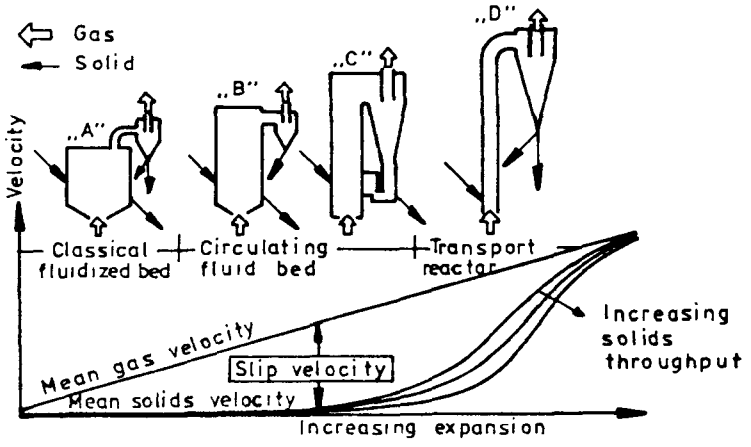

Figure 2: Bed motion as a function of SSV.

This conventional FBC system was characterized by a well defined fluidized combustion surface. As the gas velocity of the FBC system is increased, this well defined fluidized combustion surface transforms to pneumatic transport. The intermediary stage is called the circulating fluidized bed.

The advantages of the circulating fluidized bed are:

A. Further reduction in SO_2 emissions by use of fine grained limestone and combustion in various stages.

B. Reduced space requirements as compared to conventional FBC, thus greater output per unit.

Figure 2 shows the transition from the classic FBC process to the pneumatic transport process. Further development finally resulted in a pressurized FBC system which utilized the above mentioned advantages of the circulating fluidized bed to a greater degree, and, in addition, resulted in a more completely combusted ash.

A further aim of the pressurized FBC development was to operate an open cycle, coal fired gas turbine system. A simplified schematic of such a system is presented in figure 3. The heart of this system is the pressurized FBC chamber. A heat exchanger in the FBC chamber produces the steam to drive the steam turbine.

The combustion gases from the FBC boiler are expanded by a gas turbine after they have been cleaned of dust. Gas temperatures are the same as the FBC boiler temperatures about 800-950°C (1500-1750°F).

Two study groups were formed in Europe to develop the two major components of the energy recovery separately. The steam turbine process is being developed and optimized by the International Energy Agency of the OECD, with primary responsibility being exercised by the British Coal Board. The gas turbine process is being developed by a study group (AGW) which is a joint venture of the "Bergbau Forschung GmbH" and the "Vereinigte Kesselwerke A.G." in Germany.

The ultimate goal of these groups is the development of a system capable of generating a large amount of power using a combined gas/steam turbine pressurized FBC process.

GAS CLEANING AND THE PRESSURIZED FBC PROCESSES

The remainder of this paper will address the problems of cleaning the flue gas generated in a pressurized FBC process, so that this cleaned gas can be expanded in a gas turbine.

Cleaning of the flue gas is the key to an economically viable pressurized FBC process because a gas turbine requires relatively clean gas in

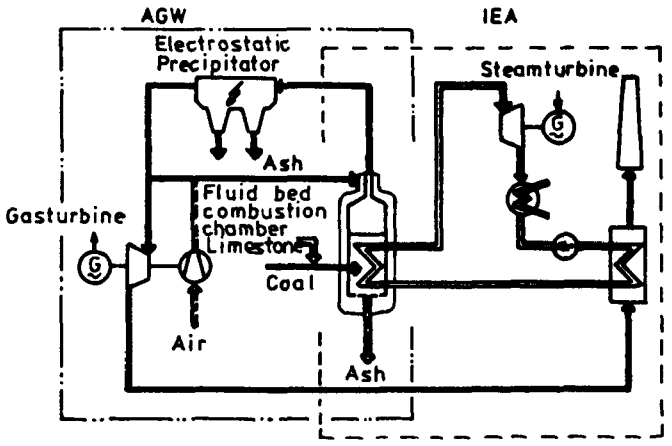

Figure 3: Flow scheme of a pressurized fluidized bed combustion plant.

order to have an acceptable operating life.

The use of electrostatic precipitators and baghouses to date has not resulted in providing a viable gas cleaning process for pressurized FBC. Tests conducted with granular filters have been equally unsuccessful. Because of this, a cyclone, a less efficient gas cleaning system was selected in Germany for the prototype plant, in conjunction with a gas turbine capable of operating with dust laden gas. Whether or not this solution will be an optimum economic and technical one is doubtful.

Even though it may not be possible, in the near future, to solve the problem of cleaning a high temperature and high pressure gas, such as that generated by a pressurized FBC system, it does seem feasable of using such a FBC boiler, with all its advantages, to generate steam. In this case a heat exchanger is placed in the pressurized FBC boiler for steam generation. In the process, the gases leaving the boiler are cooled to about 400°C (750°F).

For many years now Bischoff has successfully operated wet scrubbers for the cleaning of gas from high top pressure blast furnaces (B.F.) in conjunction with energy recovery turbines that utilize the excess temperature and pressure of the B.F. gas to generate electrical energy.

Below the use of such a wet gas cleaning system will be investigated to determine its viability for the temperatures and pressures encountered in a pressurized FBC process. A flow diagram of such a plant is presented in figure 4. The main component of a gas cleaning plant for high top pressure B.F. is the Bischoff annular gap scrubber, a differential pressure cleaning system. The heart of the system, as the name implies, is the annular gap element, an adjustable conical center body in a conical shell. A cross-section is shown in figure 5.

The Bischoff annular gap scrubber, "The Bischoff" for short, is not only able to provide a highly efficient gas cleaning system for varying operating conditions but is also able to maintain a pre-determined gas pressure in the system to a high degree of accuracy.

PERFORMANCE ANALYSIS

We shall consider two different processes for comparision:

A. Expansion of a high temperature gas in a gas turbine.

B. Expansion of a cooled and saturated gas in a gas turbine.

The results presented below will consider the required and recovered energy on the gas side of the pressurized FBC process. The calculations are based on the following gas analysis:

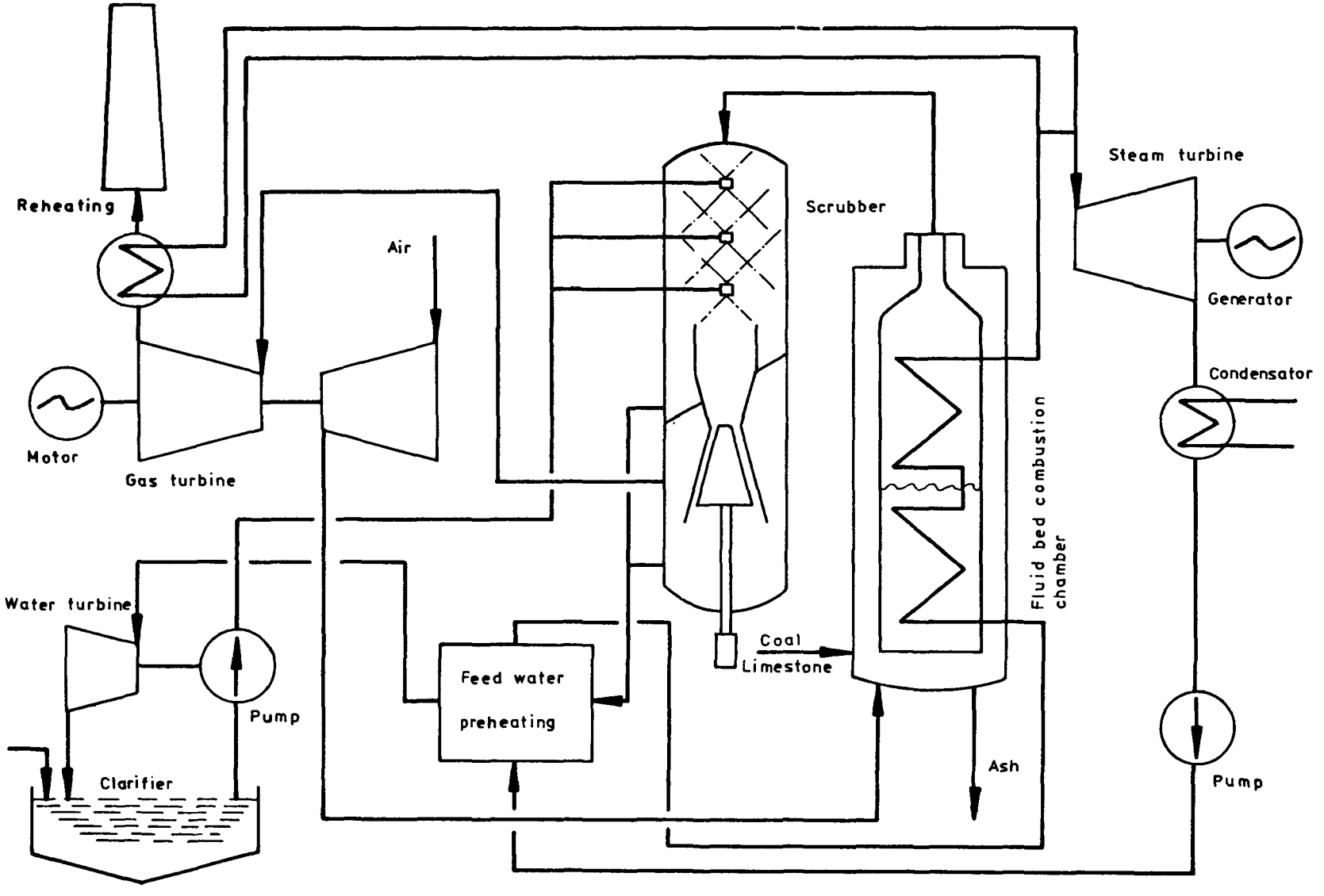

Figure 4: Flow diagram of a pressurized fluid bed combustion plant.

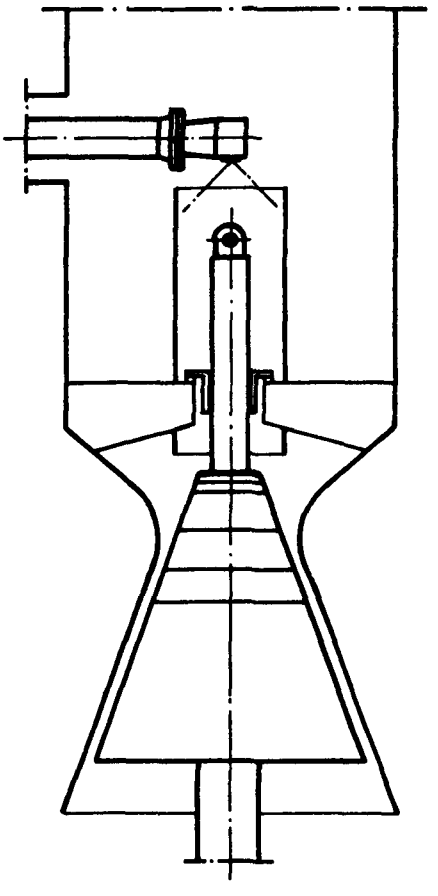

Figure 5: Bischoff Annular Gap Scrubber

CO_2 = 19,02%	N_2 = 71.112%
CO = 0.588%	SO_2 = 0.027%
O_2 = 4.836%	H_2O = 4.317%

The calculations will compare the performance of an expansion turbine downstream of the pressurized FBC boiler to the performance of an expansion turbine with a wet gas cleaning system inserted between the boiler and the turbine.

Figure 6 shows an enthalpy - moisture diagram for the case of expanding a high temperature gas in a gas turbine. Inlet (E) and exit (A) conditions for the isentropic expansion of the gas through a turbine are shown. The saturation lines (φ = 1.0) are indicated for the FBC discharge pressure P_1 = 10 bar (145 psi) and turbine discharge pressure P_2 = 1.1603 bar (16.8 psi). υ_o is the FBC discharge temperature, corresponding to turbine inlet temperature, and υ_2 is the turbine discharge temperature.

The moisture content X_o is calculated from the indicated water content in the flue gas.

Figure 7 shows the same diagram after insertion of the wet scrubber. Point W is the gas discharge condition from the FBC boiler; point S, the gas condition after cooling and saturation; point E, turbine inlet conditions, and finally point A, turbine discharge conditions after isentropic expansion.

υ_s is the saturation temperature of the gas and υ_1 and υ_2, the turbine inlet and discharge temperatures respectively. X_s, X_1, and X_2 are the corresponding moisture content values.

Values for gas temperature versus pressure at the turbine discharge for the two cases, as well as scrubber water discharge temperature are shown in figure 8. For these calculations an inlet water temperature of 80°C (175°F) was selected based on settling tank considerations and optimization of turbine performance. A flue gas volume of 100,000 m^3/h (62,100 scfm) and a cooling water use of 200 m^3/h (880 gpm) was selected.

Figure 9 compares the power output of the two cases as a function of FBC pressure and temperature. Also shown is the power requirement of the FBC compressor. Turbine and compressor efficiency were selected at 85% and 80% respectively.

Theoretical values for the thermal powers of the turbine discharge gas and the scrubber water as a function of pressure are given in figure 10, for the without and with wet scrubbing cases respectively.

For the case of expanding a high temperature gas in a turbine, a turbine discharge temperature of 100°C (212°F) is assumed. For the wet scrubbing case it is assumed that the flue gas must be reheated to 75°C

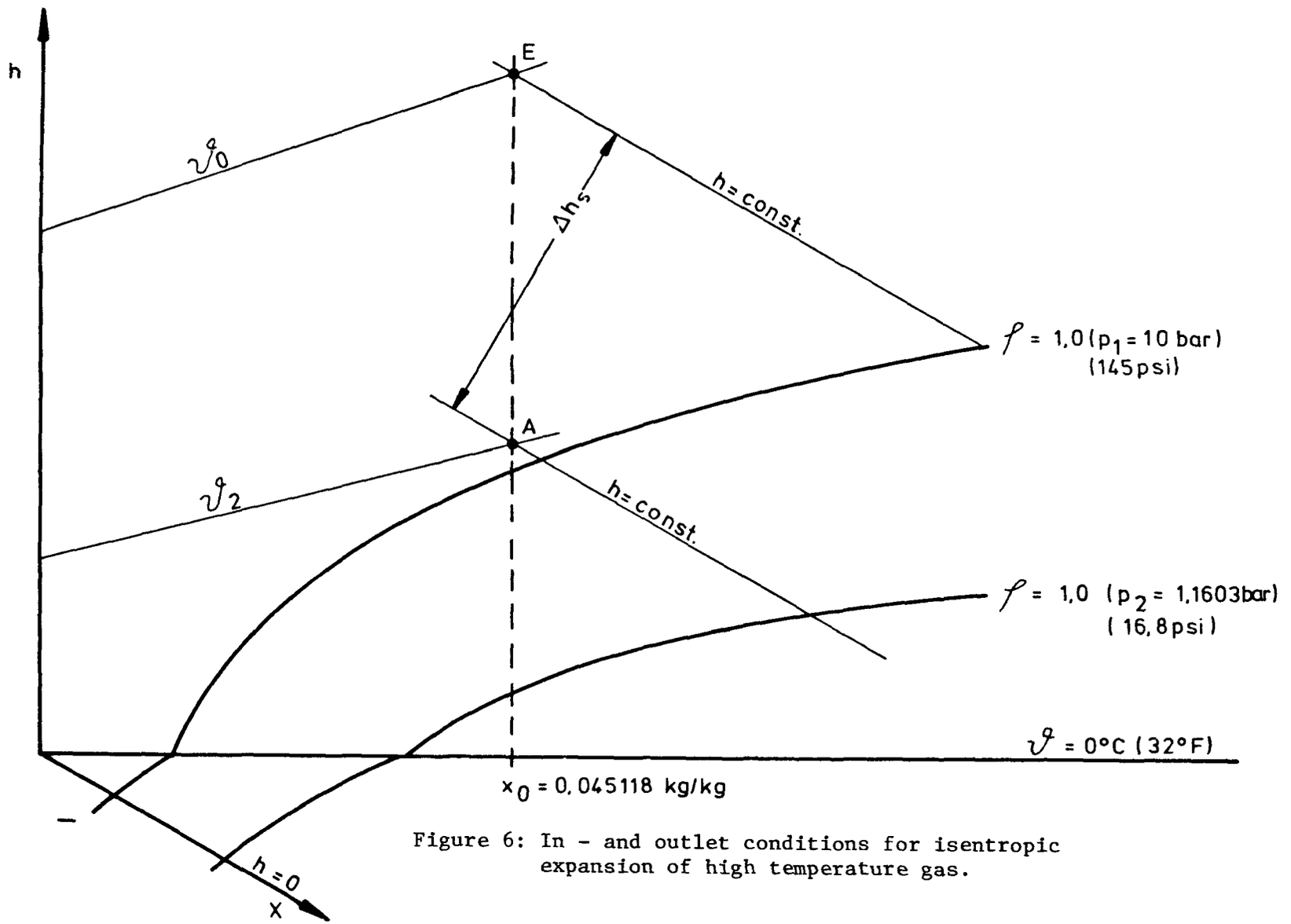

Figure 6: In - and outlet conditions for isentropic expansion of high temperature gas.

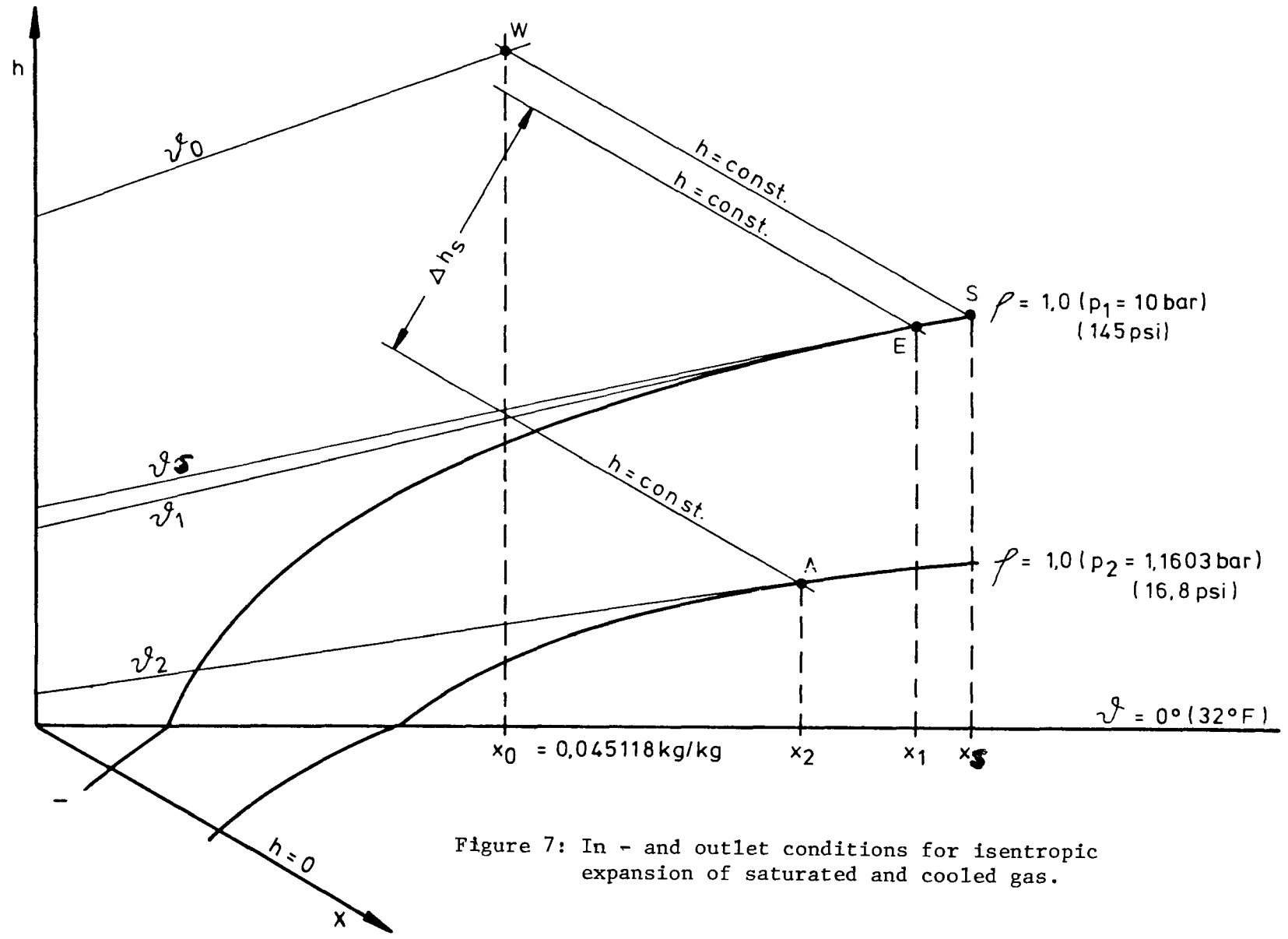

Figure 7: In - and outlet conditions for isentropic expansion of saturated and cooled gas.

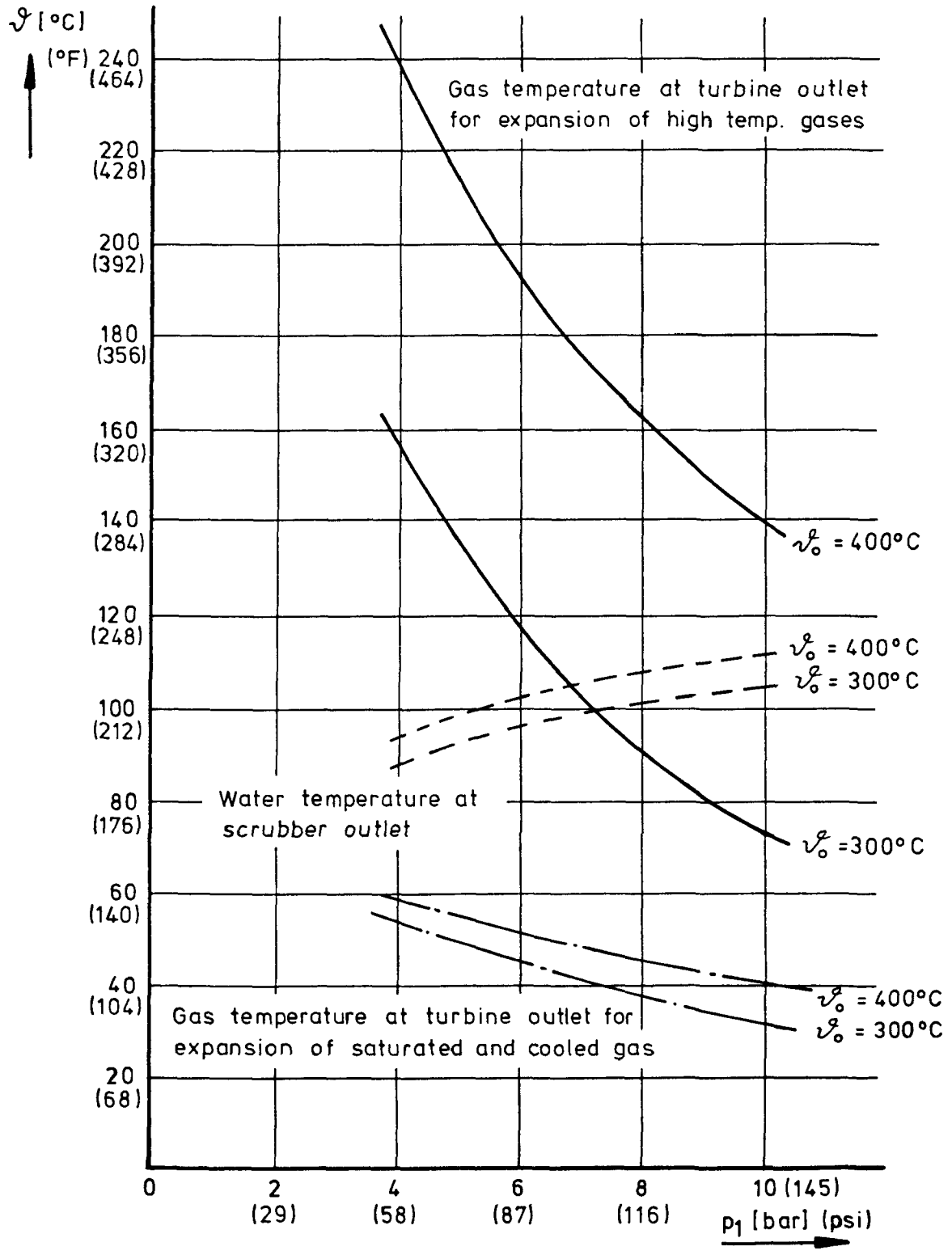

Figure 8: Temperature of gas at turbine outlet and of water at scrubber outlet.

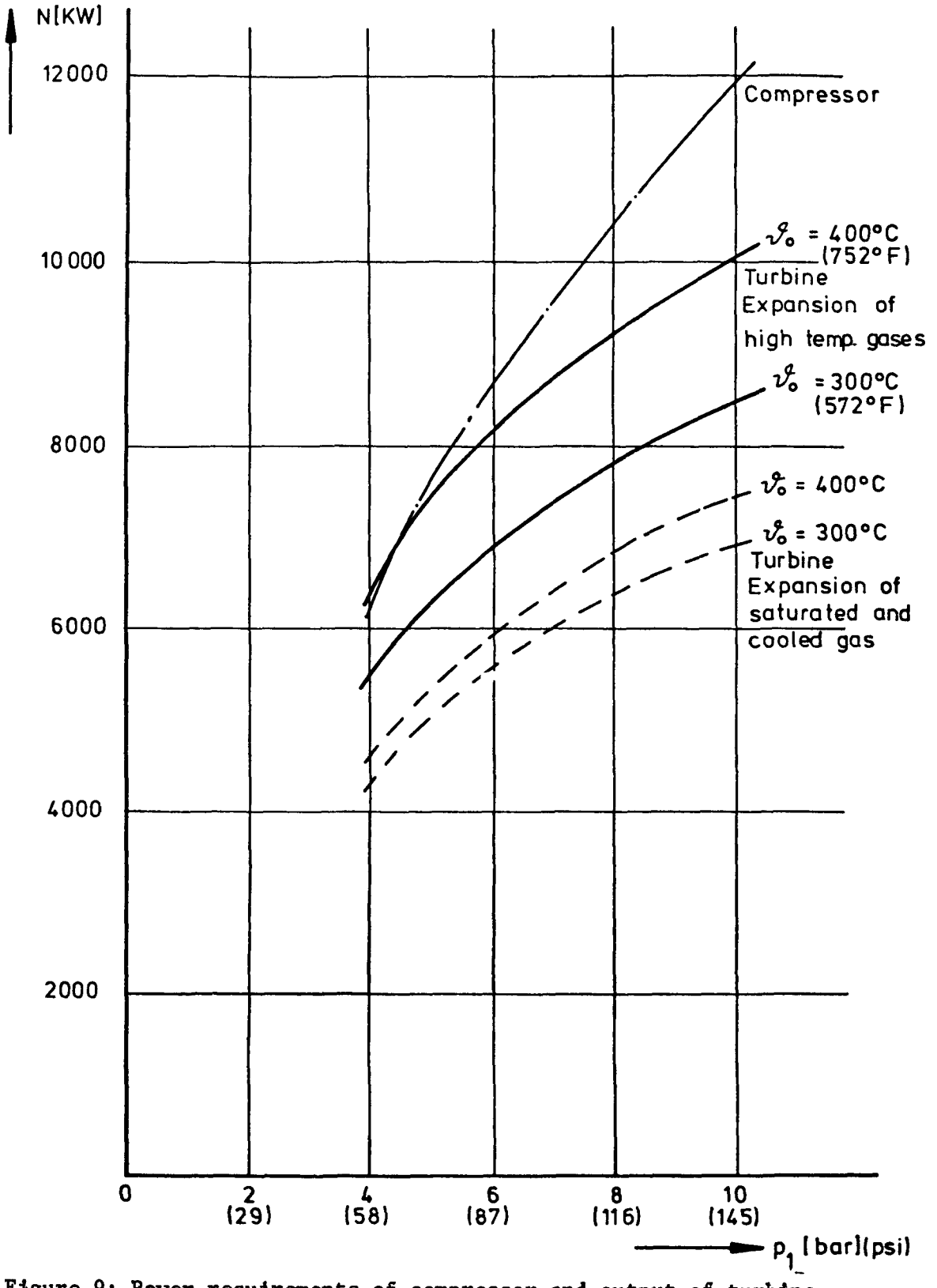

Figure 9: Power requirements of compressor and output of turbine
V_N = 100000 m^3/h (62100 scfm) η_T = 85% η_v = 80%.

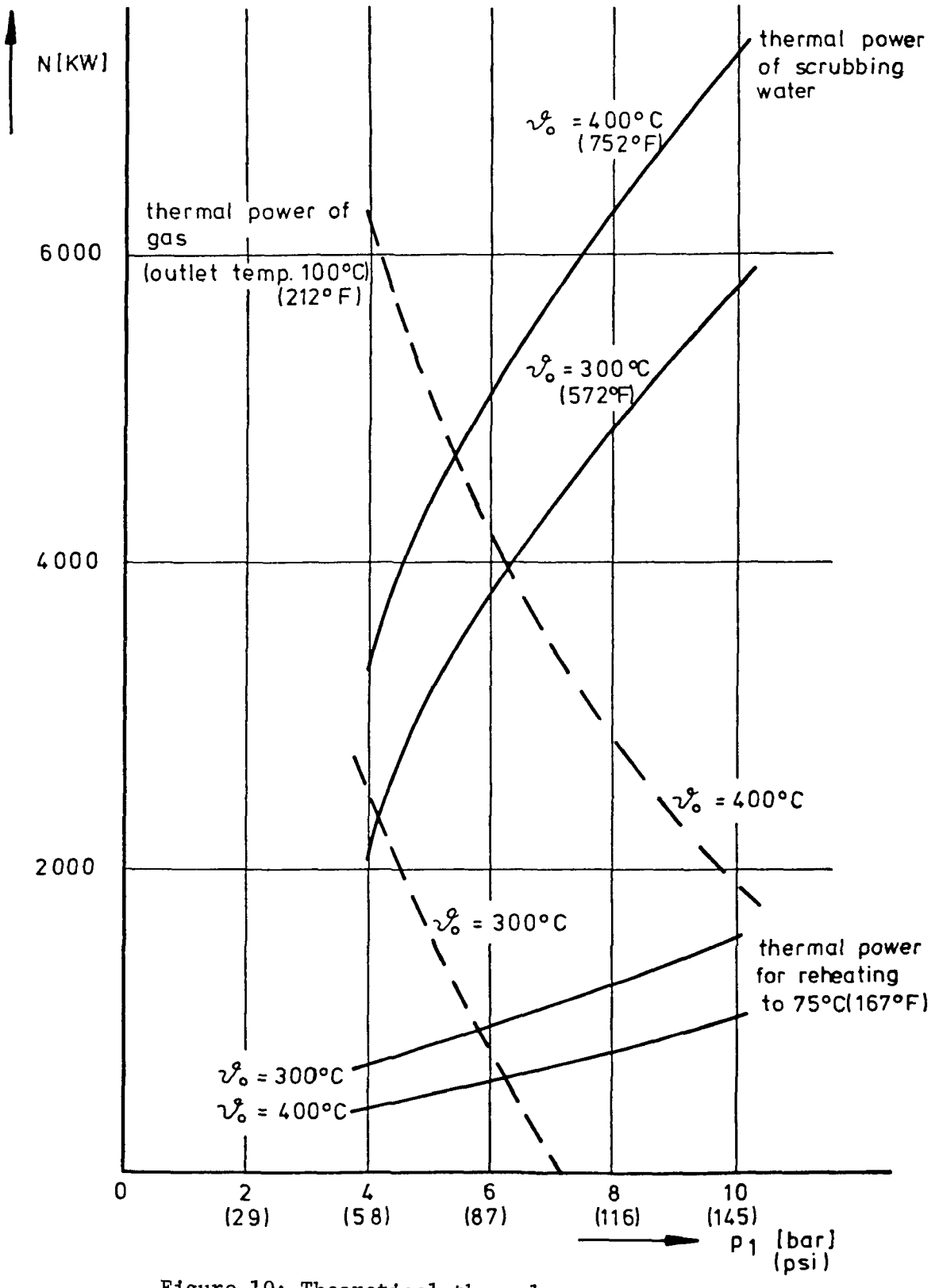

Figure 10: Theoretical thermal powers
$\dot{V}_N$ = 100000 m^3_n/h (62100 scfm)
$\dot{V}_W$ = 200 m^3/h (880 gpm)

(168°F). The energy required for this is shown.

From figure 10 we can see that FBC pressure and remaining thermal energy in the turbine discharge gas for the case without wet scrubbing is inversely proportional, whereas the thermal content of the scrubber discharge water in the wet scrubbing case and the FBC pressures is directly proportional.

Combining the results from figures 9 and 10 we obtain the values presented in figure 11.

From this figure it is clear that as the FBC operating pressure increases, the use of the wet gas cleaning system with a pressurized FBC boiler becomes a viable option.

CONCLUSION

The advantages of a pressurized FBC system are enhanced with increasing operating pressure. The above comparison has shown that wet cleaning with "The Bischoff", in conjunction with such a high pressure FBC system and an expansion turbine, is a viable alternative to the use of electrostatic precipitators, baghouses, or cyclones. This is particularly true when it is considered that "The Bischoff" represents a proven low maintanance system that is in operation on almost every high top pressure B.F. in the world today, quite a number of which also have a gas turbine for energy recovery.

The work described in this paper was not funded by the U.S. Environmental Protection Agency and therefore the contents do not necessarily reflect the views of the Agency and no official endorsement should be inferred.

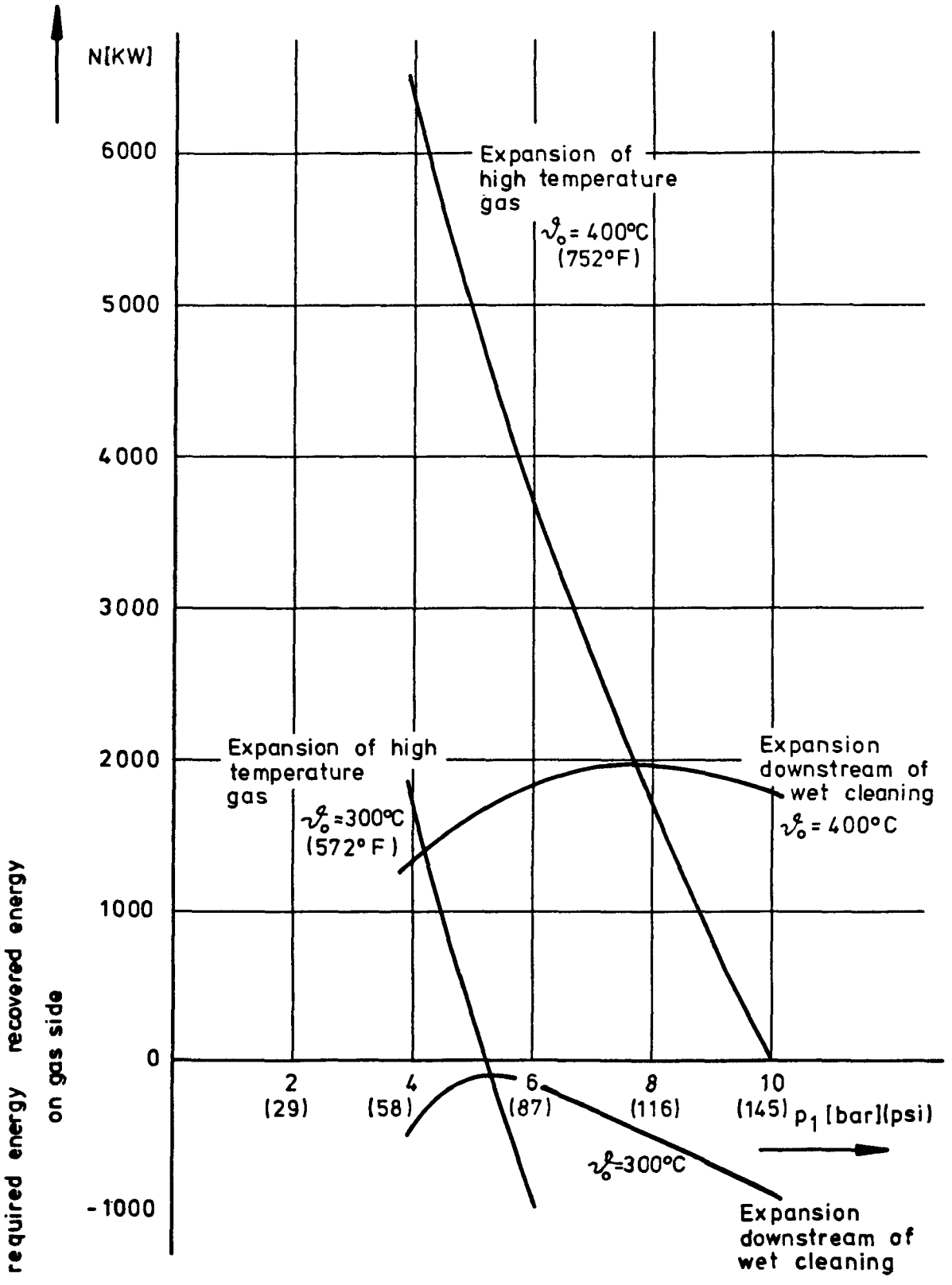

Figure 11: Comparison of power output.

DEMONSTRATION OF THE FEASIBILITY OF A MAGNETICALLY STABILIZED BED FOR THE REMOVAL OF PARTICULATE AND ALKALI

By: L. P. Golan, J. L. Goodwin, and E. S. Matulevicius
Exxon Research and Engineering Company
Florham Park, NJ 07932

ABSTRACT

This paper describes a unique panel filter bed of magnetizable particles subjected to a magnetic field used to remove particulate in the flue gas generated by a pressurized fluidized bed combustor (PFBC) to a level sufficient to prevent erosion of a gas turbine. The unique characteristics of this magnetically stabilized panel bed (MSB) high throughput rates, high particulate capture efficiency, trace metal removal, and use with a wide variety of coals.

This Department of Energy sponsored program is experimental in nature concentrating on evaluating the key factors necessary for demonstrating the feasibility of this concept, viz., the ability of the magnetic material to survive the PFBC environment, and particulate removal efficiency operating at PFBC conditions. The magnetic bed material evaluation phase has been completed. The results of the materials evaluation phase indicate that coated cobalt particles are suitable for this application. The particles have been found to possess good oxidation and attrition resistance while maintaining magnetic properties at the elevated temperatures. After 1000 hours of exposure to FBC flue gas no mechanical failure of the coating has been detected while sample magnetization was reduced only 10-20%.

The test phase of the program has been completed. The first phase of testing determined filter media flow rates at various field strengths. This was followed by a series of tests to determine the gas side pressure gradients at combinations of filter media flow and field strength. The final sequence of tests operated the filter in the semi-continuous mode. While these runs are still being analyzed, initial data appears promising.

BACKGROUND

The purpose of the program is to demonstrate the feasibility of using a bed of magnetizeable particles subjected to a magnetic field to remove particulates found in the flue gas generated by a PFBC. A typical process sequency utilizing this concept is illustrated in Figure 1. Flue gas from the PFBC combustor (1) is passed through cyclones (2) to remove the bulk of the flyash/dolomite particulates. The flue gas is then passed into a magnetized cross-flow bed consisting of an admixture of ferromagnetic particles necessary to stabilize the bed and potentially alkali metal scavenger particles such as bauxite or alumina. The downwardly moving bed acts as a filter for capturing particulates by impaction, interception, and diffusion. Trace quantities of sodium and potassium could be removed by reaction or adsorption with the scavenger bed material. As the concentration of flyash increases on the bed, it is removed from the bottom of the bed (4) and circulated by a gas transfer line to, first, a rough cut cyclone (5) which removes any flyash which has been detached from the bed material and, then, if necessary, to an elutriator (6) where the remaining flyash is removed from the bed material. Bed material is returned to the bed (8) while the dust laden gas from the elutriator is combined with the transfer line gas and sent to a cyclone (7) where the dust is separated from the gas. The remaining gas is either cleaned further in a bag filter (11) and sent to a stack, or recirculated (10) to the combustor as makeup air.

As trace metals build up on a non-magnetic material, they are removed by "bleeding" a side-stream of particles and subsequently removing the scavenger bed meterial (12). This separation should be easily accomplished by using a magnetic separation.

The key feature of this concept is the use of the magnetic field to maintain integrity of the cross-flow bed. Preliminary cold flow studies conducted at Exxon have shown that such a bed is capable of contacting the solid bed material with gas at velocities four times greater than possible in the cross-flow moving bed filters without the imposed magnetic field. The advantages for the concept developed through the cold flow studies are:

- Increased throughput. The gas velocity before bed material is entrained or "blown out" of the bed is significantly increased because of the orientation and structuring of the bed material by the magnetic field.

- Lower pressure drop. The structuring and the orientation of the bed results in a higher void fraction and hence lower pressure drag per unit thickenss of the bed when compared with a conventional moving granular bed operating at the same conditions.

- Increased collection efficiency. The collection efficiency is increased significantly over conventional beds especially for smaller (10 μm) particulate.

For the magnetized panel bed concept to be possible a filter media capable of withstanding the FBC environment was needed. The materials requirements for the filter media are demanding. Most importantly the material must be ferromagnetic at the operating temperature of the filter (~830^{0}C). The Curie temperature (that temperature where a metal loses its ferromagnetic properties) of most ferromagntic materials is lower than PFBC operating temperatures; the sole exception being cobalt. Pure cobalt however is a soft metal that is easily oxidized. Since the process environment is both corrosive and oxidative, a coating must be employed to protected the cobalt. In addition to being oxidation and corrosion resistant, the coating must also be attrition resistant. The filter material will be subjected to an attrition promoting environment when it leaves the panel bed vessel and enters the elutriator cleanup cycle. A protective coating was develped by Exxon prior to the initiation of this program which was shown to prevent oxidation of the cobalt.

ATTRITION RESISTANCE

As part of a preliminary evaluation, the coated cobalt particles were subjected to an attrition resistance test. The test consisted of vigorously fluidizing a bed of the coated cobalt for 100 continuous hours at 830°C and a fluidizing velocity of 2.1 m/s (1.6 times minimum fluidizing velocity). SEM photomicrographs of cross-sectioned spheres showed no signs of wear, chipping, oxidation or separation of the coating. Magnetic property measurements indicated that the magnetic induction force was unaffected by the 100 hours of exposure. These tests demonstrated that a material capable of satisfying the panel bed requirements was possible.

MAGNETIC MATERIAL EVALUATION

As part of the current DOE program, a materials evaluation task was conducted to assess the corrosion resistance of the filter media under high temperature FBC flue gas conditions. Small samples of filter media were exposed at FBC conditions for periods up to 1000 hours. For the testing, a small 250,000 BTU/hr AFBC unit was used (Figure 2). Flue gas from the combustion of coal passed through three sample locations yielding three different exposure temperatures. The first site was in the combustor tower approximately one foot above the fluidized bed; the temperature was approximately 830°C. The second sample site was at the tower outlet; the temper-

ature was approximately 740°C. The final site was downstream of the cyclone cleanup train; the gas temperature here was approximately 615°C. By selectively removing and replacing samples at 100 hour intervals multiple sample exposure times at temperature were achieved. The particles were generally spherical in shape and approximately 800-1400 μm in diameter.

The 1000 hours was accumulated in 14 runs. The samples cooled between runs. This was taken to be a more severe test since the particles were subjected to cooldown and heatup stresses which would not noramlly be encountered in actual PFBC operation.

A summary of the operating conditions for all runs is presented in Figure 3 including flue gas composition and materials exposure temperature. (The average flue gas composition was O_2 4.1%, SO_2 310 ppm, NO 700 ppm, CO 580 ppm and CO_2 16%.)

During the materials evaluation two different filter media samples were exposed. Both materials were pure cobalt generally spherical in shape which were coated using the same process. The difference in the filter media was the supplier and subsequently the method of manufacture of the cobalt particle. The samples were designated either N or P. The material N was used during the attrition tests conducted by Exxon. The material from a second supplier is designated by P and is the material used as filter media in the magnetically stabilized bed.

Material N was exposed for the entire 1000 hours period. The new material (P) was exposed for only 774 hours.

To facilitate identification of the samples with respect to their supplier, exposure location, and length of exposure the following nomenclature was adopted:

- first letter - identify supplier, N or P
- second letter - identify exposure location
  - A - exposed above bed at 830°C
  - B - exposed before cyclones at 740°C
  - C - exposed after cyclones at 615°C
- numbers - indicate hours of exposure

changes had occurred. The conclusion was that neither hot gas corosion of the coating nor metallurgical changes due to the high temperature of exposure affect the life of the particle.

Did the Magnetic Properties Change?

In addition to the changes in the particle metallurgical properties, changes in magnetic properties as a function of time and temperature were also determined. The magnetic properties were measured by using a Perkin-Elmer thermal microbalance, TGS II. The principle of measurement was the Faraday method. When a small magnetic sample is placed in a non-uniform magnetic field, a translational force is exerted on the sample according to the following equation:

$$\frac{F}{V} = \frac{1}{4\pi} \quad M \frac{dH}{dX}$$

where F is the translation force in dynes, V the volume of sample in cm^3, M the magnetic induction of the sample in gauss, and dH/dX the magnetic field gradient of the non-uniform applied field in oersted/cm. A schematic diagram of the setup is shown in Figure 6. A small portion of the magnetic particle sample, S, about 10 mg, was placed in the sample pan, P, on the microbalance. A sample of three beads was used. The beads were placed in a row to approximate a cylinder which helped to reduce the effect of depolarization. The environmental tube, E, for the sample was then placed in position and purged with nitrogen. When a steady state flow of the inert gas was reached, the weight of the sample was measured on the microbalance and recorded in mg. A horseshoe permanent magnet, N, was then placed around the sample at a distance X, in mm, from the center line as shown. The magnetic field strength, H, of the magnet was measured and the field gradient, dH/dX, calculated. The force exerted on the sample due to the field gradient in the direction could be measured directly on the microbalance in mg. The sample magnetization in M was then calculated using the above equation.

By placing the magnet, N, at a specific position, a corresponding force, F, could be measured. Without altering the set-up, the temperaure of the sample can be varied by controlling the heater of the furnace, C. Therefore, the temperature dependence of the magnetization could be evaluated. Measurements were made over a range of temperatures (20-1000°C).

The magnetic induction properties of samples of the cobalt particles which had been exposed to FBC flue gas conditions for various time periods were measured to evaluate the effect of exposure time on magnetization. For these measurements, a consistent procedure was used and the magnet was always placed in the same position. Measurements were made at room tempeature (25°C) and at 830°C, the exposure temperature at location A. Due to the variability of the spheres (size, shape, and magnetic property) at least two measurements (two different sets of beads)

were made for each sample evaluated. In some cases, the variance was large so additional measurements were made to assure representative values were obtained. The magnetic induction force as measured is expressed as mg of force/mg of sample. The object of the magnetic evaluation is to determine if the magnetization of the sample has decayed as a result of FBC exposure. A normalized plot of the magnetic induction force, F, versus exposure time was used to indicate whether and to what extent the magnetization has decayed. The normalized magnetic induction force is the ratio of F at time τ, and F at zero exposure. Figures 7 and 8 show the normalized plots for materials N and P respectively.

In Figure 7 we see the normalized ratio plot for samples N-A-119, 327, 530, 774, 1000 and N-original. Magnetic measurements were made at 25°C and 830°C. The data scatter is not surprising and can be attributed to the particle variability. The magnetic induction force has decreased by less than 15% over the 100 hours of exposure with no indication of decay after the first 100 hours of exposure of flue gas. Also, there is no evidence of a continuing decay with time.

Figure 8 is a similar plot for the P material. After 774 hours of exposure, there was approximately a 20% decrease in magnetization. With both materials, it appears that the major loss of magnetization occurs during the first 100 hours of exposure. The magnetization appears to stabilize after the initial drop.

The temperature dependence of the magnetiziation of the sample can be measured by continuously recording the magnetic induction force of the sample as it is heated from room temperature to 950°C. The temperature dependence for two materials, N-unexposed and P-unexposed, are shown in Figure 9. Again, a normalized ratio is used, this time the force at temperaure, F_T divided by the force at room temperature, $F_{25°C}$. The P material is only slightly affected by the temperature indicating a Curie temperature higher than 950°C. The normalized ratio drops to zero at the Curie temperature. The N sample however exhibits a decrease in magnetization with increasing temperature. The magnetic properties of the two materials were affected differently by increasing temperature. this can be attributed to the difference in the method of manufacture and the amount of diffusion that occurred during the coating process. The trends seen here are consistent with the other samples of materials N and P tested.

The metallurgical examination and magnetic evaluation of the exposed samples indicate that these particles are suitable for MSB application under the conditions at which they were evaluated. No failure of the particle coating was seen; any defects seen in the particles were inherent, not a result of the exposure testing. Only a limited amount of diffusion had taken place in the most severe case. The loss of particle magnetization which occurred during the initial 100 hours was 20% or less which is an acceptable level since most of the change occurred early in the test and, a lower rate of loss of magnetization, if any, could be assumed for long exposures.

KEY ISSUES:

Did Metalurgical Changes Occur?

All exposed samples of both materials look unaffected to the naked eye. Selected samples were submitted for cross-sectioning and photomicrographs to examine the condition of the coating. Samples of material N which were exposed for 0, 327, 530, 774 (exposure location C at 734 hours), and 1000 hours were submitted for examination. Samples of material P which were exposed for 0, 101, 304, 508, and 774 hours were also submitted for examination. Figure 4 shows cross-sections of material N particle at 0, 530, and 1000 hours of exposure at 830°C. In Figure 5, the cross-sectioned particles material P are shown for 0, 101, 304, and 774 hours of exposure at 830°C. The fissures (grain boundaries) and small voids seen in the particles remain from the manufacturing process and are not a result of the exposure testing.

Comparison of the unexposed particle with the exposed particle sample indicates no failure of the coating had occurred. It shoud be noted that due to the method of manufacture, material N is very spherical and has a narrow size distribution with a majority of the spheres having a 1000 micron diameter. The P material is less spherical with more rod and elongated pieces and cover a larger size distribution (800-1400 μm).

Energy dispersion x-ray (EDX) analysis was performed on selected particles to determine the extent of diffusion of the coating into the Co core. This was important because diffusion of the coating material into the cobalt would lower the magnetic Curie temperature of the cobalt application. Two techniques were used; one was the line scan method whereby the concentration profile of an element of interest along a particular line trace could be obtained to indicate locations of high concentration. The other method was semi-quantitative analyses of all the elements at a particular point of interest, such as the center of particle.

The samples submitted for EDX analysis were N-original, N-A-1000, P-B-304, and P-A-774. The EDX analyses indicate that a minimal amount of diffusion of the coating into the cobalt core had occurred even after 1000 hours of exposure at the most severe conditions of the materials test. The semi-quantitative EDX results also indicated that the N material contained some Fe contamination (up to 10% in the semiquantitative tests). The P material had an insignificant amount of Fe contamination. A small amount of Fe is not expected to affect the overall performance of the Co particles. In fact, the use of a Fe-Co alloy as the particle core material for this application had been studied earlier because of economic considerations. The result of this evaluation showed that little metallurgical

FILTER OPERATION

The pilot plant facility for once through operation is shown in Figure 10. The PFBC combustor which will generate the particulate ladden flue gas has an ID of 11.4 cm. It operates at 870°C and ten atmospheres pressure generating 1.5-2 sm^3/min of flue gas. Lock hoppers located above and below the filter vessel are used to supply and collect the filter media as it passes through the filter. Key features of the unit are:

1. Removable cyclones to allow variation in flue gas particulate loading.

2. A methane injection system to make up any flue gas heat loss.

3. An electric air preheater which will bring the filter up to temperature prior to filtration.

4. Particulate sampling stations before and after the filter to measure capture efficiencies.

5. Total particulate filters for integrated capture efficiencies.

6. Extensive system to measure pressure differential through the filter bed.

The filter bed internals are a variation on conventional designs used in the earlier studies of panel beds. Dirty flue gas enters down the center of filter vessel and passes radially through the openings (Figure 11). The louvers are designed such that the material will not flow out the openings when a modest magnetic field is applied. A radial gas flow pattern flowing from inside to out will be used to allow a high gas velocity at the bed inlet but a decreased velocity through the bed. The high inlet velocity will prevent duct laydown in the flue gas distributor; the lower velocity in the bed will improve capture efficiency. Pressure taps have been incorporated along the length distributor and across the distributor for measuring system pressure drop. Mathematical flow modeling of the distributor suggests that the flow maldistribution for this design should be less than 20% with a 20% slot open area. In addition the flue gas jets penetrate approximately 25% of the bed depth.

PRELIMINARY RESULTS

Filtration tests for both a stationary bed and moving bed have been completed for a range of temperatures and loadings of particulate. Results are being evaluated. However, several important conclusions have emerged.

- No plugging of the filter face has occurred. The large openings possible because of ability to hold the particles in the bed magnetically precludes the bridging of ash found in conventional panel bed filters.

- Overall efficiency has averaged approximately 90%. In addition, the efficiency did not significantly vary with particulate size but increased with loading.

- High flue gas throughputs were shown to be feasible.

- Captured particulate were shown to be easily removed from the cobalt spheres in a subsequent cleaning operation.

Final analysis of the data is currently underway. A final report will be issued by December 30, 1982.

ACKNOWLEDGEMENT

Funding for this program is provided by U. S. Department of Energy under contract No. DE-AC21-ET 15055.

The work described in this paper was not funded by the U. S. Environmental Protection Agency and therefore the contents do not necessarily refect the views of the agency and no official endorsement should be inferred.

Figure 1
Conceptual Plant Flow Sheet

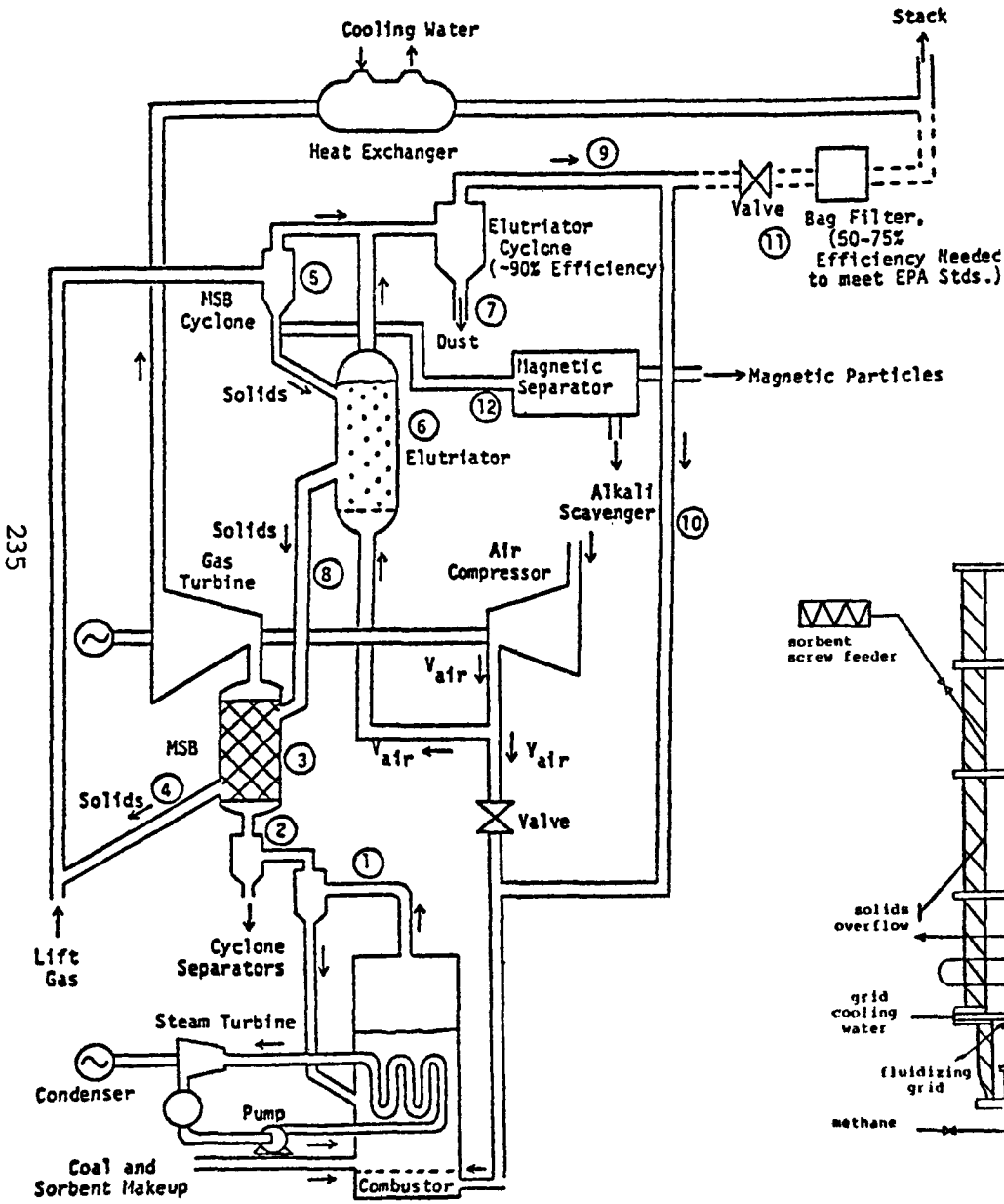

FIGURE 2 -
ATMOSPHERIC FLUIDIZED BED COMBUSTOR
FOR MATERIALS EVALUATION PROGRAM

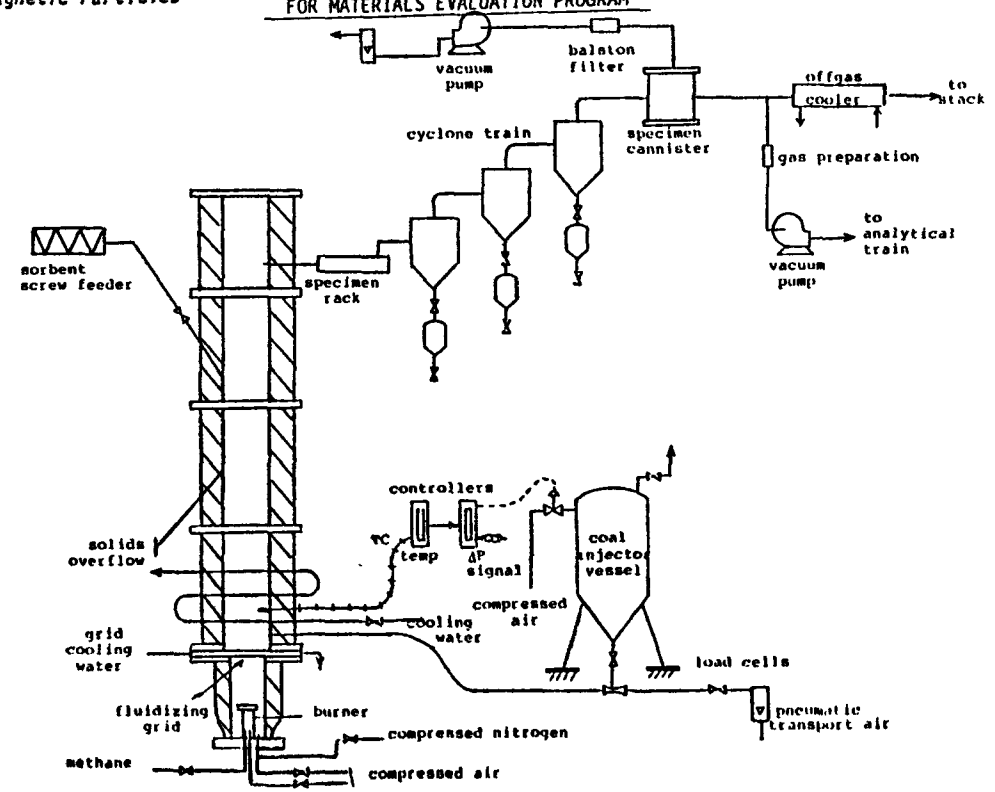

FIGURE 3

Operating Conditions for Materials Exposure Testing

Run	Date	Run Length, hrs	Pressure kPa	Air Flow Rate, m^3/min	Avg. Bed Temp., °C	Superficial Velocity, m/s	Expanded Bed Height, m	Coal Feed Rate, Kg/hr	Excess Air,* %	Average Flue Gas Emission					Materials Exposure Temp., °C		
										SO_2, ppm	NO, ppm	CO, ppm	CO_2, %	O_2, %	Above Bed	Tower Outlet	After Cyclone Train
1	1/28/81	5	110.3	0.54	890	1.45	0.50	4.1	18	900	1250	1300	16.5	3	803	759	636
2	1/29/81	5	113.3	0.54	874	1.41	0.53	4.1	21	90	1000	1000	17.5	3.5	786	745	619
3	1/30/81	7	113.7	0.54	881	1.42	0.54	4.5	19	100	1000	900	17.5	3.2	788	749	617
4	3/2-6	102	112.6	0.54	878	1.43	0.67	3.9	30	180	420	550	16.5	4.6	826	772	645
5	3/27	5	113	0.54	878	1.43	0.71	4.3	19	120	---	750	17.5	3.2	773	704	581
6	3/2-6	102	113	0.54	880	1.43	0.68	3.6	25	160	---	500	16.5	4.0	806	739	611
7	3/16-20	101	108	0.54	879	1.43	0.65	3.6	24	250	530	430	16.0	3.9	816	749	628
8	3/30-4/3	102	108	0.52	877	1.43	0.75	3.5	25	180	550	430	16.0	4.0	823	745	611
9	4/13-17	101	107	0.52	877	1.46	0.77	3.5	26	200	530	500	16.5	4.2	821	745	605
10	5/4-8	101.5	107	0.52	878	1.45	0.73	3.3	27	350	510	560	16.0	4.3	821	745	605
11	5/18-22	102.5	108	0.52	876	1.44	0.79	3.3	27	390	1050	520	16.0	4.3	806	741	612
12	6/1-5	101.75	108	0.53	877	1.45	0.76	3.5	25	370	950	490	16.0	4.0	811	741	614
13	6/15-22	92	110	0.52	877	1.41	0.71	3.2	26	360	975	450	16.0	4.2	796	732	601
14	6/29-7/2	72.25	110	0.52	877	1.41	0.73	3.5	25	750	750	460	15.5	4.0	809	739	604

*Calculated from flue gas composition

NOTE: All runs made using Champion Coal and Phizer Dolomite

FIGURE 4

MSB MAGNETIC MATERIALS EVALUATION
PHOTOMICROGRAPHS OF CROSS-SECTIONED
FILTER BED MEDIA PARTICLES

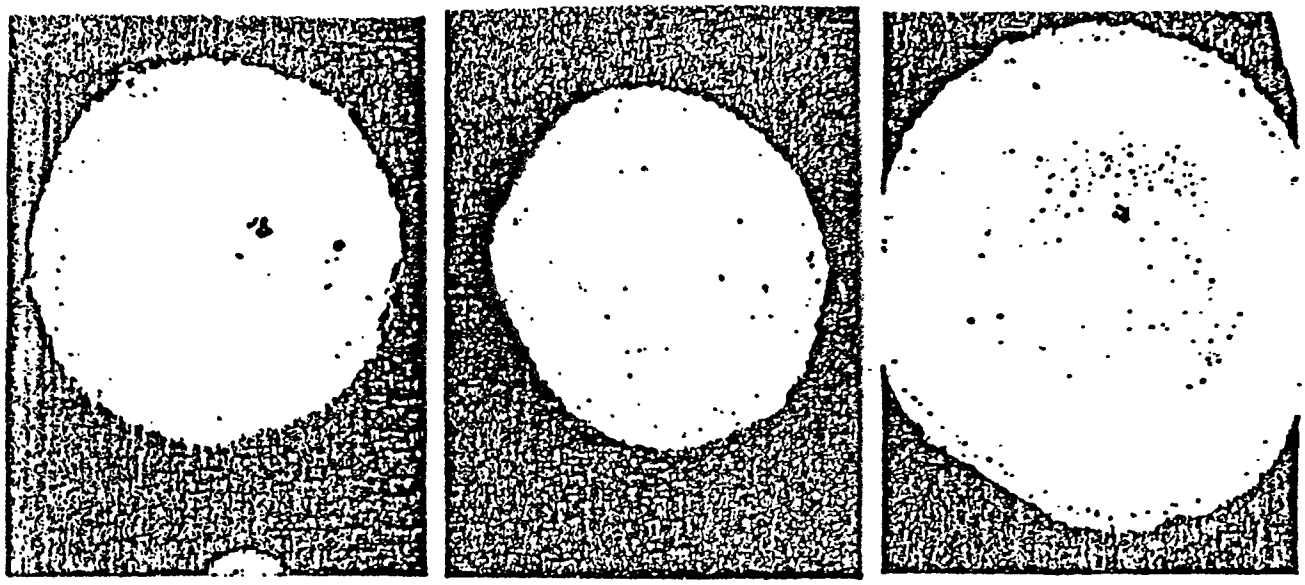

UNEXPOSED | 530 HRS EXPOSURE | 1000 HRS EXPOSURE

MATERIAL N - 100X NOMINAL
830°C

FIGURE 5

MSB MAGNETIC MATERIALS EVALUATION
PHOTOMICROGRAPHS OF CROSS-SECTIONED
FILTER BED MEDIA PARTICLES

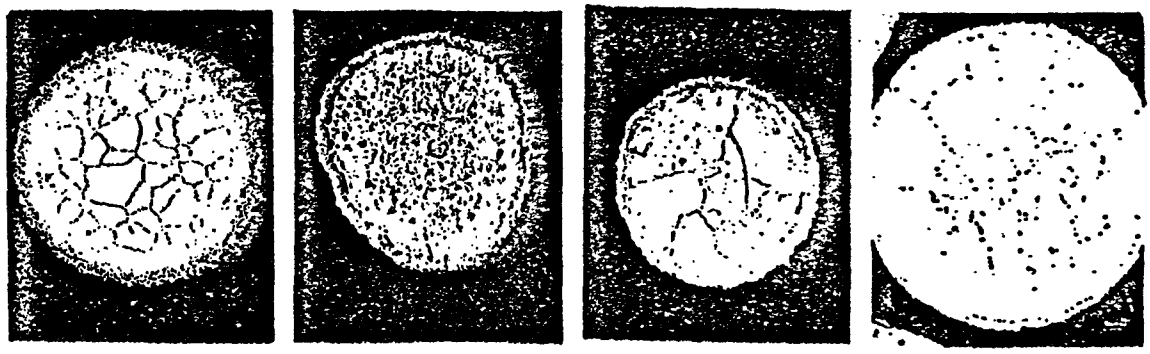

UNEXPOSED | 101 HRS EXPOSURE | 304 HRS EXPOSURE | 774 HRS EXPOSURE

MATERIAL P - 100X NOMINAL
830°C

FIGURE 6

SCHEMATIC DIAGRAM OF THE PERKIN-ELMER TGS II SET UP AS A FARADAY BALANCE FOR MAGNETIC PROPERTIES MEASUREMENT

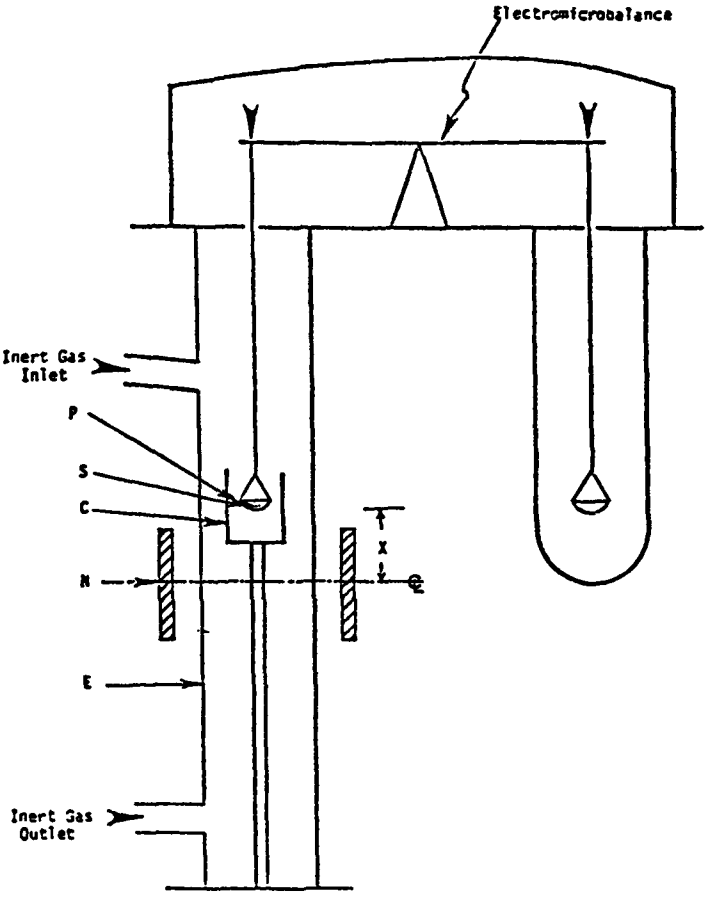

FIGURE 7

NORMALIZED FORCE RATIO VERSUS EXPOSURE TIME FOR MATERIAL N

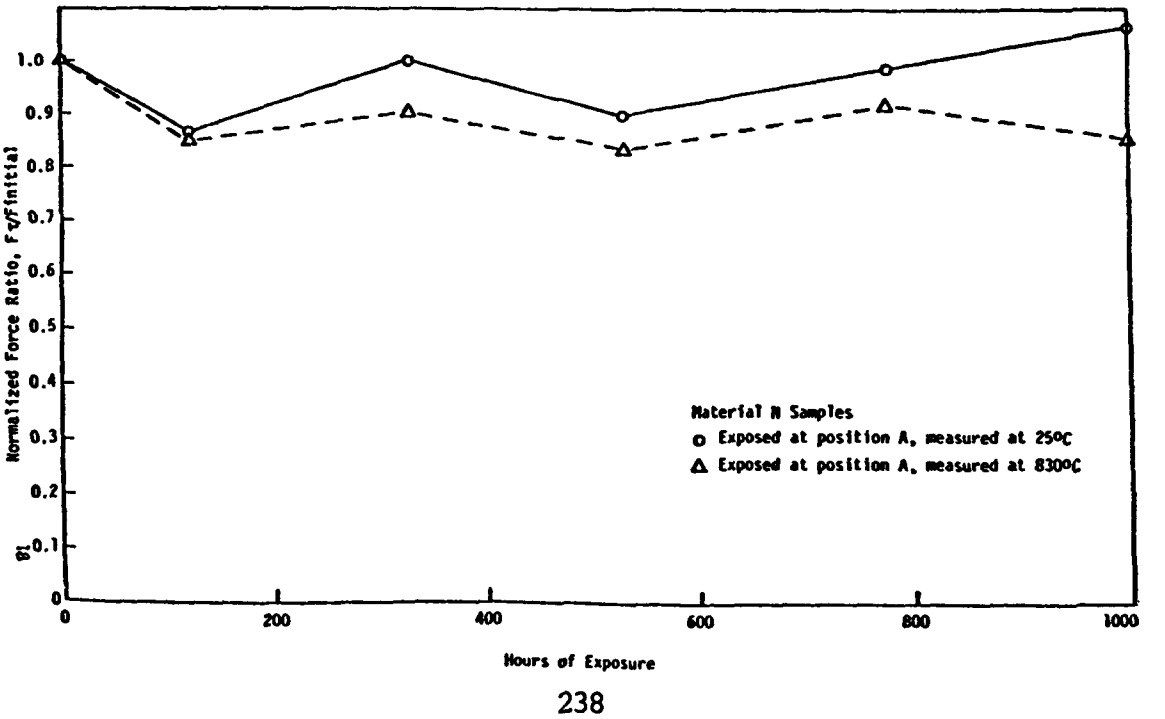

FIGURE 8
NORMALIZED FORCE RATIO VERSUS EXPOSURE TIME
FOR MATERIAL P

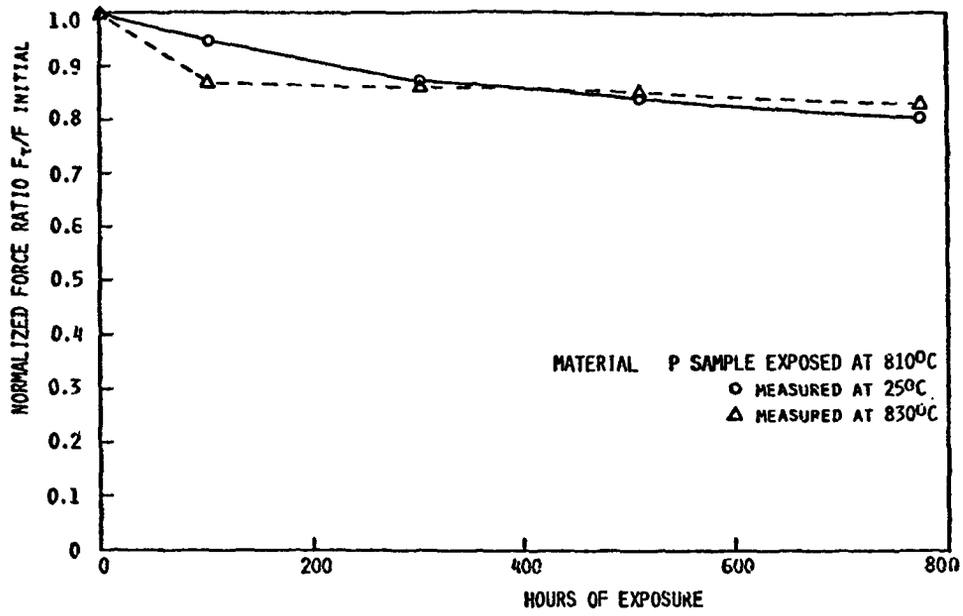

FIGURE 9
NORMALIZED FORCE RATIO VERSUS MEASUREMENT TEMPERATURE

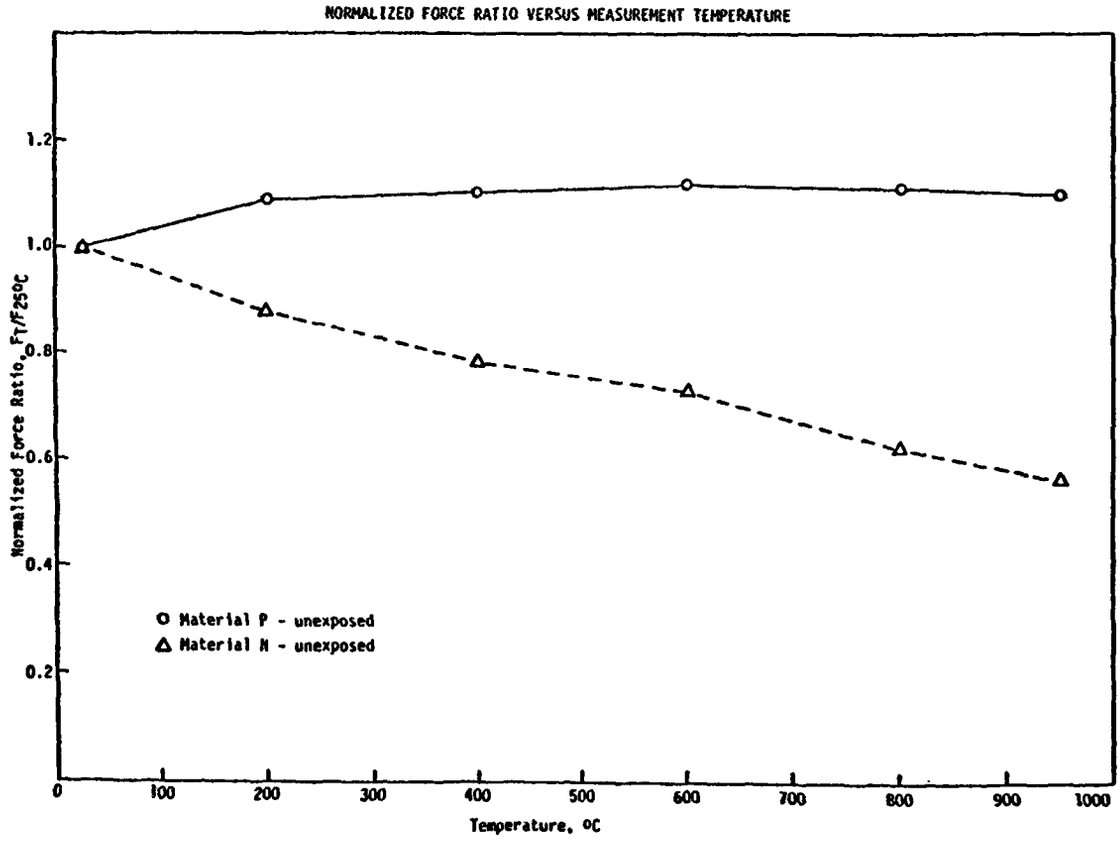

FIGURE 10
MAGNETICALLY STABILIZED BED FILTRATION SYSTEM FLOW PLAN

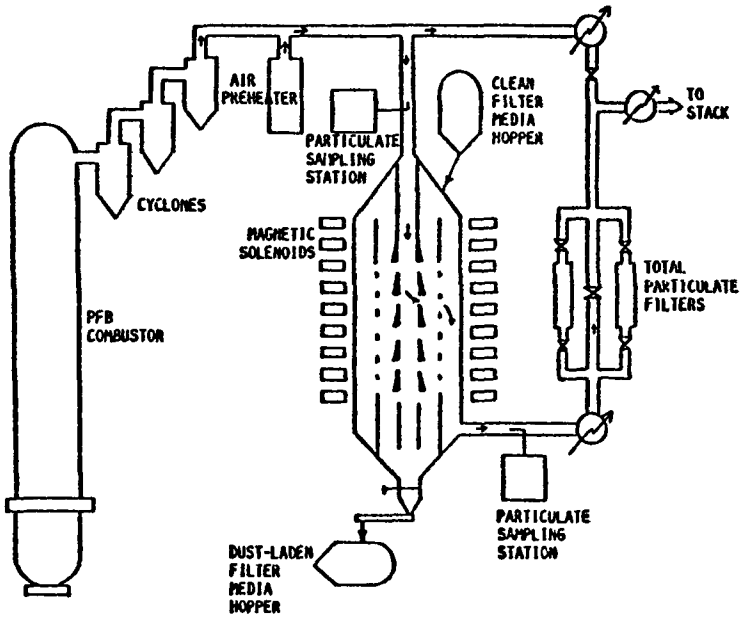

FIGURE 11
CUTAWAY VIEW OF MSB FILTER VESSEL AND BED INTERNALS

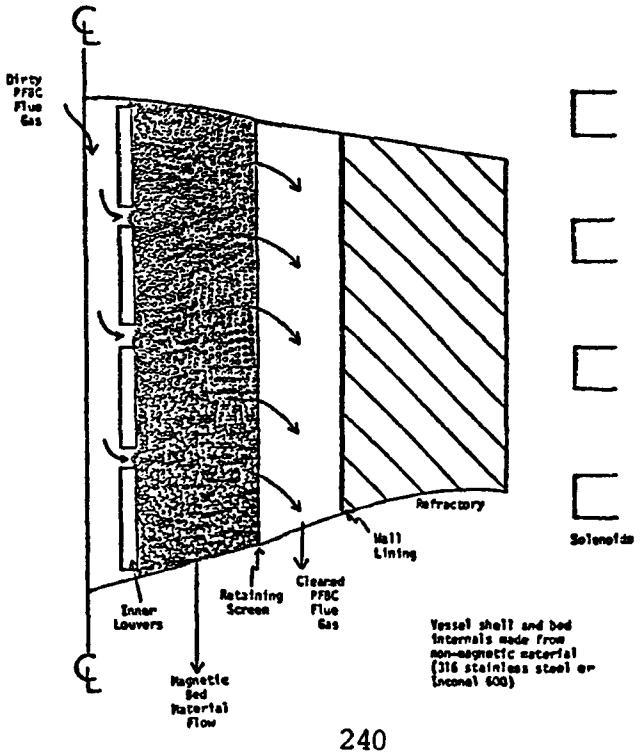

TEST RESULTS OF A HIGH TEMPERATURE, HIGH PRESSURE ELECTROSTATIC PRECIPITATOR

D. Rugg, G. Rinard, J. Armstrong, T. Yamamoto, M. Durham;
Denver Research Institute, University of Denver

ABSTRACT

The electrostatic precipitator (ESP) is being considered as a final gas cleanup device for pressurized fluidized bed combustion (PFBC) combined cycle power plants. In order to investigate the practical feasibility of ESP's applied to high temperature, high pressure (HTHP) gas streams, a pilot scale unit has been developed. This unit has been operated over a spectrum of gas temperatures, pressures, and dust loadings, which can be encountered in PFBC systems.

The electrical characteristics for a wire electrode and two electrodes designed by Research-Cottrell are reported. Flyash from the Curtiss-Wright PFBC was redispersed in the unit for these tests. The test results are being used to quantify the performance of HTHP ESP's and should also provide needed information for other PFBC gas cleanup devices which employ electrostatic augmentation.

INTRODUCTION

The electrical characteristics of three corona electrodes were measured under clean and dirty conditions in the experimental high temperature-high pressure electrostatic precipitator (HTHP-ESP) located at the Denver Research Institute's Cherry Creek Field Site facility. Clean voltage-current (VI) measurements were made on each of the three corona electrodes at several temperatures and pressures at and near the Curtiss-Wright pressurized fluidized bed combustor (PFBC) operating conditions of 640 kPa (6.4 atm) and 870°C (1600°F). Dust from the Curtiss-Wright PFBC was then redispursed into the gas stream. VI measurements were again made on the three corona electrodes at 640 kPa and 870°C.

These electrical characteristics measurement were made to determine if a region between corona onset and sparkover existed where stable operation

of the ESP could be achieved. The effects upon the electrical characteristics of dust on the corona electrode and collector tube were also measured. Determining the operating field strengths and current densities that could be achieved with each electrode were the other objectives of the test.

DESCRIPTION OF THE HTHP-ESP FACILITY

The test facility described by Rinard, et al (1981) was designed to simulate a wide range of PFBC operating conditions for the evaluation of electrostatic precipitation at high temperatures and pressures. Figure 1 shows a schematic of the test facility.

The HTHP-ESP is capable of operating at temperatures up to 980°C (1800°F) and pressures up to 1 MPa (10 atm) with a flow rate of 0.074 m^3/sec (156 ACFM) at these conditions. Collector tube electrodes up to 35 cm (14 in.) in diameter can be tested in the unit.

The pressure vessel consists of a multi-sectioned, flanged carbon steel pressure shell having an overall length of 7.52 m (24.7 ft) and an outside diameter of 0.91 m (3.0 ft). The hot gases enter near the bottom and exit near the top of the vessel. Except for the top and bottom sections of the pressure shell, which are cooled by means of water jackets, the interior of the shell is lined with a castable refractory thermal insulation 22.9 cm (9 in.) thick. Sufficient insulation and cooling is provided to maintain a maximum temperature of 110°C (230°F) on all carbon steel components and welds. The vessel is designed and rated to a pressure of 1.2 MPa (175 psig) and a temperature of 150°C (300°F). A blanket thermal insulation is used between the shell sections. As a safety precaution, the exterior of the vessel is coated with a temperature-sensitive paint.

The power supply for the HTHP-ESP is a 150 kV and 50 mA supply with reversible polarity and is equipped with meters to measure the applied voltage and current. A high voltage feedthrough of high density alumina is located on the top of the ESP. Due to considerations involving the possible electrical breakdown of a dust-coated electrical insulator, a maximum design temperature of 260°C (500°F) was established for the top vessel section housing the high voltage feedthrough. The top section is cooled by means of fins on the inside of the pressure shell and a water jacket outside. Radiation shields on the corona electrode support rod are also provided to prevent radiant heat from reaching the high voltage feedthrough. The pressure vessel head also contains an instrumentation feedthrough and three mechanical feedthroughs for supporting the rapping rods from which the ESP collector tube is suspended.

The pressure vessel bottom section is funnel shaped and forms the hopper of the ESP. The hopper is emptied after a test series when the entire unit is at ambient pressure and temperature. The bottom section also contains a corona electrode stabilizer bar. This alumina bar is cooled by physical connection to the water cooled shell section.

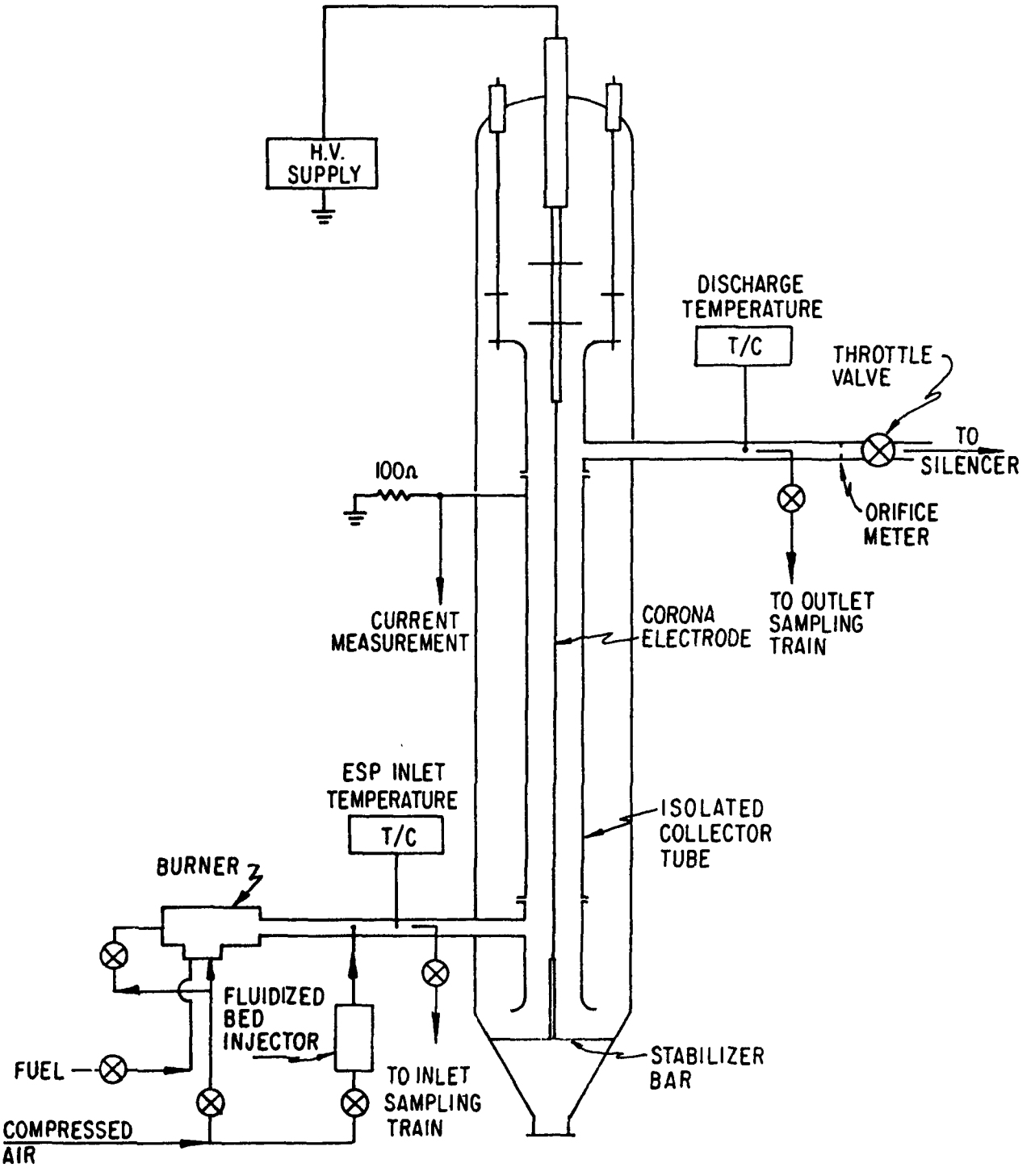

FIGURE 1. SCHEMATIC DIAGRAM OF HTHP ESP SYSTEM

The collector tube used during the tests was 30.5 cm (12 in.) in diameter. A section 2.1 m (6.9 ft.) long between inlet and outlet is electrically isolated from ground. A 100 ohm resistor is connected between the isolated tube section and ground. The corona current to the 2.0 m^2 (21.7 ft^2) isolated section is determined by measuring the voltage across the 100 ohm resistor.

Flyash can be injected into the HTHP-ESP by means of a specially designed redispersion system. A screw feeder is used to meter the dust into a fluidized bed of glass beads where the dust is redispersed in a pressurized air stream. The screw feeder and fluidized bed are housed in a pressure vessel equipped with a quick disconnect flange. The redispersed dust flows from this pressure vessel to an ESP pressure vessel injection port located just downstream of the burner. A baffle downstream of the injection port enhances mixing. The dust mass loading in the test stream can be varied from 0.23 to 11.5 g/Nm^3 (0.1 to 5 grains/scf).

A monitoring and safety interlock system has been designed to maintain safe operating conditions, assure the collection of all temperature data, and provide for an alarm and emergency shutdown should any of the critical parameters of the HTHP-ESP facility exceed their specified limits.

THE CORONA ELECTRODE TESTS

In the corona electrode tests, the flow rate in the precipitator was maintained at 0.078 m^3/sec (165 acfm) and the velocity through the collector tube was 1.07 m/sec (3.5 ft/sec). The collector tube had a specific collection area of 25.7 sec/m (130 ft^2/kacfm). The inlet gas temperature as well as the discharge gas temperature were measured and the gas temperature in the ESP collector tube was determined from these values.

Sketches of three corona electrodes that were tested are shown in Figure 2. The first corona electrode was a smooth wire 7.9/mm (5/16 in.) in diameter. The second corona electrode was a scalloped electrode designed by Research Cottrell (R-C) for possible use in an HTHP-ESP at the Curtiss-Wright PFBC facility (Feldman (1977)). Scalloped fins were attached to a 2.5 cm (1 in.) tube. The 2.5 cm (1 in.) scalloped fins produced an electrode 7.6 cm (3 in.) in diameter. The third or star electrode which was also designed by R-C, is similar to the scalloped electrode except that the 2.5 cm (1 in.) fins which are attached to the 2.5 cm (1 in.) tube are not scalloped. The latter two corona electrodes were designed to be rigid so that if the electrode were suspended by a rigid mounting at the top, it would not require a stabilizer bar at its lower end to prevent swinging when high voltage is applied. However, since the stabilizer bar was available in the unit, it was used to insure that the electrodes were centered.

RESULTS AND DISCUSSIONS

The operating conditions of the HTHP-ESP during the determination of the electrical conditions of the clean corona electrodes are shown in Table

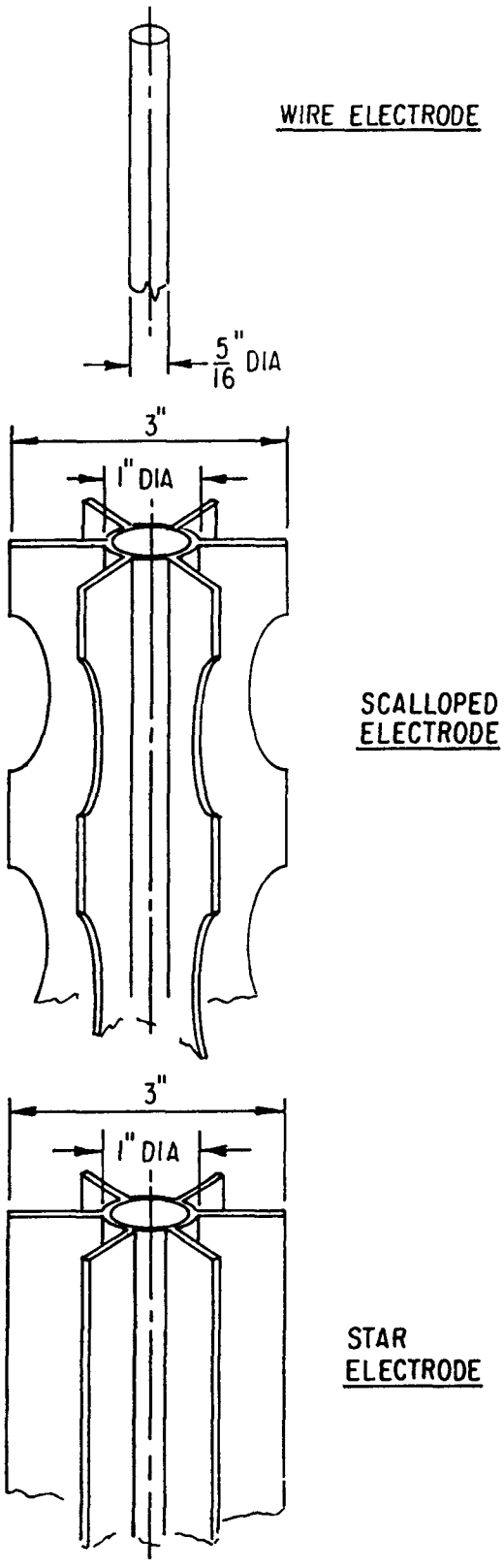

FIGURE 2. CORONA ELECTRODES

1. These test conditions were centered around 870°C (1600°F) and 640 kPA which produces a relative gas density of 1.65. First the temperature was held constant at 650°C (1200°F) while the pressure was changed from 510 to 640 kPa to determine the effects of pressure. Then the pressure was held constant at 640 kPa and the temperature was set at three additional values to determine the effects of temperature.

TABLE 1. TEST CONDITIONS FOR CLEAN CORONA ELECTRODES

Test No.	Pressure	Temperature	Relative Gas Density
1	510 kPa	650°C (1200°F)	1.65
2	640 kPa	650°C (1200°F)	2.04
3	640 kPa	845°C (1550°F)	1.69
4	640 kPa	870°C (1600°F)	1.65
5	640 kPa	900°C (1650°F)	1.61

Figure 3 shows the clean VI characteristics of the wire electrode with negative corona at a constant pressure of 640 kPa. The scales for current density over the isolated section of the collector tube and the average field strengths between corona electrode and collector tube are also shown. Field strengths above 9 kV/cm and current densities up to 0.70 $\mu A/cm^2$ were recorded. The maximum voltage was limited by the power supply and not by sparkover. The three curves show that at a constant voltage, an increase in temperature produces an increase in current. Figure 4 shows the clean VI characteristics of the wire electrode with positive corona at two temperatures. With positive corona the current increase due to increased temperature was less than with negative corona, and sparkover occurred at lower corona currents and lower corona voltages.

The VI characteristics of the scalloped electrode with both negative and positive corona at 660°C (1220°F) are shown in Figure 5. The diameter of the corona electrode was assumed to be 7.6 cm (3 in.) in determining average field strength. The current density for the scalloped electrode was about twice as high as with the wire electrode. With positive corona the curves are sparkover limited and with negative corona the curves were power supply limited. For both positive and negative corona, at a constant voltage, an increase in pressure caused a decrease in current.

Figure 6 shows the effects of temperature on the same electrode with negative corona. At the higher temperatures, there was a measurable corona current at low corona voltages. Figure 7 is the same as Figure 6 except that the corona was positive. Changing the temperature from 845°C (1550°F) to 905°C (1660°F) did not change the positive corona VI characteristics any significant amount.

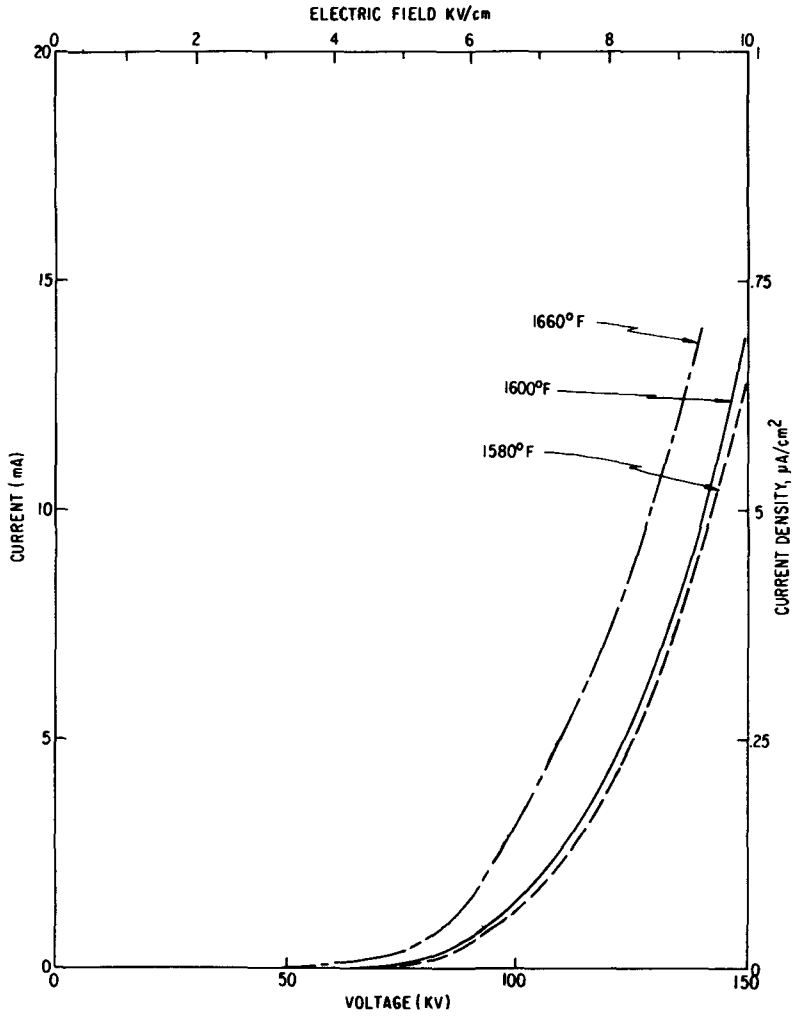

FIGURE 3. CLEAN WIRE ELECTRODE WITH NEGATIVE CORONA AT CONSTANT PRESSURE OF 6.4 ATM

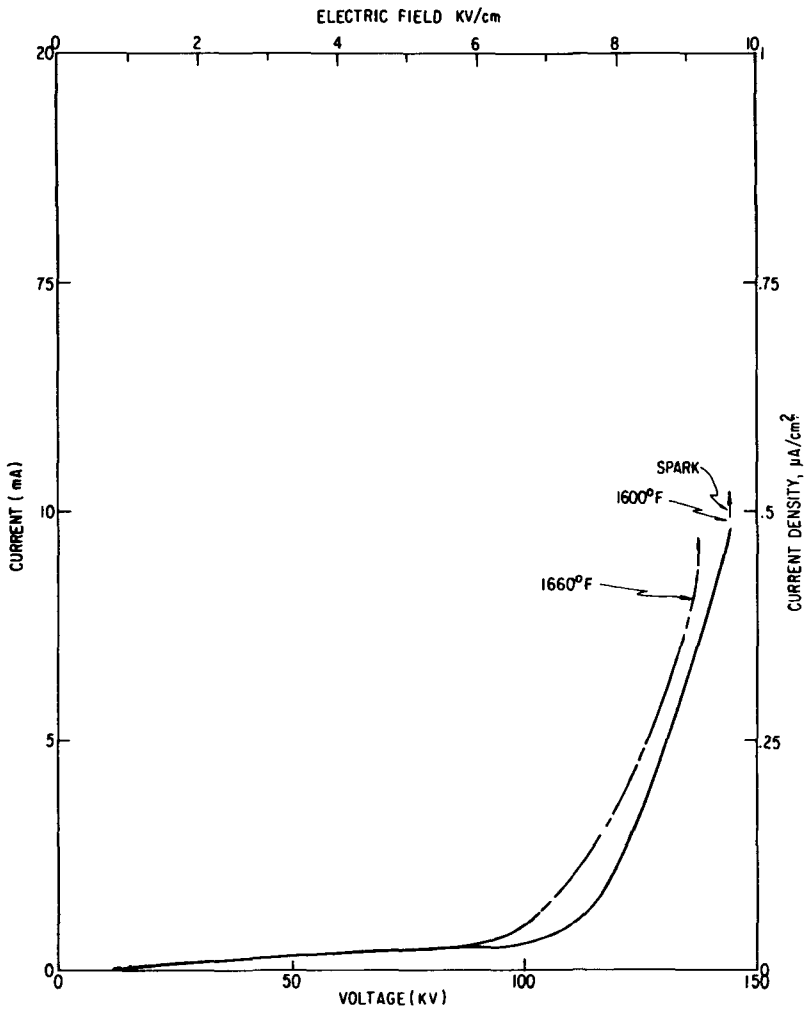

FIGURE 4. CLEAN WIRE ELECTRODE WITH POSITIVE CORONA AT CONSTANT PRESSURE OF 6.4 ATM

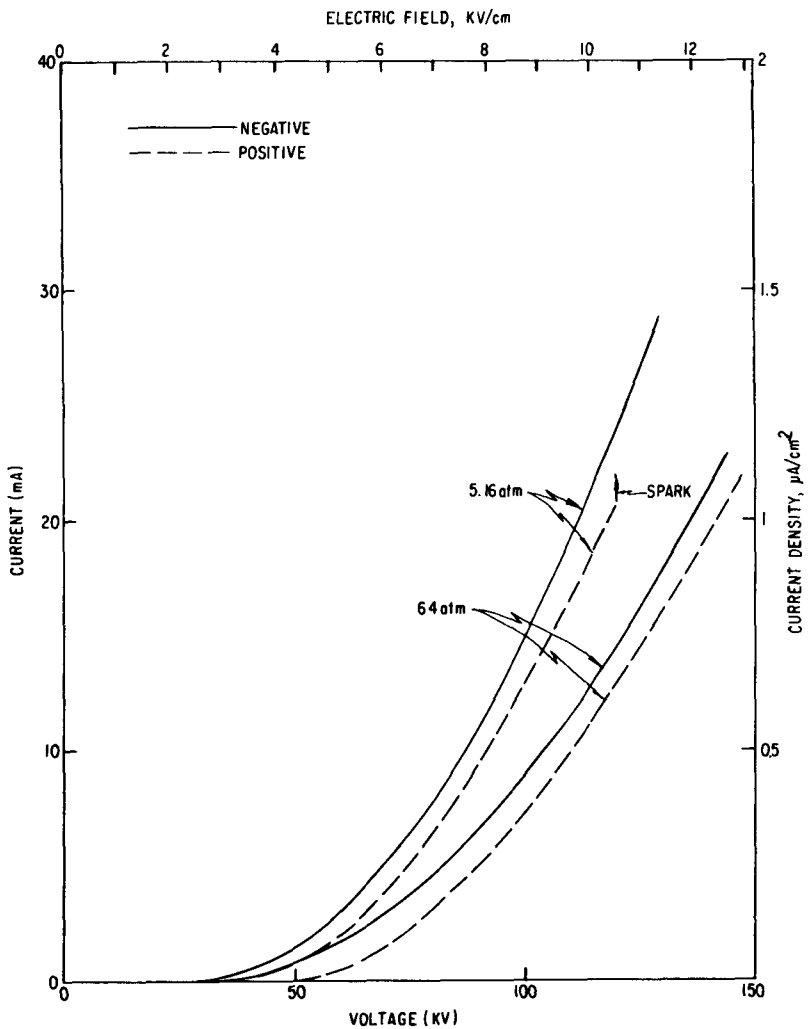

FIGURE 5. CLEAN SCALLOPED ELECTRODE AT 1220°F

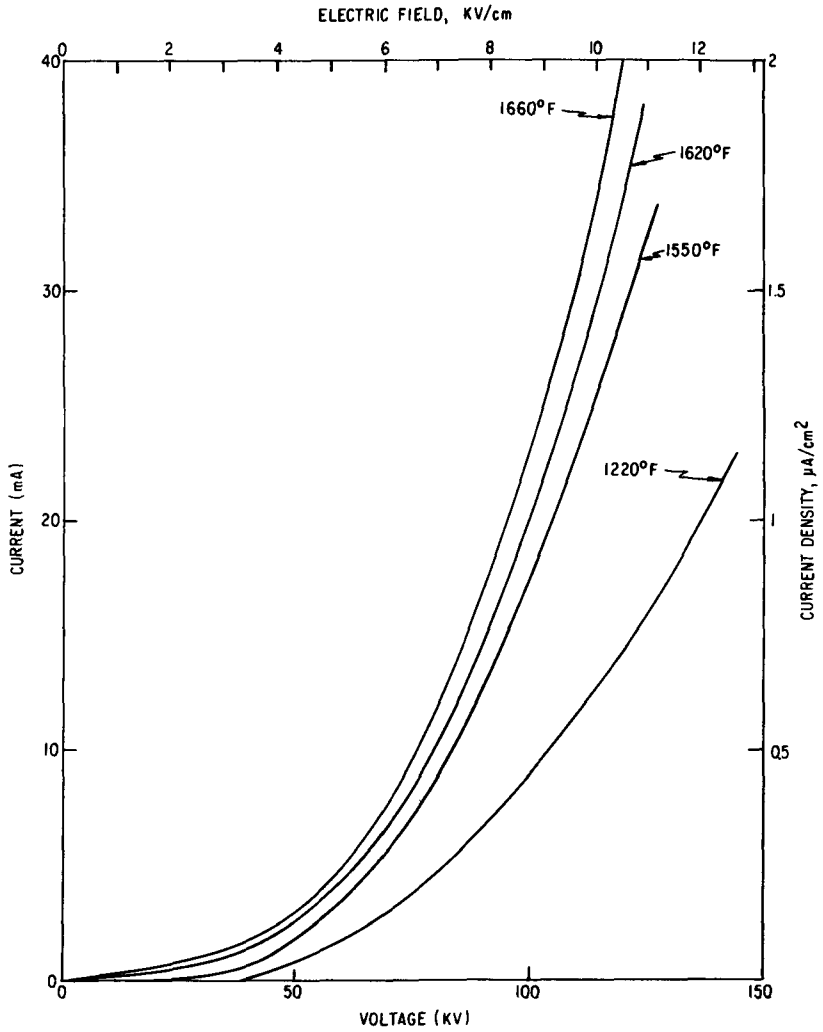

FIGURE 6 CLEAN SCALLOPED ELECTRODE WITH NEGATIVE CORONA AT CONSTANT PRESSURE OF 6.4 ATM.

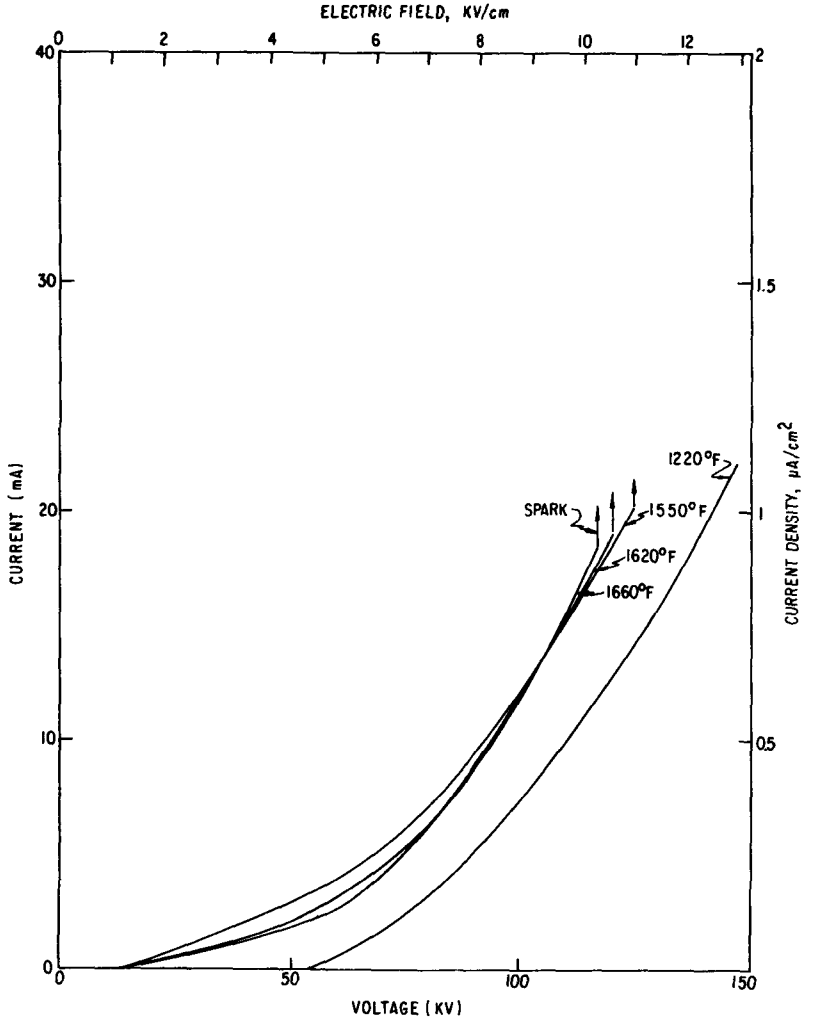

FIGURE 7 CLEAN SCALLOPED ELECTRODE WITH POSITIVE CORONA AT CONSTANT PRESSURE AT 6.4 ATM.

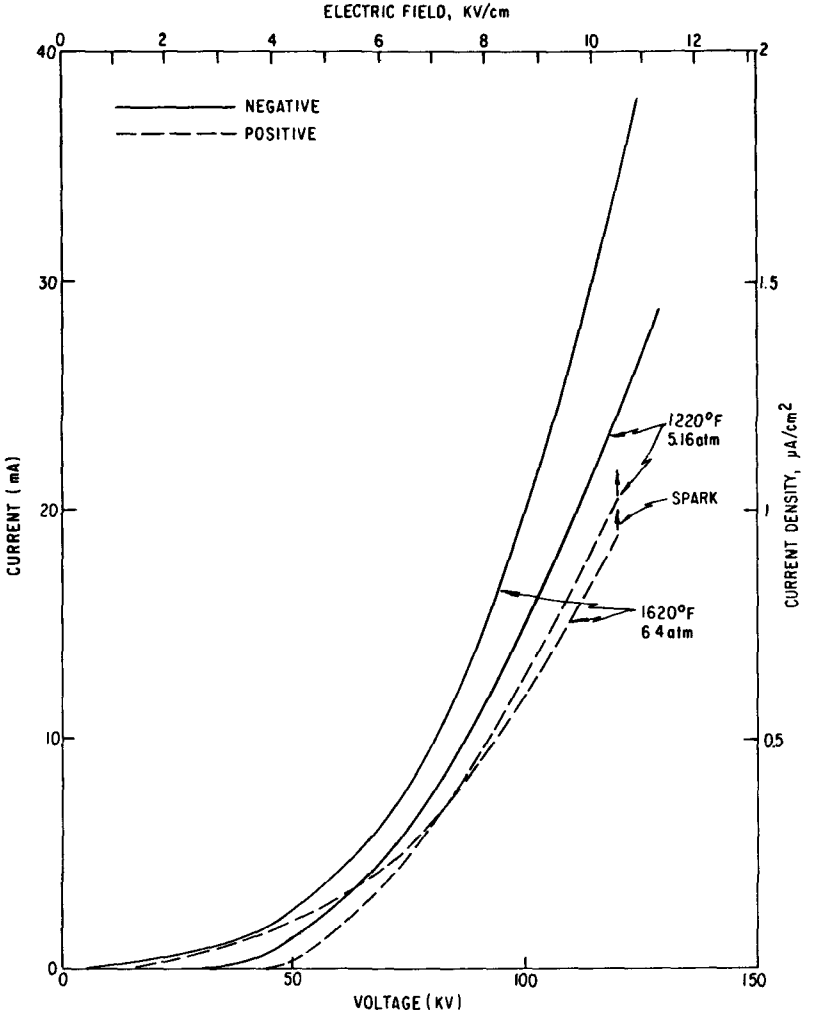

FIGURE 8 CLEAN SCALLOPED ELECTRODE AT CONSTANT RELATIVE GAS DENSITY OF 1.63

Figure 8 shows VI curves for the same relative gas density at two temperatures. For negative corona, the current increased as the temperature increased. For positive corona, the VI curves at constant relative gas density are essentially independent of temperature.

Some of the VI curves for the star electrode are shown in Figure 9. In all cases the current from the star electrode was less than the current from the scalloped electrode. However, the data showed the same dependence upon temperature, pressure, and relative gas density.

A comparison of the clean VI characteristics of the three electrodes at 870°C (1600°F) is shown in Figure 10. The curves in Figure 10 show that the current from the scalloped electrode was considerably larger than the current from either the wire or star electrode.

After the clean VI measurements were completed, dust was injected into the HTHP-ESP. The dust which was used in these tests was from the second cyclone of the Curtiss-Wright PFBC system. The elemental analysis of the ash is presented in Table 2 and the particle size distribution is shown in Table 3.

TABLE 2. ELEMENTAL ANALYSIS OF C-W ASH

SiO_2	25.46
Al_2O_3	12.72
TiO_2	0.36
Fe_2O_3	15.96
CaO	17.08
MgO	11.22
Na_2O	0.21
K_2O	0.77
P_2O_5	0.10
SO_3	18.12
TOTAL	102.00

With the ESP dirty, the measurements at 870°C (1600°F) and 640 kPa were repeated with negative corona. These measurements are shown in Figure 11 for both dust off and dust on conditions. The reduction in current due to particle space charge when the dust is turned on is shown. The size of particles in an ESP in an actual PFBC operating system would be much smaller than in the dust used for these tests. Large particles of the size shown in Table 3 would not create large space charge between corona wire and collector tube. Therefore the ash from the Curtiss-Wright second cyclone is being ground in a fluid mill to reduce particle size. The mass

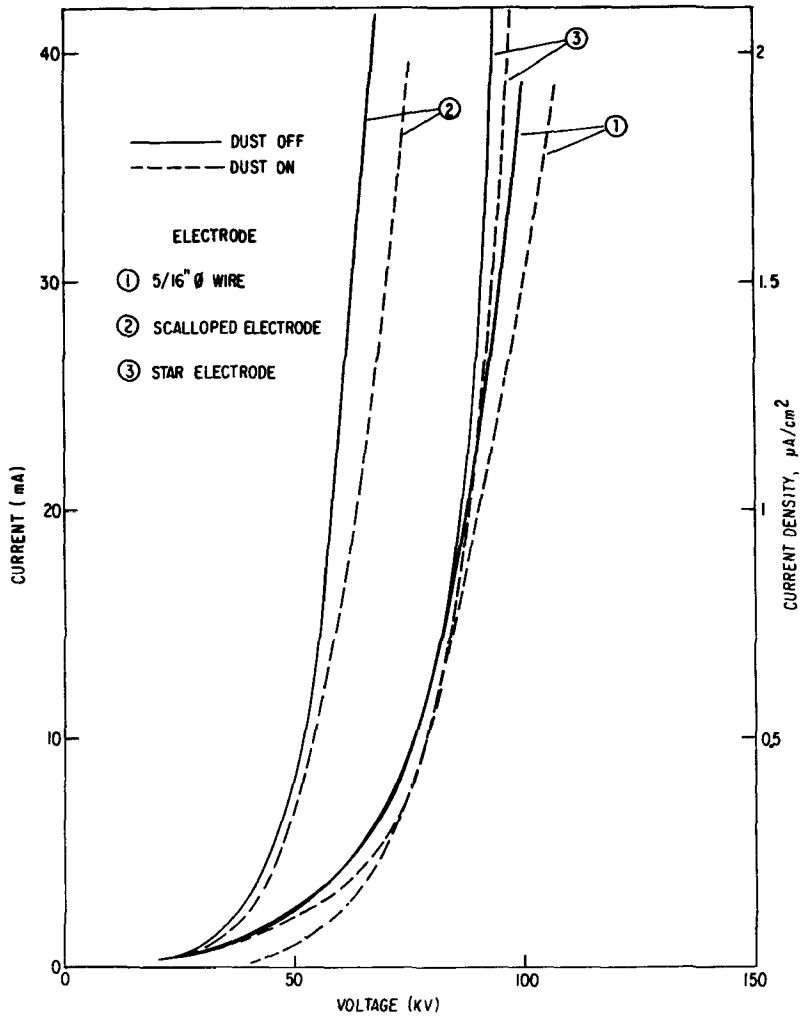

FIGURE 11. DIRTY VI CURVES, NEGATIVE CORONA, FOR CURTISS-WRIGHT CONDITIONS OF 1600°F, 6 4 ATM.

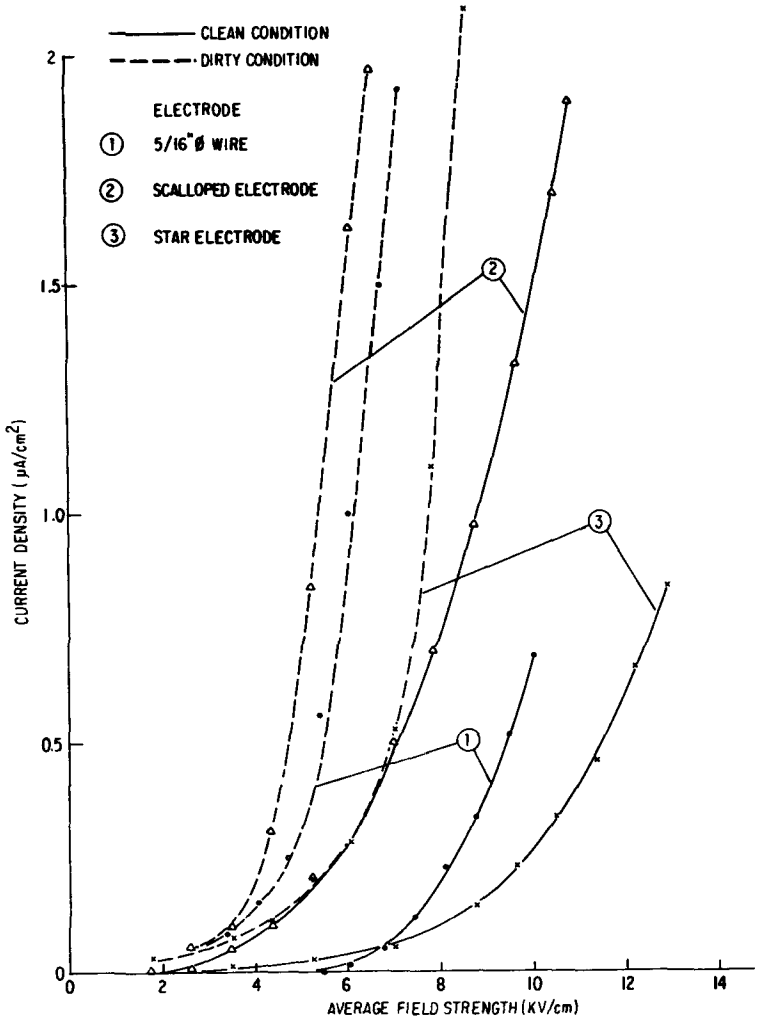

FIGURE 12. FIELD STRENGTH vs CURRENT DENSITY FOR NEGATIVE CORONA AT CURTISS-WRIGHT CONDITIONS OF 1600°F, 6 4 ATM.

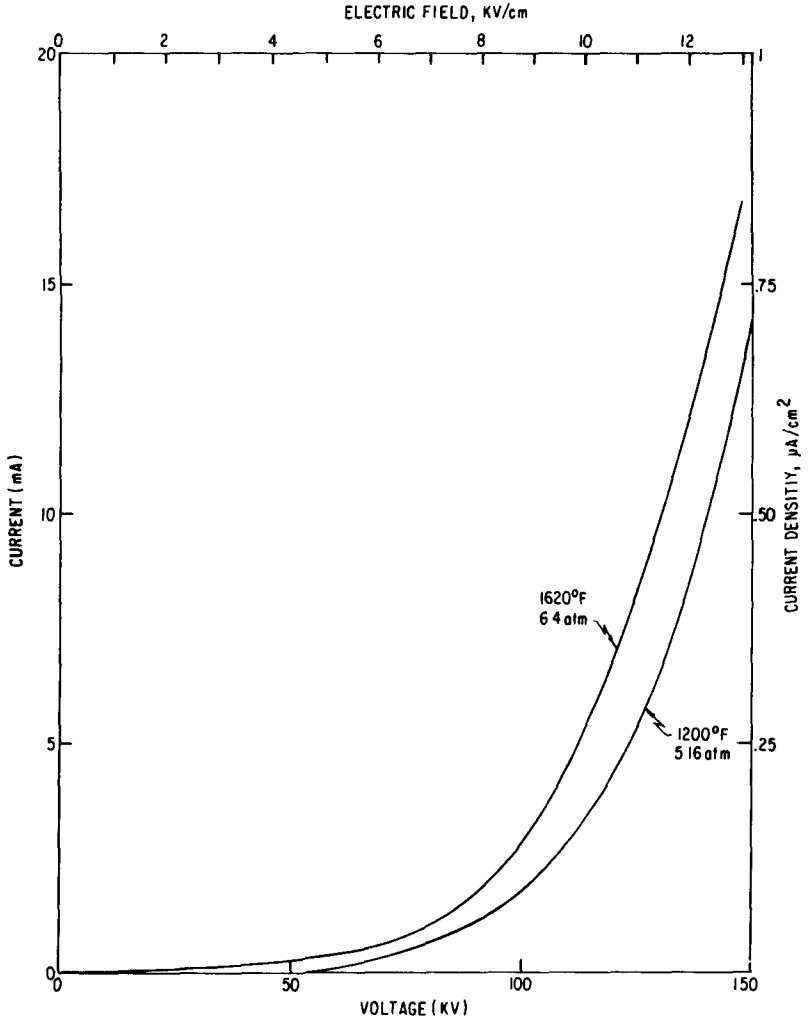

FIGURE 9. CLEAN STAR ELECTRODE WITH NEGATIVE CORONA AT CONSTANT RELATIVE GAS DENSITY OF 1.63

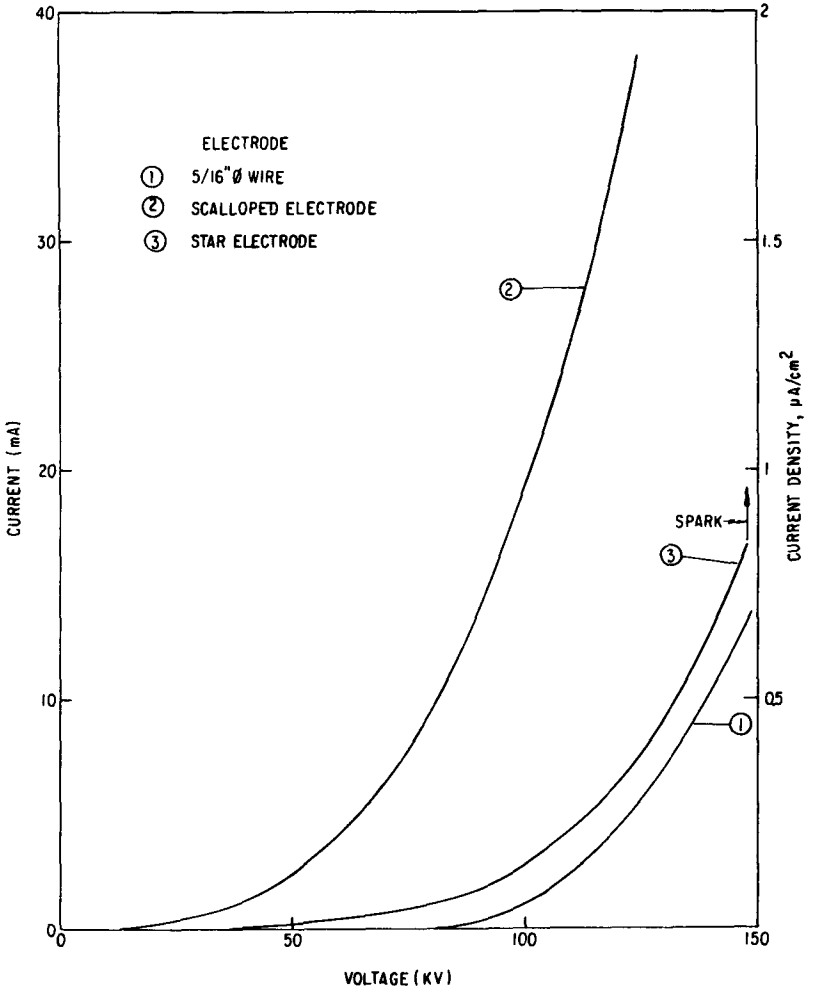

FIGURE 10. CLEAN VI CURVES, NEGATIVE CORONA, FOR CURTISS-WRIGHT CONDITIONS OF 1600°F, 6.4 ATM

mean diameter is being reduced to 2 or 3 microns and the maximum size is 10 to 12 microns. The smaller size particles will be used in future tests in order to more realistically measure the effects of particle space charge.

TABLE 3. PARTICLE SIZE DISTRIBUTION OF C-W ASH

MICRON SCREEN ANALYSIS	Above Stated Micron (By Weight)
420	0.00
210	0.00
105	0.00
45	6.38
COULTER COUNTER	
40.30	6.88
32.00	7.38
25.40	7.98
20.20	13.98
16.00	25.16
12.70	39.96
10.08	55.58
8.00	70.08
6.35	82.60
5.04	91.76
4.00	95.05
3.17	98.10
2.52	98.40
2.00	98.78
1.59	99.25
1.26	99.50
1.00	100.00

The current under dirty conditions increased for all three electrodes. This increase in current under dirty conditions also appeared in the data of Brown and Walker (1971) and Shale and Fasching (1969). Shale and Fasching were making tests at 800°C (1470°F) and 650 kPa. Injection of dust into the system lowered the corona voltage from about 42 kV to 37 kV for the same corona current. Under clean conditions, Brown and Walker operating at 900°C (1650°F) and 800 kPa, achieved voltages of 75 kV. Under dirty conditions, the voltage was only 44.5 kV for the same current level. In the measurements by DRI on the three different corona electrodes at 870°C (1600°F) and 640 kPa, the corona voltage was lowered by almost a factor of 2 when the system was dirty. Additional tests are planned which may explain this effect of dust on the electrodes.

Corona current density as a function of average field strength is shown for each of the three electrodes under clean and dirty conditions in Figure 12. The highest field strengths were achieved with the star elec-

trode. The smooth corona wire produced the next highest fields and the scalloped electrode the lowest field strengths.

CONCLUSIONS

The measurements of electrical characteristics showed that there was a voltage range between corona onset and sparkover where stable ESP operation can be achieved with each of three corona electrodes using either positive or negative corona within the range of temperatures and pressures tested. With positive corona, sparkover occurred at slightly lower voltages and lower current densities than with negative corona. Also, with positive corona, the VI characteristics appear to depend upon relative gas density while with negative corona, current increases with temperature for a constant gas density.

Changing the design of the corona electrode changes the VI characteristics of the ESP. However, the introduction of dust into the precipitator modified the VI characteristics to a greater extent than changing the design of the corona electrode. Additional measurements will be made in an attempt to explain the increase in current that occurs when dust is injected.

With the precipitator dirty, average field strengths up to 8 kV/cm and current densities larger than 1.5μ A/cm^2 were achieved.

The next tests in the evaluation of the HTHP-ESP as a final gas clean-up device for PFBC power plants will include determining the collection efficiency as a function of field strength and current density. Rapping reentrainment will also be studied.

The work described in this paper was not funded by the U.S. Environmental Protection Agency and therefore the contents do not necessarily reflect the views of the Agency and no official endorsement should be inferred.

REFERENCES

Brown, R.F. and A.B. Walker (1971) "Feasibility Demonstration of Electrostatic Precipitation at 1700°F), Journal of the Air Pollution Control Association 21:615-20.

Feldman, P.L. (1977) "High Temperature, High Pressure Electrostatic Precipitator", EPA/ERDA Symposium on High Temperature/Pressure Particulate Control, Washington, D.C.

Rinard, G., M. Durham, J. Armstrong, and R. Gyepes (1981) "The DRI High Temperature/High Pressure Electrostatic Precipitator Test Facility", Proceedings: High Temperature, High Pressure Particulate and Alkali

Control in Coal Combustion Process Streams, DOE/METC Contractor's Meeting, Morgantown, WV

Shale, C.C. and G.E. Fashing (1969) "Operating Characteristics of a High-Temperature Electrostatic Precipitator", Bureau of Mines Report of Investigations RI 7276.

COAL-ASH DEPOSITION IN A HIGH TEMPERATURE CYCLONE

by

K. C. Tsao

University of Wisconsin-Milwaukee
Milwaukee, Wisconsin

A. Rehmat and D. M. Mason

Institute of Gas Technology
Chicago, Illinois

ABSTRACT

Experimental evidence indicated that the increase of particulate removal efficiency in a high temperature agglomerating cyclone is hampered by the formation of cyclone wall deposits. The cyclone collection efficiency has been observed in a laboratory hot cyclone to meet the designated performance when the temperature of the dust ladden gas is increased to near its coal-ash fusion temperature. Factors that are affecting the wall deposition process are examined and estimation of the relative importance of the operating parameters are presented. A simple mathematical model for the wall deposition mechanism is tentatively proposed. Experimental results on the occurrence or absence of wall deposits will be discussed.

The work described in this paper was not funded by the U.S. Environmental Protection Agency and therefore the contents do not necessarily reflect the views of the Agency and no official endorsement should be inferred.

INTRODUCTION

In the course of studying the performance of a high temperature agglomerating cyclone, the deposition and altering of flow stream at the cyclone jet impingement surface have caused the cyclone in-operational while the cyclone displayed a collection efficiency of 92% and higher. Attempts were made to analyze the basic principles of adhesion at low temperature (1 - 11) and at high temperature (12 - 14), yet much remains to be investigated. Characterization of the adhesion mechanism of coal-ash near the softening/melting point though initiated (12, 13), of coal-ash is far from fully understood.

Development of coal conversion reactors, hot gas cleaning equipment, and desposition on gas turbine blades and other energy conversion apparatus usually encounters the problems of clogging, erosion and ash agglomeration/adhesion of submicron-sized particles. These difficulties arise mostly from the high temperature and severe environment where those equipments are exposed. The products of coal gas reactors are in a form of raw, low to medium heating value fuel for industrial plant or directly for power generation. The gas stream contains a complex element but also includes particles of ash char and dust of added absorbent materials. The physical and chemical properties of those small and submicron particles usually deposited along its flow path. Softening, melting and even evaporation would accelerate the deposition process when the device is operated near the fusion temperature of the coals.

This study was undertaken to investigate the conditions affecting deposition of coal ash in the high temperature cyclone of a fluidized bed coal gasifier, in the process the cyclone removes char from the product gas and returns it to the bed for completion of its gasification. Some initial but important experimental results of the coal ash deposition are reported here.

This study also presents some initial experimental observations on adhesion phenomena. A simple but effective mathematical model is tentatively proposed to analyze the relative effect of some of the factors which may enhance the wall deposition. Among the parameters examined, it was found that the momentum of the particle, the gas and the wall temperatures, and the pseudo-molten layer thickness are the important operating variables affecting the adhesion phenomena.

EXPERIMENTAL OBSERVATION

The experimental high temperature agglomerating cyclone (14) demonstrated previously as an effective particulate removal device is adopted for deposition study. The experimental set-up consisted of a controllable high temperature gas burner, an experimental cyclone made of 314 stainless steel, an external electrical heater, a coal ash feeder, an exhaust gas analyzer and a particulate sampler. A photograph of the experimental facilities is

shown in Figure 1. The inlet section of the cyclone is double jacketed, thus allows the control of cyclone wall temperature in the range between 150 to 1600°F. The burner section was operated to obtain a reducing atmosphere as evidenced by the presence of carbon monoxide and the absence of oxygen in the exhaust gases. The dust sample was prepared by comminuation and sieving of ash deposits laid down in a pilot plant run. The composition of feed dust, Table 1, is iron rich alumina silicates which were selectively deposited from the whole ash containing on the average of 20 weight percent iron oxide as Fe_2O_3.

Table 1 Composition of Dust Sample

Composition	Wt. % of Ash
SiO_2	44.0
Al_2O_3	15.2
Fe_2O_3	35.2
TiO_2	0.85
CaO	2.26
MgO	0.81
Na_2O	0.36
K_2O	1.76
SO_3	0.47
Total	100.9

A 0-38 μm fraction of the dust was fed in most of the laboratory cyclone tests results which are reported here; and a 10 - 38 μm fraction was used in some earlier tests.

During the experimental runs, a cohesive deposit appeared only at the inlet section of cyclone where entering gas impinges at the wall. The light grayish deposit adheres strongly to the metal surface and cannot be brushed away, shook off and has to be mechanically scraped away for weighing. A photo of such deposit is shown in Figure 2. While the cause of formation is not truly understood, the occurrence or the absence of these impingement deposits have been observed and related to the cyclone operating gas and wall temperatures as shown in Figure 3. The data of forty-three tests covering the gas temperatures between 1650 and 2000°F and wall temperatures from 200 to 1500°F indicates, Figure 3, that a tentative demarcation line for deposition appears plausible. It suggests that the deposition at the jet impingement surface opposing gas inlet can be prevented if proper gas-wall temperature relationship is being observed. That is, the higher the particle ladden gas temperature, the lower must be the cyclone wall temperature. A reference line for equal gas and wall temperature is added for comparison though experimental data on where deposition may occur has not been established. Note that the experimental points as indicated by the half darkened square deposit an extremely thin film of deposits, but no accumulation, was ob-

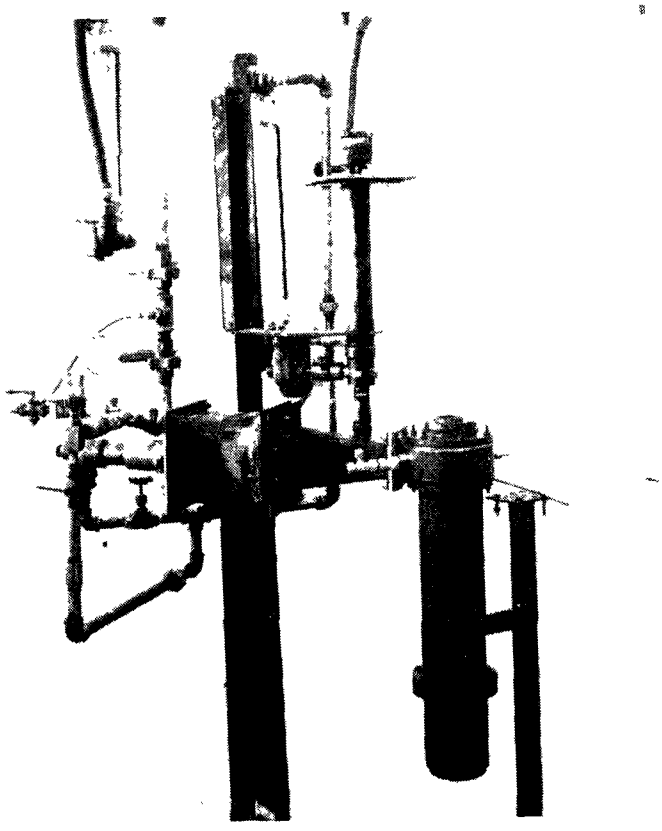

Figure 1 Experimental set up

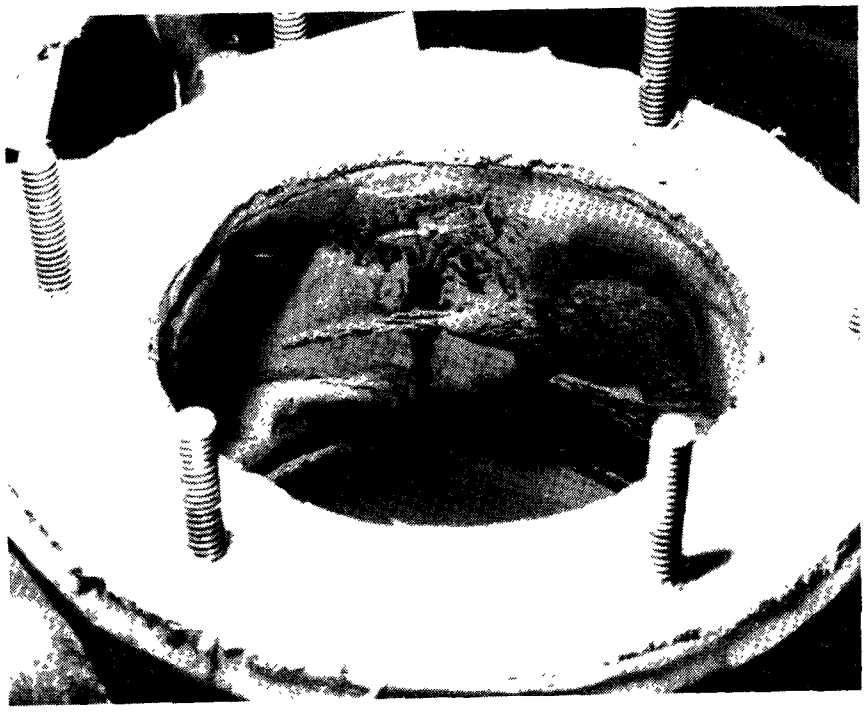

Figure 2 Sample impingement deposit

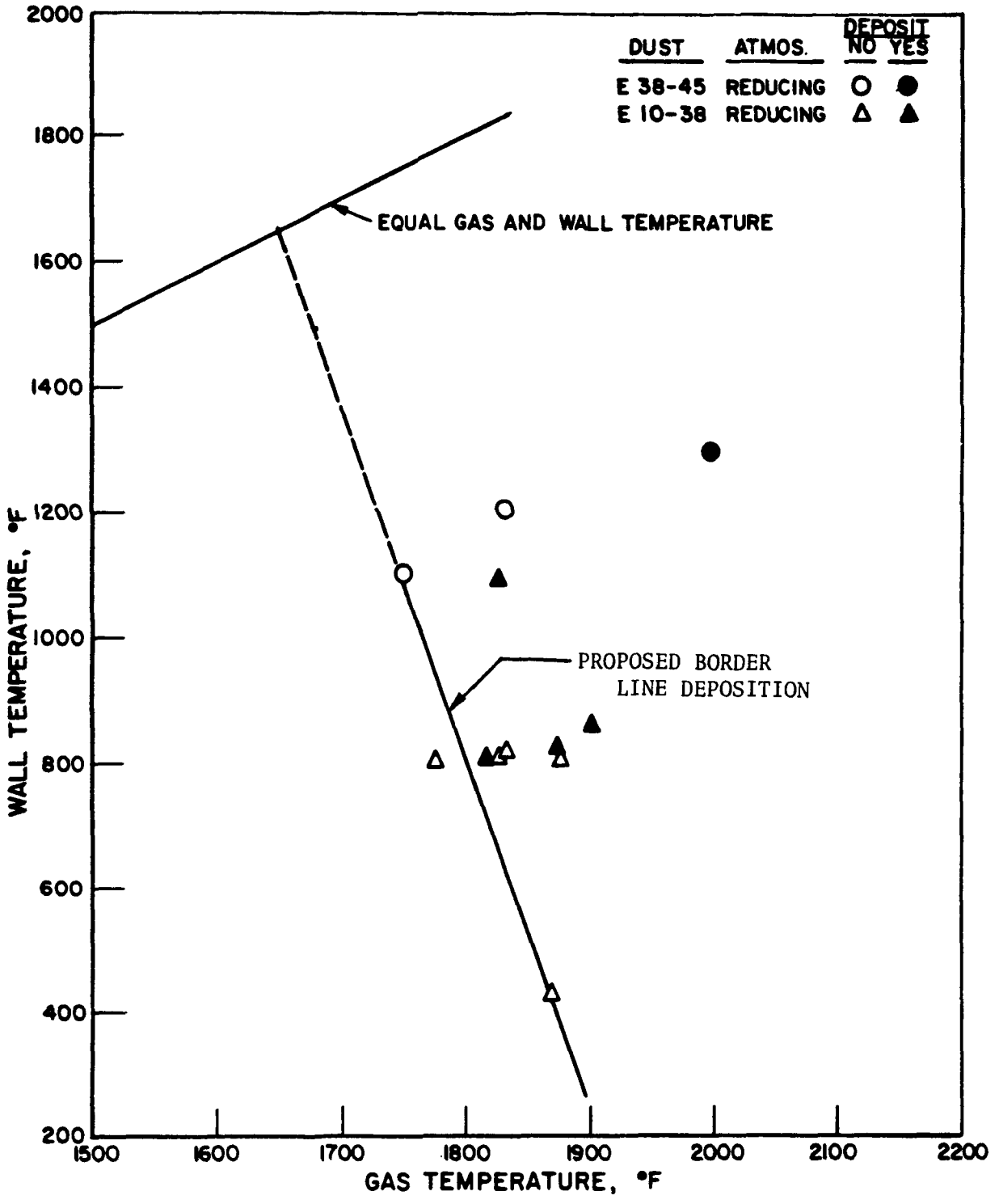

Figure 3 Sample impingement deposit

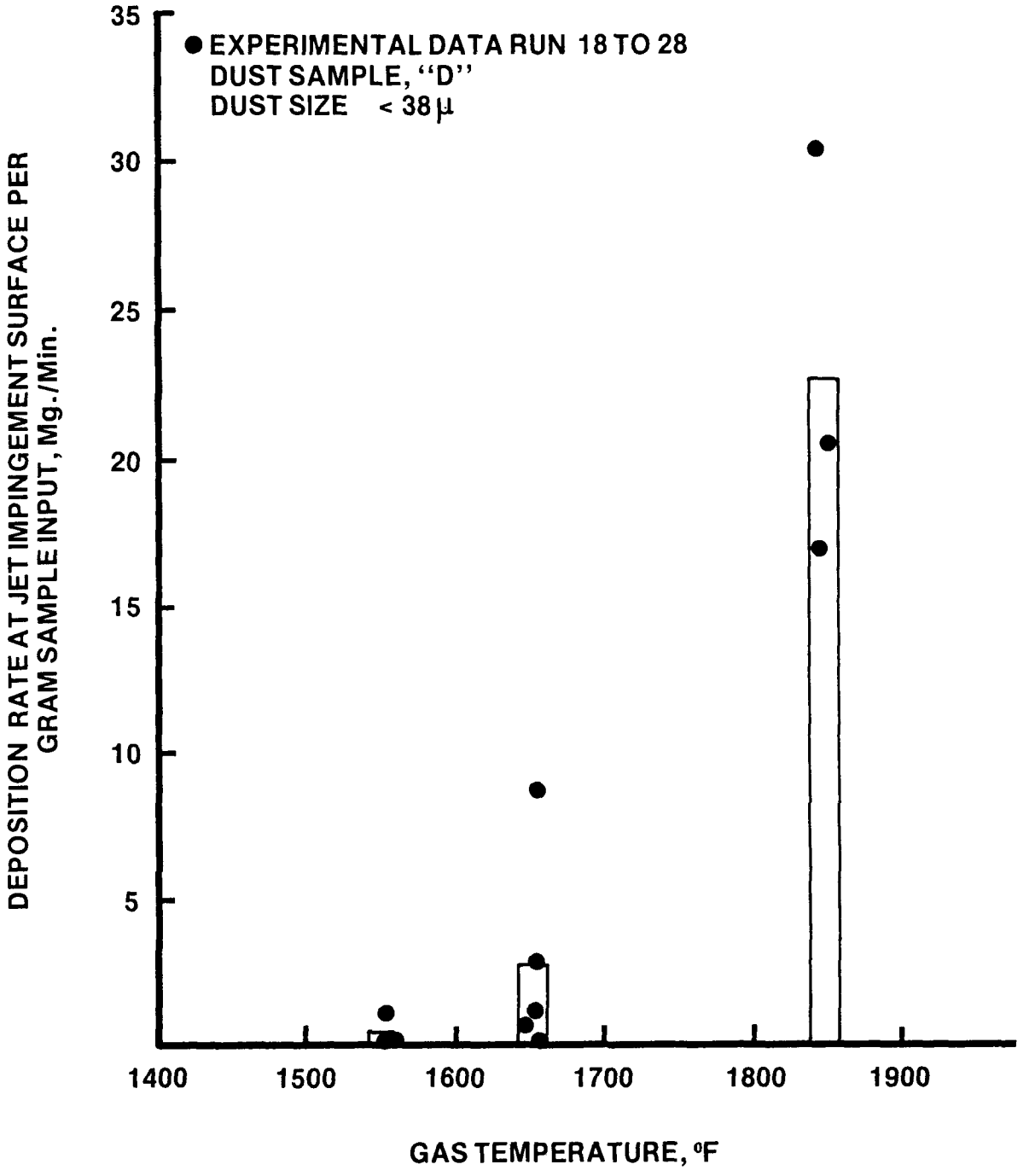

Figure 4 Bar graph showing deposition rate for 'D' dust

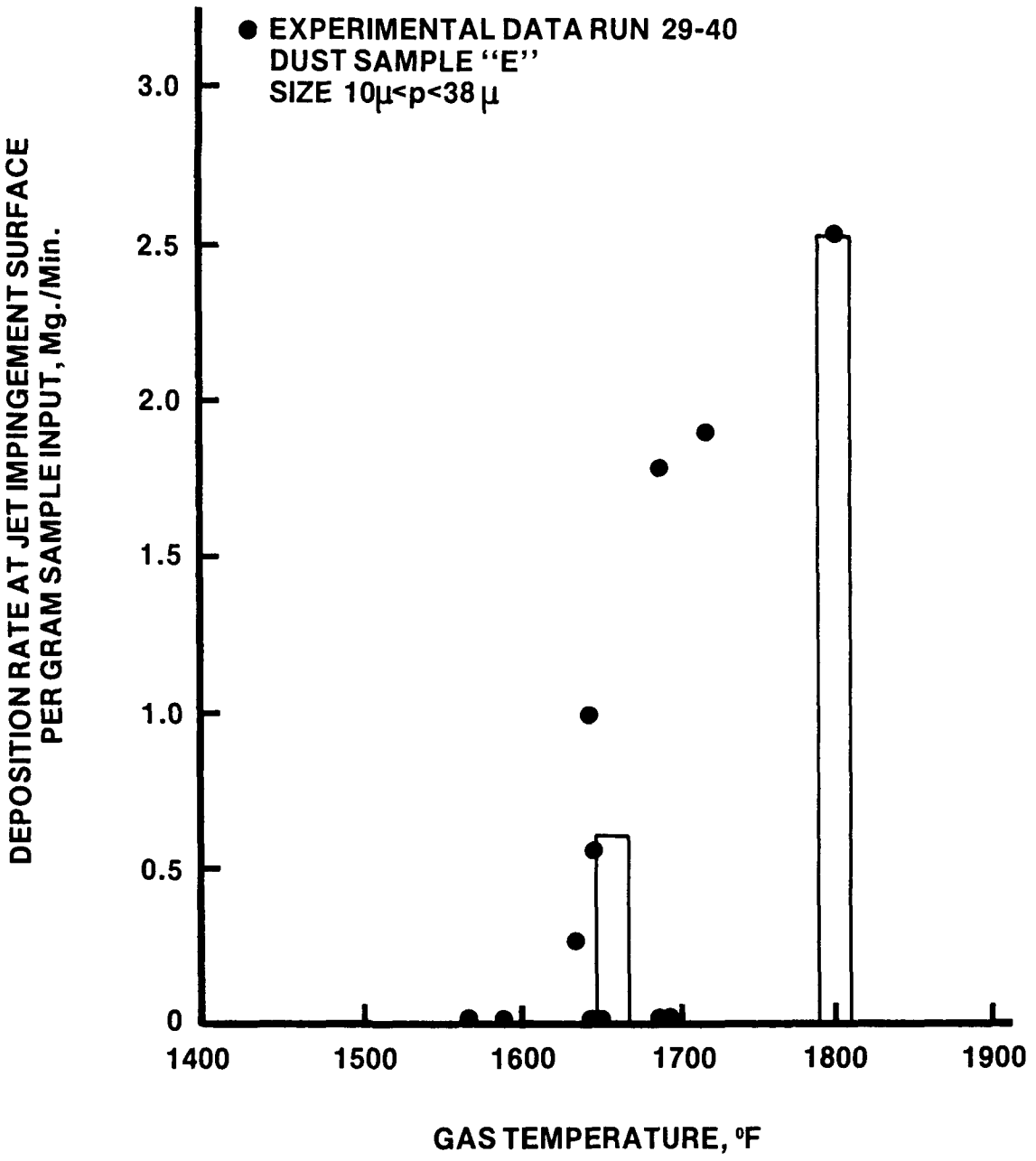

Figure 5 Bar graph showing deposition rate for 'E' dust

served at the termination of 30 minute test runs. Two types of dust of fractional size below 38 μm and similar chemical composition were employed, and the data appears consistent.

Deposits at the cyclone impingement surface were collected and weighed through a microbalance. The rate of deposition per gram of dust fed is shown in Figures 4 and 5. Figure 4 shows the deposition rate for dust particles of less than 38 μm sieved through No. 400 mesh screen. Figure 5 was plotted for particle sizes larger than 10 μm but smaller than 38 μm. It is not clear whether the deposition rate, Figure 4, of one order of magnitude greater is due to the effect of gas velocity. The average gas velocity at cyclone inlet is 26.3 to 37.6% higher in Run No. 18 to 28.

ANALYTICAL CONSIDERATION

The study of particle wall adhesion near the ash fusion temperature was attempted in a laboratory hot cyclone for enhancing the particulate removal efficiency of submicron particles. The particle trajectory under various controlling force in conjunction with coal ash physical-chemical properties will determine whether they will collide and stay together as agglomerates or whether these strike at wall surface will adhere as deposits. Consider the collision mechanism of a particle of radius R, with molten layer thickness δ, strikes at a wall, Figure 6. The force of separation that would cause rebounding are the initial momentum of the particle prior to collision and the thermal gradient across the gas film between the particle and the wall surface. Forces which would foster adhesion are the surface tension of molten layer that the particle must dash through and the Van der Waals molecular force should the interfacial distance reach 100 Å during collision. Other factors such as the electrostatic and the universal attraction are considered to be negligible.

The liquid solid bridge formed during the collision and subsequent detachment from a plane surface as shown in Figure 6, is of great importance in evaluating the surface tension and the viscous drag effect. Precise determination of the liquid-solid interfacial contour is difficult and not available in open literature. We have assumed that the force due to surface tension, F_{st}, following reference (12, 15) is

$$F_{st} = 4\pi\sigma\,[R^2 - (R-\delta)^2]^{1/2} \qquad (1)$$

where R is the radius of the semi-molten particle, δ, the molten layer thickness enclosing the solid particle core, and σ, the surface tension of the molten layer per unit length.

The effect of Van der Waal's attractive force is significant if the interfacial particle-wall distance falls within 4 to 104 Å during collision. According to Rumpf (16), the Van der Waal's force effect F_{vdw} can be approximated by

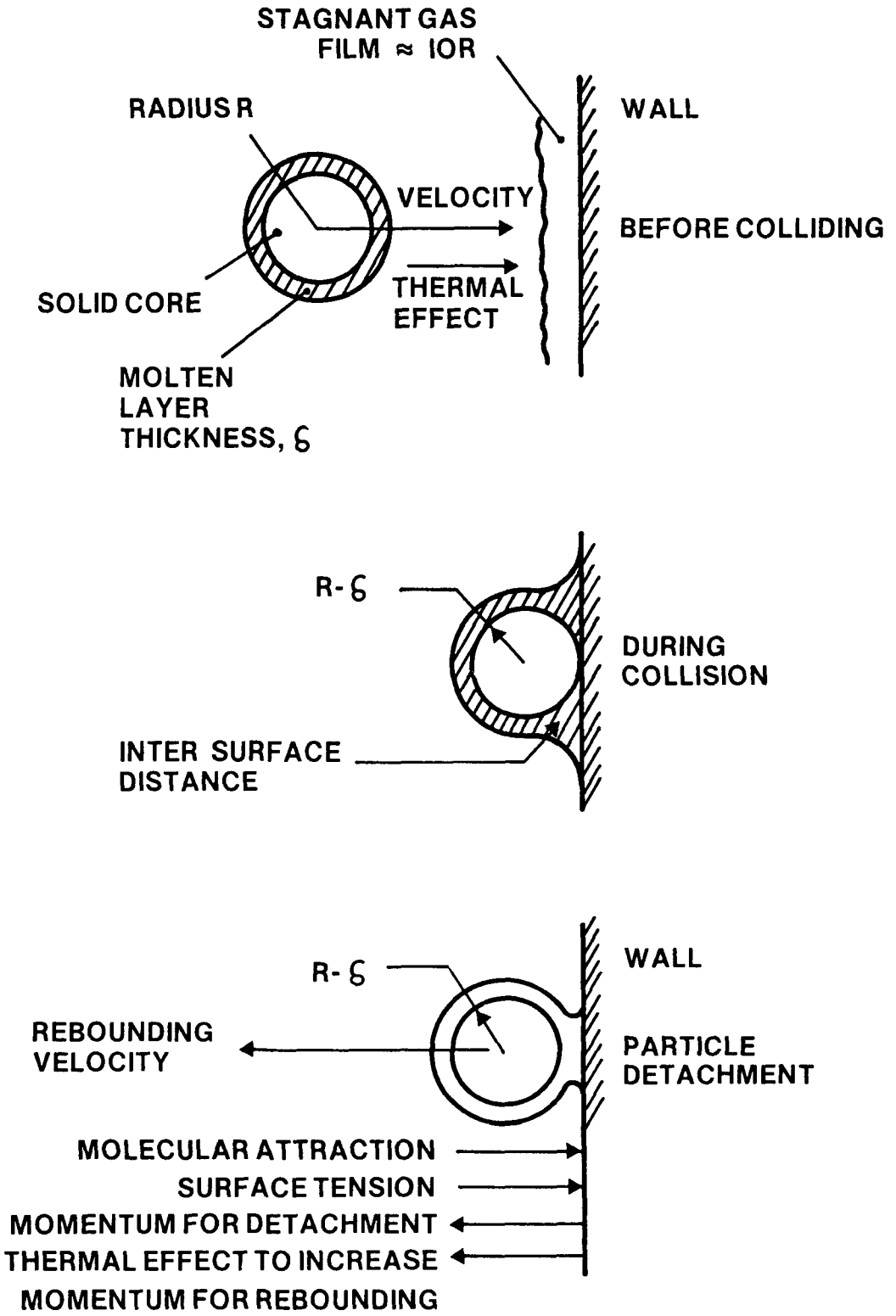

Figure 6 Schematic diagram of particle-wall collision

$$F_{vdw} = \frac{(hw)\ R}{8\pi\ (H + Z_o)^2} \tag{2}$$

where hw is the Lifshitz constant, H, the distance between the particle surface and wall, and Z_o is the limiting molecular separation length typically taken to be 4 Å.

Detachment of a particle after striking at the relatively cooler wall is accelerated due to the effect of a thermal force between the particle and wall. The thermal force increases the kinetic energy of a particle toward the plane wall prior to impaction. Epstein (17) has estimated the thermal force, F_t, as

$$F_t = - \frac{9\ \pi R \mu^2}{\rho_g T(2 + \frac{K_f}{K_p})} (\frac{\Delta T}{\Delta x}) \tag{3}$$

where μ the viscosity of gas, ρ_g, the density of gas, T, the gas temperature, K_p and K_f, the thermoconductivities of particle and gas respectively, and $(\Delta T/\Delta x)$, the thermal gradiant within the thermal boundary layer thickness.

The cause for rebounding and detachment after collision is the initial momentum carried with the particle. The inertia force, F, associated with the momentum of the particle is the rate of change of the product of particle mass, m, and velocity, V, i.e.,

$$F = \frac{d}{dt}\ (mv) = m\ \frac{dv}{dt} \tag{4}$$

Assume that the approaching velocity of a particle to be fixed in the thermal boundary region of gas film next to the plane wall, the rate change of velocity was computed as

$$\frac{dv}{dt} = \frac{\Delta v}{\Delta t}\ , \quad \text{or} \quad \frac{dv}{dt} = \frac{2v^2}{\Delta x} \tag{5}$$

where Δx is the thermal boundary layer thickness next to the wall and was judicially chosen in the subsequently computation to be five particle diameters.

Summing up all the effects and take the ratio of forces that enhance adhesion, F_{ad}, to the forces that cause separation and rebounding, F_{sp}, we have:

$$\frac{F_{ad}}{F_{sp}} = \frac{(F_{st} + F_{vdw})}{(F_t + m\ \frac{dv}{dt})} \tag{6}$$

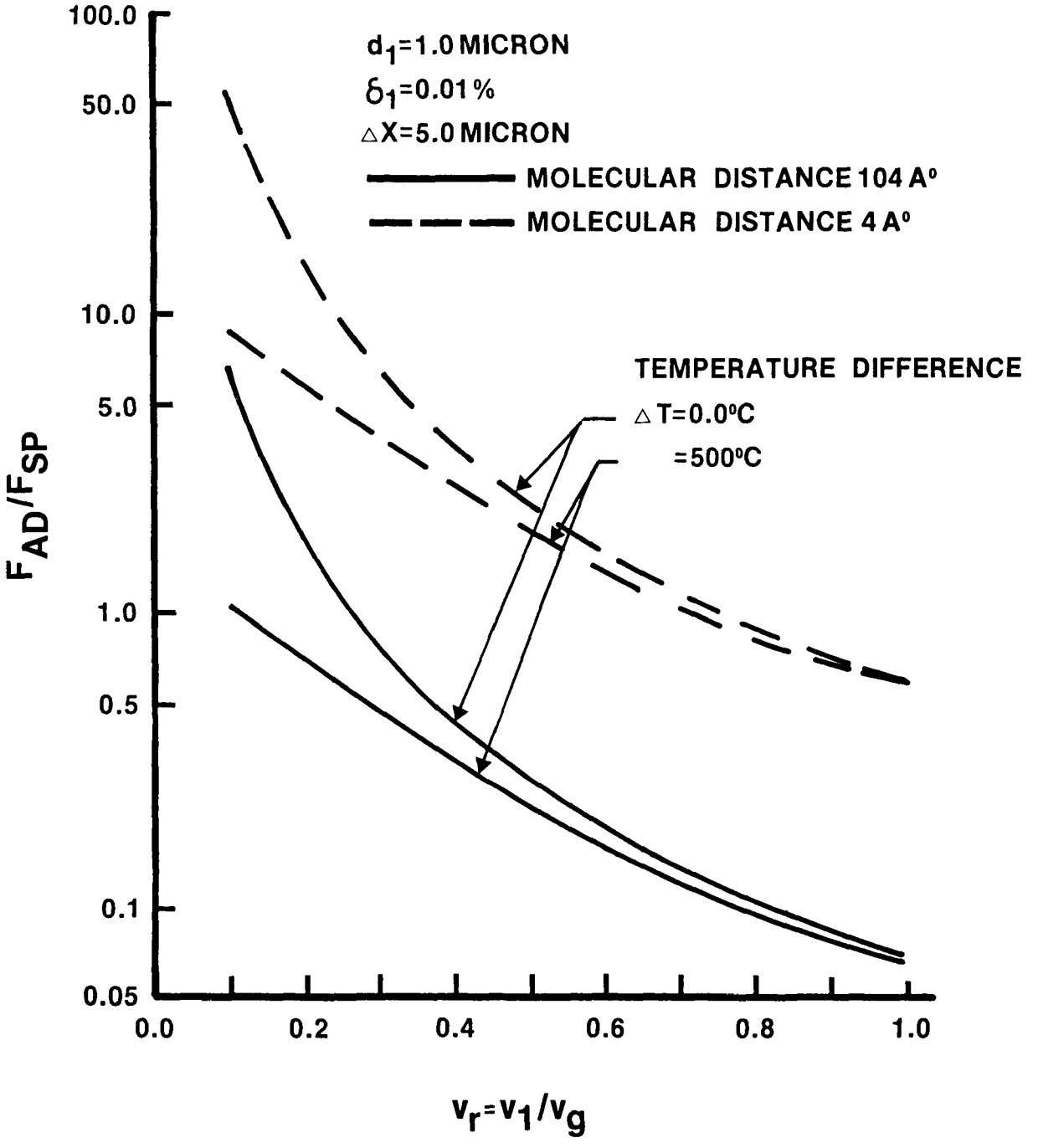

Figure 7 Effect of velocity ratio on particle wall adhesion for 1 micron particles at V_G of 36.0 m/sec.

Equation (6) is used for estimating the relative importance of operating parameters on wall impingement deposition in a high temperature cyclone.

DISCUSSION AND CONCLUSIONS

The adhesion process between a particle and a plane wall has been described physically, Figure 6, and mathematically, Equation (6). Particle-wall deposition would sustain if F_{ad}/F_{sp} is equal to or greater than unity. The ratio of forces that cause adhesion to that of separation and detachment is computed and plotted versus the velocity ratio, V_r, the velocity of the particle toward the wall to that of gas velocity at cyclone inlet. Properties of particle (18) and gas stream used in the computation are: hw = 5.0 ev, T = 1000°C, V_g = 36 m/sec, ρ_g = 0.004 gm/cm^3, $\mu_g = 0.65 \times 10^{-3}$ poise, ρ_p = 0.75 gm/cm^3, and σ = 150 dyme/cm.

Assumptions were made on those plots that the particle is moving; 1) toward the surface, 2) at same speed before and after striking at the surface and 3) at a constant speed when the particle is dashing through the stagnant gas film, Δx, next to the wall. Figures 7 to 9 demonstrate the effects of the particle momentum, the thermal gradient, the molten layer thickness enclosing the particle and the size of particles on wall deposition.

Figure 7 shows the effect of velocity ratio and the thermal gradient on particle wall adhesion for 1 μm diameter particle. The net result of increasing the temperature difference from 0°C to 500°C between the particle and wall increases the initial momentum of the particle toward the cooler wall. The larger the thermal gradient, the greater will be the force of rebounding. This is seen by comparing the two solid curves that for F_{ad}/F_{sp}=1, the detachment of a particle would occur at a velocity ratio of 0.12 and 0.27 when the temperature difference is raised from 0 to 500°C. This plot seems to agree qualitatively with observed experimental cyclone data that deposition may be prevented by cooling the wall surface, Figure 3. The intersurface distance between the particle and wall during collision appears apparent by comparing the curves of molecular distances of 4 and 104 Å. The net effect is that deposition would occur at velocity ratio of 0.12 rather than at 0.7 as particle-wall intersurface distance is varied from 104 to 4 Å.

Figure 8 shows the effect of molten layer thickness enclosing a particle on wall deposition for a 10 μm diameter particle. It is realized that while the relative importance of thermal gradient diminishes for larger size particles, the effect of molten layer thickness seems most eminent. The critical velocity ratio at which F_{ad}/F_{sp} is unity, is increased almost threefold, from 0.08 to 0.26 as the molten layer thickness is increased from 0.01% to 1%. The negative slope of border line deposition, Figure 3, seems to indicate the concept.

In conclusion the adhesion and rebounding of particles upon a plane wall is found to be function of gas and wall temperature. A simple but plausible

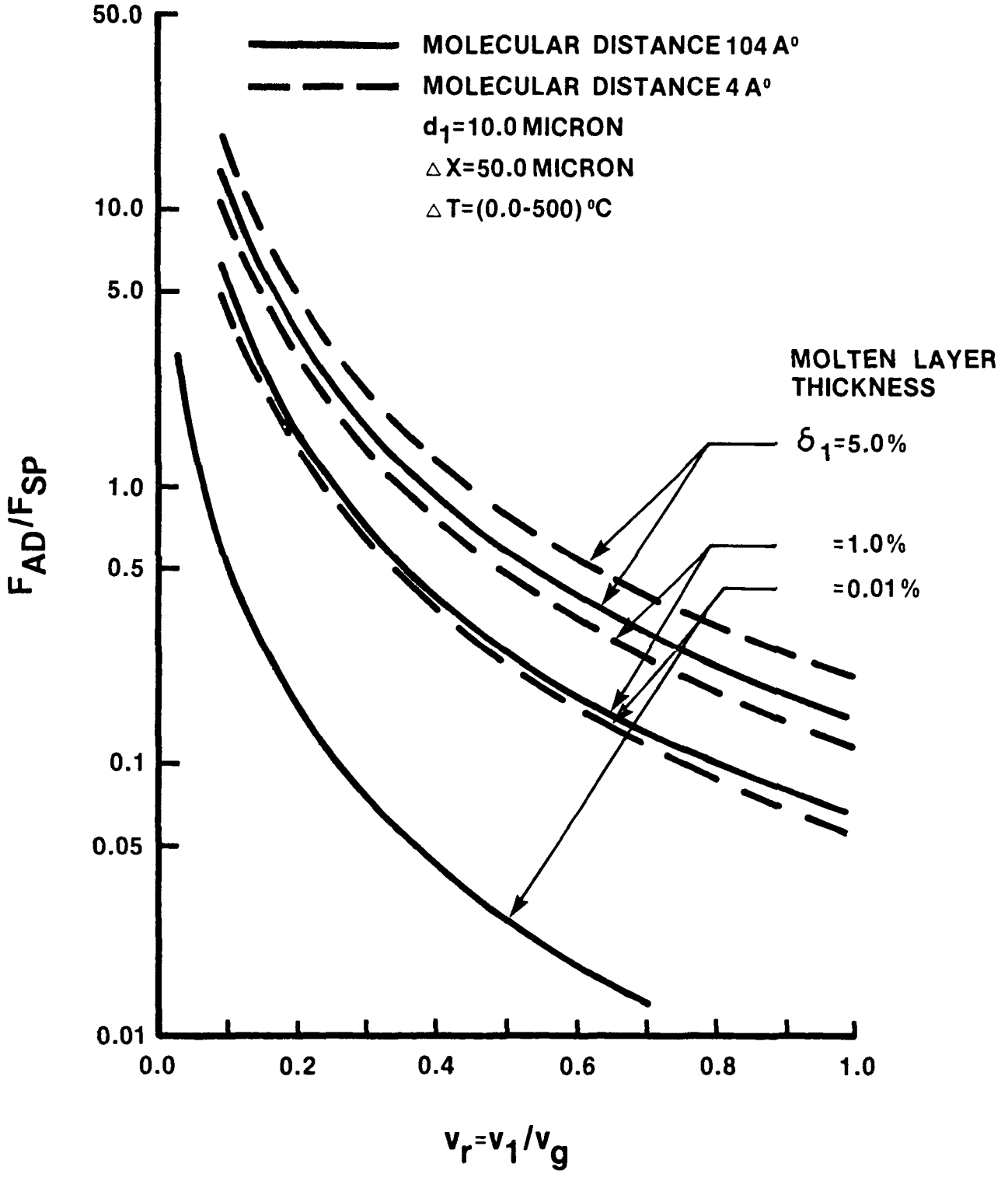

Figure 8 Effect of velocity ratio on particle wall adhesion for 10 micron particles at V_G of 36.0 m/sec.

mathematical model is tentatively proposed in assessing the coal-ash deposition process as observed in a laboratory high temperature cyclone. The effect of particle viscous drag in terms of hydrodynamic wetting which was not incorporated in this study, remains to be analyzed. Proper selection of the cyclone operating parameters namely, gas and wall temperatures, and particle-gas velocity seems to be effective in minimizing the coal-ash particle deposition.

REFERENCES

1. Browne, L.W.B., "Deposition of Particle on Rough Surfaces During Turbulent Gas-Flow in a Pipe," Atmospheric Environmental, Vol. 8, 1974, pp. 801 - 816.

2. Corn, M., "Adhesion of Particles," Chap. XI in Aerosol Sciences, edited by Davies, Academic Press, 1966, pp. 359 - 392.

3. Kneen, T. and Strauss, W., "Deposition of Dust From Turbulent Gas Stream," Atmosphere Environmental, Vol. 3, 1969, pp. 55 - 67.

4. Kordecki, M. C. and Orr, C., A.M.A. Archives of Environmental Health, Vol. 7, No. 7, 1970.

5. Gardwer, G. C., "Deposition of Particles From a Gas Flowing Parallel to a Surface," International Journal of Multiphases Flow, Vol. 2, 1975, pp. 213 - 218.

6. Gillespie, T., "On the Adhesion of Drops and Particles on Impact at Solid Surfaces I and II," Journal of Colloid Science, Vol. 10, 1955, pp. 266 - 298.

7. Hocking, L.M., "The Collision Efficiency of Small Drops," Quarterly Journal of Research for Society, Vol. 85, No. 44, 1959.

8. Lin, S. M., "Particle Deposition Due to Thermal Force in a Tube," Applied Scientific Research, Vol. 32, 1976, pp. 637 - 648.

9. Rouhiainin, P.O. and Stachiewicz, J.W., "On The Deposition of Small Particles From Turbulent Streams," Journal of Heat Transfer, ASME Transactions, 1970, pp. 169 - 177.

10. Wang, C. S., Deabor, J. J. and Lin, S.P., "Effect of Fluid Inertia on Particle Collection," Physical Fluids, Vol. 21, No. 12, 1978, pp. 2365 - 2366.

11. Soo, S.L., "Particle-Gas-Surface Interaction in Collection Devices, International Journal of Multiphase Flow, Vol. 7, 1973, pp. 89 - 101.

References (con't)

12. Tsao, K. C. and Jen, C. O., "Coal-Ash Agglomeration Mechanism and its Application in High Temperature Cyclones," Separation Science and Technology, Vol. 15, No. 3, 1980, pp. 263 - 276.

13. Tsao, K. C., Tabrizi, H., Rehmat, A. and Mason, D., "Coal-Ash Agglomeration Mechanism in a High Temperature Cyclone," Paper 82-WA/HT-29, Annual Meeting American Society of Mechanical Engineers, 1982, Phoenix, Arizona.

14. Tsao, K. C. et. al., "Particulate Collection in a High Temperature Cyclone," Proceedings - 2nd Int'l. Symposium on Transfer and Utilization of Particulate Control Technology, July, 1979, Denver, CO. Vol. 4, 1980, pp. 14 - 25.

15. Zimon, A. D., Adhesion of Dust and Power, Plenum Press, New York, 1969.

16. Rumpf, H., Particle Adhesion, Chapter 7. Agglomeration 77, pp. 97 - 129 1977.

17. Epstein, P., Z. Pysik, Vol. 54, p. 537, 1929.

18. U.S. Department of Energy, "Coal Conversion Systems Technical Data Book," HCP/T2286-01, Washington, U.S. Gov. Print. Office, 1978.

DUST FILTRATION USING CERAMIC FIBER FILTER MEDIA
-- A STATE-OF-THE-ART SUMMARY --

by: R. Chang, J. Sawyer, W. Kuby, M. Shackleton
Acurex Corporation
Energy & Environmental Division
485 Clyde avenue
Mountain View, CA 94042

O. J. Tassicker, S. Drenker
Electric Power Research Institute
3412 Hillview Avenue
Palo Alto, CA 94303

ABSTRACT

Filter media suitable for use at temperatures of >1,000°F, employing ceramic fibers in their construction, have been under development for several years. These filter media are intended for application in the development of energy production processes such as pressurized fluidized bed combustion (PFBC), but will also be suitable for many diverse industrial processes. Ceramic media development work to date has shown significant progress toward achievement of a commercially viable high temperature filter. Tests have shown that at high temperature, fine particles can be collected efficiently and pressure drop can be controlled using pulse cleaning. Accelerated durability tests produce promise for long filter life. More work is needed in durability testing to detect application related probelms and build the data base needed to move this important product development to commericalization.

INTRODUCTION

The initial development of high temperature filters were made in response to an identified need for hot gas cleaning devices in advanced coal conversion processes. One approach involved the direct combustion of coal in a pressurized, fluidized bed and generating electricity by expanding the hot flue gas through a gas turbine. Commercially proven techniques exist to remove the particulates from the hot gas stream before passing through the turbine. But to work effectively, they require that the pressure or temperature be lowered, resulting in reduced energy efficiency. Under Department of Energy (DOE) and Electric Power Research Institute (EPRI) sponsorships, several hot gas cleanup techniques are being investigated for direct particulate removal at temperatures up to 1,700°F and 10 atm. These include electrocyclones, granular bed filters, electrostatic precipitators, and ceramic filters.

With the advancement of these high-temperature particulate removal devices, potential markets unrelated to advanced coal conversion processes are emerging. For these markets, high-temperature particulate removal from a gas stream offers promise for more efficient processes, waste heat recovery and product recovery. Some examples are given in Table 1.

TABLE 1. EXAMPLES OF HIGH TEMPERATURE FILTER APPLICATIONS

Fluidized bed combustion	-- Turbine blade protection
Shale oil retort vapor	-- Vapor phase particulate removal
Wood/peat gasifiers	-- Particulate Removal
Catalytic cracking	-- Product Recovery, "expander" protection
Silicone processing	-- Silica dust removal in chlorosilane gas
Iron and steel industry	-- Waste heat recovery

In shale retorting, for example, vapor phase particulate removal of retorting fines would produce a clean shale oil stream requiring very little liquid phase solid removal which is difficult and expensive. In fluidized catalytic cracking, the catalyst is recycled using cyclones in a series. In some cases, the hot gas is then expanded across a heavy turbine called an "expander" for energy recovery. An efficient particulate removal device could offer better product recovery and extended turbine life.

HIGH TEMPERATURE CERAMIC FIBER FILTERS

Fabric filters have long been used successfully for high efficiency particulate removal from gas streams at temperatures below 500°F. The temperature limits of the filter can be extended by the use of materials capable of withstanding higher temperatures such as metallic or ceramic media. Two types of ceramic filters are currently under development; a filter with a felted media consisting of a nonwoven ceramic mat sandwiched between retaining screens and a filter woven from ceramic yarn. Some examples of potential ceramic filter media and their temperature capabilities are given in Table 2. Most of the media listed are commercially available while a few are still in the experimental and development stage. Fiberglass filters at present are limited to temperatures less than 550°F mainly because of the temperature limitations of the coating. Various methods are being explored to improve the temperture resistance of the coating and the abrasion resistance of uncoated fiberglass. Newer, stronger materials such as zirconia fibers are also in the development stage.

Both felted and woven filters have their advantages and shortcomings. A comparison is given in Table 3.

TABLE 2. EXAMPLES OF CERAMIC FIBER FILTER MEDIA

Felted	Woven
Saffil alumina (ICI) 95% AL_2O_3, 5% S_iO_2 3,000°F	Nextel (3M) 62% AL_2O_3, 14% B_2O_3, 24% S_iO_2 2,600°F
Kaowool (B&W) 47% AL_2O_3, 53% S_iO_2 2,600°F	Astroquartz (J. P. Stevens) 99.9% S_iO_2 2,000°F
Fiberfrax (carborundum) 48% AL_2O_3, 52% S_iO_2 2,300°F	Modified fiberglass 1,200°F developing
AB-312 (3M) experimental	Zirconia developing

TABLE 3. COMPARISONS OF WOVEN AND FELTED CERAMIC FILTERS

Felted	Woven
Very high collection efficiencies >99.9%	High collection efficiencies >99.9%
High face velocity operations possible. Up to 20 ft/min.	Low face velocity operations 1 to 6 ft/min
Requires relatively high cleaning energy	Relatively low energy cleaning required
Generally pulse cleaned	Can be pulse cleaned, mechanically shaken, or reverse air cleaned

In general, the felted filters have higher collection efficiencies and can operate at higher face velocities than woven filters so that the size of the overall filter unit can be reduced. However, they are more difficult to clean and usually require higher cleaning energy compared to woven filters. In pulse cleaned units, the filter lengths are also limited to less than 15 feet. At Acurex there are various programs to explore and develop both types of filters for DOE, EPRI, and industrial customers.

SUMMARY OF SOME RECENT RESULTS

ACUREX BENCH-SCALE TEST RESULTS WITH FELTED FILTERS

Under DOE sponsorship, a bench scale test program was undertaken to evaluate the felted ceramic filter concept. A schematic of the test facilities is given in Figure 1. The system is capable of operating at temperatures up to 1,500°F and pressures up to 10 atm with one filter. The types of dusts used were a variety of redispersed PFBC flyash injected via a turntable dust feeder. The mass median diameter of the various flyash used ranged from 5 to 20 μm. Cleaning was initiated on either a fixed time interval basis or a set pressure drop across the filter using a short-duration, high-pressure pulse jet of air. The duration was generally kept at 0.05 to 0.1s. Overall mass collection efficiency was determined by measuring the amount of dust penetrating the filters versus the amount of dust fed. To determine the amount of dust penetration, a total filter made of a high-efficiency fiberglass mat was used downstream of the filter unit to collect the penetrating dust. A total of about 1,000 hours of test time have been accumulated under various conditions and a summary of the test results are given in Table 4.

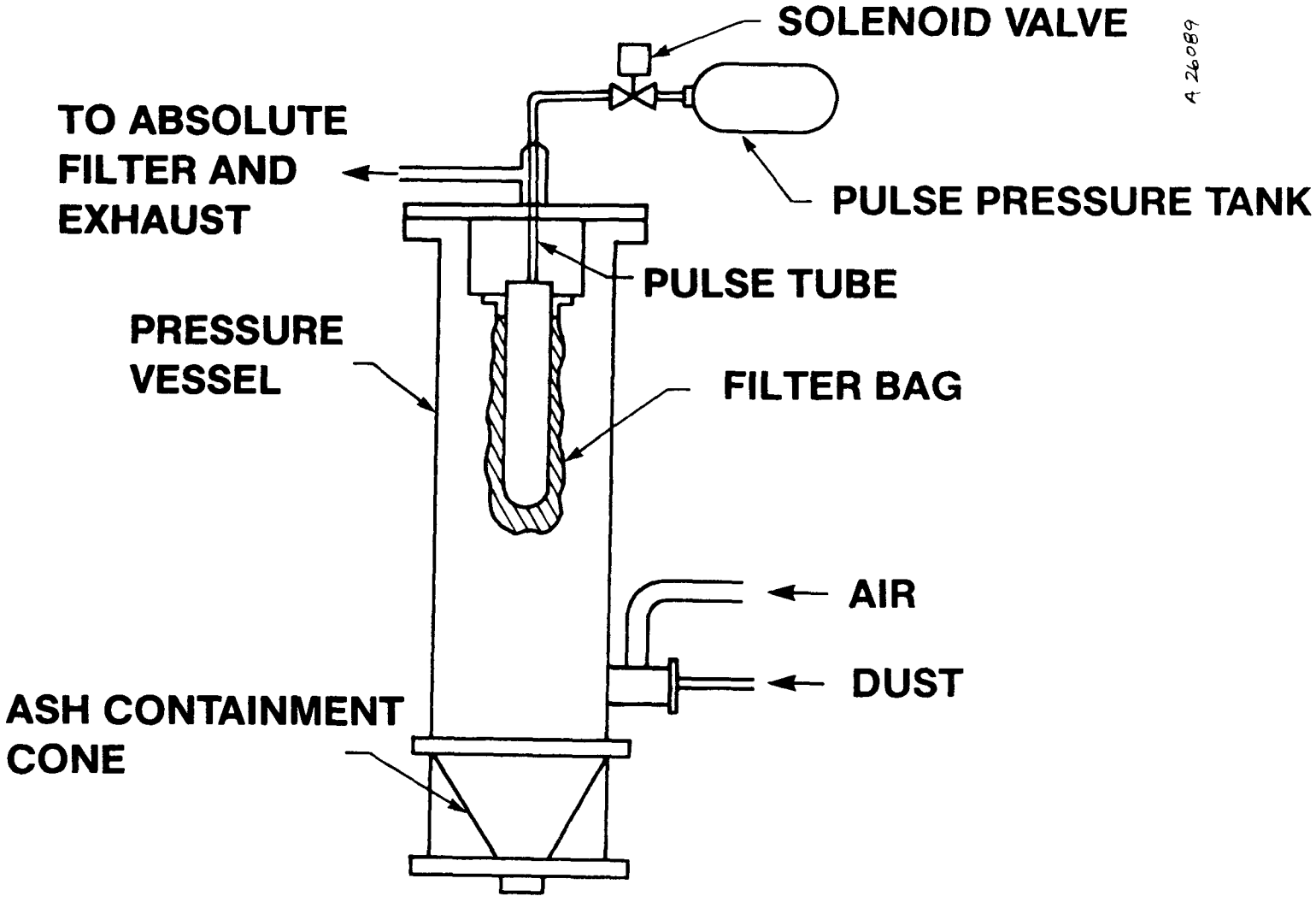

Figure 1. Test facilities schematic.

TABLE 4. BENCH SCALE TEST SUMMARY

Filter dimensions:	3 to 6 in. diameter, 3 to 8 ft. long
System pressure:	1 to 10 atm
System temperature:	Ambient to 700°F
Dust loading:	0.1 to 0.5 g/ACF
Air/cloth ratio:	5 to 18 ft/min
Maximum pressure drop across dirty filter before cleaning:	5 to 20 in. H_2O
Baseline pressure drop:	3 in. H_2O
Collection efficiency:	99.89 to 99.999 percent

Having established high collection efficiency and good cleanability, the durability of the filter was tested by subjecting the filter to a series of rapid pulses in a dusty environment. A summary of the results is provided in Table 5.

At the end of the 100,000 cleaning cycles (equivalent to 4 years of operation cleaning every 20 minutes), the overall mass collection efficiency was greater than 99.9 percent.

SCALEUP TESTING AT WESTINGHOUSE

Further evaluation of the filters were conducted on a larger scale 520 ACFM at Westinghouse under simulated PFBC conditions (150 psia, 1,500°F) using redispersed flyash. The unit contained five filters, 8 inches diameter by 5 feet and was operated under dust loadings of 1 to 2 gr/ACF and face velocities 8 to 15 ft/min.

Cleanability of the filters was generally good over a total of 77 hours of test time. An overall baseline pressure drop of about 8 inches H_2O was achieved from a pressure drop set point for cleaning 15 inches of H_2O. Overall collection efficiencies were initially high (greater than 99.9 percent) but dropped after about 20 hours of testing. Still, the collection efficiency stayed above 95 percent throughout most of the test. At the conclusion of the test it was found that in many places along the filters the saffil filter media had been blown away. It was determined that a combination of overpulsing and large outer screen openings were the major

TABLE 5. SUMMARY OF RAPID PULSE DURABILITY TESTING

Filter dimensions:	3 in. by 5 ft
System temperature:	700°F
System pressure:	35 psia
Air/cloth ratio:	5 ft/min
Cleaning pressure:	190 psia
Cleaning duration:	50 msec
Number of cleaning cycles:	100,000
Overall collection efficiency:	>99.9 percent

cause of saffil blowout. The pulse duration was set at 250 msec, the shortest possible setting on the timer but still significantly higher than normal settings of about 50 msec. This caused excessive high pressure backflow during pulsing. The large outer screen openings also did not help to retain the fibers of the mat. The inner screen held up quite well and was the primary reason why a relatively high collection efficiency could still be maintained.

SUBPILOT TESTING AT CURTISS-WRIGHT

A subpilot filter unit consisting of 15 felted filters 6-inch diameter by 8 feet long (Figure 2) was tested at the Curtiss-Wright (Wood Ridge, N.J.) PFBC facilities.

The PFBC was started with preheat air followed by kerosene addition and then coal. A final temperature of about 1,460°F and pressure of about 71 psig was achieved at a gas flow of about 940 ACFM to the filter vessel. The filters operated quite well during the first 70 hours of overall operation, including 20 hours on coal and then seemed to fail abruptly. In terms of particulate collection (Figure 3), the filters were >99.6 percent efficient on the average before failure. The pressure drop characteristics of the filter (Figure 4) also show that they have good cleanability. At a set point for cleaning 25 inches of H_2O, the baseline ΔP seem to be maintained at rather steady levels. During preheat, baseline was kept at 2 to 3 inches H_2O while during coal feed operations, the baseline was around 7 inches H_2O.

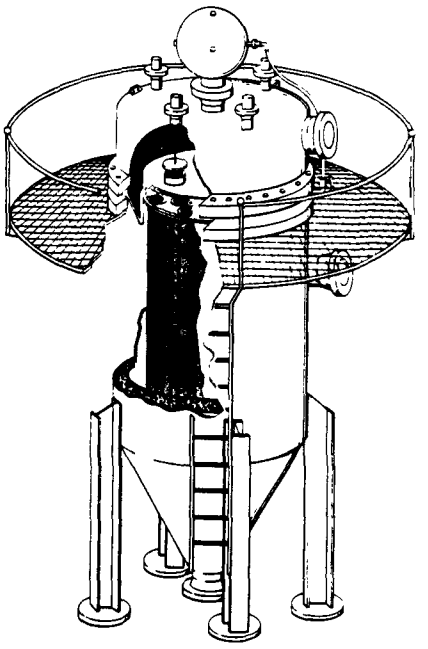

Figure 2. Schematic of pressure vessel for Acurex Ceramic Filter unit installed at Curtiss Wright.

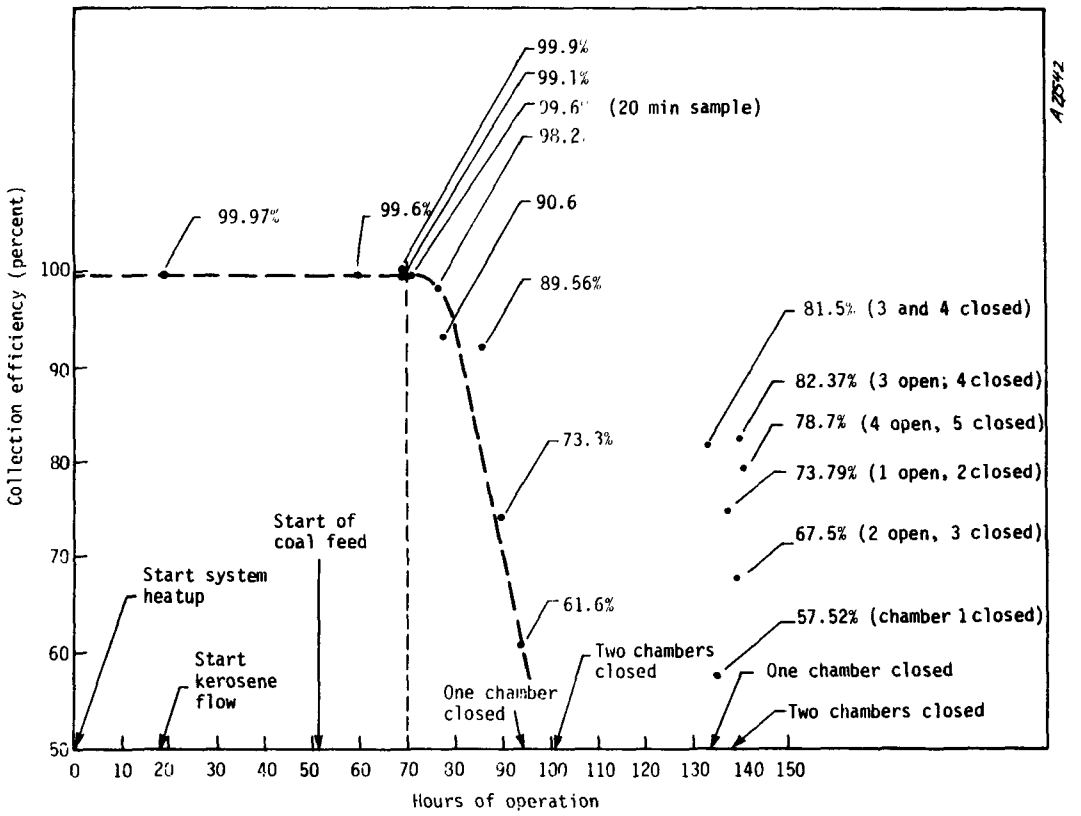

Figure 3. Collection efficiency of filters vs. hours of operation.

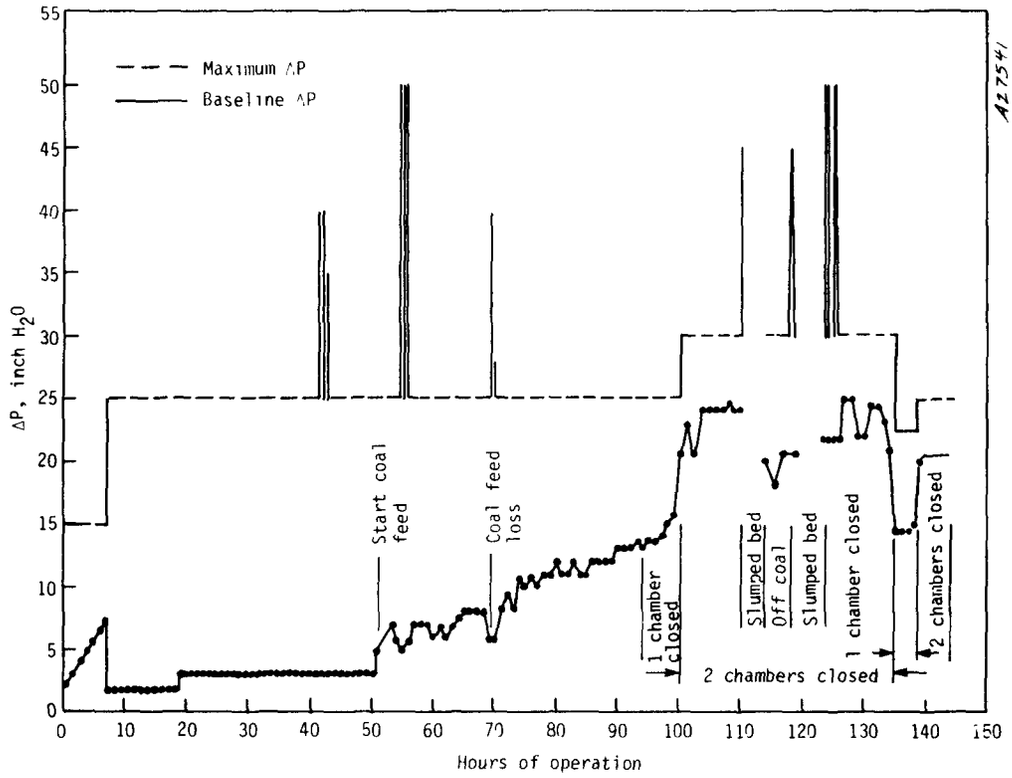

Figure 4. Pressure drop across filter with time of operation.

A detailed examination of the filters and the data indicated that the filter inner screen failed abruptly about 70 hours into operation. The failure occurred simultaneously with a disturbance to the PFBC which caused a surge in airflow and perhaps fuelflow. Failure also occured when the temperature encountered by the filter was the highest (1,460°F) since the start of operation. Failure was therefore probably related to the disturbance or the high temperature or both. One possibility is that the ceramic filter is clamped at both ends of the metal cage, consequently, the metal elongates with temperature, the filter is streched and finally tears. Another possibility is that hot spots on the filter caused by fuel carryover caused ash fusion and inner screen deterioration. Detailed analysis is being conducted by electric microscopy and chemical analysis to confirm some of the postulates. Preliminary results using scanning electron microscopy analysis located where the inner screen failed indicated that ash fusion did occur which embrittled the fabric. In any event, modification in the cage design is needed to keep a constant uniform tension on the filter. This would prevent overstretching of the filter media as well as keep dust from accumulating under the outer screen, a phenomena which was observed with most of the filters.

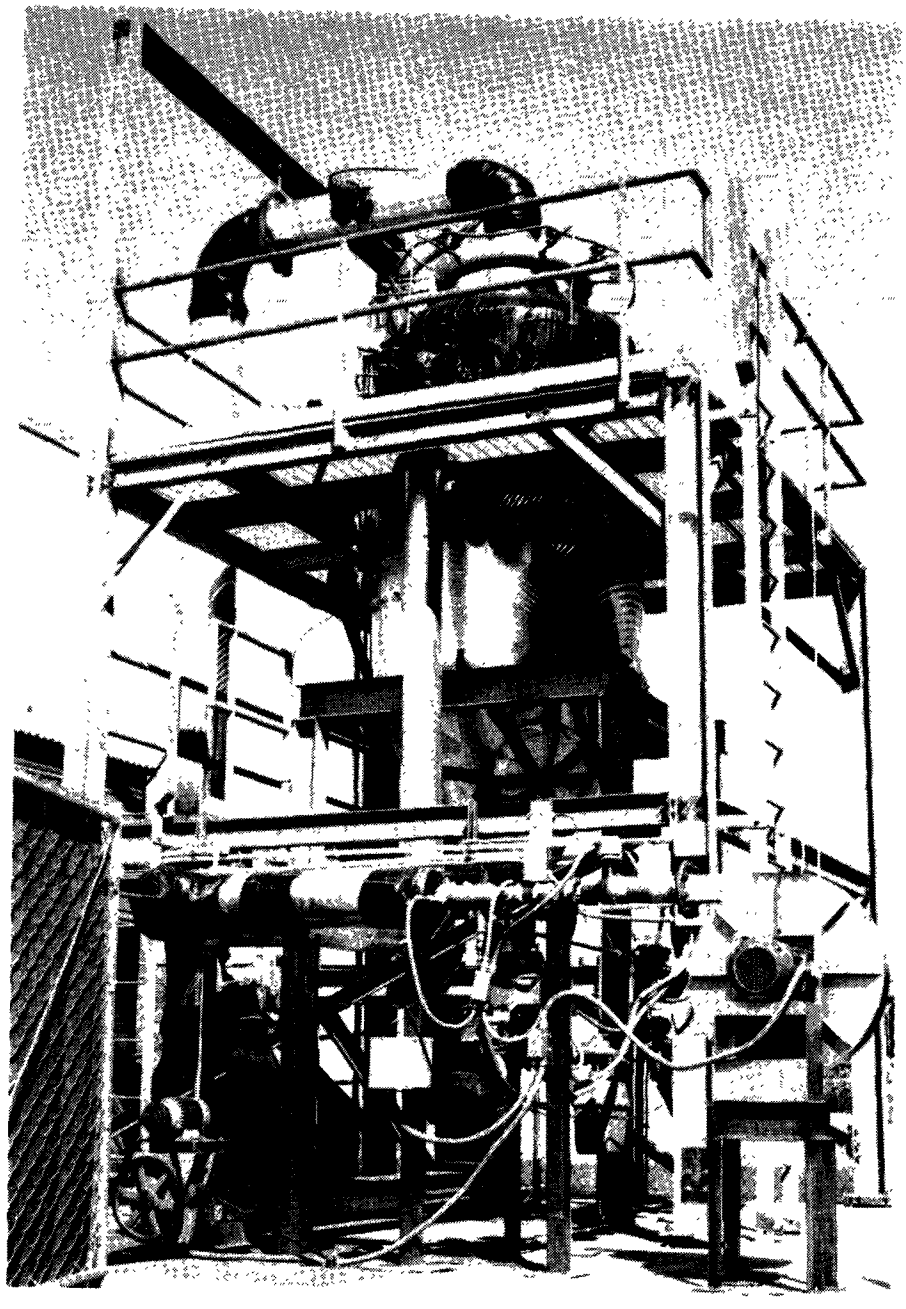

Figure 5. Durability test rig.

DURABILITY TESTING OF WOVEN CERAMIC FILTERS

A program sponsored by EPRI is underway to test ceramic filters woven from 3M Nextel® yarns. The test will be conducted for 6,000 hours at 800°F and atmospheric pressure using re-entrained PFBC dust. Thirteen filters 6 inches diameter and 5 feet long will be used. A summary of expected test conditions is given in Table 6. While the basic objective of the test is to evaluate filter durability under steady-state conditions, several advanced concepts and devices such as a filter cake mass detector and a real time particulate analyzers will also be tested. Figure 5 shows a photograph of the durability test rig. This major test is scheduled to begin during October 1982.

TABLE 6. CERAMIC FABRIC FILTER LIFE CYCLE TEST FACILITY

Temperature:	700K (800°F)
Pressure:	1 atm
Dust loading:	13.9 g/acm (5.9 grains/acf)
Flowrate:	24 acm/min (840 acf/min)
Air/Cloth ratio:	2.4 m/min (8 ft/min)
Number of filters:	13
Filter dimensions:	15.2 cm (6 in.) diameter 1.5 m (5 ft) long
Cleaning method:	Online reverse pulse

ACKNOWLEDGEMENT

This work is partially supported by a Contract DE-AC01-80ETIT092 from the Department of Energy, Morgantown, West Virgina and Contract RP-1336-4 from the Electric Power Research Institute, Palo Alto, California.

The work described in this paper was not funded by the US Environmental Protection Agency and therefore the contents do not necessarily reflect the view of the Agency and no official endorsement should be inferred.

HIGH TEMPERATURE AND PRESSURE PARTICULATE FILTERS FOR FLUID-BED COMBUSTION

by: D. F. Ciliberti, T. E. Lippert
Westinghouse Research and Development Center

O. J. Tassicker, S. Drenker
Electric Power Research Institute

ABSTRACT

The only technological barrier to the commercialization of Pressurized Fluid-Bed Combustion (PFBC) is the efficient removal of particulates at high temperature and pressure. The Electric Power Research Institute has sponsored work at the Westinghouse Research and Development Center to investigate several filtration devices for this application. This effort has included high pressure and temperature pilot-scale testing of multielement ceramic bag filters of both the woven and felted type. The current program also includes screening testing of high alloy sintered metal and tubular porous ceramic filter candles at temperatures in the range of 800-900°C and at pressures of 11 atm. Subsequent to these tests long duration life testing of a single woven ceramic bag will be carried out to optimize bag life with respect to cleaning regimen.

The work described in this paper was not funded by the U. S. Environmental Protection Agency and, therefore, the contents do not necessarily reflect the views of the Agency and no official endorsement should be inferred.

INTRODUCTION AND BACKGROUND

The successful removal of particulates from high temperature and pressure gas streams is a goal that is important to many advanced coal conversion technologies both from an operational process point of view and for environmental considerations. The economics of processes such as electric power production from low-Btu coal gasification could be greatly enhanced by a viable hot gas cleaning system, while the commercial development of power production from pressurized fluid-bed combustion critically depends on an effective hot gas cleaning system that will result in adequate turbine life. As such the hot gas cleaning problem has been identified as the single technological barrier to the commercial development of PFBC. To address this technology gap both the Electric Power Research Institute (EPRI) and the Department of Energy (DOE) recently have sponsored a broad range of research and development programs in the area of hot gas particulate removal. These programs have covered many variations of high temperature filters (granular, porous ceramic, sintered metal, and ceramic fiber bag filters), as well

as advanced cyclone concepts, electrostatic precipitators and solid particle scrubbers.

TEST FACILITIES

Since Westinghouse is a major supplier of gas turbines we have actively participated in such programs directed at the solution of the hot gas cleaning problem and subsequent commercialization of combined-cycle plant concepts. In support of this participation we have (with the aid of DOE, EPRI, and EPA) developed two high pressure and temperature particulate control test facilities. One is a flexible bench-scale unit for the development of novel concepts and the other a pilot-scale test facility in which more advanced concepts can be tested at signifiant scale.

The bench-scale test facilities was constructed by Westinghouse in conjunction with the execution of the DOE-sponsored program to develop a ceramic cross-flow filter. The original operating equipment, instrumentation, and controls were purchased and installed under the DOE cross-flow filter contract. The test facility as configured for the this work is shown schematically in Figure 1. The range of operating conditions is presented in Table 1.

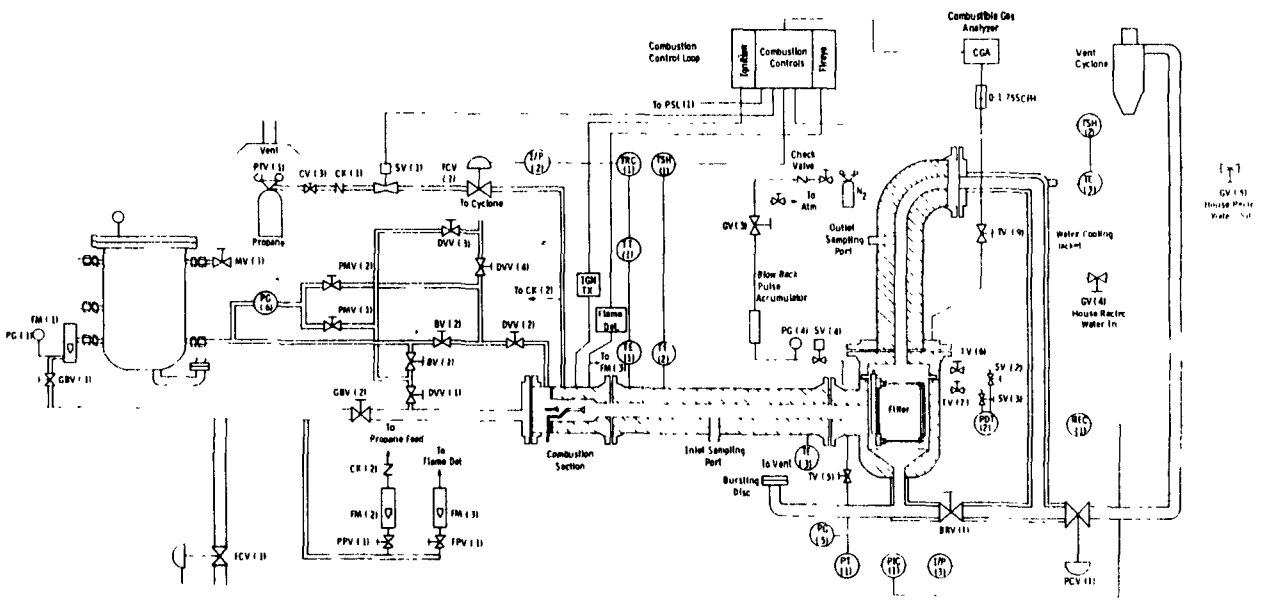

Figure 1. Bench-scale HTHP test loop.

TABLE 1 - OPERATING PARAMETERS FOR THE WESTINGHOUSE BENCH SCALE HIGH TEMPERATURE AND PRESSURE TEST FACILITY

Temperature	950°C
Pressure	18 atm
Air Flow	225 Nm^3/hr
Dust Concentrations (typical)	1,000-10,000 ppm

Under EPRI sponsorship, and with DOE approval, the facility is currently being upgraded with the intention of making it capable of unattended operation and thereby economical for long-term testing. This has involved the installation of a natural gas compressor for fuel supply (in place of the bottled propane system previously used) and the installation of other safety-related instrumentation and control. Additionally, a minicomputer-based data aquisition and control system has been installed to facilitate operation of the system for long periods of time and to manage the consequent large amounts of test data.

There also is a need to test, at high temperature and high pressure, particle removal equipment large enough to permit extrapolation to the design of utility-scale units. Westinghouse, with the support of both EPA and DOE, designed and constructed a test facility at their Synthetic Fuel Division for evaluating particle removal equipment using simulated flue gases at temperatures up to 871°C and pressures up to 15 atm. Hot gas flows up to 5.44 kg/s can be provided. Equipment up to 1.37 m in diameter and 2.44 m in length can be mounted within an insulated pressure shell for testing.

A functional schematic of the test passage is presented in Figure 2. The high-pressure air for the system is supplied by either or both of the available compressors. A 1500 kW centrifugal compressor can supply 3.4 kg/s of air at 21 atm. A second, three-stage, 900 kW reciprocating compressor can be run in parallel, providing flows up to 5.86 kg/s. The high pressure air flows from the compressor building to the laboratory, where it can be heated to temperatures up to 650°C by either of two natural-gas-fired air preheaters.

The pressurized, preheated air then flows through a combustor where No. 2 fuel is burned to raise the gases to the desired temperature. The combustor fuel is pumped from the fuel-blending building where several tanks are available for blending either corrosion inhibitors or promoters (combustible alkali organometallic compounds). From the combustor the hot pressurized gases enter the test passage piping. The passage piping and valving are arranged to allow a great deal of flexibility in the manner in which the gases are introduced to and exit from the pressure vessel, allowing virtually any device that will fit in the pressure vessel to be tested.

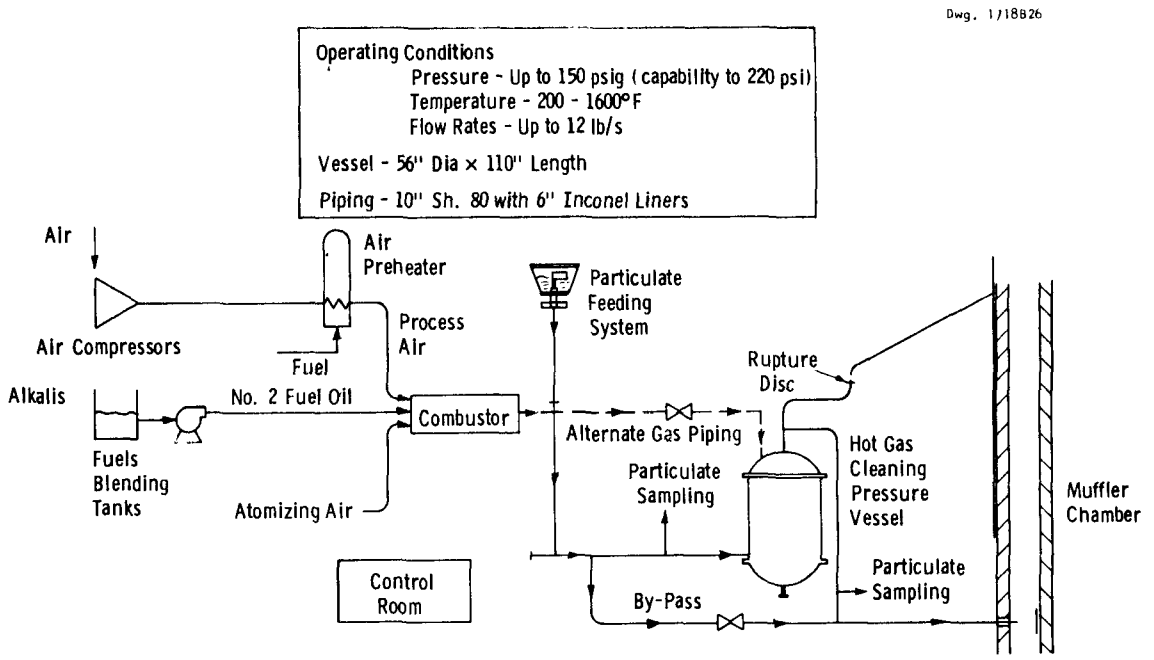

Figure 2. Schematic of Westinghouse hot gas cleanup facility.

CURRENT AND RECENT HOT GAS CLEANING PROGRAMS IN WHICH WESTINGHOUSE HAS PARTICIPATED.

Over the past several years we have focused our efforts on the development of high temperature filter systems since we believe that such systems can be designed to meet or exceed both turbine tolerance and environmental requirements. To this end Westinghouse has participated in the development of and or testing of six different filter concepts over the past three years. Table 2 presents a very brief summary of this work including some qualitative comments. In general all of the filtration devices tested have demonstrated very high collection efficiencies at moderate pressure drop. It is also true, however, that all of the filter systems have unresolved questions concerning their cleanability, be it reflected in filter life or in gradual blinding or loss of the filter medium. All the filter systems listed has displayed potential for successful application to PFBC, but none have been demonstrated to date.

Development of the last three systems shown in Table 2 has most recently been supported by DOE. Testing of the first three devices listed has been sponsored by EPRI, and these devices are the primary topic of this report.

TABLE 2 - FILTER DEVICES TESTED BY WESTINGHOUSE

Typical Operating Parameters

Dwg 4256B8E

Device	Test Scale m^3/hr	Filter Velocity, m/min	Base Pressure Drop kPa	Efficiency %	Comments
Schumacher Ceramic Candles EPRI	85	3	2	99.9+	• Mechanically sound corrosion resistant • High efficiency • Potential blinding
Pall Sintered Metal EPRI	85	3	2	99.9+	• Mechanical sound • High eff/low Δp • Potential for blinding • Potential corrosion
3M Woven Ceramic Bag EPRI	850	85-1.7	5	99	• Easy to clean/low Δp • Bag life uncertain
Acurex Felted Ceramic EPRI/DOE	850	3	5	99.9+	• Very good eff/med Δp • Cleaning trade-off
Ducon Granular Bed DOE	850	12	7-10	99	• Moderate efficiency • Blowback cleaning still to be demonstrated
Westinghouse/Coors Ceramic Crossflow DOE	85	2	1-2	99.9+	• High eff/low Δp • Compact system/good economics • Mounting and mechanical properties need improvement

PILOT-SCALE WOVEN CERAMIC BAG FILTER TESTING

The testing of filter bags woven from yarns of ceramic fiber was accomplished through the cooperative effort of the 3M Company, Buell Envirotech, and Westinghouse under EPRI sponsorship. Westinghouse R&D was EPRI's prime contractor and carried out the actual HTHP test program at their pilot-scale test facility, which is operated by the Westinghouse Synthetic Fuels Division. 3M supplied the woven ceramic bag filters and Buell Envirotech fabricated the bag mounting system and blowback equipment which was installed at the test site.

WOVEN CERAMIC BAG FILTER UNIT DESCRIPTION

The general arrangement drawing of the woven ceramic filter unit is shown in Figure 3. The unit consisted of a 19-bag array that was suspended from a canister support assembly that incorporated a top support flange and conical section, which in turn was gasketed and bolted between the pressure vessel flange. The conical section was designed to accommodate differential thermal expansion and was attached to the canister body that shrouded the bags. Gas flow was introduced at the bottom of the pressure vessel, around and through the perforated wall of the bag canister, up between the bags, in through the bags, up the inside of the bag and perforated bag support cage, and out the top of the pressure vessel. The conical section and top support flange served to separate the clean and dusty gas sides of the pressure vessel.

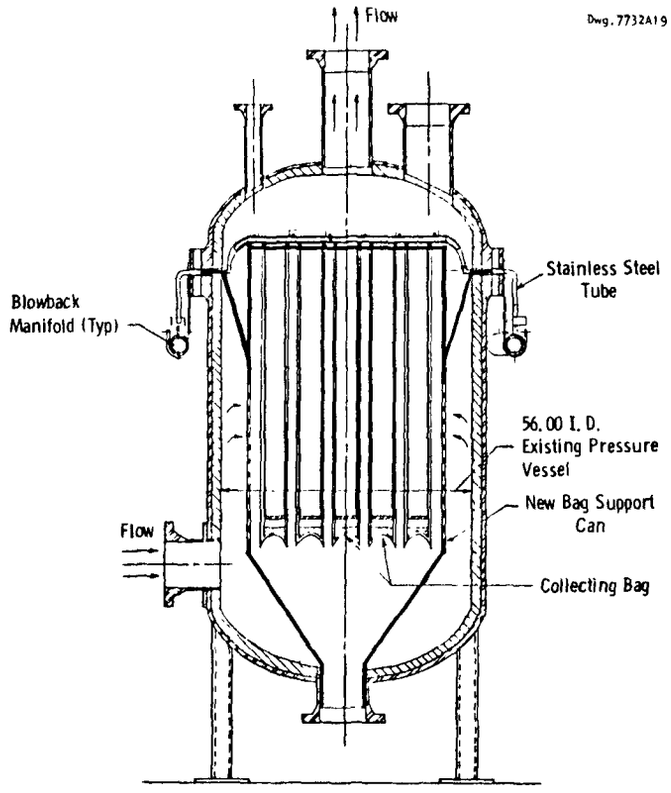

Figure 3. General arrangement drawing of the woven ceramic bag filter - front view.

The individual ceramic bags were fitted over perforated bag support cages. The cages measured 15.2 cm od by 1.4 m long. The bags were made taut against the support cage by a pocket of sand in the lower part of the bag and clamped to the top of the support cage with a metal compression band. The support cage perforations were 0.63 cm diameter holes on 0.79 cm centers, providing an approximately 58% open area. Each bag support cage was flanged at the top to seat and seal (using a special high-temperature gasket) against the canister top flange.

The filter bags themselves were made from 3M ceramic fibers AB-312 in an 8-harness weave. These fibers are nonoxidizing, nonconductive, and heat resistant, and can withstand temperatures in excess of 1096°C.

Each bag was cleaned by a 0.97 cm pulse jet nozzle located at the top of the bag. The nozzles of the 19-bag assembly were manifolded to two high-pressure reservoirs located externally to the test unit and presure tank assembly. For cleaning the bags were manifolded in groups of two and three to eight solenoid control valves programed to actuate sequentially upon initiation of the cleaning cycle. The duration of the back flush pulse could be set between 0.02 and 0.180 s.

RESULTS FROM THE WOVEN CERAMIC FILTER UNIT TESTS

Hot-gas cleanup tests were conducted on the woven ceramic filter unit at two temperatures, 427°C and 815°C. Table 3 summarizes the overall test results for the lower temperature condition. Data included in the table are the nominal test passage operating conditions, the measured filter unit pressure drop characteristics, the test average inlet and outlet dust loadings, and corresponding overall collection efficiencies. During any one test day several (up to four) outlet samples were obtained. From each of these an outlet dust loading from the filter unit was determined. The overall collection efficiency values listed in Table 3 are average values for a given day of testing. At the lower temperature condition tests were conducted at two mass flow rates corresponding to filter face velocities of 0.85 m/min and 1.71 m/min.

TABLE 3 – SUMMARY OF RESULTS FROM WOVEN BAG FILTER TESTS, 427°C (800°F)

Dwg 1715879

Test Identification	Test Conditions	No. of Cleaning Cycles	Bag ΔP, kPa (in H_2O)		Dust Loading, ppm (gr/scf)		Overall Collection Efficiency (Test Average)
			Before Cleaning	After Cleaning	Inlet	Outlet	
12-5-79 2nd Cyclone Ash	P = 1138 kPa (165 psia) T = 427°C (800°F) m = 0.91 kg/s (2.0 lb/s) Q = 9.8 m^3/min (346 ft^3/min) Air-to-Cloth = 0.85 m/min (2.8 ft/min)	1	0.47 (1.9)	0.02 (0.1)	6726 (3.8)	26.5 (0.015)	99.6%
12-7-79	P = 1138 kPa (165 psia) T = 427°C (800°F) m = 0.91 kg/s (2.0 lb/s) Q = 9.8 m^3/min (346 ft^3/min) Air-to-Cloth = 0.85 m/min (2.8 ft/min)	1	0.95 (3.8)	0.02 (0.1)	5487 (3.1)	11.3 (0.0064)	99.8%
12-11-79	P = 1138 kPa (165 psia) T = 427°C (800°F) m = 0.91 kg/s (2.0 lb/s) Q = 9.8 m^3/min (346 ft^3/min) Air-to-Cloth = 0.85 m/min (2.8 ft/min)	3	0.52 (2.1) 0.60 (2.4) 0.40 (1.6)	0.02 (0.1) 0.07 (0.3) 0.07 (0.3)	11,328 (6.4)	<1 (0.0005)	99.9%
12-13-79	P = 1138 kPa (165 psia) T = 427°C (800°F) m = 0.91 kg/s (2.0 lb/s) Q = 9.8 m^3/min (346 ft^3/min) Air-to-Cloth = 0.85 m/min (2.8 ft/min)	1	1.62 (6.5)	0.07 (0.3)	8337 (4.71)	~0 (~0)	~100%
12-19-79 Ash + Limestone	P = 1138 kPa (165 psia) T = 427°C (800°F) m = 0 91 kg/s (2.0 lb/s) Q = 9.8 m^3/min (346 ft^3/min) Air-to-Cloth = 0.85 m/min (2.8 ft/min)	3	0.50 (2.0) 0.62 (2.5) 1.37 (5.5)	0.17 (0.7) 0.02 (0.1) 0.10 (0.4)	8638 (4.88)	2.1 (0.0012)	99.9%
12-21-79 Ash + Limestone	P = 1138 kPa (165 psia) T = 427°C (800°F) m = 1.82 kg/s (4.0 lb/s) Q = 19.6 m^3/min (692 ft^3/min) Air-to-Cloth = 1.7 m /min (5.6 ft/min)	6	1.12 (4.5) 1.12 (4.5) 1.54 (6.2) 1.24 (5.0) 1.00 (4.0) 1.37 (5.5)	0.55 (2.2) 0.45 (1.8) 0.17 (0.7) 0.17 (0.7) 0.17 (0.7) 0.17 (0.7)	3894 (2.2)	15.9 (0.009)	99.6%

The initial testing of the filter unit corresponded to a period of "bag conditioning" where the relatively large spaces between the fiber weave partially filled with dust particles, preparatory to establishing an identifiable filter cake. During this bag-conditioning period, the outlet dust loading decreased dramatically with time. After about 6 or 7 hours of filter unit operation, an apparent steady-state operation was indicated. During this steady-state period of time, at the lower face velocity tests, at relatively high inlet loading, the overall collection efficiency was measured as 99.9% or greater.

The last test conducted in the low temperature sequence was at a filter face velocity twice the previous runs, corresponding to 1.71 m/min. At this condition, the overall collection efficiency was measured at 99.6%, somewhat reduced from the lower velocity, steady-state runs.

The pressure drop characteristics of the filter unit are also indicated in the table and show relatively low filtration Δp. In these tests the maximum Δp was not permitted to exceed 1.6 kPa, although system operation at higher Δp may prove to be more desirable. At the operating pressure drop in these tests, the filtration cake thickness was observed to be about 0.63 cm. The effectiveness of the pulse-jet cleaning is indicated by the very low Δp measured after bag blowback. The effectiveness of bag cleaning was found to be dependent on the pressure ratio between the bag operating conditions and pulse-jet reservoir pressure as opposed to the pressure difference. Unsuccessful cleaning was identified when multiple pulses would not result in the lowering of the bag Δp. Successful cleaning is identified for those data where a few or single pulses would result in the bag Δp reducing to its previous low base-line value. Effective bag cleaning was achieved if the pulse-jet pressure was maintained at about 3 times the filter ambient. This apparent dependence on pressure was tested at total pressures of 1114 and 709 kPa and is consistent with conventional ambient bag filtration wisdom where cleaning pulses are on the order of 203 to 405 kPa. At the lower filter bag Δp a somewhat lower cleaning pressure ratio may be indicated.

The most significant dust penetration was observed to occur during and/or immediately following the cleaning cycle. This was supported by filter samples that included periods of blowback and samples that did not include blowbacks. Two 815°C tests runs were made, one at a relatively low filter face velocity, 1.0 m/min, and the second intended to be at a higher face velocity of 2.0 m/min. During this second high temperature test, a malfunction occurred in the passage combustion system, forcing operation at less than desired conditions. Additionally, during this test, one of the filter bags failed at a sewn seam. This resulted in our inability to build system pressure drop, and tests were halted at this point.

Inspection of the failed bag by 3M Company indicated the following:

- That the top layer of Nextel fabric in a double-stitched French seam broke at the crease

- That there is no gross evidence of chemical attack, fusion via eutectic formation, etc.

- That only one bag failed in this manner

- That numerous warp thread crossings in the eight-harness weave fabric showed fiber breakage in the form of tufts of fluffy protrusions at the point of each crossover of fill yarn by warp yarn; that some general abrasion is shown by random broken fiber protrusion

- That two to four gently curved longitudinal wrinkles are heat set into the fabric of each bag. These are about 0.64 cm wide and about 0.64 cm high.

A judgmental interpretation of these observations suggests:

- That the seam should be made somewhat wider

- That cleaning be accomplished more gently to reduce abrasion wear, should this prove to limit life.

CURRENT WOVEN CERAMIC BAG FILTER PROGRAM

Subsequent to the completion of this test phase, EPRI has supported a continued effort in the development of the woven ceramic bag filter. The current program is a parallel effort being carried out by Westinghouse and Acurex for the primary purpose of exploring bag life characteristics. The Acurex effort consists of high temperature but low pressure testing using the 19-bag unit originally installed at Westinghouse.

The testing at Westinghouse will be carried out at both high pressure and temperature in the bench-scale test unit on a single bag configuration. The bench-scale test facility has been modified to accomodate a single full size filter bag, as shown in the pressure vessel assembly drawing, Figure 4. It is our intention to carry out testing on various cleaning strategies to determine the cleaning regimen that optimizes bag life. The data generated will be correlated with the low pressure test results in hopes that eventually less costly low pressure testing can be used to predict high pressure performance. To this end a detailed mathematical model of the cleaning process has been developed and will hopefully serve as the basis for correlation of high and low pressure test results.

It should be noted that 3M has pursued improvements both in the basic ceramic fiber used in the bag cloth and in the sewing techniques employed. We are currently considering the use of a new zirconia fiber that has demonstrated the potential for greatly improved abrasion resistance.

HIGH PRESSURE AND TEMPERATURE TESTING OF CANDLE FILTER

As part of the current EPRI test program we have had the opportunity to briefly examine two different types of "candle" filters in our bench-scale HTHP test facility. One was a porous ceramic candle

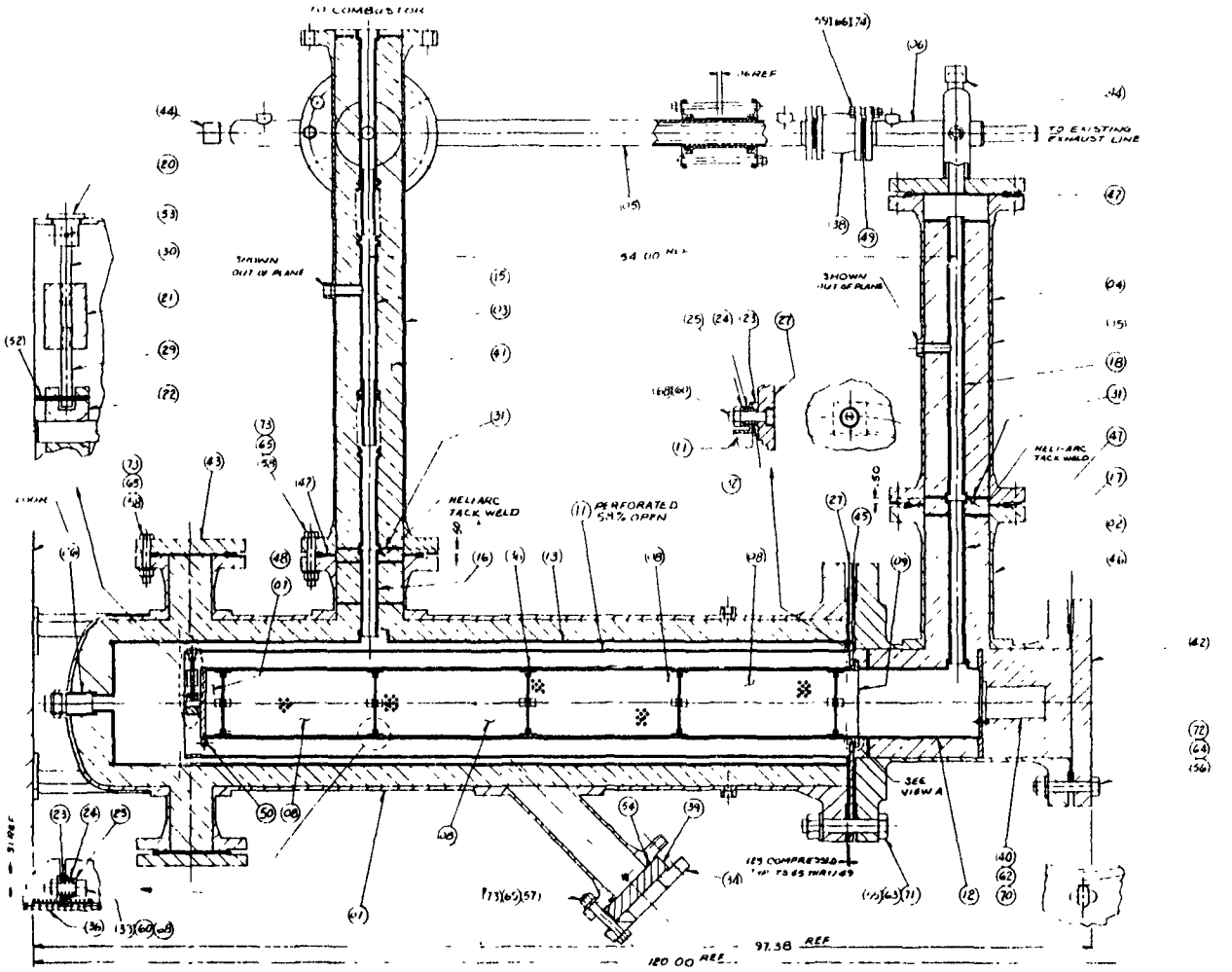

Figure 4. Single bag filter HTHP test vessel.

filter, while the other filter examined was a more or less conventional sintered metal filter.

POROUS CERAMIC CANDLE FILTERS

The porous ceramic candle filters tested were manufactured by Schumacher'sche Fabrik of Bieligheim, West Germany, and are denoted as Schumacel HTHP. These filters are formed by incorporating very small pockets of pure mineral fibers in a dense matrix of silicon carbide. The interconnecting pockets of these small diameter (3 μm) fibers gives rise to very reasonable pressure drops in spite of the rather thick and

rugged wall of the tube. The tubular filters we tested were nominally 50 cm long with an OD of 6 cm and ID of 4 cm. The active filter area was estimated as 0.072 m^2, based on the outer area.

In the course of the preliminary testing that we carried out, we tested a relatively porous element that had an ambient air resistance to flow of 0.25 kPa at a face velocity of 0.67 m/min and a relatively dense element that had essentially twice that resistance to flow at the same velocity.

TABLE 4 - SUMMARY-CERAMIC CANDLE PERFORMANCE AT 770-800°C, 11 atm

Dwg. 7772A04

Test No.	Test Time, hr	Flow, kg/min	Filter Velocity, m/min	Dust Concentration, Inlet, ppm	Measured Dust Collection Efficiency, %
Series 1 - Porous Element					
4. 22. 82	2. 0	0. 72	2. 52	2, 707	99. 90
4. 26. 82	4. 0	1. 44	5. 35	3, 811	99. 98
4. 28. 82	4. 0	1. 44	5. 20	3, 329	99. 97
5. 3. 82	9. 8	1. 44	5. 13	2, 807	99. 99
5. 4. 82	5. 0	1. 44	5. 10	3, 010	99. 99
5. 6. 82A	1. 0	1. 44	5. 31	3, 151	99. 99
5. 6. 82B	8. 5	0. 72	2. 65	6, 302	99. 99
Series 2 - More Dense Element					
8. 18. 82	4. 0	0. 83	3. 35	5, 206	99. 97
8. 24. 82	4. 0	0. 83	3. 35	5, 149	99. 96
8. 26. 82	5. 5	0. 83	3. 35	5, 499	99. 35*
8. 31. 82	9. 0	0. 83	3. 35	5, 468	99. 98

* Leaks in gasket seal

During the first series of tests with the more porous filter candle, the test temperature and pressure were constant at 775°C and 11 atm. During this series seven tests were conducted accumulating a total of about 35 hours of actual filtration time and slightly more than 100 operating cycles (blow back sequences). The filter face velocities examined ranged from 2.5 to 5.3 m/min. The test dust used was a redispersed ash from the Curtiss-Wright PFBC and had a mass mean diameter of approximately 10 μm. Dust concentrations were in the range from 2700 to 3300 ppm. The results of these tests are summarized in Table 4. The overall efficiency measurements were made using an isokinetic outlet sampler and in all cases indicated a penetration smaller than we were able to resolve. A typical pressure drop/time curve for a test is presented in Figure 5. The performance shown here is typical of the behavior observed throughout this period of testing,

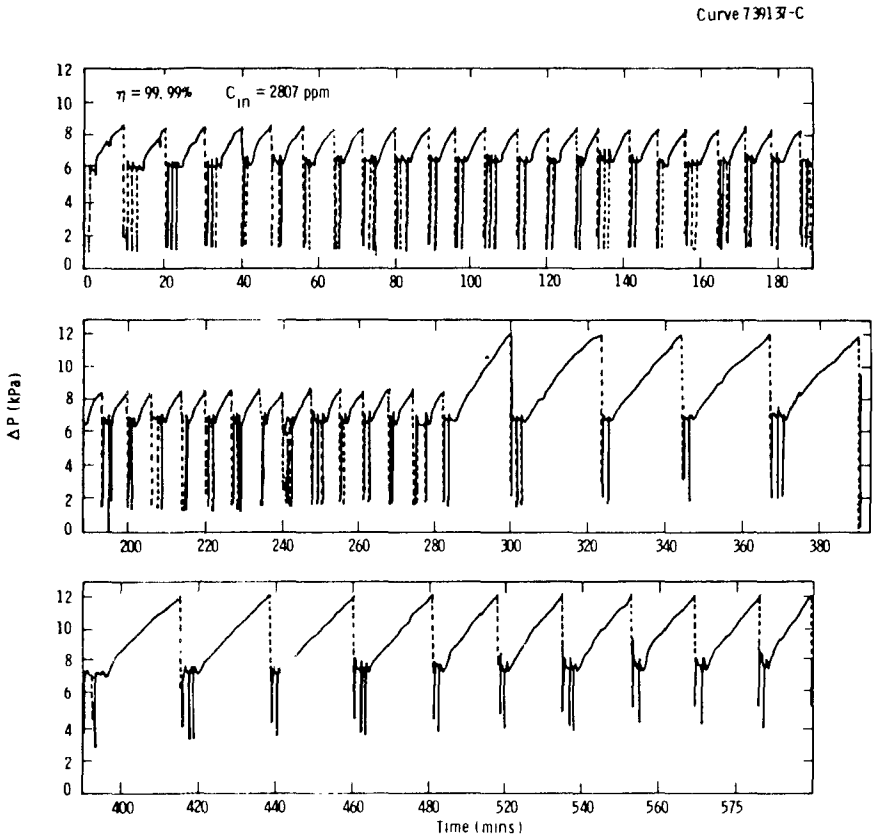

Figure 5. Δp vs time for ceramic candle filter.

that is, of gradual shortening of cycle time and slowly increasing base line pressure drop. The cleaning regimen employed for these tests was 0.5 sec reverse pulse of air from a 2.1ℓ reservoir charged to a pressure of 35 atm and discharged through a 0.75 cm diameter nozzle centered above the clean side of this filter element. This pulse typically gave rise to a 30 to 50 kPa differential pressure from the clean to dirty side of the element. Posttest examination of the filter revealed that a thin "cratered" deposit of dust remained on the filter surface, as shown in Figure 6. This dust layer was not sticky or hard and was easily removed, as shown in the photograph. We hypothesize that the nonuniformity arises from the local areas of high porosity at the imbedded fiber pocket surface sites.

Subsequently a series of tests were carried out with the more dense high pressure drop element. The only system modifications were the insertion of a venturi section in the outlet of the candle in an effort to improve cleaning and an increase in the pulse accumulator volume to 8.4ℓ. The test pressure and temperature remained essentially the same as in previous tests, but the dust concentration was somewhat higher at 5100 to 5500 ppm. Approximately 25 hours of actual filter test time and 95 cleaning cycles were accumulated over four test days

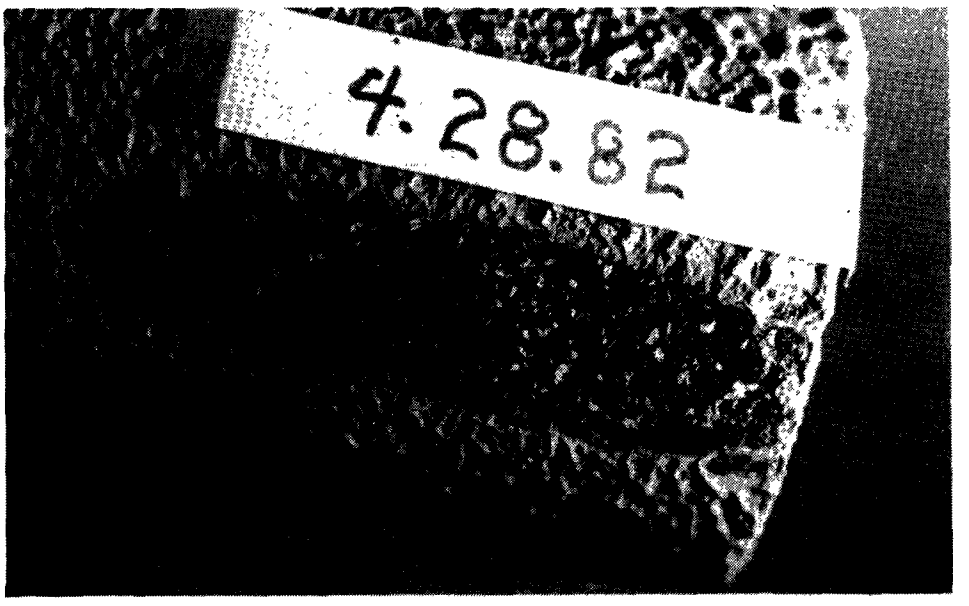

Figure 6. Posttest surface condition of porous ceramic candle filter.

with the more dense filter candle. The results of these tests are summarized in Table 4, where it can again be observed that the filter elements behaved essentially as absolute filters. As in the previous tests the pressure drop/time curves generated revealed a gradual shortening of cycle time and a slowly increasing baseline pressure drop. The inclusion of the venturi section and the larger pulse reservoir did not seem to significantly alter the pressure rise in the filter during blowback, and cleaning remained somewhat incomplete.

Figure 7 focuses on the observed cleaning problem. This figure presents a measure of the cleaned filter permeability (filter velocity divided by the freshly cleaned baseline pressure drop) as a function of operating cycles. Both elements are gradually becoming less permeable at an apparently constant rate of about 0.0024 (m/min-kPa-cycle) for the more dense element and at 1.4 times that rate for the more porous element. It is apparent that if this constant decrease in permeability persists in spite of any operating modifications, then the filter system would not be viable. It should be emphasized that we do not feel that enough operating time has been accumulated nor have a wide enough range of operating parameters been explored to conclude that the system will not provide adequate life. Rather, we are encouraged by the filter element's high collection efficiency, at modest pressure drop and high operating velocity. Another positive consideration is the mechanical strength of the elements, their resistance to thermal shock, and the ease with which they can be mounted in a conventional filter assembly.

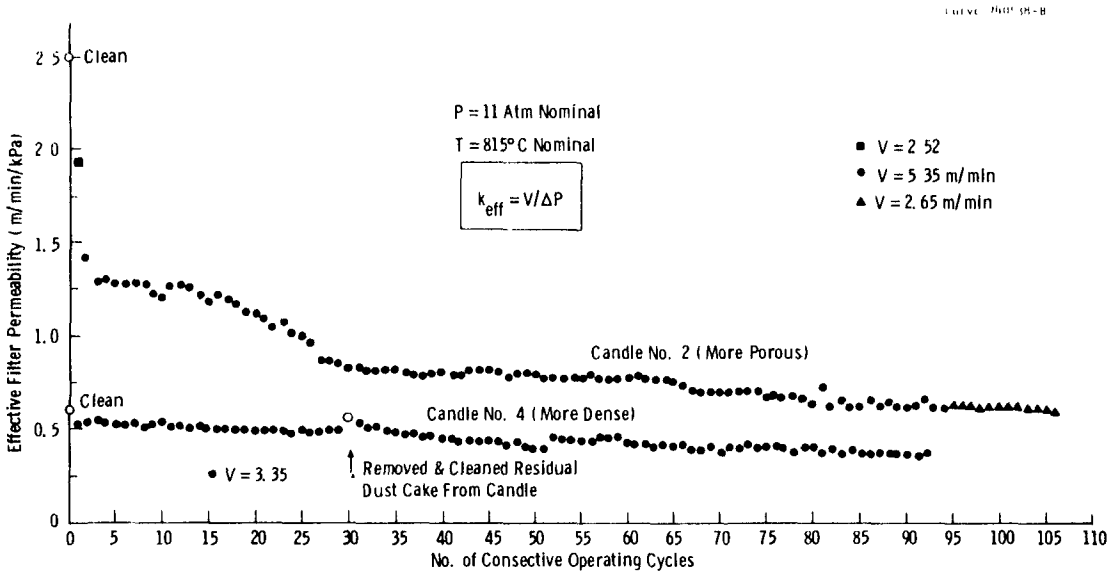

Figure 7. Effective permeability of ceramic candle and residual dust cake in HTHP PFBC simulation tests.

SINTERED METAL CANDLE FILTERS

The porous sintered metal filters tested in this program were supplied by the Pall Trinity Micro Corporation. The elements were 7.6 cm in diameter and had an active length of 38 cm, yielding a filter surface of 0.091 m^2. The material used for fabrication of the elements was a Grade F, 20 μm absolute, sintered Hastelloy X rated for service to 900°C.

Through the entire series of sintered metal filter tests the temperature was maintained at 815°C and the system pressure was held at 11 atm. During the first six test days a 3-element configuration was tested at filter face velocities from 1.22 to 2.44 m/min and dust loadings from 1600 to 4500 ppm. During the last two days of testing one of the three filter elements was removed so that the range of velocities could be extended to 3.7 m/min. A total of about 58 hours of test time were accumulated, representing 62 cleaning cycles. Table 5 presents a summary of the test experience with the sintered metal filters. As with the ceramic candle filters, virtually no reliable, measurable penetration was observed in any of the tests.

Blowback cleaning of the filters for the first 6 tests consisted of 0.5 sec pulses from a 2.1ℓ reservoir charged to pressures between 21 and 28 atm. The pulse nozzles were 0.75 cm diameter and centered over the element outlet. Each element was supplied with a venturi in the

TABLE 5 - SUMMARY OF SINTERED METAL FILTER TESTS

Dwg. 7772A05

Date	Test Time, hr	Passage Flow, kg/hr	Filter Velocity, m/min	Inlet Dust Concentration, ppm	Overall Collection Efficiency, %
5/26/82	4.5 (2 cyc)	72.64	1.22	2962	99.98
5/28/82	11.0 (5 cyc)	72.64	1.22	2508	99.98
6/3/82	11.0 (8 cyc)	72.64	1.22	3869	99.99
6/7/82	3.5 (2 cyc)	72.64	1.22	4447	99.97
	3.5 (6 cyc)	145.28	2.44	1827	99.97
6/10/82	9 (13 cyc)	145.28	2.44	1625	99.97
6/15/82*	1.5 (1 cyc)	72.64	1.22	3139	99.77
	2.0 (2 cyc)	108.9	1.83	2093	99.99
	1.5 (2 cyc)	145.28	2.44	1569	99.96
6/21/82**	0.8 (2)	97.1	2.48	1139	99.44
	0.7 (1)	97.1	2.48	1406	99.97
	2 (10)	48.6	1.22	3490	99.99+
7/1/82**	1.8 (3)	48.6	1.22	1186	99.80
	3.5 (5)	145.28	3.71	1096	99.99*

* On line cleaning test
** Two filter modules only

filter outlet to enhance the blowback effectiveness. During these tests two modifications to the blowback system were made. After the sixth test (6/15/82) the pulse reservoir volume was increased in volume by a factor of 4 to 8.4ℓ. After the seventh test (6/21/82), there was some concern that there might be some misalignment between the pulse nozzle and the venturi throat due to thermal expansion in the blowback lines. A new set of nozzles and method for maintaining alignment were therefore installed for the final test. This precaution did not result in any observable increases in internal filter pressure rise during blowback, as this rise remained at about 45 kPa for a 28 atm pulse.

During the first several days of testing the filter velocity was maintained at 1.22 m/min. During this time the filter appeared to condition and settle into stable operation as shown in Figure 8. In subsequent tests, operation at higher velocities was explored and these seemed to result in a very gradual decrease in both cycle time and permeability as shown in Figure 9.

As was the case with the ceramic filter, the shortened operating cycles appear to be a consequence of a decreasing filter permeability.

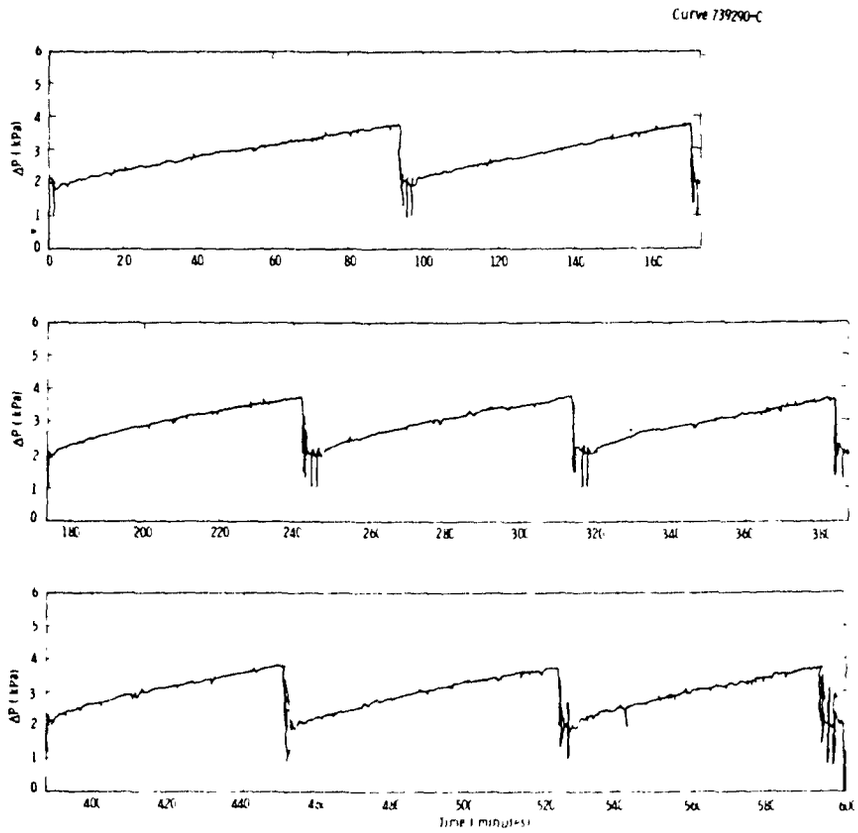

Figure 8. Pressure drop vs time for sintered metal filter conditions 6/3/82.

This decrease was essentially constant over the period of testing at a rate of 0.015 m/(min-kPa-cycle) or nearly six times the observed rate for dense ceramic candle filter.

During the final test the system was operated first for a few cycles at a face velocity of 1.22 m/min and then at 3.7 m/min. During the high velocity segment of this test, the baseline pressure drop increased rapidly from about 17 kPa to 19 kPa in the course of 4 cycles. Posttest examination of the elements revealed the fact that the dust deposit on one of the elements was quite different in appearance from any observed to date. Figure 10 shows this difference. The element on the right looks normal, while the one of the left appears to have a much heavier deposit. Although we were unable to discover the reason for this difference, we feel certain that it explains the unstable behavior observed in the last test.

In spite of the brief nature of this program, we can conclude that the sintered metal filters are capable of providing very high efficiency on PFBC ash at tolerable pressure drops. Additionally, their mechanical properties and resistance to accidental breaking is a very

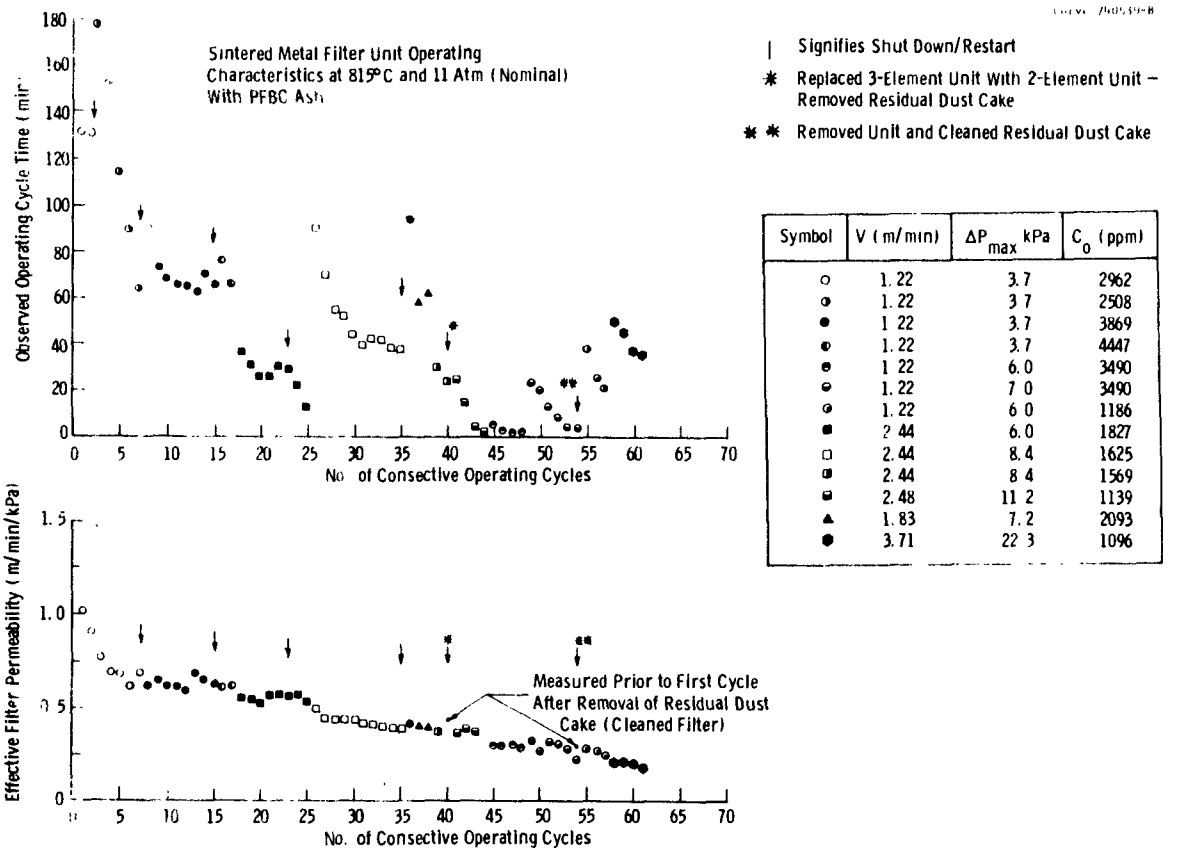

Symbol	V (m/min)	ΔP_{max} kPa	C_0 (ppm)
○	1.22	3.7	2962
◐	1.22	3.7	2508
●	1.22	3.7	3869
◐	1.22	3.7	4447
●	1.22	6.0	3490
◒	1.22	7.0	3490
◑	1.22	6.0	1186
■	2.44	6.0	1827
□	2.44	8.4	1625
◪	2.44	8.4	1569
◪	2.48	11.2	1139
▲	1.83	7.2	2093
●	3.71	22.3	1096

Figure 9. Effective permeability of sintered metal filter unit and residual dust cake at 815°C and 11 atm (nominal) with PFBC ash.

strong attribute for this type of filter, as is the ease with which they can be mounted and configured in a real system. The question of filter stability or blinding can not be definitively answered on the basis of these short-duration tests, but there was indication that stable behavior may be possible at relatively low filter velocities (1.2 m/min) as well as the possibility of unstable behavior at higher velocities. A final issue that was not addressed is the corrosion resistance of sintered metal filters in actual coal-burning applications where various sulfur and alkali metal compounds exist.

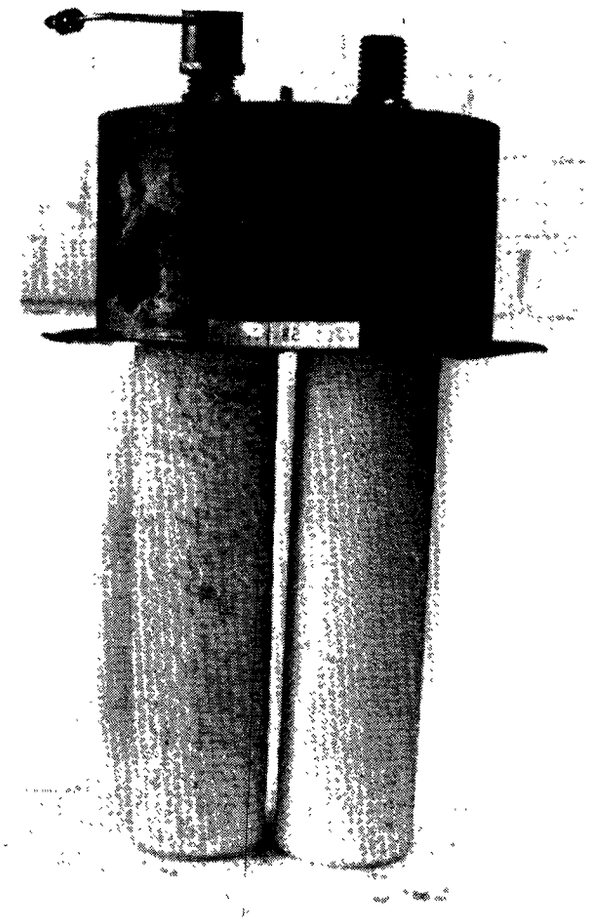

Figure 10. Posttest condition of sintered metal filters.

MOVING BED-CERAMIC FILTER FOR HIGH-EFFICIENCY PARTICULATE AND ALKALI VAPOR REMOVAL AT HIGH TEMPERATURE AND PRESSURE

By: D. Stelman, A. L. Kohl, C. A. Trilling
Rockwell International Corporation
Energy Systems Group
8900 De Soto Avenue
Canoga Park, California 91304

ABSTRACT

A moving bed-ceramic filter for high-temperature gas cleanup is described. The concept employs a high-efficiency ceramic filter that is cleaned continuously by the slow downward motion of a thin layer of granular material. Laboratory tests have been conducted with a variety of dusts carried in gas at temperatures up to 1500°F and at atmospheric pressure. The observed particle removal efficiency from a 1500°F gas containing 1 grain/scf of 1.6 micron median diameter particles was found to exceed 99.96%. The pressure drop across the filter was only 3.5 in. of water at a gas velocity of 13 ft/min. It remained essentially constant as a result of the continuous removal of the filter cake from the face of the ceramic filter by the slowly moving granular bed. In addition to particle removal, the filter offers the potential for alkali vapor removal through the use of reactive getters in the moving bed material.

INTRODUCTION

Coal-fired combined gas turbine-steam turbine cycles such as a fluidized bed combustion combined cycle or a low- or medium-Btu coal gasification combined cycle offer the potential for improved thermal efficiency and reduced cost with acceptable environmental impact. However, the combustion products or fuel gases produced by these processes must be purified because they contain particles and vapors that are corrosive and erosive to a gas turbine. The main problem is that for maximum thermal efficiency the purification should be performed at high temperature and pressure. For long-term turbine operation, the principal impurities that have to be removed are erosive particles and corrosive alkali compounds that are present both as particles and vapors.

This problem has stimulated interest in a variety of potential high-temperature filtration techniques, some directed at removing particles and others at removing alkali vapor. In the case of particle removal by fabric filtration, the high temperatures involved in this application dictate the use of ceramic fiber filter media.

Removing the dust cake from ceramic bags can be a problem. Ceramic fibers for high-temperature applications are brittle, and attempts to employ pulse-jet cleaning have encountered problems with ceramic fiber bags rupturing or tearing. In light of these difficulties, it is reasonable to explore alternative methods of cleaning high-temperature ceramic filters.

The Rockwell filter system uses a continuous-duty ceramic fiber filter that does not use a back pulse to clean the dust cake from the filter. Rather, it uses a thin moving bed of sand-like particles to continuously and gently remove deposited dust particles from the surface of the ceramic fiber sheet.

DESCRIPTION OF ROCKWELL MOVING BED-CERAMIC FILTER CONCEPT

The moving bed-ceramic filter concept is shown in Figure 1. The right side of Figure 1 shows a single filter element; the left side shows the filter elements arranged in interlocking leaves. The filter is a combination of a moving granular bed and a ceramic filter. Dirty gas is introduced into a downward moving bed through a set of louvers. The gas flows perpendicularly to the moving bed and exits through the ceramic filter sheet. A small portion of the dust is removed by the bed, and the balance by the ceramic filter sheet. The concept eliminates the damaging back pulse. The moving bed continuously and gently scrubs the deposited dust particles from the surface of the ceramic filter sheet.

Moving bed filters alone do not show adequate particle removal efficiencies (1). Since the moving bed, in the Rockwell design, is not the primary filter, it can be much thinner than "conventional" granular bed filters. The bed material does not need to be free of fines. In fact, the

presence of some relatively fine particles in the bed aids filtration. The interlocking leaf design permits a large filtration area to be contained in a relatively small pressure vessel.

The system does not require pulsing or interruptions in the flows of gas or bed material, operations that tend to cause "spikes" of dirty gas and require high-temperature, high-pressure valves in other systems.

A reactive or adsorbent material can be added to the bed to remove vapor-phase impurities. The filter is thus expected to remove alkali vapors from the gas with high efficiency by using a variety of adsorbent materials (2-5). The filter will also remove traces of tar without plugging. The tar can be removed from the bed by combustion or solution in light hydrocarbons.

In summary, the Rockwell filter is basically a fabric filter except that it uses an unconventional cleaning method (i.e., a moving granular bed). The cleanup of the gas is done almost entirely by the ceramic filter. The function of the moving bed is to clean the filter, although it does remove some of the particles. The advantages of the moving bed-ceramic filter are:

1) High-efficiency particulate removal at high temperature-high pressure.
2) High gas throughput with low pressure drop and no increase in pressure drop with time.
3) Continuous filtration without pulsing or flow interruptions.
4) No need to have the bed free of fines.
5) Vapor-phase impurity (sodium, potassium) removal capability through use of reactive or adsorbent material.
6) Removal capability for traces of tar.

EXPERIMENTAL RESULTS

The objectives of the experimental program conducted to date have been to:

1) Demonstrate filter operation at high temperature.
2) Evaluate the effect of the moving bed on dust cake removal.
3) Establish overall filter performance, collection efficiency, pressure drop, and pressure drop increase with time.
4) Investigate different dusts, bed materials, and filter materials.

LABORATORY TEST APPARATUS

The laboratory test apparatus is shown in Figures 2 and 3. The test procedure consisted of (1) injecting about 1 grain/scf of dust particles into the inlet stream; (2) heating the gas stream to the test temperature;

(3) measuring the pressure drop across the filter versus time with no bed, with a stationary bed, and with a moving bed; and (4) measuring the particle concentration in the outlet gas stream.

The materials tested are listed in Table 1.

TABLE 1. MATERIALS TESTED

Dusts	1.6-micron alumina (Glennel Corporation)
	3-micron salt fume (from Rockwell Molten Salt Test Facility)
	25-micron alumina (Buehler, Ltd.)
	50-micron fly ash (Ottertail Power Company)
Bed Materials	28 by 48 mesh alumina
	40 by 70 mesh silica
Ceramic Filter	Saffil alumina paper (ICI America)

Figure 4 shows the size distribution of the redispersed test dusts as measured with a cascade impactor in the inlet gas stream.

The face of the test filter was 2 in. wide and 1 ft long. The bed was 7/8 in. thick. The hopper on the dust feeder had a 2-h capacity.

The test conditions and results are summarized in Table 2. The results are discussed in more detail below.

TABLE 2. SUMMARY OF TEST CONDITIONS AND RESULTS

Conditions	
Temperature	900 to 1500°F
Air-Cloth Ratio	9 to 14 acfm/ft^2 (afpm)
Inlet Dust Loadings	0.8 to 3.8 grains/scf
Moving Bed Velocity	3.1 to 7.5 ft/h
Results	
Outlet Dust Loadings	Below detection limit
Removal Efficiency	>99.96%
Pressure Drop	1.5 to 4.7 in. water

EXPERIMENTAL VERIFICATION OF DUST CAKE REMOVAL BY MOVING BED

In these experiments, the system was operated with and without dust particles and with no bed, stationary bed, and moving bed. The effect of these variables on the pressure drop across the filter was observed. (The buildup of a dust deposit causes the pressure drop to rise. However, if the moving sand continuously removes the dust deposit, the pressure drop remains constant.)

Since fluctuations in the gas flow rate or temperature also affect the pressure drop, such extraneous variables can obscure the observation of the desired effect. Therefore, the results are presented in terms of the "flow resistance" rather than the pressure drop. The "flow resistance" is independent of the flow rate and temperature,[1] but does increase as dust deposits accumulate. The flow resistance is defined as the ratio of the pressure drop to the air-to-cloth ratio:

$$\text{flow resistance} = \frac{\Delta P \text{ (in. } H_2O)}{\text{air/cloth (afpm)}} \, . \tag{1}$$

The flow resistance of the system filtering fly ash with initially clean Saffil when no bed material was present is shown in Figure 5. The plot shows what happens when the dust feeder was turned on, off, on again, and finally off. As expected, the flow resistance increased during the first 40 minutes due to the buildup of a dust layer. When the dust feed was shut off, the resistance remained constant. When the dust feed was turned on again, the flow resistance again increased until the dust feed was turned off.

Figure 5 shows that the accumulating dust layer caused the pressure drop to rise at the rate of 0.88 in. H_2O/h. (The pressure drop is equal to the flow resistance times the air-to-cloth ratio.) Thus, if nothing were done to remove the dust layer, the pressure drop would continue to rise, and eventually, the filter would become useless.

The dust layer was left on the Saffil paper, and silica sand was added to the system slowly over a 1-day period. Point A in Figure 6 shows the condition of the system after the sand had been added. The drop in the flow resistance from 0.29 in. H_2O/afpm at the end of the test as shown in Figure 5 to 0.21 in. H_2O/afpm at Point A in Figure 6 was due to part of the dust layer having been knocked off during the addition of the sand. From A to B, the sand was stationary, and the flow resistance was constant. At Point B, the sand feeder was turned on. The flow resistance immediately dropped as the dust layer was removed by the moving sand. The flow resistance leveled out at 0.123 in. H_2O/afpm and remained there. At Point C, the dust feeder was turned

---

[1] There is actually a temperature-dependent viscosity effect, but for the small temperature fluctuations in these experiments, the correction is negligible and was ignored.

on. The flow resistance rose slightly for 10 minutes and then remained constant thereafter at 0.133 in. H_2O/afpm. Without the moving sand, in about 2 h the pressure drop would have more than doubled (Figure 5). Instead, the pressure remained constant to better than +0.7% at 1.46 in. H_2O.

To summarize, Figure 5 showed the formation of a dust cake on the back surface (since there was no sand in the bed at that time). Figure 6 showed the removal of that dust cake from the back face by the motion of sand through the device (Point B to Point C). From Point C to Point D, the figure shows that when dust is being fed, the motion of the sand bed kept the pressure drop from rising, presumably because the dust cake was being removed continuously by the moving sand bed.

We now turn our attention to the performance of the complete filter, that is, to experiments where there is sand in the bed from the outset.

As shown in Figure 7, pressure taps were located at the filter inlet, in the moving bed just in front of the ceramic filter sheet, and at the outlet of the filter. Using three differential pressure gauges as shown in the figure, the combined pressure drop across the louvers and the sand bed, the pressure drop across the ceramic filter sheet, and the total pressure drop across the filter were obtained. The bed extended beyond the edges of the louvers and the ceramic filter sheet so that the gas could not short circuit the sand bed by a low-resistance path along the side walls.

Figure 8 shows test results obtained at 1500°F with coarse (25-μm mass median diameter) alumina dust using an alumina bed. Figure 8 starts with the alumina bed flowing. Note that the main pressure drop was across the ceramic filter sheet. When the dust feeder was turned on, there was an initial perturbation, but after 10 min, the flow resistance returned to its initial value and remained constant until the bed flow was stopped. With the bed stationary, the total pressure drop instantly started to increase at an average rate of 2.6 in. H_2O/h. Note that the dust cake formed on the front face when the sand flow was stopped. With dust still being fed, the bed feed was restarted. There was an instant drop in the flow resistance, followed by a steady decline toward the initial value.

When the sand flow was restarted, the dust cake on the front face broke up. The incoming dust no longer accumulated on the front face. The incoming dust, together with the dust from the disintegrating dust cake, was swept through the thin moving bed (7/8 in. thick) by the gas flow (13 ft/min). The gas carried the dust to the back face where, instead of accumulating on the ceramic filter sheet, the dust was continuously removed by the moving bed (4 ft/h).

In tests with 50-μm fly ash, 25-μm alumina dust, and 3-μm salt fume at bed velocities of about 4 ft/h, we found no increase in pressure drop with time. With finer dust (1.6-μm alumina), however, the pressure drop did increase continuously with time at the same bed velocity (4 ft/h) used with the larger particle-size dusts. This indicated that finer dusts require a higher bed velocity to clean the dust cake off the ceramic filter sheet. The

data for 1.6-μm alumina dust at two bed velocities (4.0 and 7.5 ft/h) are shown in Figure 9.

At both velocities, the main pressure drop was across the back half. At the 4-ft/h bed velocity, the total pressure drop increased with time. As the figure shows, the pressure drop across the front face was relatively constant. The increase was occurring on the back face, probably because the dust cake on the ceramic filter was building up at a rate faster than the bed could remove it. When the bed velocity was increased from 4 to 7.5 ft/h, there was no effect on the front face, but the pressure drop across the back face dropped significantly, presumably because of the increased rate of removal of the dust cake from the ceramic sheet. The corresponding decrease in the total pressure drop was, therefore, due entirely to the increased rate of cleaning of the ceramic sheet.

Thus, the filtration process and the pressure drop occurred primarily at the back face. The removal of the dust cake from the ceramic sheet and achievement of a constant low total pressure drop were adequately controlled by the velocity of the moving bed. Test results indicate that very fine dusts require a higher bed velocity than coarser dusts in order to clean the dust off the ceramic filter sheet.

To summarize, the effect of the moving bed on the performance of the filter as illustrated in Figures 5 through 9 can be described as follows:

1) Without the sand bed or with a stationary sand bed, there was a continuous rise in the pressure drop.
2) With the moving bed, the pressure drop remained constant.
3) The moving bed provided continuous cleanup of the ceramic filter, even when there is an initial dust cake.

EXPERIMENTAL COLLECTION EFFICIENCY

The outlet dust loading was measured by passing the entire outlet stream through a 6-in.-diameter Gelman Type A/E glass fiber aerosol filter. The change in weight was measured on an analytical balance with 0.2-mg sensitivity. In every case (even for test with 1.6-μm alumina dust or 3-μm salt fume), the downstream dust concentration was less than the amount that could be detected. Therefore, at the present time, only a lower limit to the efficiency can be given. Based on the sensitivity of the instruments used for all of the tests conducted so far, this lower limit on the efficiency is conservatively established as 99.96%. For those tests which ran longer and used higher inlet loadings such as shown in Figure 8, the lower limit on the efficiency was 99.999%.

EROSION CONSIDERATIONS

When any two surfaces are rubbed together, they will erode and ultimately wear out. This would not be acceptable for a practical filter.

In the preceding experiments, we were primarily concerned with determining whether or not a constant pressure drop could be established by the action of the moving bed. We chose to keep the pressure drop at its initial dust-free value. Operating in this way, we can expect the filter to wear out. Considering this fact, it becomes clear that it is not desirable to completely remove the dust cake from the back face. Instead, a bed velocity should be chosen such that the pressure drop is allowed to rise to some acceptable value in order to form a protective steady-state dust cake on the ceramic filter. By choosing a bed velocity such that the dust cake is never completely removed, the bed material will never come in direct contact with the ceramic filter element. The only erosion that would be expected to take place would be steady-state erosion of the surface of the dust cake. The portion of the cake that erodes is replaced by incoming dust. In this way, even soft filter materials may be rendered immune to erosion.

Since the top of the filter receives the least amount of dust from the inlet gas stream, it will be helpful to have some fines circulated with the bed material for the purpose of augmenting the protective dust cake at the top of the filter. Consequently, when the bed material is reused, it should only be partially cleaned so that some fines remain in it.

BED MATERIAL RECYCLE

In the present study, the bed material was used once and discarded. In applications where the bed material is reused, it will be necessary to separate some, but not all, of the collected dust from the bed material. As discussed in the previous section, it is desirable to retain some fines in the bed material.

In traditional moving beds, the media must be cleaned completely of all dust. This is accomplished by fluidizing the mixture (6,7). Because the dust is much finer than the bed material, the dust is entrained in the fluidizing gas and is carried off while the bed material remains behind.

A practical example of such a bed cleaning and recycle system shown in Figure 10 consists of a pneumatic circulation system that withdraws the dirty bed material from the bottom of the filter and transports the material to an overhead deentrainment vessel (a large-diameter section of pipe or a cyclone), where the bed material and part of the dust drops out and feeds by gravity into a fluidized bed where the bed material has the last traces of dust removed (6). The dust-laden transport and fluidizing gas goes to a bag filter where the dust is collected. The cleaned bed material flows by gravity from the bottom of the fluidized bed back into the filter. The system has no moving parts, making it ideal for circulating and cleaning the hot bed material.

In the present case where it is desirable to retain some of the dust in the bed media, the same system with the fluidized bed omitted seems appropriate for the purpose.

It is not always necessary or desirable to recycle the bed material. For example, in the application of the Rockwell filter to a fluidized bed combustion combined cycle, the Rockwell filter should be able to use the spent dolomite or limestone sorbent discharged from the PFBC, as illustrated conceptually in Figure 11. The spent sorbent would already be hot and at pressure, so there would be no heat losses associated with the moving bed and no additional lock hoppers required. In this application, any alkali vapor getter added to the system would be added to the coal-sorbent mixture and injected directly into the PFBC.

ALKALI VAPOR REMOVAL CAPABILITY

A reactive or adsorbent material can be added to the bed to remove vapor-phase impurities. The filter is thus expected to remove alkali vapors from the gas with high efficiency by using a variety of adsorbent materials.

The gettering of alkali vapor by a reactive bed has been extensively studied experimentally by others (2-5). The techniques used involve the use of materials capable of chemically or physically absorbing alkali vapors. Suitable materials include clay minerals, silicas, aluminas, aluminosilicates, ash from certain coals, and industrial glasses. A wide variety of such materials has already undergone testing.

For example, Argonne National Laboratory has obtained 98% alkali vapor removal in 3-in.-thick fixed beds of -8 +10-mesh diatomaceous earth at gas velocities of 50 ft/min (4a). They have also achieved 98% alkali vapor removal with activated bauxite (4b).

Thus, it appears that it is not only technically feasible to remove alkali vapors by using reactive bed materials in the Rockwell filter, but also that the dimensions of the bed and the gas velocities in this filter offer contact times similar to those stated above.

In a recent study (8), laboratory data for various getters were scaled up to commercial size. It was calculated that a fixed bed 1 to 10 m (3 to 33 ft) thick would be required to prevent alkali vapor breakthrough for a period of 1 year. The use of such a thick fixed bed probably represents an undesirably large pressure drop.

If the Rockwell moving bed-ceramic filter were used for alkali vapor removal rather than a thick fixed bed, the main difference would be that the getter passes through the Rockwell filter in 1 to 2 h and not 1 year. For simplicity, if we scale the values given above linearly, then taking a worst case of 10 m (33 ft) thick with breakthrough in 6 months (4000 hours) would correspond to the requirement of a bed 0.20 in. thick to prevent breakthrough of alkali vapor for 2 h.

In the present experiments, the bed thickness was arbitrarily chosen at 7/8 in. That value can be increased or decreased to suit other purposes without adversely affecting the performance of the filter for particle removal. However, it appears that such thin beds would also be acceptable for

alkali removal. One would expect the Rockwell filter to perform both tasks in a single pressure vessel at a lower overall pressure drop.

COMPARISON WITH PRESENT STATE OF THE ART

In this section, the performance of the moving bed-ceramic filter is compared to (1) conventional commercial low-temperature fabric filters and (2) state-of-the-art high-temperature fabric filters.

COMPARISON WITH CONVENTIONAL LOW-TEMPERATURE FILTERS

The Rockwell high-temperature filter is basically a fabric filter except that it employs an unconventional cleaning method (i.e., a moving bed). Therefore, it is of interest to compare its efficiency, air/cloth ratio, and pressure drop to those of conventional low-temperature commercial fabric filters. On the basis of the experimental results discussed above, it can be seen that the efficiency of the Rockwell high-temperature filter (>99.96%) is about the same as that of commercial low-temperature fabric filters.

A comparison of the air/cloth ratio and pressure drop is given in Table 3.

TABLE 3. COMPARISON OF AIR/CLOTH RATIOS AND PRESSURE DROPS

Fabric Filter Type	Air/Cloth Ratio (afpm)	Pressure Drop (in. H_2O)
Commercial Low Temperature		
Reverse Air Type	1 to 2	3 to 6
Shaker Type	2 to 4	3 to 10
Pulse Jet Type	5 to 15	6 to 10
Rockwell High-Temperature Filter (900 to 1500°F)	9 to 14	1.5 to 4.7

Thus, the Rockwell filter operating in the high-velocity range of commercial fabric filters shows a very low pressure drop. Because of this low pressure drop, it is expected that the filter can be operated at higher air/cloth ratios than were used in these tests. Therefore, one must conclude that it will be smaller in size than the most compact commercial low-temperature fabric filters currently available.

COMPARISON WITH HOT MOVING BED FILTERS

The Rockwell filter employs a moving bed to clean the dust cake off the ceramic filter. Therefore, it has some similarity to the CPC moving bed filter; however, when one considers that a 16-in.-thick CPC moving bed

achieves 86 to 99.5% efficiency (6) while the 7/8-in.-thick Rockwell filter achieves >99.96% efficiency, it is clear that the similarity is superficial. The ceramic filter and not the moving bed is responsible for the high efficiency of the Rockwell filter.

COMPARISON WITH HOT FABRIC FILTER

Table 4 compares the performance of the Rockwell filter to that of hot fabric filters under development. Acurex tested filter bags made from ceramic papers, felts, and woven cloths but found that they burst when back-pulsed (9). For that reason, they finally selected 1-cm-thick thermal insulation blankets made of Saffil. Three test programs using Saffil blankets were carried out as shown in the table (10-12). The earliest test reported much higher efficiencies than subsequent tests. The reason for this difference is that the dust used in the first test had no fines in it. It was dust from the second and third cyclone catches at the Exxon Miniplant and did not include the fine particles that are not collected by the cyclones. The second Acurex test was done on-line, downstream from the second cyclone at the Exxon Miniplant, and thus contained the complete particle size distribution. The third test used the second cyclone catch with added fines (12). These results indicate that some of the finer particles pass through the Acurex ceramic blanket.

TABLE 4. COMPARISON OF HOT CERAMIC FILTERS

	Face Velocity (ft/min)	ΔP (in. H_2O)	Temp (°F)	Mass Mean Particle Diameter (μm)	Efficiency (%)	Longest Test Duration (h)
Acurex (10)	5-18	<3 cyclic	1500	4 & 19	99.96-99.99	200
Acurex (11)	8-16	1-40 cyclic	1300-1500	4	96-99.5	17
Acurex (12)	10	28-52 cleaned*	800-1500	15	99.5-99.8	50
Buell/3M (12)	2-6	1-6 cyclic	800-1500	15	99.2-99.9+	50
Rockwell	9-14	1.5-4.7 steady	900-1500	1.6	>99.96	41

*Pressure drop after the cleaning cycle at 10 and 50 hours, respectively

The Buell/3M filter uses a woven ceramic fiber bag which has been cleaned by shaking, reverse flow, and back-pulsing. The reported design face velocity is 2 ft/min (13). This means that the Buell/3M filter is larger than the other filters by a factor of approximately 4 to 10. The Buell/3M filter was tested for EPRI at Westinghouse (12).

Of the three filters, the Rockwell filter was challenged by the finest dust. Even so, it appears to have an efficiency equal to or greater than the other filters.

There are several subtle differences between a conventional fabric filter and the Rockwell moving bed-ceramic filter. In a conventional filter, the thickness of the dust cake increases with time, causing the pressure drop to rise. When the pressure drop becomes excessive, a back pulse is applied. Except as indicated in the footnote to the table, the high and low points in the cleaning cycle of the Acurex and Buell/3M filters are given in the table. The average pressure drop was somewhere between these limits. In the Rockwell filter, the dust cake was continuously removed by the moving bed. For a given dust load and sand velocity in the filter, the dust layer reached a steady-state thickness and then remained constant. The pressure drop also remained constant at that point. The constancy of the pressure drop and the absence of pulsing are responsible for the difference in behavior of the two types of filter with regard to the relationship between the gas velocity and the pressure drop and collection efficiency.

If the dust cake has a constant thickness, the pressure drop varies as the first power of the velocity. In a conventional filter, the thickness of the cake increases with time and the rate of change of the cake thickness is directly proportional to the gas velocity. The net result is that the pressure drop across the changing dust cake in a conventional filter varies as the square of the gas velocity. Thus, while the pressure drop of a conventional filter varies as the square of the velocity (14,15), that of the Rockwell filter (with its constant thickness cake) varies as the first power of the gas velocity. For this reason, the Rockwell filter should have a lower pressure drop than a conventional filter. This appears to be borne out in Table 4 when one takes into account the fact that the other filters were cycling between the high and low values and the Buell/3M filter is being operated at a much lower velocity.

The second difference is the dependence of efficiency on gas velocity. When a conventional filter is pulsed, it temporarily loses its dust cake. Pulsing also causes some of the deposit to sift through the cloth; therefore, the greater the pulse activity, the lower the average collection efficiency (14). Since the pressure drop increases as the square of the velocity, the corresponding pulse frequency also increases as the square of the velocity. As a result, the efficiency of conventional filters normally decreases with increasing gas velocity (14). The Rockwell filter does not employ pulses and, therefore, should not suffer a loss of efficiency with increased velocity.

CONCLUSION

The Rockwell moving bed-ceramic filter has demonstrated its ability to remove even submicron particles at high temperatures with very high efficiencies. In tests at 900° to 1500°F using a variety of dusts, including 1.6-micron mass median diameter dust, the outlet dust concentration was so low that it could not be detected with the instrumentation being used. Therefore, only a lower limit on the removal efficiency can be given at the present time. The instruments were capable of detecting 3×10^{-4} and possibly

5×10^{-5} grain/scf under the conditions of the tests.[1] Depending on the test conditions (i.e., inlet grain loading and duration of the tests), the lower detection limit in the various tests corresponded to removal efficiencies of 99.96 to 99.999%.

The gas velocity in these tests was 9 to 14 afpm, and the pressure drop was 1.5 to 4.7 in. of water. Compared to commercial low-temperature fabric filter operation, these test velocities are equal to the upper velocity limit of commercial fabric filters, but the pressure drop of the Rockwell filter is less than half that of commercial fabric filters. Because of its low pressure drop, it is expected that the Rockwell filter can be operated at higher velocities than those used in these tests. Therefore, one must conclude that it will be smaller in size than the most compact commercial low-temperature fabric filters available.

The system provides continuous filtration without pulsing or interruptions in the flows of gas or bed material, operations that tend to damage ceramic bags, cause "spikes" of dirty gas; and require high-temperature, high-pressure valves in other systems.

Since the moving bed in the Rockwell design is not the primary filter, it can be much thinner than "conventional" granular bed filters. The bed material does not need to be free of fines. In fact, the presence of some relatively fine particles in the bed aids filtration and the formation of a protective dust cake. In some applications, such as PFBC, it is not necessary to clean or recirculate the bed material. The filter should be able to use the hot spent dolomite sorbent discharged by the PFBC. This would also eliminate the need for additional lock hoppers.

A hot-gas cleanup system suitable for a combined cycle must remove both particles and alkali vapors. The Rockwell filter has the distinct advantage of having the potential to satisfy both these needs. The use of an alkali getter material in the moving bed is expected to make the Rockwell filter capable of removing both particles and alkali vapor.

The work described in this paper was not funded by the U.S. Environmental Protection Agency and therefore the contents do not necessarily reflect the views of the Agency and no official endorsement should be inferred.

[1] The value of 3×10^{-4} grain/scf corresponds to a weight gain five times greater than the sensitivity of the balance on which the sampling filter was weighed.

REFERENCES

1. Squires, A. M., et al. Panel Bed Filters. J. Air Poll. Control Assoc. 20:534 (1970); 21:204 (1971); 21:272 (1971).

2. Phillips, K. E. Energy Conversion from Coal Utilizing CPU-400 Technology. FE-1536-30, Vol. 1, March 1977.

3. Chamberlin, R. M., et al. An Investigation of Hot Corrosion and Erosion in Fluid Bed Combustor-Gas Turbine Cycle Using Coal as Fuel. FE-1536-30, Vol. 2, Appendix B, May 5, 1977.

4. Johnson, L., et al. Support Studies in Fluidized-Bed Combustion. (a) ANL/CEN/FE-78-3, March 1978; (b) ANL/CEN/FE-77-11, January 1978.

5. Chamberlin, R. M., et al. Advanced Coal Gasification System for Electric Power Generation. FE-1514-45, January 1976.

6. Wade, G., et al. Granular Bed Filter Development Program Final Report. FE-2579-19, April 1978.

7. Stringer, J., et al. Assessment of Hot Gas Cleanup Systems and Turbine Erosion/Corrosion Problems in PFBC Combined Cycle Systems. ASME Gas Turbine Conference, San Diego, California, March 12-15, 1979.

8. Mulik, P. R., et al. High-Temperature Removal of Alkali Vapors in Hot Gas Cleaning Systems. DOE/METC Second Annual Contractors' Meeting on Contaminant Control in Hot Coal Derived Gas Streams, February 17-19, 1982, Morgantown, W. Virginia.

9. Shackleton, M. A. and Kennedy, J. Ceramic Fabric Filtration at High Temperatures and Pressures. In: EPA/DOE Symposium on High Temperature High Pressure Particulate Control, Washington, D.C., September 20-21, 1977. p. 194.

10. Shackleton, M. A. and Drehmel, D. C. Barrier Filtration for HTHP Particulate Control. In: Symposium on the Transfer and Utilization of Particulate Control Technology, Denver, Colorado, July 24-28, 1978. Vol. 3, p. 441.

11. Ernst, M., et al. A Regenerative Limestone Process for Fluidized Bed Coal Combustion and Desulfurization. Monthly Report 107, EPA Contract 68-02-1312, March 7, 1979.

12. Ciliberti, D. F. and Lippert, T. E. Evaluation of Ceramic Fiber Filters for Hot Gas Cleanup in Pressurized Fluidized-Bed Combustion Power Plants. EPRI CS-1846, May 1981.

13. Furlong, D. A. and Shevlin, T. S. Fabric Filtration at High Temperatures. In: Proc. of the Sixth International Conference on Fluidized Bed Combustion, Atlanta, Georgia, April 9-11, 1980. Vol. 2, p. 294.

14. Lucas, R. L. Gas-Solid Systems. Chemical Engineer's Handbook, 5th edition, Perry & Chilton (ed.). McGraw-Hill, New York, 1973. Chapter 20.

15. Billings, C. E., et al. Handbook of Fabric Filter Technology, Vol. 1, Fabric Filter System Study. PB200648, December 1970.

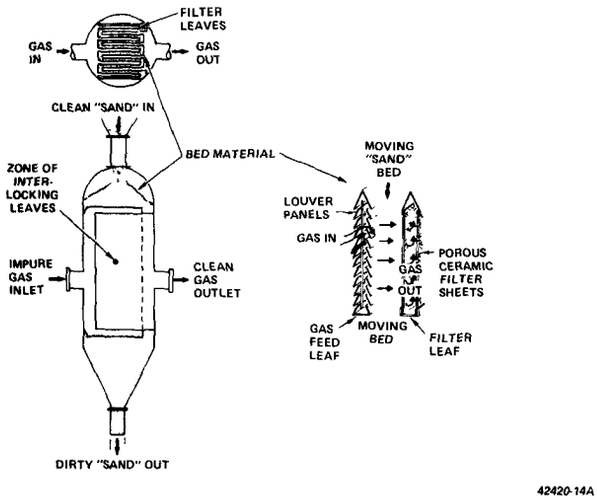

Figure 1. Rockwell Moving Bed — Ceramic Filter System Concept

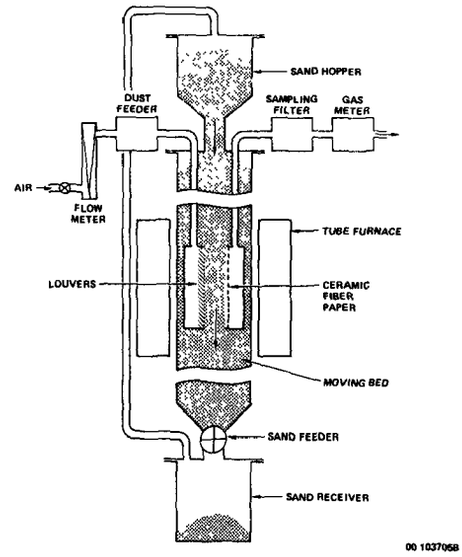

Figure 2. Moving Bed — Ceramic Filter Test System

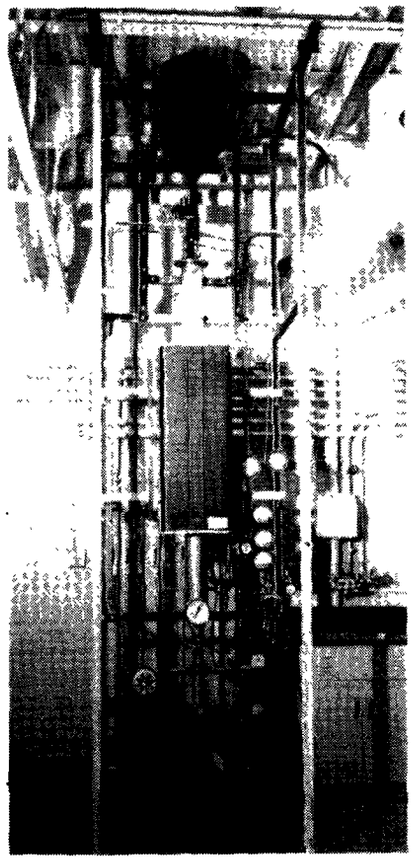

Figure 3. High Temperature Moving Bed — Ceramic Filter Test System

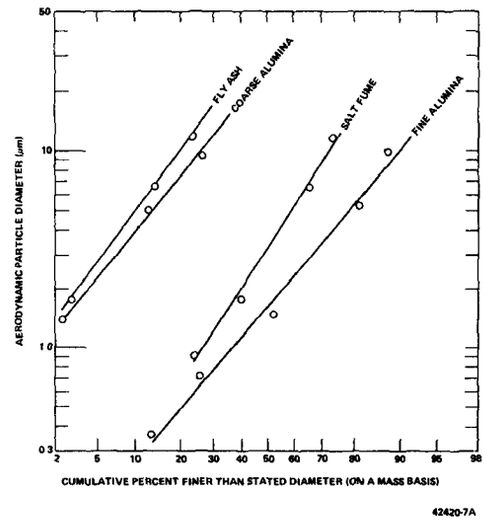

Figure 4. Size Distribution of Re-dispersed Test Dusts as Measured with Cascade Impactor in the Inlet Gas Stream

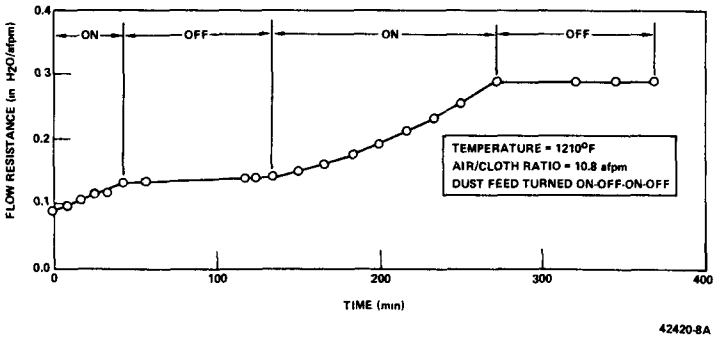

Figure 5. Filtration of Fly Ash with Clean Saffil Alumina Paper and No Bed

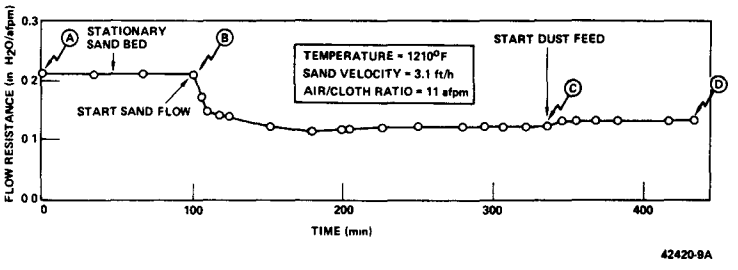

Figure 6. Filtration of Fly Ash with Initially Dirty Saffril Paper and Moving Silica Sand

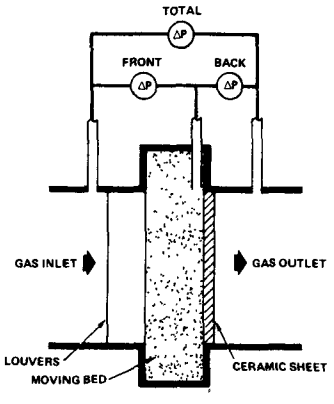

Figure 7. Top View Showing the Location of the Three Pressure Taps

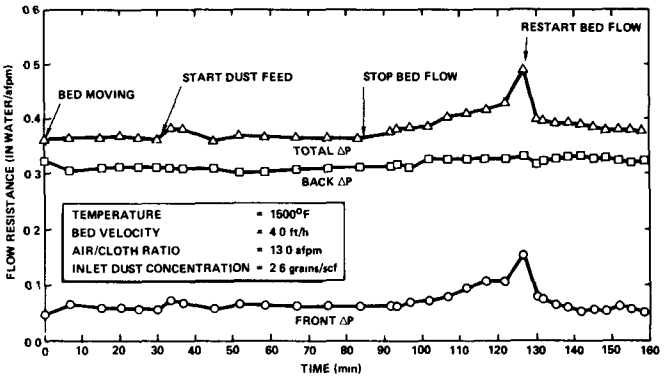

Figure 8. Filtration of Coarse Alumina Dust with Saffil Paper and Moving Alumina Bed

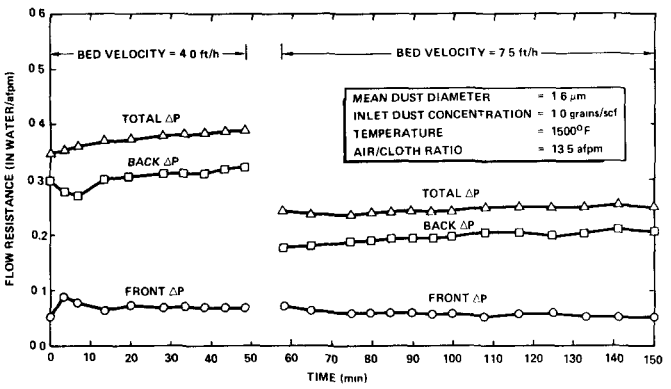

Figure 9. Filtration of 1.6 μm Fine Alumina Dust with Saffil Paper and Moving Alumina Bed at Two Bed Velocities

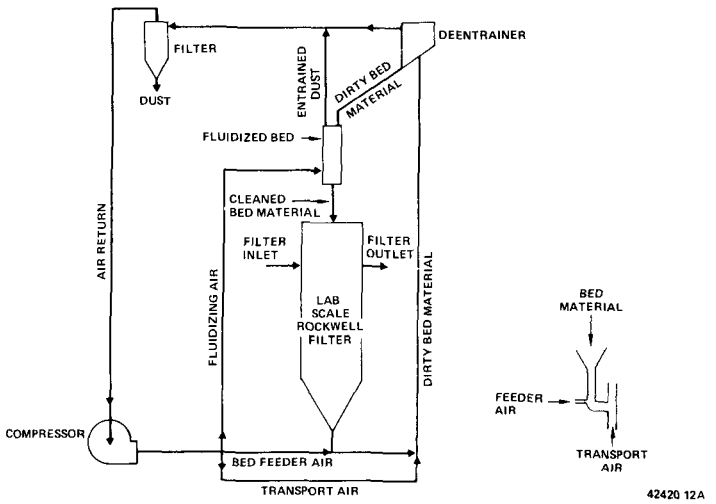

Figure 10. Bed Recycle System for Separating Dust from Bed and Recycling Cleaned Material to the System

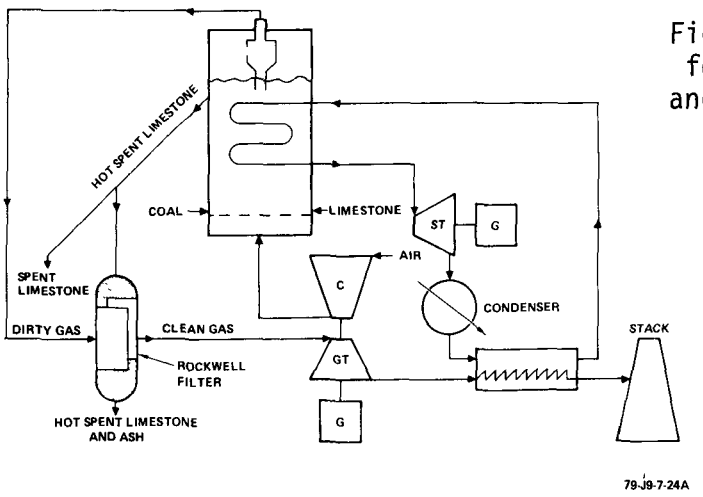

Figure 11. Non-Regenerative Fluidized Bed Combustor Combined Cycle System

TESTING AND VERIFICATION OF GRANULAR BED FILTERS FOR REMOVAL OF PARTICULATES AND ALKALIS

T. E. Lippert, D. F. Ciliberti, R. O'Rourke
Westinghouse Electric Corporation
Pittsburgh, PA 15235

The work described has been funded by the Department of Energy (DOE) under Contract DE-AC21-80ET17093.

ABSTRACT

The Granular Shallow Bed Filter (GBF) is proposed as a device to clean particulates from Pressurized Fluidized Bed Combustion (PFBC) gas streams. The GBF is a device in which the dust-laden gas passes through a shallow granular bed, depositing the particulate matter on the surface of the granular media. The bed medium is cleaned by a reverse flush that gently fluidizes the bed and elutriates the collected particulate matter from the system. Described herein are analyses and data that reflect on the GBF concept as it would apply to a PFBC and preliminary results of testing done on a six-element subpilot-scale GBF unit.

Results of systems analysis have shown an overall economic incentive for the GBF in PFBC compared to all-cyclone gas cleanup. Based on this analysis, performance goals for the GBF have been identified. A six-element, 24-bed, subpilot-scale GBF has been built and tested at both ambient and simulated PFBC conditions. Ambient flow tests were used as a basis to characterize the backflush system and evaluate candidate bed media. At simulated PFBC conditions, the test unit has been operated over 170 hours (cumulative), through 475 cleaning cycles in three test phases. Test variables have included bed media, filter flow face velocity, backflush conditions, and dust loading.

The work described in this paper was not funded by the U.S. Environmental Protection Agency and therefore the contents do not necessarily reflect the views of the Agency and no official endorsement should be inferred.

INTRODUCTION

The Westinghouse Electric Corporation with Ducon, Inc., and Burns & Roe Inc. are conducting a test and evaluation program of the Ducon Granular-Bed Filter (GBF) for gas cleaning applications in Pressurized-Fluidized Bed Combustion (PFBC) Power Plants.

Figure 1 shows a schematic diagram of one element of the subpilot-scale Ducon Granular-Bed Filter. The element shown consists of four parallel operating filter compartments or beds. Each compartment contains a granular filter bed through which the ash and dust-laden gas pass (Figure 1-a), depositing the ash and dust particles on the surface of the filter medium. With increasing deposits of the particulates, the system pressure drop increases until a point is reached when it is no longer practical or economic to operate. The GBF system is then cleaned by sequentially backflushing each element (Figure 1-b). For this purpose, a backflush motive air is introduced into an eductor at the outlet (clean-air side) of a filter element. The motive air passes through the eductor (inducing additional clean gas from the clean-air plenum) and into the GBF element housing, up through each filter bed at a velocity sufficient to gently fluidize each bed and dislodge the accumulated ash and dust material. The dislodged ash is elutriated and expelled from the element by passing back through the inlet opening provided at the top of each compartment. Figure 1 shows a four-bed element. Commercial-scale GBF systems would consist of multiple elements, each comprised of ten, twelve, or more parallel operating beds.

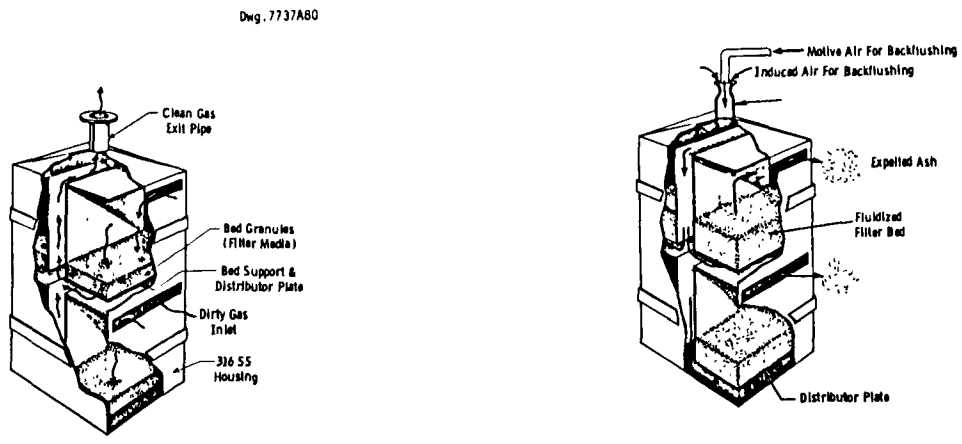

1a. GBF Element - Filtration Mode 1b. GBF Element - Cleaning Mode

Figure 1. Shallow bed GBF concept.

The major advantage for PFBC of the GBF over other advanced tertiary devices is its overall ruggedized construction, simplicity, and low operating costs. Its major technical issues are its ability to be effectively cleaned without dislodgement of filter media, and sustaining a high collection efficiency while maintaining a stable baseline pressure drop. Described herein are analysis and data that reflect on the GBF concept as it would apply to a PFBC and preliminary results of testing done on a subpilot-scale multielement GBF unit.

PFBC SYSTEMS WITH GRANULAR BED FILTERS

Gas cleanup for PFBC will require the removal of particulate to meet both turbine erosion tolerance and new source particulate emission standards and removal of alkali to reduce or minimize metal corrosion potential. The assessment of gas cleanup options for a PFBC must be based on technical feasibility and plant economics. For the GBF, a preliminary evaluation has been made of its relative economics and performance for two PFBC plant concepts, the PFBC Steam-Boiler and PFBC Indirect Air Cooled Plants, and a comparison made with PFBC plant designs that would utilize state-of-the-art cyclones for hot gas particulate clean-up. Overall conceptual designs for these plants are provided in References 1 through 6 and have been modified and used in this study. Table 1 provides a summary of the design basis for each plant concept. As indicated, there exist different assumptions between the PFBC concepts concerning combustor and turbine inlet design parameters. Thus comparison of PFBC concepts is not emphasized.

TABLE 1. PFBC PLANT CONCEPTUAL DESIGN BASIS

Dwg. 4756879

Design Parameter	Steam Cooled PFBC		Air Cooled PFBC	
	GBF	All-Cyclone	GBF	All-Cyclone
Standards	NSPS	NSPS	NSPS	NSPS
Coal Type	Eastern High S	Eastern High S	Eastern High S	Eastern High S
Net Power (MW_e)	648	648	462	462
Combustor Temperature (°F)	1750	1750	1650	1650
Combustor Pressure Ratio	11.5	11.5	7	7
Turbine Inlet Temperature (°F)	1664	1664	1600	1600
Gas Clean-Up				
Particulate	2 Stages Cyclone + GBF	3 Stages Cyclone & Stack Gas Filter	2 Stages Cyclone + GBF	3 Stages Cyclone & Stack Gas Filter
Alkali	Fixed Bed	Fixed Bed	Fixed Bed	Fixed Bed
Steam Conditions (psig/°F/°F)	2400/1000/1000	2400/1000/1000	835/800/700	835/800/700

In this study, plant cost comparisons are made only for the particulate removal systems. Figure 2 shows the overall economic incentive that would exist for the hot gas cleaning of particulates for the GBF as compared to all-cyclone systems. In the all-cyclone cases the gas cleanup costs include stack gas particulate removal to meet NSPS and costs for turbine stator and rotor blade replacement due to particle erosion. The all-cyclone case for each PFBC concept is shown for two different turbine-life assumptions. A six-month and one-year blade life is taken for the steam-cooled plant and a one- and two-year assumption for the indirect air-cooled plant. These differences in turbine life assumptions reflect differences in the expected dust loading at the turbine inlet of the respective plants.

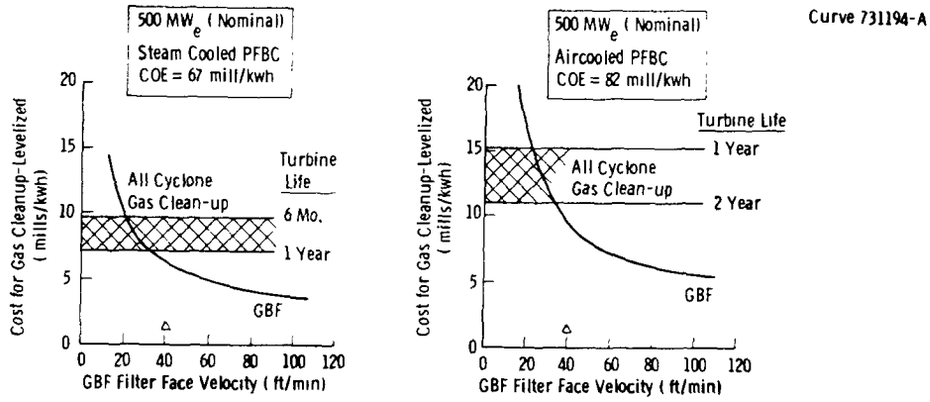

Basis: • Gas Clean-up Train Includes Primary Cyclone Thru to Expander Inlet
• Costs for Stack Gas Particulate Removal Included if Required to Meet NSPS
• Costs for Turbine Stator/Rotor Reblading

Figure 2. Comparison of gas cleanup costs for PFBC plants employing GBF or all-cyclones.

For the GBF case, gas cleanup costs are shown as a function of the assumed gas filter face velocity. The design point is taken at 40 ft/min. At this condition the particulate gas cleaning cost of electricity (COE) are shown as about 6.0 and 9.0 mill/kWh for the steam- and air-cooled designs respectively. The higher costs associated with the air-cooled case are the result of the larger volumetric gas flow per kilowatt that passes through the particulate removal system. In either case, the GBF costs (at design point) represent about 8 to 11 percent of total plant costs. As seen from the figure, operating at lower filter velocities significantly increases the gas cleaning costs. The increased number of filter units at the lower velocity along with the added cost and complexity associated with the gas piping act to nearly double the COE at 20 ft/min over the 40 ft/min case. Moving toward higher face velocities above 40 ft/min reduces costs, but the effects are less dramatic. The diminishing return at the higher velocities results from assumptions on maximum piping sizes and limiting gas velocities. These results suggest that pursuing high filter face gas velocity designs for GBF that impose increased technical risks may not

be justified in view of the relatively small incremental improvement in plant COE that is gained.

At the 40 ft/min nominal design point, the GBF cases are shown to be lower in costs than the most optimistic all-cyclone case. Lower turbine blade life and/or increased filter face velocities can significantly enhance the incentive for the GBF case. Real cost differences of 3 or 4 mills/kWh represent capital expenditures on the order of 35 to 50 million dollars.

The PFBC plant economics summarized above are based on assumed performance levels for GBF and its components. The choice of operating parameters for the GBF are not arbitrary, but with consideration of their overall impact on PFBC plant performance. Coupling the GBF with the PFBC plant must be in consideration of such parameters as inlet dust loading, system pressure drop, and backflush cycle and flow. A simplified PFBC systems model has been formulated that incorporates appropriate models for predicting the major process operations of the GBF and the equations for describing the overall PFBC system effects (7).

Results from this modeling have been used to identify test operating conditions for the GBF subpilot unit test program that would be representative of operating requirements for commercial-scale units. For this purpose, one concern has been the design and performance level necessary for the backflush eductor in the commercial-scale unit compared to what can be achieved on the smaller subpilot test unit. The sensitivity of the GBF eductor performance with both backflush time (t_{bf}) and average pressure drop (Δp_{avg}) is shown in Figures 3 and 4 for the steam-boiler PFBC concept. Similar analyses have also been conducted for the air-cooled plant design (7). The ordinate axis in Figure 3 shows the net energy penalty associated with GBF at the particular GBF operating point compared to a case where no GBF would be used. The quantity of motive air for the GBF backflush is dependent on the performance level of the eductor. Eductor performance is defined as X, the ratio of induced flow to motive flow. The total backflush flow requirement (motive + induced) is set by the bed medium fluidization and dust elutriation characteristics. The GBF operating pressure drop depends on its filtration and cleaning cycle, dust loading, and gas face velocity.

Results from the parametric analysis show (1) a rather pronounced sensitivity to backflush time with an indicated "optimum" between three and six seconds, (2) an "optimum" system pressure drop (different for the different plant concepts), and (3) near the optimum backflush time and pressure drop conditions, a general decreasing sensitivity to the performance of the backflush eductor.

The indicated optimums in the curves showing backflush time (Figure 3) result as a consideration of the physical design of the GBF elments and the assumed elutriation characteristics of the deposited

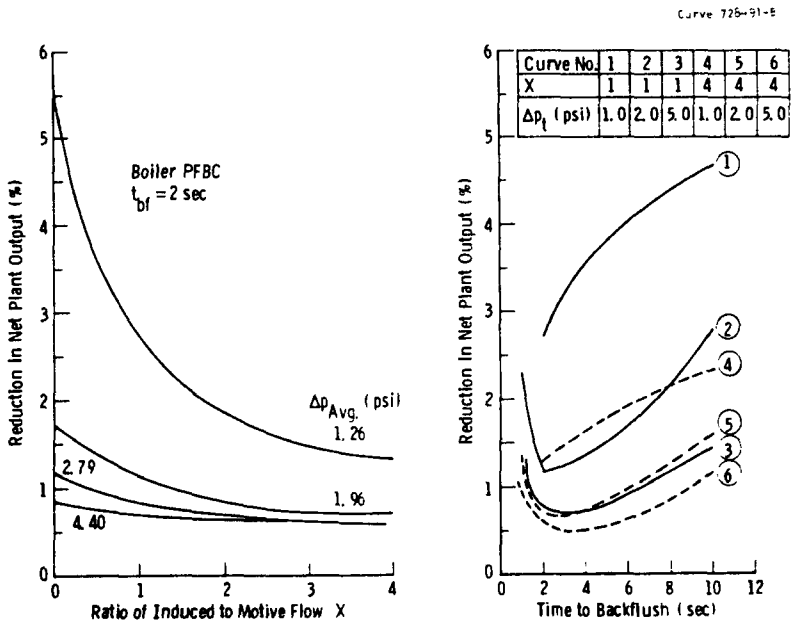

Figure 3. Effect of eductor performance and backflush time on PFBC cycle performance for boiler PFBC.

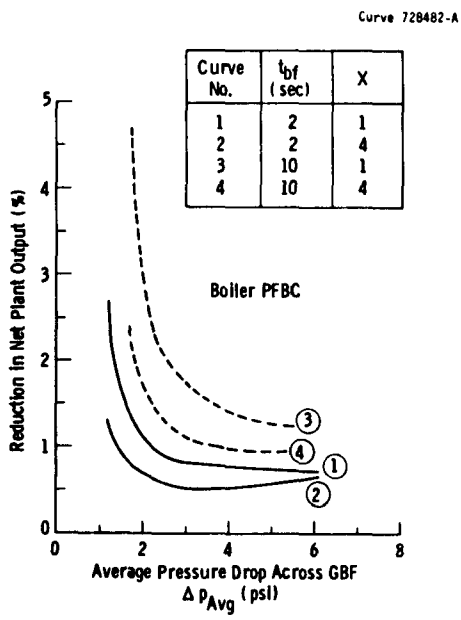

Figure 4. Effect of GBF operating pressure drop on PFBC plant performance for the boiler PFBC cycle.

dust cake. Below approximately a one-second backflush time, no cleaning would occur because of the finite time required for the elutriated dust to reach the opening in the element housing at the top of the freeboard. From about one second to the minimum point between three and six seconds, the effectiveness in elutriating dust is most pronounced, and the trade-off in compressor power (and the other factors) between shorter operating cycles or further cleaning favors the latter. Since the dust elutriation is itself dependent on the in-bed dust concentration, this trade-off shifts once sufficient dust has been removed from the bed. It should be emphasized, therefore, that the results indicated will be dependent on the validity of the elutriation model assumed. As the curves suggest, should the actual time to elutriate the dust from the individual GBF beds differ significantly from the indicated optimum, the sensitivity to both the eductor performance level and the GBF pressure drop on plant performance increases.

The GBF backflush cycle characteristics are dependent on the inlet dust loading, gas velocity, and allowed pressure drop. Pressure drop has both systems performance and element design implications. At the high operating temperatures (1600°F) in PFBC applications, low system pressure drop is favored to reduce mechanical design complexity and capital cost. For a fixed dust loading, low pressure drop implies a short filtration cycle and, as seen from the curves in Figure 4, results in a larger reduction in plant performance. The sensitivity of plant performance to eductor performance is aso increased. Increasing the system pressure drop increases total cycle time and, therefore, the fraction of time the GBF is on backflush is reduced, resulting in a reduced system loss. At some point, depending on plant design, this trend is reversed, and the impact of increased system pressure drop on plant performance becomes more detrimental. Although not indicated in the set of curves shown, it would be expected that lowering the inlet dust loading would shift the indicated ΔP_{avg} "optimums" towards lower values.

The principal conclusions for the GBF drawn from the above described analysis are as follows:

1. There exists an optimum set of GBF system operating parameters that correspond to minimum plant impact. At the optimum point, the overall penalty of the GBF on plant performance is approximately one percent or less.

2. GBF cleaning cycles of between three and six seconds appear optimum. These times represent considerably shorter backflush cycles than previously tested or thought necessary. Should significantly longer backflush times prove necessary to accomplish cleaning, larger overall plant performance penalties may be incurred.

3. The optimum operating pressure cycle for the GBF system varies with plant concept and inlet dust loading. Tolerable levels of

in-bed dust fines and operating temperature level may also be constraining factors.

4. The attainment of high eductor performance levels, i.e., ratio of induced to motive backflush flows greater than 3 or 4, would not appear to be a necessary objective for commercial GBF application in PFBC. The overall impact of the eductor performance appears relatively small except at frequent cleaning cycles. Flow ratios between one and two should be adequate if the indicated optimum backflush times are achievable.

GBF SUBPILOT SCALE TEST RESULTS

TEST UNIT DESIGN AND INSTRUMENTATION

The six-element, shallow bed granular filter test unit is shown in Figures 5 and 6. The test unit design is premised on a nominal flow of 500 acfm at 1600°F (870°C) temperature and operation at 11 atm pressure. The unit consists of six filter elements, each element containing four filtering compartments or beds as schematically illustrated in Figure 7. As the photograph of the test unit in Figure 6 shows, each GBF element attaches to the eductor section at flange connections. The eductors are each fixed (welded) to the dished head and flange support section. The dished head and flange support section separate the dirty and clean gas sides of the filter unit. The flange section clamps between the vessel and vessel dome section Figure 5. In each bed of each element there exist provisions for both a thermocouple

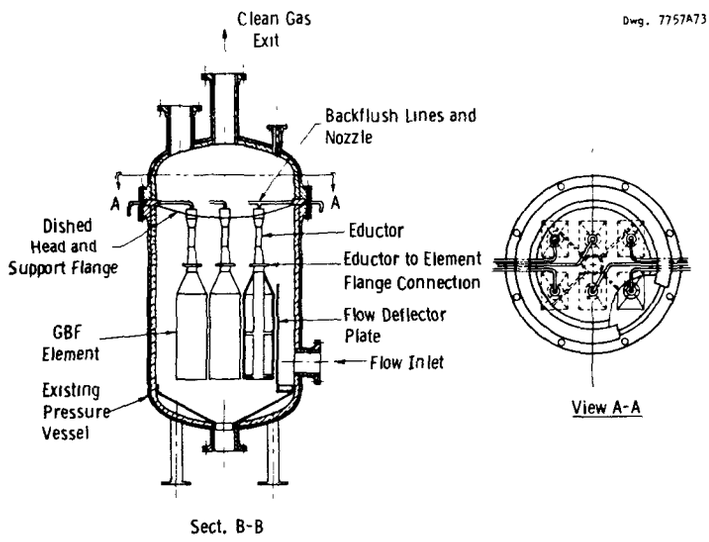

Figure 5. General arrangement of six-element GBF subpilot-scale test unit.

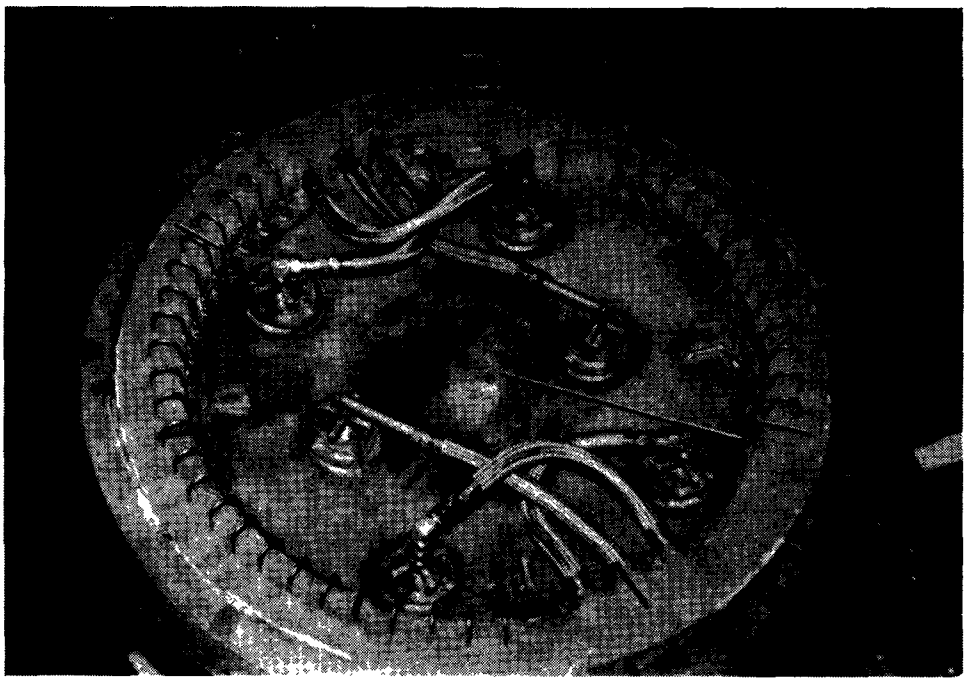

6a. Top view

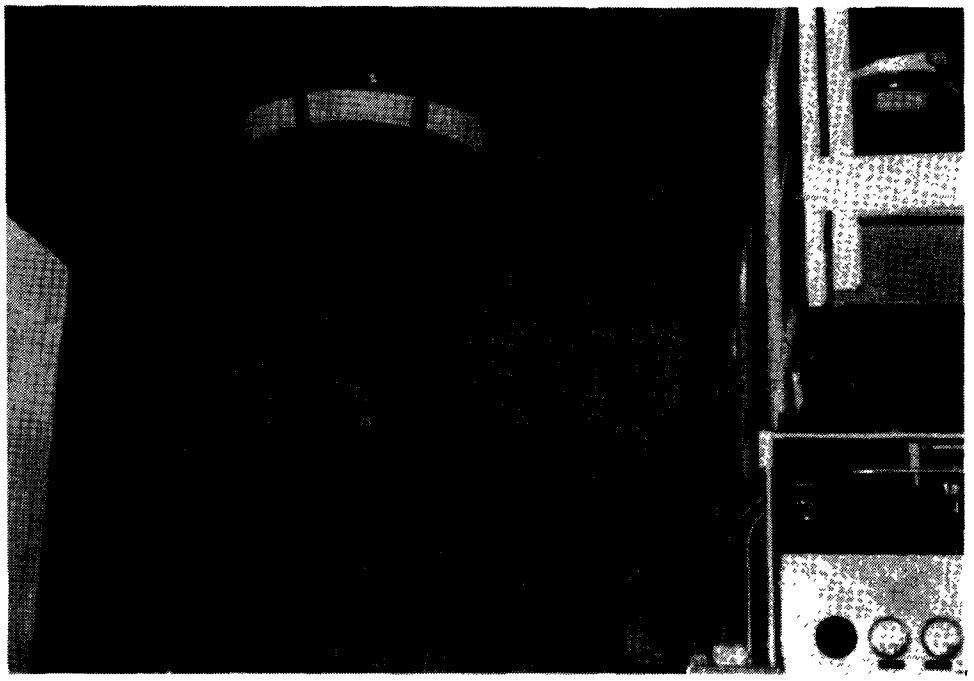

6b. Test unit being lifted to test facility pressure vessel.

Figure 6. GBF Subpilot test unit.

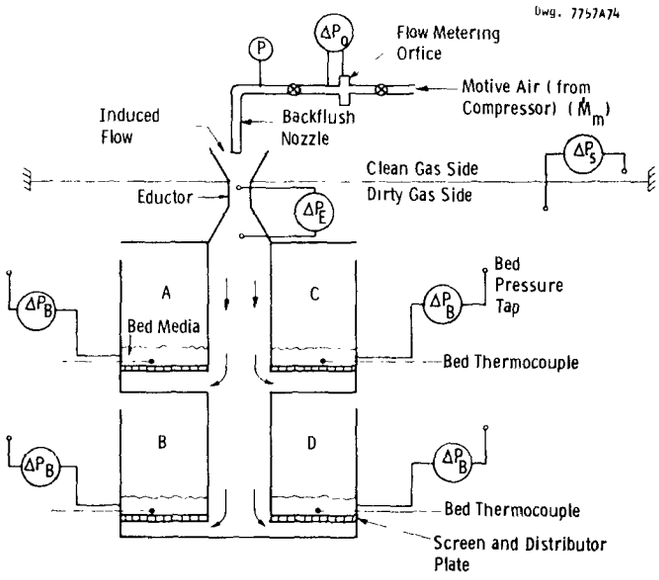

Figure 7. Schematic representation of GBF flow, pressure, and temperature measurements.

and pressure tap. Pressure taps are also provided across the eductor section of each element. Figure 7 also illustrates the instrumentation provided each GBF element. The backflush lines, visible in Figure 6, are one-inch diameter tubing sections that pass through the ring flange and connect to one-inch diameter flexible stainless steel tubing. These in turn are fastened to the inlet section of each eductor, positioned and held by the spider arrangement shown. The flexible tubing is used to accommodate thermal expansion during heat-up and backflush temperature transients. This test unit design was used through test Phase II. For test Phase III, modifications were made to the GBF unit to circumvent problems experienced in the earlier test phases in uniformly distributing the backflush flow between parallel operating filter beds. Figure 8 illustrates the test unit modifications.

HOT GAS TEST RESULTS

A series of tests on the six-element GBF subpilot test unit have been conducted at the Westinghouse Synfuels Division's (W SFD) Test and Development Center (TDC). These tests have been conducted using a test facility that simulates PFBC operating conditions. The test passage, schematically illustrated in Figure 9, was operated at 1600°F (850°C) nominal gas temperature and up to 150 psig (11 atm) pressure and a mass flow corresponding to about 500 acfm. This provides a GBF filter face velocity of 40 ft/min. Reentrained PFBC ash is injected into the test passage through a specially designed pressurized-brush dust feeder. The dust in these tests was the second-stage cyclone catch obtained from the Curtiss-Wright PFBC Technology Rig.

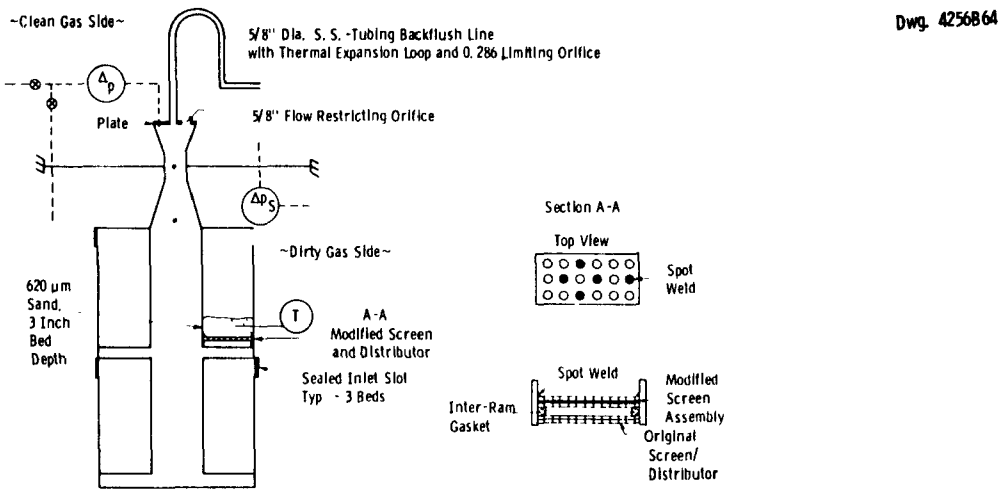

Figure 8. Test unit modifications.

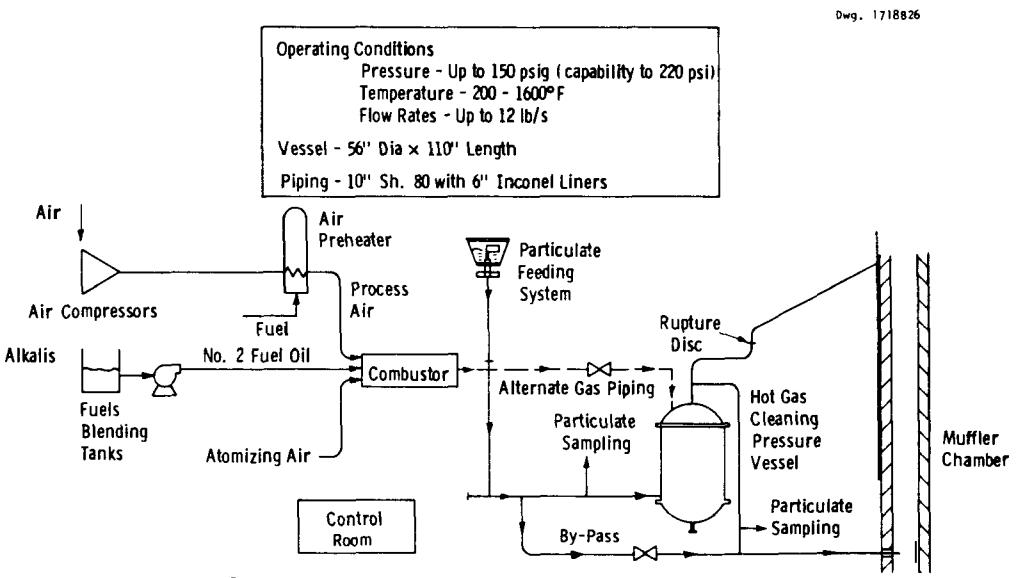

Figure 9. Schematic of hot gas cleanup facility.

Three distinct series of hot gas testing were conducted, and overall results and accomplishments of the test program are summarized in Table 2. The tests were conducted in 8 to 12 hour segments and covered a cumulative time interval of 170 hours with approximately 475 cleaning cycles attained. During the early test phases, test operations were plagued by several mechanical problems that occurred to the test unit. These included leaks in the gasket seal between each of the GBF elements and their respective eductor section. Also, several of the fittings on the backflush lines had detached or leaked. These problems were subsequently corrected before the second test phase was initiated.

The overall operational performance of the test unit is determined by its baseline pressure drop, overall dust collection

TABLE 2. SUMMARY OF GBF TEST ACCOMPLISHMENTS THROUGH PHASE III

D86-86

Test Phase & Configuration	Test Conditions (Nominal)	Major Findings: Accomplishments	Major Findings: Limitations
- I - • 6 Element/24 Bed • 1370 μm Alumina Media	• 1600°F/165 psi • 50 Hrs Operation • 103 Cycles • 40 Ft/Min	• *Integrated GBF Operation* With On-Line Cleaning • Backflush Times As Low As 6 Sec. • Low Baseline Δp (10 In. H_2O)	• *Gasket Seal Leaks* • Failed Backflush Lines
- II - • 6 Element/24 Bed • 1370 μm Alumina Media	• 1600°F/165 psi • 50 Hrs. Operation • 90 Cycles • 20 To 40 Ft/Min	• Confirmed Baseline Δp & Cleaning On-Line • Overall Dust Colletion Efficiency = 97.3%	• Significant Bed Media Loss • Warping Of Distributor Plate Assembly
- III - • 6 Element/6 Bed • 620 μm Sand Media	• 1500°F/125 psi • 71 Hrs Operation • 282 Cycles • 50 To 100 Ft/Min	• Stable Baseline Δp But Higher (40 To 80 In. H_2O) • Overall (Test Average) Dust Collection Efficiency = 99.2%	• Relatively Inflexible Test Constraints • Off-Line Cleaning Required • Some Bed Media Loss (18 To 30%)

efficiency, and demonstrated backflush cycle. Figure 10 shows a segment of the GBF pressure drop measured during system operation in Phase I. The top portion of the trace shows test segments where the duration of the backflush cycle is altered from 30 seconds to 6 seconds. In these tests dust was fed to the GBF unit until a prescribed system pressure drop was achieved (about 15 to 20 in H_2O) at which time the dust feed was halted. With the hot gas still flowing, each element of the test unit was sequentially backflushed. The dust remained turned off to enable the baseline pressure (pressure drop after backflush) to stabilize. Several such cycles were repeated for each backflush time indicated. From these test results it appeared that a stable baseline could be established even for the 6-second test conditions. Thus, it would appear that each operating bed was successfully backflushed and the dust expelled from the filter unit would settle into the containment vessel (as opposed to being carried into one of the other operating elements). The 6-second backflush cycle time corresponds to the near optimum established from the PFBC system studies (Figures 3 and 4).

The lower portion of the figure show a reproduced segment from the pressure drop trace where dust is continuously fed in a manner simulating actual PFBC operation. In this test segment, the backflush cycle was set at 6 seconds. Four operating cycles are shown corresponding to Δp's from 10 to about 30 in. of H_2O, with cycle times ranging from about 10 to 20 minutes. Conditions for these tests correspond to 1600°F, 150 psig (870°C, 11 atm), 40 ft/min filter face

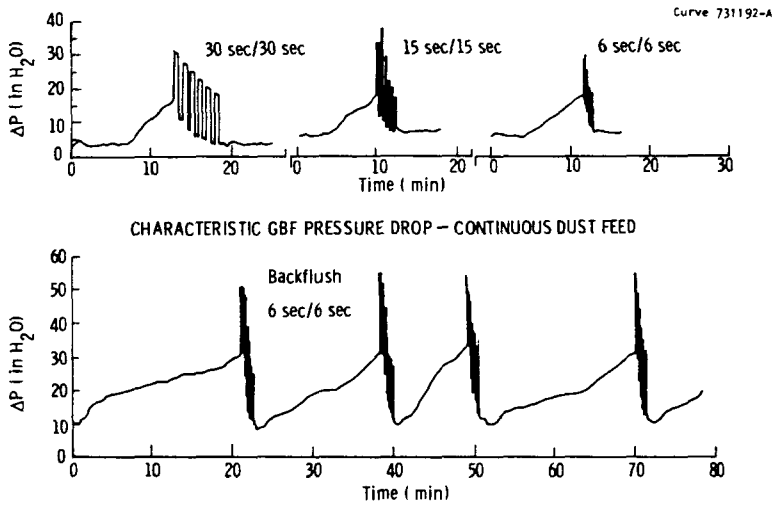

Figure 10. Characteristic GBF pressure drop for different backflush cycles.

velocity with an average inlet dust loading of about 7500 ppm. This dust loading is considerably higher than would be expected in a PFBC at the exit of a second-stage cyclone and even higher than might be experienced at the exit of a nonrecycle primary cyclone unit. The high dust loadings in these tests provide for achieving a large number of operating cycles in relatively short test times.

Test data taken during the latter portion of Test Phase I and throughout Test Phase II showed that during the backflush cleaning cycle, the backflush flow was not distributing uniformally between the filter compartments in each element. This was suggested during test operations by the bed temperature measurements. Figure 11 shows an example trace of the bed temperature measurements made in one element. During filtration, the bed thermocouples in each filter compartment (A,B,C, and D) show bed temperature close to the hot gas conditions. During backflush, relatively cold motive flow is provided that passes through the filter beds, causing a momentary temperature transient. As indicated by the recorded temperatures shown in Figure 11, only the A and C beds appear to show any temperature transient during the backflush cycle. These results (typical of all six operating elements of the GBF unit) suggest that the B and D beds in each elenent (half the total filter beds) were not seeing any significant backflush flow. In addition, those beds being backflushed did not appear to receive equal flow based on the magnitude of the recorded temperature transient.

The consequence of operating through a large number of backflush cycles with high backflush flow and poor (or no) flow distribution between beds is high superficial gas velocity and the possibility of elutriating bed medium on backflush. Subsequent inspection of the test unit at the end of Test Phase II confirmed this observation. In all six

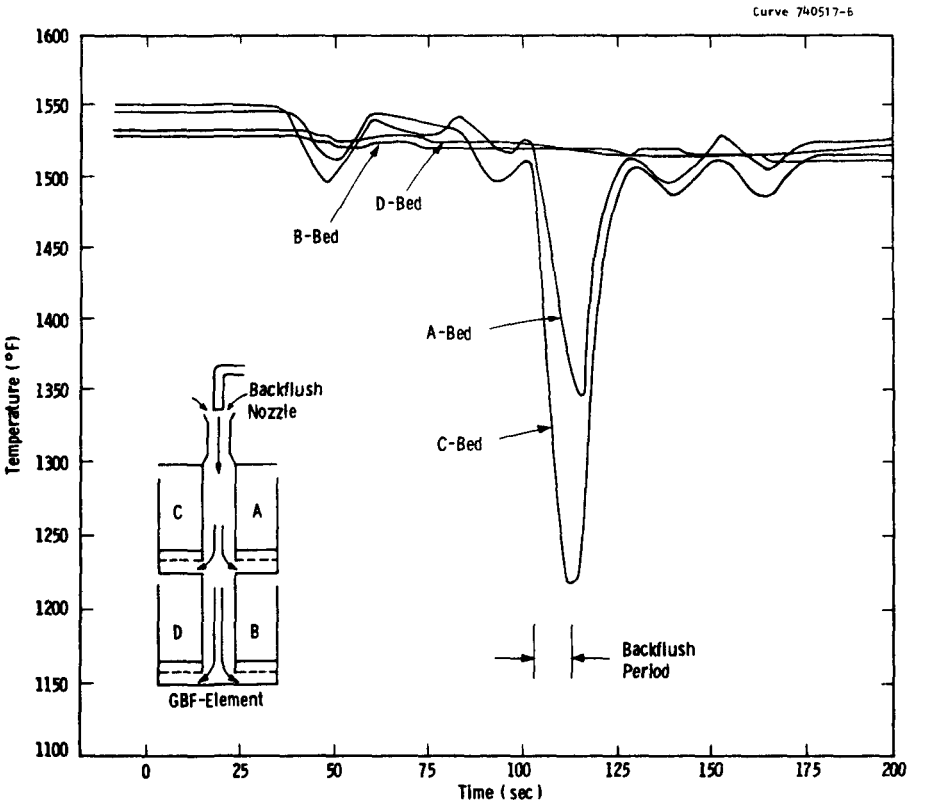

Figure 11. Measured bed temperatures during GBF operation, element 4.

GBF elements, the "C" beds showed nearly complete loss of the alumina bed medium. Likewise, most of the "A" beds showed all or substantial bed medium loss. The poor distribution of backflush flow also results in the inability to clean those beds that are starved of backflush flow. This in turn can overload the cleaned beds during the filtration cycle. In Test Phase III, the problem of the distribution of backflush flow was circumvented by eliminating three of the four filter compartments in each GBF element (see Figure 8).

Even though a significant maldistribution of backflush flow was evident over the course of the Phase I and Phase II test programs, relatively stable baseline pressure drops (i.e., operating pressure drop over the filter unit after cleaning) were achieved. These ranged from between 5 and 10 in. H_2O for the 1370 μm alumina bed medium. In test Phase III significantly higher operating baseline pressure drops were experienced. These ranged from between 40 to 60 in. H_2O and are the result of utilizing the modified GBF test unit that incorporated a double distributor plate assembly and the 620 μm sand as filter medium. Phase III testing was also conducted at somewhat higher filter face velocities and required the test unit to be cleaned off line, a

result of the modification made to circumvent the distribution of backflush flow problem experienced earlier in Test Phases I and II. Under these conditions and slightly modified backflush parameters, a steady operating baseline pressure drop was achieved. PFBC systems analysis suggests that GBF operating pressure drops of 40 to 60 in. H_2O would not significantly affect system performance or economics.

Dust sampling taken during the early portion of Test Phase II for the 1370 μm alumina medium and throughout Test Phase III for the 620 μm sand medium have been used to evaluate filter dust collection efficiency. Figure 12 shows the measured grade efficiency curves for each medium and the test basis. Table 3 gives a preliminary comparison of the GBF test results with PFBC requirements and includes comparison with an all-cyclone case. Neither the all-cyclone case nor the GBF with the 1370 μm bed medium appear to provide sufficient particle collection to meet PFBC system requirements. The GBF tests with the 620 μm sand medium show performance levels considerably improved and more than sufficient to meet New Source Performance Standards based on total particulate as well as a projected turbine life exceeding two years. These test results show considerable promise for the GBF for hot gas cleanup.

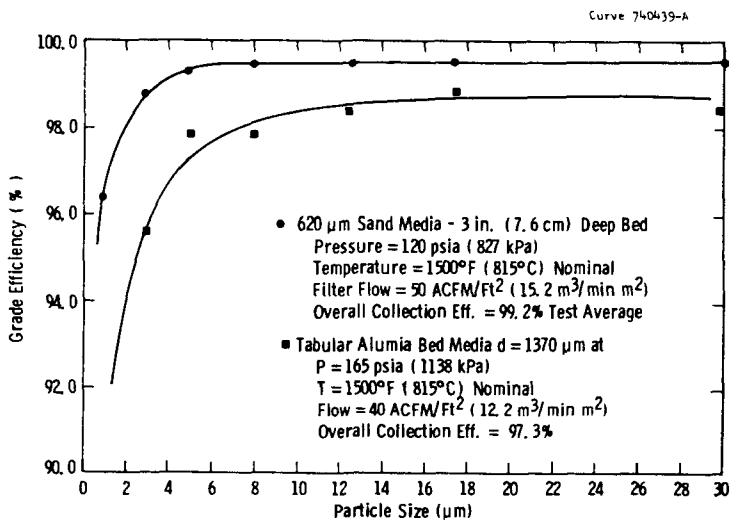

Figure 12. Measured grade efficiency curve for granular bed filter.

CONCLUSIONS

Preliminary test results on the GBF and analysis show that the GBF should be capable of performance levels sufficient to meet PFBC hot gas particulate cleaning requirements. Testing with a six-element, six-bed test unit arrangement, overall collection efficiencies averaged 99.2 percent under simulated PFBC conditions. Overall system pressure drops and backflush cleaning parameters achieved in test operations appear

TABLE 3. COMPARISON OF GBF TEST RESULTS WITH PFBC REQUIREMENTS

Dwg. 7771A51

Case	Ash	$\eta_{Overall}$	Projected Outlet Loading gr/scf	NSPS = .013 gr/scf (.03 lb/10^6 Btu)	Projected Turbine Life
GBF Alumina 1370 μm	C. W. - 2nd Stage Cyc. Ash $\bar{d}_{50}$ = 10 μm	97.3% (2)	0.027 (4)	No	< 1 Yr.
GBF 620 μm Sand	Mixed Ash (1) $\bar{d}_{50}$ = 7.7 μm	99.2% (3)	0.008 (3)	Yes	> 2 Yr.
All Cyclones	PFBC Combustor	87.5 to 96.3%	0.06	No	1 Yr.

(1) 66% by Wt. C. W. Ash Mixed with 33% by Wt. Ground Second Stage Catch from Exxon Mini Plant

(2) Representative of Best Data - Phase I & II

(3) Test Average - Phase III

(4) Assumed Inlet Loading = 1.0 gr/scf

consistent with the requirements for a commercial-scale unit for economic operation. Further testing and analysis are planned to further substantiate the GBF design basis and to pursue still higher performance levels.

REFERENCES

1. "Engineer, Design, Construct, Test and Evaluate a Pressurized Fluidized Bed Pilot Plant Using High Sulfur Coal or Production of Electric Power", Curtiss-Wright Corporation, Woodridge, NJ, 07075, FE-1726-20A, March 15, 1977.

2. "Preliminary Assessment of Alternative PFBC Power Plant Systems", Burns & Roe, Inc., Woodbury, NJ, 11797, EPRI CS-1451, Research Project 1645-2, July 1980.

3. CFCC Development Program, DOE Commercial Plant Economic Analysis (Task 1.6), Contract No. EX-76-C-01-2357, General Electric Co., Schenectady, NY, Preliminary, June 1979.

4. CFCC Development Program, DOE Commercial Plant Design Definition (Task 1.2), Contract No. EX-76-C-01-2357, General Electric Co., Schenectady, NY, March 1978.

5. "Design of Advanced Fossil Fuel Systems Study, Air-Cooled Pressurized Fluidied Bed Power Plant", Draft Report, Prepared for ANL Contract No. 37-109-38-6212 by Bechtel Group, Inc., December 1981.

6. "Design of Advanced Fossil Fuel System Study, Steam-Cooled Pressurized Fluidized Bed Power Plant", Draft Report, Prepared for ANL Contract No. 37-109-38-6212, by Bechtel Group, Inc., November 1981.

7. "Testing and Verification of Granular Bed Filters for the Removal of Particulate and Alkalies", Third Quarterly Project Report, April 1, 1981 through June 30, 1981, DOE Contract DE-AC21-80ET17093.

BAGHOUSE OPERATION IN GEORGETOWN UNIVERSITY COAL-FIRED, FLUIDIZED-BED BOILER PLANT, WASHINGTON, D.C.

by: Victor Buck
Pope, Evans and Robbins Incorporated
New York, New York 10004

and

David Suhre
Georgetown University
Washington, D.C. 20057

ABSTRACT

Since 1979, Georgetown University has operated the nation's first commercial sized, coal-fired, fluidized-bed boiler plant for over 10,000 hours, utilizing a baghouse for particulate emissions control.

In plant startup, the bags are first coated with limestone dust by operating the forced draft and induced draft fans to fluidize the bed. This is followed by firing of No. 2 fuel oil to preheat the boiler and the limestone bed. Upon achieving 100 psig boiler steam pressure, coal is introduced into the preheated bed and ignited by the oil burner to initiate boiler operation.

The baghouse has proven to be an efficient particulate collector. However, excessive pressure drop cross the baghouse has proven to be an ongoing problem. Various baghouse modifications have been implemented and different bags tested. This paper presents the results of this operation.

INTRODUCTION

Georgetown University has operated its 100,000 pounds per hour, 625 psig, coal-fired, fluidized-bed boiler plant in Washington, D.C. since July 1979. This is a national demonstration plant funded by the Department of Energy for the two-fold purpose of:

- Operating an atmospheric fluidized-bed boiler burning high-sulfur coals in an environmentally acceptable manner in an urban institutional complex, and

- Obtaining sufficient information from the prototypical operation to encourage industry to move directly into the design and construction of commercially warranted industrail size fluidized-bed boiler units.

Table 1 indicates the design basis for the Georgetown boiler.

TABLE 1. DESIGN BASIS - GEORGETOWN UNIVERSITY FLUIDIZED BED BOILER

STEAM FLOW	100,000 lbs/hr
OUTLET TEMP./PRESS	Saturated 414°F/275 psig, or 493°F/625 psig
DESIGN COAL	Bituminous
Heating Value	12,750 Btu/lb
Ash %	7.97%
Moisture %	5.0%
Sulfur %	3.29%
DESIGN PARAMETERS	
Bed Operating Temperature	1594F
Ca/S Ratio (for SO_2 Compliance)	3/1
COAL FEED SYSTEM	Stoker (2) - Side Wall Mount
COAL SIZE	1-1/4" x 1/4"
COAL FLOW RATE	9,565 lbs/hr
LIMESTONE SIZE	1/8" x 16 Mesh (0.0469")
LIMESTONE FLOW RATE	3,133 lbs/hr
RE-INJECTION FLOW RATE	7,500 lbs/hr
FLUE GAS FLOW	120,000 lbs/hr
MAXIMUM BAGHOUSE FLUE GAS TEMPERATURE	400°F
INDUCED DRAFT FAN FLOW RATE	44,430 ACFM
INLET PRESSURE AT INDUCED DRAFT FAN	(-) 18"

The boiler burns eastern bituminous coal which, in practice has had a sulfur content averaging between 2 and 2-1/2 percent, an ash content of from 10 to 16 percent, 25 percent and greater volatiles, and up to 5 percent moisture. Coal is sized 1-1/4 inch x 3/8 inch for overbed stoker feed into the boiler. The proportion of fines (< 1/4 inch) has at times reached 70 percent. As a result, a considerable amount of unburned carbon is elutriated with the flue gas stream by the upward flow of combustion air thorugh the boiler bed.

Limestone, which constitutes the basic bed material in the boiler for purposes of sulfur capture, averages about 1300 microns in size. By design intent, delivered limestone is sized to fall within the limits indicated in Table 2. These limits were based on early developmental work and had been found to insure optimum sulfur capture.

TABLE 2

DELIVERED LIMESTONE SIZE (DESIGN BASIS)

1/4"	100 %
6 Mesh (0.132")	98-100%
8 Mesh (0.094")	85-95 %
10 Mesh (0.079")	70-80 %
16 Mesh (0.047")	20-40 %
20 Mesh (0.033")	10-20 %
30 Mesh (0.023")	3-5 %

In operation, limestone is delivered by gravity into the two boiler beds as shown on Figure 1. In the presence of heat, the limestone is calcined and the calcined lime in turn reacts with the sulfur dioxide (SO_2) produced by burning coal to form calcium sulfate ($CaSO_4$) thus limiting sulfur dioxide emissions in the manner expressed by the following reactions:

$$CaCO_3 \text{ (limestone)} + \text{Heat} = CaO + CO_2$$

$$CaO + SO_2 + 1/2\ O_2 = CaSO_4$$

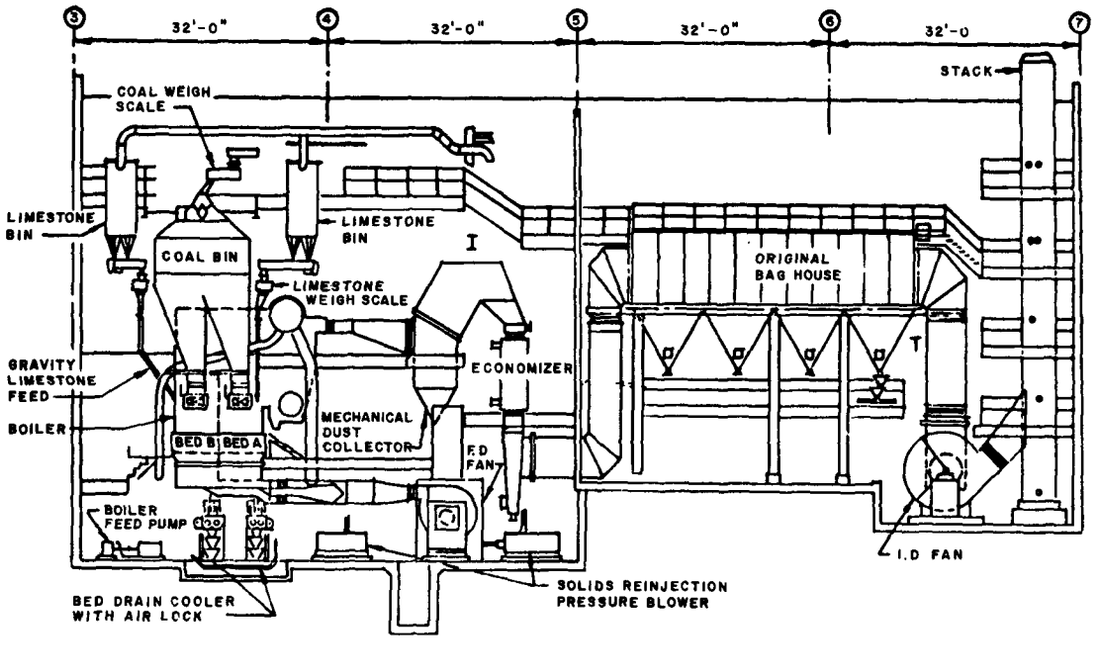

FIGURE 1

PLANT CROSS SECTION
THROUGH FLUE GAS STREAM

Combustion air entering the boiler from below serves to place the bed in suspension, i.e. the bed is fluidized. In the process, fine particles of bed material as well as of the coal fuel is driven off in the flue gas stream.

Immediately downstream of the boiler, a mechanical cyclone collector removes the bulk of the large entrained particles from the flue gas for reinjection back into the boiler bed. This serves to improve boiler efficiency by achieving more complete coal combustion and by increasing the amount of sulfur capture per unit of limestone used.

Smaller flue gas particles which pass the mechanical collector are directed to the baghouse for final cleanup.

INITIAL PLANT OPERATION

The baghouse initially installed in the plant was manufactured by Enviro-Systems and Research, Inc. It consisted of a 22 cell structure, with each cell containing 36-5 inch diameter by 8 feet 6 inch long bags - a total of 792. Bag cleaning was performed off-line by reverse air. The air to cloth ratio was 4.60 with one cell cleaning; 4.39 with all cells active. The cleaning cycle was initiated automatically whenever the pressure drop across the baghouse exceeded 4 inches. It continued to subject the bags (in one cell at a time in sequence) to reverse air cleaning until the pressure drop reduced below 4 inches. In the original installation, the first six cells were fitted with Nomex glass bags and the remaining 16 cells with Teflon felt bags.

Boiler lightoff involves preheating the boiler and the limestone bed by means of a No. 2 fuel oil igniter until a drum pressure of about 100 psig is reached. Coal feed is then initiated. The overall lightoff period, until the boiler is operational producing steam, has averaged about 4 hours. As a precautionary measure against bag fouling due to condensing of volatile hydrocarbons, the bags were precoated with limestone dust by operating the forced draft and induced draft fans before beginning lightoff.

Problems developed early due to increasing pressure drop across the baghouse. At boiler loads of less than 50 percent, this drop reached 13 to 14 inches, well in excess of the expected 4 inch drop at full load. The Teflon felt bags, in particular, were blinding and became impossible to clean by the reverse air method.

Early in 1980, the manufacturer modified the baghouse by the addition of a pulse jet cleaning system which would operate coincident with the reverse air cleaning cycle in each cell. In theory, the pulse jet would dislodge the particles while the more sustained reverse air flow would drive the particles further from the bags and thereby assure that a greater proportion of dislodged material would not be recaptured on the bag when the cell was returned to the cleaning mode. Coincident with this modification, the manufacturer also replaced the Teflon felt bags with Nomex glass as the latter type, though limited to a 400°F operating temperature, had given evidence of better cleaning characteristics.

This modification appeared to have succeeded in reducing the pressure drop across the baghouse but in time, as the boiler was operated at ever increasing loads, the drop across the baghouse again reached unacceptably high levels. Various attempts at improving operations by adjusting the application of the pulse jet to various points in the reverse air cleaning period did not appear to improve bag cleaning and reduce the pressure drop. In addition, bag failures became a significant problem with the Nomex fabric and replacements were made with Teflon felt bags.

During this entire operating period, the demonstration boiler plant operation was also undergoing refinements, many of which interacted with the baghouse operation. Included among those changes were flyash reinjection improvements, and improved boiler instrumentation leading up to automatic operation. The flyash reinjection system required modifications to determine equipment which was capable of reinjecting all fines collected in the mechanical collector back into the boiler. Obviously, when the mechanical collector hoppers filled up, all flyash passed through to the baghouse for final collection. In general, this had the following effect upon the flyash entering the baghouse:

- Larger average particle size,
- Higher carbon content,
- Higher calcined lime content.

By late 1980, the installation of an air lock below one of the five mechanical collector hoppers resulted in full reinjection of collected flyash from this point. Air locks were subsequently installed on all hoppers, and have been operational since July 1981.

Boiler instrumentation required modifications and refinements before automatic operation of the plant was attainable. Due to poor performance of the gas analyzer systems at the beds and stack, operators had a tendency to operate with a higher than design level of both excess air and also limestone feed for sulfur capture. Higher excess air rates increased the flue gas flow rate through the baghouse above design levels for a given boiler load. Higher limestone feed rates than required for maintaining emissions level below allowable led to higher dust loadings in the flue gas stream due to fines elutriation. Both factors served to hamper evaluation of baghouse pressure drops, but were not considered to be governing factors. Final instrumentation changes were implemented in the early summer of 1982 and the boiler is now capable of sustained operation in the full automatic mode.

INTERIM MODIFICATIONS

In April 1981, spot modifications were made to the baghouse as follows:

- Modified pulse jet system in one cell to inject more air during cleaning cycle;
- Added "Staclean" diffusers with venturies to all bags in one cell to improve distribution of the pulse during cleaning.
- Added "Staclean" diffusers without venturies to one row (6 bags) in a separate cell.

During a subsequent 12 day operating period, the baghouse was cleaned continuously with both pulse jets and reverse air in which a 0.1 second pulse was imposed upon the bags 3 seconds into the reverse air cleaning cycle. The reverse air flow continued for 2 seconds after the pulse.

Tests on the bags following this experiment indicated that bags subjected only to reverse air cleaning were cleaned the least. The greatest improvement was found in cells in which the pulse jet volume was increased. In a follow-on test, the reverse air cleaning was then eliminated and further improved bag cleaning was noted using only the modified pulse jet system.

Based on these tests, the baghouse was modified throughout to increase the pulse jet air flow into each bags. However, operations following this modification did not bear out the expectations envisioned from the above tests as shown in Figure 2.

Late in August 1981, the decision was made to replace all remaining Nomex glass bags with the original Teflon felt in order to reduce further bag losses. Nomex, while responding better than Teflon to bag cleaning, was succeptible to bag damage due to flue gas temperature excursions above 400°F, and to excessive bag wear in this particular baghouse.

Throughout the latter part of 1981, in addition to the above bag replacements, the University made adjustments in the operation of the baghouse including those listed below:

- Duration of pulse,
- Pulse Header Pressure,
- Timing of pulse with respect to reverse air,
- Increasing number of pulses during cleaning cycle from one to two, and
- Eliminating the reverse air function.

None of these changes resulted in significant improvements in the baghouse pressure drop which continued to increase to a point where boiler load was limited to 50% full rated capacity.

Through 1981, the bags employed at this installation were predominantly either of Teflon felt or Nomex glass. In late 1981, all bags were replaced with Goretex Teflon B fiberglass as a last measure to obtain acceptable pressure drops across this baghouse. Subsequent operations indicated that with the Goretex bags, the boiler could be operated at 90 percent output, but with a drop across the baghouse in excess of 10 inches. Whereas these bags were in service for just two months, no reliable information on bag failure could be obtained. It was noted that in this period, a boiler tube leak caused a plant shutdown and upon returning to operation 10 days later, the bags reverted to the pressure drop that existed prior, an indication that despite high moisture content in the flue gas stream, the bags were capable of responding to the cleaning cycle. The overall results of this experiment, however, led to the conclusion that in order to reduce the drop across the baghouse to acceptable levels at all loads, the baghouse would require major modification.

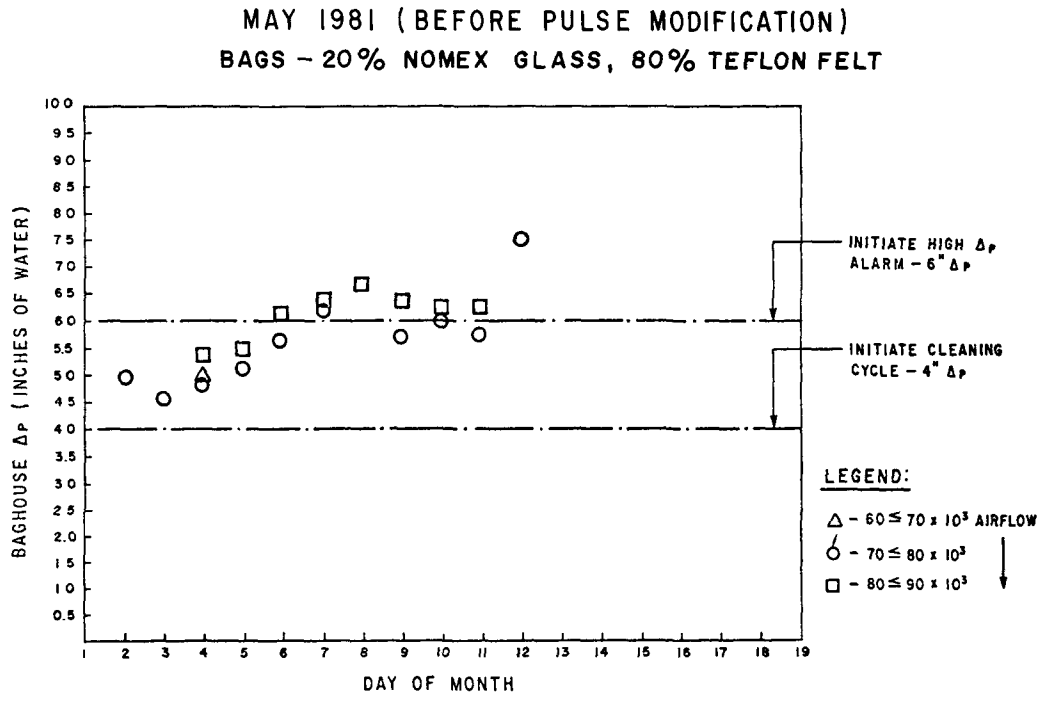

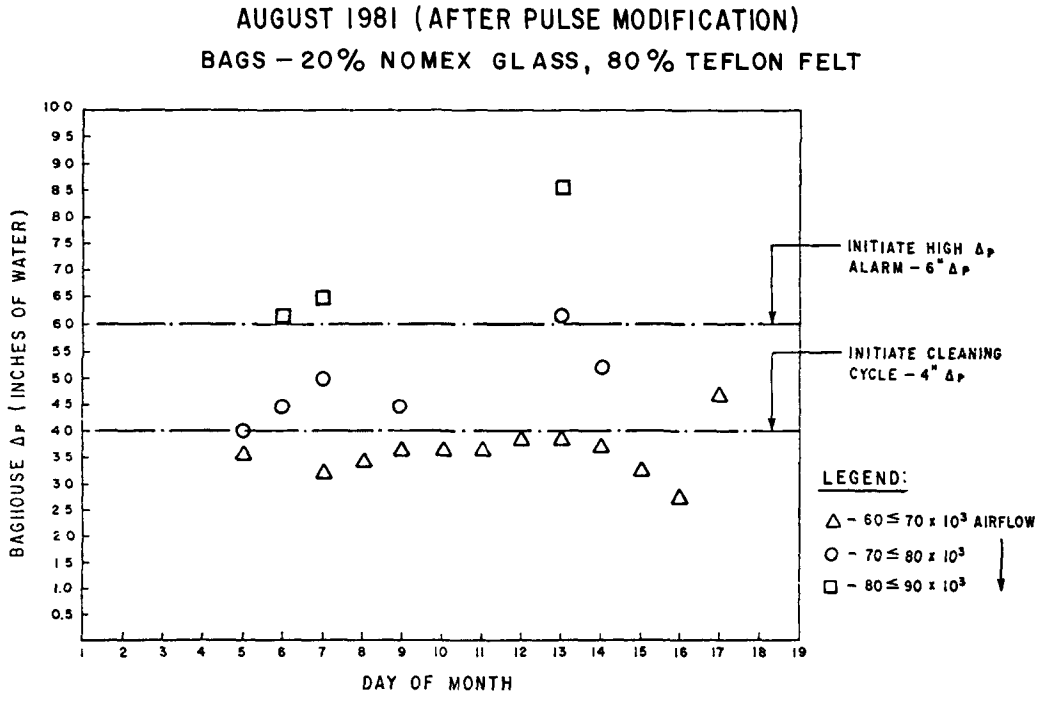

FIGURE 2

BAGHOUSE Δ VS. TOTAL AIR FLOW (lbs / hr)
BEFORE AND AFTER PULSE MODIFICATION

FINAL MODIFICATION

Based upon a report prepared by Davy McKee, Consultants to DOE, the baghouse at Georgetown University was completely rebuilt between April and July 1982. Salient features of the revised baghouse as constructed by Mikro-Pul Corporation are:

1. Four cell construction with capability of isolating one cell for maintenance or inspection without interrupting operation;
2. 308 bags per cell, each bag 4.5 inches in diameter by 10 feet in length;
3. Pulse jet cleaning in on-line mode;
4. Air to cloth ratio of 3.07:1 (on-line cleaning);
5. Compressed air requirement - 80 cfm @ 100 psig (on-line cleaning);
6. Bags - Felted Fiberglass "BWF" 25 oz/sq yd.

The new baghouse configuration is shown on Figure 3.

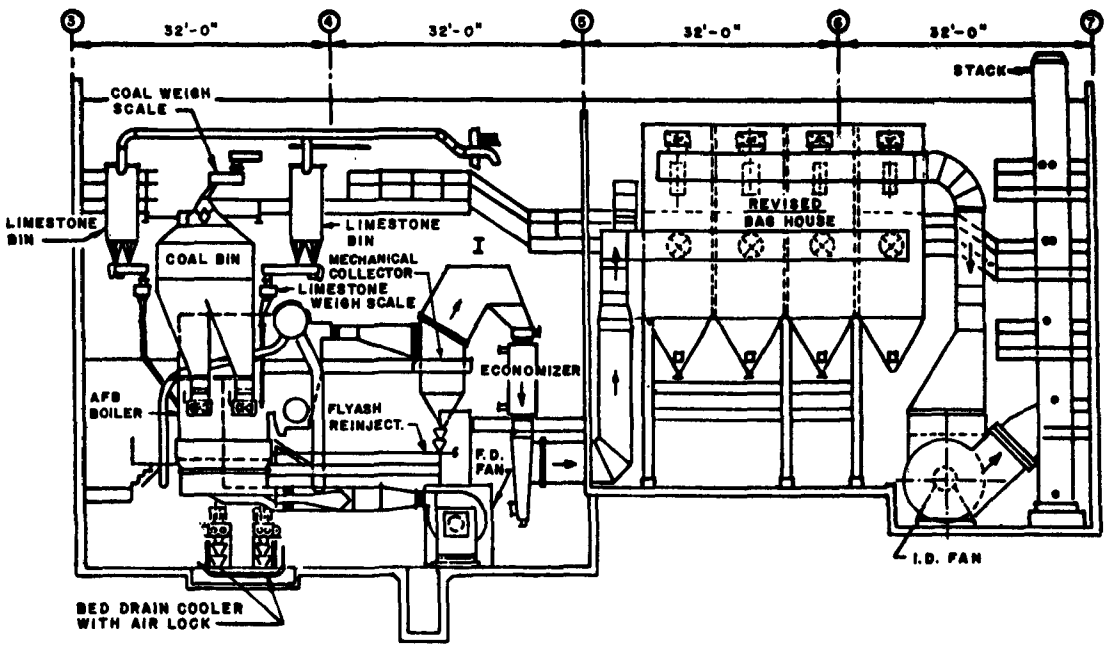

FIGURE 3

PLANT CROSS SECTION
AFTER 1982 BAGHOUSE RECONSTRUCTION

Since plant operations were resumed in early August 1982, a total of 1,100 hours of steam generation have been logged up to October 1 at output levels ranging between 55 and 100 percent of boiler rated output. The pressure drop across the baghouse has remained well within operational limits. Figure 4 depicts the pressure drops through the flue gas system for a three week period in September 1982. It is expected that the cleaning cycle will require some further adjustment until a stable operating point is reached that will permit sustained operation at up to boiler full load without excessive drop.

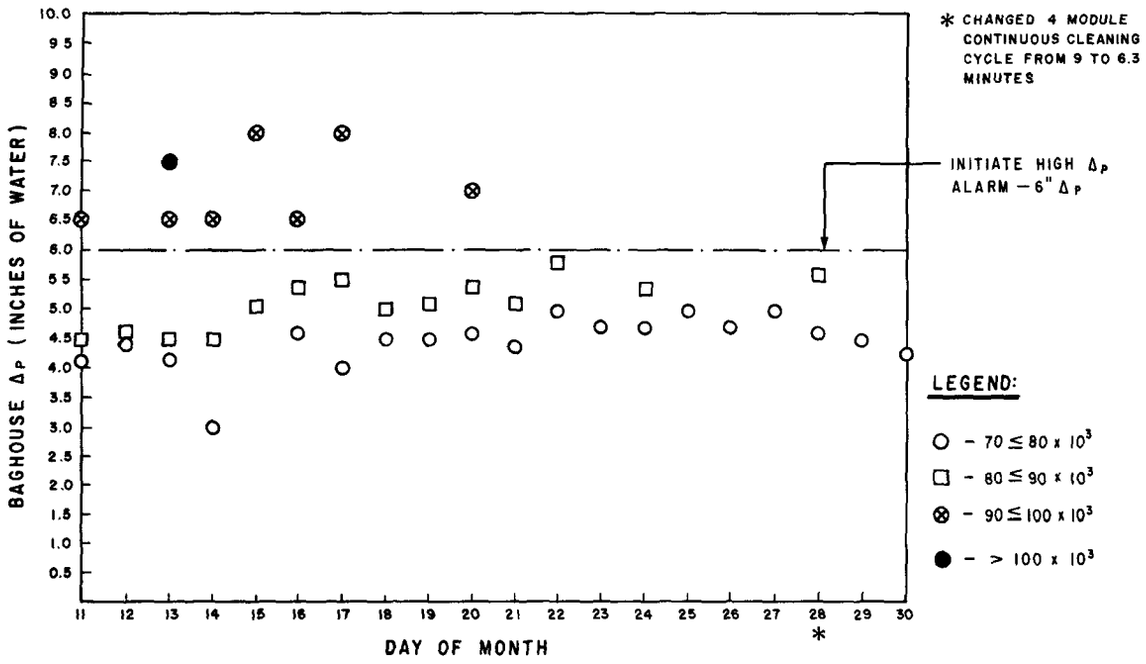

FIGURE 4

BAGHOUSE ΔP VS TOTAL AIR FLOW (lbs/hr)
SEPTEMBER 1982 (WITH REBUILT BAGHOUSE)

FLY ASH COMPOSITION

In fluidized bed combustion, the fly ash composition may vary considerably within a given plant, the composition largely determined by the type, quantity, size and make-up of the coal and limestone delivered to the boiler.

At Georgetown University, samples of flyash were taken from the flyash silo at intervals and analyzed by the DOE laboratory in Alexandria, Virginia. The tabulation in Table 3 below summarizes the results and demonstrates the variations that are found.

TABLE 3

FLYASH SAMPLES ANALYSES (%)

Measured Value	Range	Mean
C (total)	20.55-35.61	31.31
S	1.65-2.68	2.25
CaO	14.81-20.58	17.26
$CaSO_4$	8.11-11.38	9.53
SiO_2	20.27-26.19	22.84
Al_2O_3	7.95-10.60	9.42
Fe_2O_3	4.47-8.96	6.34
MgO	0.13-1.06	0.56
L.O.i	29.77-37.16	34.58
HHV (Btu/lb)	3303-5163	4473
Bulk Density (lb/cf)	28.4-36.5	32.33
Ave. Micron Size	37.6-51.8	43.16

A word of caution applies in interpreting the above values. The samples were taken from the ash silo and therefore may have undergone further reaction from the time that the material was collected at the baghouse. After collection, the samples were not always analyzed promptly and hence the opportunity existed for further reactions to take place before the analysis was made. They are indicative, however, of the range that may be encountered in this type of plant.

CONCLUSIONS

The baghouse at Georgetown University's fluidized bed boiler plant has performed to limit particulate emissions well below D.C. allowable limits. The problem of excessive pressure drop across the baghouse appears to have been overcome with the rebuilding of the baghouse. However, the performance evaluation of bags now in place must await further periods of operation. The operating experience at Georgetown has been documented in a series of quarterly reports issued by DOE and listed in the References below. The results cannot be considered typical of all fluidized bed boiler plants due to differences from plant to plant in the type of boiler, coal and limestone; the size and method of feeding coal and limestone; and other factors. It is

expected, however, that with the accumulation of similar information on other operational fluidized bed boiler plants, the selection of a baghouse and bag material for this type of plant can be made in the future with assurance that the initial selection will operate successfully over the full range of boiler output.

ACKNOWLEDGEMENTS

Capital funding for this project was provided by the U.S. Department of Energy.

The work described in this paper was not funded by the U.S. Environmental Protection Agency and therefore the contents do not necessarily reflect the views of the Agency and no official endorsement should be inferred.

REFERENCES

1. Davy McKee Corporation, Fabric Filter Design for Application in the Fluidized Bed Combustion of Coal, DOE/ET/10123-1171.

2. Georgetown University, Industrial Application of Fluidized Bed Combustion, Quarterly Technical Progress Report, July-September 1979, DOE/FE/2461-13.

3. Georgetown University, Industrial Application of Fluidized Bed Combustion, Quarterly Technical Progress Report, October-December 1979, HCP/T2461-13, UC-9UE.

4. Georgetown University, Industrial Application of Fluidized Bed Combustion, Quarterly Technical Progress Report, January-March 1980, HCP/T2461-13, UC-9UE.

5. Georgetown University, Industrial Application of Fluidized Bed Combustion, Quarterly Technical Progress Report, April-June 1980, HCP/T2461-13, UC-9UE.

6. Georgetown University, Industrial Application of Fluidized Bed Combustion, Quarterly Technical Progress Report, July-September 1980, METC/DOE/10381/135.

7. Georgetown University, Industrial Application of Fluidized-Bed Combustion, Quarterly Technical Progress Report, October-December 1980, HCP/T2461-13, UC-9UE.

8. Georgetown University, Industrial Application of Fluidized Bed Combustion, Quarterly Technical Progress Report, January-March 1981, EO/ET/10381-197 (DE 81030272).

9. Georgetown University, Industrial Application of Fluidized Bed Combustion, Quarterly Technical Progress Report, April-June 1981, DOE/ET/10381-1109 (DE 82006241).

10. Georgetown University, Industrial Application of Fluidized Bed Combustion, Quarterly Technical Progress Report, July-September 1981, DOE/ET 10381-1143.

11. Georgetown University, Industrial Application of Fluidized Bed Combustion, Quarterly Technical Progress Report, October-December 1981 (In printing).

12. Georgetown University, Industrial Application of Fluidized Bed Combustion, Quarterly Technical Progress Report, January-March 1982 (In preparation).

13. Georgetown University, Industrial Application of Fluidized Bed Combustion, Quarterly Technical Progress Report, April-June 1982 (In preparation).

14. Pope, Evans and Robbins Incorporated, Baghouse Test Program Final Report, April 1980 (Prepared for U.S. Department of Energy).

PARTICLE CAPTURE MECHANISMS ON SINGLE FIBERS IN THE PRESENCE OF ELECTROSTATIC FIELDS

by: M.B. Ranade, F-L. Chen, and D.S. Ensor
Research Triangle Institute
Research Triangle Park, NC 27709

L.S. Hovis
Industrial Environmental Research Laboratory
U.S. Environmental Protection Agency
Research Triangle Park, NC 27711

ABSTRACT

Fabric filtration, although simple mechanically, is a complex phenomenon. As part of an effort to isolate the mechanisms significant in fabric filtration, simple experiments have been devised to evaluate the effects of electrostatic fields on particle capture. A series of experiments, with charged and neutral particles with various applied fields, were conducted to determine the location of deposits on the fiber. In particular, the location of the attachment of the aerosol, with respect to the direction of flow, was found to be strongly dependent on the applied field. The implications of these data, comparison to theory, and implications when applied to fabric filtration are described.

This paper has been reviewed in accordance with the U.S. Environmental Protection Agency's peer and administrative review policies and approved for presentation and publication.

INTRODUCTION

Filtration using media composed of fibers is one of the most efficient processes for fluid/particle separation. To predict the performance of the media, it is necessary to understand the process by which particles are deposited on the individual fibers.

Deposition of particles on a collector is the preliminary step leading to particle collection in a fibrous or fabric filter. In general, most of the past theoretical studies in fibrous filtration were based on the idealized single-fiber concept and were confined to the initial filtration period; i.e., before significant particle buildup. Thus, they do not deal with the more important period when deposition is at an advanced stage. It is known that deposited particles not only distribute themselves on the surface of the fiber but also may build up chain-like agglomerates called dendrites.

In this work, the quantitative characteristics of monodisperse particles deposited on a single metal fiber were investigated under three situations: 1) neutral particles and neutral fibers; 2) non-neutralized particles and neutral fibers; and 3) neutral particles and neutral fibers in a variable electric field.

BACKGROUND

The theory of filtration by fibrous filters is based on the concept of the capture efficiency of a single fiber and supposes that the fibrous layer is composed of such single fibers. In the past, experiments conducted to prove the above theory assumed that the packing density was very small and that effects from neighboring fibers could be neglected. No experiments were applied to determine the deposition efficiencies and to describe the dendrite formation of particles collected by a single fiber until 1966.

Billings (1) used a single glass fiber to collect neutral polystyrene latex particles and obtained photographs of the particle dendrite formation. He observed that particle deposition on a collector was not uniform but varied along the angular sectors of the collector. Also, the collection efficiency increased as the number of particles on the collector increased. These dendrites were apparently better aerodynamic targets than the bare fibers.

Several models have been published by different authors to explain the particle dendrite formation on a single fiber. Payatakes and Tien (2) and Payatakes (3, 4, 5) have developed deterministic expressions for dendrite growth by solving successive differential equations. Payatakes and Gradon (6, 7) extended this model to include different dominant mechanisms such as interception (Payatakes [3, 4]), interception and inertial impaction (Payatakes and Gradon [7]), and the Brownian diffusion effect (Payatakes and Gradon [6]). With these models, the configuration of individual particle dendrites and the rate of growth of these dendrites, as a function of deposition age and angular coordinates on the fiber surface, can be predicted.

Tien et al. (8) and Wang et al. (9) have made a study of particle dendrite growth using stochastic simulation. The number of dendrites formed on a given length of fiber and their size and shape were determined by the location of individual particles arriving from upstream and their order of arrival. The stochastic simulation method will serve as a tool for testing the hypothesis and will be a guide for the development of particle collection models. Kanaoka et al. (10, 11) have developed a similar method to predict the growing process of a dendrite and to determine the collection efficiency of a single fiber under dust loading conditions. The Kanaoka model was simple in structure and could generate a statistically sufficient number of simulations in short computation time.

Several researchers have utilized experimental equipment and methods to study the phenomena of particle deposition on a collector. Their results have indicated that the number of particles collected by a fiber is a function of deposition age, particle concentration, particle dendrite structure, Stokes number, and external forces. Beizaie (12), Bhutra and Payatakes (13), and Barot et al. (14) collected particles on a single fiber by interception and inertial impaction mechanisms. They observed that particle distribution on a single fiber is not uniform and significantly depends on the angular sector of the fiber. Wang et al. (15) accumulated solid particles on single cylinders in an electric field. They observed that dendrites formed straight chains and that collection efficiency markedly increased under the electrostatic effect. Oak and Saville (16) did an experiment to consider the deposition of weakly charged particles on a collector in a strong external field. They observed results similar to Wang's and concluded that the particle-particle bonds were stronger than the particle-fiber bonds on a fiber.

EXPERIMENTAL WORK

EXPERIMENTAL APPARATUS

The experimental apparatus was designed and built to enable deposition and observation of fine particles on a single fiber under well-defined and controlled conditions. It consisted of a particle generator, a particle collector, and monitoring devices. The different parts of the experimental apparatus are shown schematically in Figure 1.

The vibrating-orifice aerosol generator, TSI Model 3050, was used to produce well characterized monodisperse aerosols. It was supplied with a constant feed of solution of methylene blue dissolved in 2-propanol. For the first part of the experiment, the solid methylene blue particles generated were neutralized effectively by passing them through a TSI Model 3054 neutralizer containing a Krypton-85 source. For the second part, charged particles were generated by the above method except that the neutralizer was not used. The particles were negatively charged with an average 850 electron units charge per particle.

The aerosol was then passed into a specially designed chamber under laminar flow conditions. The chamber was similar to the one used by Bhutra and Payatakes (13). As shown in Figure 2, a smooth cylindrical tungsten

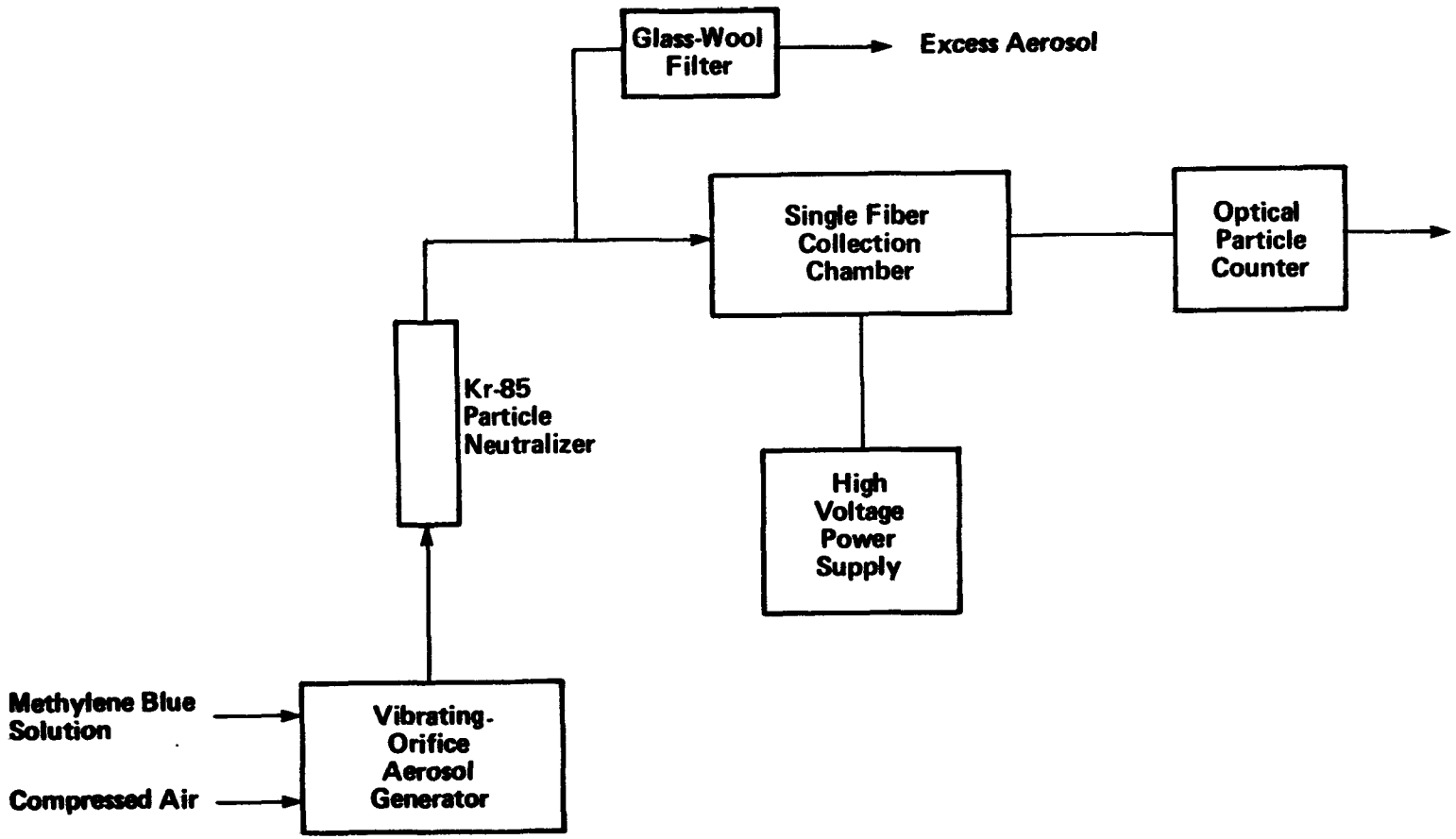

Figure 1. Arrangement of equipment to collect neutral particles on a single fiber in an electric field.

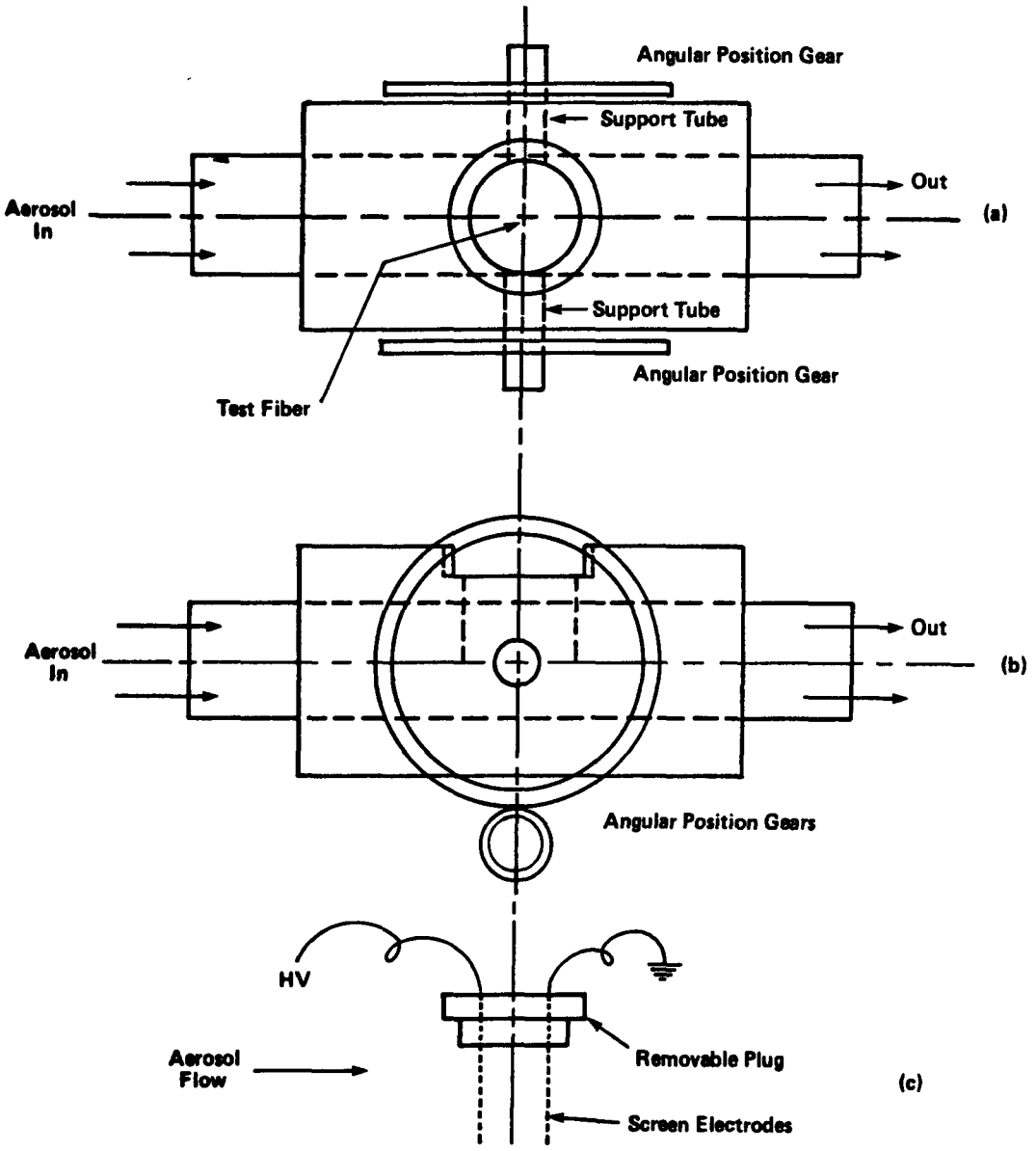

Figure 2. Single fiber aerosol collection chamber--a) top view; b) side view; and c) electrode assembly.

metal fiber was supported by two copper tubes and could be rotated without torsion using the gear arrangement. The chamber had an opening just above the fiber, which could be sealed with a removable plug. To create a field around the fiber parallel to the aerosol flow, two screens, 0.6 cm apart, were added to the plug and a high voltage power supply was connected to them.

After the particles were collected for a predetermined time, the plug was removed and the objective lens of the microscope camera system was lowered to examine the fiber. The microscope camera system was mounted on a stable base and could be moved with a control knob to scan the length of the fiber. Using the gear arrangement, the fiber could be rotated and photographed at different angles.

A Climet 208 optical particle analyzer and a Climet CI-210 multi-channel monitor were used to obtain the particle concentration. The Climet 208 was operated at the same flowrate as that of the aerosol stream approaching the fiber.

EXPERIMENTAL PROCEDURE

At the beginning of an experimental run, a new fiber was supported in the fiber holder across the path of the aerosol. In the first part of the investigation, neutral particles were collected on a fiber which was not subjected to an external electric field. After a period of time, the aerosol feed was stopped, the plug was removed from the fiber holder, and the objective lens of the microscope was lowered into position. Several parameters in the generation and collection of the methylene blue particles were kept constant during all three parts of the experiment and are listed in Table 1. The fiber diameter, particle size, and the fluid velocity were so chosen that a direct comparison could be made with the results reported by Bhutra and Payatakes (13) in absence of an electric field. The velocity is considerably higher than expected for fabric filtration, but is well within practical filtration range such as in depth filtration (17).

Photographs of dendrite structures were taken at desired locations, and the film and frame numbers were recorded. After all the dendrites in the field of view had been examined, the objective lens was retracted, the plug was set in position, and the entire procedure was repeated. The same area on the fiber was examined to follow the growth of individual dendrites since the previous viewing. Several runs were needed to accumulate enough information for a given set of data.

In the second part of the investigation, non-neutralized particles were collected on the fiber. The procedure was identical to that of the first part, except the particle neutralizer was not used. An electrometer was used to measure the amount of charge on the particles.

In the third part of the investigation, neutral particles were collected on the fiber placed in an external electric field directed parallel to the flowstream. The procedure was identical to that of the first part of the experiment, except that two screens were attached to the removable plug, as shown in Figure 2, and were connected to a high voltage supply with the downstream screen grounded.

RESULTS

Extensive data were collected from each of the three parts of this investigation: 1) neutral particles versus neutral fibers; 2) non-neutralized particles versus neutral fibers; and 3) neutral particles versus neutral fibers in an external electric field.

From the series of photographs which were taken of the same section of fiber, it is apparent that particle number and dendrite length both increase with time. However, the distribution of this growth between the various sectors is different for each of the three parts of the experiment. Figure 3 shows the particles deposited on the same degree sector and the same exposure time of the fiber under the different electrical conditions.

TABLE 1. PARAMETER VALUES USED IN THE EXPERIMENT

Particle Diameter	:	3 μm
Fiber Diameter	:	35 μm
Fiber Length	:	700 μm
Particle Density	:	1.2 g/cm^3
Viscosity	:	0.0000183 Pa•s
Velocity of Flow	:	41 cm/sec
Reynolds Number of Fiber	:	1.0116
Stokes Number	:	0.8
Interception Parameter	:	0.086

For the neutral particles in absence of an external electric field, particle deposition on a fiber was entirely due to inertial impaction and interception. All of the particle deposition occurred in the upstream sector.

For the non-neutralized particles, deposition was observed on the downstream side of the fiber. Their presence was due to the image forces between the slightly charged particles and the neutral fibers. However, since the charge on the particles was very small, the image force--significant over a small distance of the order of particle dimension--caused only a few particles to deposit on the downstream sectors.

When the fiber was subjected to the electric field, the particle deposition was more uniform over the entire fiber surface compared to the first two

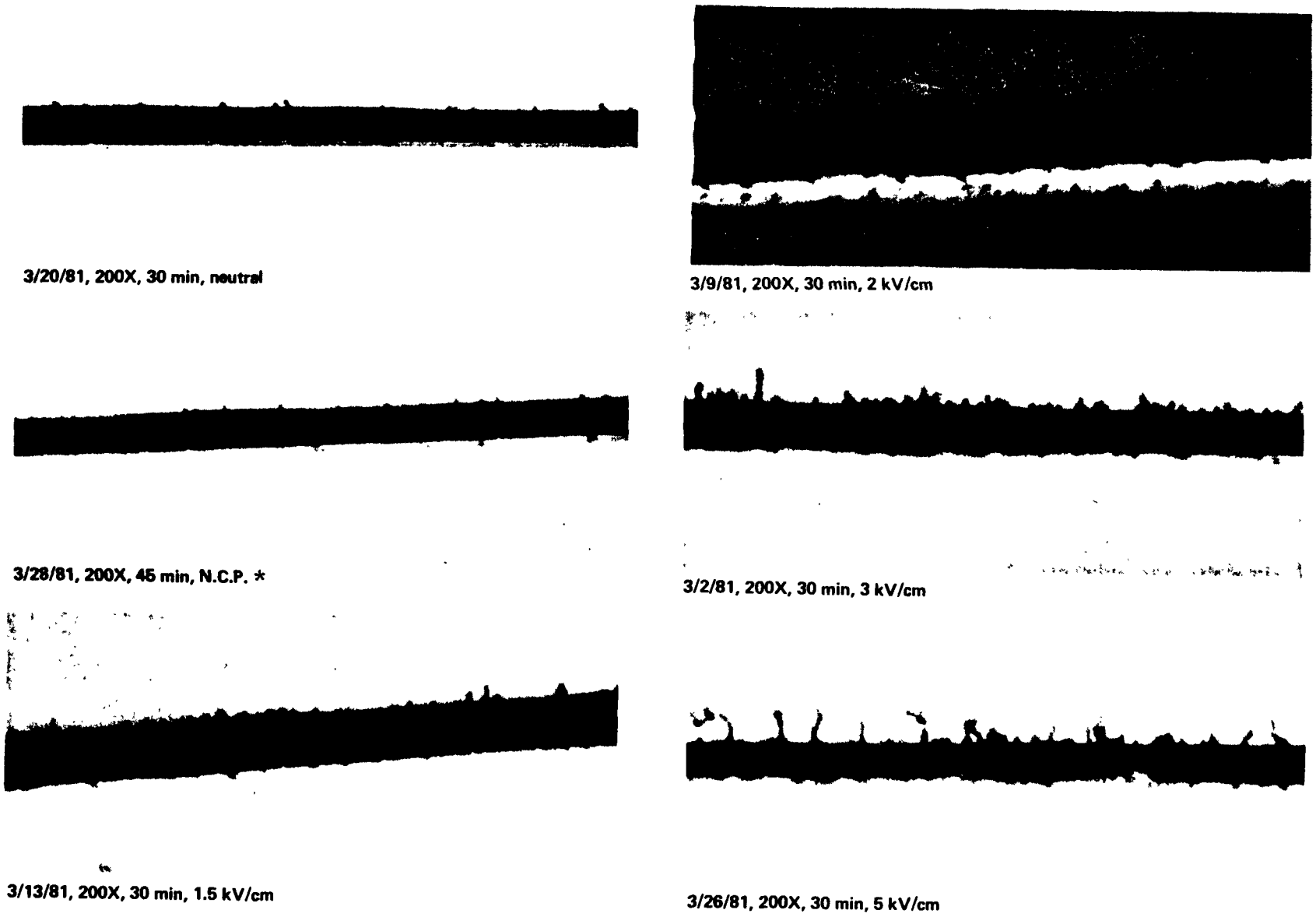

Figure 3. Particle deposits under various electrical conditions.

parts of the investigation. The electric field also affected the shape and size of the dendrites. In contrast to the branching, irregularly shaped dendrites formed in the absence of an electric field, these dendrites were much more slender and very straight. Contact between neighboring chains was very limited.

In all three parts of the investigation, the number of particles and dendrites collected on the fiber increased as the sampling time increased. For any given sampling time, many more particles were collected on the fiber when an electric field was present than when one was not present. Figure 4 shows the dendrite configuration in an electric field strength of 3 kV/cm.

The tendency of dendrite formation on the fiber surface was different for each set of conditions. As shown in Figure 5, the ratio of M_2 to M_1 reflects the probability of dendrite formation. M_2 is defined as the number of particle chains which have a minimum of two particles; that is, the number of dendrites. M_1 represents the number of particles which contact the fiber surface, regardless of whether or not they form the base of a dendrite. The neutralized particles show a greater tendency for dendrite formation than the non-neutralized particles. This may be caused by repulsion between the similarly charged non-neutralized particles, thus preventing particle linkages.

The probability of dendrite formation increased as the electric field strength was increased. In the presence of an electric field, the particles in the flowstream were polarized and were attracted by dielectrophoresis to the metal fiber with a high electric field gradient near it.

The overall collection efficiency was calculated for each experimental run. The efficiency was defined as the ratio between the number of particles collected per unit length of the particles, and the total particle flux across the cross section of the fiber, as shown in Figure 6.

The measured efficiency at zero field agreed very well with the predicted value using the Langmuir-Blodgett theory (18) based on inertial impaction. When the electric field strength was increased, the interaction force between the particle and the fiber increased and the collection efficiency of the fiber increased. Figure 6 indicates that the collection efficiency monotonically increased with electric field strength. The collection efficiency was also calculated for each degree sector of the fiber and is plotted in Figure 7. For the fiber not placed in an electric field, the collection efficiency plots for neutral and non-neutralized particles appear very similar. Both exhibit sharp peaks in the upstream portion of the fiber, and the natural charged particles show a little collection on the backside of the fiber. For the fiber placed in an electric field, the collection efficiency is higher in all degree sectors and exhibits a greater uniformity between the different sectors.

3/5/81, 200X, 2.5 hr, 3 kV/cm

Figure 4. Dendrite configuration deposited on the fiber in an electric field (270° sector).

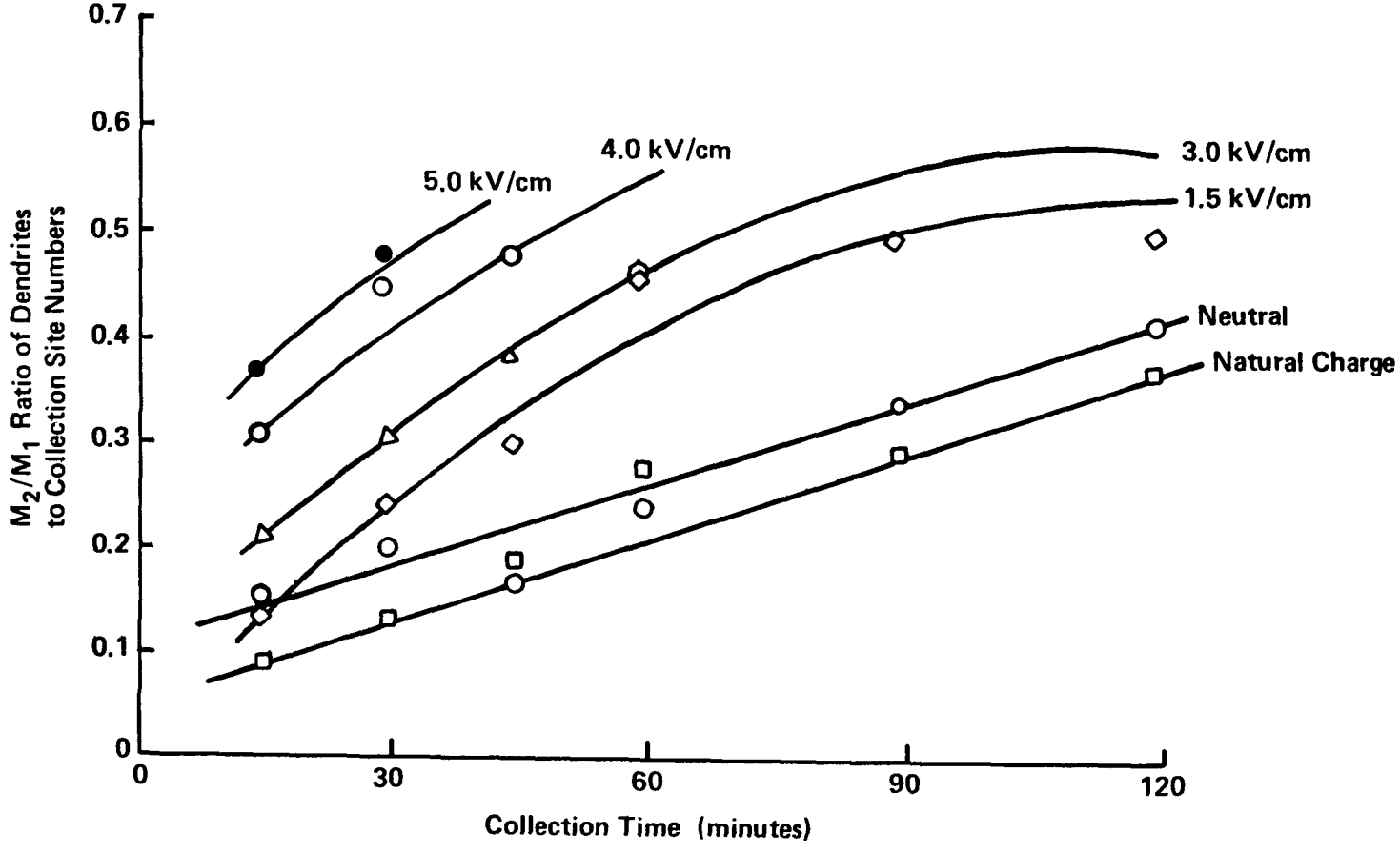

Figure 5. The ratio of dendrite count (M_2) to particle count (M_1) after different collection times.

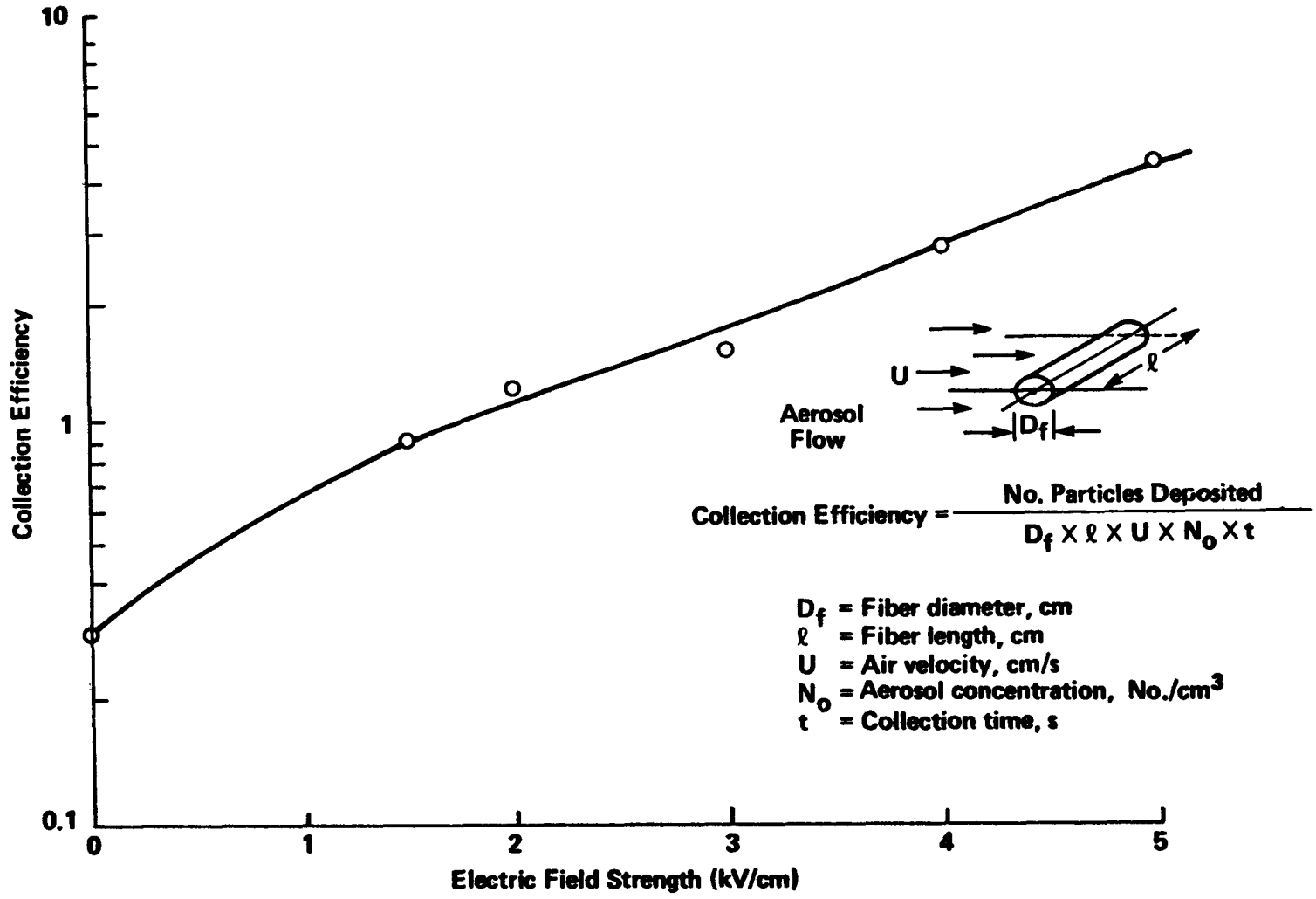

Figure 6. The collection efficiency of particles deposited on the fiber under various electrical conditions.

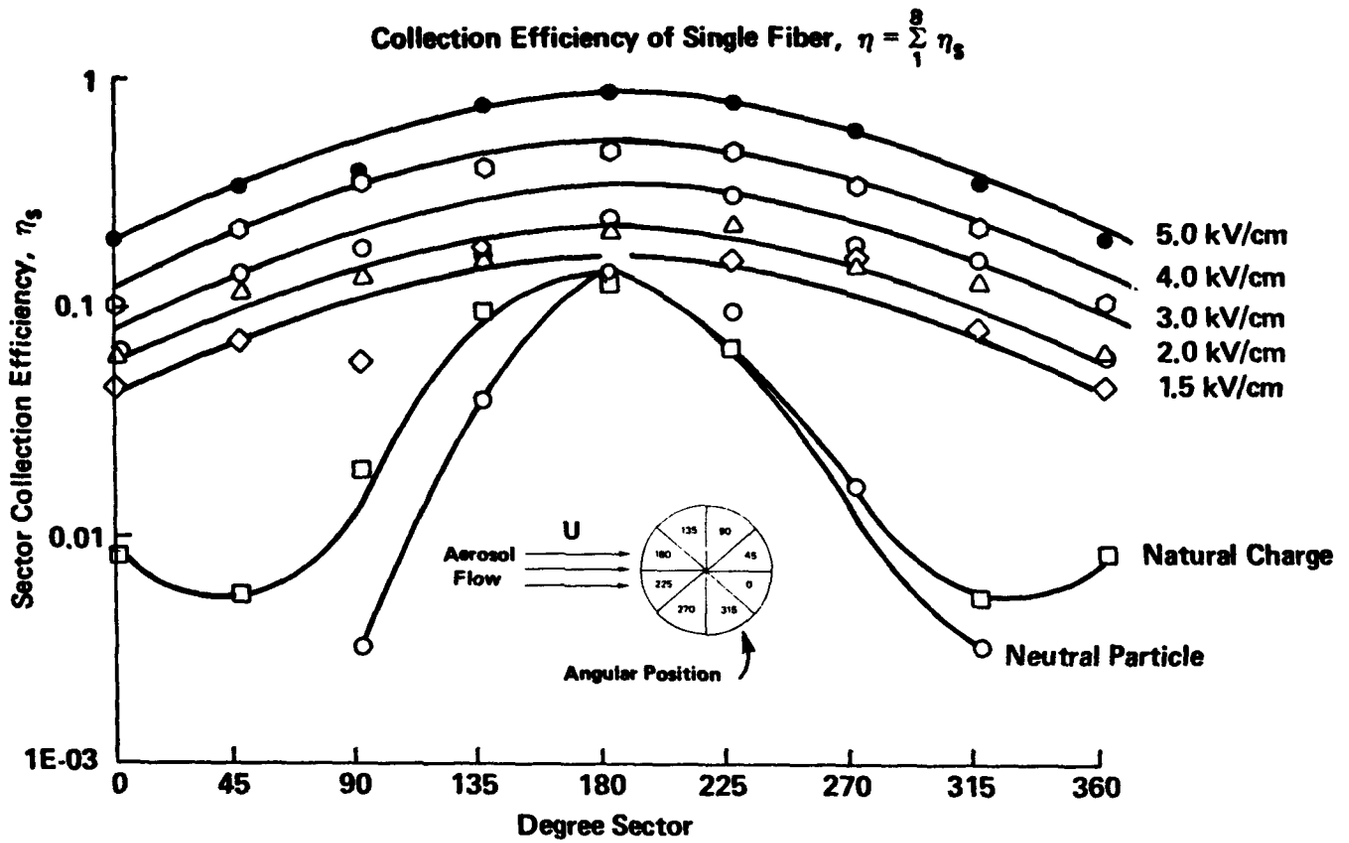

Figure 7. The collection efficiency as a function of sector under different conditions.

CONCLUSIONS

This investigation was performed to observe the quantitative characteristics of particle deposition on a single fiber under three conditions. Based on the observations, the following conclusions were reached:

1. Particle collection efficiency increases as electric field strength increases.

2. In the presence of an external electric field, deposited particles and particle dendrites are more uniformly distributed over the entire metal fiber surface than without the electric field.

3. As electric field strength increases, the probability of dendrite formation increases.

4. Dendrites formed with electric field collection are much more slender and straighter.

REFERENCES

1. Billings, C.E. Effects of particle accumulation in aerosol filtration. Ph.D. dissertation, California Inst. Technology, Pasadena, CA, 1966.

2. Payatakes, A.C. and Tien, C. Particle deposition in fibrous media with dendrite-like pattern: A preliminary model. J. Aerosol Sci. Vol. 7, 85, 1976.

3. Payatakes, A.C. Model of the dynamic behavior of a fibrous filter application to case of pure interception during period of unhindered growth. Powder Technology. 14: 267, 1976.

4. Payatakes, A.C. Model of aerosol particle deposition in fibrous media with dendrite-like pattern: Application to pure interception during period of unhindered growth. Filtration and Separation. 13: 602, 1976.

5. Payatakes, A.C. Model of transient aerosol particle deposition in fibrous media with dendritic pattern. AIChE J. 23: 192, 1977.

6. Payatakes, A.C. and Gradon, L. Dendritic deposition of aerosols by convective Brownian diffusion for small, intermediate, and high particle Knudsen numbers. AIChE J. Vol. 26, No. 3, 443, 1980.

7. Payatakes, A.C. and Gradon, L. Dendritic deposition of aerosol particles in fibrous media by inertial impaction and interception. Chem. Engineering Sci. Vol. 35, 1083, 1980.

8. Tien, C., Wang, C.S., and Barot, D.T. Chain-like formation of particle deposits in fluid-particle separation. Science. 196, 983, 1977.

9. Wang, C.S., Beizaie, M., and Tien, C. Deposition of solid particles on a collector: Formulation of a new theory. AIChE J. Vol. 23, No. 6, 879, 1977.

10. Kanaoka, C., Emi, H., and Myojyo, T. Simulation of deposition and growth of airborne particles on a filter. Kagako Kogako Ronbunshu, Japan. 4, 535, 1978.

11. Kanaoka, C., Emi, H., and Myojyo, T. Simulation of the growth process of a particle dendrite and evaluation of a single fiber collection efficiency with dust load. J. Aerosol Sci. Vol. 11, 377, 1980.

12. Beizaie, M. Deposition of particles on a single collector. Ph.D. dissertation, Syracuse University, Syracuse, NY, 1977.

13. Bhutra, S. and Payatakes, A.C. Experimental investigation of dendritic disposition of aerosol particles. J. Aerosol Sci. Vol. 10, 445, 1979.

14. Barot, D.T., Tien, C., and Wang, C.S. Accumulation of solid particles on single fibers exposed to aerosol flows. AIChE J. Vol. 26, No. 2, 289, 1980.

15. Wang, C.S., Ho, C.P., Makino, H., and Iinoya, K. Effect of electrostatic fields on accumulation of solid particles on single cylinders. AIChE J. Vol. 26, No. 4, 680, 1980.

16. Oak, M.J. and Saville, D.A. The buildup of dendrite structures on fibers in the presence of strong electrostatic fields. J. of Colloid and Interface Sci. Vol. 76, No. 1, 259, 1980.

17. Hiller, V.R. and Loeffler, F. Reinhalt Luft 40, 405, 1980.

18. Langmuir, I. and Blodgett, K. Report on Smokes and Filters. Supplement to Section I and Section II. No. 3460, U.S. Office of Scientific Research and Development, 1944.

PILOT DEMONSTRATION OF PARTICULATE REMOVAL USING A CHARGED FILTER BED

by: Paul H. Sorenson
Air Correction Divison, UOP Inc.
Norwalk, Connecticut 06856

ABSTRACT

The concept of fine particulate collection in a gas stream using a highly porous, charged fiber bed was first developed at Battelle Pacific Northwest Laboratories while studying the collection process by charged spray drops. Laboratory testing by Batelle using highly resistive, charged submicron aerosols showed that extremely high collection efficiencies were possible by this process. Air Correction Division, UOP Inc. has undertaken a program to develop the concept under field scale conditions. A transportable 4000 cfm pilot plant was constructed and installed slipstream on a lignite-fired utility boiler at the outlet of an existing precipitator. The collection efficiency of the bed was monitored as a function of bed face velocity, gas temperature, and particle charge levels. This paper reports the results of the program.

INTRODUCTION

Trends in air pollution control during the last several years have emphasized reduction in particulate emissions without appreciably increasing operating costs. Advances in electrostatic precipitator technology have reduced emissions, but success has been limited by highly resistive ash. Fabric filters have successfully reduced resistive ash emissions but only at the expense of higher operating costs. The Electrostatic Fiber Mat (EFM) filter system invented by the Battelle Pacific Northwest Laboratories (1) appeared to be a potential method for reducing high-resitivity particulate emissions at the outlet of an electrostatic precipitator without an appreciable increase in pressure loss.

To explore the potential of the EFM for collection of flyash, Air Correction Division, UOP Inc. established a program involving laboratory work and field pilot tests. UOP sponsored additional research at Battelle using their laboratory and expertise. Laboratory tests were performed using ash samples collected at boilers burning high- and low-sulfur coal and lignite. The results of these tests showed that the EFM is effective in collecting highly resistive ash with low energy consumption (2). On the basis of these tests, Air Correction Division undertook a program to verify those results under field conditions.

A field test program was established to demonstrate that the EFM was a practical device for the collection of high-resistivity ash that had penetrated an operating electrostatic precipitator. To be considered a practical device, the EFM should remove at least 90% of all incident particulate with a pressure drop of less than one inch of water column. It was also necessary to show that accumulated particulate could be removed from the mat and separated from the flue gas stream for disposal and the mat restored to service. When these criteria have been demonstrated, the EFM could be considered a potential retrofit for nonconforming precipitators. It could also be incorporated into an effective primary particulate emission control system for new installations.

Air Correction has conducted a program of field testing to demonstrate the potential of the EFM. The first site chosen to study high-resistivity ash was a utility boiler burning lignite. An EFM pilot plant was set up and a test program conducted to demonstrate the stated objectives. This paper is a report on that program.

DESCRIPTION OF THE PILOT PLANT

The pilot plant was designed as a five-to-one scale-up of the laboratory apparatus. The EFM system consisted of a particle charging section and fiber mat section with an in-situ mat-cleaning mechanism and interconnecting ductwork. A schematic of the system is shown in Figure 1.

Two particle-charging electrode configurations were tested during the program. The first electrode configuration consisted of wire emitting electrodes and rod grounded electrodes. The electrodes were spaced to emphasize particle charging and to minimize particle collection. Gas velocity in the charging section equaled mat face velocity. In the second configuration, each row of rod electrodes was replaced with a single plate. This design permitted charger operation at lower current densities and reduced electrical stress across the collected ash area.

The fiber mat itself was made of highly resistive fibers knit in an open mesh. The resulting fabric was then layered and compressed to the appropriate thickness and void fraction. Two types of fibers were tested in the field, a monofilament and a yarn. Both fibers were capable of operation up to 500°F. The mats were held between fiberglass grids. Fiberglass pins pierced the mat to provide support and were terminated in the face grids.

DESCRIPTION OF TEST METHODS

Operation of the pilot plant required control and recording of temperature and flow. Temperature was controlled by adjusting a dilution air damper on the inlet duct and was measured with a thermocouple immediately before expansion into the test cross-section. Flow was controlled by adjusting the outlet damper on the slipstream fan. Flow was monitored with a pitot tube and thermocouple located in the high-velocity duct between the test section and the fan. Velocity pressure and mat pressure drop were monitored with an inclined manometer.

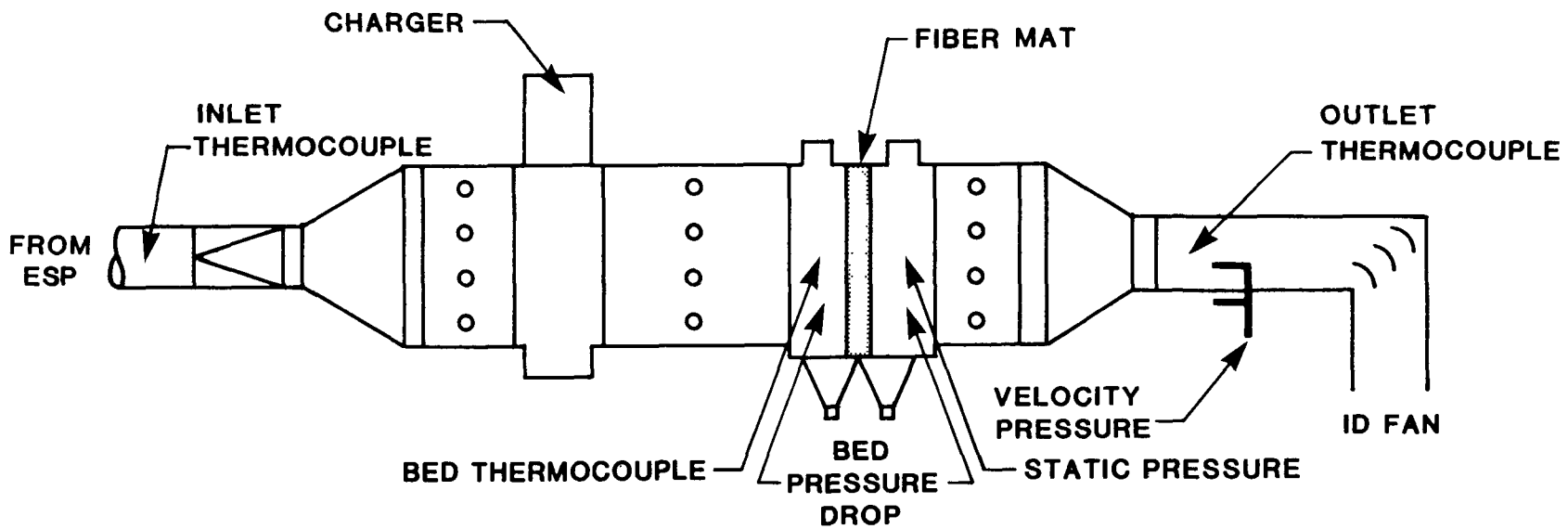

Figure 1.Pilot plant schematic.

Particle concentrations were measured with conventional mass-sampling trains. Standard buttonhook nozzles were mounted on in-line filter holders to provide in-stack particulate sampling at the system inlet and outlet locations. Because of the low velocity at the test locations, sampling rates were calculated from the velocities measured in the high-velocity duct and actual static pressure and temperature readings in the sampling area. Sampling times were calculated so that the lowest anticipated mass loading would be at least two orders of magnitude greater than the smallest division on the mass balance, i.e., approximately 1.0 milligrams when measuring to 0.01 milligrams. The sampling train consisted of probe, filter, desiccant, rotometer, pump, and gas meter. The pilot plant efficiency was calculated from the mass concentrations.

DESCRIPTION OF THE TEST SITE

The test site chosen for evaluation of the EFM with flyash from a utility power boiler burning lignite consisted of a 550 megawatt boiler supplied with lignite from a local strip mine. The pilot plant slipstream was taken from the outlet of the electrostatic precipitator and reinjected at the I.D. fan suction. The precipitator was of conventional design upgraded for increased power and better gas flow distribution. Precipitator performance was generally between 99.3% and 99.5% efficient. The plant uses a flue gas conditioning system in conjunction with the precipitator. The gas conditioning system was in operation during the test period.

A comparison was made between the flue gases entering the pilot plant and the gases leaving the stack to obtain an indication of how well the slipstream represented the plant discharge. Table 1 presents a summary of results of tests taken at the pilot plant inlet and the stack. The close agreement in the two tests shows that the pilot plant slipstream is a reasonable representation of the plant exhaust gases. The lower temperatures recorded at the pilot plant probably result from pilot plant duct in-leakage as is evident by the slight increase in oxygen content.

TABLE 1. COMPARISON OF PILOT STREAM TO STACK

	PILOT	STACK
Flow Rate, acfm	2800	2.1×10^6
Flow Rate, dscfm	1558	1.2×10^6
Temperature, ^oF	322	366
Moisture, %	13	13
CO_2, %	13	13.3
O_2, %	6	5.8
CO, %	-	-
N_2, %	81	80.8
EA %	38.8	34.9
Grains/dscf	0.06	0.075

Flyash resistivity readings were taken on samples of ash taken from the hoppers on the last stage of the precipitator. The results are shown in Table 2.

TABLE 2. RESISTIVITY OF FLYASH SAMPLES

TEMPERATURE	MOISTURE PERCENT VOLUME	
Degrees F	11.5%	16.5%
200	3.7×10^{11}	1.8×10^{11}
240	3.6×10^{11}	2.4×10^{11}
280	3.7×10^{11}	2.2×10^{11}
315	3.1×10^{11}	2.1×10^{11}
355	1.8×10^{11}	1.6×10^{11}

Resistivity in ohm-cm at 3.87 KV/cm

DISCUSSION OF RESULTS

PARTICLE COLLECTION EFFICIENCY

The test program was arranged to compare the wire-rod charger with the wire-plate charger by operating each charger with the monofilament mat and obtaining the mass efficiencies of both combinations. The charger configuration providing higher efficiency would then be operated with the yarn mat and the test series would be repeated. Each combination was tested for mat face velocities from 200 to 350 feet per minute and temperatures ranging from 200°F to 350°F.

Each charger configuration was operated with the monofilament mat over temperatures ranging from 200°F to 350°F. The collecting efficiency for the EFM increased from 81.2% for the wire-rod arrangement to 90.5 for the wire-plate arrangement. Lower efficiencies for the wire-rod configuration can be attributed to higher current densities and electrical field stress resulting in back corona. (3) Fiber mat face velocity was varied from 200 to 350 feet per minute without a noticeable change in collection efficiency.

The yarn fiber bed was then installed in the pilot plant and compared with the monofilament performance. The particle collection efficiency increased to 94.6%. The increase in efficiency can be attributed to the smaller diameter of the yarn fiber and a lower sensitivity of the material in the yarn to changes in resistivity.

Laboratory tests showed that efficiency was essentially insensitive to inlet dust loading from 0.08 to 0.12 gr/dscf. Actual inlet loadings to the pilot plant covered a wider range. Testing during periods of precipitator maintenance and other upset conditions resulted in inlet loadings ranging from 0.05 to 1.32 gr/dscf. Particle collection efficiency remained constant over the entire range of inlet concentrations. Mat dust loadings and therefore mat pressure drop increased due to the heavy accumulation within the mat during periods of heavy loading. Once the bed was cleaned, pressure drop returned to the desired operating range.

PRESSURE DROP AND MAT CLEANING

Both mat configurations were tested for pressure drop before they were contaminated with ash. The monofilament mat construction had a pressure drop of 0.21 inches of water column at 300 feet per minute and the yarn mat construction had a pressure drop of 0.46 inches of water column at 300 feet per minute. The increase in pressure drop for the yearn is a result of the difference in the diameter of the fiber and the differences in aerodynamic profile. The monofilament presents a smooth, cylindrical obstruction to the gas flow. The yarn forms a ribbon-type obstruction with its oval cross-section constantly changing orientation with respect to the flow path. In addition, while the monofilament has a smooth surface, the yarn has an irregular surface resulting from the multitude of filaments of which the yarn is composed.

Two methods of mat cleaning have been evaluated. The first method used high-velocity water sprays to remove the ash from the mat fibers. The second method used a compressed air and vacuum system where the concentrated dust cloud is drawn out of the gas duct and separation occurs in an auxiliary baghouse. Both systems removed sufficient ash to maintain a constant pressure drop across the mat of less than one inch of water column. The water systems was used exclusively with monofilament mats and the air system with yarn mats.

Inspection of the mats constructed of monofilament following several cleaning cycles showed that the wash system was effective in restoring the fibers to their clean state wherever the sprays contacted the mat. The spraying action did, however, drive some of the ash into unwashed areas, especially around the edges. These areas eventually collected sufficient ash to block off flow and resulted in increased pressure drop. Once these areas were packed, no furthur build-up was noticed. Thus, the pressure drop after cleaning increased gradually from 0.21 inches of water column to 0.28 inches of water column. All subsequent cleaning cycles returned the pressure drop to 0.28 inches. Three sample collecting/cleaning cycles for the water system with the monofilament mat are shown in Figure 2. It can be noted that the collecting time for the mat is only limited by the maximum tolerable pressure drop.

Operation of the compressed air vacuum system was considerably different from the water system. Unlike the water system, which carries all of the particulate away with the slurry, the air system momentarily resuspends collected particulate in a concentrated cloud, which is then drawn off through the vacuum system. Since the vacuum cannot draw from deep within the mat, the cleaning cycle must be timed so that the particulate is resuspended while still within reach of the vacuum. The compressed air vacuum system must therefore be used more frquently than the water system. The yarn presents an additional problem in cleaning. Because of its construction from many filaments, the yarn traps particulate within the filaments, especially when direct interception occurs. Cleaning vigorously enough to dislodge such trapped particles would at the same time destroy the integrity of the yarn. Increases in pressure loss due to this type of particle accumulation appear to diminish after eight to ten hours of operation. After this initial increase, a constant range of operation can be held. Figure 3 shows the pressure drop history for a yarn mat with compressed air vacuum cleaning The gradually increasing pressure drop due to intrafiber capture can be seen stabilizing after about seven hours of operation and several cleaning cycles.

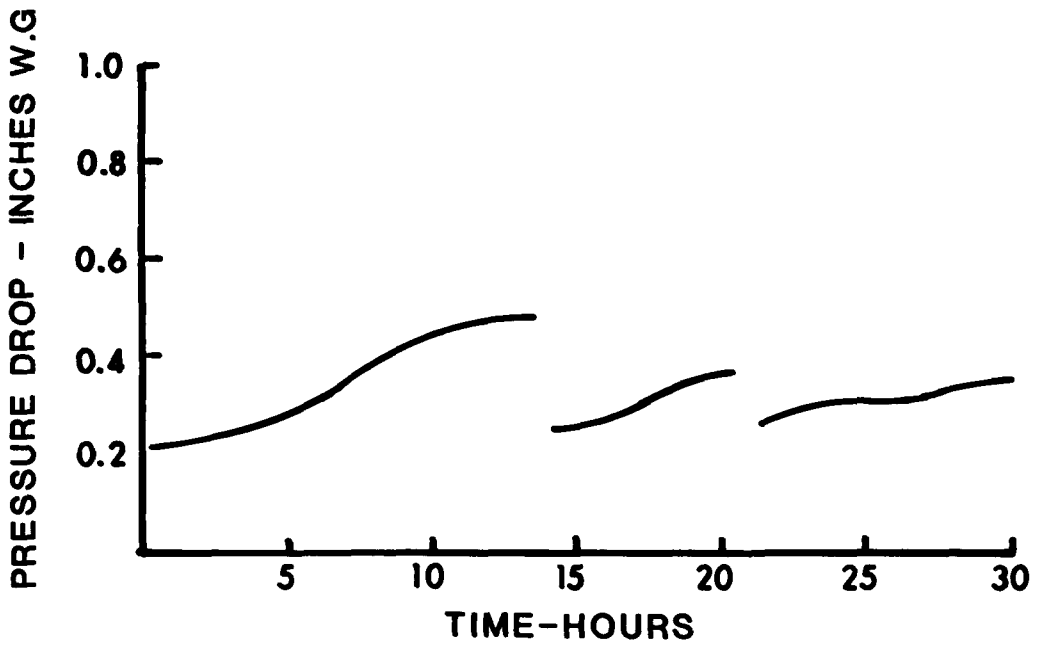

FIGURE 2
PRESSURE DROP HISTORY FOR WATER CLEANED MATS

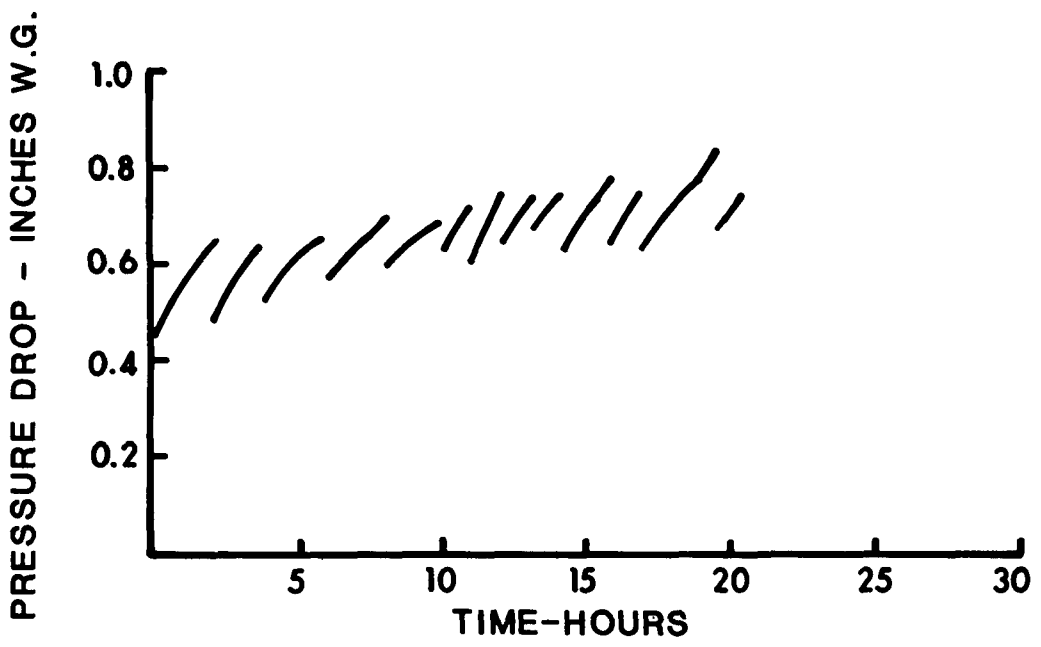

FIGURE 3
PRESSURE DROP HISTORY FOR AIR CLEANED MATS

CONCLUSIONS

The test program was designed to demonstrate that the Electrostatic Fiber Mat is a practical method of reducing highly resistive flyash emissions. The pilot plant was operated to show that practicality in efficiency, operating pressure drop, and mat cleaning techniques.

Mass efficiencies of 94% for the wire-plate charger and yarn mat system exceeded the objective of 90%. Projecting this efficiency to a full-size installation such as the host site would reduce the current average emission of 0.075 gr/dscf to less than 0.007 gr/dscf. The EFM efficiency has also been shown to apply to a range of inlet concentrations from 0.05 to 1.3 gr/dscf. The ability to retain collection efficiency during inlet upsets is especially advantageous when emissions drift out of compliance during plate rapping, soot blowing cycles, or load changes.

The practicality of this device has been further shown in the operation of the compressed air vacuum mat cleaning system. The water wash system is extremely effective in regenerating the mat. The quality of cleaning does not offset the drawbacks of sectionalization and isolation required to cool, clean, and reheat the mat assembly. The development of the air system overcomes the difficulties of the water system at the expense of reduced time between cycles. Thus, while the monofilament mat with water washing was regnerated every eight to ten hours, the yarn mat was air cleaned every two hours. The combined system of a yarn mat with compressed air vacuum cleaning therefore presents a practical method of reducing the emissions from an operating electrostatic precipitator.

The work described in this paper was not funded by the U. S. Environmental Protection Agency and therefore the contents do not necessarily reflect the views of the Agency and no official endorsement should be inferred.

REFERENCES

1. Reid, D.L. and Browne, L.M., "Electrostatic Capture of Fine Particles in Fiber Beds," EPR Report 600/2-76-132, National Technical Information Service, Springfield, VA (976)

2. Bamberger, J.R. and Winegardner, W.K., "Fiber Bed Filter System Control of Ash Particualtes," ASME paper 81-WA/APC-1, ASME Publication, New York, NY (1981)

3. White, H.J., "Resistivity Problem in Electrostatic Precipiator," APCA 24(4): 314-338 (April 1974)

4. Yu, H.S. and Teague, R.K., "Performance of Electrostatic Fiberbed," presented at the First Annual Conference of the Aerosol Research Association, February 17-19, 1982, Santa Monica, CA

PILOT DEMONSTRATION OF MAGNETIC FILTRATION WITH CONTINUOUS MEDIA REGENERATION

by: Carroll E. Ball and David W. Coy
Research Triangle Institute
Research Triangle Park, NC 27709

ABSTRACT

A mobile pilot plant with a nominal flow capacity of 3,060 m^3/hr (1,800 cfm) was designed and built to evaluate the use of high gradient magnetic filtration (HGMF) for particulate emission control on an electric arc furnace (EAF). A five-month test program was conducted at Georgetown Steel Corporation's plant in Georgetown, South Carolina, to test the performance of the HGMF. A 500-hour long-term test was scheduled and later changed in order to perform additional characterization studies.

The pilot-plant collection efficiency was less than expected for the stainless steel wool matrix packed to a density of 1.5 percent by volume. The matrix was then changed to an expanded metal, packed to a density of 3.5 percent by volume, which resulted in much lower pressure drop measurements, but even lower collection efficiencies. The expanded metal matrix was then packed to a density of 6.0 percent by volume, which gave higher collection efficiencies than the steel wool and a slightly lower pressure drop.

During the field test operations, there were no significant problems with the HGMF mobile pilot-plant equipment.

The report describes the design and construction of the continuous HGMF mobile pilot plant, as well as some of the background work in high gradient magnetic filtration done at RTI. The field start-up and performance characterization of the mobile pilot plant are discussed in detail. The experimental data and data analysis are given, as well as an economic evaluation and comparison of the HGMF with other particulate control devices.

This paper has been reviewed in accordance with the U.S. Environmental Protection Agency's peer and administrative review policies and approved for presentation and publication.

INTRODUCTION

Since the commercialization of high gradient magnetic filtration (HGMF) in the clay industry 10 years ago, the applications of magnetic separation of process streams have been steadily increasing. Some of the applications are mineral beneficiation, coal deashing, coal desulfurization, wastewater treatment, and blood component separation. From 1975 to 1977 Research Triangle Institute (RTI) conducted experimental work, funded by the U.S. Environmental Protection Agency (EPA), in the application of HGMF to air pollution control. Magnetic separation was tested in the laboratory on several dusts from the iron and steel industry. There were promising results from the following iron and steel industry sources: basic oxygen furnace (BOF); electric arc furnaces (EAF); open hearth furnace; scarfing machine; and the sinter machine.

An earlier pilot plant was designed and built by RTI and tested on a Pennsylvania sintering plant. The overall efficiency data were low for these tests, however, due to the low specific magnetization of the sinter plant dust. It was then decided to design and build a pilot plant with continuous media regeneration and test it on a dust with higher specific magnetization such as BOF or EAF dust.

In June, 1981 the pilot plant was moved to Georgetown, South Carolina and connected to a slipstream from the exhaust of three EAF's just upstream of a baghouse. After startup and debugging, the test program was begun to obtain results on the effects of filter density, applied magnetic field, and gas velocity on overall and fractional collection efficiency. Total mass and fractional collection efficiency tests were conducted, and samples of the dust entering, exiting, and captured by the pilot plant were collected for magnetic and chemical analyses.

The results of the field tests were used to make technical and economic assessments of the application of HGMF to EAF's, and to compare HGMF to other types of pollution control devices.

BACKGROUND DEVELOPMENT

BASIC CONCEPT

The fundamental concept of the HGMF process is the interaction between paramagnetic or ferromagnetic particles and ferromagnetic fibers while in the presence of an applied background magnetic field. The applied magnetic field induces a magnetic dipole in the particle and magnetizes the wire. This creates a convergence of the field near the wire resulting in a net force being applied to the particle. The magnetic force, in competition with the viscous, inertial, and gravitational forces, causes the particle to be attracted to the wire and held there until the applied field is removed.

The high gradient magnetic filter consists of several cassettes packed with ferromagnetic fibers (such as stainless steel wool or expanded metal)

which are moved into a magnetic field as the particle-laden gas is being passed through. The particle-laden gas is cleansed as the particles are attracted to and held by the fibers. When the matrix is loaded, the cassette is then moved out of the magnetic field and the particles are flushed from the fibers.

HGMF DEVELOPMENT AND APPLICATIONS

The experimental work in high gradient magnetic filtration, with the exception of the EPA sponsored development begun in 1975, has been most concerned with the magnetic separation of particles in a slurry. Oberteuffer (1), Kolm et al (2), Oder (3), and Iannicelli (4) have published excellent reviews of the process and its chronological development. A brief review of HGMF development can also be found in the EPA report "Application of High Gradient Magnetic Separation to Fine Particle Control" by Gooding et al (5).

The most extensive development of HGMF has been within the last decade in the clay industry. Here, the HGMF is used to separate small paramagnetic color bodies from kaolin clay. The successful demonstration of this process in the clay industry has sparked investigations of HGMF for many different applications.

DETAILED DESIGN AND CONSTRUCTION OF THE HGMF MOBILE PILOT PLANT

The mobile pilot plant is a continuous HGMF system housed in a 12.8 m (42 ft) freight van. The system is designed for a nominal flow capacity of 3,060 m^3/hr (1,800 cfm). Figure 1 is a flow schematic of the continuous HGMF system.

The dirty gas enters the pilot plant through a 0.267 m ID stainless steel pipe (10" schedule 5). The gas passes by test ports through which samples can be drawn to determine inlet dust concentration, chemical composition, and size distribution, and then is directed to the HGMF device. The magnetic filter is a Sala-HGMS® Carousel Model 120-05-00 (Sala Magnetics, Inc., Cambridge, MA) incorporating a magnet head and a cleaning station mounted 180° apart on a rotating carousel. The magnet coils are split into a saddle configuration to allow the carousel to be rotated through the magnetized zone by a variable speed drive. The carousel contains 48 removable cassettes which can be loaded with filter material to a depth of 0.15 m (5.8 in.). The magnet head encloses an active face area of 0.085 m^2 (133 $in.^2$) in the direction of fluid flow. The magnet head is designed to provide an applied field from 0.0 to 5.0 kG. In the range of gas velocities tested, 2 to 10 m/s, the gas residence time in the filter varied from 0.015 to 0.075s.

After passing through the magnet, the gas then passes by another set of test ports and exits the pilot plant. Once leaving the pilot plant, the gas is directed through an orifice, for velocity determination, through an induced draft blower and then is exhausted to the atmosphere through an 8 m (26 ft) high stack.

After the filter matrix has passed through the magnetized zone and collected dust from the gas stream, it then passes through the cleaning station. The filter is cleaned by backflushing with compressed air.

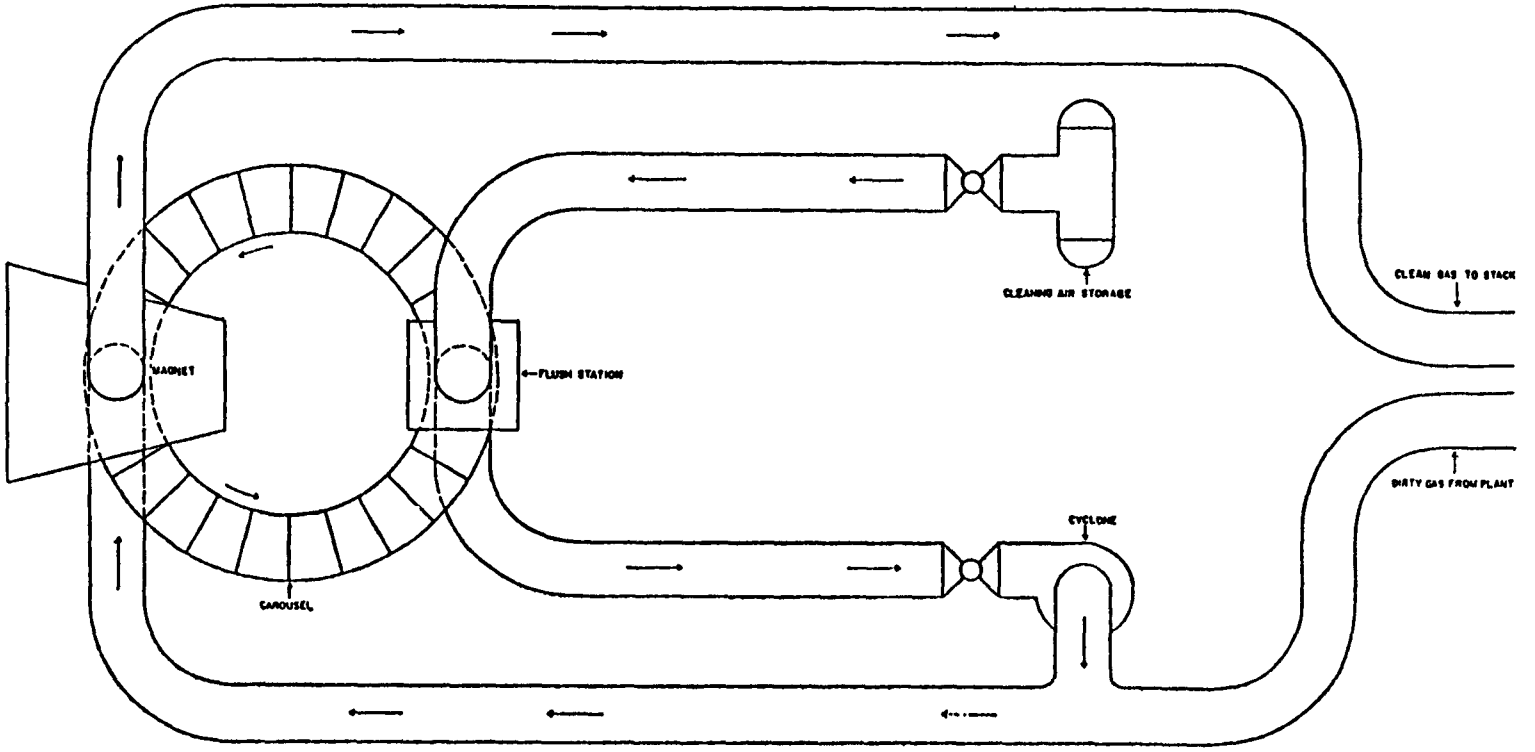

Figure 1. Flow schematic of continuous HGMF system.

The agglomerated dust that is cleaned from the filter matrix with the cleaning air pulse is sent to a cyclone. Exhaust from the top of the cyclone is recycled into the dirty gas stream. Dust can be removed from the cyclone while the pilot plant is in operation through a double-sealed valve.

The induced draft blower which moves the gas through the pilot plant is rated at 3,060 m^3/hr at a suction pressure of -13.7 kPa (-55 inches H_2O) and a temperature of 150°C. The entire system is designed to allow continuous operation at temperatures of up to 200°C. All interior and exterior pipe is insulated with jacketed fiberglass.

The utility requirements of the pilot plant are electricity and water. The main power panel has 400 ampere service at 440 ac volt input. The total connected load is 300 amperes. The major equipment operates off 440 vac and a transformer is provided to step down to 240 vac and 120 vac. Water consumption is approximately 2.3 m^3/hr (10 gpm) for magnet cooling, compressor aftercooler, and occasional use of the lab sink.

FIELD OPERATIONS

DESCRIPTION OF THE ELECTRIC ARC FURNACE AT GEORGETOWN, SOUTH CAROLINA

The dust source was an EAF shop utilizing three arc furnaces operating continuously in a staggered batch operation. The Georgetown Steel raw steel production facilities are composed of three 68 Mg (75 ton) per cycle DeMag electric arc furnaces. The charge to the furnaces consists of scrap and prereduced iron pellets. The scrap charged is obtained primarily from external sources; about 5 to 10 percent is reclaimed scrap. Prereduced pellets are produced on-site from South American iron ores. Other materials added to the furnaces during the course of the production cycle include limestone, coke, ferromanganese, and ferrosilicon.

Gas cleaning for the furnaces is provided by a positive pressure baghouse supplied by American Air Filter. A slipstream of gas was taken from the duct. The gas stream conditions at the extraction point are listed below:

Pressure	-1.7 kPa (-7 inches H_2O)
Temperature	71°C (160°F)
Velocity	17 m/s (55.65 ft/s)
Reynolds Number	4.1×10^6

PERFORMANCE CHARACTERIZATION

The test program was designed to test the effects of four parameters on collection efficiency, and the reliability of the equipment during long-term operation. The four parameters to be varied were applied field, gas velocity, filter type, and filter packing density.

Selection of an optimum set of operating conditions was the goal of the performance characterization. The selection of optimum conditions was to be based on statistical analysis of the performance data obtained under varied operating conditions. Performance under each set of conditions was to be measured by sampling the HGMF inlet and outlet particulate concentrations. Overall efficiency would be determined on a mass basis, and fractional efficiency would be determined by measuring inlet and outlet particle size distribution. Periodically during the characterization, bulk samples of the particulate were to be obtained from the inlet, the outlet, and the cyclone catch in order to obtain the chemical composition and its effect on performance and vice versa.

The applied magnetic fields were varied between 0 and 5 kG for each of three test series. Gas velocities through the filter were varied between 2 and 10 m/s.

The initial filter medium was American Iron and Steel Institute Type 430 medium grade stainless steel wool packed to a density of 0.015 (1.5 percent by volume) and came packed in the carousel from Sala Magnetics. The average fiber diameter of this material is 120 μm.

The second and third test series were run with expanded metal matrices (layers of wide mesh screen separated by spacers). The expanded metal matrix can be packed with all of the fibers perpendicular to the magnetic field and in the optimum position for particle capture. This we had hoped would allow us to obtain a higher collection efficiency for the same pressure drop as was attained with a stainless steel wool matrix.

The average fiber diameter of the expanded metal matrix is 300 μm. In the second test series, the approximate packing density of the expanded metal matrix was calculated to be 0.035. In the third test series the packing density was calculated as 0.06.

Multiple linear (slope-intercept form) regression techniques were used to analyze the overall mass efficiency data. The groups of data for each matrix type and packing density were obtained in sequence, rather than randomly, owing to the difficulty of changing the carousel cassettes. Also because of this factor, statistical analyses were performed on the data grouped by packing type and packing density. Using statistical techniques, the model found to produce the best data fit was an exponential model.

The comparative performance of the filter system for both matrices and packing densities can be seen in Figure 2. The performance data are plotted as penetration (1-efficiency) versus regression function divided by inlet mass rate. The line through each data set is a regression curve for that data set. The regression coefficients a, b, c, and intercepts for each set of data are given in Table 1. To compare the performance one must examine the penetration at low values of the regression function for each data set. Looking at the functional relation of each variable in the regression function, it is expected that best performance would be measured for low regression function values, i.e., low inlet mass, low velocity, and high field strength. Differing absolute values of the regression function occur between sets because of the different regression coefficients for each data

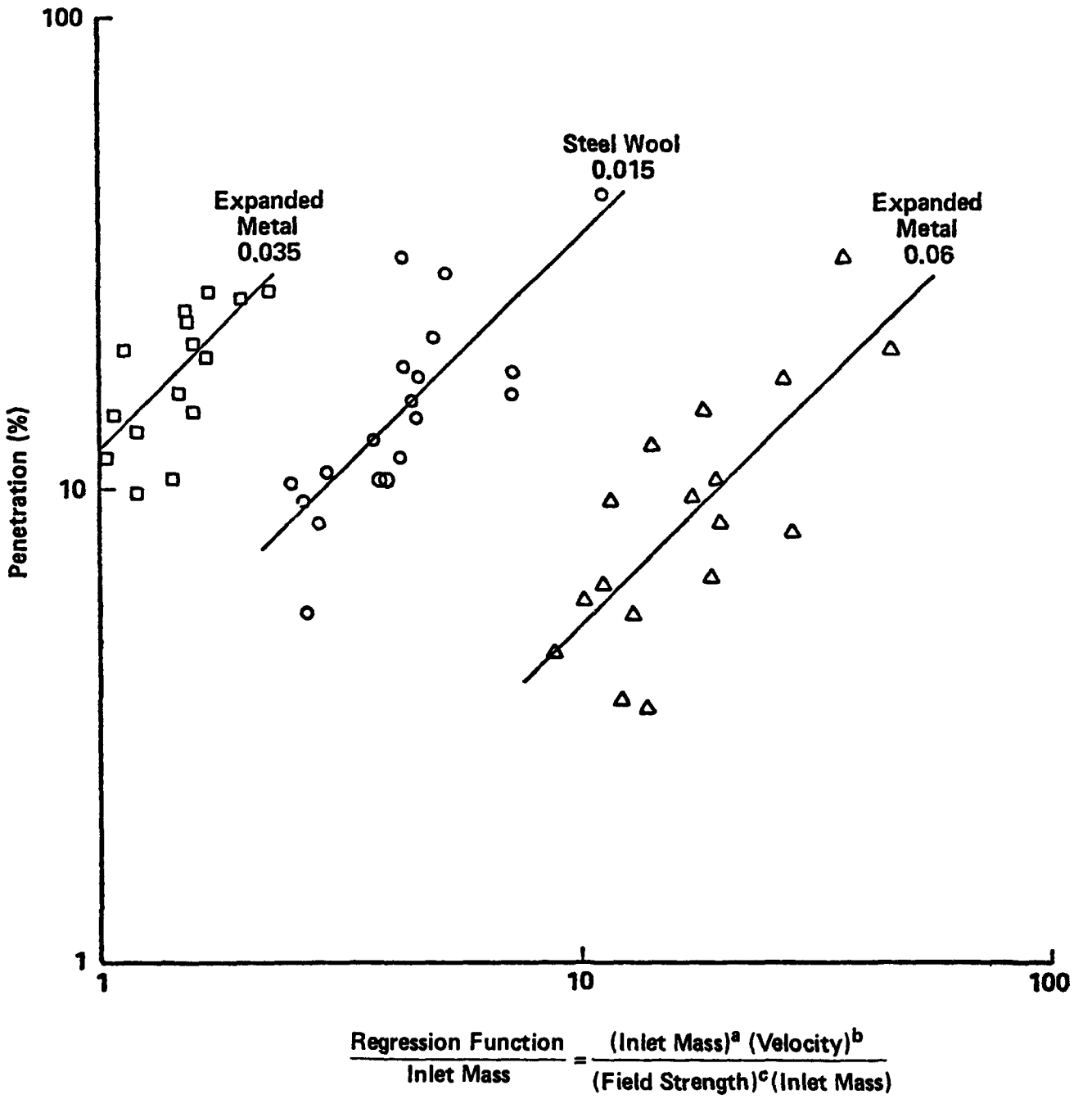

Figure 2. Georgetown Steel HGMF test--Penetration vs. regression function (all matrices and packing densities).

TABLE 1. REGRESSION COEFFICIENTS FOR EACH FILTER MATRIX AND PACKING DENSITY

Model: $\text{Outlet mass rate} = \text{Intercept} \times \frac{(\text{Inlet mass rate})^a(\text{Velocity})^b}{(\text{Field Strength})^c}$

Matrix and packing density	Intercept	Regression Coefficients a	b	c
Steel wool, 0.015	0.034	0.482	0.801	0.315
Expanded metal, 0.035	0.123	0.647	0.351	0.139
Expanded metal, 0.06	0.005	0.364	1.39	0.227

set. At low values of the regression function, poorest performance was measured for expanded metal at 3.5 percent packing density, with clearly best performance from expanded metal at 6 percent packing density.

Table 2 presents the predicted penetration based on the model and coefficients in Table 1 for both matrices and packing densities at fixed system operating conditions. Predicted penetrations are lower for expanded metal at 6 percent packing density and the observed pressure drop was also lower for this matrix than for steel wool. Pressure drop was significantly lower for expanded metal at 3.5 percent packing density, but its predicted penetration is about twice as high as that for 6 percent packing density at the higher field strengths. Based on Table 2, expanded metal at 6 percent packing density would be the preferred matrix.

TABLE 2. PREDICTED FILTER PERFORMANCE FOR EACH FILTER MATRIX AND PACKING DENSITY

Operating conditions*	Matrix and Packing Density: Steel wool 0.015		Expanded metal 0.035		Expanded metal 0.06	
	Penet.%	ΔP**	Penet.%	ΔP**	Penet.%	ΔP**
0.1 kilogauss 7m/s	26.2	38.1	22.5	25.4	15.2	30.5
2.5 kilogauss 7m/s	9.5	38.1	14.4	25.4	7.3	30.5
5.0 kilogauss 7m/s	7.6	38.1	13.1	25.4	6.2	30.5

* Inlet concentration = 1.0 gram/m^3.
**Actual pilot-plant ΔP, cm H_2O.

Performance By Particle Size

The MRI cascade impactor size data were used to generate particle size penetration curves. Simultaneously obtained inlet and outlet distribution curves were used, and in some cases data taken under duplicate conditions were combined to provide composite fractional efficiency curves.

Figure 3 shows typical fractional penetration curves for each matrix and packing density. It is evident that the filter is relatively inefficient for particle sizes below 1 μm in diameter. This leads to the question of whether inefficiency in the smaller particle size range is inherent to the design and magnet operating conditions chosen for these tests, or attributable to variation in size-related particle characteristics.

Chemical And Magnetic Characteristics Of The Dust

The chemical and magnetic characteristics of suspended dust entering and leaving the pilot plant were analyzed. The outlet dust samples contained a relatively significant amount of magnetic material. For the low field test case (0.1 kilogauss), the outlet dust specific magnetization was about 80 percent of the inlet dust value. For the 2.5 kilogauss field cases, the outlet dust specific magnetization was about 65 percent of the inlet values. In the high field case (5.0 kilogauss), the outlet value was about 50 percent of the inlet value.

Elemental chemical analyses were performed on collected inlet and outlet dust samples by atomic adsorption. In each set of samples the percentage of iron in the outlet sample was lower than in the the inlet sample, as expected. However, even in the case of the maximum magnetic field strength tests there was 6 percent by weight iron penetration. The fact that incomplete elemental iron separation occurred in the magnetic filtering process suggests complex particle chemistry.

Other studies (6) of EAF dust have shown zinc (a diamagnetic element) to be associated with iron in particles labelled mixed ferrite. Some of these particles were found in both magnetic and non-magnetic fractions. Since some of the iron occurs in ferrite particles that are non-magnetic, this offers one explanation for iron penetration not approaching zero in these pilot-plant tests.

Discussion of Performance Characterization Results

This pilot program was the first attempt at using a continuously cleaned magnetic filter unit on a gas stream as opposed to a liquid stream.

The performance data discussed, showed the best performance (efficiency), was achieved with an expanded metal matrix at 6 percent packing density. This best performance was achieved at a pressure drop lower than the second best performing matrix, steel wool. This test program was the first in the HGMF development program attempting to use an expanded metal matrix instead of steel wool. Given the better performance at lower pressure drop observed in the initial experiments, expanded metal matrices deserve further study toward additional optimization.

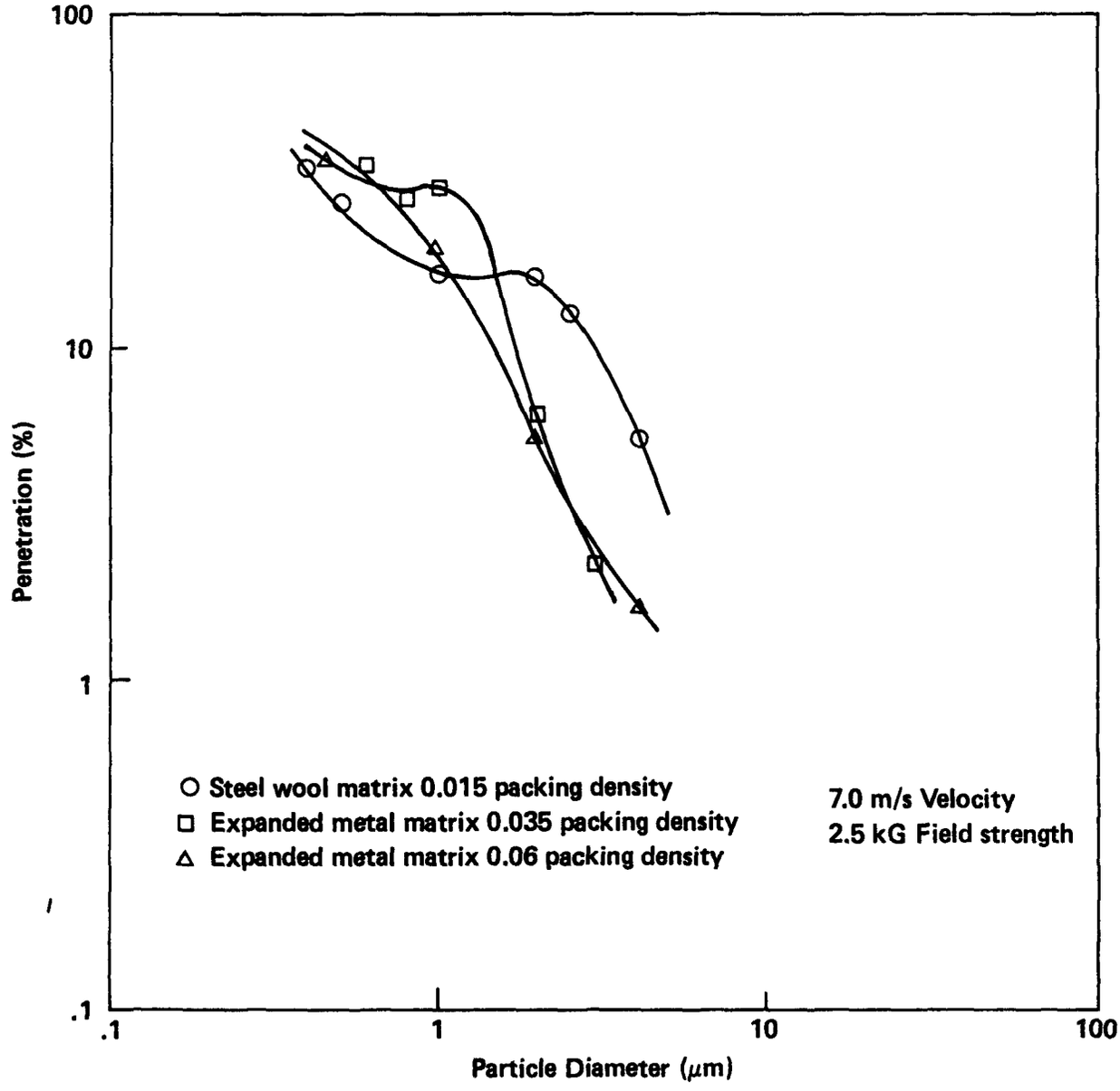

Figure 3. Georgetown Steel HGMF test—penetration vs. particle size.

For the given conditions of applied field, velocity (residence time), and inlet concentrations, the best overall efficiencies achieved were in the range of 94 to 96 percent with outlet concentrations in the range of 20 to 70 mg/m^3. The efficiency levels are much improved over those achieved in the previous pilot plant work on sinter plant emissions. The performance levels, however, are not competitive with conventional high efficiency control devices applied to electric arc furnaces. The New Source Performance Standard (NSPS) for electric arc furnaces limits particulate emissions to 12 mg/dsm^3. The HGMF outlet concentrations in these tests were 2 to 6 times the required level. State standards for existing sources vary considerably e.g. Pennsylvania equivalent to 18 mg/dsm^3, Michigan equivalent to 130 mg/dsm^3. On a performance basis, HGMF might have some limited retrofit potential.

The fractional penetration data show the HGMF was not as effective on particles below 1 μm in diameter as on those above 1 μm. In terms of fractional particle size penetration, it is not evident that any significant qualitative differences exist between HGMF and conventional control devices.

The magnetic analyses data reveal that the HGMF did not remove all of the magnetic material. The magnetic material penetrating the collector may do so because of insufficient residence time or reentrainment. The chemical analyses data reveal a significant amount of iron penetrated the filter, especially in the small particle size (below 1 μm) fraction. Penetration of the iron may be due to insufficient residence time and reentrainment. However, the recent report (6) indicating some iron in electric arc furnace dust to be present in a "non-magnetic" form (probably meaning not ferromagnetic) suggests a third mechanism for penetration. The HGMF's sensitivity to chemical composition of particles and their resulting magnetic susceptibility is analagous to the effects of chemical composition on particle resistivity and electrostatic precipitator performance.

An alternative use for HGMF not explored in this study is to separate non-magnetic components of waste EAF dust from magnetic components, i.e. ferrous and non-ferrous. At present, EAF dust is classified as hazardous waste as a result of heavy metals contamination. Separation of the ferrous portion with minor contamination by zinc might permit its recycle to steelmaking, reducing the residue for disposal. With sufficient concentration of zinc, the non-ferrous portion might be sold to zinc refiners. The association of iron and zinc in non-magnetic particles identified in the study discussed above (6) suggests that this potential application of HGMF needs further study to determine the degree of separation achievable.

ECONOMICS

Approximate costs have been developed for four different options for particulate emission control of EAF dust. The accuracy of these costs corresponds roughly to that of a study grade estimate (±30 percent) and are shown in Table 3. Although a best estimate is presented for both capital and annual expenses, it should be kept in mind that the absolute costs of the four options may depend on special process details -- plant location, and

material of construction. Consideration of these details was not within the scope of the estimate. However, the estimates were made for the following common base case:

Volumetric flow rate:	8,500 m^3/min @ 66°C
Inlet dust loading:	1,050 mg/sm^3
Outlet dust concentration:	12 mg/sm^3
Annual operation:	8,500 hr/yr

For purposes of the economic comparisons, it was assumed that HGMF performance could attain the outlet concentration needed to comply with the EAF NSPS, or 12 mg/sm^3.

TABLE 3. COSTS OF VARIOUS CONTROL OPTIONS FOR EAF PARTICULATE EMISSION $/$m^3$/s

	Total capital costs	Total annualized costs 10 yr[1]	20 yr[1]	Direct operating costs[2]
HGMF[3]				
2 m/s	31.31	7.06	5.64	0.71
5 m/s	20.99	5.21	4.26	0.95
7 m/s	14.16	4.07	3.43	1.20
ESP	11.94[4]	3.43	2.89	1.01
Fabric Filter	11.11	3.64	3.14	1.09
Venturi scrubber	17.58	8.11	7.31	4.55

[1]Total annual costs are computed for both 10 and 20 year capital recovery periods. The capital recovery factor for 10 years is .16275 and for 20 years is .11746.
[2]Direct operating costs include operation and maintenance labor, supervisory overhead, and utility costs. It does not include capital recovery charges or taxes, insurance, and administrative charges (taxes, insurance, and administration are computed at 4 percent of the total capital costs).
[3]Values given for three separate face velocities.
[4]Capital costs for the ESP were calculated in four ways.
a)Ratio from reference (7) using empirical factors- Cost = $11.50/$am^3$/s
b)Itemized major equipment and cost factors Cost = 10.47/am^3/s
c)Escalate from reference (8) Cost = 13.11/am^3/s
d)Ratio from reference (7) using ".6 rule" Cost = 13.13/am^3/s

In addition, the following system parameters specific to each option were specified based on engineering judgment:

HGMF

		Superficial face velocity		
		7 m/s	5 m/s	2 m/s
ΔP_{HGMF}-cm H_2O		33.0	17.8	2.5
Total fan static ΔP,	design	63.5	50.8	38.1
	operating	50.8	38.1	25.4

ESP

Migration Velocity	4.6 cm/s
Specific collection area	100 $m^2/m^3/s$
ΔP_{ESP}	2.5 cm H_2O
Total fan static ΔP, design	5.9 cm H_2O
operating	3.9 cm H_2O

FABRIC FILTER

Air/cloth	1.0 cm/s
ΔP_{FF}	20.3 cm H_2O
Total fan static ΔP, design	50.8 cm H_2O
operating	38.1 cm H_2O

VENTURI SCRUBBER

L/G	93 ℓ/1,000 m^3
ΔP_{VS}	152 cm H_2O
Total fan static ΔP, design	203 cm H_2O
operating	191 cm H_2O
Water recycle ratio	0.9

The scope of the cost estimates includes flange-to-flange costs from the confluence of the particulate collection hoods (e.g., shell and canopy) to the discharge of the clean air from the control device. For the venturi scrubber, costs of sludge treatment equipment are also included. It is assumed that utilities are available at the plant site at the following rates:

Electricity	\$.05/kWh
Plant water	\$.066/1,000 ℓ
Cooling water	\$.026/1,000 ℓ
Compressed air	\$.706/1,000 m^3

CAPITAL COSTS

The total capital costs (TCC) were calculated using a modified Lang method, i.e., applying factors to the purchased equipment costs to account for direct and indirect installation costs.

A substantial amount of engineering judgment is used in formulating these factors. However, the relative order of these factors for the ESP, VS, and FF is consistent with other data (9). These factors reflect the expense necessary to install and put into operation each control option. The ratio between installation costs and purchased equipment costs for HGMF was judged to be lower than for either the ESP or FF.

Table 3 shows that HGMF is more capital intensive than either the ESP or FF. Looking at annualized costs, the venturi scrubber is not competitive with any of the other three options at the given conditions. Direct operating costs, which do not include the cost of capital over the life of the unit, are slightly higher for the HGMF at 7 m/s than for either the ESP or FF. However, the difference in both capital and direct operating costs among the HGMF at 7 m/s, ESP, and FF is well within the probable error of the estimate (±30 percent).

It is important to note that tax considerations are not part of this estimate. Investment tax credits and other tax incentives could offset some of the initially higher HGMF capital costs by reducing the total annualized costs of Table 3.

CONCLUSIONS

The following conclusions were drawn from the field operation of the HGMF mobile pilot plant:

1. Test series were performed on two types of matrices at three levels of matrix packing density. The best overall performance of the HGMF unit was achieved with the expanded metal matrix at a packing density of 6 percent. The highest efficiency level achieved was 96.4 percent with five of nine tests (excluding zero applied magnetic field tests) in the range of 93.9 to 96.4 percent.

2. In the velocity range of 4 to 8 m/s, the expanded metal matrix at 6 percent had lower pressure drops (10 cm H_2O to 46 cm H_2O) than the steel wool matrix (16 cm H_2O to 50 cm H_2O). Given the better overall performance (both efficiency and pressure drop) with the expanded metal at 6 percent packing density, it was the preferred filter matrix.

3. Particle size measurements with cascade impactors were used to measure fractional size penetration. Fractional penetration curves show performance of the HGMF to be relatively poor (85 percent efficiency or less) in the particle size range below 1 μm .

4. Elemental chemical analyses show iron removal efficiencies are higher than overall mass efficiencies as determined from thimble dust samples. However, the data show iron penetration to be as much as 6 percent when overall mass penetration is 9 percent.

5. Potential explanations for inadequate capture of iron-bearing particles include the following:

   a. magnetic forces acting on the fine particles are not sufficent to effect capture as the gas passes through the filter due to insufficient residence time,
   b. some of the iron occurs in complex compounds with zinc that is not sufficiently magnetic to be captured; this is supported by work done at Lehigh University on waste dusts from electric arc furnaces, and
   c. reentrainment.

6. The overall penetration of electric arc furnace dust through HGMF measured in this program must be reduced by a factor of 2 to 6 to compete with the performance of conventional particulate control devices applied to new sources. Standards for existing sources in some states might permit the retrofit of an HGMF.

7. Assuming HGMF performance can reach a competitive level in the configuration and operating mode tested in this program (e.g., 99 percent efficiency), comparative annualized costs for HGMF, fabric filters, ESPs, and venturi scrubbers show that HGMF can compete economically with venturi scrubbers, but is more expensive than fabric filters and ESPs. Since to achieve that level of performance on EAF dust, it would be necessary to reduce gas velocity and/or increase filter length, it will be difficult for HGMF to compete as a control device for EAF's.

REFERENCES

1. Obertueffer, J.A. Magnetic separation: A review of principles, devices, and applications. IEEE Trans. Mag. Mag-110: 223, 1974.

2. Kolm, H.H., Oberteuffer, J.A., and Kelland, D.R. High gradient magnetic separation. Sci. Am. 223: 47, Nov. 1875.

3. Oder, R.R. High gradient magnetic separation theory and applications. IEEE Trans. Mag. Mag-12: 428, 1976.

4. Iannicelli, J. New developments in magnetic separation. IEEE Trans. Mag. Mag-12: 436, 1976.

5. Gooding, C.H., Sigmon, T.W., and Monteith, L.K. Application of high-gradient magnetic separation to fine particle control. EPA-600/2-77-230 (NTIS PB 276-633), 1977.

6. Keyser, N.H., et al. Characterization, recovery and recycling of electric arc furnace dust. Paper presented at the Symposium on Iron and Steel Pollution Abatement Technology for 1981, Chicago, Illinois. October 6-8, 1981.

7. Severson, S.D., Horney, F.A., Ensor, D.S., and Markowski, G.R. Economic evaluation of fabric filtration versus electrostatic precipitation for ultrahigh particulate collection efficiency. FP-775, Research Project 834-1, prepared for EPRI by Stearns-Roger, Inc., 1978.

8. ES&T currents. Environmental Science & Technology. Vol. 12, No. 13, December 1978.

9. Neveril, R.B. Capital and operating costs of selected air pollution control systems. EPA-450/5-80-002, U.S. Environmental Protection Agency, Research Triangle Park, NC, 1978.

NOVEL PARTICULATE CONTROL TECHNOLOGY

by: Senichi Masuda
Department of Electrical Engineering,
Faculty of Engineering, University of Tokyo
7-3-1, Hongo, Bunkyo-ku Tokyo, Japan 113

ABSTRACT

A review of pulse energization and precharging is attempted in view of their inherently great potentials for particulate control and the current controversies around these two technologies. They may provide three major advantages when properly designed and applied. These are "energy-saving", "back corona correction for high resistivity dusts", and "performance enhancement for medium resistivity dusts. The physical backgrounds of these technologes are examined with a special attention on the technical potential of nanoseond pulse. Different designs and operation modes of these technologies are discussed in consideration of various application areas and dust resistivity levels, with an intention to provide a guide-line for correct use of these technologies.

INTRODUCTION

The current interests world-wide in the field of particulate pollution control may be three-fold: "Cost-Effectiveness", "Energy-Saving", and "Submicrometer Particules". To meet with these interests a number of novel technologies have been proposed. Among these are discussed in this review only on "Pulse Energization" and "Precharging", as these are currently under great arguments and controversies, yet are quite certain to provide great impacts when fully developed and properly applied.

PULSE ENERGIZATION

The advantages of "Pulse Energization" currently being expected are three-fold: "Energy-Saving", "Correction of Back Corona" and "Performance--Ehancement at Medium Dust Resistivity". These are based on its inherent feature capable of smoothly decreasing corona current level without degrading a uniformity in its distribution and a main field strength. The current emphasis in this technology is directed to its application primarily for retrofitting to existing precipitators. This is a factor causing various confusions and controversies, as the essential feature of this technology is much more involved. Therefore, a current estimation of its cost-effective-

ness should never be taken as representing its actual potential. The pulse energization is not a single unit operation, but a family of similar but different groups, each having its own specific application area. The design and operation modes of pulse energization differ greatly depending upon the target of its applicatio and dust resistivity level encountered, producing "Energy-Saving Mode", "Back Corona Corection Mode" and "Performance-Enhancing Mode". Another great difference arises from the pulse to be used itself, more exactly its duration time, t_p. These are "Millisecond-Pulse", "Microsecond-Pulse", and "Nanosecond-Pulse". The third difference appears in the construction of electrode system: the conventional "Twin-Electrode System" and "Tri-Electrode System" having an additional third electrode. The fourth difference is whether it is used for retrofitting to an existing plant or in a new plant.

Mode of Operation

a) Energy-Saving Mode: This design or operation mode is directed to the greatest current concern, and applicable in most of the precipitators with and without back corona. The "Intermittent Energization System" - MIE - commercialized by Mitsubishi Heavy Industries (1) may represents a typical example although it also produces back corona correction effect. By a periodical blocking of ac primary current with thyristors the secondary current is blocked intermittently, with a concurrent pulsation of precipitator voltage (Fig. 1). The power consumption is reduced in proportion to decrease in duty ratio, $Rc = t_1/(t_1 + t_2)$. Extensive tests made at a pilot plant and 8 full-scale plants indicate that different grades of improvement in performance can be achieved depending primarily upon the dust resistivity level. The best result is obtained for the high resistivity dusts with 10^{11} - 10^{13} ohm-cm causing severe back corona (low-sulfur low-alkali coal fly-ashes and iron ore sinter-machine dusts) with a reduction in power consumption R = 10 - 30 % and performance enhancement in terms of modified Deutsch migration velocity H = 1.1 - 1.7 at the optimum duty ratio Rc = 1/5 - 1/3. A moderate improvement is achieved for the medium resistivity dusts with 10^{10} - 10^{12} ohm-cm causing slight back corona (general overseas coal fly-ashes) with R = 30 - 50 % and H = 1.1 - 1.3 at Rc = 1/3 - 1/2. However, in the case of medium-low resistivity dusts with less than 10^{11} ohm-cm causing no back corona, the advantage of the MIE is greatly reduced, indicating a maximum of power reduction R = 50 % with a slight performance degradation H = 0.8.

b) Back Corona Correction Mode: This is the most fruitful application area of pulse energization. The pulse voltage is applied intermittently to discharge electrodes on top of a dc "Base Voltage", V_{dc}. In the case of a tri-electrode system, the dc base voltage is applied between the third and collecting electrodes, and the pulse voltage is applied across the third and discharge electrodes. Most important, it is imperative to produce corona discharge only at an instant when the pulse voltage is applied, but never in a period between two successive pulses. Otherwise, a precise control of corona current by means of pulse parameters (frequency, f_p; crest voltage V_p; duration time, t_p) necessary for correction of back corona is lost. Back corona can be corrected by lowering corona current density, i_d, so as to meet the following criterion:

$$i_d \times r_d < E_{ds} \quad (1)$$

where r_d = dust layer resistivity. The correct selection of V_{dc} is of utmost importance in this case. In the case when r_d is not too high, V_{dc} can be set close to corona inception voltage, V_c. Care must be taken, however, when r_d becomes very high, exceeding say 10^{12} ohm-cm, to cause a severe back corona and a great hysteresis in V-I curve with its inception voltage, V_c, much higher than its extinction voltage, V_e. In this case the level of V_{dc} must be set slightly below V_e (2,3). The reason for this is to avoid an uncontrollable runnaway of back corona in a form of its lateral propagation (4). The large hysteresis in V-I curve is due to both self-stabilization of local back corona and its lateral propagation to cause a time-dependent current increase. This begins to occur when the field intensity in the collection field, E, exceeds a level of streamer propagation, E_{st} (ca. 5 kV/cm in air at NTP) (2). Now, even if V_{dc} be set lower than V_c or at a value with E lower than E_{st}, stochastic fluctuations of process parameters may cause back corona at a local point somewhere in a large collection field, as well as its lateral propagation. Once this happened, it can never be extinguished unless V_{dc} be decreased below V_e. The constraint to maintain V_{dc} below quite a low level V_e produces a great difficulty as it inevitably impairs collection performance (3). This may lead to a thought that pulse energization may be useless for extremely high resistivity dusts. However, a possibility of its correction arises from a fact that it takes at least several seconds before the lateral propagation reach a detrimental level. The author and his co-workers confirmed the effectiveness of an operation called "Back Corona Quenching" which is an intermittent abrupt lowering of V_{dc} from a high level close to V_c to zero and a succeding recovery to its original level. The entire back corona is immediately quenched, and the current shows a fairly slow time-dependent rise although V_{dc} is as high as V_c. Before the current reaches a detrimental level by lateral propagation, the quenching operation is repeated. Its combination with pulse energization will be tested in more detail in the author's laboratory. It is felt that the pulse energization for better correction of back corona will require a more sophysticated control of power supply, which in turn will neccesitate the development of more advanced "Back Corona Sensors". The "Bipolar Current Probe" (5,6), enabling on-line measurement of both negative and positive ionic current desities, may meet such a requirement.

The merits of pulse energization becomes diminished with increasing dust resistivity, and completely lost beyond say 10^{13} - 10^{14} ohm-cm. First, a shortage occurs in corona current density (ion depletion) to meet the condition (1), lowering greatly the particle charging speed. This necessitates the use of a "Back Corona Free Precharger" in front of a pulsed collection field, as discussed later. Second, at an extremely high dust resistivity particle charge in a dust layer is retained to form a space charge, and this modifies greatly the field distribution inside to invalidate the above criterion (7). Back corona occurs at a certain layer thickness, called "Limiting Thickness", independent of its resistivity (even when i_d = 0 in extreme cases), so far as an externally applied field, E, exists (7). Back corona is enhanced by increasing corona current with a decrease in the limiting thickness. In other words, in the presence of corona current, back corona occurs sooner or later, unavoidable even with the pulse energization, unless dust layer be constantly cleaned. This was

cleary confirmed by using the bipolar current probe (5). Back corona at such a high resistivity takes a form of a large number of very feeble scattered glow spots (glow-mode) (5,7,8), hard to detect by visual observation, yet emitting large quantity of positive ions in total (5). The only possible electrical control means in this case is to use a two-stage precipitator consisting of a back corona free precharger and a parallel-plane collection field, as described later.

A number of pulse-energized ESP's, both of twin-electrode systems (9-12) and tri-electrode systems (13-15), indicated more or less successful results in improving correction efficiency for high resistivity dusts.

c) Performance-Enhancing Mode: This mode is for enhancing a collection performance at a medium dust resistivity causing no back corona. V_{dc} is set close to the sparking voltage, V_s, and pulse voltage is applied on its top. Since the pulse spark voltage becomes increasingly higher with decreasing its duration time, t_p, the overall crest voltage can be raised beyond the dc spark voltage, V_s. It is expected that particle charge could be raised concurrently to produce an enhancement of collection performance. The enhancement up to about H = 1.2 is reported by several investigators, while others recognize no distinct improvement. The whole story is still underlying a great controversy. More time seems to be required before a definite condition for enhancement and its extent can be more clearly identified.

Pulse Duration Time

A pulse voltage propagates along a corona transmission line, consisting of discharge and collecting electrodes (or discharge and third electrodes in a tri-electrode system), with a speed close to light velocity, i.e. about = 0.3 m/nanosecond (16) The exact speed in a lossless line is given by $v_p = 1/(LC)^{1/2}$, where L and C represent line inductance and capacity per unit length. Hence, the geometrical length on a line of a pulse voltage wave with t_p nanosecond duration time is about $l_p = 0.3 \times t_p$ m. In the case when the length of the line, L_1, is longer than about $l_p/3$ - a condition for the mulitiple-reflected portion of the wave to occupy, before decaying, only a fraction of the total wave length - the pulse voltage behaves as a travelling wave, and the line must be treated as a distributed constant circuit. Whereas, in the case when l_p is much longer than L_1, its character as a wave is lost, and the line should be treated as a circuit with lamped constants, L, C and R. Assuming L_1 = 100 m in a practical plant, the critical pulse duration time dividing these two regions is roughly t_p = 1,000 nanoseconds. In other words, the nanosecond pulse with t_p shorter about 1,000 nanoseconds should be treated as a travelling wave, whereas the microsecond and millisecond pulses necessitate a circuit handling with lamped constants. A great difference occurs concurrently in physical phenomena and engineering approach to the designs of electrode system and pulse power supply.

a) Nanosecond-Pulse: In this case the energy is concentrated in the localized travelling voltage wave. The necessary energy input from the pulse power supply into the line can become lower than the other types of pulses depending upon the level of l_p/L_1. The negative streamer coronas are triggered by this pulse wave to appear uniformly along the line (Fig. 2),

but lasting only a very short time to make spark voltage extremely high. During the course of propagation the pulse wave is gradually eroded by these streamers from its front edge of the peak (Fig. 3), finally to become impotent so as not to trigger the streamers any more. The streamers act as a plasma ion source with ion concentration of about 5×10^9 ion pairs/cm^3 (17), emitting negative ions to the charging and collection zone with the aid of dc base field. The streamers are produced in a very short time of only several nanoseconds, but its plasma life time is as long as several milliseconds, owing to a slow process of ion recombination. Hence, the corona current lasts for several milliseconds, too (17,18). The pulse energy is also consumed by ohmic loss of the line enhanced by skin-effect especially at its sharp rising front. As a result, its rising speed becomes gradually slowed down. Hence, after losing its power of producing streamers, the pulse wave becomes flattened after multiple-reflection, finally to become a dc voltage covering uniformly the entire length of the line and to be added to the dc base voltage. This part may represent a final loss as a pulse energy, but actually it is converted into a dc energy. The greatest advantage of the nanosecond-pulse is based on the facts that its short duration time is still long enogh for a streamer to be fully developed, that its energy can be fully squeezed out into corona by using novel technologies specific to its wave nature, such as wave reflection, wave compression, etc., and further that its pulse power supply can be made extremely simple, efficient and cheap, when properly desinged.

Fig. 4 illustrates one of such power supplies. The capacity of the pulse forming condenser, C_p, is very small depending upon nl_p/L_1, where n = number of parallel corona transmission lines to be pulsed, since the magnitude of C_p comparable to the electrostatic capacity of total lines is large enough in this case. Its charging is made by an ac voltage from its zero level through a rectifier and a very small protective resistance. This "AC Charging" mode greatly reduces charging loss compared to an ordinary "DC Charging". The condenser voltage after charging is held by the rectifier up to the next half cycle, when the polarity of ac voltage is reversed. Switching is made in this cycle by a rotary spark gap to the feeder cable acting as a resistive load equal to its surge impedance $Z_o = (L/C)^{1/2}$. The voltage wave is distributed from the feeder to a number of corona transmission lines in the collection field. The rush current from the ac main source after switching is interrupted by the rectifier, allowing the use of such a low protective resistance. The erosion rate of the spark elements can be made acceptably low by a correct selection of material, requiring a replacement about once a year. Fig. 5 shows a picture of one such pulse power supply (V_p = 55 kV; rise time t_r = 65 nanoseconds; t_p = 400 nanoseconds (half-peak width); f_p = 50 z; 7.75 kW output pulse power for 5 ohm surge impedance; 90 % efficiency) which is very compact in size and very high in efficiency.

"Coupling" of pulse power to a feeder at a high dc base voltage is a problem to be carefully considered. This is made in a twin-electrode system through a coupling condenser which is not only expensive but also produces a "Coupling Loss" inversely proportional to its capacity. In a tri-electrode system, however, a direct coupling can be used to remove this problem.

"Tapping" of pulse energy from a feeder to the lines also causes a problem, owing to an abrupt drop of surge impedance at each tapping point which causes a partial reflection of pulse voltage wave. A stepwise drop of pulse voltage occurs in the feeder downstream of each tapping point,

impairing uniform distributiom of pulse power. Fig. 6 illustrates a "Graded Feeder" (19) solving this problem by compensating the tapping effect with a stepwise increaese of its surge impedance.

Finally, one must also look at the "Corona Transmission Line" itself. Its terminal must be opened in any case to recover the pulse energy by reflection. The modification of pulse wave form due to corona loss, with its crest lowered and duration elongated, must be corrected so that the pulse energy can be fully squeezed out into corona formation so as to produce a longest possible active length of the corona transmission line and to reduce the cost and power consumtion of the pulse power supply. One of the possible solutions is "Pulse Compression" (20) effected by a gradual or stepwise increase of a line surge impedance. This can be made by inserting inductances (ferite cores, coils, etc.) into the line, or by lowering the line capacity with decreasing electrode width or gap. Partial reflection of voltage wave occurs on the line either continuously or in multiple steps to produce such a "Compression". Fig. 7 indicates examples of a single pulse compression made by inserting a coil in series to a 100 m zig-zag corona transmission line. A peaking produced by its open end should also be noted. The tri-electrode pulse-energized field is being developed for practical application in the author's laboratory in consideration of its advantage in eliminating the coupling condenser and its greater flexibility in electrode design and voltage control.

b) Microsecond-Pulse: In this case a precipitator behaves essentially as a capacitive load with a very high corona resistance in parallel. The entire inter-electrode capacity is fully charged by the "non-travelling" pulse voltage to store quite a large capacitive energy $(1/2)CV^2$. The pulse wave forming requires the removal of this energy from the system after a desired pulse duration time. Since this capacitive energy is much larger than that consumed by corona, it must be recovered to the tank condenser of pulse power supply, using "L-C oscillation" through a thyrister switch and a reverse rectifier (Fig. 8)(11,21). The recovery rate can be made quite high, about 70 to 90 %. However, for this energy recovery scheme to be effective, the capacity of the high voltage tank condenser should be about one order of magnitude larger than that of an entire electrode system. In addition, the twin-electrode system requires a pulse transformer or a coupling condenser for a pulse coupling (Fig. 8 (a)). The direct coupling is possible in the tri-electrode system, requiring, however, a switching element to drain the residual charge from the load capacity after each recovering cycle (Fig. 8 (b)).

An enhancement in collection performance in the range of H = 1.2 - 1.7 can be obtained by using the microsecond-pulse in both tri-electrode system (13,22) and twin-electrode system (9-12). Its effect becomes pronounced with increasing dust resistivity. The advantage of microsecond-pulse is that it can generated by using a thyrister switch, a well-proven solid-state element completely free of erosion, and that its noise levels, both sonic and electromagnetic, remain substantially lower than the spark-switch. An instantanuous power flowing through the pulse transformer is quite large, requiring a concurrently much larger current capacity than corona current itself. Its step-up ratio is restricted, so that many series-connected thyristors must be used in its primary to cope with a high primary voltage.

c) Millisecond-Pulse: A great advantage of using the millisecond-pulse is a simplicity of its power supply with its cheaper cost. This is because the pulse formation control can be made at the primary of the main transformer by simply interrupting the primary current. The "MIE System" (Fig. 1) is one of its typical examples. Of course, the circuit as shown in Fig. 8 can also be used to produce a better pulse wave form. As the pulse-induced saw-teeth voltage produces a kind of dc bias voltage, it can be omitted in this case. The millisecond pulse in both twin-electrode and tri-electrode systems, not only produces an "Energy-Saving", but also "Back Corona Correction" for high resistivity dusts (1,13-15)). However, an advantage of increasing spark voltage, specific to a narrow pulse, is lost in the millisecond pulse. Hence, an overall crest voltage is restricted to a dc spark voltage, reslting in a lower effective dc base voltage. This provides a performance limitation in the medium resistivity applications (1).

Retrofitting or New Plant Application

The current emphasis is primarily placed on a retrofitting use of pulse energization for improving substandard performance of existing plants. Hence, the conventional electrode construction poses a definite constraint on its applicable mode, often requesting a modification of sound approaches of pulse power technology. A direct pulse coupling must be excluded because of a twin-electrode design, and the use of a cost-effective, energy-saving nanosecond-pulse can not be considered. This situation is quite understandable in view of of the current urgent interests. It should not be overlooked that noticeable advantages are being obtained by such retrofitting when properly designed and applied. Anyway, it should be emphasized that the current data from retrofitting applications should not be taken as reflecting its maximum potential. Fig. 9 (c) shows one of the possibilities of introducing a nanosecond pulse technology into an existing ESP, by attaching a long non-corona wire (dotted line) close to the convetional corona wires to constitute a "Corona Transmission Line" in a form of a tri-electrode system. Figs. 9 (a) and (b) illustrate the corona transmission lines of twin- and tri-electrode systems, both applicable to a new plant.

PRECHARGING

The precharging is used in a mode of "Two-Stage Module" for "Energy--Saving", "Back Corona Correction", or "Performance-Enhancement" of the downstream ESP field. The module consists of a precharger and an ESP, either conventianal (dc-energized), or pulsed, or non-corona (parallel-plane) type. In a high resistivity application, the precharger must be, first of all, "Back Corona Free" with its absolute charging performance being the second priority. Only at a medium dust resistivity causing no back corona, the "High-Performance Precharger" comes to the highest rank.

Hardwares of Precharger

a) High Intensity Ionizer: The well-known "High Intensity Ionizer" (Fig. 10) (23) represents one of the typical "High-Performance Prechargers". The gas velocity in an annular charging zone is made very high (about 30 m/s). The thick metal rod supporting a disc-like corona electrode produces a radial controlling field. The sparking voltage in the charging zone is

extremely high, beyond say 10 - 12 kV/cm, with a concurrently very high current density of 20 - 30 mA/m^2, so that a charge-to-mass ratio obtainable at its outlet can be 20 - 100 micro-coulombs/g depending upon the particle size. This may be due to the very high gas speed to produce a downstream shift of a dense ionic and dust space charge from the critical anode region which otherwise launches spark in the presence of such field-enhancing space charge. An effective shift may be assisted by a radial field of the metal rod to confine the ionic current into a narrow disc-like pattern and to avoid its upstream divergence. The high gas speed must be slowed down at its outlet by locating a free conjunction space to a level acceptable to the succeeding collection field. Care must be taken so as not to produce a too big free volume. Otherwise, a highly charged dust cloud produces an extremely high space-charge field as to cause positive coronas at many protruding grounded points. These coronas continue to emit copious positive ions to the dust cloud to reduce its charge, and never stop till the space-charge induced local field at each point drops below a corona inception level. Thus, particle charge is self-limited to a level inversely proportional to the linear dimension of the conjunction space. This problem can only be solved by dividing the space into a number of smaller regions with metal members. High resistivity dusts can easily cause back corona at the throat surface owing to a high current density. This is corrected by injection of steam to the critical surface region of the throat to reduce dust resistivity, which however resluts in an additional cost. The High Intensity Ionizer certainly provides an enormas potential when properly applied.

b) Tri-Electrode Precharger (EPA/SoRI Precharger): Fig. 11 illustrates one of the "Back Corona Free Prechargers", called "EPA/SoRI Precharger" (24) comprizing a grid electrode close to a plate of a twin-electrode corona system. The grid is fed with a negative bias-voltage so as to avoid arrival of negative ions to cause back corona. The negative ions from the discharge electrode is allowed to pass through the grid openings to reach the plate. Back coronas on the plate are expected from the first, but positive ions are to be collected by the grid completely. When the potentials of discharge and grid electrodes are properly tuned to each other, a very good charging performance can be obtained (24). The grid bias-voltage must be high enough to avoid a back corona on it, but never exceeds a critical level to produce "Streamer-Mode Back Corona" (8) in the grid/plate interspace. Otherwise, a "Lateral Propagation" of an original corona may start, finally to produce a uniformly bi-ionized atmosphere in the entire interspace, emitting copious positive ions to the charging space so that the control of grid is completely lost. "Back Corona Quenching" control described previously, by an intermittent abrupt zero-setting of the grid voltage, proved to be effective for its correction. A micro-processor control may also provide a reliable tuning. Large scale pilot plant tests of this precharger are going at a Bull Run Power Station (25). These will bring this technology to a mature level to make its inherent potential available to a public.

c) Water-Cooled Prechargr (EPA/DRI Precharger: Fig. 12 illustrates another "Back Corona Free Precharger", called "EPA/DRI Precharger" (26) using water-cooled grounded pipes for the anodes. The resistivity of dust layer covering the pipe surface can be reduced by lowering its temperature,

so that back corona can be eliminated. A very satisfactory charging performance can be obtained, so far as the water temperature in the pipes be kept below a certain critical level. The largest attraction of this precharger is its simple construction and, possibly a lower cost. The most essential factor to be carefully considered in this precharger is an effective removal of dust deposit from the pipe surface. Otherwise, the poor heat conductivity of porous dust layer should produce, in combination with its increased thickness, a temperature rise and local increase in dust resistivity at the dust layer surface being constantly subjected to a hot gas flow, finally to produce back corona. The dust removal is made by mechanical rapping of pipes, but when applied in a large ESP, the use of mechanical scrapers may become imperative. Concentrations of SO_3 and H_2O in the flue gas are another critical factors deciding the effectiveness of this precharger.

d) Boxer-Charger: Fig. 13 illustrates the third example of the "Back Corona Free Prechargers", called "BOXER-CHARGER" (18,27-29). Unlike all other prechargers, BOXER-Charger uses an alternating field in its charging zone between two double-helix electrode units (Fig. 14 (a)). When one of them takes a negative peak of its ac voltage, a nanosecond pulse voltage is applied across its two herical wires. This proceeds as a travelling wave along a corona transmission line of the two helical wires, producing uniform streamer coronas along the line (Figs. 14 (b), 15 (b) and (c)). At first negative streamers (Fig. 15 (b)) are launched from the negative wire. Then, positive streamers (Fig. 15 (c)) are emitted from the positive wire when the pulse voltage is high enough. This is very well indicated in the streak-photograph of these streamers (Fig. 15 (a)) (18). The negative streamers produce only a small erosion in the pulse wave form ahead of its peak. Whereas the positive streamers causes a large dip downstream of its peak with a concurrently great energy loss (Fig. 16) (16). Negative ions are extracted from the streamer plasma to travel across the charging zone. When the polarity of the ac main voltage is reversed, the opposite double-helix is energized by the nanosecond pulse voltage to emit negative ions to the oposite direction. The dust particles are bombarded by these ions from both sides to be charged rapidly. A great advantage of this charging scheme lies in a possibility of periodical "Charge-Elimination" from the dust-contaminated wires of the double-helix units. The negative ions from a double-helix unit arrive at its oposite unit and accumulate on the surface of dust deposit on its two wires. The dust surface potential rises with time, and would cause breakdown (back corona) if nothing happens. Before that the polarity of the ac field is reveresed so that charge accumulation interrupted. Next, this opposite unit is energized so that plasma is produced very close to the accumulated charge. Hence, it is immediately neutralized by positive ions from the plasma, and the cycle repeats itself. Thus,BOXER-CHARGER possesses a built-in mechanism of back corona correction, when properly designed. After successful tests in a both laboratory and pilot plant, its demonstration model for testing at a larger plant will be completed by March, 1983. Fig. 14 indicates a small BOXER-CHARGER system to be tested at a pilot at an incimerator, and its power supply. It is discovered that a great-energy saving is possible in the pulse power supplies of BOXER-CHARGER by selecting a correct pulse voltage to produce only negative streamers for the plasma ion source. The negative streamers are much less energy-consuming

than positive streamers (16,18), yet can emit almost the same amount of negative ions (17). The nanosecond-pulse power supply, direct pulse coupling, graded feeders, and pulse compression technology described previously are also used in BOXER-CHARGER technology. A pilot plant test of precharging in front of a bag filter was also performed using BOXER-CHARGER with a satisfactory result.

Mode of Operation

a)Energy-Saving Mode: The combination of a precharger with a energy-saving collection field, such as a low-corona conventional field, pulsed-field, or a parallel-plane field, is getting an increased attention in view of an overall energy-saving possibility. Provided dust particles be fully charged by a precharger, only an electrostatic field (parallel-plane system) should be required for their collection. At a very high dust resistivity, beyond say 10^{13} ohm-cm, this approach is possible (30), as the particle charge is preserved in the dust layer on a collecting electrode to produce enough electrical adhesion force. At a medium resitivity, say below 10^{11} ohm-cm, the parallel-plane collection field indicates a very good performance at an initial stage of operation. However, with the growth of dust deposit on the planes a time-dependent performance degradation by dust reentrainment occurs (30). This is because the particles arriving at the dust deposit surface quickly lose their original charge at this resistivity level, and are immediately induction-charged to the opposite polarity to be strongly subjected to an electrostatic attraction force. Whereas the surface of dust deposit becomes increasingly rough with its growth, producing a concurrent reduction of its physical adhesion force and increased dust reentrainment. The use of a short water-irrigated field could provide a solution for this problem. In a "Corona Collection Field", either dc- or pulse-energized, the dust reentrainment is greatly reduced as the negative ions from corona produce an adequate electrical adhesion force.

b) Back Corona Correction Mode:

(i) Conventional Twin-Electrode Collection Field: First, let us consider a conventional twin-electrode collection field subjected to back corona activity with bi-ionized atmosphere. The highly charged particles from a precharger lose their charge with time by attachment of positive ions, and their charge finally reach a saturation level specific to the "Back Corona Severity" of this bi-ionized field, defined as the ratio of positive to negative ionic current density, i_p/i_n (5). In other words, the average charge of particles in the back corona field can be always higher than that without precharger, depending upon the back corona severity, and its space distribution in the field which determine their charge decaying velocity and the final level of charge (5). A great difference is produced by whether back corona is localized in a form of channels (lower resistivity), or it is uniformly distributed (very high resistivity). In the former case, the overall charge decaying speed becomes fairly low to produce a high average particle charge, even if a local severity of back corona be quite high. Whereas the latter type of back corona is highly detrimental. Anyway, it is highly preferable to use in series a multiple number of "Precharger/Collection Field Modules" to compensate the back corona induced degradation of

charge repeatedly. Fig. 17 (a) shows laboratory data indicating a great advantage of such a multi-module design (dotted line). This produced an enhancement of Deutsch migration velocity (not modified) as high as 2.44 (Table 1) (29).

(ii) Pulsed Collection Field: Perhaps the module out of "Precharger/Pulsed Collection Field" would represent the most favorable combination. The highly charged particles from a precharger can preserve their charge in the pulsed collection field operated in the back corona correction mode, as no positive ions exist. A slight quantity of negative ionic current can provide adequate electrical adhesion force to the dust layer on the collecting electrode to avoid dust reentrainment. Fig. 17 (b) indicates the laboratory data of this multiple-module design (dotted line), with the enhancement factor as high as 2.9 (Table 1) (29). This performance level is exactly the same as that obtained for the medium resistivity dust at normal temperature, completely free of back corona (29).

(iii) Parallel-Plane Field: In the case when dust resistivity becomes extremely high, beyond say 10^{15} - 10^{16} ohm-cm, neither a dc- nor pulse-energized collection field can perform at all after a precharger, indicating practically zero electrical collection performance. Only possible way of electrical collection is to use the parallel-plane field (30). Even Boxer--Charger loses its charging performance when operated at negative charging mode, and its normal charging performance is obtained only at positive charging mode (30).

c) Performance-Enhancing Mode: The primary interest of this mode is a retrofitting use to improve a substandard performance of an existing precipitator operating at a medium dust resistivity causeing no back corona. The second interest is on enhancing overall cost-effectiveness of a new plant for a medium resistivity dust. Emphasis in the precharger is placed primarily on its absolute charging performance, i.e. the levels of field intensity and ionic current density obtainable in its charging field. In retrofitting application, however, care must be taken in advance so as to clearly identify whether the charging is really the cause of a trouble. This is because the particle charging in a precipitator at medium dust resistivity is usually quite good, showing enough charging speed and charging level, and the substandard performance is mostly produced by other causes. such as under-sizing, non-uniform gas distribution, gas sneakage, uncorrect rapping, etc. As a result the effect of precharging may be quite small (29), or even hardly detectable. In the case of a new plant, an ideal design of precharger /collector module may be possible, combining a high-performance precharger with a "Reentrainment Free Collection Field" such as with a low-current dc- or pulse-energized field, or a parallel-plane field followed by a water-irrigated short corona section.

CONCLUSION

The present status of both pulse energization and precharging technologies are reviewed, with a special attention to the difference in their design and operation modes corresponding to the difference in their application areas and dust resistivity levels encounterd. The physical backgrounds of

various pulse technologies are discussed from a standpoint, how to take full advantage of their technical potentials. The pulse energization and precharging technologies have great potential advantages of energy-saving, back corona correction, and performance-enhancement for medium resistivity dusts. Their application areas are two-fold: retrofitting use in an existing plant, and use in a new plant. In the former applications, the existing plant poses a great constrain on the design and operation modes of the pulse energization and precharging to be used. In the latter application, theoretically most reasonable design may be possible. It should be emphasized that both technologies are still in the course improvement and elaboration, but their full advantages will surely become available in a near future.

REFERENCES

(1) T. Ando, N. Tachibana and Y. Matsumoto: A New Energization Method for Electrostatic Precipitators - Mitsubishi Intermittent Energization System, Proc. 4th EPA-Symposium on Transfer and Utilization of Particulate Control Technology (Oct., 1982 in Houston, Texas).

(2) S. Masuda, S. Obata and Y. Ogura: Lateral Propagation of Back-Discharge in a Tri-Electrode System, Inst. Phys. Conf. Ser. No. 48 (The Inst. of Phys., London), p. 9 (1979).

(3) M.D. Durham, G.A. Rinard and D.E. Rugg: Evaluation of Novel Electrostattic Precipitator Technology, Proc. 75th Annual Meeting of APCA, Paper No. 82-34.4 (June, 1982 in New Orleans, Louisiana).

(4) S. Masuda and T. Itagaki: Lateral Propagation of Back Corona in Twin-Electrode Type Precipitators, Proc. 4th EPA-Sumposium on Transfer and Utilizatio of Particulate Control Technology (Oct., 1982 in Houston, Texas).

(5) S. Masuda and Y. Nonogaki: Bi-Ionized Structure of Back Discharge Field in an Electrostatic Precipitator, Proc. IEEE/IAS 1981 Annual Conf. p. 1111 (Oct., 1981 in Philadelphia).

(6) S. Masuda and Y. Nonogaki: Sensing of Back Discharge and Bipolar Ionic Current, Journal of Electrostatics, 10 (1981) 73-80 (Elsevier).

(7) S. Masuda, A. Mizuno and K. Akutsu: Initiation Condition and Mode of Back Discharge for Extremely High Resistivity Powders, Proc. IEEE/IAS 1977 Annual Conf., p. 867 (Oct., 1977 in Los Angels, California).

(8) S. Masuda and A. Mizuno: Initiation Condition and Mode of Back Discharge Journal of Electrostatics, 4 (1977/1978) 35-52 (Elsevier).

(9) H.I. Milde and P.L. Feldman: Pulse Energization of Electrostatic Precipitators, Proc. IEEE/IAS 1978 Annual Conf., p. 66 (Oct., 1978 in Tronto, Canada).

(10) H.I. Milde and H.E. VanHoesen: Application of Fast Rising Pulses to Electrostatic Precipitators, Proc. IEEE/IAS 1979 Annual Conf., p. 158 (Oct., 1979 in Cleveland, Ohio).

(11) P. Lausen, H. Hendriksen and H.H. Petersen: Energy Conserving Pulse Energization of Precipitators, Proc. IEEE/IAS 1979 Annual Conf., p. 163 (Oct., 1979 in Cleveland, Ohio).

(12) H.H. Petersen: Application of Energy Conserving Pulse Energization for Electrostatic Precipitators - Practical and Economic Aspects, Proc. 3rd EPA-Symposium on Transfer and Utilization of Particulate Control Technology (March, 1981).

(13) S. Masuda, I. Doi, M. Aoyama and A. Shibuya: Bias-Controlled Pulse

Charging System for Electrostatic Precipitator, Staub-Reinhalt. Luft 36 (1976) No. 1, p. 19.
(14) S. Masuda, I. Doi, I. Hattori and A. Shibuya: Back Discharge Phenomena in Bias-Controlled Pulse Energization System, Proc. 4th Int. Clean Air Congress, Paper No. V-52 (May, 1977 in Tokyo).
(15) S. Masuda: Novel Electrode Construction for Pulse Charging, Proc. 1st EPA-Symposium for Transfer and Utilization of Particulate Control Technology (July, 1978 in Denver, Colorado), Vol.1 (EPA-600/7-79-044a, Feb. 1979).
(16) S. Masuda and H. Nakatani: Distorsion of Pulse Voltage Wave Form on Corona Wires Due To Corona Discharge, Proc. 4th EPA-Symposium on Transfer and Utilization of Particulate Control Technology (Oct., 1982 in Houston, Texas).
(17) S. Masuda and Y. Shishikui: Pulse Corona As Ion Source and Its Behavios in Monopolar Current Emission, ibid.
(18) S. Masuda, H. Nakatani, K. Yamada, M. Arikawa and A. Mizuno: Production of Monopolar Ions by Travelling Wave Corona Discharge, Proc. IEEE/IAS 1981 Annual Conf., p. 1066 (Oct., 1981 in Philadelphia).
(19) S. Masuda, H. Nakatani and T. Kaji: Graded Feeder for Uniform Distribution of Pulse Power to Many Loads, to be published.
(20) S. Masuda and S. Hosokawa: Pulse Compression for Regeneration of Its Energy, to be published.
(21) S. Masuda, S. Obata and J. Hirai: A Pulse Voltage Source for Electrostatic Precipitators, Proc. IEEE/IAS 1978 Annual Conf., p. 23 (Oct., 1979 in Tronto, Canada)
(22) G.W. Penny and P.C. Gelfand: The Trielectrode Electrostatic Precipitator for Collecting High Resistivity Dust, JAPCA, Vol. 28, No. 1, p. 53 (Jan., 1978).
(23) O. Tassicker and J. Schwab: EPRI Journal, June/July (1977) 56-61.
(24) D,H, Pontius, P.V. Bush and W.B. Smith: Electrostatic Precipitator for Collection of High Resistivity Ash, EPA-Report EPA-600/7-79-189 (Aug., 1979).
(25) P.V. Bush, D.H. Potius and L.E. Sparks: Pilot Demonstration of The Precharger/Collector System, Proc. 3rd. EPA-Symposium on Transfer and Utilization of Particulate Control Techanology (March, 1981)
(26) G. Rinard, M. Durham, D. Rugg and L.E. Spark: Development of A Charging Device for High Resistivity Dust Using Heated and Cooled Electrodes, ibid.
(27) S. Masuda, M. Washizu, A. Mizuno and K. Akutsu: Boxer-Charger - A Novel Charging Device for High Resistivity Powders, Proc. IEEE/IAS 1978 Annual Conf., p. 16 (Oct., 1978 in Tronto, Canada).
(28) S. Masuda, A. Mizuno and H. Nakatani: Application of Boxer Charger in Electrostatic Precipitators, Proc. IEEE/IAS 1979 Annual Conf. p. 131 (Oct., 1979 in Cleveland, Ohio)
(29) S. Masuda, A. Mizuno, H. Nakatani and H. Kawahara: Application of Boxer-Charger in Pulsed Electrostatic Precipitator, Proc. IEEE/IAS 1980 Annual Conf., p. 904 (Oct., 1980 in Cincinnati, Ohio).
(30) S. Masuda and S. Hosokawa: Performance of Two-Stage Type Electrostatic Precipitators, Proc. IEEE/IAS 1982 Annual Conf. (Oct., 1982 in San Francisco, California).

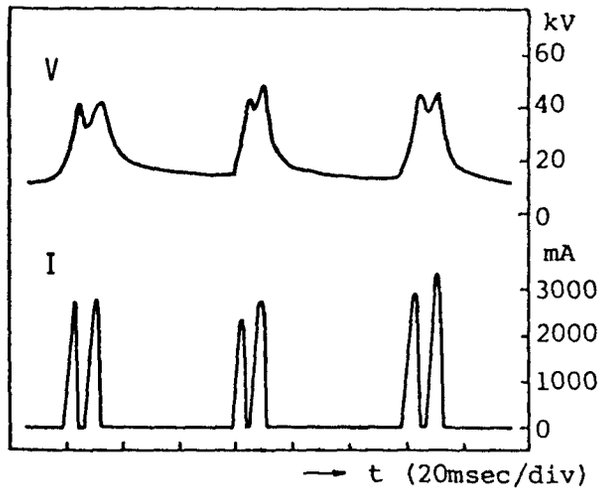

Fig. 1 Voltage and Current Wave Forms of MIE System (Rc = 1/3)

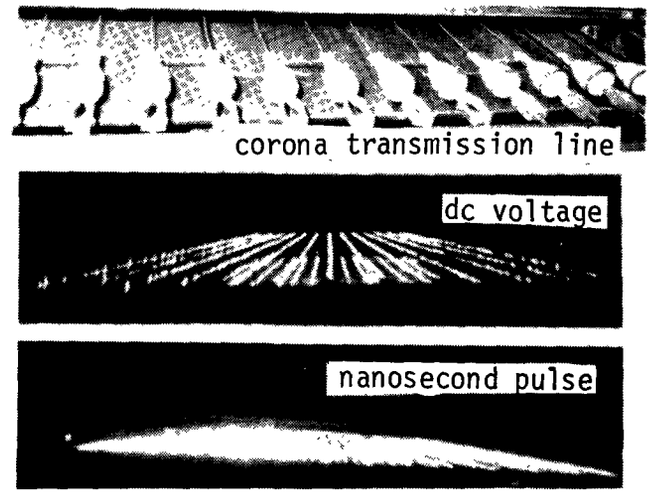

Fig. 2 Comparison between Pulse and DC Negative Coronas (L_1=200m)

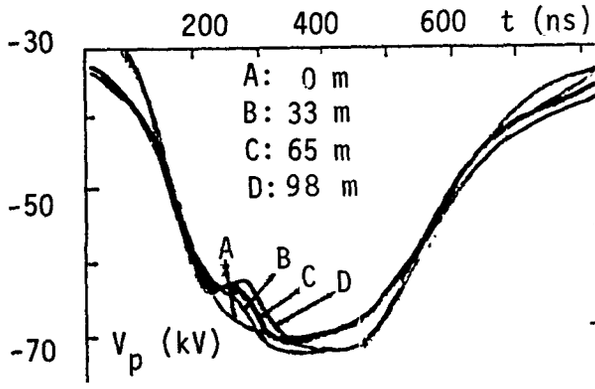

Fig. 3 Erosion of Pulse Voltage Wave by Negative Streamers (V_{dc} = - 30 kV; V_p = - 40 kV)

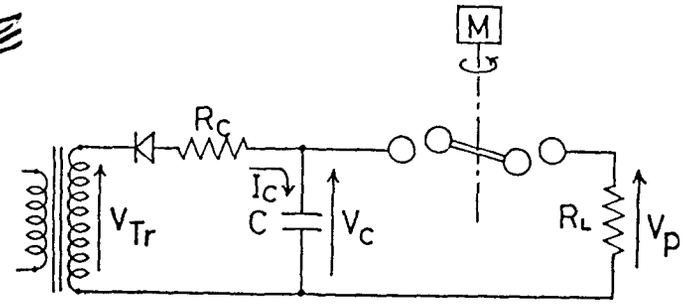

Fig. 4 Nanosecond Pulse Power Supply with AC Charging and Rotary Spark Gap (see Fig. 5)

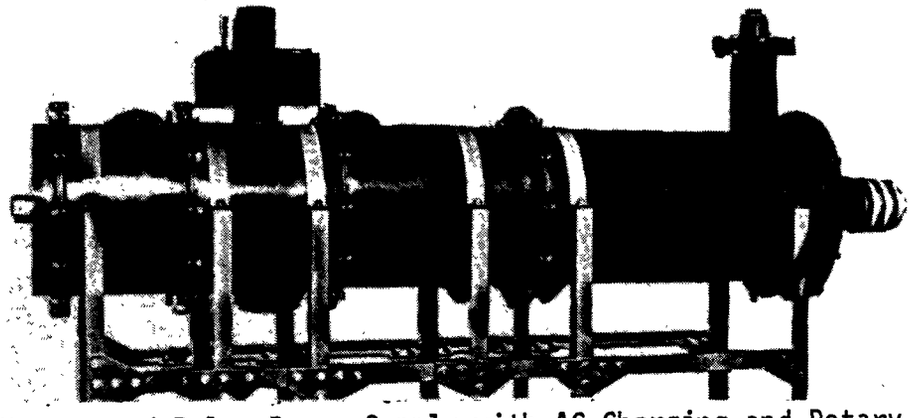

Fig. 5 Nanosecond Pulse Power Supply with AC Charging and Rotary Spatk-Switch (total length = 2173 mm; diameter = 360 mm ; Vp = 55 kV; t_r = 65 ns; t_p = 400 ns; f_p = 50 Hz; W_p = 7.75 kW; eff. = 90 %)

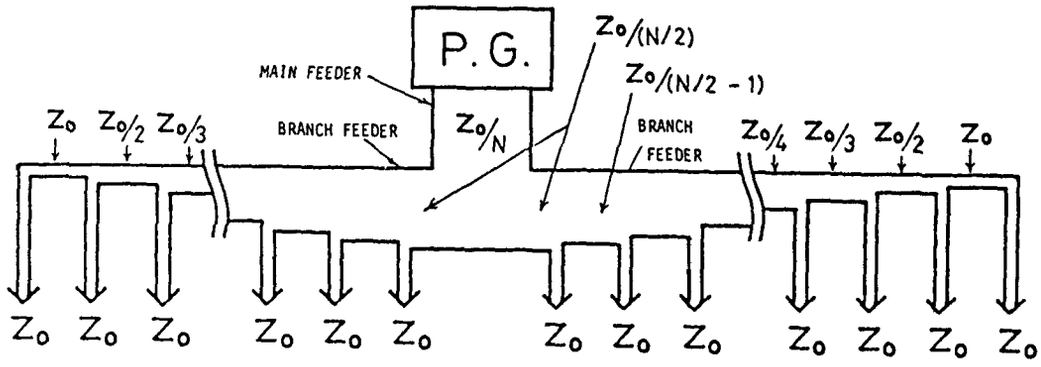

Fig.6 Graded Feeder

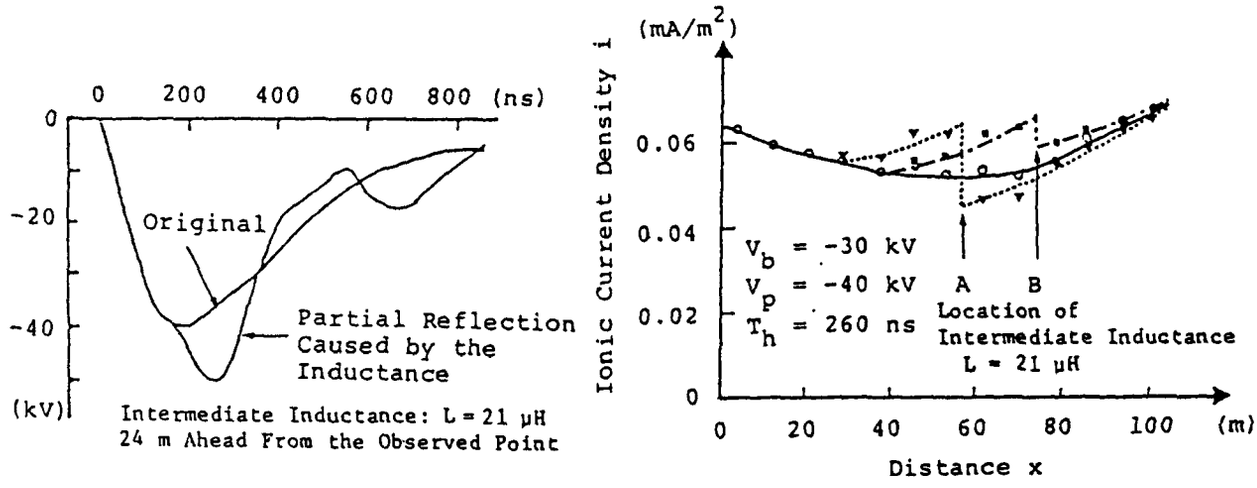

(a) Compressed Wave Form (b) Change of Current Distribution

Fig.7 Pulse Compression by Inserting a Cil (Length of Corona Transmission Line = 100 m ; Coil Inductance = 21 μH)

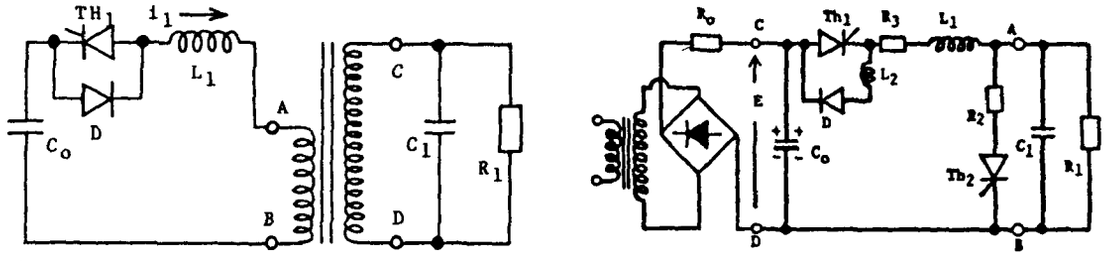

(a) Coupling by Pulse Transformer (b) Direct Coupling with Reset Switch

Fig. 8 Microsecond Pulse Power Supply with Energy Recovery by L-C Oscillation (Co: tank condenser; Th_2: reset thyristor)

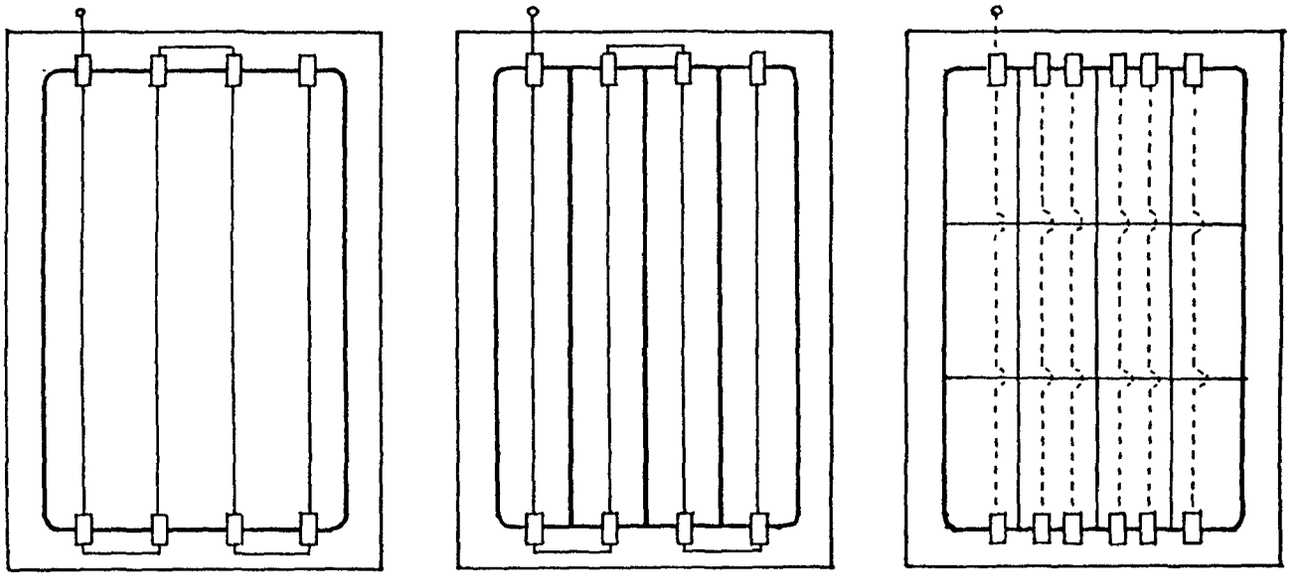

(a) Twin-Electrode System (b) Tri-Electrode System (c) Modified System

Fig. 9 Corona Transmission Line for Nanosecond Pulse Energization

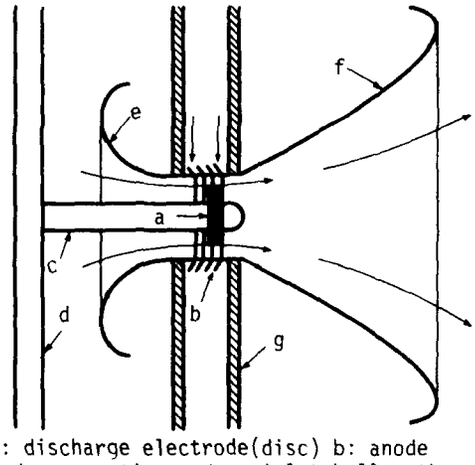

a: discharge electrode(disc) b: anode
c,d: supporting rod e: inlet bellmouth
f: outlet cone g: partition wall

Fig. 10 High Intensity Ionizer

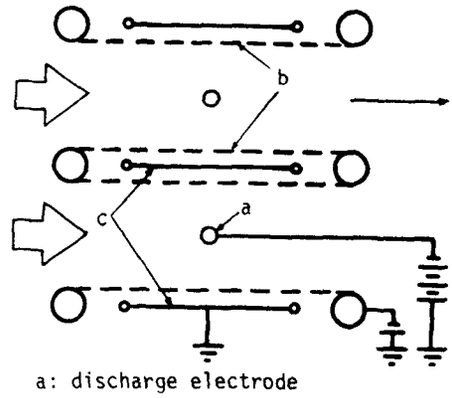

a: discharge electrode
b: grid electrode
c: collecting electrode

Fig. 11 EPA-SoRI Tri-Electrode Precharger

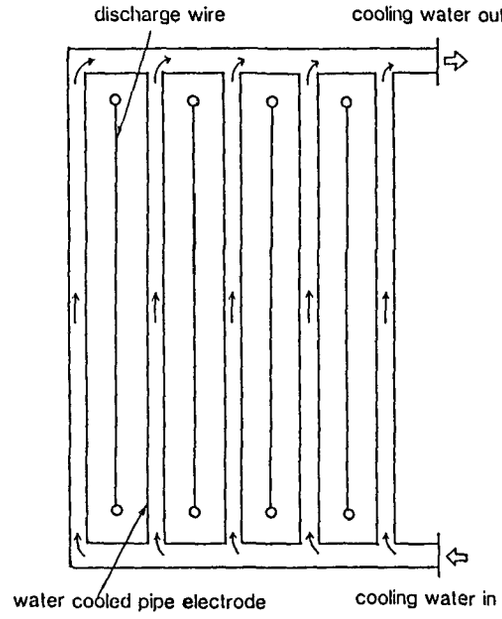

Fig. 12 EPA-DRI Water Cooled Precharger with Heat-Exchanger

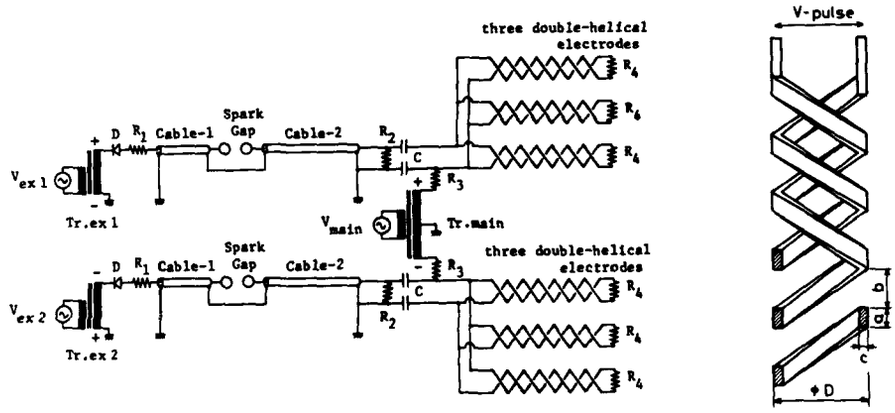

(a) Pulse and Main Voltage Sources

(b) Electrode Element

Fig. 13 BOXER-CHARGER and Its Power Supply (Principle)

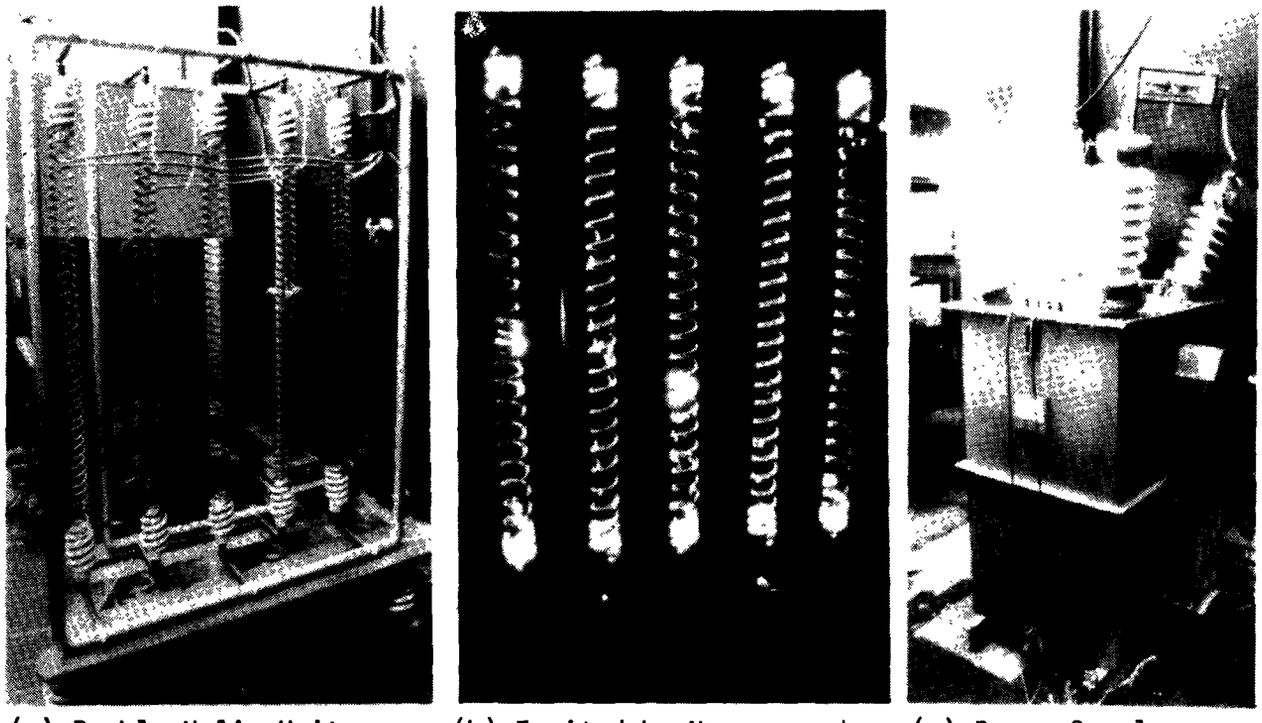

(a) Double-Helix Units (b) Excited by Nanosecond-Pulse Voltage with AC Main Voltage On (c) Power Supply

Fig. 14 BOXER-CHARGER and Its Power Supply for A Pilot Plant Test

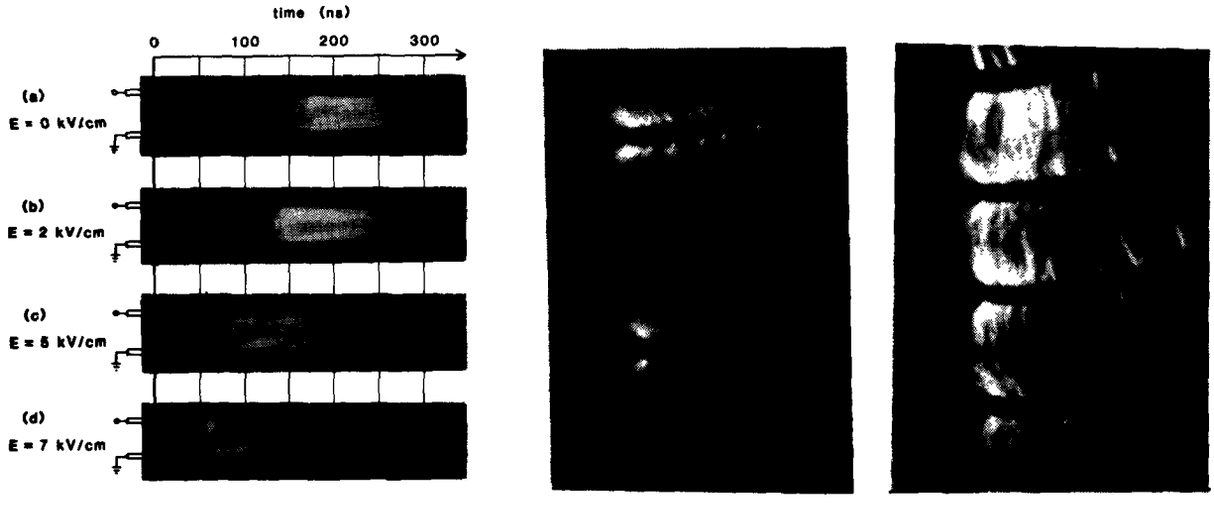

(a) Streak Photograph of Negative and Positive Streamers (b) Negative Streamers only (c) Negative and Positive Streamers

Fig. 15 Streamer Coronas on A Double-Helix Transmission Line Induced by Nanosecond Pulse Voltage

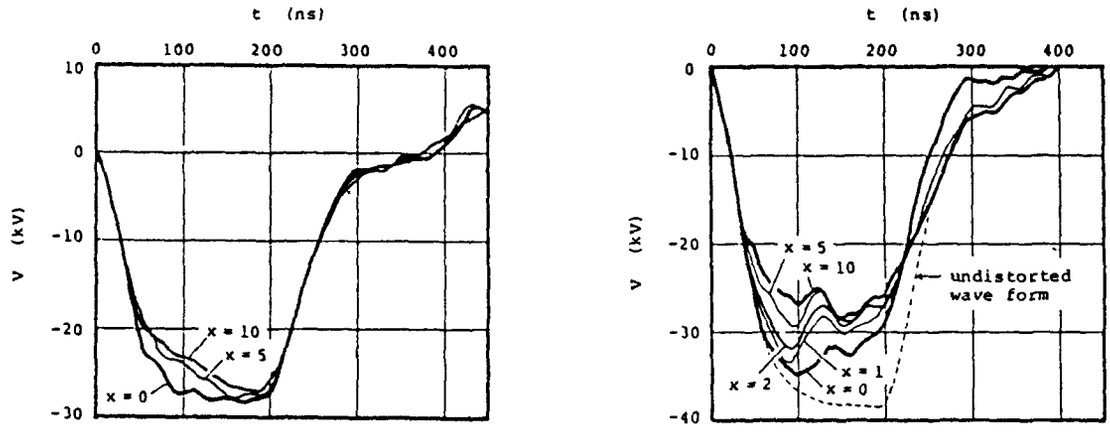

(a) Negative Streamers only (Vp = - 28 kV at inlet; E = - 5 kV/cm)

(b) Negative and Positive Streamers (Vp = - 35 kV at inle; E = - 5 kV/cm)

Fig. 16 Modification of Travelling Pulse Wave Form by Streamer Coronas

Table 1 PERFORMANCE ENHANCEMENT BY MULTI-MODULES OF TWO-STAGE ESP AT HIGH RESISTIVIT FLY-ASH

Operation Mode of Collection Fields	Tg (°C)	ρd (ohm-cm)	Dust Migration Velocity (cm/s)		Enhancement Factor
			precharging off	precharging on*	
DC Operation Mode under Back Discharge	100	10^{11} - 10^{12}	w_o = 11.7	w_1 = 28.6	w_1/w_o=2.44
DC-Puls-Pulse Operation Mode at high ρd	100	10^{11} - 10^{12}	w_p = 19.1	w_{p1} = 34.1	w_p/w_o=1.63 w_{p1}/w_o=2.91
DC OPeration Mode under No Back Discharge	20	< 10^{10}	w_b = 32.7	w_{b1} = 39.5	w_b/w_o=2.79 w_{b1}/w_b=1.21

Remarks: * ----- Repeated precharging mode, Tg = gas temp., ρd = dust resistivity

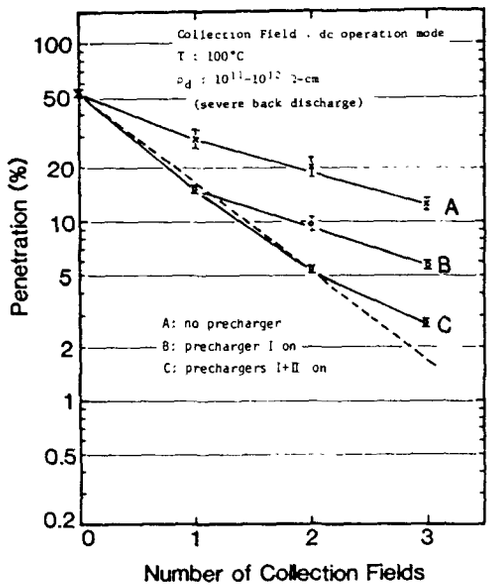

(a) Dust Penetration vs. Effective Length of DC Energized Collection Field for High Resistivity Fly Ash with Prechargers on and off (Base Line - I : 10^{11} - 10^{12} Ohm-cm ; 100 °C)

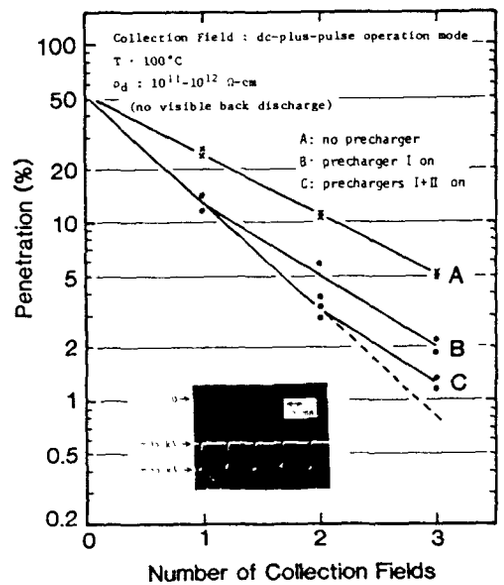

(b) Dust Penetration vs. Effective Length of Pulse-Energized Collection Field for High Resistivity Fly Ash with Prechargers on and off (10^{11} - 10^{12} ohm-cm : 100 °C)

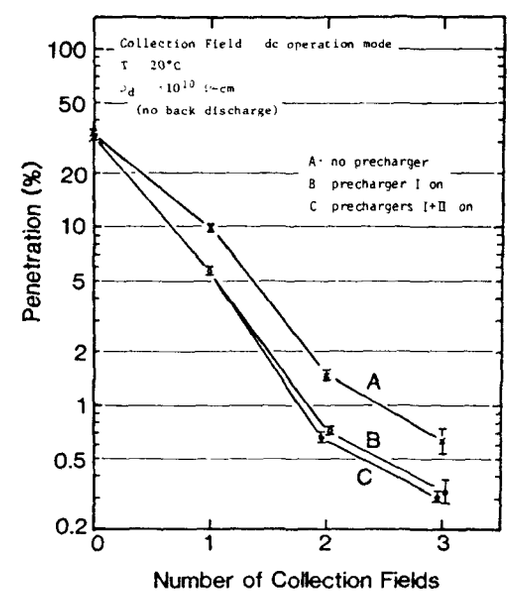

(c) Dust Penetration vs. Effective Length of DC-Energized Collection Field for Medium Resistivity Fly Ash at Room Temperature with Prechargers on and off (Base Line-II: below 10^{10} ohm-cm)

Fig. 17 Dust Penetration vs. Length of Field in Two-Stage Precipitator (Precharger: Boxer-Charger)

AUTHOR INDEX

AUTHOR NAME	PAGE
ADAIR, L.	I-460
ADAMS, R.L.	II-35
ANDO, T.	II-474
ARMSTRONG, J.	III-241
ARSTIKAITIS, A.A.	II-194
BALL, C.E.	III-370
BANKS, R.R.	I-37, I-62
BARRANGER, C.B.	I-132
BAYLIS, A.P.	II-384
BELTRAN, M.R.	II-51
BENSON, S.A.	III-97
BERGMAN, F.	III-154
BIESE, R.J.	I-446
BOSCAK, V.	III-66
BRADBURN, K.M.	II-499
BRADLEY, L.H.	II-369
BRINKMANN, A.	III-211
BUCK, V.	III-335
BUMP, R.L.	II-17
CAPPS, D.D.	I-121
CARR, R.C.	I-148
CHAMBERS, R.	I-226, I-239
CHANG, R.	III-271
CHEN, F.L.	III-347
CHEN, Y.J.	I-506
CHIANG, T.	II-184
CHRISTENSEN, E.M.	II-243
CHRISTIANSEN, J.V.	II-243
CILIBERTI, D.F.	III-282, III-318
CLEMENTS, J.S.	II-96
COE,JR, E.L.	II-416
COLE, W.H.	III-1

COOK, D.R. II-349
COWHERD,JR, C. III-183
COY, D.W. III-370
CRYNACK, R.R. II-1
CUSCINO, T. III-154
CUSHING, K.M. I-148
DAHLIN, R.S. I-192
DARBY, K. II-499
DAVIS, R.H. II-96
DAVIS, W.T. I-521
DAVISON, J.W. III-166
DELANEY, S. I-357
DEMIAN, A. III-66
DENNIS, R. I-22, III-81
DIRGO, J.A. III-26, III-81
DISMUKES, E.B. II-444
DONOVAN, R.P. I-77, I-107, I-316, I-327, I-342
DORCHAK, T.P. III-114
DRENKER, S. III-271, III-282
DRIGGERS, G.W. II-194
DUBARD, J.L. II-337
DUFFY, M.J. II-489
DURHAM, M. II-84, III-241
EBREY, J.M. II-349
ENGLEHART, P.J. III-183
ENSOR, D.S. III-347
FAULKNER, M.B. II-204, II-337
FINNEY, W.C. II-96
FORTUNE, O.F. I-482, I-494
FOSTER, J.T. I-37, I-91
FREDERICK, E.R. I-536
FRISCH, N.W. III-114
FURLONG, D.A. I-287, I-342
GARDNER, R.P. I-77, I-107
GAWRELUK, G.R. II-17
GELFAND, P. II-35

GIBBS, J.L. II-430
GILES, W.B. III-41, III-53
GOLAN, L.P. III-226
GOLDBRUNNER, P.R. II-401
GOLIGHTLEY, R.M. I-164
GOOCH, J.P. II-444
GOODWIN, J.L. III-226
GRANT, M.A. III-81
GREEN, G.P. I-192
GREINER, G.P. I-287, I-357
GRONBERG, S. III-141
GRUBB, W.T. I-62, I-91, I-179
HALL, H.J. II-459
HALOW, J.S. II-96
HANSON , P. I-460
HARMON, D. I-226, I-239, III-131
HAWKINS, L.A. II-194
HERCEG, Z. II-489
HOVIS, L.S. I-22, I-77, I-107, I-287, I-316, I-327, I-342, I-357, III-81, III-347

HOWARD, J.R. I-164
INGRAM, T.J. I-446
ISAHAYA, F. II-154
ITAGAKI, T. II-322
JACOB, R.O. I-446
JENSEN, R.M. I-431
JONES, R. I-303
KASIK, L.A. II-430
KETCHUCK, M. I-482
KINSEY, J. III-154
KOHL, A.L. III-300
KUBY, W. III-271
KUNKA, S. I-239
KUTEMEYER, P.M. III-211
LAMB, G.E.R. I-303
LARSEN, P.S. II-243

LAWLESS, P.A. II-271
LEE, W. I-303
LEITH, D. III-26
LEONARD, G.L. II-230
LEWIS, M. I-179
LIPPERT, T.E. III-280, III-318
LUGAR, T.W. II-184
MARCHANT,JR, G.H. II-444
MASON, D.M. III-256
MASUDA, S. II-139, II-169, II-322, III-386
MATSUMOTO, Y. II-474
MATULEVICIUS, E.S. III-226
MCCAIN, J.D. III-198
MCCOLLOR, D.P. III-97
MCDONALD, J.R. II-204
MCKENNA, J.D. I-210
MCLEAN, K.L. II-489
MENARD, A. I-255
MILLER, M.L. I-482
MILLER, R.L. I-494
MILLER, S.J. III-97
MITCHNER, M. II-230
MOSLEHI, G.B. II-288, II-306
MOSLEY, R.B. II-204
MOYER, R.B. I-460
MUSGROVE, J. I-382
MYCOCK, J.C. I-210
NAKATANI, H. II-169
NG, T.S. II-489
NOVOGORATZ, D. II-349
OGLESBY, S. II-534
O'ROURKE, R. III-318
PEARSON, G. I-121
PETERS, H.J. I-179
PIULLE, W. II-401
PONTIUS, D.H. II-65

PUDELEK, R.E. I-521
PUTTICK, D.G. II-126
QUACH, M.T. I-506
RAMSEY, G.H. I-316, I-327
RANADE, M.A. III-347
REED, G.D. I-521
REHMAT, A. III-256
REIDER, J.P. III-183
REISINGER, A.A. I-179
RICHARDS, R.M. I-255
RICHARDSON, J.W. I-210
RINARD, G. II-84, III-241
ROOP, R.N. I-460
ROSS, D.R. I-164
RUGENSTEIN, W.A. II-430
RUGG, D. II-84, III-241
RUSSELL-JONES, A. II-384
SAIBINI, J. I-132
SAMUEL, E.A. I-1, II-218
SANDELL, M.A. II-1
SAWYER, J. III-271
SEARS, D.R. I-192, III-97
SELF, S.A. II-230, II-228, II-306
SHACKLETON, M. III-271
SHISHIKUI, Y. II-139
SMITH, W.B. I-148
SORENSON, P.H. III-362
SPARKS, L.E. II-204, II-271, II-337
SPENCE, N. I-132
SPENCER,III, H.W. I-506
STELMAN, D. III-300
STOCK, D.E. II-261
SUHRE, D. III-335
SUNTER, T.C. I-48
SURATI, H. II-51
TACHIBANA, N. II-474

TASSICKER, O.J. III-271, III-282
THOMPSON, C.S. III-12
THOMSEN, H.P. II-243
TOKUNAGA, O. II-96
TREXLER, E.C. II-96
TRILLING, C.A. III-300
TSAO, K.C. III-256
VANN BUSH, P. II-65
VANOSDELL, D.W. I-287, I-342
WALSH, M.A. I-482
WEBER, E. II-111
WELLAN, W.G. I-420
WEXLER, I.M. II-521
WHITTLESEY, M. I-482
WILCOX, K. III-154
WILLIAMSON, A.D. III-198
YAMAMOTO, T. III-241
YEAGER, K.E. . . . . III-xv

☆ U S GOVERNMENT PRINTING OFFICE 1985 - 559-111/10739